Spacecraft Manoeuvring in the Vicinity of a Near-Circular Orbit

Andrey Baranov

Spacecraft Manoeuvring in the Vicinity of a Near-Circular Orbit

Spacecraft Manoeuvring in the Vicinity of a Near-Circular Orbit

By

Andrey Baranov

Cambridge Scholars Publishing

Spacecraft Manoeuvring in the Vicinity of a Near-Circular Orbit

By Andrey Baranov

This book first published 2022

Cambridge Scholars Publishing

Lady Stephenson Library, Newcastle upon Tyne, NE6 2PA, UK

British Library Cataloguing in Publication Data
A catalogue record for this book is available from the British Library

ISBN (10): 1-5275-8472-0
ISBN (13): 978-1-5275-8472-3

TABLE OF CONTENTS

PREFACE

In this book the author shares his more than 45-years' experience in the field of spacecraft manoeuvre determination in near-circular orbits.
In the second half of the 70s, the ballistics center of the Keldysh Institute of Applied Mathematics in the USSR Academy of Sciences was assigned a task to solve the problem of manned and unmanned spacecraft ballistics and navigation support. The greatest challenge was to solve the multiple-impulse rendezvous problem for these types of spacecraft and space stations.

The author studied the literature available at the time concerning the rendezvous problem in order to find an analytical or numerical analytical solution but there was no answer to that question. As a rule, some cumbersome numerical solutions were used.

Analytical and numerical analytical solutions presented in the works of J.-P. Marec and J.E. Prussing were only related to the nondegenerate rendezvous problem (Prussing studied the coplanar rendezvous problem on circular orbits). In addition, constraints on the impulse application moments and their orientation were not considered.

Initially a numerical solution method was designed at the Keldysh Institute of Applied Mathematics in the USSR Academy of Sciences. This method was suitable for solving the problem but did not give an explanation as to why this or that solution had been chosen, which made it difficult to use in emergency situations. A numerical analytical method was designed in the early 80s. It was intended to solve degenerate coplanar and noncoplanar rendezvous problems in the classical statement with and without constraints. A geometric interpretation of impulses in the space of eccentricity vector components provided an opportunity to explain the nature of the found solution. A graphical user interface made it easy to select a new manoeuvring scheme in case of emergency situations. The method's simplicity and reliability allowed it to be used on board spacecraft. Later, analytical solutions for coplanar and noncoplanar nondegenerate rendezvous were found. In the late 90s, a solution for rendezvous with significant initial right ascension of the ascending node (RAAN) deviation and long flight duration was found. Thus, the theory for optimal multiple-impulse rendezvous was fully developed.

The next step in the evolution of manoeuvring theory in the vicinity of circular orbits was the development of solution methods for coplanar and noncoplanar rendezvous and transfers using low-thrust engines in the 2000s. The types of optimal solutions and their existence domains were defined. The parameters of these solutions were determined using simple analytical and numerical analytical algorithms.

The almost fully developed theory of optimal manoeuvring on near-circular orbits allowed the author to find numerical analytical solutions for all of the practical problems he faced during more than 45 years of work with real spacecraft. The solution time for these problems is significantly smaller in comparison with the time needed to solve the same problems using classical numerical methods. In addition, it became possible to explain the physical nature of the found solution. This was the answer to the question that the author had been searching for since the beginning of his work on the problem, which was a long time ago.

The problems of coplanar and noncoplanar rendezvous of different duration, as well as the problems of deployment and maintaining the given configuration of satellite constellations, were solved. Lately, the primary focus has been shifted to space debris manoeuvring problems.

In addition to the fact that this book contains the accumulated knowledge of solving complex practical problems, it will also be useful for young specialists making their first steps in the field of spacecraft manoeuvring. Each theoretical section ends with an example using the specified algorithms. The author's lecturing experience in Bauman Moscow State Technical University (BMSTU) and the Academy of Engineering Faculty of the Peoples' Friendship University of Russia (RUDN) shows that it will help students to better understand the material and to learn how to solve real nonsimplified problems.

Those readers who have extensive experience in solving complex practical problems can be helped by learning new approaches to problem solutions and explanations of their nature.

INTRODUCTION

Manoeuvres play an important role in the spacecraft flight process. A manoeuvre is a target driven alteration of spacecraft orbit parameters with the help of a propulsion system. Generally, manoeuvres help to change the orbit with the necessary precision, which allows the spacecraft to fulfill its mission. The important role of manoeuvres, as well as their variety and presence practically in each space mission, determines the attention that is paid to them in the literature on space flight mechanics.

Released in 1969, F.W. Gobetz and J.R. Doll's report (Doll and Gobetz 1969, 801–834) already encompassed more than 300 articles dedicated to the optimal spacecraft manoeuvring. At the present time, there are thousands of articles related to the topic, as well as dozens of monographs including notable works by V.V. Ivashkin (Ivashkin, 1975), K.B. Alexeev, G.G. Bebenin, V.A. Yaroshevsky (Alexeev, Bebenin, and Yaroshevsky, 1970), V.A. Egorov (Egorov, 1965), T.V. Solovyev, and E.V. Tarasov (Soloviev and Tarasov, 1973). D.F. Lawden's work is considered to be the foundational one (Lawden, 1966).

The problem of optimal manoeuvring parameter determination for spacecraft in near-circular orbits holds a special place in the theory of optimal manoeuvring. Firstly, these problems are of big practical interest as most of the real spacecraft operate in these orbits. Secondly, these problems are less complicated than those in the classical statement and they can sometimes be solved using analytical and numerical analytical methods. Naturally, lots of articles are dedicated to problems of this type. Their references will be given in successive chapters. The most noticeable are the monographs by J.-P. Marec (Marec, 1979); V.A. Ilyin and G.E. Kuzmak (Il'in and Kuzmak, 1976); and M.F. Reshetnev, A.A. Lebedev, V.A. Bartenev, M.N. Krasilshikov, V.A. Malyshev, and V.V. Malyshev (Bartenev, Krasilshikov, Lebedev, Malyshev et al., 1988).

The necessary conditions of the strict local optimality of impulsive flybys in arbitrary and Newton's gravity fields were obtained on the basis of the variation approach (Il'in and Kuzmak, 1976). The solution for the transfer problem (the flyby without time constraint) between the near-circular orbits in the linearized statement and the solution for the rendezvous problem are given. A brief and sufficiently complete solution of the transfer problem in the noncoplanar near-circular orbits is given in

Edelbaum (1967, 66–73). In the work of Bartenev, Krasilshikov, Lebedev, Malyshev, et al. (1988), the problems of orbit determination and manoeuvring with high and low-thrust engines (mostly transfer problems) are considered. In J.-P. Marec's monograph (Marec, 1979) major attention is paid to the nondegenerate rendezvous problem in near-circular orbits. A fundamental up-to-date review of articles on rendezvous problems can be found in Guojin, Jin, and Yazhong (2013, 1–11).

The rendezvous problem consideration started in the mid-60s. Even now, the articles by J.E. Prussing are still cited (Prussing 1969, 928–935; Prussing 1970, 1221–1228). Prussing considered the two-spacecraft rendezvous in coplanar orbits with 1–3 revolutions duration. In the book by J.-P. Marec (Marec, 1979), research was conducted into the classic average duration noncoplanar rendezvous in near-circular orbits. It was shown which diapasons of orbit element values could be achieved while using different types of optimal nondegenerate solutions (reversed problem solutions). The difficulty in understanding the book's material was one of the reasons why its ideas were not widely used. The algorithm for the rendezvous manoeuvre parameter determination corresponding to the nondegenerate hodograph of primer vector was introduced in Jones (1976, 55–90).

In the 60s, the first spacecraft dockings were conducted. It turned out that additional constraints should be taken into account while solving practical problems: velocity impulse application time, its orientation and value, transfer orbit parameters, etc. The problem got far more complex in comparison with the classic one from the first theoretical articles. It became impossible to use the solutions from those articles. New effective numerical methods for solving practical problems were developed.

Nowadays, three major approaches for solving complex multiple-impulse spacecraft manoeuvring problems are mainly used. In the first case, the problem is divided into several simple problems. For example, the problem of manoeuvring within an orbit plane and the problem of orbit plane rotation are solved separately. The orbit plane rotation in this scheme is carried out by the single velocity impulse, which is applied on the orbit plane intersection line. Such a scheme[1] was used for the rendezvous of Shuttle and the ISS in Fehse (2003, 441–449). A similar approach is used for guiding geostationary satellites (Bulynin 2008, 73–74), and satellites in a constellation (Rylov 1985, 691–714), (Bobronnikov, Fedorov, Krasilshikov, Malyshev et al. 2001, 43–45), etc. The advantage of the scheme is its simplicity and reliability, clarity of the physical nature of each of the

[1] "Shuttle Press Kit: STS-92". Accessed March 25, 2007. http://www.shuttlepresskit.com/STS-92/

manoeuvres, and the usage of simple spacecraft orientation systems. The disadvantage of the scheme is the excessive total delta-v expenditure on manoeuvres.

In the second case, numerical methods are applied, allowing finding the optimal solution of the most complex multiple-impulse problems with different constraints. Numerical methods have been successfully used for decades for the rendezvous manoeuvre determination of “Soyuz” and “Progress” spacecraft with long-term orbital stations (Bazhinov and Yastrebov, 1978; Petrov 1985; Baranov 1986, 324–327). The articles by V.P. Gavrilov and E.V. Obuhov had a great influence on development of these methods (Gavrilov and Obukhov 1980, 163–172). Numerical methods allow finding the solutions with minimum total delta-v, which is sometimes crucial for the accomplishment of the mission. For example, the orbital module “Kvant” only docked on the “Mir” orbital station after the third attempt with almost depleted fuel tanks. If only one of three attempts had not been optimal, there would not have been a sufficient amount of fuel for docking. The simplex method is mostly used for manoeuvre parameter determination (Lidov 1971, 687–706; Lidov and Teslenko 1978, 112–141; Gavrilov and Obukhov 1980, 163–172; Gavrilov 1995; Kolegov, 2007; Bakshiyan, El'yasberg, and Nazirov, 1980). The method was first used for the abovementioned purposes by M.L. Lidov.

The disadvantage of all numerical methods is the absence of information on why we arrived at this or that type of solution and how the solution would alter with an initial condition change. It is especially critical in the case of emergency situations occurring during the flight when a new manoeuvring scheme with additional constraints is needed. Similar problems arise at the stage of development when the future manoeuvring scheme is being selected. Generally, it is easier to determine the manoeuvre parameters than the manoeuvring scheme. When choosing the scheme, we should determine the number of velocity impulses needed for an optimal solution, the intervals of manoeuvring and rendezvous duration. After that we can evaluate the manoeuvre parameters. We can name the cumbersomeness of the numerical methods as their disadvantage. This creates additional difficulties when using them on board a spacecraft. For another thing, numerical methods need a significant amount of computing time to solve problems. This factor appears to be a significant disadvantage when solving complex combined problems. Sometimes the solution of lots of conventional transfer and rendezvous problems are needed to obtain a complex optimal solution. The same problem appears when we use the space debris catalogue and need to calculate the parameters of thousands of manoeuvres.

The third approach to solving the rendezvous problem can often be found in articles from universities. This approach was first implemented in articles by P.M. Lion and M. Handelsman (Handelsman and Lion 1968, 127–132) and D.J. Jezewski and H.L. Rozendaal (Jezewski and Rozendaal 1968, 2160–2165). At the first stage of this method, the parameters of the two-impulse solution using Lambert's problem are obtained. Then the primer vector hodograph for the found solution is analyzed. If necessary, additional velocity impulses are added for the optimal solution. With this technique and gradient optimization algorithms, multiple-impulse solutions for a two-body problem were obtained (Gross and Prussing 1974, 885–889; Chiu and Prussing 1986, 17-22; Guzman, Hughes, and Mailhe 2003, 85–104). The most common and developed method of solving rendezvous problem is the use of Lambert's problem (Ohotsimsky and Sikharulidze 1990; Battin 1966; Battin 1977, 707–713; Ermilov, Ivanova, and Panushin 1977; Dashkov and Kubasov 1979; Escobal 1970; Herrick 1978). We can distinguish as a separate group the solution of multiple-revolution for Lambert's problem (Prussing 2000, 31–148; Shen and Tsiotras 2003, 50–61; Han and Xie 2004, 9–13) and the universal algorithms of its solution (Pitkin 1968, 270–27; Kriz 1976, 509–513; Sukhanov 1988, 483–491). Nowadays, the method for searching for an optimal multiple-impulse solution for the rendezvous problem based on Lambert's problem is also widespread (Guo-Jin, Hai-Yang, Ya-Zhong, and Yong -Jun 2007, 946–952).

Problems of orbital station manoeuvre parameter determination can be put in a special group, although, despite their peculiarity, they might be considered to be rendezvous problems. They are rather specific due to the long-time interval between the initial and terminal manoeuvres and multiple, often controversial, constraints on the parameters of the interim orbit. The basic research in this field was conducted by E.K. Melnikov (Melnikov 2004, 176–186; Melnikov 2009; Kolegov and Melnikov 1990, 158–165).

The purpose of this book is to introduce numerical analytical methods for solving multiple-impulse rendezvous problems in near-circular orbits to the reader. These methods combine the advantages of the first two methods. The methods are simple enough, as well as illustrative and reliable. By using them, we can obtain close-to-optimal solutions. This allows us to use the results obtained in the articles by G.E. Kuzmak, T.N. Edelbaum, and J.-P. Marec when solving actual practical problems. The suggested numerical analytical methods are several times quicker than the numerical methods and they also give an explanation as to why this or that optimal solution was obtained. They allow us to determine the existence domains of optimal solutions of different types. It is hard to determine

these domains using numerical methods. It is especially important when we choose the manoeuvring scheme: how many velocity impulses should we use and on which manoeuvring intervals can they be applied? The found solutions give us a simple geometric interpretation which simplifies their explanation and allows the use of a graphic dialogue while solving the problem.

Also, the basic problems of manoeuvring with low-thrust engines are considered. Special attention is paid to satellite constellation and satellite formation flying deployment and keeping. Problems of the determination of manoeuvres performed by an active space object, problems of space debris collision avoidance, problems of large space debris de-orbiting, and problems of the transfer of spacecraft to disposal orbit (DO) are considered.

The structure of the book is arranged in accordance with the adopted classification of manoeuvres in near-circular orbits (Doll and Gobetz 1969, 801–834).

In the first chapter a solution of linearized equations of motion system in a cylinder coordinate frame is given. The statement of the optimal manoeuvre parameter determination problem in near-circular orbits and necessary optimal conditions are presented. The iterative procedure is explained. It allows the realization of terminal conditions with the necessary accuracy and with due regard to the noncentral gravitational field, atmosphere, and spacecraft propulsion system etc. The geometric interpretation of the impulse components' influence on different orbit elements is given. The relative motion of two approaching spacecraft with different target vectors is depicted. It is shown that an impulse transversal component sum in every manoeuvring interval can be determined analytically with good precision during the spacecraft-orbital station rendezvous. The equations for the determination of optimal phase desynchronization diapason between the spacecraft and orbital station are given. The equations include options for shifting first interval manoeuvres to later revolutions and shifting the launch date. Further material is given in accordance with the adopted manoeuvre classification.

In the second chapter, the problems of transfer between coplanar (three types of two-impulse solutions) and noncoplanar orbits (three types of two-impulse solutions and one type of three-impulse solution) are considered. The equations for the determination of the manoeuvre parameters of these solutions are given. A comparison between problem solutions in linearized and accurate statements is made. Equations for the impulse components of the optimal coplanar two-impulse solution for fixed impulse application angles are given.

In the third chapter, the coplanar rendezvous is considered. Three types of possible solutions, which correspond to the point, ellipse, and cycloid primer vector hodographs, are analyzed. The existence domains for three types of solutions are determined. The algorithms for the parameter determination of two-, three-, and four-impulse solutions for each type of possible primer vector hodographs are considered. Example cases are presented. It is shown that the total delta-v of the optimal Lambert's problem solution might be two or even three times higher than the delta-v for an optimal three-impulse solution. The rendezvous problem with a constraint on transfer orbit altitude is considered. The impact of orbit determination errors and manoeuvre realization errors is analyzed. The procedure for the solution selection for the minimum influence of these errors is presented.

In the fourth chapter, a universal algorithm for a four-impulse multiple-revolution rendezvous in noncoplanar near-circular orbits manoeuvre parameter determination and a numerical analytical algorithm of long-range guidance for Soyuz- and Progress-type spacecraft manoeuvre parameter determination are shown. The six-impulse solutions which correspond to the spiral hodograph of primer vector are analyzed. The equations for the determination of optimal impulse application angles for these solutions are presented. The numerical analytical algorithm for several dozen rendezvous manoeuvres determination is shown.

There are lots of problems in practical work which are hard to solve without using numerical methods. This is why Chapter Five is dedicated to numerical methods. The numerical method, which was used over a number of years in the ballistics center of the Keldysh Institute of Applied Mathematics at the Russian Academy of Sciences for real spacecraft manoeuvre parameter determination, is also presented with selected examples.

The ballistics center of the Keldysh Institute of Applied Mathematics at the Russian Academy of Sciences, whose creator and long-term head, E.L. Akim, was the corresponding member of the Russian Academy of Sciences, participated in ballistics navigation flight support for all major scientific spacecraft. The ballistics center played an important role in the ballistics navigation support of manned spacecraft. The author of this book took part in the determination of manoeuvre parameters of "Soyuz 19" (1974), "Soyuz 20" (1975, Apollo-Soyuz Test Project), and "Soyuz 22" (1976). Over a number of years (since 1978), the ballistics center has participated in ensuring the functioning of the orbital stations "Salut-6", "Salut-7", and "Mir"; in the activities connected with the deployment of the International Space Station (ISS); and the ballistic support of the "Buran" space system. As part of these activities, the author has calculated

the manoeuvre parameters of approximately 140 spacecraft of different types: “Soyuz”, “Soyuz-M”, “Soyuz-TM”, “Progress”, and “Progress-M”, as well as the orbital modules of “Kvant”, “Priroda”, “Spectre”, “Zvezda”, and the “Buran” space system, etc. Participation in the ballistics navigation support of these flights gave the opportunity to develop and test different methods of manoeuvre parameter determination, and to choose the simplest and most reliable ones with maximum adjustment to the peculiarities of the flight of real spacecraft. Since the methods presented in this book were designed for solving practical problems, they take into account the constraints on moments of impulse application, their magnitudes and orientation, and interim orbit altitude limits, as well as meet the strongest demands in terms of performance and reliability.

Due to their advantages, the methods were chosen by CNES as a basis for their own method of calculating the manoeuvre parameters of rendezvous problem for the ATV approach to ISS (Carbonne, Chemama, Julien, Kudo et al. 2009, 1091–1106).

Emergency situations occurring in orbit proved the necessity of the graphic dialogue, which rapidly reselects manoeuvring schemes with additional constraints caused by emergency situations.

The first use of the graphical dialogue while solving the manoeuvring problem was described in the article by A.K. Platonov and R.K. Kazakova (Kazakova and Platonov 1976). Lambert’s solution was used for the manoeuvre determination. The book by Y.A. Zakharov gave the description of the graphic dialogue for the calculation of interorbital transfer with finite thrust. A transition to the solution of the problem with finite thrust from an impulsive solution was made by using nonlinear programming. Both graphical dialogues were developed at the stage of spacecraft flight design.

The graphical dialogue description, which can be used at the stage of ballistics design and during the flight in emergency situations, including space debris collision avoidance, is described in the fifth chapter. Unlike the previous two dialogues, the solution analysis and its alteration take place in the space of eccentricity vector projections, and not in the space orbits themselves.

It was assumed in the problems mentioned above that the burn duration is noticeably shorter than the orbit period. It allowed us to solve the problem in an impulsive statement and helped us to recalculate the engine regime parameter accurately with the help of an iterative procedure. Still, in a number of practical problems, the manoeuvre duration is comparable with the orbit period. For example, such a situation appears when orbital module big-sized manoeuvres are carried out with the use of docking and attitude thrusters. Another example is the usage of electric propulsion

engines. In these cases, impulsive approximation is not enough and special manoeuvre determination methods are needed.

Problems of this type have a special place among optimal spacecraft manoeuvring problems. A number of articles are dedicated to them. Articles by the group of authors led by T.M Eneev and V.A. Egorov (Beletsky and Egorov 1964, 360–391; Akhmetshin, Efimov, Eneev, and Yegorov 2000, 279–305; Ermilov, Ivanova, and Panushin 1977; Akhmetshin, Beloglazov, Belousova, Efimov et al. 1985; Egorov, Grigoriev, and Ryzhov 2005), as well as articles by M.P. Zapletin and I.S. Grigoriev (Grigoriev, Zapletina, and Zapletin 2007, 758–762; Grigoriev and Zapletin 2009, 1499–1513) can be mentioned. Several interesting monographs have been published (Grodzovski, Ivanov, and Tokarev 1966; Lebedev, 1968; Bartenev, Krasilshikov, Lebedev, Malyshev et al., 1988; Zakharov, 1984). Articles by M.S. Konstantinov (Konstantinov 1997) and V.G. Petukhov (Petukhov 2004, 250–268; Petukhov 2008, 219–232; Petukhov 2012, 249–261) can also be noted. Due to the complexity of the problems in which manoeuvring is performed by low-thrust engines, they were traditionally solved by numerical methods with the use of Pontryagin's maximum principle or by dividing the problem into simpler problems which have trivial solutions, just like the Shuttle manoeuvre calculations. In recent years, Y.P. Ulybyshev has successfully been using the method of inner point for long-duration manoeuvre problems (Sokolov and Ulybyshev 1999, 95–100; Ulybyshev 2008, 135–147; Ulybyshev 2012, 403–418).

The aspects of manoeuvring with limited thrust engines are described in Chapter 6. The algorithms of the transfer problem manoeuvre parameter determination on coplanar orbits with fixed orientation of engines in orbital and inertial coordinate frames and the algorithm of optimal engine orientation change determination are depicted. In the space of deviations of semimajor axis and eccentricity between final and initial orbits the areas with optimal engine orientation mentioned above are determined. The numerical analytical algorithm for the manoeuvre parameter determination for a noncoplanar transfer is shown. A coplanar rendezvous with manoeuvring on each revolution and on two separate intervals is considered.

In the previous theoretical articles from the 60s and early 70s, no research was conducted in the field of spacecraft manoeuvring in satellite constellations, which play an important role in modern cosmonautics. Nowadays, lots of satellite constellations differ in terms of application, the number of satellites in a constellation, the types of orbits, and the relative satellites positions used. The most common are satellite constellations on near-circular orbits. The algorithms mentioned in the previous chapters might be used for the calculation of a spacecraft manoeuvre parameter in

satellite constellations. At the same time, the manoeuvres of such satellites have their own peculiarities.

Dozens of publications have been dedicated to satellite constellations. At first, the satellite constellation configuration that can provide the necessary coverage of the Earth should be selected. In this field, the articles by G.V. Mozhaev (Mozhaev, 1968; Mozhaev 1972, 833–843; Mozhaev 1973, 59–68), J.G. Walker (Walker 1971, 369–384), B.P. Byrkov (Byrkov and Razoumny 1992, 62–68), Y.N. Razoumny (Razoumny 1993), E. Lansard (Frayssinhes, Lansard, and Palmade 1998, 555¬564), and V.K. Saulsky (Saulsky 2005, 34–51) can be noted. Recently, some articles by Y.N. Razoumny (Kozlov, Razoumny, and Razoumny 2015, 200–204; Kozlov, Razoumny, and Razoumny 2015, 196–199), and S.Y. Ylybyshev (Ulybyshev 2015, 311–¬322; Ulybyshev 2016, 1–11) concerning the multiple-tiered satellite constellations have been published. The satellites in these constellations move in circular orbits with different radii.

Despite the variety of satellite constellations, there are two basic types of optimal manoeuvre problems: satellite constellation deployment and keeping.

The first one is close to the classic rendezvous problem. Each satellite is considered separately. The satellite needs to be transferred to a specified point in the final orbit in a fixed period of time. In this case, the time of the satellite transfer to a specified point is not important and can be selected in a wide range unlike in the case of the manoeuvring problem, which is calculated when docking “Soyuz” or “Progress” to a long-term space station. It is connected with the search for a compromise solution between the transfer duration and the total delta-v expenditures. Total delta-v expenditures usually increase with the decrease of the transfer duration to a specific orbit point. Also, when dealing with low Earth orbits, we face a shift of RAAN even after the simplest satellite transfer along the orbit. And this needs to be corrected. This case is thoroughly examined in the first paragraph of Chapter 7. The algorithm of optimal impulse application angle selection and the algorithm of compromise rendezvous time selection are shown.

The problem gets more complicated when the satellite operational orbit RAAN differs from the initial orbit RAAN by dozens of degrees. For example, such a situation occurs when a single launch vehicle injects several satellites in orbit and some of them need to be transferred to different operational planes or when a spare satellite needs to be transferred to another orbit plane in order to replace the malfunctioning one. The optimal one in terms of total delta-v costs satellite transfer needs significant time (several hundreds of revolutions). The problem of satellite

transfer from the circular orbit to a specific point of analogous circular orbit with a big RAAN difference is also shown in Chapter 7.

It was shown that, with the increase of RAAN deviation, the total delta-v expenditures do not grow proportionally as might be expected. They alter in a fashion that corresponds to the sine-shaped fading law over the line corresponding to the expected proportionality. The magnitudes of these oscillations are noticeable within several degrees of variations of RAAN. In this case, the total delta-v expenditures for the compensation of a substantially bigger deviation of RAAN can be tens of percent less than the cost of the compensation for relatively small deviations.

In general, it is necessary to have a universal manoeuvre parameter computing algorithm for a long-duration rendezvous when being transferred to the given point of the final orbit from an arbitrary injection orbit. This algorithm becomes more complicated when there is a big difference in RAAN between the initial and final orbits.

It is impossible to solve this problem using the existing methods for short and medium duration rendezvous problems. In these methods, the influence of the Earth's oblateness was omitted (Prussing 1969, 928–935; Prussing 1970, 1221–1228; Jones 1976, 55–90; Marec 1968; Marec, 1979) or accounted for using the iterative procedure (Petrov 1985; Bazhinov and Yastrebov, 1978; Gavrilov, Obukhov, Skoptsov, and Zaslavsky 1975; Baranov, Gundobin, Ivanov, Kapralov et al. 1992, 26–27) when obtaining the given tolerance of terminal conditions. The Earth's oblateness can be used for the reduction of total delta-v expenditures in the problem of the satellite transfer to the given plane, whose RAAN differs from the initial one by several tens of degrees.

In the available articles, the problems of the parameter determination of satellite transfer to another operational plane were hardly considered. The two problem solving methods for a rendezvous with big initial deviations of RAAN (Bollman, D'Amario, Lee, Roncoli et al. 1999; Breeden, Guinn, and Ocampo, 2001, 1–20) were presented at international conferences held by AIAA. The methods were demonstrated for the solution to rendezvous on Mars orbit. RAAN needed to be changed by 182 degrees. The first one (Bollman, D'Amario, Lee, Roncoli et al. 1999), the NASA project, is similar to the Shuttle-to-ISS docking method. The correction of orbital elements in the orbital plane and orbital plane rotation are carried out separately. The solution obtained is not optimal (the total delta-v expenditures are 60% higher than the necessary ones). Due to the complexity of the problem, ten velocity impulses were used instead of five for NASA's classical rendezvous problem solution. The second method (Breeden, Guinn, and Ocampo, 2001, 1–20) developed by JPL and the University of Texas is numerical. It obtains the optimal solution with three

velocity impulses, but the time needed to arrive at the solution is extremely long and a good initial guess is needed. It is hard to perform multiple solutions for the problem using these methods.

In Chapter 7, a simple, reliable, and fast numerical analytical method for obtaining an optimal solution of such a type (Baranov and Baranov 2009, 256–262) is given. It allows the formulation of the dependence of the consumption of the total delta-v on the duration of the flight with a single solution to the problem. Besides, the computational process is well illustrated. It is always clear why the optimal solution has its specific look and how it alters due to the change of initial conditions. It is possible to obtain solutions which can decrease the influence of manoeuvre realization errors.

The given method was used for a number of situations including the solution to abovementioned rendezvous problem on Mars orbit, and the solution to the manoeuvre parameter problem while deploying satellite constellations (e.g., "Globalstar") and satellite formation flying. The examples of manoeuvre parameter calculations for the initialization of a cluster for atmospheric tomography and for the satellite formation flying "Aqua Train" deployment are given. Due to the close positions of satellites in formation flying, significant attention must be paid to collision avoidance while calculating the manoeuvres for their deployment. This problem was considered in (Baranov, Boutonnet, Escudier, and Martinot 2005, 913–920; Baranov, Boutonnet, Escudier, Matinot et al. 2003, 83–96; Baranov, Boutonnet, Escudier, and Martinot 2003).

Special attention is also paid to the problem of keeping the given satellite constellation configuration, which has several significant differences from the satellite constellation deployment problem. Two strategies can be distinguished: absolute and relative keeping. In the absolute keeping regime, the motion of each satellite should comply with some given motion, which allows the manoeuvres for each satellite to be calculated separately from other satellites in the constellation (Chao and Schmitt 1991; Baranov and Wang 2015, 68–83). In the relative keeping regime, the cooperative motion of all satellites in a constellation is ensured. It is significantly cheaper than the absolute regime because there is no need to correct orbit elements which practically alter in the same fashion repeatedly for all satellites in a constellation. For example, the semimajor axis reduces in practically the same fashion for all satellites due to atmospheric drag and does not need to be corrected. The only thing to do is to control the relative angular distances between the satellites which determine the satellite constellation configuration. Relative keeping is a more complicated problem as it is necessary to take into consideration the location of other constellation elements while calculating manoeuvres of

the current satellite. In the articles by G.V. Mozhaev (Mozhaev 2001, 634–647) and R.F. Murtasin (Murtazin 1998, 173–182), two keeping policies were considered and it was shown that relative keeping leads to a smaller number of manoeuvres needed and lesser total delta-v expenditures.

The problem of manoeuvre parameter calculation in the relative regime of constellation keeping has been examined by a number of authors. A simplex method (Bernussou, Brousse, Dufour, Foliard et al. 1997; Bernussou, Dufour, and Lasserre 1996, 169–174; Fedorov, Malyshev 2001, 45–46) or the numerical solution of the Riccati equation (Ulybyshev 1998, 109–115) are usually used for its solution. In these cases, the system conditions are controlled after fixed and equal time gaps. It may be needed to perform some optimal orbit element corrections before or after one of these fixed moments, which is a disadvantage of both methods. Analytical solutions were suggested in some articles; however, it was agreed that the manoeuvres were performed in the initial (Mozhaev 2001, 634–47) or in the initial and final moments of time (Murtazin 1998, 173–182). The constellation was not controlled in the intermediate moments. The numerical analytical method allows the manoeuvre parameters to be evaluated analytically; this ensures the necessary configuration keeping on the whole interval is given in Chapter 7. Taking into consideration the physical peculiarities of problems helps to decrease the number of manoeuvres used. The suggested geometrical interpretation of the maintenance process gives a comprehensive explanation of the nature of the optimal solution. Numerical solutions do not allow this.

The development of methods for the deployment manoeuvre calculation and relative satellite constellation station keeping was carried out in the work initialized and supported by CNES. J.-P. Carrou, J.-P. Bertiasse, P. Legandre, J. Folliard, P. Brousse, J.P. Guster, and F. Dufour made great contributions in organizing this and other works. The development of the universal manoeuvre parameter determination method of satellite transfer to a specified point of orbit with several dozens of degrees RAAN deviation was made together with P. Labourdette (Baranov and Labourdette 2003, 130–142; Baranov and Labourdette 2002).

Absolute keeping is used far more often and is considered in the last paragraphs of Chapter 8. The example contains the case of the absolute keeping of a microsatellite in the sun-synchronous orbit which fulfills Earth remote sensing problems.

The satellite group absolute configuration initialization and its keeping during a considerable time interval were illustrated by the satellite formation flying “Tandem”. Much attention is paid to the collision avoidance problem when maintaining orbit.

Nowadays, the spacecraft safety problem during flight draws more and more attention due to increasing space debris collision hazards. Manoeuvring problems have an important place in the space debris problem. Chapter 9 and 10 are dedicated to this issue.

The four trends in space debris manoeuvre calculating problems can be distinguished. The first and second trends are considered in Chapter 9, and the third and fourth in Chapter 10.

The first trend is the determination of manoeuvres which allow collisions with space debris to be avoided. Special collision avoidance manoeuvres are usually used. They are relatively simple. Their description is given in the beginning of Chapter 9. It would be more interesting to solve a more complicated problem like finding the solution to the rendezvous problem which will allow collisions on the phasing orbit (drift orbit) to be avoided. A safe orbit can be obtained by searching for magnitudes and times of velocity impulse applications on the first manoeuvring interval, and not by adding additional collision avoidance manoeuvres. A compromise solution can be obtained without a substantial increase of the fuel needed thanks to the abovementioned graphic dialogue with the problem.

The second trend is to determine manoeuvres performed by an active space object. The assessment and future forecasting of such manoeuvres will allow modeling an active space object movement with higher accuracy and, hence, to avoid collisions with them. Single- and two-impulse manoeuvres were assessed. The two-impulse manoeuvre parameter determination algorithm reduces the problem solution time by several orders in comparison with Lambert's solution, which is traditionally used for these purposes. The manoeuvre determination accuracy is also improved. Single- and two-impulse long duration manoeuvres were also assessed. The solution time was also decreased by several orders in comparison with traditional methods (Alfriend, Kamensky, Stepanyants, and Tuchin 2009, 3–22; Borovin, Stepanyantz, Tuchin, Tuchin et al. 2012). The assessment algorithms of short and long duration single-impulse manoeuvres with considerable errors in the determination of initial and, especially, final orbits were presented. In this case, the manoeuvre assessment helps to improve the final orbit accuracy (it is obtained by applying a calculated manoeuvre to the initial orbit) and thus helps us to increase the approach (of the protected spacecraft with the given object) determination accuracy. These algorithms can be used while assessing the impulses which occur during the setup of the given spacecraft orientation; this helps to increase the orbit forecast accuracy.

Manoeuvre assessment problem statements and approaches to their solutions have been discussed with V.M. Agapov several times.

The third trend is the transfer of the decommissioned spacecraft into orbits where they cannot be dangerous for active space objects. For geostationary orbit spacecraft, this means a transfer into orbits with altitudes 250–350 km higher than regular geostationary orbits, while, for low Earth orbits, it is the transfer to orbits where the existence time is limited to 25 years. An orbit parameter determination algorithm was given, and this type of elliptical and circular orbits evolution was considered. The dependences of elements of orbits with reduced existence time against the time of their size and orientation adjustment, ballistic coefficients etc. were considered.

The fourth trend is large space debris transfer (cross-section area is not less than 5 m2, final rocket stages, boosters) in orbits with a significantly reduced orbital lifetime which will not be dangerous to active space objects.

There are lots of projects for space debris mitigation measures. The most effective ones are the two schemes in which one of the servicer spacecraft (space vehicle collector [SV-collector]) can remove several large space objects (LSO).

The first scheme includes a successive flyby of several spacecraft with their collection or insertion in the exhaust sections of small spacecraft with their own autonomous control and enough fuel supply (thrust de-orbit kits [TDKs]) for braking and large space debris transfer to the disposal orbit (DO). The flyby is performed by an SV-collector and, when it is out of fuel and TDKs, it is refueled by a tanker spacecraft.

The second scheme suggests the usage of one spacecraft which manoeuvres between the objects and provides their transfer to the DO. This scheme is less effective, but it performs the flyby faster. Both schemes are considered and compared in Chapter 10.

Five groups of objects with close values of orbit inclinations were identified. The strategy of the flyby was chosen, and the compromise times of each flyby were found to meet the time constraints of the whole mission. The total delta-v expenditures on different flyby schemes were calculated and the most preferable schemes of each group flybys were chosen. It was determined which amount of fuel supply and the number of TDKs the SV-collector and tanker spacecraft should have. It was also estimated how many SV-collectors and tanker spacecraft were needed for the almost complete cleanup of all groups.

Practically all the algorithms described were supported by example cases. This will allow readers who intend to use the algorithms from the book to check their own realizations.

Solutions are given for the problems which can be met in practical work. In those solutions, terminal conditions were calculated with the set-

up precision using the iteration procedure described in the first chapter, which takes into consideration all the necessary perturbations.

The author thanks A.R. Golikov, M.O. Karatunov, D.A. Grishko, A.A. Budyansky, N.V. Chernov, I.S. Gundobin, M.A. Kapralov, E.O. Terehova, and D.S. Roldugin for their collaborative work and obtaining some numerical results mentioned in the book.

The author is grateful to the employees of the 5th Department of Keldysh Institute of Applied Mathematics in the Russian Academy of Sciences, who are the leading specialists in the field of spacecraft manoeuvre determination; the author would also like to extend his gratitude to his lecturers, V.V Ivashkin, A.K. Platonov, V.A. Egorov, M.L. Lidov, G.S. Zaslavsky, and R.K. Kazakov. The high scientific standards of the Department were developed by its head, the academician of Russian Academy of Sciences, D.E. Ohotsimsky, and are maintained at present by Professor U.F. Golubev.

The author is especially grateful to the book reviewer, G.A. Kolegov, for his comments and suggestions.

The author will be grateful for any critical notes from readers.

CHAPTER ONE

PROBLEM STATEMENT: GENERAL SOLUTION SCHEME

1.1. Spacecraft Equations of Motion

A particular interest in manoeuvring in near-circular orbits can be explained by the fact that most real spacecraft orbits are in this class of orbits. The circular orbital velocity in a central gravitational field can be determined as:

$$V_0 = \sqrt{\frac{\mu}{r_0}},$$

where r_0 = the circular orbital radius and μ = Earth's gravitational constant (the product of the gravitational constant by mass of the attracting body, for Earth $\mu = \gamma M \approx 3.986028 \cdot 10^5 \text{km}^3/\text{s}^2$ and for Earth's radius $R_e = 6{,}371$ km).

In practice, there are always some perturbations in real and circular orbits.

The three main groups of perturbing factors can be distinguished as:

1. Deviations in the initial conditions (by velocity, radius or angle) from the conditions which provide motion along the circular orbit;

2. Additional external forces: the influence of the noncentrality of the gravitational field; atmospheric drag; attraction between bodies; solar radiation pressure; and the influence of the magnetic field, etc.

3. Forces caused by the spacecraft's propulsion system.

These perturbations can significantly change the circularity of an orbit. However, in most practically significant cases, deviations from circular orbits are relatively small and linearized equations of motion can be used (at least as a starting point) when studying them. Here, we assume that a

circular orbit of radius r_0 is unperturbed, while the orbit under investigation is perturbed.

1.1.1. Equations of Motion in a Cylindrical Coordinate Frame

For the description of motion, we use a cylindrical coordinate frame r,u,z (Fig. 1-1). Its origin O is situated as the center of attraction. Here, r = the distance between the attraction center and the spacecraft's projection on the unperturbed orbital plane; u = the angle within the plane of the unperturbed orbit starting from an arbitrary initial Ox axis in the direction of the satellite's movement; and z = the distance between the unperturbed orbital plane and the satellite. The z axis is perpendicular to the unperturbed orbital plane. It is aligned in such a manner that if one were to follow the direction of increasing z, the satellite would move in a clockwise fashion. It is suggested that the time reference starting point (t = 0) is the moment when the satellite passes the point at which u = 0.

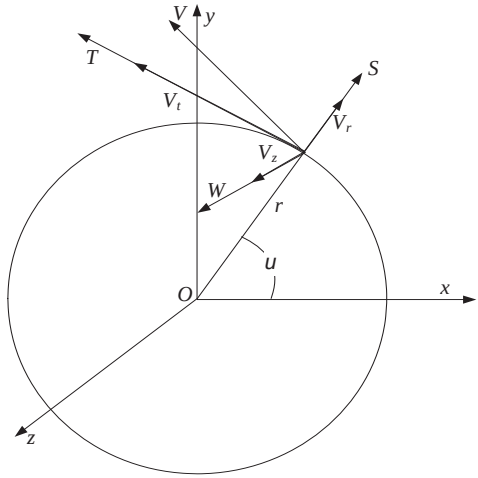

Fig. 1-1. The cylindrical coordinate frame connected to a satellite position in orbit

Here, we consider perturbing acceleration as summed acceleration caused by all forces except for the force produced by the central gravitational field ($g = \mu / r^2$). In addition, let the projection of the

perturbing acceleration be in the direction of radius-vector r; the projection of the perturbing acceleration move along a normal line to the radius vector r in the unperturbed orbital plane; and the projection of the perturbing acceleration on the z axis be *S*, *T*, and *W* (Fig. 1-1), respectively. Keeping in mind that ratio z/r is small, and neglecting the effects of the second order infinitesimal, one can obtain the satellite equations of motion relative to the introduced coordinate frame in Suslov (1946):

$$\begin{aligned} S - g &= \ddot{r} - r\dot{u}^2, \\ T &= \frac{1}{r}\frac{d}{dt}(r^2\dot{u}), \\ W &= \ddot{z} + g\frac{z}{r}. \end{aligned} \tag{1-1}$$

We will only investigate the case of the minor (with respect to the major acceleration *g*) perturbing accelerations *S*, *T*, and *W*, and minor (with respect to r_0 and V_0) deviations from circular motion caused by perturbing accelerations.

With accuracies of small quantities of the first order, the influence of deviations between the perturbed orbit and the unperturbed circular orbit in terms of the *S*, *T*, and *W* values can be omitted and these accelerations can be calculated as accelerations corresponding to the unperturbed orbit. This assumption allows us to solve the first two parts of Eq. 1-1 independently of the third equation, as the values S and T, with the accuracies of small quantities of the first order, are not affected by the lateral displacement z.

Let $V_r = \dot{r}$ and $V_t = r\dot{u}$ be the velocity vector projections on the radius vector and the normal line in the unperturbed orbital plane, respectively. By substituting these values in Eq. 1-1 we get:

$$\begin{aligned} \dot{V}_r &= S - \frac{\mu}{r^2} + \frac{V_t^2}{r}, \\ \dot{V}_t &= T - \frac{V_t V_r}{r}, \\ \dot{r} &= V_r, \\ \dot{u} &= \frac{V_t}{r}. \end{aligned} \tag{1-2}$$

This system of three differential equations with the unknown values r, V_r, V_t cannot be evaluated in a closed form with arbitrary values of the perturbing accelerations *S* and *T*.

1.1.2. Equations in Deviations from a Basic Circular Orbit

For the approximate solution of Eq. 1-2, we will assume that the basic characteristics of the perturbed motion under consideration on the time interval of interest deviate little from the corresponding characteristics of the unperturbed circular motion. Let $\Delta r, \Delta V_r, \Delta V_t, \Delta u$ be the deviations between the respective values of the perturbed and unperturbed orbits:

$$\begin{aligned} r &= r_0 + \Delta r, \\ V_r &= \Delta V_r, \\ V_t &= V_0 + \Delta V_t. \end{aligned} \tag{1-3}$$

The first equation of Eq. 1-2 for the unperturbed orbit can be stated as:

$$0 = -\frac{\mu}{r_0^2} + \frac{V_0^2}{r_0}. \tag{1-4}$$

Let us substitute Eq. 1-3 in Eq. 1-2 and subtract Eq. 1-4 from the first equation of 1-2. In this case, by using Eq. 1-4 and assuming the values $\Delta r, \Delta V_r, \Delta V_t$ to be small (with accuracy of the first order of smallness), we get the following relationships (with accuracies of small quantities of the first order):

$$\begin{aligned} &\Delta \dot{V}_r - 2\lambda_0 \Delta V_t - \lambda_0^2 \Delta r = S, \\ &\Delta \dot{V}_t + \lambda_0 \Delta V_r = T, \\ &\Delta \dot{r} - \Delta V_r = 0, \\ &\Delta \dot{u} = \frac{1}{r_0}\left(\Delta V_t - \lambda_0 \Delta r\right), \end{aligned} \tag{1-5}$$

where λ_0 = the angular velocity of satellite motion along the unperturbed orbit, which can be found by:

$$\lambda_0 = \frac{V_0}{r_0}. \tag{1-6}$$

We get the equation system of four linear differential equations with constant coefficients and a set of unknown variables $\Delta r, \Delta V_r, \Delta V_t, \Delta u$.

In a similar manner, we get the equation for the deviations of lateral displacement:

$$\ddot{z} + \lambda_0^2 z = W. \tag{1-7}$$

1.1.3. Equations of the Motion System Solution

The equation systems 1-5 and 1-7 have a solution that can be stated as follows (El'yasberg 1965):

$$\begin{aligned}
\Delta r &= (2-\cos\lambda_0 t)\Delta r_0 + \frac{\sin\lambda_0 t}{\lambda_0}\Delta V_{r_0} + \frac{2(1-\cos\lambda_0 t)}{\lambda_0}\Delta V_{t_0} \\
&+ \frac{1}{\lambda_0}\int_0^t S(\xi)\sin\lambda_0(t-\xi)d\xi + \frac{2}{\lambda_0}\int_0^t T(\xi)\left[1-\cos\lambda_0(t-\xi)\right]d\xi, \\
\Delta V_r &= \lambda_0 \sin\lambda_0 t\cdot\Delta r_0 + \cos\lambda_0 t\cdot\Delta V_{r_0} + 2\sin\lambda_0 t\cdot\Delta V_{t_0} \\
&+ \int_0^t S(\xi)\cos\lambda_0(t-\xi)d\xi + 2\int_0^t T(\xi)\sin\lambda_0(t-\xi)d\xi, \\
\Delta V_t &= -\lambda_0(1-\cos\lambda_0 t)\Delta r_0 - \sin\lambda_0 t\cdot\Delta V_{r_0} - (1-2\cos\lambda_0 t)\Delta V_{t_0} \\
&- \int_0^t S(\xi)\sin\lambda_0(t-\xi)d\xi - \int_0^t T(\xi)[1-2\cos\lambda_0(t-\xi)d\xi, \\
\Delta u &= \Delta u_0 - \frac{3\lambda_0 t - 2\sin\lambda_0 t}{r_0}\Delta r_0 - \frac{2(1-\cos\lambda_0 t)}{V_0}\Delta V_{r_0} \\
&- \frac{3\lambda_0 t - 4\sin\lambda_0 t}{V_0}\Delta V_{t_0} - \frac{2}{V_0}\int_0^t S(\xi)[1-\cos\lambda_0(t-\xi)]d\xi \\
&- \frac{1}{V_0}\int_0^t T(\xi)[3\lambda_0(t-\xi) - 4\sin\lambda_0(t-\xi)]d\xi,
\end{aligned} \tag{1-8}$$

$$z = \cos\lambda_0 t\cdot z_0 + \frac{\sin\lambda_0 t}{\lambda_0}V_{z_0} + \frac{1}{\lambda_0}\int_0^t W(\xi)\sin\lambda_0(t-\xi)d\xi,$$

$$V_z = -\lambda_0 \sin\lambda_0 t\cdot z_0 + \cos\lambda_0 t\cdot V_{z_0} + \int_0^t W(\xi)\cos\lambda_0(t-\xi)d\xi.$$

The members of the equations under the integrals determine the influence of the perturbing forces, whereas the other members of the equations determine the influence of the minor initial perturbations on the current deviations of the orbit from the unperturbed circular orbit. For now, we will consider only the influence of the minor initial perturbations. The equations for them in dimensionless form can be found below:

$$\begin{aligned}
\frac{\Delta r}{r_0} &= k_{11}\frac{\Delta r_0}{r_0} + k_{12}\frac{\Delta V_{r_0}}{V_0} + k_{13}\frac{\Delta V_{t_0}}{V_0},\\
\frac{\Delta V_r}{V_0} &= k_{21}\frac{\Delta r_0}{r_0} + k_{22}\frac{\Delta V_{r_0}}{V_0} + k_{23}\frac{\Delta V_{t_0}}{V_0},\\
\frac{\Delta V_t}{V_0} &= k_{31}\frac{\Delta r_0}{r_0} + k_{32}\frac{\Delta V_{r_0}}{V_0} + k_{33}\frac{\Delta V_{t_0}}{V_0},\\
\Delta u &= k_{41}\frac{\Delta r_0}{r_0} + k_{42}\frac{\Delta V_{r_0}}{V_0} + k_{43}\frac{\Delta V_{t_0}}{V_0} + k_{44}\Delta u_0,\\
\frac{z}{r_0} &= k_{55}\frac{z_0}{r_0} + k_{56}\frac{V_{z_0}}{V_0},\\
\frac{V_z}{V_0} &= k_{65}\frac{z_0}{r_0} + k_{66}\frac{V_{z_0}}{V_0}.
\end{aligned} \tag{1-9}$$

Here, k_{ij} $(i, j = 1,2,...,6)$ = dimensionless coefficients, which can be written as:

$$\begin{aligned}
&k_{11} = 2-\cos\varphi,\ k_{12} = \sin\varphi,\ k_{13} = 2(1-\cos\varphi),\\
&k_{21} = \sin\varphi,\ k_{22} = \cos\varphi,\ k_{23} = 2\sin\varphi,\\
&k_{31} = -(1-\cos\varphi),\ k_{32} = -\sin\varphi,\ k_{33} = -(1-2\cos\varphi),
\end{aligned}$$

$$\begin{aligned}
&k_{41} = -(3\varphi - 2\sin\varphi),\ k_{42} = -2(1-\cos\varphi),\ k_{43} = -(3\varphi - 4\sin\varphi),\\
&k_{55} = \cos\varphi,\ k_{56} = \sin\varphi,\ k_{44} = 1,\\
&k_{65} = -\sin\varphi,\ k_{66} = \cos\varphi,
\end{aligned}$$

where $\varphi = \lambda_0 t$ = the unperturbed value of the angle u.

1.2. Problem Statement

1.2.1. Velocity Impulse Impact on Deviations in the Specific Point of an Orbit

Orbit-changing impulse components $\Delta V_r, \Delta V_t, V_z$ can be treated as initial velocity deviations. Each impulse, applied at points with the angles $\varphi_i (i = 1,..., N)$, causes deviations in the orbital elements at the specified point with the angle $\varphi = \varphi_f$, which can be found using Eq. 1-9. The sum of these deviations caused by *N* impulses can be written as:

$$\sum_{i=1}^{N}\left(\frac{\Delta V_{r_i}}{V_0}\sin\left(\varphi_f - \varphi_i\right) + 2\frac{\Delta V_{t_i}}{V_0}\left(1-\cos\left(\varphi_f - \varphi_i\right)\right)\right) = \frac{\Delta r}{r_0}, \quad (1\text{-}10a)$$

$$\sum_{i=1}^{N}\left(\frac{\Delta V_{r_i}}{V_0}\cos\left(\varphi_f - \varphi_i\right) + 2\frac{\Delta V_{t_i}}{V_0}\sin\left(\varphi_f - \varphi_i\right)\right) = \frac{\Delta V_r}{V_0}, \quad (1\text{-}10b)$$

$$\sum_{i=1}^{N}\left(-\frac{\Delta V_{r_i}}{V_0}\sin\left(\varphi_f - \varphi_i\right) - \frac{\Delta V_{t_i}}{V_0}\left(1-2\cos\left(\varphi_f - \varphi_i\right)\right)\right) = \frac{\Delta V_t}{V_0}, \quad (1\text{-}10c)$$

$$\sum_{i=1}^{N}\left(-2\frac{\Delta V_{r_i}}{V_0}\left(1-\cos\left(\varphi_f - \varphi_i\right)\right) - \frac{\Delta V_{t_i}}{V_0}\begin{pmatrix}3\left(\varphi_f - \varphi_i\right)\\ -4\sin\left(\varphi_f - \varphi_i\right)\end{pmatrix}\right) = \Delta u, \quad (1\text{-}10d)$$

$$\sum_{i=1}^{N}\frac{\Delta V_{z_i}}{V_0}\sin\left(\varphi_f - \varphi_i\right) = \frac{\Delta z}{r_0}, \quad (1\text{-}10e)$$

$$\sum_{i=1}^{N}\frac{\Delta V_{z_i}}{V_0}\cos\left(\varphi_f - \varphi_i\right) = \frac{\Delta V_z}{V_0}, \quad (1\text{-}10f)$$

where $\Delta V_{r_i}, \Delta V_{t_i}, \Delta V_{z_i}$ = the radial, transversal, and lateral components of the *i*-th impulse respectively.

From Eq. 1-10, one can obtain the impulse parameters, which will meet the terminal condition requirements of entering the target orbit if the deviations on the right side of the equations are treated as deviations between the target and the initial orbital parameters. These deviations can be given by:

$$\Delta r = \Delta r_f - \Delta r_0, \Delta V_r = \Delta V_{r_f} - \Delta V_{r_0}, \Delta V_t = \Delta V_{t_f} - \Delta V_{t_0},$$
$$\Delta u = \Delta u_f - \Delta u_0, \Delta z = z_f - z_0, \Delta V_z = V_{z_f} - V_{z_0},$$

where the deviations between the circular and terminal orbits and the circular and initial orbits at the point $\varphi = \varphi_f$ are given by the indexes "*f*" and "0", respectively.

Deviations from circular orbits derived in the cylindrical coordinate frame can be used in the most efficient fashion when solving the rendezvous of two spacecraft in the final manoeuvring interval; this is when the determination of their relative position and motion is most important. At this moment, the target point is usually not the spacecraft itself, but some point in its vicinity. This shift is determined by the so-called "target vector". For example, if an active spacecraft is situated on an internal orbit relative to a target spacecraft, then some small negative radial and transversal velocity deviations can be chosen (like $\Delta r = -0.5\,\text{km}$, $\Delta V_t = -10\,\text{m/s}$, for instance). In this way we ensure a "bottom-up" approach, as the active spacecraft chases the target and approaches it from below.

A scheme for the "bottom-up" approach is described in Fig. 1-2. The scheme presents the positions of the active spacecraft (named "ch", the internal orbit) and the target spacecraft (named "tg") in the moments of time t_1, t_2, t_3, preceding the rendezvous moment, and in the rendezvous moment t_{rdv}. The line segments connect the spacecraft positions belonging to the same moments in time. The deviation $\Delta r = -0.5\,\text{km}$ ensures that no collision will occur, even if the autonomous approach hardware were to fail.

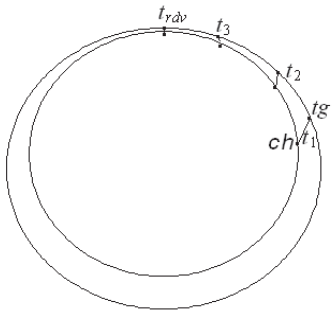

Fig. 1-2. On-orbit spacecraft approaching process

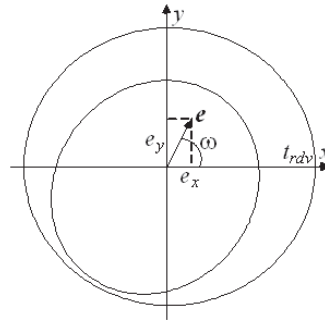

Fig.1-3. The coordinate frame used for the solution of the rendezvous problem

The change in the active spacecraft's position from the inner to the outer orbit leads to the alteration of the signs of the specified deviations from the target point and reverses the approach scheme (the so-called "from-above" approach).

1.2.2. Velocity Impulse Impact on Deviations of the Keplerian Orbital Elements

It is more preferable in most cases to determine orbits by their elements. Let us introduce an *Oxyz* coordinate frame with the origin as the center of attraction; the *Ox* axis pointing to the point in which the deviations are evaluated (Fig. 1-3); and the *Oy* axis lying within the orbital plane. The connection between the deviations introduced earlier and the orbital elements can be given by the equation system from El'yasberg (1965):

$$\begin{aligned} \Delta a &= 2\left(\Delta r + \frac{\Delta V_t}{\lambda_0}\right) \\ e_x &= \frac{\Delta r}{r_0} + 2\frac{\Delta V_t}{V_0} \\ e_y &= -\frac{\Delta V_r}{V_0} \end{aligned} \quad , \tag{1-11}$$

where a = the semimajor axis; Δa = its difference from r_0; e = orbital eccentricity; and e_x, e_y = eccentricity vector projections on the x and y axes. An eccentricity vector e is a vector with magnitude e, which points to the orbital pericenter (Fig. 1-3). The orbital focus is the Earth's center. The deviations can be evaluated at any point, but it is convenient to use the rendezvous point in the case of the rendezvous problem.

Thus, for near-circular motion the dimensionless conditions of reaching the specified point in the target orbit can be described as follows:

$$\sum_{i=1}^{N} \left(\Delta V_{ri} \sin\varphi_i + 2\Delta V_{ti} \cos\varphi_i\right) = \Delta e_x, \tag{1-12a}$$

$$\sum_{i=1}^{N} \left(-\Delta V_{ri} \cos\varphi_i + 2\Delta V_{ti} \sin\varphi_i\right) = \Delta e_y, \tag{1-12b}$$

$$\sum_{i=1}^{N} 2\Delta V_{ti} = \Delta a, \tag{1-12c}$$

$$\sum_{i=1}^{N} \left(2\Delta V_{ri}\left(1-\cos\varphi_i\right)+\Delta V_{ti}\left(-3\varphi_i+4\sin\varphi_i\right)\right) = \Delta t, \tag{1-12d}$$

$$\sum_{i=1}^{N} -\Delta V_{zi}\sin\varphi_i = \Delta z, \tag{1-12e}$$

$$\sum_{i=1}^{N} \Delta V_{zi}\cos\varphi_i = \Delta V_z, \tag{1-12f}$$

where $\Delta e_x = e_f\cos\omega_f - e_0\cos\omega_0$, $\Delta e_y = e_f\sin\omega_f - e_0\sin\omega_0$, $\Delta a = (a_f - a_0)/r_0$, $\Delta t = \lambda_0(t_f - t_0)$, $\Delta z = z_0/r_0$, $\Delta V_z = V_{z0}/V_0$, $\Delta V_{ri} = \Delta V_{ri}^*/V_0$, $\Delta V_{ti} = \Delta V_{ti}^*/V_0$, and $\Delta V_{zi} = \Delta V_{zi}^*/V_0$.

Here, "*f*" and "0" = indexes corresponding to the target and initial orbits; e_f, e_0 = the orbital eccentricities; a_f, a_0 = the semimajor axes; ω_f, ω_0 = the angles between the direction towards the pericenter of the specified orbit and the direction towards the specified point on the target orbit (the *Ox* axis is the heading to this point); t_f = the time necessary for the transfer to this point; t_0 = the moment when the radius-vector projection on the target orbit (while moving along the initial orbit) appears to be situated on the beam that intersects the specified point; z_0 = the deviation of the spacecraft on the initial orbit from the target orbital plane at the moment t_0; V_{z_0} = the lateral relative velocity at this moment; V_0, λ_0 = the orbital and angular velocities of motion along the reference orbit with radius $r_0 (r_0 = a_f)$; N = the number of velocity impulses; φ_i = the angle of application of the *i*-th impulse, which is measured in the direction on the specified point towards the motion of the spacecraft; and $\Delta V_{ri}^*, \Delta V_{ti}^*, \Delta V_{zi}^*$ = the radial, transversal and lateral components of the *i*-th impulse, respectively. One should bear in mind that the angles φ_i are negative, it being agreed that in the specified point $\varphi_f = 0$ (this is one of the reasons why the minus sign is used in the 5th equation).

1.2.3. Optimization Problem Goals

The manoeuvring intervals $F_1,...,F_N$ for impulse applications are usually defined by the revolution number and the initial and terminal latitude arguments. There are constraints on the impulse application angles:

$$\varphi_1 \in F_1,...,\varphi_N \in F_N, \tag{1-13}$$

where $F_1,...,F_N$ = the specified manoeuvring intervals.

Thus, the problem of finding the optimal manoeuvring parameters can be stated as follows:

We determine $\Delta V_{ri}, \Delta V_{ti}, \Delta V_{zi}, \varphi_i$ $(i = 1,...,N)$, ensuring the minimum ΔV, which satisfies the constraints 1-12 and 1-13.

$$\Delta V = \sum_{i=1}^{N} \Delta V_i = \sum_{i=1}^{N} \sqrt{\Delta V_{ri}^2 + \Delta V_{ti}^2 + \Delta V_{zi}^2}.$$

Not all of the aforementioned constraints can be used when speaking about the specified problem.

1.2.4. Geometric Interpretation of the Velocity Impulse

According to eqs. 1-12a and 1-12b, alteration of the orbital eccentricity vector through the application of the transversal component ΔV_{ti} of the *i*-th impulse on the plane e_x, e_y can be depicted as vector *AB* (Fig. 1-4). The magnitude of this vector is $2\Delta V_{ti}$ and the angle between the vector and the e_x axis is φ_i. The alteration caused by the radial component ΔV_{ri} is depicted by vector *BK* (Fig. 1-4). The magnitude of this vector is ΔV_{ri} and the angle between the vector and e_x is $1.5\pi + \varphi_i$. It is apparent that vectors *BK* and *AB* are perpendicular to each other. Vector *AK* on plane e_x, e_y corresponds to an impulse and shows the alteration of the eccentricity vector after the application of an impulse with these radial and transversal components. The equations 1-12e and 1-12f demonstrate that vector *A'K'* with magnitude ΔV_{zi} and angle φ_i to the V_z axis corresponds to the lateral component of the *i*-th impulse on plane $V_z, -z$ (Fig. 1-5).

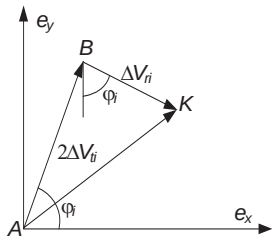

Fig. 1-4. Eccentricity vector alteration after impulse application

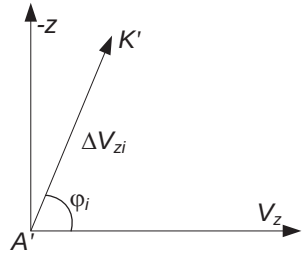

Fig. 1-5. Deviation from the orbital plane due to lateral impulse component application

Thus, the broken lines correspond to a multiple-impulse solution of the problem for the coordinates e_x, e_y and $V_z, -z$. Examples of such broken lines for the two-impulse solution with zero radial impulse components are presented in figs. 1-6 and 1-7.

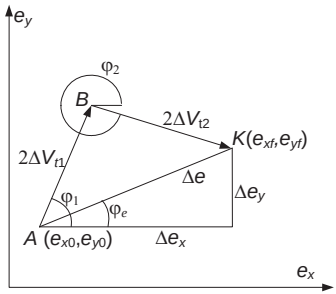

Fig. 1-6. Two-impulse alteration of the eccentricity vector

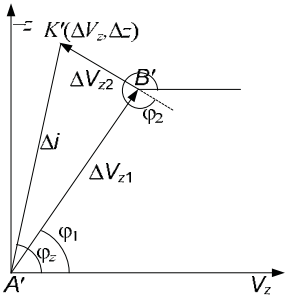

Fig. 1-7. Two-impulse rotation of the orbital plane

The angles φ_e, φ_z, which form the direction of optimal correction of the eccentricity vector deviation and the correction of the orbital plane deviation respectively, are marked in the figures. These angles can be given by:

$$tg\varphi_e = \frac{\Delta e_y}{\Delta e_x}, \qquad (1\text{-}14a)$$

$$tg\varphi_z = -\frac{\Delta z}{\Delta V_z}, \tag{1-14b}$$

The angle $\Delta\varphi$ is worthy of particular attention. It is the angular difference between the direction of optimal eccentricity vector deviation correction and the orbital plane deviation correction:

$$\Delta\varphi = \varphi_e - \varphi_z, \tag{1-14c}$$

Δi = the minimum impulse (in dimensionless form) necessary for the alignment of the orbital planes. It can be evaluated as:

$$\Delta i = \sqrt{\Delta z^2 + \Delta V_z^2}. \tag{1-14d}$$

1.2.5. Relative Orbit

Equation 1-12 describes the orbital element deviations in the rendezvous point, but not the element values. This means that the transfer from the initial to the target elliptical orbits with parameters (e_{x_0}, e_{y_0}, a_0) and (e_{x_f}, e_{y_f}, a_f) is formally equivalent to the transfer from the reference orbit with radius r_0 to the elliptical orbit with parameters $(\Delta e_x, \Delta e_y, a = r_0 + \Delta a)$, where $\Delta e_x = e_{x_f} - e_{x_0}$, $\Delta e_y = e_{y_f} - e_{y_0}$, and $\Delta a = a_f - a_0$. Hereon, we assume that an elliptical orbit with such elements is *relative*. Furthermore, the transfer from point (0, 0) to point ($\Delta e_x, \Delta e_y$) in plane e_x, e_y will be depicted instead of the transfer from point (e_{x_0}, e_{y_0}) to point (e_{x_f}, e_{y_f}).

1.3. Single Impulse Manoeuvres

It is apparent that a single impulse transfer from the initial to the final orbit is possible only when the orbits osculate or intersect with each other. In other cases, only some of the elements of the target orbits can be shaped using single-impulse manoeuvres.

The equation system 1-12 allows us to make some clear conclusions about the alterations of orbital elements due to a single impulse.

1.3.1. Semimajor Axis Correction

A semimajor axis alteration occurs only due to the transversal component of the impulse and the variation value does not depend on the moment of application of the impulse. The radial component does not affect the semimajor axis. The transversal component can be found from Eq. 1-12c:

$$\Delta V_t = \frac{1}{2}\Delta a.$$

1.3.2. Eccentricity Correction

Alteration to the eccentricity value occurs due to both components. The variation value depends strongly on the moment of application of the impulse. It is evident that the most effective way is to alter the eccentricity by applying the transversal impulse component at the pericenter $(\varphi = \varphi_e)$ or the apocenter $(\varphi = \varphi_e + \pi)$ of the relative orbit. The transversal component can be found from Eq. 1-12a. The plus sign corresponds to the impulse applied at the pericenter and the minus sign corresponds to the impulse applied at the apocenter:

$$\Delta V_t = \pm\frac{1}{2}\Delta e,$$

where $\Delta e = \sqrt{\Delta e_x^2 + \Delta e_y^2}$. Consequently, the signs of the eccentricity variation values will differ too.

The radial component can also alter the eccentricity value. It is half as effective when used, but the semimajor axis remains unchanged. The impulse can be applied in $\varphi = \varphi_e + \frac{\pi}{2}\left(\Delta V_r = \Delta e\right)$ or $\varphi = \varphi_e - \frac{\pi}{2}\left(\Delta V_r = -\Delta e\right)$.

1.3.3. Single-Impulse Transfer

If the orbits lie in one plane and intersect with each other, then it is possible to transfer from the initial orbit to the target one using a single impulse applied at one of the points of orbital intersection. As has already

been mentioned, the broken line corresponds to the problem solution on plane e_x, e_y. It starts at the center of the coordinate frame (point *A*) and ends at point *K*, corresponding to the relative orbital eccentricity vector (Fig. 1-8).

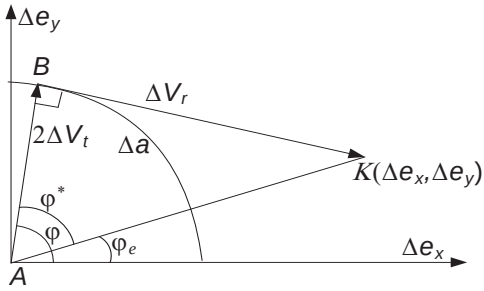

Fig. 1-8. Single-impulse transfer between intersecting orbits

The broken line consists of two pieces as the solution involves both the transversal and radial components of the impulse. The transversal component can be found from Eq. 1-12c: $\Delta V_t = \Delta a / 2$. A circle with radius Δa (Fig. 1-8) will be the geometric locus of the points (on plane e_x, e_y), which can be reached using this component, because the impulse application angle is not defined while the transversal component has a known value. As was mentioned before, the line segment corresponding to the radial component is perpendicular to the line segment corresponding to the transversal component. This means that the line segment that is tangential to the circle must correspond to the radial impulse component. It is necessary to form the given eccentricity vector (i.e. it is necessary to transfer from point *A* to point *K* using two components), which is why line segment *BK* should correspond to the radial component and line segment *AB* should correspond to the doubled transversal component (Fig. 1-8). Using the geometric solution of the problem, the radial component value and the angle of application φ can be found:

$$\Delta V_r = \sqrt{\Delta e^2 - \Delta a^2},$$
$$\varphi = \varphi_e \pm \varphi^*,$$

where $\sin\varphi^* = \Delta V_r / \Delta e$. Then, the delta-v necessary for the transfer can be given as:

$$\Delta V = \sqrt{\Delta e^2 - \frac{3}{4}\Delta a^2}.$$

With the help of the radial component, point *K* can be reached only if it is outside the circle, i.e. *AK>AB*, which is equivalent to the condition $\Delta e > |\Delta a|$. However, on the other hand, the single-impulse solution exists only if the orbits intersect and, hence, the orbits intersect if the condition $\Delta e > |\Delta a|$ is satisfied. Note that the equation for the impulse application angle in the single-impulse transfer to the target orbit can be used for the *determination of the orbital intersection point.*

1.3.4. Orbital Plane Rotation

As can be seen in Fig. 1-7, the orbital planes can also be aligned with the use of a single impulse, which can be applied at $\varphi = \varphi_z$:

$$\Delta V_z = \Delta i$$

or at $\varphi = \varphi_z + \pi$:

$$\Delta V_z = -\Delta i$$

Here, $\Delta i, \varphi_z$ can be found using eqs. 1-14d and 1-14b. It is evident that these impulses are applied on the line of the initial and target orbital intersection.

The angle alteration Δi can be determined without evaluating the deviations $\Delta z, \Delta V_z$ if the angle $\Delta\gamma$ between the orbital planes is known:

$$\Delta i = 2\sin\frac{\Delta\gamma}{2}.$$

Most of cases in this book deal with the small angles between orbital planes. Thus, the equation can be simplified:

$$\Delta i = \Delta\gamma.$$

Taking into account the aforementioned simplification, Δi can be treated as an angle between orbital planes. $\Delta\gamma$ and u_z (u_z = the latitude argument of the impulse application point for the orbital plane alignment) can be determined using the initial orbital inclination i_0, the target orbital inclination i_f, and the RAAN difference of these orbits $\Delta\Omega$:

$$\cos\Delta\gamma = \cos i_f \cos i_0 + \sin i_f \sin i_0 \cos\Delta\Omega,$$
$$\sin u_z = \frac{\sin i_f \sin\Delta\Omega}{\sin\Delta\gamma}.$$

A particularly simple equation can be obtained if only one of the parameters needs to be corrected as i or $\Delta\Omega$:

$$\Delta\gamma = i_f - i_0, u_z = 0^\circ \text{ or } 180^\circ \text{ (equator), or}$$
$$\Delta\gamma = \Delta\Omega, u_z = 90^\circ \text{ or } 270^\circ \text{ (orbital apex or vertex).}$$

1.3.5. Semimajor Axis Correction in the Case of an Elliptical Orbit

Naturally, if only one of the orbital elements needs alteration, more accurate equations (in comparison to the equations for the near-circular motion) can be used. For example, the alteration of the semimajor axis for an elliptical orbit can be calculated as:

$$\Delta a = \frac{2a^2V}{\mu}\Delta V_T,$$

where ΔV_T = the tangential component of the velocity impulse and V = the velocity at the impulse application point. It can be easily seen that for optimal semimajor axis alteration, the impulse must be oriented tangentially, reaching its maximum at the orbital pericenter (the spacecraft's velocity is at its maximum here).

The simple equations of linearized motion will be helpful in obtaining the analytical problem solution, in which several of the orbital elements need to be corrected simultaneously.

1.4. Change in Orbital Size Due to the Application of a Velocity Impulse

Let us depict the alteration of the orbital size and along-the-orbit shifts, which occur under the influence of various impulse components (El'yasberg 1965).

1.4.1. Impact of the Radial Velocity Impulse Component

In Fig. 1-9, the orbit after the application of the positive radial impulse component is pictured using dashed lines. The orbital pericenter is situated at point $\varphi_0 = 1.5\pi$. The absolute values of radial deviations at the apocenter and pericenter are equal and can be evaluated as:

$$\left|\Delta r_\alpha\right| = \left|\Delta r_\pi\right| = r_0 \frac{\Delta V_r}{V_0}.$$

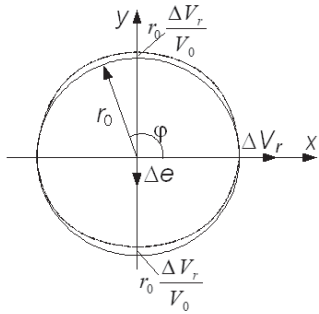

Fig.1-9. Orbital size alteration after radial impulse component application

In Fig. 1-10, one can see the shifts along the orbit during a revolution.

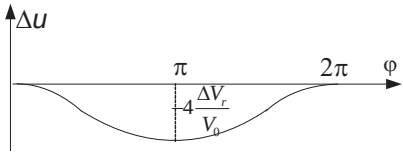

Fig.1-10. Along-the-orbit shift after radial impulse component application

As we can see, the lag from the unperturbed motion appears to be at its maximum after half a revolution:

$$\Delta u = -4\frac{\Delta V_r}{V_0},$$

but it becomes zero by the end of the revolution. This indicates the absence of a secular perturbation.

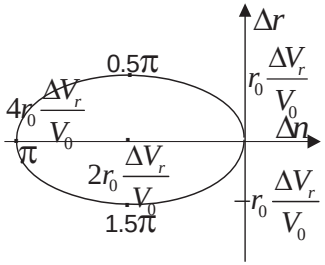

Fig. 1-11a. Relative motion after radial impulse component application

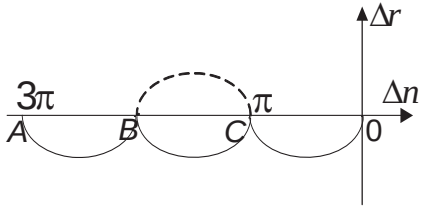

Fig.1-11b. Radial impulse component approach

The results obtained can be used for representing the motion of an active spacecraft (or an object thrown away from a station) relative to the station. This motion can be easily described in an orbital coordinate frame with the origin at the station's center of mass. The axis r points along the radius-vector and the axis n lies on the orbital plane and points in the direction of the spacecraft's motion.

The relative motion caused by the application of the positive radial impulse component can be seen in Fig. 1-11a. The positive radius deviation achieves its maximum after a quarter of a revolution. The along-

the-orbit lag achieves its maximum after half a revolution. The deviation of the radius is zero at this point. A quarter of a revolution later, the radial deviation achieves its maximum negative value and the object returns to the initial point after a full revolution.

Sometimes the difference in the radial velocity component can be used in the approach to a target spacecraft. For example, if an active spacecraft is inserted at a point in the target orbit behind the target spacecraft (point *A* in Fig. 1-11b), then, the active spacecraft approaches the target with the help of the application of the negative radial impulse component (we use only the lower halves of the ellipse in Fig. 1-11a) (Carbonne, Chemama, Julien, and Kudo et al. 2009, 1091-1106). This strategy has some advantages, for example, if the impulse is not located at point *C* (Fig. 1-11b), the spacecraft can return to point *B* and continue its motion without the secular perturbation of position relative to the target spacecraft. The approach process can be continued as needed.

1.4.2. Impact of the Transversal Velocity Impulse Component

In Fig. 1-12, the orbit is plotted using a dashed line, which was obtained after the application of the positive transversal component.

The orbital pericenter is at point $\varphi_0 = 0^\circ$, and the radial deviation at the apocenter is:

$$\Delta r_\alpha = 4r_0 \frac{\Delta V_t}{V_0}.$$

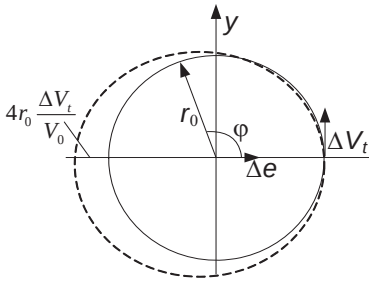

Fig.1-12. Orbital alteration after transversal impulse component application

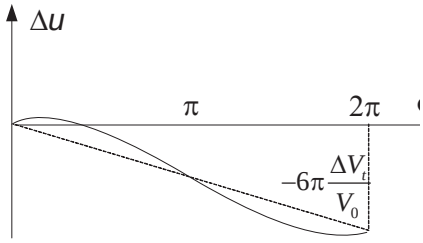

Fig.1-13. Shift along the orbit after transversal impulse component application

The along-the-orbit shift is shown in Fig. 1-13. The shift is initially positive and reaches its maximum as:

$$\Delta u \approx 0.4776 \frac{\Delta V_t}{V_0},$$

when $\varphi = 41^\circ 24'35''$, then, the shift decreases and after $\varphi = 73^\circ 05'32''$ the unperturbed motion lag starts.

Per revolution, the lag can be evaluated by:

$$\Delta u = -6\pi \frac{\Delta V_t}{V_0}.$$

This means that, in fact, the spacecraft starts to move backwards with an average speed of $3\Delta V_t$ after the velocity impulse application ΔV_t is pointed forward.

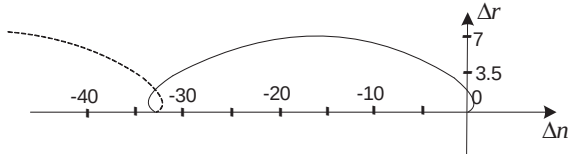

Fig.1-14. Relative motion after transversal impulse component application

The relative motion, caused by the application of the positive transversal impulse component ($\Delta V_t = 2$ m/s, orbital radius $r_0 = 6{,}700$ km) is shown in Fig. 1-14. As we can see, an object thrown forward from the station will move forwards and up. It will continue moving up with a simultaneous backwards motion before descending and reaching the level of the station; however, it will now be behind the station (the same movement during the second revolution is shown by the dashed line).

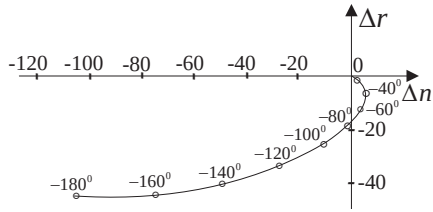

Fig. 1-15. Relative motion of the "Soyuz" spacecraft while approaching the orbital station

The theoretical movement of the "Soyuz" spacecraft relative to the orbital station after the last application of the velocity impulse (180º before the target point) is shown in Fig. 1-15. It is supposed that the deviation at the target point (the target vector) is $\Delta V_t = -12.5$ m/s. As we can see, the spacecraft chases the station at a range of angles from –180º to approximately –73º (it approaches the station from the bottom); then, the spacecraft slightly overruns it; during the last phase, the station chases the spacecraft (the angle range is from –41º to 0º). In fact, the autonomous rendezvous equipment starts working when the angle range reaches 100º and the real movement of the spacecraft will differ from the one shown in Fig. 1-15.

1.4.3. Impact of the Lateral Velocity Impulse Component

Figure 1-16 shows the influence of the lateral impulse component.

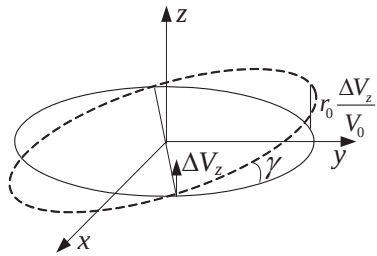

Fig. 1-16. Influence of the lateral impulse component

As we can see, this leads to rotation in the orbital plane at angle:

$$\gamma \approx \frac{|\Delta V_z|}{V_0}.$$

Thus, the maximum deviation from the orbital plane will be:

$$\Delta z = r_0 \frac{|\Delta V_z|}{V_0}.$$

As such, no along-the-orbit shift occurs. The relative motion consists of an oscillating motion along the *z* axis, which is perpendicular to the orbital plane.

Let us undertake some training and use the results obtained for the solution of the problem given in the exams of the Moscow Institute of Physics and Technology.

EXERCISE. Which direction should you avoid while shooting from a spacecraft in order not to be hit by your own bullets?

SOLUTION. The bullets will hit the spacecraft if the period of their orbit is the same. The radial and lateral impulses do not change the orbital period in case of the near-circular motion and, hence, it is prohibited to shoot in the plane, which holds the radial vector and the vector perpendicular to the orbital plane.

1.4.4. Orbital Element Change for Various Circular Orbital Radii

Table 1-1 presents the orbital element alterations for circular orbits of various radii due to the application of a 1m/s transversal impulse component (the first five elements) and a 1m/s lateral impulse component (the last two elements).

The orbital height above the Earth's surface is given in the first column. The changes to the other elements are given in the following columns: Δa = the semimajor axis alteration; Δe = the eccentricity alteration; ΔP = the period alteration; ΔU = the along-the-orbit angular shift per revolution; ΔL = the along-the-orbit linear shift per revolution; $\Delta\gamma$ = the angle of orbital plane rotation; and Δz = the maximum deviation from the orbital plane.

Table 1-1

H km	Δa km	Δe	ΔP s	ΔU deg	ΔL km	$\Delta \gamma$ deg	Δz km
200	1.689	0.000256	2.042	-0.138	-15.826	0.0073	0.844
400	1.765	0.00026	2.166	-0.140	-16.589	0.0074	0.880
800	1.924	0.00027	2.432	-0.143	-17.928	0.0077	0.968
1,500	2.212	0.00028	2.930	-0.149	-20.465	0.0080	1.102
10,000	6.635	0.00040	12.674	-0.218	-62.210	0.0114	3.274
20,000	13.566	0.00051	32.887	-0.278	-127.899	0.0146	6.725
36,000	27.428	0.00065	84.077	-0.351	-258.471	0.0186	13.704

Some of the deviations are not listed in the table, but they can be easily evaluated with the help of these values. For instance, the maximum radial deviation is equal to the doubled semimajor axis deviation, etc. The deviations due to the application of the radial component can be easily evaluated with the use of the deviations caused by the transversal component. In addition to single-impulse manoeuvres, multiple-impulse ones can also be approximately calculated using this table.

1.5. Manoeuvre Assessment and Initial Phase Range Selection

1.5.1. Features of Soyuz Spacecraft Manoeuvres

As an example, let us estimate the sum of transversal impulse components of the first and second manoeuvring intervals of the four-impulse approach manoeuvre between the "Soyuz" spacecraft and an orbital station. The first manoeuvring interval is located on the third and fourth revolutions, while the second interval starts one revolution before the target point. The target point is set at the end of the 33rd revolution.

Let us assume that, in the moment of the "Soyuz" spacecraft's insertion, the station is $\Delta u_0 = 197^\circ$ ahead (this range of angles is sometimes called the "initial phase" or simply "phase"). The "Soyuz" spacecraft's orbit (initial orbit) has the heights $h_{\min} = 192\,\text{km}$ and $h_{\max} = 238\,\text{km}$, while the station's orbit (the target orbit) has the heights $h_{\min} = 330\,\text{km}$ and $h_{\max} = 341.5\,\text{km}$.

The average orbital radial difference is $120.75\,\text{km}$. As one can see from the table, a transversal impulse of magnitude $\frac{120.75}{1.69} \approx 71.4\,\text{m/s}$ is

needed to eliminate this difference. With the existing difference between the orbit's semimajor axes, the angle range (the phase) will decrease to $197^\circ - 0.139 \cdot 71.4 \cdot 3 = 167.218^\circ$ due to the motion before the first manoeuvring interval, which is on the third revolution. The impact of a fixed impulse with magnitude $2\,\text{m/s}$, applied at the 17th revolution and serving the purpose of fixing first impulse realization errors in phase deviation, can be estimated as $0.139 \cdot 2 \cdot 14 = 3.892^\circ$, where 14 = the number of revolutions between the first manoeuvring interval and the fixed impulse application. Thus, in order to "catch" the station in 29 revolutions, the phase difference should decrease by $\frac{167.218 - 3.892}{29} \approx 5.632^\circ$ per revolution. In order to satisfy this condition, the required semimajor axis difference must be equivalent to the transversal impulse with magnitude $\frac{5.632}{0.139} \approx 40.52$ m/s. The calculated value should be decreased by the target vector magnitude $(-12.5\,\text{m/s})$ since this deviation is not compensated for by the burns. As a result, the sum of the transversal impulse components of the second manoeuvring interval will be $\Delta V_{t_{II}} = 40.52 - 12.5 = 28.02$ m/s. The sum of the transversal impulse components of the first interval will be $\Delta V_{t_I} = 71.4 - 2 - 12.5 - 28.02 = 28.88$ m/s. An accurate analytical solution of the problem (see Example 1, Chapter 5) gives the following values: $\Delta V_{t_{II}} = 28.67$ m/s, $\Delta V_{t_I} = 32.1$ m/s. As we can see, the phase condition allows us to determine the impulse values with good precision as the sums of the transversal impulse components of the second manoeuvring interval (calculated analytically and numerically) do not differ by much. The sums of the transversal impulse components of the first interval differ significantly. This can be explained by the omission of the notable influence of atmospheric drag on the spacecraft due to its relatively low orbit.

Simple equations can be used to assess the influence of atmospheric drag on the spacecraft's motion in a circular orbit. The atmospheric drag force is given by:

$$R_x = c_x F_m \frac{\rho V_{rel}^2}{2},$$

where c_x = the dimensionless atmospheric drag coefficient; F_m = the spacecraft's cross-section (the maximum spacecraft section, perpendicular to the velocity vector of the flight relative to the atmosphere); ρ = the atmospheric density; and V_{rel} = the absolute value of the flight velocity vector relative to the atmosphere. A spacecraft moving along a circular orbit suffers deceleration, which can be calculated using the following equation:

$$T = -\frac{R_x}{m} = -c\rho V^2 = -\frac{c\rho\mu}{r},$$

where $c = \frac{c_x F_m}{2m}$ = the ballistic coefficient, which is refreshed during flight. Alterations to the height and period per revolution on a circular orbit can be found in El'yasberg (1965):

$$\delta r = -4\pi c\rho r^2,$$
$$\delta P = -\frac{12\pi^2}{\sqrt{\mu}} c\rho r^{5/2}.$$

The atmospheric density depends on many factors and there are different static and dynamical (including the influence of solar pressure) atmospheric models.

We can use table 1-2 to assess the atmospheric influence (El'yasberg 1965). The alterations of δP and δr for circular orbits versus different heights H above the Earth's surface have been calculated for a spacecraft with the ballistic coefficient $c = 0.1$ (the CIRA 1961 static atmospheric model was used).

Table 1-2

H km	150	200	250	300	350
δP s	11	2.4	$7.0\cdot10^{-1}$	$2.3\cdot10^{-1}$	$8.7\cdot10^{-2}$
δr km	9.2	2.0	$5.8\cdot10^{-1}$	$1.9\cdot10^{-1}$	$7.1\cdot10^{-2}$
H km	400	500	600	700	800
δP s	$3.7\cdot10^{-2}$	$8.6\cdot10^{-3}$	$2.7\cdot10^{-3}$	$9.6\cdot10^{-4}$	$3.8\cdot10^{-4}$
δr km	$3.0\cdot10^{-2}$	$7.1\cdot10^{-3}$	$2.1\cdot10^{-3}$	$7.6\cdot10^{-4}$	$3.0\cdot10^{-4}$

The basic parameters of this atmospheric model (density, pressure, temperature, and molecular weight versus different heights) are listed in El'yasberg (1965).

Using table 1-2, one can estimate the decrease in height for 33 revolutions. Here, the average orbital height after the first manoeuvring interval is 265 km (corresponding to $\Delta V_{t_1} = 28.88$ m/s). The orbital radius decreases by 0.46 km per revolution for a spacecraft with the ballistic coefficient $c = 0.1$. The "Soyuz" spacecraft has the approximate ballistic coefficient 0.039. As such, after 33 revolutions the height has decreased by $\Delta r = \frac{0.46 \cdot 0.039 \cdot 33}{0.1} = 5.92$ km. In order to compensate for this loss in height, it is necessary to increase the sum of the transversal components for the first manoeuvring interval by $\frac{5.92}{1.69} = 3.5$ m/s. Thus, we get $\Delta V_{t_1} = 28.88 + 3.5 = 32.38$ m/s, which agrees well with the numerical result.

1.5.2. Initial Phase Range at Launch Time

The angular range between the spacecraft and the orbital station in the moment of the spacecraft's orbital insertion Δu (initial phase) has a significant influence on the delta-v expenditure distribution between the manoeuvring intervals. Let us assume that primary manoeuvring occurs at the beginning and the end of a flyby, lasting N revolutions. If the spacecraft did not manoeuvre at all, then the along-the-orbit dimensionless deviation at the rendezvous point would be:

$$u_f = \Delta u^* - \frac{3}{2}\Delta a N,$$

where Δa = the semimajor axis difference between the spacecraft and the orbital station and Δu^* = the initial phase, measured in fractions of a revolution ($\Delta u^* = \frac{\Delta u}{2\pi}$). To eliminate this deviation, the sum of the transversal impulse components of the first manoeuvring interval should be:

$$-3N\Delta V_{t_I} = \Delta u^* - \frac{3}{2}\Delta aN,$$

$$\Delta V_{t_I} = \frac{1}{2}\Delta a - \frac{\Delta u^*}{3N}.$$

Hence, the sum of the transversal impulse components of the last manoeuvring interval will be:

$$\Delta V_{t_{II}} = \frac{1}{2}\Delta a - \Delta V_{t_I} = \frac{\Delta u^*}{3N}.$$

Thus, the initial phase and rendezvous duration unambiguously define the sum of the transversal impulse components of the second manoeuvring interval and the lasting of the semimajor axis deviation will be eliminated by the manoeuvres of the first interval.

In Fig. 1-17, $\Delta V_{t_{II}}$, as a function of Δu^*, is depicted by the dashed line; ΔV_{t_I}, as a function of Δu^*, is depicted by the dash-dotted line; and total delta-v is depicted by the solid line. As a result, an optimal range of the initial phase values exists: $\Delta u^* \in [0, \Delta u_m^*]$, where $\Delta u_m^* = \frac{3}{2}N\Delta a$. The total delta-v is constant in this range and equals the minimum value $\Delta V = \frac{1}{2}\Delta a$.

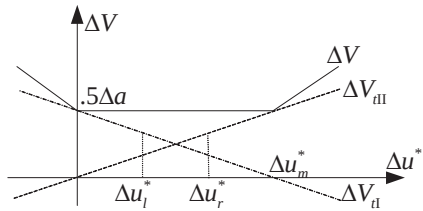

Fig. 1-17. ΔV as a function of the initial phase

While selecting the initial phase, one should bear in mind that in the case of abnormal situations there must be the possibility of rescheduling the first manoeuvres to a back-up revolution. If the back-up manoeuvring interval is *n* revolutions behind the first interval, then the sums of the

transversal impulse components of the first and second manoeuvring intervals can be found by:

$$\Delta V_{t_I} = \frac{\Delta aN}{2(N-n)} - \frac{\Delta u^*}{3(N-n)},$$
$$\Delta V_{t_{II}} = \frac{\Delta a}{2} - \frac{\Delta aN}{2(N-n)} + \frac{\Delta u^*}{3(N-n)}.$$

With the increase in n, the sum of the manoeuvring transversal components in the first interval increases and the sum of the manoeuvring transversal components of the second interval decreases; ΔV_{t_I}, however, should not exceed $\frac{1}{2}\Delta a$. This condition helps us discover the left boundary of the allowed range Δu_l^*:

$$\Delta u_l^* = \frac{3}{2} n \Delta a.$$

The 13th revolution used to be the backup revolution for the first "Soyuz" spacecraft. The first manoeuvring interval was on the 3rd and 4th revolutions, the second one was on the 32nd revolution, and docking occurred on the 33rd revolution. Thus, for this scheme $n \approx \frac{1}{3}N$. The left boundary of the allowed range Δu_l^* shifts by the third part of the optimal range length to the right.

We may encounter a situation where the spacecraft launch is rescheduled. For the "Soyuz" spacecraft, the backup launch date is usually scheduled two days later (after the scheduled revolutions). In this case, the initial phase increases if the station period is less than 90 minutes. The phase change Δu_{st}^* can be evaluated by:

$$\Delta u_{st}^* = \left\{ \frac{3\pi m}{\nu T} \right\} (\mathrm{mod}\, l),$$

where m = the number of revolutions by which the launch date is shifted; $\nu = \omega_E + \dot{\Omega}_{J_2}$, ω_E = Earth's angular speed of movement; and $\dot{\Omega}_{J_2}$ = the

change rate of Ω accounting for the second gravitational field zonal harmonic.

If the initial phase increases, the right boundary of the permitted range Δu_r^* should be shifted by Δu_{st}^* leftwards from Δu_m^* in order to maintain the phase inside the optimal range after the change in the launch date.

In addition, there may be some restrictions on the acceptable values of the impulse sum of the second manoeuvring interval, which can also shift the right boundary of the allowed range leftwards.

1.6. Optimality Conditions

A single impulse is not enough if it is necessary to correct all the elements of the orbit. Two or more impulses are used in this case. The number of control parameters ($4N$, where N = the number of impulses) usually exceeds the number of constraints in the equation system 1-12. This can be changed if additional restrictions on impulse orientation and/or on the moments of their application are introduced. The problem of searching for the optimal solution appears. To find the solution, one can use the necessary optimality conditions from the primer vector theory (Lawden 1966).

1.6.1. Equations of Motion in Dimensionless Form

After the conversion of variable t to the independent angular variable θ, the equations of motion in dimensionless form for the mass point in the cylindrical coordinate frame (eqs. 1-5 and 1-7) will be as follows (Il'in and Kuzmak 1976):

$$\frac{d\Delta\tilde{r}}{d\theta} = \Delta\tilde{V}_r, \tag{1-15a}$$

$$\frac{d\Delta\tilde{t}}{d\theta} = \Delta\tilde{r} - \Delta\tilde{V}_t, \tag{1-15b}$$

$$\frac{d\Delta\tilde{z}}{d\theta} = \Delta\tilde{V}_z, \tag{1-15c}$$

$$\frac{d\Delta\tilde{V}_r}{d\theta} = 2\Delta\tilde{V}_t + \Delta\tilde{r} + n_r, \tag{1-15d}$$

$$\frac{d\Delta\tilde{V}_t}{d\theta} = -\Delta\tilde{V}_r + n_t, \tag{1-15e}$$

$$\frac{d\Delta\tilde{V}_z}{d\theta} = -\Delta\tilde{z} + n_z, \tag{1-15f}$$

$$\frac{d\tilde{q}}{d\theta} = n, \tag{1-15g}$$

Here, $\Delta\tilde{r}, \Delta\tilde{t}, \Delta\tilde{z}, \Delta\tilde{V}_r, \Delta\tilde{V}_t, \Delta\tilde{V}_z, \tilde{q}$ = the dimensionless variables; $q = c \ln \frac{m_0}{m}$ = the characteristic velocity (c = the exhaust velocity; m_0 and m = the initial and current masses; and n_r, n_t, n_z and $n = \sqrt{n_r^2 + n_t^2 + n_z^2}$ = the components of jet acceleration and its modulus divided by gravitational acceleration $g(r_0)$).

1.6.2. Co-state Equation System

The co-state equation system for Eq. 1-15 will be as follows (Il'in and Kuzmak 1976):

$$\frac{dp_r}{d\theta} = -s_r - p_t, \tag{1-16a}$$

$$\frac{dp_t}{d\theta} = 0, \tag{1-16b}$$

$$\frac{dp_z}{d\theta} = s_z, \tag{1-16c}$$

$$\frac{dp_q}{d\theta} = 0, \tag{1-16d}$$

$$\frac{ds_r}{d\theta} = s_t - p_r, \tag{1-16e}$$

$$\frac{ds_t}{d\theta} = -2s_r + p_t, \tag{1-16f}$$

$$\frac{ds_z}{d\theta} = -p_z, \tag{1-16g}$$

Here, the vector $\mathbf{s} = (s_r, s_t, s_z)$ and the velocity vector $\mathbf{V} = (V_r, V_t, V_z)$ are conjugated vectors and p_r, p_t, p_z and $\Delta r, \Delta t, \Delta z$ are conjugated variables.

The solution of this system can be given by:

$$p_r = 2\lambda_1 + \lambda_2 \sin\theta + \lambda_3 \cos\theta - 3\lambda_6\theta, \quad (1\text{-}17a)$$

$$p_t = \lambda_6, \quad (1\text{-}17b)$$

$$p_z = \lambda_5 \sin\theta - \lambda_4 \cos\theta, \quad (1\text{-}17c)$$

$$p_q = -1, \quad (1\text{-}17d)$$

$$s_r = -\lambda_2 \cos\theta + \lambda_3 \sin\theta + 2\lambda_6, \quad (1\text{-}17e)$$

$$s_t = 2\lambda_1 + 2\lambda_2 \sin\theta + 2\lambda_3 \cos\theta - 3\lambda_6\theta, \quad (1\text{-}17f)$$

$$s_z = \lambda_4 \sin\theta + \lambda_5 \cos\theta, \quad (1\text{-}17g)$$

where $\lambda_1, \lambda_2, \lambda_3, \lambda_4, \lambda_5, \lambda_6$ = arbitrary constants.

The problem Hamiltonian can be written as:

$$H = [(\mathbf{s}, \mathbf{n}) + p_q n] + s_r(2\Delta V_t + \Delta r) + s_t(-\Delta V_t) + s_z(-\Delta z) + \\ + p_r \Delta V_r + p_t(\Delta r - \Delta V_t) + p_z \Delta V_z. \quad (1\text{-}18)$$

1.6.3. Necessary Optimality Conditions

Let the primer vector be the vector function $\mathbf{s}(s_r, s_t, s_z)$, conjugated with the velocity vector. D. F. Lawden (1966) showed that the primer vector should not exceed a unity in the modulus while on the optimal trajectory; the impulses are applied at those moments when the primer vector is a unity in the modulus and the impulse vector and the primer vector are aligned in this point of the trajectory. This means that the primer vector hodograph of the optimal solution does not exceed the boundaries of the unit sphere (the spatial problem), or the boundaries of the unit circle (the flat problem). The optimal solution impulses are applied at those moments when the hodograph osculates with a sphere (a circle)—the inner impulses—or intersects it (the initial and the terminal moments of the flyby interval)—the two outer impulses.

Hence, we only need the variables to conjugate the velocity vector. The labels λ, μ, ν are often used for these variables. Equations 1-17e to 1-17g can be converted into a more convenient form (Edelbaum 1967, 66-73):

$$\lambda = \sqrt{\lambda_2^2 + \lambda_3^2}\, \sin(\theta - \theta_0) + 2\lambda_6, \quad (1\text{-}19a)$$

$$\mu = 2\lambda_1 + 2\sqrt{\lambda_2^2 + \lambda_3^2}\cos(\theta - \theta_0) - 3\lambda_6\theta, \quad \text{(1-19b)}$$

$$\nu = \frac{\lambda_3\lambda_4 - \lambda_2\lambda_5}{\sqrt{\lambda_2^2 + \lambda_3^2}}\sin(\theta - \theta_0) + \frac{\lambda_2\lambda_4 + \lambda_3\lambda_5}{\sqrt{\lambda_2^2 + \lambda_3^2}}\cos(\theta - \theta_0), \quad \text{(1-19c)}$$

$$tg\,\theta_0 = \frac{\lambda_2}{\lambda_3}. \quad \text{(1-19d)}$$

The impulse will be optimally oriented in the moment θ_i if the conditions below are satisfied:

$$\frac{\Delta V_{r_i}}{\Delta V_i} = \lambda(\theta_i); \frac{\Delta V_{t_i}}{\Delta V_i} = \mu(\theta_i); \frac{\Delta V_{z_i}}{\Delta V_i} = \nu(\theta_i). \quad \text{(1-20)}$$

The conditions 1-19 and 1-20 can be obtained using the Lagrange multiplier method. The Lagrange function L will consist of ΔV and Eq. 1-12 multiplied by the Lagrange multipliers $\lambda_1,...,\lambda_6$. After differentiation of L by $\Delta V_{r_i}, \Delta V_{t_i}, \Delta V_{z_i}$, and equalizing the results of differentiation by zero, we get the conditions 1-20.

Normally, eqs. 1-19a to 1-19d describe a spiral in the dimensions λ, μ, ν or a cycloid on the plane μ, λ. If $\lambda_6 = 0$, the primer vector hodograph can degenerate to an ellipse, a circle, a line segment, or a point. Each hodograph type has a corresponding type of optimal solution. A new designation for the angle (θ instead of φ) is used for the conjugated variables. The primer vector hodograph type defines the possible types of optimal solution, and the problem's peculiarities determine the concrete choice of the type of solution.

The dependences between the primer vector modulus *s* and the time for the cases when the hodograph is an ellipse and when it is a one-and-half-revolution long cycloid are given in Fig. 1-18.

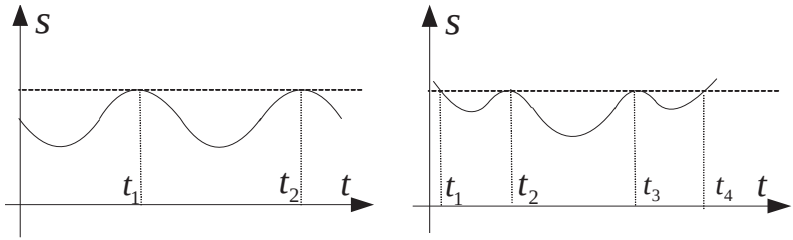

Fig. 1-18. Primer vector modulus as a function of time for hodographs in the form: (*a*) ellipse; (*b*) cycloid

1.7. General Solution Scheme

The linearized equations of motion are used in the problem stated in section 1.2. The noncentrality of the gravitational field, the atmospheric influence, and velocity impulse durations are not taken into account. This leads to insufficient accuracy in the terminal conditions 1-12. An iterative scheme from the work of Bazhinov and Yastrebov (1978), Gavrilov, Obukhov, Skoptsov, and Zaslavsky (1975), and Petrov (1985) can be used to solve the problem with higher accuracy. The scheme consists of several steps:

0. In the beginning, an "accurate" prediction of the spacecraft's movement in the initial and terminal orbits to the rendezvous point using all the necessary perturbation models is made. Deviations between the initial and target orbit parameters are calculated.

1. The next step involves solving the "approximate" problem. With the aforementioned simplifying assumptions, we determine the parameters of the impulses, shaping the "target" orbit. On the first iteration, the "target" orbit coincides with the terminal orbit.

2. After this, using the calculated impulses and models of all necessary perturbations, an "accurate" prediction of the spacecraft's movement is made and the parameters of the new orbit are found.

3. The deviations between the new orbit and the corresponding parameters of the terminal orbit are calculated.

4. If the deviations exceed tolerable limits, the "target" orbit parameters are changed to values of parameters with the summed up deviations and the next iteration is performed.

The procedure ends when the terminal conditions are satisfied.

As a rule, numerical and/or analytically numerical integrations are used for “accurate” prediction. It is possible to use different prediction methods on different iterations, but the accuracy of the prediction should get higher with each successive iteration.

The gravitational field’s noncentrality, and the atmospheric and solar radiation pressure influence, etc., are taken into account while performing numerical integration and the work of the spacecraft propulsion system is also modeled. Hence, despite the fact that the manoeuvring parameters are evaluated on each iteration with the use of simple models, the results of the iteration procedure ensure the acquisition of a solution with the desired precision.

The flowchart of the iteration procedure is given below. We can see that use of this iteration procedure does not guarantee that the found solution is optimal. The search for an optimal solution has been carried out with some simplifying assumptions. Determination of a possible deviation from the optimal solution on the first iteration can be found in table 2-1 (paragraph 2.1.6). However, firstly, the alteration of the terminal conditions of the problem during the iteration process and some special techniques (for example, the alteration of the order of the impulse application, see 2.1.6) allow us to get close to the real optimal solution. Secondly, during the solution of the real problem, the first priority takes the accuracy of adjustment of the given orbit as well as the reliability and the speed of the solution’s acquisition. This scheme gives all this to the user and it is acceptable to have a few percent difference between the found and the optimal solutions. In practice, the simplicity and reliability of the solution is sometimes worth a 40 % loss of total delta-v. Furthermore, the results demonstrate that the difference between the found solutions of real problems using this procedure and the solutions found using the cumbersome numerical methods hardly exceed 1 %.

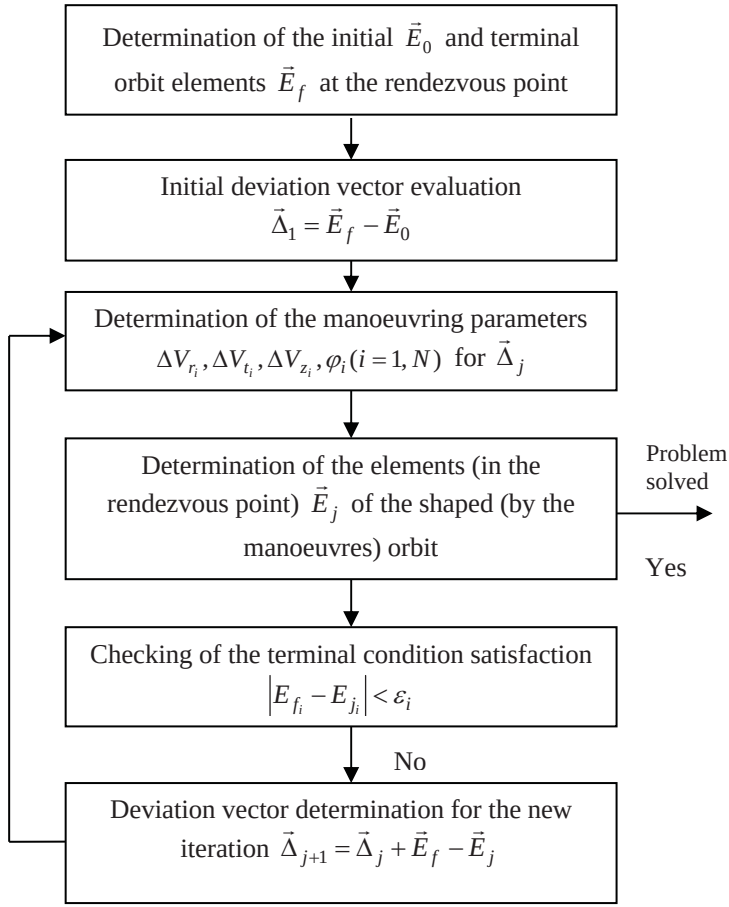

Using the numerical methods without this iteration procedure, it is hard to provide the desired accuracy in the satisfaction of the terminal condition and strict minimization of total delta-v. Also, problems with the selection of the solution for the start of the minimization process and the search for the local minimum appear. High speed or reliability can be provided by this approach in the acquisition of the solution.

The aforementioned explains why this iteration procedure is widely used in ballistic centers all over the country.

Reliability is the key feature of practical problem solving methods. This is why the convergence of the iterative procedure plays a primary role.

This solution scheme is quite promising. The deviations between the orbit and the relative orbit can reach several hundred kilometers and the manoeuvre duration can reach 2-3 tens of degrees by the latitude argument, which is noticeably far from the initial impulse supposition. For the majority of practical problems, this procedure converges fast and with certainty. For example, it is enough to pass through the five iterations to get the manoeuvring parameters for the "Soyuz" and "Progress" spacecraft. However, when the omitted perturbations become considerable or the perturbation group starts to produce a more substantial effect, problems of convergence appear. In this case, some perturbations need to be taken into account. For example, the influence of the second harmonic of the gravitational field's potential expansion and the long duration of spacecraft engine firing should be taken into account during manoeuvre parameter determination. There is also an option to use the techniques invented by the author. Drawing on 45 years of experience with actual projects, these can help ensure the required reliability and convergence speed for all the numerous practical problems.

1.8. Main Types of Optimal Spacecraft Manoeuvring Problems

The problem of the optimal near-circular orbital manoeuvring parameter search has been stated in general terms. Several types of problems, which have to be solved while supporting real spacecraft, can be distinguished. Naturally, each problem has its own solution. Even more simple solutions can be found for different well-known particular cases.

Two basic types of spacecraft optimal manoeuvring problems in near-circular orbits can be distinguished:

I. The interorbital transfer problem, when the transfer time from the initial to the target orbit is not fixed (as a rule, two-impulse solutions).

II. The rendezvous problem, when the transfer time to the given point in the terminal orbit is fixed (sometimes two-impulse solutions, but, as a rule, requiring multiple-impulse solutions (three or more)).

Each of these types of problem has two manoeuvring subtypes:

Coplanar manoeuvres (where the terminal and initial orbits lie in the same plane).

Non-coplanar manoeuvres (where the orbital planes do not coincide).

Hence, there are four different types of problems for impulse manoeuvres. It should be noted that each of problems has three of four types of possible solutions.

We have the same types of problems for manoeuvres performed by low-thrust engines, where the burning intervals take up considerable parts of the revolutions.

Similar problems can be encountered while evaluating transfer manoeuvres between highly eccentric orbits.

The described classification of manoeuvres can be found in the scheme.

Those problems that correspond to the dashed arrows are not considered in this book. They deal with transfers when at least one orbit is highly eccentric. All the problems corresponding to the solid arrows are considered rather thoroughly.

In this scheme, division by the eccentricity value 0.1 is nominal. In fact, as already mentioned, the iterative procedure converges with higher eccentricity values.

Similarly, it is hard to accurately distinguish those problems that can be solved with the approximation of the impulse manoeuvres and those problems that can be solved by taking into account the real manoeuvre duration.

The impulse manoeuvres of transfers between coplanar and non-coplanar orbits are considered in Chapter 2. The rendezvous problems in the coplanar and non-coplanar orbits are examined in the 3rd and the 4th chapters. The 5th chapter presents the numerical methods for the solution of near-impulse rendezvous problems and finally manoeuvring with low-thrust engines is considered in Chapter 6.

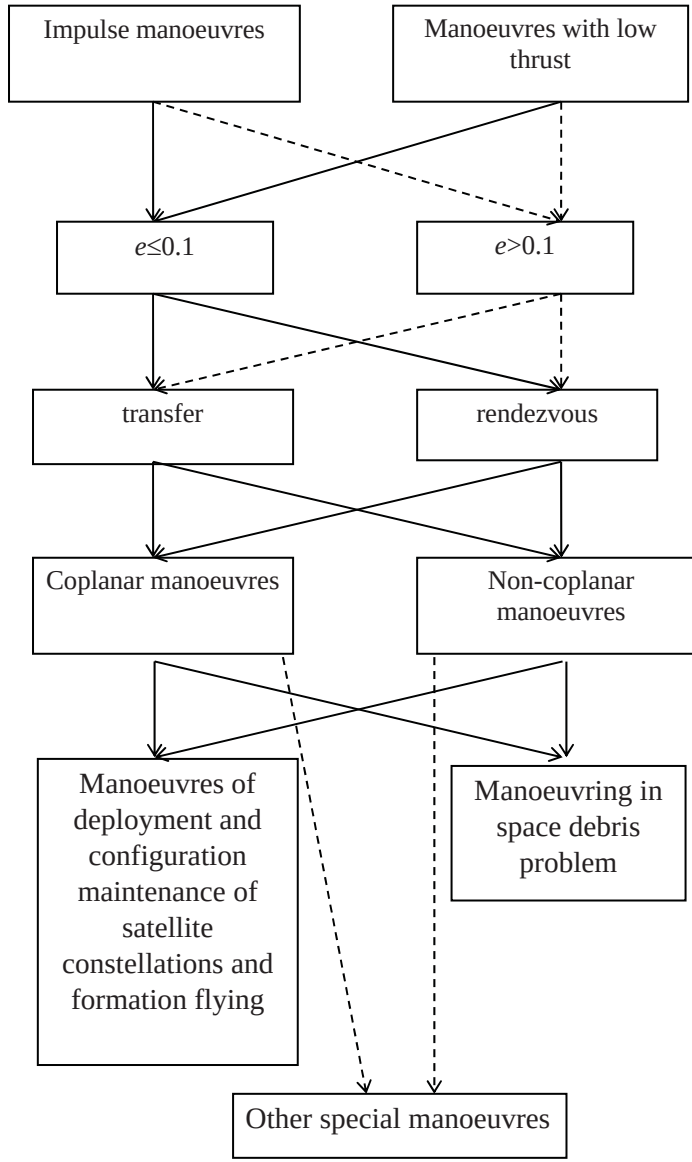

The problems enumerated in the first six chapters are used for the deployment and station-keeping (attitude control) of satellite constellations; manoeuvre determination for collision avoidance with space debris; and the assessment of manoeuvres performed by active space objects, as well as lots of others. Some of these problems are also mentioned in the presented scheme.

The 7th chapter describes manoeuvring peculiarities while forming set configurations of satellite constellations and satellite formation flying. The problems in the general statement, as well as some particular cases like the alteration of a satellite's position in a satellite constellation in circular orbits (including the transfer to a different operational plane), are considered. In the 8th chapter, problems of the absolute and relative station-keeping of a satellite constellation and formation flying are given. Manoeuvres for space debris collision avoidance, including solution alteration, helping to avoid collisions in the reference orbit, are considered in Chapter 9. The algorithms, which help us to estimate single and two-impulse manoeuvres of small and big durations performed by active spacecraft, including cases when the terminal orbit is determined with considerable errors, are given.

In the 10th chapter, spacecraft transfer to a disposal orbit is examined. The evolution of these types of orbits is considered. An examination of the problem of de-orbiting large-size space debris is given. The five compact groups of large-size space debris are distinguished and two schemes for the transfer of space debris to disposal orbits are considered. The quantity assessment of spacecraft, needed for the transfer of the majority of the elements of these groups, is also given.

CHAPTER TWO

TRANSFER MANOEUVRES

2.1. Coplanar Transfers

2.1.1. Problem Statement

The lateral motion and time constraints are not taken into account during the transfer manoeuvre parameter determination. Thus, the conditions for the transfer to the desired orbit (Eq. 1-12) will be

$$\sum_{i=1}^{N}(\Delta V_{r_i}\sin\varphi_i + 2\Delta V_{t_i}\cos\varphi_i) = \Delta e_x, \qquad (2\text{-}1a)$$

$$\sum_{i=1}^{N}(-\Delta V_{r_i}\cos\varphi_i + 2\Delta V_{t_i}\sin\varphi_i) = \Delta e_y, \qquad (2\text{-}1b)$$

$$\sum_{i=1}^{N} 2\Delta V_{t_i} = \Delta a, \qquad (2\text{-}1c)$$

The problem of the optimal manoeuvre parameter determination for the transfer between the coplanar orbits can be stated as "find $\Delta V_{r_i}, \Delta V_{t_i}, \varphi_i$ $(i = 1,..., N)$, which ensure the minimum total delta-v

$$\Delta V = \sum_{i=1}^{N}\sqrt{\Delta V_{r_i}^2 + \Delta V_{t_i}^2}$$

with the constraints 2-1a–2-1c".

The problem solution does not depend on the time. Thus, $\lambda_6 = 0$ in the necessary optimality conditions 1-19a–1-19d. On the other hand, $\lambda_4 = 0, \lambda_5 = 0$, due to the fact that these are coplanar manoeuvres. Hence, the equations for the primer vector will be

$$\lambda = \sqrt{\lambda_2^2 + \lambda_3^2}\,\sin(\theta - \theta_0),$$
$$\mu = 2\lambda_1 + 2\sqrt{\lambda_2^2 + \lambda_3^2}\,\cos(\theta - \theta_0),$$
$$tg\,\theta_0 = \frac{\lambda_2}{\lambda_3}.$$

There are three types of possible solutions which satisfy the necessary optimal conditions:

1. The primer vector hodograph on the plane μ, λ is and *ellipse*; the center of the ellipse belongs to the μ axis, but it is shifted from the center of the coordinate frame; the ellipse touches the unit circle at the point *C* (Fig. 2-1a) if the center is shifted to the right, *or* it touches the unit circle at the point *B* if the center of the ellipse is shifted towards the opposite direction;

2. The primer vector hodograph turns to the *point* that coincides with the point of the intersection with the unit circle of the μ axis; this is point *B or* point *C*;

3. The primer vector hodograph is an *ellipse* with the center in the origin of the coordinate frame, which touches the unit circle at *two* points– –*B* and *C* (Fig. 2-1b).

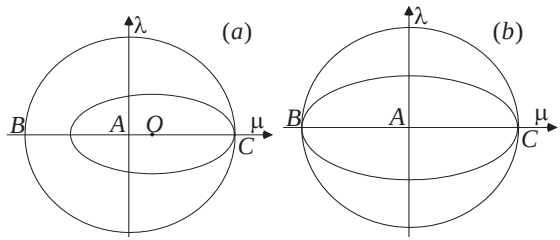

Fig. 2-1. Primer vector hodograph for the coplanar transfer.

Let us remember that the angles in Eq. 1-12 are negative, and the deviations are calculated at the rendezvous point. The deviations can be estimated in the arbitrary point of the orbit in the transfer case but, usually, they are estimated in the ascending node on the equator or on the apsidal line of the relative orbit. We can switch from negative angles, which are estimated in a clockwise manner from the chosen direction (for instance, from the node line), to impulse application moments, to positive angles, which are estimated in the reverse direction (that is not exactly right, but it

is more habitual). It means that, in the first case, when the deviations are estimated on the node line, the values of the angles φ_i will coincide with the latitude arguments of the impulse application points u_i, which is rather convenient. In the second case, when the *x* axis coincides with the apsidal line of the relative orbit, $\Delta e_y = 0, \Delta e_x = e$, and for the determination of the impulse magnitudes which are applied on the apsidal line of the relative orbit, it is enough to solve the equation system:

$$2\Delta V_{t_1} - 2\Delta V_{t_2} = \Delta e,$$
$$2\Delta V_{t_1} + 2\Delta V_{t_2} = \Delta a.$$

The impulse magnitudes are found from this equation system:

$$\Delta V_{t_1} = \frac{1}{4}(\Delta a + \Delta e)$$
$$\Delta V_{t_2} = \frac{1}{4}(\Delta a - \Delta e)$$

2.1.2. Coplanar Transfers between Osculating Orbits

If $\lambda_1 \neq 0$ and $\lambda_2^2 + \lambda_3^2 \neq 0,$ the primer vector hodograph will be the ellipse, which has been shifted from the center of the coordinate frame. The ellipse would coincide with the unit circle on the plane μ, λ if the condition $2\lambda_1 + 2\sqrt{\lambda_2^2 + \lambda_3^2} = 1$ (with $\lambda_1 > 0$), or $2\lambda_1 - 2\sqrt{\lambda_2^2 + \lambda_3^2} = -1$ (with $\lambda_1 \leq 0$) is satisfied. The hodograph osculates with the circle in one point, which is situated on the μ axis ($\mu = 1, \lambda = 0$). Thus, according to Eq. 1-20, the solution with one transversal impulse will be optimal. It is worth mentioning that the necessary conditions would be satisfied again after one revolution and two revolutions, etc.; hence, this impulse can be divided into the parts, which can be performed on different revolutions, but in the same location. The option of impulse division is available for all transfer problems, but the solutions with the minimum number of impulses have a higher priority. These solutions will be analyzed further.

The found single-impulse solution is only feasible for transfers between *osculating* orbits. The magnitude of this impulse can be found from Eq. 2-1c

$$\Delta V_t = \frac{1}{2}\Delta a,$$

or from eqs. 2-1a and 2-1b

$$2\Delta V_t \cos\varphi = \Delta e_x,$$
$$2\Delta V_t \sin\varphi = \Delta e_y,$$
$$\left|\Delta V_t\right| = \frac{1}{2}\Delta e.$$

Thus, for the osculating orbits, $\Delta e = \left|\Delta a\right|$.

The paradoxical feature of the optimal solution of this type draws our attention. The specific solution, which is only true for osculating orbits, corresponds to the basic appearance of the primer vector hodograph (lots of ellipses exist, which osculate with the circle in one point). Most often in practical work the transfers between the intersecting and nonintersecting orbits correspond to the particular appearances of the primer vector hodograph (when it degenerates to the point or ellipse with the center in the reference frame origin). As will be shown in Chapter 6, this paradoxical feature disappears if one considers long-duration manoeuvres, and not impulsive ones.

2.1.3. Coplanar Transfers between Nonintersecting Orbits: Coplanar Singular Solutions

A primer vector hodograph degenerating to a point will belong to the unit circle, if $\lambda_2 = \lambda_3 = 0, \lambda_1 = \pm 0.5$. The point coordinates are (1, 0) or (-1, 0); hence, the impulses are transversal ($\Delta V_{r_i} = 0$). All impulses are accelerating ($\Delta V_{t_i} > 0$), if $\mu = 1$, and decelerating ($\Delta V_{t_i} < 0$), if $\mu = -1$. The hodograph does not depend on θ; therefore, for this type of solution, it is not possible to determine the impulse application angles and their minimum number from the equations for the primer vector. Let these solutions be coplanar singular solutions (CSS) in accordance with the terminology introduced by Edelbaum for noncoplanar solutions.

Since the signs of all transversal components coincide, solutions of this type are only possible for transfers between nonintersecting orbits for which the inequality $\left|\Delta a\right| > \Delta e$ is true. It is known that, for transfers between the intersecting orbits, one of the impulses should be accelerating

and the other one decelerating. From Eq. 2-1c, one can determine the total delta-v of the manoeuvre

$$\Delta V = \sum_{i=1}^{N} \left| \Delta V_{t_i} \right| = \frac{|\Delta a|}{2}.$$

The solution does not depend on the angle θ, as there are lots of solutions of this type with an equal total delta-vs, but with the different application angles and impulse magnitudes.

In order to find the solution parameters of this type, one of the impulse application angles can be fixed; for example, $\varphi_1 = \varphi_{1_f}$. From eqs. 2-1a–2-1c, one can determine the second impulse application angle φ_2 and the magnitudes of the transversal impulse components $\Delta V_{t_1}, \Delta V_{t_2}$

$$\Delta V_{t_1} = \frac{\Delta e^2 - \Delta a^2}{4(\Delta e_y \sin \varphi_{1_f} + \Delta e_x \cos \varphi_{1_f} - \Delta a)}, \tag{2-2a}$$

$$\Delta V_{t_2} = \frac{\Delta a}{2} - \Delta V_{t_1}, \tag{2-2b}$$

$$tg\,\varphi_2 = \frac{\frac{\Delta e_y}{2} - \Delta V_{t_1} \sin \varphi_{1_f}}{\frac{\Delta e_x}{2} - \Delta V_{t_1} \cos \varphi_{1_f}}. \tag{2-2c}$$

All other optimal transfer parameters can be found by choosing the most suitable magnitude φ_{1_f}.

If we alter the angle φ_1, then on the plane e_x, e_y the geometric locus, which corresponds to the eccentricity vector of the transfer orbit and was obtained after the first impulse application, will be the ellipse (Fig. 2-2) (Bushuev and Krasovski 1969, 48–-489). The solution which meets the additional constraints can be chosen from the set of solutions with equal total delta-vs. The additional constraints include the constraints on the transfer orbit eccentricity, and the constraints on the impulse magnitudes or the angles of their application, etc. For example, the curved line *ADK* with *AD=DK* corresponds to the solution with equal impulse magnitudes.

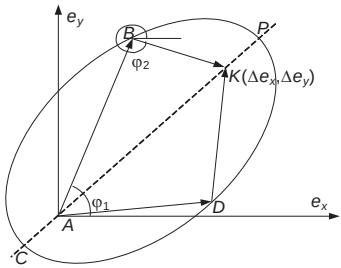

Fig. 2-2. Relative orbit eccentricity vector locus.

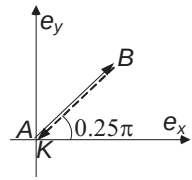

Fig. 2-3. Hohmann's transfer.

Please note that the famous Hohmann's transfer is the simplest particular case for this solution. Since the initial and the final orbits are circular for the Hohmann's transfer, $\Delta e_x = \Delta e_y = \Delta e = 0,$ and, hence, $\Delta V_{t_1} = \Delta V_{t_2} = 0.25\Delta a, \varphi_2 = \varphi_1 + \pi.$ An example of such a solution for $\varphi_1 = 0.25\pi$ is depicted in Fig. 2-3. The line segment *AB* corresponds to the first impulse and the line segment *BK* corresponds to the second impulse.

2.1.4. Coplanar Transfers between Intersecting Orbits: Coplanar Apsidal Solutions

The ellipse with the center in the reference frame origin as the primer vector hodograph on the plane μ, λ corresponds to the optimal transfers between the intersecting orbits ($\Delta e > |\Delta a|$). The ellipse osculates with the unit circle in the points (1, 0) and (-1, 0) (Fig. 2-1[*b*]). It is necessary that $\sqrt{\lambda_2^2 + \lambda_3^2} = \frac{1}{2}, \lambda_1 = 0$ for such an osculation. Since $\lambda = 0$ in both osculating points, the impulses of this solution will be transversal again ($\Delta V_{r_i} = 0$). The two-impulse solution will be optimal if the first impulse is braking (the left osculating point corresponds to it [$\mu = -1$ ']) and the second impulse is accelerating (the right osculating point corresponds to it [$\mu = 1$]). The impulse application angles φ_1, φ_2 differ from each other by half a revolution.

For solutions with no radial impulse components, on the plane e_x, e_y the locus, which corresponds to the eccentricity vector of the transfer orbit

(obtained after the application of the first impulse), will be hyperbolic lines (Fig. 2-4a) (Bushuev and Krasovski 1969, 485–489). The impulse magnitudes and the angles of their application can be determined by Eq. 2-2, but one of the impulses will be braking.

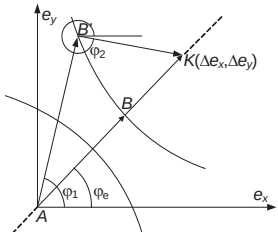

Fig. 2-4a. Relative orbit eccentricity vector locus.

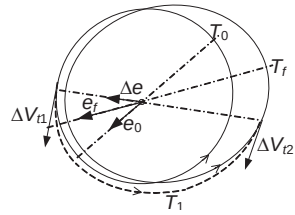

Fig. 2-4b. Transfer between intersecting orbits.

The choice of the hyperbolic line is determined by the order of the accelerating and the braking impulse applications. Out of the obtained solutions, the optimal one will be the solution with line segments that correspond to the impulses directed along the symmetry line of the hyperbole ($2\Delta V_{t_1} = AB, 2\Delta V_{t_2} = BK$ [Fig. 2-4a]), i.e., the impulses are applied in the pericenter and the apocenter of the relative orbit.

The impulse parameters (for the solution *ABK*) can be found by

$$\Delta V_{t_1} = \frac{1}{4}(\Delta a + \Delta e), \tag{2-3a}$$

$$\Delta V_{t_2} = \frac{1}{4}(\Delta a - \Delta e), \tag{2-3b}$$

$$\varphi_1 = \varphi_e, \varphi_2 = \varphi_e + \pi, \tag{2-3c}$$

where φ_e is determined by Eq. 1-14a.

It is obvious that the order of the impulse application can be changed

$$\Delta V_{t_1} = \frac{1}{4}(\Delta a - \Delta e), \tag{2-4a}$$

$$\Delta V_{t_2} = \frac{1}{4}(\Delta a + \Delta e), \tag{2-4b}$$

$$\varphi_1 = \varphi_e + \pi, \varphi_2 = \varphi_e. \tag{2-4c}$$

The total delta-v value can be obtained by

$$\Delta V = \sum_{i=1}^{N} \left| \Delta V_{t_i} \right| = \frac{\Delta e}{2},$$

which does not depend on the impulse application order.

Let us remember that if the single-impulse solution with the impulse in the point of the orbit intersection is used, the total delta-v expenditures can be determined by the following equation:

$$\Delta V = \sqrt{\Delta e^2 - \frac{3}{4}\Delta a^2}.$$

The comparison of two equations shows that the total delta-v of the single-impulsive manoeuvre is higher, because $\Delta e > |\Delta a|$ for the intersecting orbits.

Let us call the two-impulse solutions of this type coplanar apsidal solutions (CAS).

2.1.5. Example

Find the parameters of the impulse transfer between the orbits from Table 2-1.

Table 2-1

Elements	Initial orbit	Target orbit
$H_{\min}$ km	180	340
$H_{\max}$ km	210	360
u_{prg} deg	20	150

The basic constants are: $R_e = 6{,}371.0$ km; $\mu = 3.986028 \cdot 10^5$ km^3/s^2.

The semimajor axis and the orbit eccentricity can be given by

$$a = R_e + \frac{H_{\max} + H_{\min}}{2}, e = \frac{H_{\max} - H_{\min}}{2a}.$$

The relative orbit is chosen as the drift orbit. The parameters of the relative orbit are shown below:

$$r_0 = \frac{a_i + a_t}{2}; V_0 = \sqrt{\frac{\mu}{r_0}}; \lambda = \frac{V_0}{r_0}.$$

The semimajor axis deviation is calculated by

$$\Delta a^* = a_t - a_i, \Delta a = \frac{\Delta a^*}{r_0},$$

and the eccentricity vector:

$$\begin{cases} \Delta e_x = e_t \cos u_{prg_t} - e_i \cos u_{prg_i} \\ \Delta e_y = e_t \sin u_{prg_t} - e_i \sin u_{prg_i} \end{cases},$$
$$\Delta e = \sqrt{\Delta e_x^2 + \Delta e_y^2}.$$

The calculation results:

$a_i = 6{,}566.0$ km, $a_t = 6{,}721.0$ km, $e_i = 0.00228$, $e_t = 0.00149$,

$\Delta a^* = 155.0$ km, $\Delta a = 0.02333$,

$\Delta e_x = -0.00344$, $\Delta e_y = -0.00004$, $\Delta e = 0.00344$.

The found eccentricity vectors and their difference vector are depicted in the below figure:

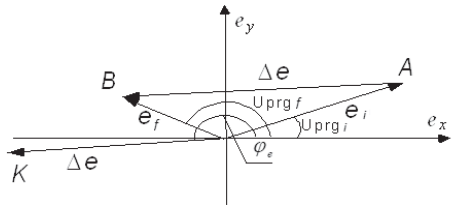

It is needed to calculate the two nonintersecting orbit transfer parameters $(\Delta a > \Delta e)$. The primer vector hodograph degenerates to the point and, hence, the two positive transversal impulses should be applied in order to obtain the optimal transfer. The apsidal solution, which is suitable for nonintersecting and intersecting orbits, is chosen from the set of the possible solutions which meet the constraint $2\Delta V_{t_1} + 2\Delta V_{t_2} = \Delta a$.

The impulse application angles for this solution can be obtained by the following equations:

$$\varphi_1 = \varphi_e = \operatorname{arctg} \frac{\Delta e_y}{\Delta e_x},$$

$$\varphi_2 = \varphi_e + \pi.$$

$$\Delta V_{t_1} = \frac{1}{4}(\Delta a - \Delta e),$$

$$\Delta V_{t_2} = \frac{1}{4}(\Delta a + \Delta e).$$

The calculation results: $\varphi_1 = \varphi_e = 180.624^\circ$ (the quadrant of φ_e should be controlled and it is determined by the signs of Δe_x and Δe_y), $\varphi_2 = 360.6240^\circ$.

The impulses, which correspond to these angles, can be obtained with the use of eqs. 2-4a and 2-4b.

The calculation results: $\Delta V_{t_1} = 38.5273$ m/s, $\Delta V_{t_2} = 51.8327$ m/s.

2.1.6. Comparison with the Results Obtained after the Problem Statement Refinement

It should be noted that the statement that the total delta-v of the transfer between the intersecting orbits does not depend on the order of the accelerating and decelerating impulse application is only true for the linearized spacecraft equations of motion. It can be seen that the total manoeuvre delta-v would be a little bit different if one makes the manoeuvre parameters more accurate with the help of the iterative procedure from Chapter 1 in order to satisfy the terminal conditions with high accuracy. The same thing can be said about the transfers between the nonintersecting orbits but, here, the optimal transfer needs to be found among the set of transfers with the equal total delta-vs $\Delta V = |\Delta a|/2$ in the linearized statement. The theoretical results obtained for the optimal transfers between the elliptical orbits may help when choosing the genuine optimal manoeuvre (Ivashkin, 2012).

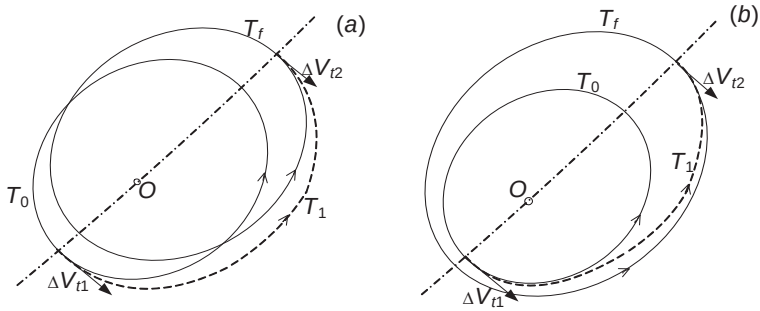

Fig. 2-5. Transfers between coaxial orbits:
(*a*) intersecting orbits; (*b*) nonintersecting orbits.

During the research into the transfers between the coplanar elliptical orbits, it was found that in the case of the transfer between the freely oriented orbits, the delta-v impulse expenditures will be minimal for the equally coaxial orbit orientation when the apsidal lines are directed along one line and the directions between the center of the attraction and the pericenter are equal $(\omega_f = \omega_0)$. The transfer along the curve of the half-ellipse, which connects the more distant apocenter with the other orbit pericenter, will be optimal (Figs. 2-5a and 2-5b).

For the counter-axial intersecting orbits (the apsidal lines are aligned and the directions from the center of attraction to the pericenter are opposite), the transfer from the apocenter to the apocenter will be optimal (the curve T_1 in Fig. 2-6a). If the counter-axial orbits do not intersect, the analogous transfer from the apocenter to the apocenter (the curve T_1 in Fig. 2-6b) or the pericenter-to-pericenter transfer (the curve T_2 in Fig. 2-6b) will be optimal.

In order to assess the difference between the optimal and the nonoptimal solutions, we will calculate the total delta-v of the transfers on the curves T_1 and T_2 (Fig. 2-6a) for the case of counter-axial intersecting orbits with perigee $h_\pi = 200$ km and apogee $h_\alpha = 400$ km, respectively.

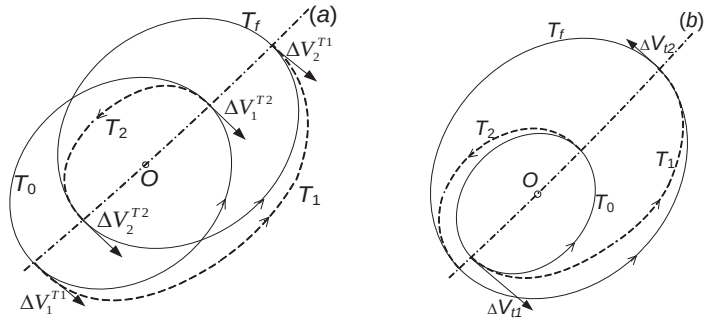

Fig. 2-6. Transfers between counter-axial orbits:
(*a*) intersecting orbits; (*b*) nonintersecting orbits.

For the considered case of the counter-axial intersecting orbit solution, the energetic difference will be maximum. The semimajor axes, the eccentricities, and the focal parameters are

$$a = \frac{r_\alpha + r_\pi}{2} = r_0 + \frac{h_\alpha + h_\pi}{2} = 6{,}671\,\text{km},$$
$$e = \frac{r_\alpha - r_\pi}{2a} = 0.015,\ p = a(1-e^2) = 6{,}669.5\,\text{km}$$

The orbit perigee and apogee velocities are

$$V_\pi = \sqrt{\frac{\mu}{p}}(1+e) = 7{,}730.756 \cdot (1+0.015) = 7{,}846.717\ \text{m/s},$$
$$V_\alpha = \sqrt{\frac{\mu}{p}}(1-e) = 7{,}730.756 \cdot (1-0.015) = 7{,}614.795\ \text{m/s}.$$

By using the equation for the semimajor axis alteration (see Section 1.3.5)

$$\Delta a = \frac{2a^2 V}{\mu}\Delta V_T,$$

one can find the magnitude of the first impulse for the apocenter-to-apocenter transfer

$$\Delta V_1^{T_1} = \frac{\Delta a \mu}{2a^2 V_\alpha} = \frac{100 \cdot 398{,}600}{2 \cdot 6{,}671^2 \cdot 7.614795} \cdot 1{,}000 = 58.81 \text{ m/s},$$

and for the pericenter-to-pericenter transfer

$$\Delta V_1^{T_2} = \frac{\Delta a \mu}{2a^2 V_\pi} = \frac{-100 \cdot 398{,}600}{2 \cdot 6{,}671^2 \cdot 7.846717} \cdot 1{,}000 = -57.07 \text{ m/s}.$$

On the first stage, we have a difference of 1.74 m/s for the same semimajor axis alteration, which comprises approximately 3% of the impulse magnitude. The transfer orbit semimajor axes noticeably differ for the transfer along the curve T_1 $a_1 = 6{,}771$ km and for the transfer along the curve T_2 $a_2 = 6{,}571$ km. Both transfer orbits are circular with the velocity of motion along the curve T_1 is $V_1 = 7.67259$ km/s and the velocity of motion along the curve T_2 is $V_2 = 7.78848$ km/s.

Now, the magnitudes of the second impulses can be determined by

$$\Delta V_2^{T_1} = \frac{\Delta a \mu}{2a_1^2 V_1} = \frac{-100 \cdot 398{,}600}{2 \cdot 6{,}771^2 \cdot 7.67259} \cdot 1{,}000 = -56.65 \text{ m/s},$$

$$\Delta V_2^{T_2} = \frac{\Delta a \mu}{2a_2^2 V_2} = \frac{100 \cdot 398{,}600}{2 \cdot 6{,}571^2 \cdot 7.78848} \cdot 1{,}000 = 59.26 \text{ m/s}.$$

The total delta-v for the transfer along the curve T_1 is $\Delta V_1 = 58.81 + 56.65 = 115.46$ m/s, while the total delta-v for the transfer along the curve T_2 is $\Delta V_2 = 57.07 + 59.26 = 116.33$ m/s. Their difference is 0.87 m/s, which comprises 0.75% of the total transfer delta-v. As can be seen, the difference in magnitudes of the particular impulses can reach up to several per cent, but the total delta-v of the transfers themselves differ slightly. By using the equations for the near-circular motion, we can obtain the impulse magnitudes, which are equal for both transfers:

$$\Delta V_{1,2} = \frac{\Delta a V}{4a} = \frac{200 \cdot 7.72988}{4 \cdot 6{,}671} \cdot 1{,}000 = 57.936 \text{ m/s}.$$

Thus, the total transfer delta-v is $\Delta V = 115.87$ m/s . Both magnitudes of impulses and the total delta-v of the solution, which were obtained with

the help of the equations for near-circular motion, are within the diapasons of the analogous variable magnitudes of the two exact solutions.

The accuracy of forming of the given orbit, which was obtained with the use of equations for near-circular motion (for example, for the apocenter-to-apocenter transfer), can also be assessed. Due to the application of the first accelerating impulse of 57.936 m/s

$$\Delta r = \frac{4a^2 V_\alpha}{\mu}\Delta V_{1,2} = \frac{4\cdot 6{,}671^2 \cdot 7.614795}{398{,}600}\cdot 0.057936 = 197.02 \text{ km}$$

the pericenter of orbits became higher by 197.02 km instead of the necessary 200 km. The braking impulse of the magnitude 57.936 m/s, which was performed at the opposite point, lowers the orbit apocenter

$$\Delta r = \frac{4a_1^2 V_1}{\mu}\Delta V_{1,2} = \frac{4\cdot 6{,}771^2 \cdot 7.67259}{398{,}600}\cdot 0.057936 = 204.51 \text{ km}$$

by 204.51 km instead of the necessary 200 km. Thus, a considerable error when adjusting the orbit apocenter and pericenter exists, but the error of the semimajor axis is smaller by 2–3 times at only 1.5 km. It can be stated that the errors comprise 2–3% of the caused alteration of the corresponding values. They can be easily eliminated with the help of the iterative procedure from Chapter 1.

The order of the impulse applications, which ensures the optimal solution is obtained, can be chosen for the analytical problem solution. The distances to the apocenters and pericenters for each orbit can be easily calculated because their orbit elements are known. The difference between the known ω_f, ω_0 allows us to assess the proximity of orbit apsidal line orientation to the co-axial or the counter-axial orientation. Then the optimal solution is chosen out of the two possible solutions with the help of the aforementioned algorithm. The apsidal solutions can also be optimal for nonintersecting orbits. The curved lines *ACK* and *APK* correspond to them in Fig. 2-2. The parameters of these solutions are determined by Eq. 2-4. If there is the option, it is better to obtain accurate solutions for both successions of the apsidal impulses with the help of the iterative procedure and then choose the optimal one.

Table 2-2 shows the results of the analogous calculations for the different orbit heights and different height deviations in the pericenter and the apocenter. The results for the apocenter-to-apocenter and pericenter-

to-pericenter flybys are listed in the first line of each cell; the results, which were obtained by the approximate equations and the relative error, are listed in the second line of each cell.

Table 2-2

H km	Δh = 50 km		Δh = 100 km		Δh = 300 km	
300	57.832	58.049	115.47	116.34	-	-
	57.937	0.0038	115.87	0.0075	-	-
600	54.143	54.388	108.11	108.89	322.62	329.66
	54.237	0.0036	108.47	0.0072	325.42	0.0218
1,000	49.801	49.97	99.448	100.13	296.82	302.95
	49.883	0.0034	99.765	0.0068	299.3	0.0206
1,500	45.136	45.28	90.142	90.716	269.11	274.3
	45.206	0.0032	90.412	0.0064	271.24	0.0193
19,100	7.7617	7.7694	15.516	15.547	46.463	46.738
	7.7655	0.001	15.531	0.002	46.593	0.0059
36,000	3.6183	3.6205	7.2346	7.2431	21.679	21.756
	3.6194	0.0006	7.2388	0.0012	21.716	0.0035

Table 2-2 Continued

H km	Δh = 500 km		Δh = 1,000 km	
300	-	-	-	-
	-	-	-	-
600	-	-	-	-
	-	-	-	-
1,000	492.98	510.16	-	-
	498.83	0.0349	-	-
1,500	446.96	461.51	891.47	952.1
	452.06	0.0326	904.12	0.068
19,100	77.309	78.072	154.06	157.13
	77.655	0.0099	155.31	0.0199
36,000	36.093	36.307	72.008	72.864
	36.194	0.0059	72.388	0.0119

2.1.7. Solution with Fixed Velocity Impulse Application Angles

In some cases, it is necessary to find a problem solution with fixed impulse application angles. Such a necessity occurs, for example, if there are constraints on the permitted manoeuvring intervals, and also when the transfer problem solution appears to be the part of the solution algorithm for the more complex rendezvous problem.

The problem solution with the fixed impulse application angles is given in Gavrilov, Obukhov, Skoptsov, and Zaslavsky (1975). In this work, the equations for the transversal and radial impulse components for the minimum manoeuvre total delta-v are depicted. But they are given in the deviation of the coordinates and velocities at the point of the second impulse application, which is not convenient. It can be shown that the equation is true if one uses the results from the work of Gavrilov, Obukhov, Skoptsov, and Zaslavsky (1975):

$$\frac{\Delta V_{r_1}}{\Delta V_{t_1}} = \frac{\Delta V_{r_2}}{\Delta V_{t_2}}.$$

By using this equation and the conditions for the transfer to the final orbit (Eq. 2-1), we can obtain the equations for the impulse components:

$$\Delta V_{t_2} = 0.5 \cdot \Delta a \frac{a - \Delta e_x \cos\varphi_1 - \Delta e_y \sin\varphi_1}{2a - \Delta e_x(\cos\varphi_1 + \cos\varphi_2) - \Delta e_y(\sin\varphi_1 + \sin\varphi_2)},$$

$$\Delta V_{t_1} = 0.5 \cdot \Delta a \frac{a - \Delta e_x \cos\varphi_2 - \Delta e_y \sin\varphi_2}{2a - \Delta e_x(\cos\varphi_1 + \cos\varphi_2) - \Delta e_y(\sin\varphi_1 + \sin\varphi_2)},$$

$$\Delta V_{r_2} = \frac{2\Delta V_{t_2}(\Delta e_x - a\cos\varphi_1 + 2\Delta V_{t_2}(\cos\varphi_1 - \cos\varphi_2))}{2\Delta V_{t_2}(\sin\varphi_1 + \sin\varphi_2) - a\sin\varphi_1},$$

$$\Delta V_{r_1} = -\frac{2\Delta V_{t_1}(\Delta e_x - a\cos\varphi_1 + 2\Delta V_{t_2}(\cos\varphi_1 - \cos\varphi_2))}{2\Delta V_{t_2}(\sin\varphi_1 + \sin\varphi_2) - a\sin\varphi_1},$$

which will ensure the solution optimality.

2.2. Noncoplanar Transfers

2.2.1. Problem Statement

The problem of the optimal transfer between the noncoplanar orbits has been investigated in works by many authors including Kuzmak (Il'in and Kuzmak, 1976) and Marec (Marec, 1979). The fullest, the most compact, and the simplest solution to the problem was given by Edelbaum (1967, 66–73). However, it is necessary to note that there are no equations for the parameter determination of the third-type solution presented in this work (it is only mentioned that this type of solution exists).

The final orbit transfer conditions for this problem can be written as

$$\sum_{i=1}^{N} (\Delta V_{r_i} \sin\varphi_i + 2\Delta V_{t_i} \cos\varphi_i) = \Delta e_x, \tag{2-5a}$$

$$\sum_{i=1}^{N} (-\Delta V_{r_i} \cos\varphi_i + 2\Delta V_{t_i} \sin\varphi_i) = \Delta e_y, \tag{2-5b}$$

$$\sum_{i=1}^{N} 2\Delta V_{t_i} = \Delta a, \tag{2-5c}$$

$$\sum_{i=1}^{N} -\Delta V_{z_i} \sin\varphi_i = 0, \tag{2-5d}$$

$$\sum_{i=1}^{N} \Delta V_{z_i} \cos\varphi_i = \Delta i. \tag{2-5e}$$

It is supposed here that the deviations are calculated in the coordinate frame with the x axis directed along the line of the orbit plane intersection. As a consequence, the right-hand side of Eq. 2-5d is equal to zero.

It can be taken that Δi is approximately the angle between the orbit planes, and its magnitude can be determined by Eq. 1-14d $\Delta i = \sqrt{\Delta z^2 + \Delta V_z^2}$. The angle $\Delta\varphi$ between the line of orbit plane intersection and the relative orbit apsidal line is evaluated by Eq. 1-14c.

Find the impulse parameters $\Delta V_{r_i}, \Delta V_{t_i}, \Delta V_{z_i}, \varphi_i$ $(i = 1,..., N)$ for the minimum total delta-v of the transfer

$$\Delta V = \sum_{i=1}^{N} \sqrt{\Delta V_{r_i}^2 + \Delta V_{t_i}^2 + \Delta V_{z_i}^2}$$

with the constraints 2-5a–2-5e.

The equations for the primer vector for noncoplanar transfers are listed below:

$$\lambda = \sqrt{\lambda_2^2 + \lambda_3^2}\,\sin(\theta - \theta_0), \tag{2-6a}$$

$$\mu = 2\lambda_1 + 2\sqrt{\lambda_2^2 + \lambda_3^2}\,\cos(\theta - \theta_0), \tag{2-6b}$$

$$\nu = \frac{\lambda_3\lambda_4 - \lambda_2\lambda_5}{\sqrt{\lambda_2^2 + \lambda_3^2}}\sin(\theta - \theta_0) + \frac{\lambda_2\lambda_4 + \lambda_3\lambda_5}{\sqrt{\lambda_2^2 + \lambda_3^2}}\cos(\theta - \theta_0), \tag{2-6c}$$

$$tg\,\theta_0 = \frac{\lambda_2}{\lambda_3}. \tag{2-6d}$$

Eqs. 2-6a–2-6d are ellipse equations in three-dimensional space.

There are three primer vector hodograph configurations in the form of an ellipse, which allow the hodograph to have more than one maximum, and, hence, osculate with the unit circle in two or more points (Edelbaum 1967, 66–73). The first configuration is the family of solutions with the center of ellipse in the reference frame origin (Fig. 2-7a). The two equivalent maximums are situated on the ellipse major axis and, hence, the distance between the impulse application angles is half a revolution.

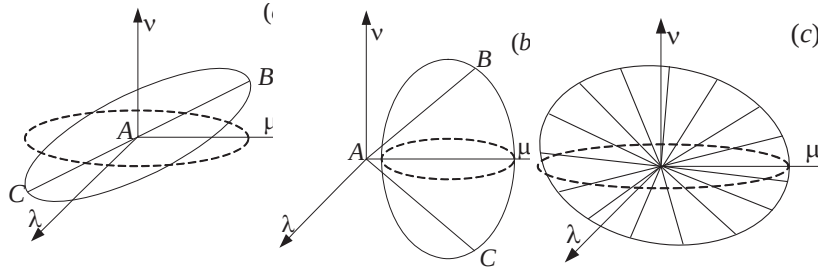

Fig. 2-7. Primer vector hodograph for noncoplanar transfer:
a) nodal case; *b*) nondegenerate case; *c*) special case.

The following equations describe this case, which is called the *nodal case* (NC):

$$\lambda_1 = 0, \tag{2-7a}$$

$$\theta_2 = \theta_1 + \pi, \tag{2-7b}$$

$$\left.\begin{aligned}\lambda(\theta_1) &= -\lambda(\theta_2)\\ \mu(\theta_1) &= -\mu(\theta_2)\\ \nu(\theta_1) &= -\nu(\theta_2)\end{aligned}\right\}. \tag{2-7c}$$

The second configuration, which holds the two identical primer vector maximums, corresponds to the case when the two points of an ellipse and its center belong to the μ axis and the ellipse center is shifted from the reference frame origin (Fig. 2-7b). This case, which was called the *nondegenerate case* (NDC), is presented by the following equations and inequalities:

$$\lambda_2\lambda_4 = -\lambda_3\lambda_5, \tag{2-8a}$$

$$\theta_2 - \theta_0 = \theta_0 - \theta_1, \tag{2-8b}$$

$$\left.\begin{aligned}\lambda(\theta_1) &= -\lambda(\theta_2)\\ \mu(\theta_1) &= \mu(\theta_2)\\ \nu(\theta_1) &= -\nu(\theta_2)\end{aligned}\right\}, \tag{2-8c}$$

$$\cos(\theta_1 - \theta_0) = \frac{4\lambda_1(\sqrt{\lambda_2^2 + \lambda_3^2})^3}{(\lambda_3\lambda_4 - \lambda_2\lambda_5)^2 - 3(\lambda_2^2 + \lambda_3^2)^2}, \tag{2-8d}$$

$$3(\lambda_2^2 + \lambda_3^2)^2 < (\lambda_3\lambda_4 - \lambda_2\lambda_5)^2, \tag{2-8e}$$

$$4\lambda_1\sqrt{\lambda_2^2 + \lambda_3^2} \le (\lambda_3\lambda_4 - \lambda_2\lambda_5)^2 - 3(\lambda_2^2 + \lambda_3^2)^2. \tag{2-8f}$$

The third configuration is the combination of the first two. The primer vector hodograph is a circle and the primer vector has the same magnitude in all orbit points (Fig. 2-7c). This *singular case* (SC) is described by the following equations, where the primer vector magnitude is unity:

$$\lambda_1 = 0, \tag{2-9a}$$

$$\lambda_2\lambda_4 = -\lambda_3\lambda_5, \tag{2-9b}$$

$$3(\lambda_2^2 + \lambda_3^2)^2 = (\lambda_3\lambda_4 - \lambda_2\lambda_5)^2 = \frac{3}{4}, \tag{2-9c}$$

$$\lambda = \frac{1}{2}\sin(\theta - \theta_0), \tag{2-9d}$$

$$\mu = \cos(\theta - \theta_0), \tag{2-9e}$$

$$\nu = \pm\frac{\sqrt{3}}{2}\sin(\theta - \theta_0)\ (+\text{if } \Delta i < 0). \tag{2-9f}$$

By solving simultaneously eqs. 2-5a–2-5e, 1-18, and 2-7a–2-7c or 2-8a–2-8f or 2-9a–2-9f. one can obtain the transfer impulse parameters, which correspond to one of the possible optimal solutions.

The easiest way is to do it for the nodal case, where the impulse parameters can be obtained geometrically.

2.2.2. Nodal Solution

As always, let us depict the transfer on the plane e_x, e_y. Point *K*, as usual, corresponds to the relative orbit parameters. Due to the fact that the impulse application angles differ by half a revolution (Eq. 2-7b), the orbit planes can only be aligned if the impulses are applied in the moment of the orbit plane intersection; hence, the impulse application angles will be *0* or π. Thus, line segments, which represent the transversal impulse components, will be parallel to the e_x axis, and the line segments, which represent the radial impulse components, will be parallel to the e_y axis (Fig. 2-8).

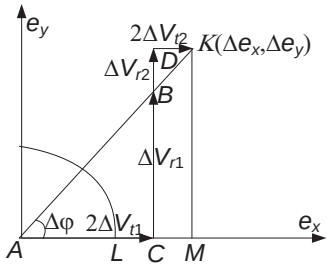

Fig. 2-8. Nodal solution

Let us draw the circle of radius $|\Delta a|$ with the center in the reference frame origin. Let the e_x axis-circle intersection point be *L*, and the point *K* projection on the e_x axis be *M*. The magnitude of the transversal component of the first impulse can be found with the help of the following equation (the equality *LC* = *CM* should be satisfied):

$$2\Delta V_{t_1} = AC = \frac{1}{2}(\Delta a + \Delta e_x).$$

The radial component magnitude can be found with the help of the following equation:

$$\Delta V_{r_1} = CB = -(\Delta a + \Delta e_x)\frac{\Delta e_y}{2\Delta e_x}.$$

Point *B*, which corresponds to the eccentricity of the orbit and was obtained after the application of the first impulse, should belong to the line segment *AK*.

After that, the transversal and the radial component magnitudes of the second impulse can be easily found:

$$2\Delta V_{t_2} = DK = \frac{1}{2}(\Delta a - \Delta e_x),$$

$$\Delta V_{r_2} = BD = -(\Delta a - \Delta e_x)\frac{\Delta e_y}{2\Delta e_x}.$$

The components of the same type have different signs, but the impulse application angles differ by π; this is why the vectors that depict the impulse components on the plane $e_x, e_y,$ are pointed in the same direction.

Similarly, we divide Δi correction into two parts with the lateral impulse components:

$$\Delta V_{z_1} = \frac{(\Delta a + \Delta e_x)\Delta i}{2\Delta e_x},$$

$$\Delta V_{z_2} = \frac{(\Delta a - \Delta e_x)\Delta i}{2\Delta e_x}.$$

By knowing the impulse components, the transfer total delta-v can be obtained:

$$\Delta V = \sqrt{\Delta i^2 + \frac{1}{4}\Delta e_x^2 + \Delta e_y^2}.$$

The found solution would meet the constraints of 2-7c, if point *C* is situated to the left of point *M*; hence, the condition,

$$\Delta a^2 \le \Delta e_x^2,$$

which denotes that the solution is only possible for transfers between the intersecting orbits (the inequality $\Delta e > |\Delta a|$ is true for this type of orbits), should be true.

The primer vector should be maximum in the impulse application point; hence, the second condition can be written as

$$3\Delta e_y^2 \le \Delta i^2.$$

2.2.3. Nondegenerate Solution

We have to solve the complex equation system 2-5a–2-5e, 1-18, and 2-8a–2-8f for the *nondegenerate case*. The solution procedure, the equations for ΔV, and the coefficients, $\lambda_1, \lambda_2, \lambda_3, \lambda_4, \lambda_5$, can be found using the results from the work by Edelbaum:

$$\Delta V = \sqrt{\frac{1}{2}}\sqrt{\Delta i^2 + \Delta e_x^2 + \Delta e_y^2 - \Delta a^2 + \sqrt{(\Delta i^2 - \Delta e_x^2 - \Delta e_y^2 + \Delta a^2)^2 + 4\Delta i^2 \Delta e_y^2}},$$

$$\lambda_1 = \frac{\Delta a}{2\Delta V}\left[-\frac{1}{2} + \frac{\Delta i^2 - \Delta e_x^2 - \Delta e_y^2 + \Delta a^2}{\sqrt{(\Delta i^2 - \Delta e_x^2 - \Delta e_y^2 + \Delta a^2)^2 + 4\Delta i^2 \Delta e_y^2}}\right],$$

$$\lambda_2 = \frac{\Delta e_y}{2\Delta V}\left[1 - \frac{-\Delta i^2 - \Delta e_x^2 - \Delta e_y^2 + \Delta a^2}{\sqrt{(\Delta i^2 - \Delta e_x^2 - \Delta e_y^2 + \Delta a^2)^2 + 4\Delta i^2 \Delta e_y^2}}\right],$$

$$\lambda_3 = \frac{\Delta e_x}{2\Delta V}\left[1 - \frac{\Delta i^2 - \Delta e_x^2 - \Delta e_y^2 + \Delta a^2}{\sqrt{(\Delta i^2 - \Delta e_x^2 - \Delta e_y^2 + \Delta a^2)^2 + 4\Delta i^2 \Delta e_y^2}}\right],$$

$$\lambda_4 = -\frac{\Delta e_y}{2\Delta V}\left[\frac{2\Delta i \Delta e_x}{\sqrt{(\Delta i^2 - \Delta e_x^2 - \Delta e_y^2 + \Delta a^2)^2 + 4\Delta i^2 \Delta e_y^2}}\right],$$

$$\lambda_5 = \frac{\Delta i}{2\Delta V}\left[1 + \frac{\Delta i^2 - \Delta e_x^2 + \Delta e_y^2 + \Delta a^2}{\sqrt{(\Delta i^2 - \Delta e_x^2 - \Delta e_y^2 + \Delta a^2)^2 + 4\Delta i^2 \Delta e_y^2}}\right].$$

With the knowledge of these coefficients, one can obtain θ_0 from Eq. 2-6d, and then, from Eq. 2-8d, the impulse application moments can be determined. The impulse orientation can be found from eqs. 2-6a–2-6d. By knowing ΔV, the impulse magnitude distribution can be determined from Eq. 2-5c.

The existence domain of the problem solutions is described by the following inequalities:

$$\Delta a^2 \geq \Delta e_x^2,$$

$$\Delta a^2 \geq \Delta e_x^2 + \Delta e_y^2 + \frac{2}{\sqrt{3}}\Delta i \Delta e_y - \Delta i^2.$$

2.2.4. Singular Solution

For the *singular case* with the help of the passage to the limit from the nondegenerate case, one can find the total delta-v

$$\Delta V = \frac{1}{4}\sqrt{(\sqrt{3}\Delta i + \Delta e_y)^2 + \Delta e_x^2}$$

the existence domain

$$\Delta i^2 \leq 3\Delta e_y^2,$$

$$\Delta a^2 \leq \Delta e_x^2 + \Delta e_y^2 + \frac{2}{\sqrt{3}}\Delta i \Delta e_y - \Delta i^2,$$

and the θ_0 magnitude

$$tg\theta_0 = \frac{\sqrt{3}\Delta i + \Delta e_y}{\Delta e_x}. \tag{2-10}$$

The initial equation system should be simplified in order to obtain the impulse magnitudes and their application angles. For this purpose, we will rotate the coordinate frame by the angle θ_0 from Eq. 2-10. Let the new projections of the eccentricity vector $\Delta e_{x_n}, \Delta e_{y_n}$ be

$$\Delta e_{x_n} = \Delta e_x \cos\theta_0 + \Delta e_y \sin\theta_0,$$
$$\Delta e_{y_n} = -\Delta e_x \sin\theta_0 + \Delta e_y \cos\theta_0,$$

Let us introduce the new variables, a_s, x_s, y_s, ψ, which are related with the variables $\Delta a, \Delta e_{x_n}, \Delta e_{y_n}, \varphi$ by the following equations:

$$a_s = \frac{1}{2}\Delta a, x_s = \frac{2}{3}(2\Delta V - \Delta e_{x_n}), y_s = \frac{2}{3}\Delta e_{y_n}, \psi = \varphi - \theta_0.$$

The equations for the terminal constraints will be

$$\sum_{i=1}^{N} \Delta V_i = \Delta V, \tag{2-11a}$$

$$\sum_{i=1}^{N} \Delta V_i \cos\psi_i = a_s, \tag{2-11b}$$

$$\sum_{i=1}^{N} \Delta V_i \sin^2\psi_i = x_s, \tag{2-11c}$$

$$\sum_{i=1}^{N} \Delta V_i \sin\psi_i \cos\psi_i = y_s, \tag{2-11d}$$

where ΔV_i = the magnitude of i-th impulse.

The equation system 2-11 has fewer equations in comparison with Eq. 2-5, since the two equations from Eq. 2-11 turned out to be linear combinations of the other equations and were excluded. Hence, the variable replacement was made.

The analytical solution for the parameters of the two-impulse solution cannot be obtained from a seemingly simple equation system: it can only be shown that it exists, which is why Edelbaum suggests using the three-impulse solution. No concrete equations are presented because lots of three-impulse solutions exist. However, it is important to have the equations for the calculations and we will go into greater detail by showing one of the possible ways of obtaining one of these solutions.

Assume that the angle of the first impulse application coincides with $\theta_0 (\varphi_1 = \theta_0)$, and that the angle of the second impulse application differs by half a revolution, i.e., $\psi_1 = 0, \psi_2 = \pi$. Then, from eqs. 2-11c and 2-11d, one can determine the application angle and the magnitude of the third impulse

$$\operatorname{tg} \psi_3 = \frac{x_s}{y_s}, \tag{2-12a}$$

$$\Delta V_3 = \frac{x_s^2 + y_s^2}{x_s}. \tag{2-12b}$$

Then the magnitudes of the first and the second impulses can be found from eqs. 2-11a and 2-11b:

$$\Delta V_1 = \frac{1}{2}(\Delta V + a_s - \Delta V_3 \cos \psi_3 + \Delta V_3), \tag{2-13a}$$

$$\Delta V_2 = \frac{1}{2}(\Delta V - a_s + \Delta V_3 \cos \psi_3 - \Delta V_3). \tag{2-13b}$$

The geometric interpretation of the solution is given in Fig. 2-9. Only the transversal components of the first two impulses are not zeros. The impulse application angles are $\varphi_1 = \theta_0, \varphi_2 = \theta_0 + \pi$. The line segments *AB* and *BC* correspond to these impulses.

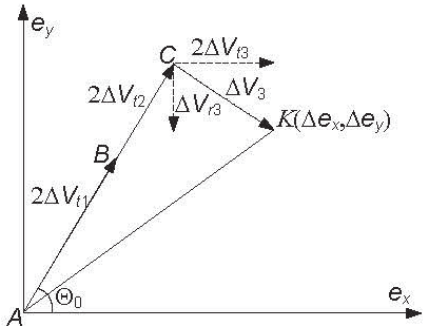

Fig. 2-9. Singular solution

The third impulse lateral component is equal to Δi, as it is the only impulse that changes the attitude of the orbit plane and, hence, its application angle is $\varphi_3 = 0$. The segment, which is parallel to the e_x axis, corresponds to the transversal component of this impulse. The ratio of the radial and transversal components should have a magnitude which ensures the perpendicularity between line segment *CK*, which depicts the influence of the third impulse, and line segment *AC*.

2.2.5. Solution Existence Domains

This type of optimal solution, which corresponds to the particular deviations between the initial and the final orbits, can be found with the help of the following diagram:

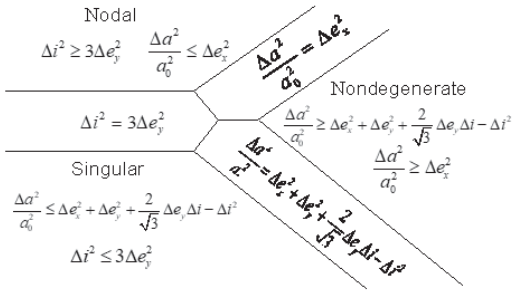

The existence domain areas of different type solutions depend on the deviations $\Delta a, \Delta e_x, \Delta e_y, \Delta i$.

The specific look and the locations of the existence domains for the different type solutions are depicted in Figs. 2-10a–2-10f.

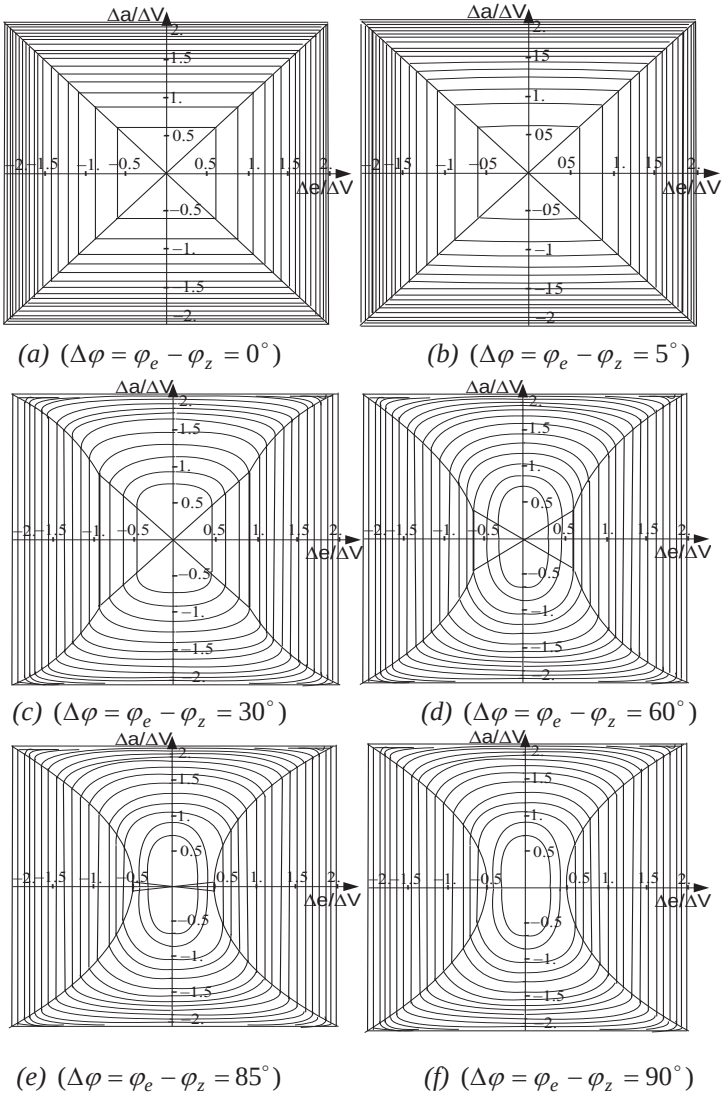

Fig. 2-10. Different types of solution existence domain.

The close-ended contours correspond to various values of $\Delta i / \Delta V$, which alter with the 0.05 step from the zero value (on the boundary of the figures) to the unity in the reference frame origin. Every figure has the caption with the difference between the angles φ_e and φ_z (Eq. 1-14) under them. In Fig. 2-10a, the node solution existence domain is the set of two triangles, the bases of which are the vertical boundaries of the quadrate, and the apexes of the triangles are situated in the reference frame origin.

The existence domain of the nondegenerate solutions is the remaining two triangles with the bases as the horizontal boundaries of the quadrate and confluent apexes.

In Fig. 2-10b, the singular solution existence domain appears near the vertical boundaries of the quadrate and the node solution occupies the triangle area, which adjoins to the singular solution area. The existence domain of the nondegenerate solutions occupies the rest of the figure.

The nodal solution existence domain rapidly decreases with the increase of the difference between the angles φ_e and φ_z (Figs. 2-10c–2-10e); meanwhile, the singular solution's existence domain increases. As a result, in Fig. 2-10f, the existence domain of the node solutions is completely absent.

2.2.6. Optimal Solution without the Radial Velocity Impulse Components

The solution with the zero radial impulse components was mentioned by Edelbaum but was never distinguished as a self-consistent type of optimal solution. The first figure in the set (Fig. 2-10) corresponds to it $(\Delta\varphi = \varphi_e - \varphi_z = 0)$; hence, the point *K* in Fig. 2-8 belongs to the abscissa axis, and it means that the radial impulse components are equal to zero. It can be shown that the solution without the radial impulse components can be classified as the fourth possible type of optimal solution (Baranov 2012, 141–151).

Eqs. 1-17e–1-17g with $\lambda_2 = \lambda_3 = \lambda_6 = 0$ can be presented as

$$\lambda = 0,$$
$$\mu = 2\lambda_1,$$
$$\nu = \sqrt{\lambda_4^2 + \lambda_5^2}\cos(\theta - \theta_1),$$
$$\operatorname{tg}\theta_1 = \frac{\lambda_4}{\lambda_5}.$$

The primer vector hodograph degenerates to the line segment, which is parallel to the ν axis and crosses the μ axis (Fig. 2-11, the line segment *BC*). The optimality conditions are satisfied, since the primer vector hodograph does not exceed the unit circle boundaries and osculates with it in the two points.

A solution of this type cannot be classified as a particular case of the nondegenerate solution because Eq. 2-8e is violated and Eq. 2-8d cannot be used. This new solution will have

$$\frac{\nu(\theta_1)}{\mu(\theta_1)} = -\frac{\nu(\theta_2)}{\mu(\theta_2)},$$

i.e., $\frac{\Delta V_{z_1}}{\Delta V_{t_1}} = -\frac{\Delta V_{z_2}}{\Delta V_{t_2}}$. Such a solution exists if the relative orbit apsidal line coincides with the plane intersection line for the initial and the target orbits ($\varphi_e = \varphi_z, \Delta\varphi = 0, \Delta e_y = 0$). The impulse application angles differ by 180° ($\theta_1 - \theta_2 = 180^\circ$). In Fig. 2-10a, this solution (not the nondegenerate solution) exists in the triangles with the horizontal bases. The nondegenerate solution occurs in these areas when the condition $\varphi_e = \varphi_z$ is violated, which is why it was the only mentioned solution in the description of the different types of solution existence domains.

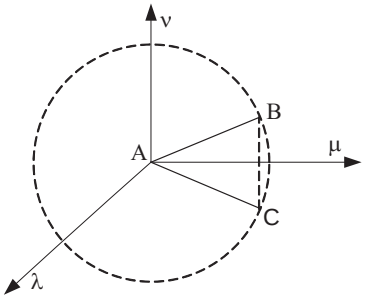

Fig. 2-11. Primer vector hodograph in the line segment form.

It may seem that a solution of this type can be rarely met in practical work, as it is hard to imagine the case when the node and apsidal lines fully coincide with each other. However, this solution for the first manoeuvring interval is often part of the four-impulse solution for the

rendezvous manoeuvres of “Soyuz”- and “Progress”-type spacecraft and the orbital station. The existence conditions for this simple and optimal solution on the first interval can be created by the two impulses of the second manoeuvring interval.

2.2.7. Manoeuvres without Radial Components: Universal Solution

During the calculation of the spacecraft manoeuvres, we have to deal with the constraints on orientation and the moments of impulse application, and the parameters of the transfer orbit, etc. A prohibition on the use of the radial impulses can be often met.

Let us consider the two-impulse transfer manoeuvre parameter determination procedure between the *arbitrary* noncoplanar orbits without radial impulse components (in the previous paragraph it was supposed that the apsidal line of the relative orbit coincides with line of the initial and the target orbit intersection).

In this case, there are six unrestricted variables (the two angles of the impulse application, φ_1, φ_2, the four impulse components $\Delta V_{t_1}, \Delta V_{z_1}, \Delta V_{t_2}, \Delta V_{z_2}$), and five constraints in the equality forms 2-5a–2-5e. We can fix the value of one of the variables, for example, $\varphi_1 = \varphi_{1_f}$, and determine the values of the variables $\Delta V_{t_1}, \Delta V_{t_2}, \varphi_2$ with the help of eqs. 2-2a–2-2c, and then find the lateral impulse components from eqs. 2-5d and 2-5e:

$$\Delta V_{z_1} = -\frac{\Delta i \sin\varphi_2}{\sin(\varphi_1 - \varphi_2)}, \tag{2-14a}$$

$$\Delta V_{z_2} = \frac{\Delta i \sin\varphi_1}{\sin(\varphi_1 - \varphi_2)}. \tag{2-14b}$$

Then it is enough to make the optimization by one variable φ_1 in order to find the optimal solution parameters. If there are no constraints on angles of the impulse application, the enumeration is carried out on the interval $[0, \pi]$. If the constraints are present, then φ_1 is enumerated in the permitted diapason and the solutions with φ_2, which do not meet the imposed restrictions, will be excluded.

The close-to-optimal solution parameters can be found analytically among the solutions with zero radial impulse components. We will suppose that the impulse components of this solution are connected with each other via the equation:

$$\left|\frac{\Delta V_{z_1}}{\Delta V_{t_1}}\right| = \left|\frac{\Delta V_{z_2}}{\Delta V_{t_2}}\right|. \tag{2-15}$$

This demand is pretty natural, as the majority of the previously considered optimal solutions, which meet the necessary optimality conditions, have this attribute.

We will call the solutions with the following characteristics *universal*: $\Delta V_{r_1} = \Delta V_{r_2} = 0,$ the transversal and lateral impulse components are connected with each other by Eq. 2-15, and $\theta_1 - \theta_2 \neq 180^\circ.$ They can be used either with or without the constraint on the usage of the radial impulse components. The geometric method can also be used for the universal solution parameter determination (Baranov 2008, 430–439).

Let us suppose again that point *K* corresponds to the elements of the relative orbit on the plane e_x, e_y and the e_x axis corresponds to the direction of the optimal orbit plane correction. Let us draw the line *CM* through the middle of line segment *AK* (through the point *C*). *CM* is parallel to the e_x axis (Fig. 2-12).

Let us find point *B* on this line, which meets the constraints $AB + BK = \Delta a,$ if $|\Delta a| > \Delta e$ or $AB - BK = \Delta a,$ and if $|\Delta a| < \Delta e.$ The curved line *ABK* will correspond to the solution of the flat problem ($AB = 2\Delta V_{t_1}, BK = 2\Delta V_{t_2}$). Let us extend the line segment *KB* until it intersects with the e_x axis (point *L*). Let us draw the line segment *AL′* ($AL' = \Delta i$) on the e_x axis and the line segment *L′B′*, which is parallel to the line segment *LB*.

The line segments *AB′* and *B′L′* have the same inclinations as the line segments *AB* and *BK*; hence, the curved line *AB′L′* corresponds to the lateral deviation correction ($AB = \Delta V_{z_1}, B'L' = \Delta V_{z_2}$). It can easily be seen that $\frac{AB'}{AB} = \frac{B'L'}{BK};$ hence, $\frac{\Delta V_{z_1}}{\Delta V_{t_1}} = \frac{\Delta V_{z_2}}{\Delta V_{t_2}}.$ Thus, a solution with the desired characteristics is found.

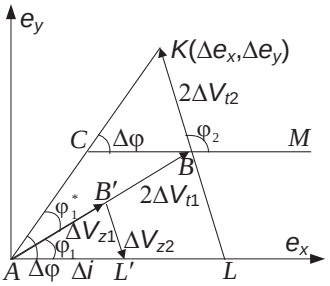

Fig. 2-12. Universal solution.

By knowing the geometric interpretation, we can find, for example, the first impulse application angle of this solution (Baranov 2008, 430–439):

$$\begin{aligned} \varphi_1 &= \Delta\varphi - \varphi_1^*, \\ \Delta\varphi &= \varphi_e - \varphi_z, \\ \operatorname{tg}\frac{\varphi_1^*}{2} &= \left(1 - \frac{\Delta e}{\Delta a}\right)\cdot\left(-\operatorname{ctg}\Delta\varphi + \sqrt{\operatorname{ctg}^2\Delta\varphi + \frac{\Delta a^2}{\Delta a^2 - \Delta e^2}}\right), \end{aligned} \tag{2-16}$$

and then, with the help of eqs. 2-2a–2-2c, 2-14a, and 2-14b, we can obtain the other manoeuvre parameters.

The numerical research showed that the total delta-v of this simplest solution is close enough to the total delta-v of the aforementioned optimal solutions, especially to the nondegenerate case solution. Thus, this analytical solution can be used for the solution of the majority of the practical noncoplanar optimal transfer problems. Furthermore, when the solution with the satisfied terminal conditions with the given tolerance is found with the help of iterative procedure, then sometimes the usage of the universal solution in the iterative procedure gives smaller total delta-v value in comparison with the usage of the optimal solution. Besides, in the complex problems from Chapter 7, the usage of the universal solution in the iterative procedure allows us to substantially reduce the number of iterations needed to obtain the given accuracy for the terminal condition satisfaction.

It is obvious from this section that the impulse application order can be changed for every solution. Furthermore, the impulses can be divided into parts and these parts can be applied on different revolutions, but on the same latitude argument. This allows the reduction of, for example, the

impulse realization error magnitude. However, just like in the case of the coplanar transfers, it is necessary to remember that the statement about the arbitrary impulse application order is only fair in the linear approximation. If there is the option, it is better to obtain the accurate solutions for both successions of the impulses with the help of the iterative procedure and then choose the optimal one.

2.2.8. Example

Determine the parameters of noncoplanar impulse transfer for the parameters listed in Table 2-3:

Table 2-3

Elements	Initial orbit	Final orbit
$H_{\min}$ km	180	340
$H_{\max}$ km	210	360
u_{prg} deg	20	150
i deg	51.7	51.69
Ω deg	17.49	17.5

The information about the orbit inclination and the RAANs was added to the first example solution in this chapter.

The calculation results from the first example solution: $\Delta a = 0.02333, \Delta e_x = -0.00344, \ \Delta e_y = -0.00004, \Delta e = 0.00345.$

The evaluated RAANs and inclinations: $\Delta\Omega = 0.01^\circ, \Delta i = -0.01^\circ.$

By using the equations for the spherical triangle, one can find the angle between the orbit planes $\Delta\gamma$ and the node line latitude argument u_z :

$$\left.\begin{aligned}\Delta\Omega &= \frac{\sin u_z}{\sin i}\Delta\gamma \\ \Delta i &= \cos u_z \Delta\gamma\end{aligned}\right\} \Rightarrow tgu_z = \sin i \frac{\Delta\Omega}{\Delta i}.$$

We get $\Delta\gamma = -0.0127^\circ, u_z = -38.1240^\circ.$

Between the two possible optimal lateral correction angles one should choose the closest to φ_e : $\varphi_z = 180^\circ + u_z = 141.8760^\circ.$

The angle between the optimal eccentricity correction direction and the optimal lateral correction direction $\Delta\varphi$ is evaluated: $\Delta\varphi = \varphi_e - \varphi_z = 180.624^\circ - 141.876^\circ = 38.748^\circ$.

It is necessary to keep in mind that all angles in the equations are in radians; the velocities and the other variables are dimensionless.

By using Eq. 2-16,

$$tg\frac{\varphi_1^*}{2} = \left(1 - \frac{\Delta e}{\Delta a}\right)\left(-ctg\Delta\varphi + \sqrt{ctg^2\Delta\varphi + \frac{\Delta a^2}{\Delta a^2 - \Delta e^2}}\right)$$

we get φ_1^* = first impulse application angle, starting from the line $\varphi_e = const, \varphi_1^* = 34.004^\circ$. The angle φ_1 of the first impulse application starting from the x axis: $\varphi_1 = \varphi_e - \varphi_1^*, \varphi_1 = 146.620^\circ$. The transversal impulse components and the angle of the second impulse application are determined for the angle φ_1 using Eq. 2-2: $\Delta V_{t_1} = 50.3461$ m/s, $\Delta V_{t_2} = 40.0139$ m/s, $\varphi_2 = 315.9030^\circ$.

Then the magnitudes of the lateral impulse components are found with the use of eqs. 2-14a and 2-14b: $\Delta V_{z_1} = -0.9616$ m/s, $\Delta V_{z_2} = 0.7643$ m/s, where $\varphi_i^z = \varphi_i - \varphi_z$.

The sum of the lateral components is $\Delta V_z = \left|\Delta V_{z_1}\right| + \left|\Delta V_{z_2}\right| = 1.7259$ m/s.

The sum of all components is $\Delta V = 90.37$ m/s.

The minimal possible expenditure on the orbit plane rotation (with node line correction) is $\Delta V_{z_{\min}} = V_0\Delta\gamma = 1.7185$ m/s.

The found solution is close to optimal, and ΔV_z practically coincides with $\Delta V_{z_{\min}}$.

The ratios' equality is checked for control purposes $\left|\frac{\Delta V_{z_1}}{\Delta V_{t_1}}\right| = \left|\frac{\Delta V_{z_2}}{\Delta V_{t_2}}\right|$.

The found values are $\left|\frac{\Delta V_{z_1}}{\Delta V_{t_1}}\right| = 0.0191, \left|\frac{\Delta V_{z_2}}{\Delta V_{t_2}}\right| = 0.0191$.

The ratios are equal; therefore, the found solution is correct.

CHAPTER THREE

COPLANAR RENDEZVOUS

3.1. Problem Statement

Determine the manoeuvre parameters that ensure the flyby to the given point of the target orbit for a fixed time.

The conditions of the transfer to a given point of the target orbit for a fixed time in the case of the coplanar rendezvous problem can be presented as follows:

$$\sum_{i=1}^{N} (\Delta V_{r_i} \sin\varphi_i + 2\Delta V_{t_i} \cos\varphi_i) = \Delta e_x, \qquad (3\text{-}1a)$$

$$\sum_{i=1}^{N} (-\Delta V_{r_i} \cos\varphi_i + 2\Delta V_{t_i} \sin\varphi_i) = \Delta e_y, \qquad (3\text{-}1b)$$

$$\sum_{i=1}^{N} 2\Delta V_{t_i} = \Delta a, \qquad (3\text{-}1c)$$

$$\sum_{i=1}^{N} (2\Delta V_{r_i} (1-\cos\varphi_i) + \Delta V_{t_i} (-3\varphi_i + 4\sin\varphi_i)) = \Delta t. \qquad (3\text{-}1d)$$

The impulses are applied on two manoeuvring intervals. The first interval starts from the moment when the possibility to perform the manoeuvre occurs, while the second interval ends right before the rendezvous point. Each interval has the length of one revolution; the gap between the intervals is several revolutions. The division of the manoeuvring intervals into several revolutions has its advantages. In the case when the total rendezvous ΔV_{rdv} exceeds the total transfer ΔV_{trf} due to the considerable difference in the initial positions of spacecraft along the orbit, the long flight interval on the drift orbit significantly brings ΔV_{rdv} closer to ΔV_{trf}. Besides, the possibilities of the orbit determination after the first manoeuvring interval and the second manoeuvre parameter

update (for the error compensation after the first impulse applications) appear. If necessary, additional burns, which correct errors in the orbit determination and the realization of the first impulses (a special manoeuvre to avoid colliding with space debris, can be added. In real missions, the manoeuvring intervals are separated from each other by a considerable number of revolutions. For example, for the "Soyuz" and "Progress" spacecraft, the first and the last manoeuvring intervals are separated by approximately 30 revolutions. There are more than 40 revolutions for the "Shuttle" and several dozens of revolutions for the European ATV etc. The relatively short rendezvous scheme (the several revolution approach) which can be found in works by Murtazin (2012, 14–2149; 2014, 162–175) also has its own advantages. It is mainly connected with the convenience of the cosmonaut habitability. However, the permitted phase diapason (the difference between the latitude arguments of the target spacecraft and the active spacecraft in the initial moment of the flyby) becomes extremely narrow, which adds significant constraints on the possible launch windows. Thus, the multiple-revolution rendezvous is preferable for automatic spacecraft, and both variants are possible for manned spacecraft. For manned spacecraft, the transition from the short scheme to the conventional multiple-revolution scheme is fulfilled in emergency situations.

The impulse belonging to the given manoeuvring intervals can be presented as follows:

$$\varphi_1 \subseteq F_1,...,\varphi_{N_1} \subseteq F_1, \varphi_{N_1+1} \subseteq F_2,...,\varphi_{N_1+N_2} \subseteq F_2, \qquad (3\text{-}2)$$

where N_1, N_2 = numbers of impulses on the first and the second manoeuvring intervals and $(N = N_1 + N_2)$, F_1, F_2 = the first and the second manoeuvring intervals, respectively.

The problem of the optimal coplanar rendezvous manoeuvre parameter determination can be stated as follows:

Find the components $\Delta V_{r_i}, \Delta V_{t_i}, \varphi_i (i = 1,..., N)$, which ensure the minimal total manoeuvre ΔV:

$$\Delta V = \sum_{i=1}^{N} \sqrt{\Delta V_{r_i}^2 + \Delta V_{t_i}^2}$$

with the constraints 3-1a–3-1d, 3-2.

The equations for the primer vector are listed below:

$$\lambda = \sqrt{\lambda_2^2 + \lambda_3^2}\,\sin(\theta - \theta_0) + 2\lambda_6, \tag{3-3a}$$

$$\mu = 2\lambda_1 + 2\sqrt{\lambda_2^2 + \lambda_3^2}\,\cos(\theta - \theta_0) - 3\lambda_6(\theta - \theta_0), \tag{3-3b}$$

$$tg\,\theta_0 = \frac{\lambda_2}{\lambda_3}, \tag{3-3c}$$

or

$$\lambda = A(\cos(\theta - \theta_0) + 2B), \tag{3-4a}$$

$$\mu = A(-2\sin(\theta - \theta_0) - 3B(\theta - \theta_0) + \frac{C}{A}), \tag{3-4b}$$

$$tg\,\theta_0 = \frac{\lambda_2}{\lambda_3}, \tag{3-4c}$$

where $A = \sqrt{\lambda_2^2 + \lambda_3^2}$, $B = \frac{\lambda_6}{A}$, $C = 2\lambda_1$.

Normally, eqs. 3-4a and 3-4b in the plane μ, λ describe the cycloid. The cycloid form depends only on the constant *B*, while the constant *A* determines the hodograph scale. The closed loop of the cycloid disappears for $B > 2/3$. The cycloid turns into an ellipse with $B = 0$. It degenerates to the point with $A = 0, B = 0$. Thus, three types of the optimal solutions are possible:

A) The hodograph degenerates to the point; hence, just like for coplanar *transfers*, the impulses will only have transversal components ($\lambda = 0$), which will all be accelerating (if $\mu = 1$) or decelerating (if $\mu = -1$). In the previous chapter, these solutions were designated as *coplanar special solutions* (CSS).

B) The hodograph turns into an ellipse. Similar to coplanar transfers, the impulses only have transversal components ($\lambda = 0$), *some of them* are accelerating ($\mu = 1$), while the rest of them are decelerating ($\mu = -1$). The impulses are located on the apsidal line of the drift orbit. These solutions are called *coplanar apsidal solutions* (CAS).

C) The hodograph is the cycloid. The impulses have radial components ($\lambda \neq 0$); the impulses applied on the first manoeuvring interval are decelerating (the transversal components are negative [$\mu < 0$]), and the impulses applied on the other interval are accelerating (the transversal

components are positive [$\mu > 0$]). Let these solutions be *coplanar nondegenerate solutions* (CNS).

In the first two cases, the total rendezvous problem ΔV_{rdv} is equal to the total transfer problem ΔV_{trf} ($\Delta V_{rdv} = \Delta V_{trf}$),; in the third case, $\Delta V_{rdv} > \Delta V_{trf}$.

The existence conditions for each of these three possible types of rendezvous problem solutions will be formulated in the fourth paragraph of this chapter.

First, we will consider the parameter determination procedures for each type of solution.

3.2. Rendezvous in Coplanar Nonintersecting Orbits: The Coplanar Singular Solution

Solutions of this type exist when the rendezvous can be performed by the corresponding division of impulses (which are necessary for the transfer between orbits) between the first and the second manoeuvring intervals. For example, the active spacecraft is situated in the inner orbit, while the target spacecraft is situated in the outer orbit ahead of the active spacecraft (but not too far). The manoeuvres, which increase the orbit's semimajor axis and change the eccentricity vector appropriately, are performed for the active spacecraft on the first interval. Then a process occurs which is usually called "phasing". The active spacecraft stays in the inner orbit and gradually, revolution by revolution, approaches the target spacecraft. When it is practically under the target spacecraft, the manoeuvres on the second manoeuvring interval, which ensure the two spacecrafts' rendezvous, are performed. If the active spacecraft was in the outer orbit, the target spacecraft should have been behind the active spacecraft in the initial moment of time. Then, similar to the previous case, the braking manoeuvres are performed, then the phasing stage follows, and finally the concluding braking manoeuvres are performed.

The primer vector hodograph in the form of the point corresponds to the considered special solution CSS. The optimal solution to the rendezvous problem has impulses with only transversal components, which are all either accelerating or decelerating. The primer vector does not give any information about the impulse application angles. The total delta-v of such rendezvous manoeuvres coincides with the total delta-v of the transfer manoeuvres (the group of rendezvous manoeuvres is a particular case in the transfer manoeuvres group):

$$\Delta V = \sum_{i=1}^{N} \left| \Delta V_{t_i} \right| = \frac{|\Delta a|}{2}.$$

Two-, three-, and four-impulse solutions are considered. The solution parameter searching procedures for the various numbers of impulses differ from each other. Solutions with more than four impulses do not gradually differ from four-impulse solutions.

3.2.1. The Two-Impulse Solution

We will start the two-impulse solution parameter determination with the impulse assessment. Eq. 3-1d shows that, for the considered flybys with a duration of several revolutions the major influence on the time of the arrival to the rendezvous point is caused by the transversal component of the first impulse. This allows approximately determining its magnitude:

$$\Delta V_{t_1}^{*} \approx -\frac{\Delta t}{3\varphi_{10}}, \tag{3-5}$$

Where φ_{10} = arbitrary point of the first interval permitted for the manoeuvring. Here, we used the fact that the length of the first manoeuvring interval is considerably smaller than the distance to the rendezvous point. We will further mark with asterisk the manoeuvre parameters for which the condition 3-1d is approximately satisfied. The geometric condition 3-5 indicates that, on the plane e_x, e_y, the point *B* (Fig. 3-1a), which corresponds to the drift orbit eccentricity vector (the orbit obtained after the application of the impulses of the first manoeuvring interval, also called the “phasing orbit”), should belong to the circle with the radius $R_1 = 2\left|\frac{\Delta t}{3\varphi_{10}}\right|$ and the center in the point *A*, because the magnitude of the first impulse is known, but its application angle is still unknown.

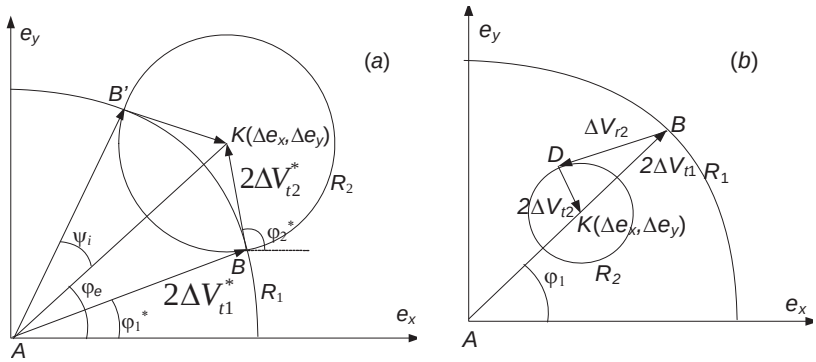

Figure 3-1. Two-impulse solutions:
(*a*) both impulses are transversal (*b*) second impulse has radial component

That means that the line segments on the plane e_x, e_y with lengths of $2\Delta V_{t_1}^*$ (plotted from the point A with various angles to the e_x axis) correspond to the impulses with magnitudes $\Delta V_{t_1}^*$ which were applied in the various points of the initial orbits. The geometric locus of the ends of these line segments will be a circle with the radius R_1.

It follows from eqs. 3-1c and 3-5 that

$$\Delta V_{t_2}^* \approx \frac{1}{2}\Delta a + \frac{\Delta t}{3\varphi_{10}}, \tag{3-6}$$

Thus, the point B must also belong to the circle of the radius $R_2 = \left|\Delta a + 2\frac{\Delta t}{3\varphi_{10}}\right|$ with a center in point K (Fig. 3-1a). It follows that it is necessary to transfer to point K with the second impulse of known magnitude $\Delta V_{t_2}^*$, but the application angle of this impulse is still unknown; hence, we can transfer to point K with the help of this impulse from an arbitrary point of a circle with the radius R_2.

The two-impulse solution with zero radial components exists if the circles intersect, i.e., the below conditions are satisfied:

$$R_1 + R_2 \geq \Delta e, \tag{3-7a}$$

$$\left|R_1 - R_2\right| \le \Delta e. \tag{3-7b}$$

The equality of the signs of the transversal impulse components of the first and the second manoeuvring intervals should be fulfilled in order to rank the found two-impulse solution as the CSS. The parameters of the orbits for this case will be determined in the fourth paragraph of this chapter.

It is obvious that the intersections of the circles give the two two-impulse solutions *ABK* and *AB'K* (Fig. 3-1a). The impulse application angles φ_1^*, φ_2^*, in which the intersection of the circles occur can be found from eqs. 3-1a and 3-1b:

$$\varphi_i^* = \varphi_e \pm \psi_i - 2\pi n_i + \frac{1}{2}\pi(1 - \operatorname{sign}\Delta V_{t_i}^*)\,(n_i = 0,1,2,...), \tag{3-8}$$

where

$$\varphi_e = \arccos\left(\frac{\Delta e_x}{\Delta e_y}\right)\operatorname{sign}\Delta e_y,$$

$$\psi_i = \arccos\frac{\Delta e^2 + 4\cdot(-1)^i\cdot(\Delta V_{t_2}^{*2} - \Delta V_{t_1}^{*2})}{4\Delta V_{t_i}^{*2}\Delta e}\,(i = 1,2).$$

In Eq. 3-8 the upper indexes correspond to the point *B'*, and the lower indexes correspond to the point *B*. The constants n_1 and n_2 are chosen in a way that the angles φ_1^*, φ_2^* would belong to the first and the second manoeuvring intervals, correspondingly.

The found angle values can be used as the initial guess for the iterative procedure (Baranov 1989, 689–697), which determines the parameters of the manoeuvre, for which the condition 3-1d would be fulfilled with the given tolerance.

On the consecutive iterations of this procedure, the magnitudes of the transversal impulse components $\Delta V_{t_1}^*, \Delta V_{t_2}^*$ are determined by eqs. 3-1c and 3-1d, where the impulse application angles φ_1^*, φ_2^* were calculated on the previous step. Then, with the help of Eq. 3-8, one can update the impulse application angle magnitudes. The calculations continue if the right and the left parts of Eq. 3-1d do not coincide with each other with the given tolerance for the found values of $\varphi_1^*, \varphi_2^*, \Delta V_{t_1}^*, \Delta V_{t_2}^*$.

It can be shown that the procedure converges if the condition below is satisfied:

$$\left| 2 \frac{\operatorname{tg} \frac{(\varphi_1 - \varphi_2)}{2}}{(\varphi_1 - \varphi_2)} \right| < 1,$$

Hence, the intersection of the circles in the small vicinity of the line *AK* is not allowed but, in this area, simple apsidal solutions are optimal. Their parameters will be determined below.

If the circles with radii R_1 and R_2 do not intersect, then the two-impulse transfer with zero radial components of both impulses is not possible. This is possible for nonintersecting orbits when one of the circles is located entirely inside of the other. For this problem, a manoeuvre with a nonzero radial component and with a lower (by magnitude) value than the transversal component will have the least total delta-v (Fig. 3-1b). The iterative procedure, which determining the parameters of such manoeuvres, is described in Baranov (1985). The total delta-v of these manoeuvres is greater than the minimal possible $|\Delta a|/2,$. Therefore, if the circles do not intersect, then it is necessary to use three- or four-impulse manoeuvring schemes for obtaining the optimal solution.

The aforementioned manoeuvre parameter determination method is quite convenient for the qualitative solution assessment. However, the researchers, who usually carry out this assessment, as a rule, have the orbit parameters in the first (before the first manoeuvring interval) moment of time, and not in the final one. With a rendezvous duration of several dozens of revolutions, the eccentricity vectors and the semimajor axes alter insignificantly, which is why one can use their deviations, which correspond to the initial moment of time, in the aforementioned equations. It is convenient to transit from Δt to Δu (Δu = difference in the angular positions between the target spacecraft and the active spacecraft in the initial moment of time [the initial phase]). Then, instead of $\Delta V_{t_1}^*$, we can find the approximate value of $\Delta V_{t_2}^*$

$$\Delta V_{t_2}^* \approx -\frac{\Delta u}{3\varphi_{10}},$$

then the value of $\Delta V_{t_1}^*$, and then the values of φ_1^*, φ_2^* etc.

3.2.2. The Three-Impulse Solution

In the analysis of three-impulse manoeuvres, we will assume that a single impulse is applied on the first manoeuvring interval. The variant with two impulses on the first interval can be evaluated in analogous fashion. It is reasonable to make the assumption that one impulse is applied on the first manoeuvring interval while the two other impulses are applied on the second manoeuvring interval. In the moment of manoeuvre parameter determination, an error in the orbital elements of the active and target spacecraft exists. The manoeuvres of the first interval will be fulfilled with errors as well. All these factors will lead to there being a difference between the active spacecraft's real orbit and the estimated orbit before the second manoeuvring interval. This is why a single impulse will not be enough for the transfer to the final orbit and thus it is necessary to use two burns in this interval.

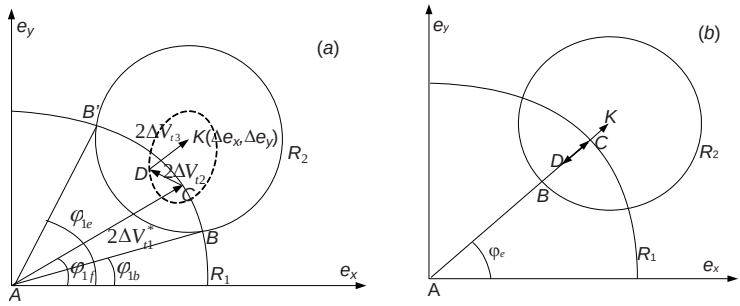

Fig. 3-2. Three-impulse solutions:
(*a*) basic solution (*b*) apsidal solution

The magnitude of the transversal component of the first impulse can be approximately determined by Eq. 3-5, while the sum of the transversal impulse components of the second interval can be determined in the same fashion as Eq. 3-6:

$$\Delta V_{t_{II}} = \Delta V_{t_2}^* + \Delta V_{t_3}^* \approx \frac{\Delta a}{2} + \frac{\Delta t}{3\varphi_{10}}. \tag{3-9}$$

We suppose that the circles with radii $R_1 = 2\left|\Delta V_{t_1}^*\right|$ and $R_2 = 2\left|\Delta V_{t_{II}}\right|$ intersect (Fig. 3-2a) and the signs $\Delta V_{t_1}^*$ and $\Delta V_{t_{II}}$ coincide, which is possible for flybys between nonintersecting orbits with optimal values of Δt.

For the existence of the CAS-type solutions considered, it is necessary for all the signs of the transversal impulse components of the second manoeuvring interval to coincide, which is possible with $\left|\Delta V_{t_i}^*\right| \le \left|\Delta V_{t_{II}}\right|$ (i = 2, 3). The application angles of these impulses may be arbitrary and, hence, point *C*, which corresponds to the *drift orbit* eccentricity vector, should belong to the circle with radius R_2 and its center at point *K* (Fig. 3-2a). This is connected to the fact that the transfer to point *K* on the second manoeuvring interval is fulfilled by a two-section curved line of length $2\Delta V_{t_{II}}$ (since the two impulses are applied on the second manoeuvring interval, the application angles may be arbitrary), not by the single line segment of length $2\Delta V_{t_{II}}$ (as in the two-impulse scheme with one impulse on the second manoeuvring interval). An example of such a line is the curved line *CDK* in Fig. 3-2a. Thus, point *C* can lie not only on the circle of radius R_2, but also inside it. In the meantime, it should belong to the circle with radius R_1. As such, point *C* should belong to the curve *BB′* of the circle with radius R_1 (Fig. 3-2a). The set of solutions, which differ by the application angles and the magnitudes of the second and third impulses, but have equal total delta-v magnitudes $\left|\Delta a\right|/2$, correspond to the position of point *C* on curve *BB′*. The three-impulse example solution is presented in Fig. 3-2a by the curved line *ACDK*. Point *D*, which corresponds to the orbital eccentricity vector (obtained after the application of the first impulse on the second manoeuvring interval), should belong to an ellipse with focus points *C* and *K*. The semimajor axis of this ellipse is equal to $\Delta V_{t_{II}}$ (Fig. 3-2a).

There are six variables (three transversal impulse components and three angles of their application) and four constraints in the equality forms in the considered three-impulse rendezvous problem. Additionally, if we fix the values of two out of the six variables, the values of the rest can be determined using eqs. 3-1a to 3-1d.

Let us fix the application angles of the first and second impulses $\varphi_1 = \varphi_{1_f}, \varphi_2 = \varphi_{2_f}$. A solution of the required type can be obtained if

$\varphi_{1_f} \subseteq (\varphi_{1_b}, \varphi_{1_e})$ is true, i.e. point *C* belongs to curve *BB'*. Naturally, φ_{1_f} and φ_{2_f} should belong to the first and second manoeuvring intervals, respectively. Since φ_1 is fixed and $\Delta V_{t_1}^*$ can be determined from Eq. 3-5, the position of point *C* is known (the drift orbit eccentricity vector is known). The last two impulses ensure a transfer without the time constraint on the second manoeuvring interval (the transfer from point *C* to point *K*). The application angle of the first of these impulses is fixed and, with the use of eqs. 2-2a to 2-2c, one can determine $\Delta V_{t_2}^*, \Delta V_{t_3}^*$ and φ_3^*:

$$\Delta V_{t_2}^* = \frac{\Delta\tilde{e}^2 - \Delta\tilde{a}^2}{4(\Delta\tilde{e}_y \sin\varphi_{2_f} + \Delta\tilde{e}_x \cos\varphi_{2_f} - \Delta\tilde{a})}, \tag{3-10a}$$

$$\Delta V_{t_3}^* = \frac{\Delta\tilde{a}}{2} - \Delta V_{t_2}^*, \tag{3-10b}$$

$$\mathrm{tg}\,\varphi_3 = \frac{\frac{\Delta\tilde{e}_y}{2} - \Delta V_{t_2}^* \sin\varphi_{2_f}}{\frac{\Delta\tilde{e}_x}{2} - \Delta V_{t_2}^* \cos\varphi_{2_f}}, \tag{3-10c}$$

where

$$\Delta\tilde{e}_x = \Delta e_x - 2\Delta V_{t_1}^* \cos\varphi_{1_f}, \Delta\tilde{e}_y = \Delta e_y - 2\Delta V_{t_1}^* \sin\varphi_{1_f}, \Delta\tilde{a} = \Delta a - 2\Delta V_{t_1}^*.$$

By using $\Delta V_{t_1}^*, \Delta V_{t_2}^*, \Delta V_{t_3}^*, \varphi_3^*$ as the initial guess, we can evaluate the manoeuvre parameters that would satisfy condition 3-1d with the desired accuracy. For this purpose, let us put the fixed application angles and the found impulse parameters in the left part of Eq. 3-1d and determine Δt^*. Then, we substitute Δt to $\Delta t - \Delta t^*$ ($\Delta t := \Delta t + \Delta t - \Delta t^*$) in Eq. 3-1d and repeat the calculations. The procedure ends when $\left|\Delta t - \Delta t^*\right| \le \varepsilon$, where ε = the accuracy of Eq. 3-1d. Since we have the outer iterative procedure (presented in Chapter 1), which ensures that all perturbations are taken into account, the accuracy of this iterative procedure, as a rule, should be by an order of magnitude more accurate than the fulfillment of the time condition in the outer procedure.

The impulse application angle fixation is usually dictated by the flight conditions. If there are no constraints on the moments of impulse

application, then it is better to use the simplest solution for the sake of simplicity and reliability. The impulses of the simplest solution are applied on the apsidal line of the relative orbit (the apsidal solution). We can assume, for example, that the third impulse has the same application angle φ_e (Eq. 1-14a) on its revolution as the first impulse had on its revolution, and the application angle of the second impulse differs by 180º from the angle of application of the third impulse. The line segments *AC*, *CD*, and *DK* correspond to the impulses of such a solution in Fig. 3-2b. The angular values φ_i can easily be calculated if we know the impulse application angles on the revolution:

$$\varphi_1 = \varphi_e + 2\pi(N_I - N_{as}) - u_{as}, \tag{3-11a}$$

$$\varphi_2 = \varphi_e - \pi + 2\pi(N_{II} - N_{as}) - u_{as}, \tag{3-11b}$$

$$\varphi_3 = \varphi_e + 2\pi(N_{II} - N_{as}) - u_{as}, \tag{3-11c}$$

where N_{as}, u_{as} = the number of revolutions and the target point latitude argument and N_I, N_{II} = the numbers of revolutions on which impulses of the first and the second manoeuvring intervals are applied, respectively.

The transversal impulse component magnitudes can be evaluated from Eq. 3-1:

$$\Delta V_{t_2} = \frac{1}{4}(\Delta a - \Delta e), \tag{3-11d}$$

$$\Delta V_{t_1} = \frac{\Delta t - k_2 \Delta V_{t_2} - \frac{1}{4} k_3 (\Delta a + \Delta e)}{(k_1 - k_3)}, \tag{3-11e}$$

$$\Delta V_{t_3} = \frac{1}{4}(\Delta a + \Delta e) - \Delta V_{t_1}, \tag{3-11f}$$

where $k_i = 4\sin\varphi_i - 3\varphi_i$ (i = 1, 2, 3).

Depending on the location of the second manoeuvring interval, there may be a solution with the reverse order of impulse application. The application angle of the first impulse of the second manoeuvring interval is φ_e, and the second impulse is applied half a revolution later.

It is important to note that, during the determination of the apsidal solution parameter, the concept of the rendezvous having a multiple-revolution nature was not used. As such, the found analytical solution can

be used for the manoeuvre parameter determination of a rendezvous of arbitrary duration.

We can use Eq. 3-11f, instead of Eq. 3-5, for the assessment of the first impulse magnitude.

The considered solutions exist if the circles with radii R_1 and R_2 intersect, or the circle of radius R_1 is entirely situated inside the circle with radius R_2. If the opposite situation occurs, with the circle of radius R_2 situated entirely inside the circle of radius R_1, three-impulse CSS solutions exist only if two impulses are applied on the first manoeuvring interval.

If one of the circles lies entirely inside the other and three-impulse CSS solutions exist, one can distinguish the four simplest three-impulse apsidal solutions from among them (if two of the three impulses can be placed on the first or on the second manoeuvring interval). The parameters of these solutions can be determined unambiguously from Eq. 3-1 as well. As shown in Chapter 2, the real (after the manoeuvre parameter update with the help of the iterative procedure from the first chapter) total delta-vs of these solutions can differ. If the lengths of each of the permitted manoeuvring intervals do not exceed one revolution, only two possible apsidal solutions remain.

3.2.3. Example

Here, in considering the three-impulse rendezvous, one of the impulses is applied on the first manoeuvring interval and the other two impulses are applied on the second. The initial and target orbital elements are listed in the table. They are similar to the orbital elements from solution 2.1.5, but the information about the active and target spacecraft latitude arguments in the initial moment of time, the numbers of revolutions of both spacecraft for that moment N_{0in} and N_{0f}, and the numbers of revolutions for the rendezvous moment N_{asi} and N_{ast}, are added. The three variants are considered. They differ from each other by the target spacecraft's location.

Elements	Initial orbit	Target orbit
$H_{\min}$ km	180.0	340.0
$H_{\max}$ km	210.0	360.0
u_{prg} deg	20.0	150.0

u_1 deg	60.0	5.0
u_2 deg	60.0	210.0
u_3 deg	60.0	355.0
N_0 (initial revolution)	1	201
N_{as} (rendezvous revolution)	17	217

The rendezvous point is at the beginning of the 17th revolution, i.e. $u_{as} = 0$ is the target point latitude argument and $N_{as} = 17$ is the target point revolution number. The first manoeuvring interval is on the 1st revolution, while the second manoeuvring interval is on the 16th revolution. The manoeuvring scheme can be found in the figure.

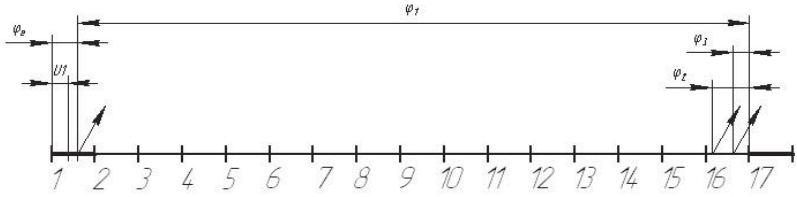

The simplest apsidal solution will be used. The angles φ_i, which start from the target point, determine the impulse application moments:

$$\varphi_1 = \varphi_e + 2\pi(N_I - N_{as}) - u_{as},$$
$$\varphi_2 = \varphi_e - \pi + 2\pi(N_{II} - N_{as}) - u_{as},$$
$$\varphi_3 = \varphi_e + 2\pi(N_{II} - N_{as}) - u_{as},$$

where N_I, N_{II} = the numbers of revolutions on which the impulses of the first and second manoeuvring intervals are applied, respectively.

In our case, $N_I = 1, N_{II} = 16.$

The calculated results are:

$\varphi_1 = -97.3784, \varphi_2 = -6.2723, \varphi_3 = -3.1307.$

The approximate value of the parameter Δt (the resynchronization of the arrival times at the rendezvous point of the active and target spacecraft) is evaluated. The revolution periods of the active and target spacecraft can be determined as:

$$T_{IN} = 2\pi a_{IN}\sqrt{\frac{a_{IN}}{\mu}}, T_F = 2\pi a_F\sqrt{\frac{a_F}{\mu}}.$$

The time of arrival of the spacecraft to the rendezvous point is:

$$t_{IN} = T_{IN}\left(N_{asi} - N_{0in} - 1 + \frac{360 - u_{IN}}{360}\right)$$

(with a distance of 15 revolutions plus remaining for the completion of the full revolution during the motion from the initial point).

The calculated results: $t_{IN} = 83{,}836.54\ s.$

For the target spacecraft:

$$t_{Fi} = T_F\left(N_{asf} - N_{0f} - 1 + \frac{360 - u_{Fi}}{360}\right)$$

Δt_i can be determined as: $\Delta t_i = (t_{Fi} - t_{IN})\lambda_0.$

The exact Δt_i value can be obtained with the help of numerical prediction of the rendezvous point for the active and target spacecraft orbits while accounting for all perturbations, just as in the practical problem solution.

The transversal impulse component magnitudes can be determined from eqs. 3-11d to 3-11f, where $k_i = 4\sin\varphi_i - 3\varphi_i$ (i = 1, 2, 3), $k_1 = 292.0919, k_2 = 18.86044, k_3 = 9.348559.$

The problem solution:

1) $U_{K1} = 5^\circ$ $T_{K1} = 87{,}660.38\ s$ $\Delta t_1 = 4.458352\ (3{,}823.84\ s)$
$\Delta V_{t_1} = 117.8551$ m/s, $\Delta V_{t_2} = 38.5273$ m/s, $\Delta V_{t_3} = -66.0223$ m/s,

2) $U_{K2} = 210^\circ$ $T_{K2} = 84{,}537.82\ s$ $\Delta t_2 = 0.8176375\ (701.2713\ s)$
$\Delta V_{t_1} = 18.1158$ m/s, $\Delta V_{t_2} = 38.5273$ m/s, $\Delta V_{t_3} = 33.7169$ m/s,

3) $U_{K3} = 355^\circ$ $T_{K3} = 82{,}329.17\ s$ $\Delta t_3 = -1.757502\ (1{,}507.37\ s)$
$\Delta V_{t_1} = -52.4314$ m/s, $\Delta V_{t_2} = 38.5273$ m/s, $\Delta V_{t_3} = 104.2641$ m/s.

Conclusions:

1) In the first case, the target spacecraft "stays behind" the active spacecraft ($U_{K1} = 5^\circ$, $U_I = 60^\circ$). In order to reduce this lag, it is necessary to gradually increase the spacecraft's orbital semimajor axis (see the figure). This will allow the target spacecraft to "catch up" with the active spacecraft while moving along the orbit with a smaller period. The necessary drift orbit is obtained thanks to a highly-accelerating impulse and is plotted in the first figure with the dashed line. Then, with the help of the accelerating impulse performed on the second manoeuvring interval, an orbit that osculates with the target spacecraft orbit is formed. The last braking impulse completes the transfer to the target spacecraft's orbit. Such a flyby is not optimal, as one of the impulses is decelerating and the flyby energetics are higher in comparison to the case when all the impulses are accelerating. On the other hand, it is impossible to implement the reverse scheme and let the active spacecraft "chase" the target spacecraft because the number of revolutions for the flyby is limited.

2) In this case, the active spacecraft is behind the target spacecraft ($U_{K1} = 210^\circ$, $U_I = 60^\circ$). The phase difference lies in the optimal range and, hence, all three impulses are accelerating. The optimal manoeuvre (the phasing orbit semimajor axis plotted with a dashed line in the second figure) lies between the semimajor axes of the initial and target orbits.

3) In this case, the active spacecraft is far behind the target spacecraft ($U_{K1} = 5^\circ$, $U_I = 355^\circ$). In order to chase it down in the fixed number of revolutions, the active spacecraft orbital period needs to be decreased even more (see the figure below). As a result of this step, the required drift orbit appears (the dashed line in the third figure). The second and third impulses are accelerating and adjust the target orbit.

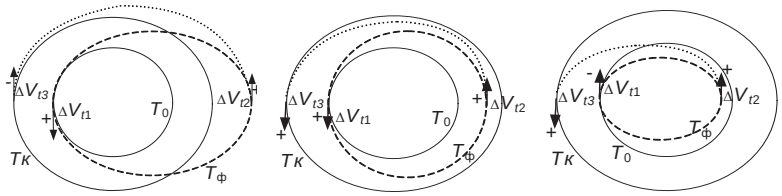

1) $U_{K1} = 5^\circ$ 2) $U_{K2} = 210^\circ$ 3) $U_{K3} = 355^\circ$

3.2.4. The Four-Impulse Solution

The use of the four-impulse scheme allows for two impulses on each manoeuvring interval and, thus, does not depend on the relative positions

of the circles with radii R_1 and R_2 (it does not matter which of the circles will be inside the other). Besides, the presence of new free variables allows us to meet different and additional constraints on the manoeuvre parameters.

Let us approximately assess the sum of the transversal impulse components of each manoeuvring interval in the same way as was done for the two and three-impulse manoeuvre solutions:

$$\Delta V_{t_I} = \Delta V_{t_1}^* + \Delta V_{t_2}^* \approx -\frac{\Delta t}{3\varphi_{10}}, \tag{3-12a}$$

$$\Delta V_{t_{II}} = \Delta V_{t_3}^* + \Delta V_{t_4}^* \approx \frac{\Delta a}{2} + \frac{\Delta t}{3\varphi_{10}}. \tag{3-12b}$$

Let us suppose that the circles, which have the radii $R_1 = 2\left|\Delta V_{t_I}\right|$ and $R_2 = 2\left|\Delta V_{t_{II}}\right|,$ intersect and the signs of ΔV_{t_I}, $\Delta V_{t_{II}}$ coincide. In this case, the set of solutions with equal total manoeuvre delta-vs $\left|\Delta a\right|/2$ exists. Point *C*, which corresponds to the parameters of the drift orbits of such solutions, should belong to set *G* (the intersection of the circles with radii R_1 and R_2, respectively (Fig. 3-3)). This is necessary for the sign equality of the transversal impulse components on each manoeuvring interval. The values of eight variables $\varphi_i, \Delta V_{t_i}\,(i = 1,...,4)$ with four constraints are determined in the problem. As such, the four additional constraints should be added in order to solve the problem unambiguously. One should bear in mind that the obtained solution should remain a CSS-type solution. For example, the three impulse application angles and the impulse magnitude ratio of one of the intervals can be fixed. Let us assume that, for example, $\varphi_1 = \varphi_{1_f}$, $\varphi_3 = \varphi_{3_f}$, $\varphi_4 = \varphi_{4_f}$, $m = \dfrac{\Delta V_{t_3}}{\Delta V_{t_3} + \Delta V_{t_4}}$. The constraint on the impulse magnitude distribution on the second manoeuvring interval is often met in practical work during the manoeuvre parameter determination of the “Soyuz” and “Progress” spacecraft.

Fixation of the impulse application angles on the second manoeuvring interval means that point *C*, which corresponds to the drift orbit

eccentricity vector, should belong to line segment *LN'* (Fig. 3-3a), and not to the entire circle with radius R_2, for the second manoeuvring interval.

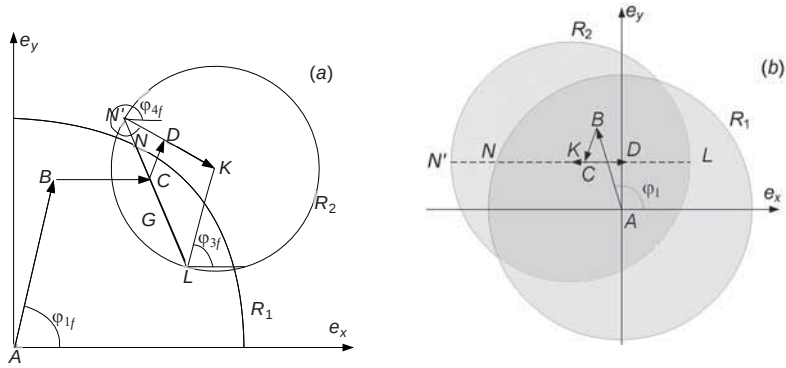

Fig. 3-3. Four-impulse solutions:
(*a*) general solution (*b*) typical "Soyuz" spacecraft solution

In the meantime, point *C* should belong to the circle with radius R_1, and, hence, it should by all means belong to line segment *LN*. Since the ratio of the impulse magnitudes for the second manoeuvring interval is given and their sum is known (3-12b), then the magnitudes of these impulses $\Delta V^*_{t_3}, \Delta V^*_{t_4}$ are known. Thus, the location of point *C* on line segment *LN* is known.

The first two impulses ensure the transfer to point *C* without the time constraint. The application angle of one of the impulses is fixed and the impulse magnitudes and the application angle of the second impulse can be determined by the equations, which are similar to eqs. 3-10a to 3-10c, just as for the second manoeuvring interval of three-impulse transfers. The indexes should be replaced in eqs. 3-10a to 3-10c: "3" to "2" and "2" to "1". The values $\Delta\tilde{e}_x, \Delta\tilde{e}_y, \Delta\tilde{a}$ should be determined by the equations:

$$\begin{aligned}
\Delta\tilde{e}_x &= \Delta e_x - m\Delta V_{t_{II}} \cos\varphi_{3_f} - (1-m)\Delta V_{t_{II}} \cos\varphi_{4_f}, \\
\Delta\tilde{e}_y &= \Delta e_y - m\Delta V_{t_{II}} \sin\varphi_{3_f} - (1-m)\Delta V_{t_{II}} \sin\varphi_{4_f}, \\
\Delta\tilde{a} &= \Delta a - 2\Delta V_{t_{II}}.
\end{aligned} \qquad (3\text{-}13)$$

The curved line *ABCDK* corresponds to the found solution (Fig. 3-3a).

The values of $\Delta V_{t_1}^*, \Delta V_{t_2}^*, \Delta V_{t_3}^*, \Delta V_{t_4}^*$ and φ_2^* are used as the initial guess for the iterative procedure, which is analogous to the procedure for the three-impulse problem and allows us to deal with constraint 3-1d with the desired tolerance.

3.2.5. Peculiarities of the Manoeuvring Scheme for the Soyuz and Progress Spacecraft

During the flight of the "Soyuz" spacecraft, the application angles of the last two impulses are fixed at one revolution and half a revolution before the rendezvous point. Thus, with the help of the impulses of the first manoeuvring interval, it is necessary to transfer to line segment *LN*, which is parallel to the abscissa axis (Fig. 3-3b). The constraint of approximate equality on the impulse of the last manoeuvring interval is often added. This means that point *C*, which corresponds to the eccentricity vector of the drift orbit, should be situated on line segment *LN* in the vicinity of point *K*, when line segment *CD* (the third impulse) is approximately equal to line segment *DK* (the fourth impulse). The application angle of one of the impulses of the first manoeuvring interval is often fixed in order to force the application of this impulse on the line of the orbital plane intersection of the "Soyuz" spacecraft and the orbital station. Thus, four constraints are added, which allow the unambiguous determination of the magnitudes of all impulses of the four-impulse coplanar rendezvous. The depiction in Fig. 3-3b corresponds to the real solution and the real relative position of the circles for the four-impulse problem, which is solved during ballistic support of the "Soyuz" spacecraft flight.

The manoeuvring schemes, which had been used for the docking of the "Soyuz" and "Progress" spacecraft with the orbital station in the late 1970s and the early 1980s, differed from the schemes that were used later. Indeed, a one-day docking scheme, rather than a two-day scheme, was used for the docking of the "Soyuz" spacecraft. The biggest discrepancy is found for the docking scheme of the "Progress" spacecraft, which was a two-day rendezvous scheme with considerable constraints on thrust engine orientation.

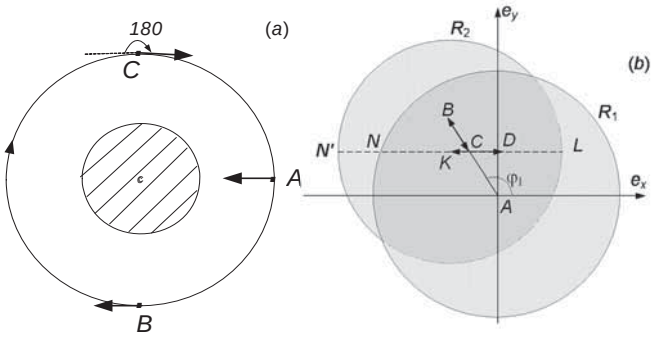

Fig. 3-4. Manoeuvring scheme of the first "Progress" spacecraft: (*a*) orientation setting and manoeuvre performance scheme (*b*) example solution for the first "Progress" spacecraft

An orientation on the center of the Earth is set up with the help of the infrared vertical 22.5 minutes before the start of the estimated manoeuvre (Fig. 3-4a, point *A*). Then, 22.5 minutes later (Fig. 3-4a, point *B*), when the set orientation becomes close to the transversal, the first impulse is applied (it can be accelerating or decelerating). 45 minutes later, one more estimated earlier impulse is applied, which is also close to the transversal one (Fig. 3-4a, point *C*). In order to have two accelerating impulses, the thrust vector is rotated by 180º before ignition.

The thrust engine orientation on the second manoeuvring interval can be set in the same fashion. Thus, the coplanar rendezvous problem is solved with the following constraint: the second impulse is performed approximately half a revolution after the first one and the fourth impulse is performed half a revolution after the third one. If the application angle of the third impulse is fixed (one revolution before the rendezvous point), then one free parameter stays—the application angle of the first impulse. By altering this angle, one can obtain solutions with the desired attributes. For example, we can obtain a solution with approximately equal magnitudes for the last two impulses (Fig. 3-4b). Such a solution can be found analytically or by enumerating the application angles of the first impulse and solving Eq. 3-1 with the fixed angles of application of the rest of the impulses. Thus, the solution of the four-impulse coplanar rendezvous problem can be found with the help of the simplest single-axis orientation to the center of the Earth.

3.2.6. The Apsidal Four-Impulse Solution

Similar to the case of the three-impulse solution, if there are no constraints, it is better to use the simplest solution with the impulse application on the apsidal points of the relative orbit. However, unlike the case of the three-impulse solution, there will be options available in choosing the drift orbit eccentricity vector magnitude, i.e. point *C* can be anywhere on line segment *LN* (Fig. 3-5).

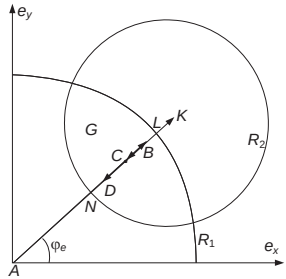

Fig. 3-5. Four-Impulse apsidal solution

In order to eliminate this uncertainty, it is necessary to choose point *C* in the middle of line segment *LN*. Then, the magnitudes of the two impulses, applied at points $\varphi_e + \pi$ on their corresponding revolutions, will be equal and have the value $(\Delta a - \Delta e)/8$, i.e. their sum will be equal to the impulse magnitude of the three-impulse solution applied in the same direction. The magnitudes of the two remaining impulses of the four-impulse solution can be unambiguously determined from the last two equations of Eq. 3-1. The example of such a solution is depicted in Fig. 3-5.

Line segment *AB* corresponds to the first impulse (its application angle is φ_e); line segment *BC* corresponds to the second impulse (its application angle is $\varphi_e + \pi$); line segment *CD* corresponds to the third impulse (its application angle is $\varphi_e + \pi$); and line segment *DK* corresponds to the fourth impulse (its application angle is φ_e). In this case, when we speak about the impulse application angles, their positions on the corresponding revolution are implied. The position of point *C* on the line segment (and, hence, the eccentricity magnitude and the drift orbit focal parameter) can be chosen as well in order to provide the necessary drift orbital RAAN

evolution. This opportunity will be used in the second paragraph of Chapter 6.

It is important to mention that, just as in the three-impulse case, during the determination of the apsidal solution, the parameter for the multiple-revolution rendezvous was not used. The analytical solution found can be used for the manoeuvre parameter determination of a rendezvous with arbitrary duration.

The real (after updating the manoeuvre parameters with the help of the iterative procedure) total delta-vs of the various apsidal solutions can differ.

3.3. Rendezvous in Coplanar Intersecting Orbits: The Coplanar Apsidal Solution

The coplanar apsidal solution (CAS) takes place if the circles, having radii R_1 and R_2, do not intersect and neither circle lies inside the other, i.e. the condition $|R_1| + |R_2| \leq \Delta e$ is satisfied. This is possible for transfers between intersecting orbits with some values of $\Delta t(\Delta u)$. The existence domains of different types of solutions will be discussed more thoroughly in the fourth paragraph of this chapter

Let us consider three-impulse manoeuvres with two impulses applied on the second manoeuvring interval. All the impulses are applied on the relative orbital apsidal line and, hence, their application angles are known (eqs. 3-11a to 3-11c). Thus, using Eq. 3-1 we can unambiguously determine the impulse magnitudes. The equations for the apsidal three-impulse solution from the previous section (eqs. 3-11d to 3-11f) are used for this purpose, but it is worth paying attention to the fact that ΔV_{t_2} will be negative. The advantage of the apsidal solutions is that they offer an opportunity to use the same equations for both intersecting and nonintersecting orbits. Figure 3-6a presents the obtained solution. Line segment *AB* corresponds to the first burn; line segment *BC* corresponds to the second burn; and line segment *CK* corresponds to the third burn. It follows from eqs. 3-5 and 3-9 that $AB \approx R_1$, and $CK - BC \approx R_2$.

For four-impulse apsidal manoeuvres, the line segments, which correspond to the impulses, also belong to line segment *AK*, which connects the centers of the circles (Fig. 3-6b). Line segment *AB* corresponds to the first impulse; line segment *BC* corresponds to the second impulse; line segment *CD* corresponds to the third impulse; and

line segment *DK* corresponds to the fourth impulse. According to eqs. 3-12a and 3-12b, $AB - BC \approx R_1, DK - CD \approx R_2$.

The exact values of the transversal component are determined from eqs. 3-1a to 3-1d. Since the number of the equations is smaller than the number of unknown variables, it is necessary to add one more constraint. For example, we may fix the position of point *C* on line segment *EL*, which corresponds to the drift orbit eccentricity vector, fix the ratio of the impulse magnitudes of one of the manoeuvring intervals, or apply any other analogous constraint; however, it is worth remembering that point *C* must always belong to line segment *EL*, which connects the nearest points of the circles. If there are no additional constraints, one can use the simplest solution with point *C* situated in the middle of line segment *EL*. Such a solution parameter determination procedure is described in the following paragraph.

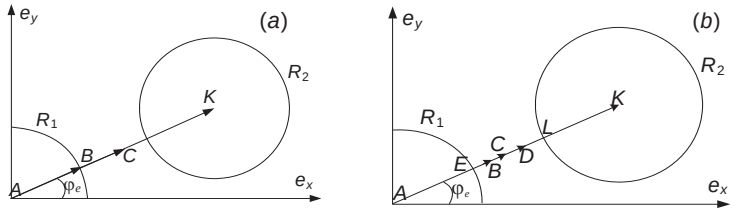

Fig. 3-6. Apsidal solutions:
(*a*) three-impulse solution (*b*) four-impulse solution

Depending on the order of the impulse applications, two possible three-impulse CAS solutions and four four-impulse apsidal solutions can be distinguished. If the length of each of the permitted manoeuvring intervals does not exceed one revolution, only one possible apsidal solution remains. Thus, in order to find the genuine optimal solution, which depends on the impulse application sequence, the length of each of the manoeuvring intervals should be one and a half revolutions. The length of one revolution for a manoeuvring interval is enough if we narrow our consideration with the linearized equations of motion, from which it follows that the impulse application sequence is not important. The real (after the manoeuvre parameter update with the help of the iterative procedure) total delta-v of the various apsidal solutions may differ.

As in the case of nonintersecting orbits, during the apsidal solution, parameter determination using the concept of the multiple-revolution nature of the rendezvous was not used. The found analytical solution can

be used for the manoeuvre parameter determination of a rendezvous with arbitrary duration.

3.4. Nondegenerate Coplanar Solution

If there is a considerable initial difference between the spacecraft positions along the orbit, the total rendezvous ΔV_{rdv} exceeds the total transfer ΔV_{trf}, and the nondegenerate solution will be optimal. For example, if the target spacecraft is situated too far ahead of the active spacecraft, which is situated on the inner orbit. As such, it will be necessary to reduce the semimajor axis in order to catch the target spacecraft during the phasing process and then increase the semimajor axis to the desired value with the help of the second manoeuvring interval impulses. For solutions of this type, we use accelerating impulses on one interval and braking impulses on the other.

Coplanar nondegenerate solutions (CNS) exist if the circles with radii R_1 and R_2 intersect in the case of a flyby between intersecting orbits, or where one of the circles lies entirely inside the other during a flyby between nonintersecting orbits.

For the nondegenerate solution, the primer vector hodograph is a cycloid. The hodograph must be symmetrical relative to the λ axis (Prussing 1969, 928-935) in order to meet the required optimality conditions for the four-impulse flyby. Hence, the center of the coordinate frame should lie either in the middle between the closed loops of the hodograph (Fig. 3-7) (let us call such a solution a “first-type hodograph”) or on the axis of the closed loop (a “second-type hodograph”).

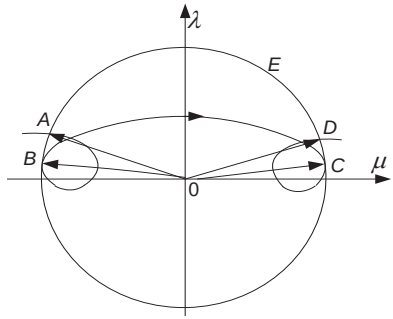

Fig. 3-7. Primer vector hodograph for a coplanar rendezvous

The first-type hodograph exists if $C = 0, \theta_0 = (\theta_b + \theta_f)/2$ in eqs. 3-4a and 3-4, while the second-type hodograph exists if $C = 3BA\pi, \theta_0 = (\theta_b + \theta_f)/2 + \pi$. The angle θ_b corresponds to the start of the first manoeuvring interval (point *A*, Fig. 3-7), while θ_f corresponds to the end of the second manoeuvring interval (point *D*, Fig. 3-7).

The constraints on the manoeuvring parameters follow from the solution symmetry:

$$\theta_2 - \theta_1 = \theta_4 - \theta_3, \tag{3-14}$$

$$\frac{\lambda(\theta_1)}{\mu(\theta_1)} = -\frac{\lambda(\theta_4)}{\mu(\theta_4)}, \tag{3-15}$$

$$\frac{\lambda(\theta_2)}{\mu(\theta_2)} = -\frac{\lambda(\theta_3)}{\mu(\theta_3)}. \tag{3-16}$$

Thus, for an optimal four-impulse solution, the first impulse should be applied at the beginning of the first manoeuvring interval $\theta_1 = \theta_b$, and the last impulse should be applied at the end of the second manoeuvring interval $\theta_4 = \theta_f$, the angle between the application moments of the first and second impulses is equal to the angle between the application moments of the third and fourth impulses (Eq. 3-14). The simple eqs. 3-15 and 3-16 also connect the impulse orientations to each other.

It follows from the symmetrical nature of the hodograph that, if the necessary optimality conditions are satisfied for the first and second impulses, they will also be satisfied for the third and fourth impulses.

3.4.1. Parameter Determination for the Four-Impulse Solution

Let us write down the intersection condition of the primer vector hodograph with the unit circle for the first impulse and the conditions of the osculation of the hodograph and the circle for the second impulse:

$$\lambda^2(\theta_1) + \mu^2(\theta_1) = 1, \tag{3-17}$$

$$\lambda^2(\theta_2) + \mu^2(\theta_2) = 1, \tag{3-18}$$

$$\lambda(\theta_2)\dot{\lambda}(\theta_2) + \mu(\theta_2)\dot{\mu}(\theta_2) = 0, \tag{3-19}$$

$$\lambda^2(\theta) + \mu^2(\theta) \le 1 \; \forall \, \theta \in [\theta_b, \theta_f]. \tag{3-20}$$

Let $\Delta\theta$ be $\Delta\theta = \theta_2 - \theta_1, \tilde{\theta} = \frac{1}{2}(\theta_b - \theta_f) = \frac{1}{2}(\theta_4 - \theta_1)$. Then, the equation system 3-17 to 3-19 can be written as:

$$A^2(\pm\cos\tilde{\theta} + 2B)^2 + A^2(\mp 2\sin\tilde{\theta} - 3B\tilde{\theta})^2 = 1, \tag{3-21}$$

$$\begin{aligned} &A^2(\pm\cos(\tilde{\theta} - \Delta\theta) + 2B)^2 \\ &+ A^2(\mp 2\sin(\tilde{\theta} - \Delta\theta) - 3B(\tilde{\theta} - \Delta\theta))^2 = 1, \end{aligned} \tag{3-22}$$

$$\begin{aligned} &(-\cos(\tilde{\theta} - \Delta\theta) \mp 2B)\sin(\tilde{\theta} - \Delta\theta) + (\mp 2\sin(\tilde{\theta} - \Delta\theta) \\ &- 3B(\tilde{\theta} - \Delta\theta))(\mp\cos(\tilde{\theta} - \Delta\theta) - 3B) = 0, \end{aligned} \tag{3-23}$$

where the upper indexes correspond to a hodograph of the first type and the lower indexes correspond to a hodograph of the second type.

Deriving *B*, *A* from eqs. 3-21 and 3-22, and substituting them in Eq. 3-23, yields the equation for the determination of $\Delta\theta$ with fixed $\tilde{\theta}$. This equation, for both hodographs of the first and second types, is written as:

$$\begin{aligned} &9B^2(\tilde{\theta} - \Delta\theta) + (4\sin(\tilde{\theta} - \Delta\theta) \\ &+ 6(\tilde{\theta} - \Delta\theta)\cos(\tilde{\theta} - \Delta\theta)B \\ &+ 3\sin(\tilde{\theta} - \Delta\theta)\cos(\tilde{\theta} - \Delta\theta) = 0, \end{aligned} \tag{3-24}$$

where $B = \frac{B_1}{B_2}$,

$$\begin{aligned} B_1 &= 3\sin(\tilde{\theta} - \Delta\theta)\cos(\tilde{\theta} - \Delta\theta)(\tilde{\theta}^2 - (\tilde{\theta} - \Delta\theta)^2) \\ &- 3(\tilde{\theta} - \Delta\theta)(\sin^2\tilde{\theta} - \sin^2(\tilde{\theta} - \Delta\theta)), \\ B_2 &= 12(\tilde{\theta} - \Delta\theta)(\tilde{\theta}\sin\tilde{\theta} - (\tilde{\theta} - \Delta\theta)\sin(\tilde{\theta} - \Delta\theta)) \\ &+ 4(\tilde{\theta} - \Delta\theta)(\cos\tilde{\theta} - \cos(\tilde{\theta} - \Delta\theta)) \\ &- (\tilde{\theta}^2 - (\tilde{\theta} - \Delta\theta)^2) \\ &\cdot (6(\tilde{\theta} - \Delta\theta)\cos(\tilde{\theta} - \Delta\theta) + 4\sin(\tilde{\theta} - \Delta\theta)). \end{aligned} \tag{3-25}$$

The constant *A* can be determined from Eq. 3-21:

$$A = ((\pm\cos\tilde{\theta} + 2B)^2 + (\mp 2\sin\tilde{\theta} - 3B\tilde{\theta})^2)^{-1/2}. \tag{3-26}$$

Equation 3-24 is solved numerically. It can have up to 6 solutions, but some of them are eliminated due to Eq. 3-20. The correspondence to the hodographs of the first and/or the second type equation roots stays.

By altering $\tilde{\theta}$ and determining the corresponding $\Delta\theta$, one can obtain the dependencies between the distance between the impulses of one manoeuvring interval $\Delta\theta$ and the flyby interval length $2\tilde{\theta}$.

These dependencies are depicted in Fig. 3-8.

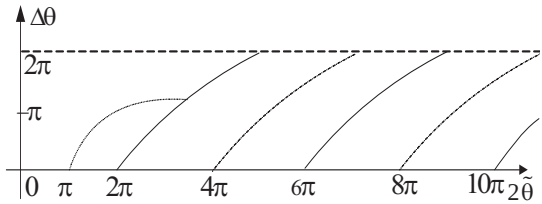

Fig. 3-8. Distances between impulses as a function of flyby duration

The solid lines correspond to a hodograph of the first type and the dash-dot lines correspond to a hodograph of the second type. The continuous existence interval length of each of the solutions is 3π. With the angular distance of the flyby $[2\pi n, 2\pi n + \pi]$, the solutions of both types exist. On the intervals $[3\pi + 4\pi(N-1), 4\pi N]$, the solutions for a hodograph of the first type exist, while on the intervals $[5\pi + 4\pi(M-1), 6\pi + 4\pi(M-1)]$, the solutions for a hodograph of the second type exist. The first dependency plotted with dots, which corresponds to the hodograph "with one closed loop", is an exception (Prussing 1969, 928-935). In the following discussion, the values of *N* and *M* will be used as the ordinal item of the continuous curves, corresponding to hodographs of the first and second types.

The dependency $\Delta\theta = f(\tilde{\theta})$ can be conveniently written as a function of two variables: $\Delta\theta = f^*(\tilde{\theta}^*, N)$, where $\tilde{\theta}^* = \tilde{\theta} - 2\pi - 4\pi(N-1)$, $\tilde{\theta}^* \in [0, 3\pi]$. As depicted in Fig. 3-8, the dependencies are close to each other: the function f^* has a weak dependency on *N* and the alteration $\Delta\theta$ on the interval $[0, 3\pi]$ is determined mainly by the value $\tilde{\theta}^*$. Fig. 3-9a presents the dependency between $\Delta\theta$ and $\tilde{\theta}^*$ for *N* = 5. Its difference from the dependencies, obtained for a large value of *N*, do not exceed 0.2°

on all intervals $[0,3\pi]$, while the difference to the dependencies for smaller N is depicted in Fig. 3-9b. A similar situation occurs for dependencies obtained for the second-type hodograph.

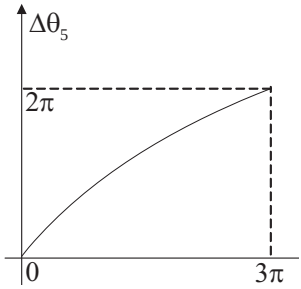

Fig. 3-9 (a). Angular distance between impulses as a function of flyby duration for $N = 5$

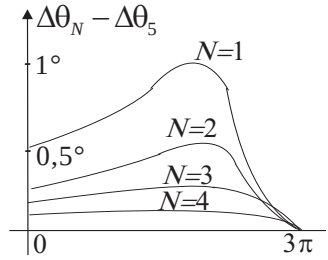

Fig. 3-9 (b). Difference in angular distances between impulses vs. various values of N

Besides the impulse application angles, the primer vector hodograph allows us to determine the impulse orientation. After evaluating $\Delta\theta$ from Eq. 3-24, the constants A and B are determined with the help of eqs. 3-25 and 3-26, λ, μ in the points θ_1, θ_2 are calculated. The dependencies between the pitches $\vartheta = \operatorname{arctg}\dfrac{\lambda}{\mu}$ and $\tilde{\theta}^*$ for the outer impulses are depicted in Fig. 3-10a. Similar dependencies for the inner impulses are depicted in Fig. 3-10b.

According to the figure, the ratio λ/μ is small for the inner impulses, and they can be assumed to be purely transversal. In the case of the outer impulses, it is necessary to account for their radial components.

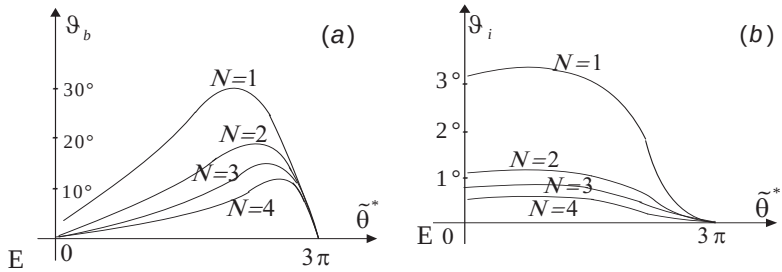

Fig. 3-10. Pitches of impulses as a function of flyby duration:
(*a*) outer impulses (*b*) inner impulses

In order to quicken the optimal flyby parameter determination process, the dependencies $\Delta\theta(\tilde{\theta})^*$ and $\frac{\lambda}{\mu}(\tilde{\theta}^*)$, for hodographs of the first and second types, can be approximated with the analytical equations (Baranov and Terekhova 1995, 382-387). These equations should be both accurate and relatively simple. The function $\Delta\theta(\tilde{\theta})^*$ can be approximated with the cubic parabola:

$$\Delta\theta = a(\tilde{\theta}^*)^3 + b(\tilde{\theta}^*)^2 + c\tilde{\theta}^* + d. \qquad (3\text{-}27)$$

In the meantime, the dependency between $\Delta\theta$ and *N* or *M* can be neglected due to the proximity of the curves to each other with various values for *N* and *M*. There is a common dependency of $\tilde{\theta}^*$ for all curves, corresponding to the first-type hodograph. Its coefficients, *a*, *b*, *c*, and *d*, have been determined with the help of the least squares method: $a = -0.00125, b = 0.003475, c = 0.74309, d = 0$. For the function, which corresponds to the second-type hodograph, the coefficients *a*, *b*, *c*, and *d* will have the following values:
$a = -0.001213, b = 0.00302, c = 0.74444, d = 0.$
For a hodograph "with one closed loop":
$a = 0.00575, b = -0.11271, c = 1.15557, d = -2.52301.$

The difference between $\Delta\theta$, obtained from Eq. 3-27, and $\Delta\theta$, obtained from Eq. 3-24, does not exceed 0.7º for the hodograph of the first type and 0.55º for the hodograph of the second type. The peculiar distribution of $\Delta\theta = \Delta\theta_{num} - \Delta\theta_{analyt}$, as a function of $\tilde{\theta}^*$ for $N = 3$, is depicted in Fig. 3-11.

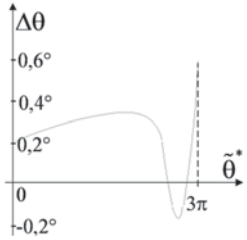

Fig. 3-11. Discrepancy in the difference of the application angle for analytical and numerical solutions

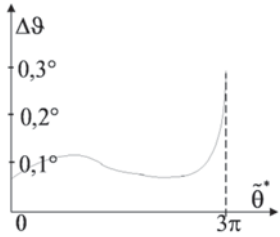

Fig. 3-12. Difference between impulse pitches for analytical and numerical solutions

Thus, a very simple and sufficiently accurate equation for the analytical determination of the impulse application angle of the optimal solution is found.

For the analytical approximation of the function $\frac{\lambda}{\mu}(\tilde{\theta}^*)$ for the outer impulses, we can use the equation:

$$\frac{\lambda}{\mu}\left(\tilde{\theta}^*\right) = l\left(3\pi - \tilde{\theta}^*\right)^{g \cdot e^{f(3\pi - \tilde{\theta}^*)}}, \tag{3-28}$$

where the coefficients *l*, *g*, and *f* depend on *N* (for the hodograph of the first type) or *M* (for the hodograph of the second type). For the hodographs of the first type:

$$l = 0.3605805\, e^{-0.2073523\, N} + 0.1938393\,, \tag{3-29a}$$

$$g = 0.7413017 e^{-0.6305316 N} + 1.1037093 e^{-0.04167616 N}, \tag{3-29b}$$

$$f = -0.1733134 e^{0.0305692 N} - 0.55892376, \tag{3-29c}$$

and for the hodographs of the second type:

$$l = 0.39946973\, e^{-0.19462509\, M} + 0.18542422\,, \tag{3-30a}$$

$$g = 0.90946358 e^{-0.5468307 M} + 1.0936807 e^{-0.03895865 M}, \tag{3-30b}$$

$$f = -0.24736464 e^{0.259488 M} - 0.48186975. \tag{3-30c}$$

With equal values of *N* and *M* greater than 10, the values $\frac{\lambda}{\mu}$ for the hodographs of the first and the second types practically coincide. The dependence between the coefficients *l*, *g*, *f*, and *N* for the first-type hodograph can be described as:

$$l = 0.2918171\, e^{-0.05347094\, N} + 0.0622614\,, \tag{3-31a}$$

$$g = 0.8709496 e^{-0.03271924 N} + 0.09475382, \tag{3-31b}$$

$$f = 0.0000574 N^2 - 0.0040646 N - 0.7591687. \tag{3-31c}$$

The same equations can be used for the second-type hodograph, but the replacement of *N* by *M* is needed.

Equation 3-28 approximates $\frac{\lambda}{\mu}(\tilde{\theta}^*)$ with good accuracy (≈1 %) for $0 \le \tilde{\theta}^* \le 2.22\pi$. The error increases with increasing $\tilde{\theta}^*$, but on the interval $2.22\pi \le \tilde{\theta}^* \le 3\pi$ it does not exceed 10 % of $\frac{\lambda}{\mu}$ (for dependencies with $N \le 50$). The distribution of $\Delta\vartheta = \Delta\vartheta_{num} - \Delta\vartheta_{analyt}$, as a function of $\tilde{\theta}^*$ for $N = 20$, is presented in Fig. 3-12, where $\vartheta = \text{arctg}(\frac{\lambda}{\mu})$.

With magnitudes of $N > 50$ on the interval $0 \le \tilde{\theta}^* \le 2.45\pi$, the value $\vartheta = \text{arctg}(\frac{\lambda}{\mu})$ does not exceed 0.1º and the maximum ϑ on the interval $2.45\pi \le \tilde{\theta}^* \le 3\pi$ does not exceed 3º. This allows us to assume that the outer impulses of the optimal solution for a flyby with a duration greater than 100 revolutions are purely transversal. The hodograph with "one closed loop" $\frac{\lambda}{\mu}$ as a function of $\tilde{\theta}^*$ can be described with the equation:

$$\frac{\lambda}{\mu}(\tilde{\theta}^*) = (1.15557\tilde{\theta}^{*2} - 6.06497\tilde{\theta}^* + 9.51334)^{-1}. \qquad (3\text{-}32)$$

As such, with a fixed angular distance of transfer $\theta_f - \theta_b$, the application and orientation angles of the impulses of the optimal four-impulse manoeuvre can easily be found using eqs. 3-27 and 3-28. Then, using eqs. 3-1a to 3-1d, we can unambiguously determine the impulse magnitudes. If the signs of the transversal impulse components of one manoeuvring interval coincide, the solution will belong to the considered CNS class and will be locally optimal.

It is worth mentioning that the simplification of the parameter determination process for the four-impulse nondegenerate rendezvous problem was attempted in the work of Alvarez and Carter (2000, 109-117). The material in section 3.4.1 has previously been published in the work of Baranov and Terekhova (1993) and Baranov and Terekhova (1995, 382-387) (Russian and English versions).

3.4.2. Parameter Determination for the Two and Three-Impulse Solutions

In order to find the globally optimal solution, it is necessary to find more two and three-impulse solutions that meet the necessary optimality constraints and compare the total delta-vs of these solutions.

We can use the iterative procedures in paragraph 3.2 for the parameter determination of this type of solution. Since the pitches of the inner impulses are small, the intersection points of the circles with radii R_1 and R_2 (only the signs of ΔV_{t_1} and ΔV_{t_2} are different) correspond to the two-impulse solution as well. The parameter determination procedure for these solutions was described earlier. The start of the first manoeuvring interval $\varphi_1 = \varphi_{I_l}$ and the end of the second manoeuvring interval $\varphi_3 = \varphi_{II_r}$ (for the two impulses, the first one and the last one are applied at points where the cycloid intersects with the circle) are taken as the fixed angles of the impulse application for the three-impulse solution. Then, with the help of eqs. 3-11a to 3-11c, the magnitudes of the transversal impulse component and the application angle of the inner impulse φ_2 are determined. If three-impulse solutions of this type exist, then the moment of osculation of the cycloid and the circle correspond to this angle. The manoeuvre parameters are updated with the help of the iterative procedure.

The procedure of searching for the parameter solution with a single impulse applied on the boundary and the other two applied at points of the osculation of the cycloid with the circle is more complicated. On the interval in which two manoeuvres are applied, one of the impulses should also be applied on the outer boundary of the interval φ_{II_r}. Hence, the application moment of this impulse is known $\varphi_3 = \varphi_{II_r}$. The application moment of the second impulse of this interval is chosen inside the interval $\varphi_2 = \varphi_{II_f}$. The approximate value of the transversal impulse component of the first manoeuvring interval ΔV_{t_1} can be determined by Eq. 3-5, or, more accurately, by Eq. 3-11e. After this the application angle of the first impulse φ_1 and the impulse magnitudes ΔV_{t_2} and ΔV_{t_3} are evaluated by eqs. 3-1a to 3-1c (Baranov 1985):

$$\varphi_1 = \arccos\left(\frac{\Delta e_y}{2\Delta V_{t_1}} \sin\frac{\varphi_2+\varphi_3}{2} + \frac{\Delta e_x}{2\Delta V_{t_1}} \cos\frac{\varphi_2+\varphi_3}{2} + \right.$$

$$\left. + \left(1 - \frac{\Delta a}{2\Delta V_{t_1}}\right) \cos\frac{\varphi_3-\varphi_2}{2}\right) - \frac{\varphi_3-\varphi_2}{2} - 2\pi n,$$

$$\Delta V_{t_3} = (\Delta e_x + (2\Delta V_{t_1} - \Delta a)\cos\varphi_2 -$$

$$- 2\Delta V_{t_1}\cos\varphi_1) \frac{1}{2(\cos\varphi_3 - \cos\varphi_2)},$$

$$\Delta V_{t_2} = \frac{1}{2}\Delta a - \Delta V_{t_1} - \Delta V_{t_3}.$$

As always, the manoeuvre parameters are updated with the help of the iterative procedure in order to solve the fourth equation of Eq. 3-1 with the desired tolerance. After the manoeuvre parameter determination, the total delta-v solution is calculated. By varying the position of the second impulse on the manoeuvring interval, one can find the optimal solution of this type. The simple point enumeration from the corresponding manoeuvring interval with a constant step can be used for this purpose.

3.4.3. Examples

As an example of implementing the method mentioned above, let us consider the optimal manoeuvre parameter determination problem, which leads to the alteration of the spacecraft's position on the circular orbit and the transfer to the set point for the fixed time (the orbital plane orientation alteration that occurs is not important here). The problem in this statement has been considered in the works of a number of authors.

By using the aforementioned equations, we can analytically find the parameters of optimal four-impulse solutions. It is interesting to compare the total delta-vs of the obtained solutions with the total delta-vs of the two-impulse and the "rational" four-impulse manoeuvres in the works of Ivashkin and Raykunov (1991, 352-374) and Ivashkin and Raykunov (1994, 33-46). The inner impulses are half a revolution distant for the "rational" four-impulse manoeuvres.

For this problem, $\Delta e_x = \Delta e_y = \Delta a = 0$. The angle $\tilde{\theta}^*$ fully determines the nature of the optimal solution, Δt determines only the sums of the impulse magnitudes of the first and the second manoeuvring intervals (

$\Delta t = 0.01$ was chosen for the calculations). The research was conducted using $N = 1$, and $\tilde{\theta}^*$ was taken in the range $\left[0^\circ, 360^\circ\right]$

It turned out that the optimal four-impulse solutions exist for $\tilde{\theta}^* \in \left[0^\circ, 339^\circ\right]$. Figure 3-13 presents the appearances of the optimal solutions for various $\tilde{\theta}^*$.

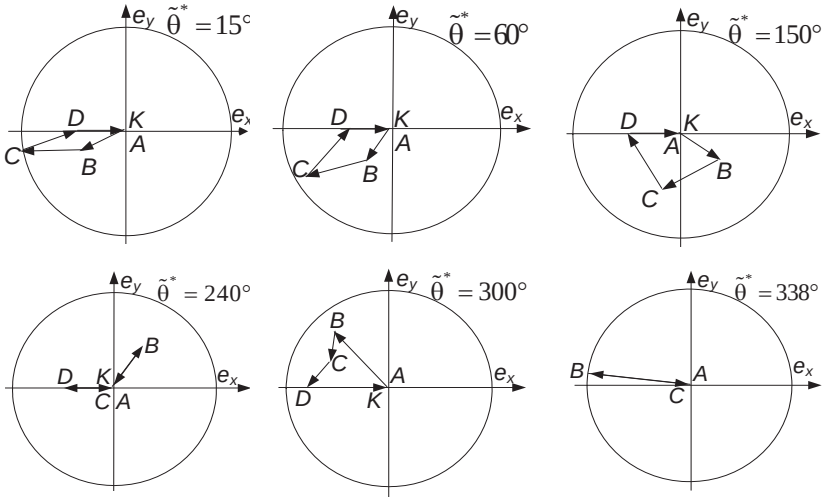

Fig. 3-13. Optimal solutions for various transfer distances

From Fig. 3-13, it follows that there are no optimal three-impulse solutions for the circular orbit change in position problem. It does not matter which are the first impulses to be used (to which the line segments *AB* and *BC* correspond), line segment *CK* should correspond to the third impulse, but the application angle of this impulse does not coincide with the possible optimal impulse application angles, to which the line segments *CD* and *DK* correspond (besides, the third base of the triangle would have to be equal to the sum of the other two, which is impossible).

Table 3-1 gives the total delta-vs of the optimal (ΔV_{opt}) and the "rational" (ΔV_{r4}) four-impulse solutions, and also the total delta-vs of the two-impulse solutions (ΔV_2) and their ratio in percent. The "rational" scheme has equal impulses. The magnitudes of the outer impulses differ from the magnitudes of the inner impulses for the optimal scheme.

Table 3-1

$\tilde{\theta}^*$ deg	ΔV_{opt}	ΔV_{r4}	$\frac{\Delta V_{opt}}{\Delta V_{r4}}$	ΔV_2	$\frac{\Delta V_{opt}}{\Delta V_2}$
5	1.060	2.065	51.35	1.070	99.1
15	1.0598	1.698	54.10	1.113	95.22
30	1.0594	1.819	58.24	1.242	77.88
45	1.058	1.698	62.32	1.452	72.89
60	1.0569	1.592	66.40	1.546	68.35
90	1.0506	1.415	74.26	2.870	36.59
120	1.050	1.273	82.46	6.400	16.41
150	1.0385	1.158	89.72	47.780	2.12
180	0.9857	1.061	92.90	5.000	19.72
210	0.9389	0.979	95.86	2.52	37.26
240	0.8745	0.9095	96.15	1.59	55.00
270	0.7900	0.849	93.07	1.09	72.48
300	0.6850	0.796	86.08	0.78	87.82
330	0.5620	0,749	75.03	0.593	99.77
338	0.5269	0.737	71.45	0.563	93.60
355	-	0.714	-	0.5303	-
360	-	0.796	-	0.5305	-

With small $\tilde{\theta}^*, \Delta\theta (\Delta\theta \approx \frac{2}{3}\tilde{\theta}^*)$ is small as well. Hence, the first two impulses are applied at the beginning of the flyby and the last two impulses are applied at the flyby's end. The total delta-v of the optimal scheme is close to the total delta-v of the two-impulse scheme. Due to the considerably longer duration of the motion along the drift orbit, we get a notable gain in total delta-v in comparison to the "rational" scheme.

With the increase in $\tilde{\theta}^*, \Delta\theta$ increases and, hence, the optimal solution total delta-vs get closer to the total delta-vs of the "rational" solutions, but the total delta-vs of the two-impulse solutions worsen considerably.

With $\tilde{\theta}^* \approx 240^\circ$, when $\Delta\theta \approx 180^\circ$, the total delta-vs of the optimal and "rational" solutions practically coincide. With the further increase of $\tilde{\theta}^*, \Delta\theta$ keeps on increasing, but the total delta-vs of the optimal solutions become considerably smaller than the total delta-vs of the "rational" solutions due to the increase in the outer impulse magnitude and the decrease in the inner impulse magnitudes, once again. The total delta-vs of

the optimal solutions get closer to the total delta-vs of the two-impulse solutions. When $\tilde{\theta}^*$ becomes equal to approximately 339º (the exact value depends on *N*), the magnitude of the inner impulses decreases to zero. The optimal four-impulse solution degenerates to a two-impulse solution. With a further increase in $\tilde{\theta}^*$, the optimal-by-primer-vector four-impulse solutions cease to exist. For the interval $\left[339^\circ, 360^\circ\right]$ a two-impulse flyby is optimal.

As can be seen from the table, the optimal four-impulse solution results in maximum profit with $\tilde{\theta}^* = 60^\circ$. With these angles, the optimal solution total delta-vs are more than 30 % smaller than the delta-vs of the "rational" or two-impulse solutions.

With the increase in *N*, when the duration of presence on the drift orbit increases, the difference between the total delta-vs of the optimal and "rational" schemes decreases. For example, for $N = 10, \tilde{\theta}^* = 30^\circ$, the total delta-v of the optimal scheme is only 5 % smaller than the total delta-v of the "rational" scheme.

The change in position problem on the circular orbit draws our attention. It has been considered many times in the works of a number of authors and will continue to be considered in the future. It appears that the report by Trofimov (2014, 140-141) is one of the most recent. In this work, a comparison of the four-impulse and two-impulse solutions has been conducted. A similar comparison is listed in the last column of table 3-1 in Baranov and Terekhova (1993).

3.5. Existence Domains of Various Solution Types

Analysis of the relative positions of the circles with radii R_1 and R_2 and various values of Δu (the difference of the angular positions of the target and active spacecraft in the initial moment of time (the initial phase)) can help us identify the existence domains of various solution types.

3.5.1. Nonintersecting Orbits

First of all, let us consider the variant when the orbits do not intersect. We will assume that $\Delta e_y = 0,\ \Delta e_x > 0,$ and $\Delta a > \left|\Delta e_x\right|$ for the sake of certainty. We suppose the target spacecraft, which is situated on the outer orbit, is behind the active spacecraft in the initial moment, i.e. $\Delta u < 0,$ for

example, $\Delta u = \Delta u_I$ (Fig. 3-14a). Then, it is necessary to apply impulses with the positive transversal components on the first manoeuvring interval with the sum value ΔV_{t_I}, which is greater than $|\Delta a|/2$, in order to transfer to the orbit with a semimajor axis greater than the target spacecraft orbit's semimajor axis. This will allow the target spacecraft to catch up to the active spacecraft. Impulses with the sum value of $\Delta V_{t_{II}} < 0$ should be applied on the final interval.

The circle of radius R_2 is entirely located inside the circle of radius R_1 (Fig. 3-15a) for all $\Delta u < 0$. In this figure, the large circle corresponds to the impulses of the first manoeuvring interval, while the smaller one corresponds to the impulses of the second manoeuvring interval; the signs of ΔV_{t_I} and $\Delta V_{t_{II}}$ are different and, thus, the nondegenerate solution (CNS) will be optimal. Since the circles do not intersect, only the three and four-impulse solutions are possible. The three-impulse solution is possible only with two burns on the first manoeuvring interval.

The existence domains of various solution types and the number of possible-to-use impulses are depicted in Fig. 3-14a (Baranov 1989, 689-697). The digit "2" in the brackets before the digit "3" means that two impulses of the three-impulse solution should be applied on the first manoeuvring interval. The digit "2" in the brackets after the digit "3" means that two impulses should be applied on the second manoeuvring interval.

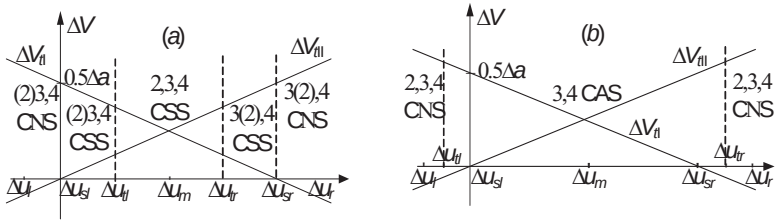

Fig. 3-14. Various type-solution existence domains:
(*a*) nonintersecting orbits (*b*) intersecting orbits

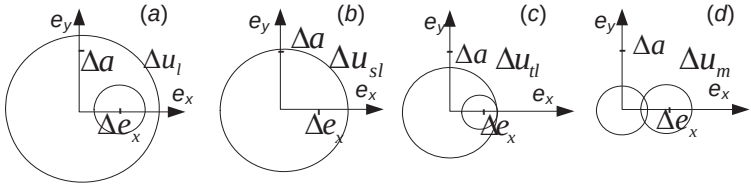

Fig. 3-15. Alteration of circle positions, corresponding to the sum of the transversal impulse components of the first and second manoeuvring intervals for nonintersecting orbits with alteration of the initial phase value

If $\Delta u = \Delta u_{sl} \approx 0$ (hereafter, we will denote the moments when the radius of one of the circles is zero by the index "*s*" and we will denote the moments when the circles osculate by the index "*t*"). Then, we can transfer to the required point of the final orbit by the impulses of the first manoeuvring interval. Certainly, only the qualitative manoeuvring picture is considered and the flyby time to the final orbit is not accounted for. The positions of the circles in Fig. 3-15b correspond to this case. The radius of the second circle, decreasing with the increase in Δu, becomes zero at this moment.

When $\Delta u_{sl} < \Delta u < \Delta u_{tl}$, the impulses on the first manoeuvring interval produce only a part of the necessary alteration of the semimajor axis, the rest is produced by the impulses of the second manoeuvring interval. The signs of ΔV_{t_I} and $\Delta V_{t_{II}}$ coincide and CSS solutions are available. After Δu_{sl}, the radius of the second circle increases with the increase in Δu. The circles, which correspond to Δu from this interval, do not intersect and, thus, only three and four-impulse CSS solutions are possible (Fig. 3-14a). The first manoeuvring interval should contain two impulses, just as in CNS solutions. The moment of the circles' osculation $(\Delta u = \Delta u_{tl})$ is depicted in Fig. 3-15c.

The circles intersect on the interval $\Delta u_{tl} < \Delta u < \Delta u_{tr}$, hence, the two, three, and four-impulse CSS solutions exist (Fig. 3-14a). The moment when the circles have equal radii $(\Delta u = \Delta u_m)$ is depicted in Fig. 3-15d.

With $\Delta u > \Delta u_m$ the picture becomes symmetrically mirrored, i.e. the same types of solutions exist, but ΔV_{t_I} and $\Delta V_{t_{II}}$ change places.

When $\Delta u > \Delta u_{sr}$, the target spacecraft is situated too far ahead of the active spacecraft. Firstly, the semimajor axis of the active spacecraft

should be decreased in order to catch up to the target spacecraft during phasing; then, the semimajor axis can be increased up to the required value by the impulses of the second manoeuvring interval. For these values of Δu, the three or four-impulse nondegenerate CNS solutions will be optimal.

The values of Δu, which lead to the alteration of the signs ΔV_{t_I} or $\Delta V_{t_{II}}$ and, correspondingly, to the change in the solution type, can be assessed. The sum of the transversal impulse components of the first manoeuvring interval ΔV_{t_I} changes its sign with $\Delta u = \Delta u_{sl} \approx 0$, while the sum of the transversal impulse components of the second manoeuvring interval $\Delta V_{t_{II}}$, changes its sign with $\Delta u = \Delta u_{sr} \approx 3\pi\Delta a N$, where N = the number of revolutions from the beginning of the first manoeuvring interval up to the rendezvous point.

The osculation of the circles for the case when the radius of the first circle is greater than the radius of the second (Fig. 3-15c), occurs with:

$$\Delta V_{t_I} = \frac{1}{4}(\Delta a + \Delta e), \tag{3-33a}$$

$$\Delta V_{t_{II}} = \frac{1}{4}(\Delta a - \Delta e), \tag{3-33b}$$

Hence,

$$\Delta u_{tl} = \frac{3}{2}\pi N(\Delta a - \Delta e). \tag{3-34}$$

The osculation of the circles in the case when the radius of the second orbit is greater than the radius of the first, occurs with:

$$\Delta V_{t_I} = \frac{1}{4}(\Delta a - \Delta e), \tag{3-35a}$$

$$\Delta V_{t_{II}} = \frac{1}{4}(\Delta a + \Delta e). \tag{3-35b}$$

Hence,

$$\Delta u_{tr} = \frac{3}{2}\pi N(\Delta a + \Delta e). \tag{3-36}$$

3.5.2. Intersecting Orbits

Figure 3-14b gives the dependencies between the values $\Delta V_{t_I}, \Delta V_{t_{II}}$ and Δu for the intersecting orbits. We also assume $\Delta a > 0$ for certainty.

The examples of the locations of the circles with radii R_1 and R_2 for the phase differences $\Delta u_l, \Delta u_{tl}, \Delta u_{sl}, \Delta u_m$ are depicted in Fig. 3-16. The ratio of the circle radii will be inverted for those moments of time that are symmetrical relative to Δu_m.

As can be seen from the figure, with $\Delta u < \Delta u_{tl}$ and $\Delta u > \Delta u_{tr}$ the circles intersect (3-16a) and $\Delta V_{t_I} \Delta V_{t_{II}} < 0$, hence, the CNS-type solution will be optimal. Two, three, and four-impulse solutions are possible.

With $\Delta u_{tl} < \Delta u < \Delta u_{tr}$, the circles do not have common points and, thus, the three and four-impulse CAS solutions will be optimal. The calculation of the magnitudes $\Delta u_{tl}, \Delta u_{tr}$ is undertaken by the same equations, 3-34 and 3-36. The different type-solution existence domains and the number of burns, which can be used for the acquisition of the optimal solution, are listed in Fig. 3-14b.

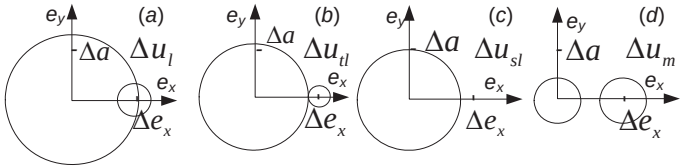

Fig. 3-16. Alteration of the circle locations, which correspond to the sum of the transversal impulse components of the first and second manoeuvring intervals for intersecting orbits with alteration of the initial phase

Summing up this chapter, the following simplest algorithm for optimal solution parameter searching can be suggested. The magnitudes $\Delta u_{tl}, \Delta u_{tr}$ can be found using eqs. 3-34 and 3-36. By comparing them to the magnitude of deviation by the phase Δu, we can determine which manoeuvring interval should have two impulses. The parameters of the apsidal three-impulse solution can be found unambiguously from eqs. 3-1a to 3-1d. If the obtained solution is of the CSS or CAS-type and fulfills the constraints on the moments of impulse application, then the problem is solved. Otherwise, the algorithms from the third paragraph of this chapter should be used in the search for the optimal solution.

3.6. Four-Impulse Nondegenerate Solution Existence Domains

As has been already mentioned, the CNS solution exists if the circles of radii R_1 and R_2 have common points and the signs of ΔV_{t_I} and $\Delta V_{t_{II}}$ do not coincide. It is obvious that the greater the area of the circles that is occupied by their intersection, the more different CNS solutions exist. The relative positions of the circles depend on the difference between the eccentricities Δe, determining the distance between their centers, and on Δa and $\Delta t / 3\varphi_{10}$, determining the magnitudes of their radii. For the determination of the four-impulse nondegenerate solution existence domain, one can fix Δe and investigate the dependency of the existence of the CNS from Δa and $\Delta t / 3\varphi_{10}$, as only the relative area of the circles' intersection is important. The research was conducted for $\Delta e = 0.01$. The four-impulse CNS solution existence domains are depicted in figs. 3-17 and 3-18 (Baranov and Terekhova 1993).

As has already been noted, the major influence on the primer vector hodograph is caused by $\tilde{\theta}^*$. This variable, which is crucial for the existence of the CNS solution, is put on the *x* axis on all the graphs. The angle $\tilde{\theta}^*$ alters in the range 0 to 360º. On this interval, solutions of both types exist in the range 0 to 180º and the solution of one type exists in the range 180 to 360º (Fig. 3-7). It is more convenient to investigate the existence of the hodograph of one type (in this case, the second type) on the interval 0 to 540º. This is acceptable because the first-type hodograph versus $\tilde{\theta}^*$ on the interval 0 to 180º practically coincides with the second-type hodograph versus $\tilde{\theta}^*$ on the interval 360 to 540º. The primer vector hodograph depends weakly on *N* and the radii of the circles depend on *N* only by the ratio $\Delta t / 3\varphi_{10}$, allowing us to conduct an investigation into the constant value of $N = 10$, while the alteration of the ratio $\Delta t / 3\varphi_{10}$ is undertaken by changing Δt. The values of Δt are depicted in the upper right corner of each graph. The values of Δa in the bottom of the figure belong to all graphs from the corresponding columns. The existence of CNS-type solutions strongly depends on the angle ω, which sets the orientation of the apsidal line relative to the direction on the rendezvous point. This angle is put on the *y* axis on graphs.

Let us consider how the appearance of the CNS existence domain depends on Δt and Δa. Narrow S-like areas can be seen for small Δt (the first figure in each column). This is connected to the smallness of the radius of the first

circle; it can be assumed that the major influence on the existence of the solution is due to the impulse locations of the second manoeuvring interval.

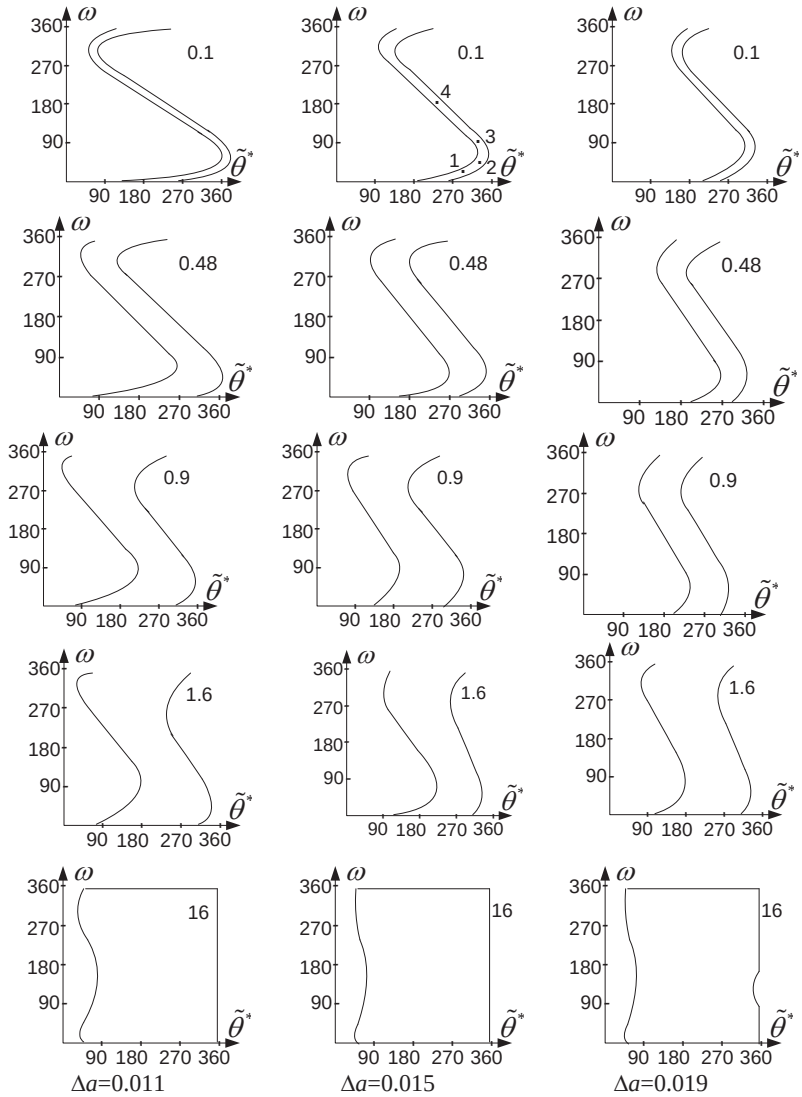

Fig. 3-17. Existence domains of four-impulse nondegenerate solutions for nonintersecting orbits

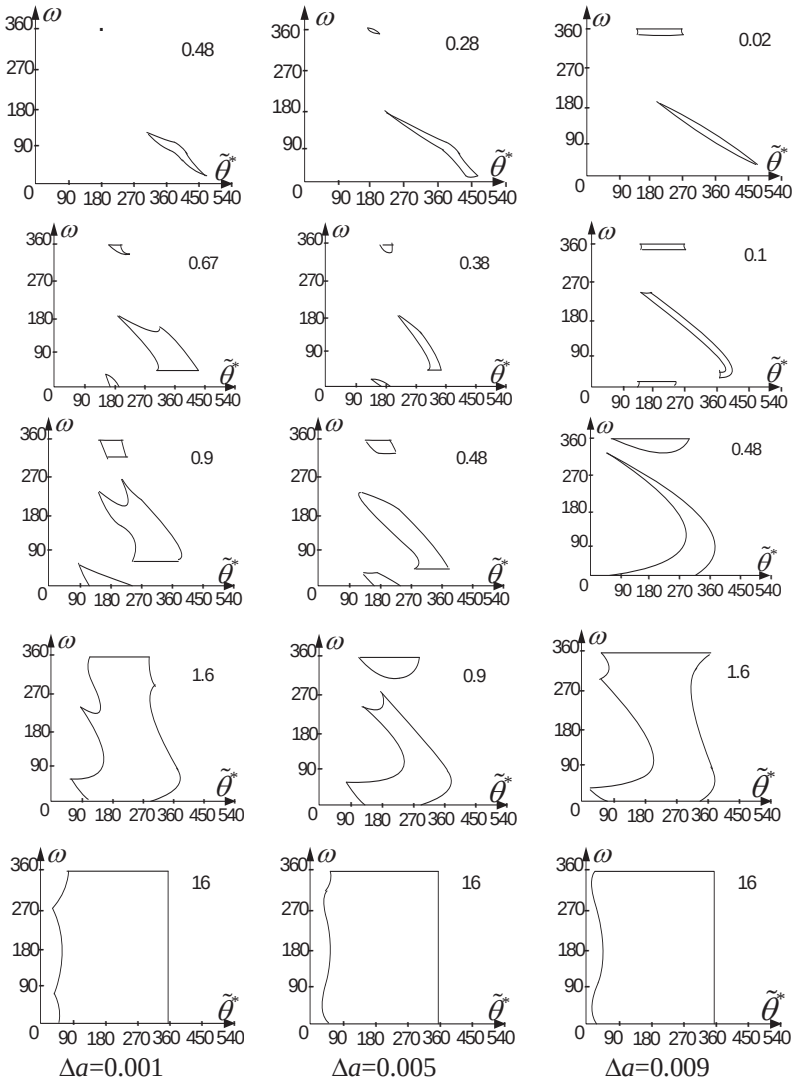

Fig. 3-18. Existence domains of four-impulse nondegenerate solutions for intersecting orbits

Let us draw the solutions, which correspond to the different points from Fig. 3-17 (the point marked with the digits), on one figure (Fig. 3-19). We will assume that the transfer is always fulfilled to one point $(\Delta e_x,0)$. With this representation, the line segment corresponding to the last impulse turns out to be rotated by angle ω relative to axis e_x (in reality, the line segment depicting this impulse is parallel to axis e_x and the line segment, which connects the reference frame origin with the point $(\Delta e_x, \Delta e_y)$, is rotated by angle ω).

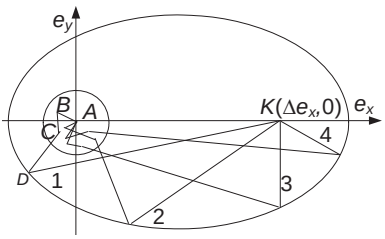

Fig. 3-19. Four-impulse nondegenerate solutions for various values of angle ω with small $\Delta t/3\varphi$

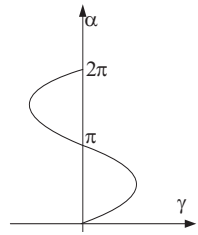

Fig. 3-20. Inclination angle between the focal radius and the main axis of the ellipse as a function of the angle between the radii

The sums of the impulses of the last manoeuvring intervals of these solutions are approximately the same $(\Delta V_{t_3} + \Delta V_{t_4} \approx \frac{1}{2}\Delta a - \frac{\Delta t}{3\varphi_{I_0}})$. The point of the line segment's start, which depicts the third impulse, is close to the reference frame origin due to the smallness of the radius of the first circle. Thus, the end of this line segment lies in the vicinity of the ellipse with the points of focus $(0,0)$ and $(\Delta e_x,0)$. Hence, angle ω, as a function of angle $\Delta\theta$ between the third and fourth impulses, is close to angle α (the inclination angle between the focal radius r_2 and axis e_x) as a function of angle γ (the angle between the focal radii of the ellipse). This function has a particular S-based appearance (Fig. 3-20). The appearance of the curved line depends on the parameters of the ellipse: the greater the magnitude of the semimajor axis with the constant distance between the focuses, the less curved the line is. The function $\omega(\tilde{\theta}^*)$ can be considered

as a complex function $\omega(\Delta\theta(\tilde{\theta}^*))$. Since the function $\Delta\theta(\tilde{\theta}^*)$ is close to the linear function (see figs. 3-8 and 3-27), the appearance of the curved line $\omega(\tilde{\theta}^*)$ is determined basically by the function $\omega(\Delta\theta)$. Changes in the appearance of the CNS solution existence domains can be explained by the increase in Δa (see Fig. 3-17).

The smoothing of the curved line due to the increase in the radius of the second circle also occurs with the increase in $\Delta t(\Delta a = \text{const})$. In this case, the radius of the first circle increases, leading to an increase in the number of acceptable solutions due to greater uncertainty in the position of the left focus of the ellipse. It can be seen in Fig. 3-17 that the CNS existence domain area widens with the increase in Δt.

The similar appearance and the dependency of Δa and Δt can be seen in the graphs for the variant $\Delta e > \Delta a$ (Fig. 3-18). In this case, the impulses of the first manoeuvring interval have greater influence and must transfer point *C* to the area of the circles' intersection. If this does not happen (as a rule it happens for small Δt and $\omega > 180^\circ$), then the solutions, which are present on the graphs for $\Delta e < \Delta a$, are not present on the graphs with $\Delta e > \Delta a$.

The common feature of the graphs in figs. 3-17 and 3-18 is the absence of solutions with small $\tilde{\theta}^*$ and the absence of solutions with $\tilde{\theta}^* > 360^\circ$ for big values of Δt.

The absence of solutions with small $\tilde{\theta}^*$ is evident because, due to the small $\Delta\theta$, the four-impulse solutions do not differ much from the two-impulse solutions. They exist only for transfers between the two points on the same circular orbit, or for transfers between the intersecting orbits in a narrow range of angles.

With big magnitudes of $\Delta t / 3\varphi_{10}$, the radii of the circles considerably exceed the distance between their centers. With the flyby, the angles $\tilde{\theta}^*$ close to 2π magnitudes of the outer impulses considerably exceed the magnitudes of the inner impulses (Fig. 3-21a). Thus, the existence of CNS solutions depends on the relative orientation of the outer impulses.

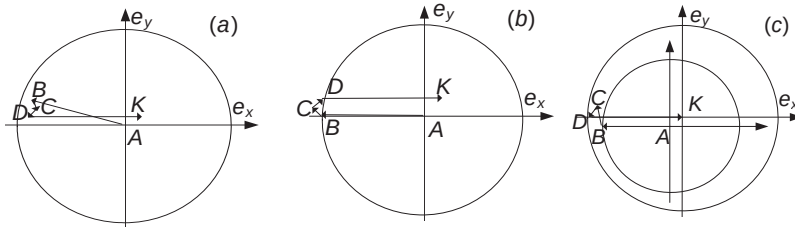

Fig. 3-21. For solutions with angles in the flyby of $\tilde{\theta}^*$ close to 2π, the values of the outer impulse solutions are considerably greater than the values of the inner impulses:
(*a*) $\tilde{\theta}^* < 2\pi$ optimal solution;
(*b*), (*c*) $\tilde{\theta}^* > 2\pi$ nonoptimal solutions.

With $\tilde{\theta}^* < 2\pi$, point *B*, being the end of the line segment and depicting the first impulse, is above the line segment depicting the last impulse. Since $\Delta\theta \approx 240^\circ$ in this case, the transfer from point *B* to point *D* is fulfilled by the inner impulses, which have the same signs of the transversal impulses as the outer impulses of the corresponding manoeuvring interval. These solutions are CNS-type solutions. If $\tilde{\theta}^* > 2\pi$, then point *B* lies below line segment *DK*. In this case, either one (Fig. 3-21c) or both (Fig. 3-21b) transversal impulses have the signs of the transversal components; these do not coincide with the signs of the transversal components of the outer impulses, which correspond to the manoeuvring intervals, hence, these are not CNS-type solutions.

As was previously mentioned, for this example, the solutions of the second type on the interval 360 to 540º correspond to the solutions of the first type on the interval 0 to 180º. It can be seen in the graphs that the solutions of both types do not exist simultaneously, not even for considerable values of $\Delta t / 3\varphi$, when the existence domains of the second-type CNS solutions practically fill the total area of 0 to 360º.

3.7. Lambert's Problem: Advantages and Disadvantages of the Two-Impulse Solution

The solution of Lambert's problem is a well-known and often-used method for the rendezvous solution (two-impulse manoeuvre parameter determination with fixed moments of impulse application). It is interesting

to compare its capabilities with the capabilities of the previously mentioned methods. In the fourth paragraph of this chapter, it was shown that an *optimal* two-impulse solution does not exist for all values of the initial phase deviation Δu. Let us assess the magnitude of the difference between the total delta-v of the two-impulse solution and the total delta-v of the optimal three-impulse solution.

Lambert's problem has a trivial solution for near-circular motion. We have the equation system containing four linear equations (eqs. 3-1a to 3-1d) with the four unknown variables $\Delta V_{r_1}, \Delta V_{t_1}, \Delta V_{r_2}, \Delta V_{t_2}$ (for the coplanar rendezvous) for the fixed impulse application moments $\varphi_1 = \varphi_{1_f}, \varphi_2 = \varphi_{2_f}$. By solving this equation system and determining the values of the impulse components, one can find the total delta-v of the manoeuvres. By enumerating all of the possible combinations of φ_1, φ_2 a close-to-optimal rendezvous solution can be found. The more combinations φ_1, φ_2 we consider, the more accurate an optimal solution we get.

Such a two-impulse rendezvous solution method has two advantages. Firstly, any constraints on the moments of impulse application can be satisfied. Secondly, this method is both reliable for a multiple-revolution rendezvous and for a small-duration rendezvous. However, there is a problem with the optimality of the found solution. Two-impulse solutions with total delta-vs that close to optimal (both impulses are practically transversal) exist only when the circles with radii R_1 and R_2 intersect. This intersection occurs for some CSS solutions for nonintersecting orbits and for the CNS-type solutions for intersecting orbits.

A totally different situation occurs if the circles of radii R_1 and R_2 do not intersect. In this case, as mentioned before, optimal two-impulse solutions do not exist (both impulses of which are transversal) and, hence, Lambert's problem will lead us to a nonoptimal solution with any number of the considered set of the points φ_1, φ_2.

The difference between the total delta-v of the optimal three-impulse solution and the total delta-v of the two-impulse solution will be greater with an increase in the distance between the points of the circle. This can take place when $\Delta e >> |\Delta a|$ or $|\Delta a| >> \Delta e$. For intersecting orbits, with an increase in the limit of the difference between Δe and $|\Delta a|$, the two-impulse manoeuvre will practically solve the problem with the sole help of the radial velocity components. In Fig. 3-22a, the curved line *ABCK* corresponds to the two-impulse manoeuvre and line segment *BC*

corresponds to the radial component of the first impulse. The optimal three-impulse manoeuvre (the CAS-type solution) only uses the transversal components and, hence, the total delta-v for the solution of Lambert's problem $(\Delta V \approx \Delta e)$ will be two times greater than the total delta-vs of the optimal three or four-impulse solutions $(\Delta V = \Delta e / 2)$.

For nonintersecting orbits, the difference can get up to triple the value. The optimal manoeuvre from among the two-impulse manoeuvres is presented in Fig. 3-22b.

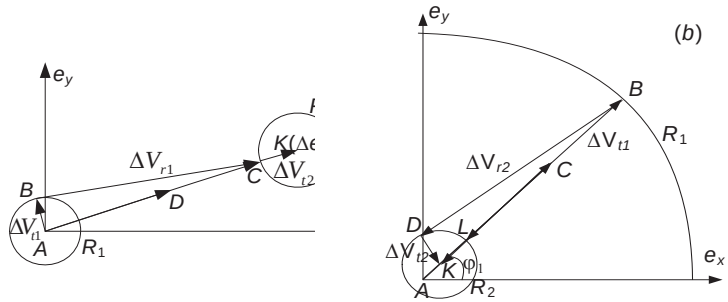

Fig. 3-22. Lambert's problem solution:
(*a*) intersecting orbits (*b*) nonintersecting orbits

The curved line *ABDK* corresponds to it. This is connected to the fact that a radial impulse component with magnitude $\Delta V_{r_2} \approx 2\Delta V_{t_1} \approx \Delta a$ occurs. The total delta-v expenditure of the two-impulse manoeuvre can be estimated as $\Delta V \approx \left|\Delta V_{r_2}\right| + \left|\Delta V_{t_1}\right| = \frac{3}{2}|\Delta a|$, and the three-impulse transversal manoeuvre has $\Delta V \approx \Delta V_{t_1} \approx \frac{|\Delta a|}{2}$. Such a variant occurs for solutions that correspond to the deviations of Δu close to the values Δu_{sl} or Δu_{sr} in Fig. 3-14a.

3.8. Manoeuvres with Drift Orbit Altitude Constraints

The previous paragraphs presented problems without any constraints on the orbital elements; however, in practical work one can meet problems with these constraints. Let us consider, for example, drift orbit manoeuvres that lie in the desired "ring" with the center as the center of attraction:

$$r_{\min} \le r_p \le r_a \le r_{\max}, \tag{3-37}$$

where $r_{\min}, r_{\max}$ = the radii of the inner and outer ring circles and r_p, r_a = the radii of the drift orbit pericenter and apocenter, respectively.

Constraints of this type can often be met while solving the rendezvous problem. For example, in order to catch up to the target spacecraft (which is far ahead), the active spacecraft needs to gradually decrease the period of its drift orbit. This may lead to a considerable decrease in the minimal orbit altitude and, hence, to a dangerous level of atmospheric deceleration. There are also other numerous grounds for the introduction of such constraints.

Figure 3-23 gives the example of a flyby from an initial orbit (denoted by T_0) to a target orbit (denoted by T_f), in which the constraint on the minimum altitude $r_{\min}$ is crucial for the drift orbit (denoted by the dashed line T_d). The following sequence has been carried out in order to catch the target spacecraft over a fixed time duration: application of the braking impulse ΔV_{t_1}, transfer to the drift orbit, which osculates the circular orbit with the radius $r_{\min}$, and the application of the two impulses ΔV_{t_2} and ΔV_{t_3} on the last manoeuvring interval in order to transfer to the target orbit at the required point.

Because of their importance, many publications have been dedicated to the solution of manoeuvring problems with altitude constraints on the drift orbit. The most fundamental results can be found in the work of Ivashkin (1975), in which the transfers between elliptical orbits were analyzed. The many peculiarities of multiple-revolution flybys between near-circular orbits have been considered in this work, which can be used for the acquisition of an analytical solution.

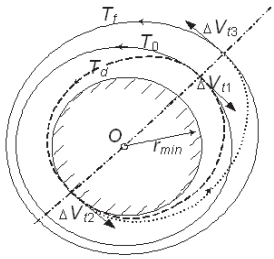

Fig. 3-23. Flyby with constraint on drift orbit altitude

As mentioned before, condition 3-1d allows for the approximate assessment of the magnitude of the transversal impulse component sum of the first manoeuvring interval $\Delta V_{t_1}^{*}$ of the multiple-revolution flyby and, hence, approximately determining the magnitude of the drift orbit semimajor axis:

$$a_d = a_0 + 2\Delta V_{t_1}^{*},$$

where a_d = the drift orbit semimajor axis; a_0 = the initial value of the active spacecraft orbit semimajor axis; and $\Delta V_{t_1}^{*}$ is determined by Eq.3-12a.

It is assumed that Eq. 3-1d is replaced with the approximate Eq. 3-12a for further analysis of the problem. The values of the optimal manoeuvring parameters (for which condition 3-1d will be fulfilled with the desired tolerance), as usual, can be carried out with the help of the iterative procedure.

It is apparent that the problem stated previously has a solution, if:

$$r_{\min} \le a_d \le r_{\max}, \tag{3-38}$$

Otherwise the spacecraft will arrive at the rendezvous point at the fixed time, but without fulfilling one of the constraints (3-37).

Since the semimajor axis of the drift orbit is known, the constraint on the eccentricity of the drift orbit is equivalent to constraint 3-37:

$$e_d \le e_s, \tag{3-39a}$$

$$e_d \le e_b, \tag{3-39b}$$

where e_d, e_s, e_b = the drift orbit eccentricity; the eccentricity of the orbit with the semimajor axis a_d, which osculates with the lower boundary of the ring; and the eccentricity of the orbit with the semimajor axis a_d, which osculates with the upper boundary of the ring, respectively. The magnitudes of e_s, e_b can be evaluated by:

$$e_s = \frac{a_d - r_{\min}}{a_d}, \tag{3-40a}$$

$$e_b = \frac{r_{\max} - a_d}{a_d}. \tag{3-40b}$$

The orientation of the orbit's apsidal line is not important. We cannot increase the drift orbit eccentricity more than the lesser value of the magnitudes e_s, e_b, while maintaining the set value of the semimajor axis, because the orbit will exceed the boundaries of the restraining ring.

Thus, it follows from inequalities 3-39a and 3-39b that the geometric locus on the plane e_x, e_y will be a circle with radius R_m (Fig. 3-24), which is equal to the smaller of the values e_s, e_b (Baranov 1985). The points from this geometric locus correspond to the acceptable values of the drift orbit eccentricity vector. The center of the circle is situated in the reference frame origin.

Let us draw circles with radii $R_1 = 2\Delta V_{t_I}^*, R_2 = 2\Delta V_{t_{II}}^*$ ($\Delta V_{t_{II}}^*$ is evaluated by Eq. 3-12b) with centers at point A (e_{x_0}, e_{y_0}) and point K (e_{x_f}, e_{y_f}). Let us remember that point *A* corresponds to the eccentricity vector of the active spacecraft's orbit and point *K* corresponds to the eccentricity vector of the target spacecraft's orbit. In the case when set *G* in Fig. 3-24a (the set of the points of the intersection of the circles with radii R_1 and R_2) has common points with the circle of radius R_m, it is easy to point out the two, three, and four-impulse variants, for which the aforementioned points will correspond to the acceptable values of the drift orbit eccentricity vector, among the solutions, investigated in the previous paragraphs. This is point *B* for the two-impulse solution; curve *BC* for the three-impulse solution with the two impulses on the second manoeuvring interval; and area *BCD* for the four-impulse solution. Since the conditions 3-39a and 3-39b are met for the found solutions, then condition 3-37 is satisfied too. The solution parameters are updated with the help of the aforementioned iterative procedures, which ensure the satisfaction of condition 3-1d with the desired tolerance.

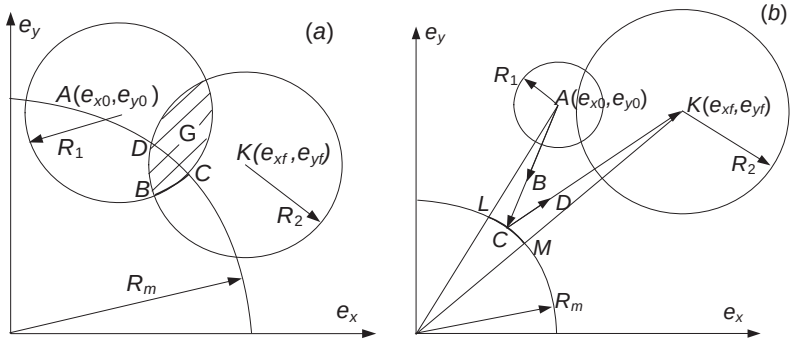

Fig. 3-24. Relative positions of circles corresponding to the sum of the transversal impulse components of the first and second manoeuvring intervals and permitted values of the drift orbit eccentricity vector: *(a)* solutions with fulfillment of the constraint on the drift orbit altitude from among the conventional rendezvous problem solutions; *(b)* special solutions need to be searched for.

The variant when the circles of radii R_1 and R_2 have common points (they intersect or one of them is inside the other) is mostly typical for problems in which it is necessary to account for constraints on the drift orbit altitude. As a rule, we have to account for constraints on altitude when the sums of the transversal impulse components of the first and second manoeuvring intervals have different signs (the presence of common points is a necessary condition for the circles of radii R_1 and R_2).

If the constraint on the altitude is severe (a_d is slightly different from $r_{\min}$ or $r_{\max}$), then the drift orbit eccentricity (the radius of circle R_m) will be small. If the initial and final orbits in this problem have relatively big eccentricity values, and the differences between their semimajor axes and the eccentricity vectors are small, then there may be no common points between the three circles (Fig. 3-24b). In this case, the four-impulse manoeuvre will be optimal and the curved line *ABCDK* corresponds to it (Fig. 3-24b). Point *C*, which corresponds to the drift orbit eccentricity vector, should belong to curve *LM* (curve *LM* is the part of the circle with radius R_m, which is limited by line segments, connecting the centers of the circles with radii R_1 and R_2 with the reference frame origin).

If the initial and final orbits intersect, then the variant is possible in which only the inner points of line segment E_1E_2 (Fig. 3-25) belong to the

circle with radius R_m. In this case, among the optimal solutions without accounting for the constraint (Eq. 3-37), only the four-impulse solutions, for which the points of line segment *LN* would correspond to the permitted values of the drift orbit eccentricity vectors, fulfill constraint 3-37.

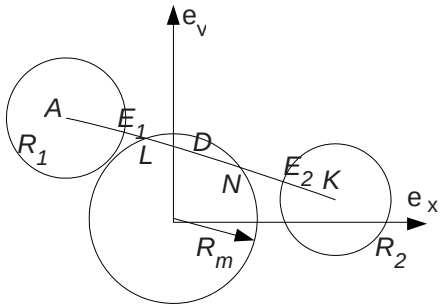

Fig. 3-25. Four-impulse solutions fulfilling the constraints on drift orbit altitude and existing among the optimal solutions

When neither set *G* nor line segment E_1E_2 have common points with the circle of radius R_m, the total delta-v of the acceptable solution will exceed the total delta-v of the solution, obtained without accounting for constraint 3-37.

We can determine which points of the circle of radius R_m can correspond to the acceptable values of the drift orbit eccentricity vector, obtained after the optimal manoeuvring performance in this case.

We now consider four-impulse manoeuvres. We assume that point *C* (Fig. 3-26), which corresponds to the drift orbit parameters, is the inner point of the circle with radius R_m. It does not belong to set *P* (which is the set of intersection points of the circles with radii R_m and R_2). For such a manoeuvre, the value of minimal total delta-v is equal to $\Delta V_c = 0.5(AC + CK)$. The minimal expenditures for the transfer through the arbitrary point *C*', which belong to curve L_1L_2 (Fig. 3-26), are smaller than ΔV_c, since $AC'+C'K<AC+CK$.

Among the manoeuvres to which points of set *P* correspond, the minimal expenditures will result in a manoeuvre that is closest to point *A* of set *P*. This point corresponds to the drift orbit parameters. For the case depicted in Fig. 3-26, point *N* will be such a point. The optimality of this solution follows from the statement that the total impulse delta-v of the second manoeuvring interval is equal to $0.5R_2$ for all points of set *P* and

the minimal impulse delta-v of the first manoeuvring interval is equal to the half the distance to point *A*.

Thus, the point of circle with radius R_m, which lies on curve L_1N, corresponds to the optimal transfer. The positions of the points of this set can be set with angle ω_d (Fig. 3-26).

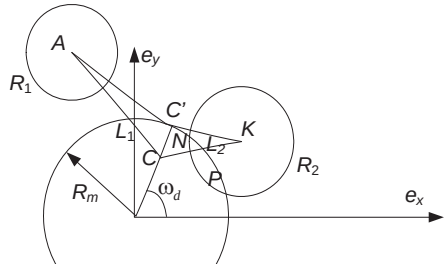

Fig. 3-26. Case when the altitude constraint changes optimal solution

Through the minimization of total delta-v by ω_d, one can find the drift orbit parameters. Then, with the help of the iterative procedure, one can find the optimal manoeuvre parameters, which fulfill constraint 3-1d with the desired accuracy.

3.9. The Impact of Error in Performing the Manoeuvre

Errors always arise in discovering the spacecraft's orbital elements and there are always errors in the performance of manoeuvres during flight. Accounting and compensating for the influence of these errors is of great importance in a multiple-revolution rendezvous. The first priority is to take into account errors of a secular nature. The influence of these errors is usually investigated using the Monte Carlo or analogous methods. In some cases, it is possible to account for errors analytically for near-circular motion.

Firstly, we will consider the influence of manoeuvre realization error. Inaccuracies in the moments of thrust engine ignition, errors in the magnitudes of the applied impulses, and errors in thruster orientation can all be highlighted.

Errors in the moments of starting the engine burn Δt_0 and/or finishing the engine burn Δt_f, lead to the alteration of the moment of impulse application (in comparison to the modeled one), by the angle $\Delta\varphi$:

$$\Delta\varphi = \frac{\Delta t_0 + \Delta t_f}{2T},$$

and to the magnitude alteration of this impulse by δV:

$$\delta V = \frac{\Delta V(\Delta t_f - \Delta t_0)}{\Delta t},$$

Here, T = the orbital period; Δt = the manoeuvre duration; and ΔV = the impulse magnitude.

Let us consider the influence of this error on the alteration of the eccentricity vector. On the plane e_x, e_y, the vector, corresponding to the impulse, is rotated by angle $\Delta\varphi$. The vector length also alters by $\frac{2\delta V}{V_0}$ in the case of the transversal impulse. An error in impulse orientation also leads to the rotation of this vector (and to a small alteration of its magnitude). An error in the impulse magnitude leads to an additional alteration of vector length.

Thus, during the realization of the first manoeuvre, for example, the three-impulse solution *ABCK* (one impulse is applied on the first manoeuvring interval), vector *AB*′ (Fig. 3-27a) may correspond to the first impulse instead of the determined vector *AB*. Point *B*′ belongs to an ellipse with its center at point *B*. If the error in the orientation of the thrust engines is considerable, then the semimajor axis of the ellipse is perpendicular to the line segment, which corresponds to the nominal value of the impulse (for example, the ellipse in Fig. 3-27a with point *B* as its center). If the error in the magnitude of the manoeuvre is considerable, then the semimajor axis of the ellipse is directed along the line segment, which corresponds to the nominal value of the impulse (the ellipse in Fig. 3-27a with point *D* as its center). The error ellipse has such a position, for example, if there is an error in the moment of engine burn start or finish, or if these errors have different signs $(\Delta t_0 \Delta t_f < 0)$.

3.9.1. Effects on CSS and CNS-Type Solutions

Let us consider the influence of the impulse realization error on the first manoeuvring interval of CSS-type solutions. We need to remember that the problem has lots of three and four-impulse solutions of this type with equal total delta-vs. The curve of the circle corresponds to the acceptable drift orbit eccentricity vector values of the three-impulse solutions and the area of the intersection of the circles with radii R_1 and R_2 corresponds to the acceptable values of the drift orbit eccentricity vector for four-impulse solutions. If the ellipse with the impulse realization errors of the first manoeuvring interval belongs to the circle with radius R_2 and a center at point *K*, then, with the use of the impulses of the second manoeuvring interval, one can optimally transfer from an arbitrary point of the ellipse to point *K*. In the initial moment, if line segment *AB* corresponds to the impulse, and accounting for the realization error, we change it to line segment *AB*′ (point *B*′ does not belong to the circle with its center at point *K* (Fig. 3-27a)), then, the total manoeuvre delta-v expenditure of the second interval and, hence, of the flyby, will be greater than in the case where no accounting for errors has been conducted.

In order to put the error ellipse inside the circle with its center at point *K*, the point, which corresponds to the drift orbit eccentricity vector, should be placed closer to point *K*. If only one impulse is used on the first manoeuvring interval, the opportunities for this are limited. For example, the case to which point *D* corresponds in Fig. 3-27b. In this example, if the impulses are to be performed exceeding the nominal value, then point *D*′ may be outside the limits of the circle with its center at point *K*. However, if two impulses are used on the first manoeuvring interval and point *K* is situated inside the circle of radius R_1 with its center in the reference frame origin, then point *B*, which corresponds to the drift orbit eccentricity vector, can be placed as close as possible to point *K* (Fig. 3-27b). The error ellipse will be situated at its maximum depth inside the circle with its center at point *K*. Strictly speaking, the error ellipse obtained after the realization of two impulses on one manoeuvring interval, will not take the form of the ellipse. However, it is preferable to put this figure (the superposition of the two ellipses) as deep as possible inside the circle with its center at point *K*.

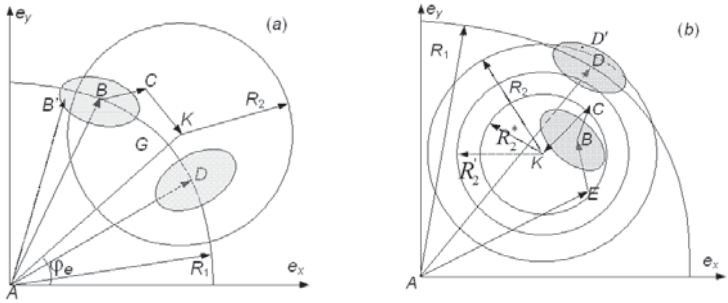

Fig. 3-27. Influence of impulse errors applied on the first manoeuvring interval for CSS-type solutions

If point *B* is situated right next to point *K*, then the impulses of the second interval will be equal in magnitude and their angles of application will differ by 180º. Such a solution is less sensitive to both manoeuvre realization errors in the first manoeuvring interval and errors in the second manoeuvring interval.

During the evaluation of the four-impulse manoeuvres of the "Soyuz" spacecraft, the application angle of the third impulse is fixed one revolution before the rendezvous point, while the application angle of the fourth impulse is fixed half a revolution before the rendezvous point. The constraint that the impulses of the second manoeuvring interval should be approximately equal is often added. These constraints lead to a situation in which point *B*, which corresponds to the drift orbit eccentricity vector, is very close to point *K*. Thus, we get the aforementioned solution, which is the least sensitive one to manoeuvre realization errors for both intervals. Certainly, the additional constraint increases the total delta-v expenditure of the manoeuvres of the first interval on the orbital plane rotation; however, as will be shown in Chapter 4, when points *B* and *K* are very close, it becomes easier to correct the errors in the impulse lateral components on the second manoeuvring interval.

As a matter of fact, it is not necessary to place point *B*, which corresponds to the drift orbit eccentricity vector, as close as possible to point *K*. Instead, the point *B* area of possible positions can be determined with a reasonable level of accuracy. Let us remember that for the multiple-revolution rendezvous sum of the transversal impulses, the components of the first manoeuvring interval ΔV_{t_1} can be determined by Eq. 3-12a. If the maximum error (3σ) in the orientation of the impulse $\Delta\varphi_{\max}$, and the maximum error (3σ) in the magnitude of the impulse k ($k = 0.01$

corresponding to a possible error in the magnitude of the impulse of 1 %) are known, then the semimajor axis magnitudes of the error ellipse $a = \Delta V_{t_1} \sin \Delta\varphi_{\max}, b = k\Delta V_{t_1}$ can be determined. Let us denote c as the maximum of a and b. If point B belongs to the circle of radius $R_2^{'} = R_2 - c$ with its center at point K (the circle plotted by points in Fig. 3-27b), then the error ellipse will belong to the circle of radius R_2 with its center at point K and, hence, it will be possible to optimally transfer from the arbitrary point B' to point K with the help of the manoeuvres of the second interval.

Errors in the impulse magnitudes influence not only the position of the point corresponding to the drift orbit eccentricity vector, but also the radius of the circle with its center at point K. If the real magnitude of the performed impulse manoeuvres on the first manoeuvring interval exceeds the estimated magnitudes by $k\Delta V_{t_1}$, then, on the second manoeuvring interval, the magnitudes of the impulses should be smaller than the estimated ones by $k\Delta V_{t_1}$, in order to ensure the necessary alteration of the semimajor axis. Thus, it is desirable to locate point B in the circle of radius $R_2^* = R_2 - c - b$ with its center at point K (the dashed circle in Fig. 3-27b), in order for the ellipse corresponding to the impulse errors of the first manoeuvring interval to be inside the circle of smaller radius.

The apsidal solutions, the parameters of which are determined in the easiest fashion, are, at the same time, the solutions that are least sensitive to the errors of impulses of the first manoeuvring interval because they allow us to find the maximum approach between points B and K with a corresponding distribution of the impulse magnitudes of this interval.

The solution starts with a comparison of the magnitudes ΔV_{t_1} and Δe (the length of line segment AK). If $2\Delta V_{t_1} < \Delta e,$ then it is better to use one transversal impulse on the first manoeuvring interval. If $2\Delta V_{t_1} > \Delta e,$ then two transversal impulses are used on the first manoeuvring interval. The magnitudes of these impulses are connected to each other by the equation $\frac{\Delta V_{t_2}}{\Delta V_{t_1}} = \frac{2\Delta V_{t_1} - \Delta e}{2\Delta V_{t_1} + \Delta e},$ which ensures the proximity of points B and K. The magnitudes of all the impulses can be found from eqs. 3-1a to 3-1d.

The influence of the impulse realization errors on the alteration of the eccentricity vector has also been considered. However, their distribution on the correction of the semimajor axis is usually not that important. An

error in the moment of engine burn start and burn finish with the maintenance of the total duration of the manoeuvre does not lead to a deviation from the estimated semimajor axis alteration because it can be corrected equally effectively at any point of the orbit (for the linearized equations of motion).

The small error in the orientation of the impulse also does not lead to a considerable alteration of the transversal component magnitude and thus to a considerable alteration of the semimajor axis. The basic contribution to the semimajor axis correction error is made by the error in the magnitude of the impulse. However, this error does not lead to an increase in the total delta-v of the manoeuvres for the CAS-type solutions, when the total delta-v of the rendezvous manoeuvres is equal to the total delta-v of the transfer manoeuvres between these orbits and the primer vector hodograph degenerates to the point. In this case, the error in the correction of the semimajor axis by the impulses of the first manoeuvring interval can be compensated with a corresponding alteration of the impulses of the second manoeuvring interval without any increase of the total delta-v for all manoeuvres.

If the primer vector hodograph is cycloid (CNS-type solution), then the total delta-v of the rendezvous manoeuvres is greater than the total delta-v of the transfer manoeuvres between these orbits. In this case, the error in the correction of the semimajor axis by the impulses of the first manoeuvring interval may lead either to an increase in the total delta-v of the manoeuvres (if the alteration of the semimajor axis is greater than the estimated one), or to its decrease (if the alteration of the semimajor axis is smaller than the estimated one). However, in both cases, just like for the CSS-type solutions, this error in the semimajor axis alteration leads to an error in the time of arrival at the rendezvous point.

For a multiple-revolution rendezvous, this error, caused by errors in the correction of the semimajor axis by the impulses of the first manoeuvring interval, is the most important one.

The arrival at the rendezvous point time miss can be evaluated by the equation:

$$\Delta t_I = -6\pi N \Delta V_{t_{I_{err}}},$$

where $\Delta V_{t_{I_{err}}}$ = the error in the sum of the transversal components of the impulses of the first manoeuvring interval that caused the error in the semimajor axis correction.

It is impossible to eliminate this error by the necessary analogous alteration of the impulse magnitudes of the last manoeuvring interval $\delta V_{II} = \Delta V_{t_{I_{err}}}$ without only altering the moments of the impulse application of this manoeuvring interval. The corresponding alteration of the impulse magnitudes gives the alteration of the time of the arrival at the rendezvous point, which does not exceed the value:

$$\Delta t = 6\pi\delta V_{II}.$$

This error can be eliminated with the help of the alteration of the impulse application moments performed on the second manoeuvring interval. For the case when points *B* and *K* are close and, hence, the magnitudes of the third and fourth impulses are practically equal to each other $(\Delta V_{t_3} \approx \Delta V_{t_4})$, the alteration of the arrival time at the rendezvous point due to the alteration of the application angle of one of the impulses by $\Delta\varphi_{ch}$, and the alteration of the application angle of another impulse of close magnitude, can be evaluated by the equation:

$$\Delta t_{II} = 3\Delta\varphi_{ch}\Delta V_{t_{II}},$$

where $\Delta V_{t_{II}}$ = the sum of the transversal impulse components of the second manoeuvring interval.

The maximum alteration of the application angle of one of the impulses does not exceed half a revolution (it is suggested that the length of the manoeuvring interval is approximately one revolution). Thus, the maximum alteration of the arrival time at the rendezvous point is given by:

$$\Delta t_{II} = 3\pi\Delta V_{t_{II}}.$$

As a rule, only small alterations of the impulse locations on the second manoeuvring interval can be done, narrowing the magnitude Δt_{II} even further.

If $\Delta t_I > \Delta t_{II}$, it is impossible to eliminate the error in the time of arrival at the rendezvous point by altering the moments of performing the manoeuvre in the second interval.

In order to effectively eliminate the deviation in the time of arrival at the rendezvous point, caused by errors in the impulse realization of the first manoeuvring interval, additional manoeuvres are usually used.

For example, for the “Soyuz” spacecraft we can use an additional manoeuvre on the 17th revolution between the first manoeuvring interval on the 3rd-4th revolutions and the second interval on the 32nd revolution. During the parameter determination of the four-impulse manoeuvre on the 3rd and 32nd revolutions, a transversal accelerating impulse with a fixed magnitude 2 m/s on the 17th revolution has been accounted for. The magnitude of this impulse should be twice as great (since the distance between this impulse and the rendezvous point is twice as small as the distance between this point and the first manoeuvring interval) as the maximum error in the magnitude of the sum of the impulses of the first manoeuvring interval $\Delta V_{t_{I_{err}}}$. After the determination of the orbit before the 17th revolution, the parameters of the three-impulse solution are determined: the first impulse is performed on the 17th revolution, while the second and third impulses are performed on the 32nd revolution. Thus, the updated magnitude of the additional impulse is calculated, which allows the compensation of errors in the first manoeuvring interval. If the first impulses were performed with an error towards increasing $\Delta V_{t_{I_{err}}}$, then the magnitude of the additional impulse will decrease by $2\Delta V_{t_{I_{err}}}$ after the update. If the first impulses were performed with a shortfall in the required magnitude, then the mid-impulse magnitude (additional) will be increased by double the magnitude of the error after the update.

It is very important to correctly choose the magnitude of the mid-impulse for this scheme. If we make it too big, then the sum of the transversal components of the first manoeuvring interval will decrease by half of its magnitude and these impulses contribute most to the necessary rotation of the orbital plane. Thus, the total delta-v of the manoeuvres will increase. If we make it too small, then, after the update its magnitude can become negative, which will also increase the total delta-v of the manoeuvres.

The optimal magnitude of the mid-impulse is:

$$\Delta V_{mid} = 2k\Delta V_{t_{I_{\max}}},$$

where $\Delta V_{t_{I_{\max}}}$ = the maximum value of the sum of the transversal impulse components of the first manoeuvring interval. Its magnitude depends on the maximum possible difference between the semimajor axes of the initial and the target orbits, and on the initial phase Δu_I^* (see section 1.5.2).

In order to find the practically optimal and resistive to errors of the impulse realization solution, one can divide each of the impulses ΔV_i by $2(1-k)\Delta V_i$ and $k\Delta V_i$ (k = the maximum error in the magnitude of the impulse). The impulse $(1-k)\Delta V_i$ is applied on the primary revolution and the impulse $k\Delta V_i$ is applied on the following revolution. The application point on the revolution and the orientation of the mid-impulse are analogous to the corresponding values of the basic impulse. Thus, for example, instead of a four-impulse solution we get an eight-impulse solution. The division is made after the solution of the approximate four-impulse problem, while accounting for the influence of the division through the help of the iterative procedure from the first chapter, which ensures the fulfillment of the terminal conditions with the desired tolerance. With this scheme, even if the manoeuvre were to be fulfilled with the maximum error, leading to an increase in the given value, the additional manoeuvre can be omitted because it was already performed by this maximum error. If the primary manoeuvre were to be performed with the maximum error leading to a decrease in its value, the magnitude of the additional manoeuvre will be doubled. Such a scheme allows us to compensate for the errors of the basic manoeuvres and not spend additional fuel. If high accuracy is needed for the terminal orbit, for example, during satellite formation flying deployment, then we have to divide the additional impulses of the second manoeuvring interval with the same proportions (Baranov, Boutonnet, Escudier, and Martinot 2005, 913-920).

The parameters of the CNS-type solutions are determined unambiguously. If the error ellipse of the manoeuvres of the first interval, corresponding to this solution, belongs to the circle with its center at point *K*, then, with the help of the manoeuvres of the second interval, one can transfer to the final orbit without significant losses. If the ellipse considerably exceeds the limits of the circle, then it is worth solving it through the use of the CSS-type solution, but with different signs of the transversal components on the first and second manoeuvring intervals. Then the appropriate solution can be chosen from the set of solutions. This solution has impulses on the first manoeuvring interval, situated closer to the beginning of this interval (for a decrease in total delta-v expenditure), and the point, which corresponds to the eccentricity vector of the drift orbit, is situated closer to point *K* (for a decrease in the influence of the error).

3.9.2. Effects on the CAS-Type Solution

Let us consider the influence of errors in manoeuvre realization on the total delta-v of CAS-type solutions. The vectors, which correspond to the impulses of these solutions, lie on the line segment that connects points *A* and *K* (Fig. 3-28).

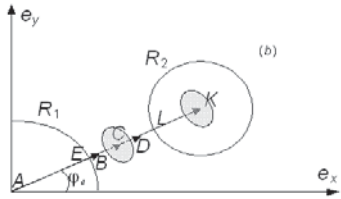

Fig. 3-28. Influence of impulse errors applied in the first manoeuvring interval on CAS-type solutions

Point *E* corresponds to the drift orbit eccentricity vector of the three-impulse solution (one manoeuvre is performed on the first interval), while point *C* (which belongs to line segment *EL*) corresponds to the drift orbit eccentricity vector of the four-impulse solution. These points are equal in terms of total delta-v expenditure-per-flyby, but the choice of the concrete location of point *C* exercises a substantial influence on the distribution of errors in the first and second manoeuvring intervals. The closer point *C* is to point *E*, the fewer errors there are in the first manoeuvring interval (as the magnitude of impulses of this interval decreases) and the greater the errors in the second manoeuvring interval. By placing point *C* in the middle of line segment *AK*, we get a solution with the maximum equal possible errors on the first and second manoeuvring intervals (Fig. 3-28). If we happen to choose point *C* so that the error ellipse of the first manoeuvring interval will not have common points with the circles of radii R_1 and R_2, then the error in the magnitude of the manoeuvres of the first interval insignificantly increases the total delta-v expenditure in the second interval. If the errors of the second manoeuvring interval are not important, for example, because the equipment used for the autonomous approach can easily compensate for them, it is better to place point *C* closer to point *E*, but the error ellipse should not share common points with the circle of radius R_1. This will result in the decreased influence of the error in the orientation of the impulses of the first interval on the total delta-v of the manoeuvres of the second interval.

It is harder to eliminate the error in the time of arrival at the rendezvous point, which adds error to the correction of the semimajor axis

by the manoeuvres of the first interval, for CAS-type solutions than for CSS-type solutions. The second interval impulse application angles belong to angle φ_e (Eq. 1-14a). We can only move the moment of velocity application by one revolution, which is not always allowed. A considerable shift in the moments of impulse application, necessary for the compensation of an error in the time of arrival at the rendezvous point, leads to a considerable increase in the total delta-v of the manoeuvres of the second interval. The use of one or several additional impulses may solve this inconvenience, but it is better to have them factored into the manoeuvring scheme in advance.

In the multiple-revolution manoeuvring scheme, since the orbit is determined one more time before the fulfillment of the manoeuvres of the second manoeuvring interval and the magnitudes of the impulses are recalculated, the influence of the realization errors is basically calculated in the same fashion. Only the secular influence of the error in the magnitudes of the transversal components of the impulses is missing.

CHAPTER FOUR

NONCOPLANAR RENDEZVOUS

4.1. Problem Statement

The conditions of the transfer to the given orbit for the noncoplanar rendezvous problem can be written as

$$\sum_{i=1}^{N} (\Delta V_{ri} \sin \varphi_i + 2\Delta V_{ti} \cos \varphi_i) = \Delta e_x, \tag{4-1a}$$

$$\sum_{i=1}^{N} \left(-\Delta V_{ri} \cos \varphi_i + 2\Delta V_{ti} \sin \varphi_i\right) = \Delta e_y, \tag{4-1b}$$

$$\sum_{i=1}^{N} 2\Delta V_{ti} = \Delta a, \tag{4-1c}$$

$$\sum_{i=1}^{N} \left(2\Delta V_{ri}\left(1-\cos \varphi_i\right) + \Delta V_{ti}\left(-3\varphi_i + 4\sin \varphi_i\right)\right) = \Delta t, \tag{4-1d}$$

$$\sum_{i=1}^{N} -\Delta V_{zi} \sin \varphi_i = \Delta z, \tag{4-1e}$$

$$\sum_{i=1}^{N} \Delta V_{zi} \cos \varphi_i = \Delta V_z, \tag{4-1f}$$

where the deviations are evaluated in the rendezvous point (the *x*-axis is directed towards the rendezvous point).

Impulses, just like in the coplanar problem case, are applied on the two manoeuvring intervals, the length of each interval is one revolution, and the distance between the intervals is several revolutions long.

The impulses belonging to the set of manoeuvring intervals can be stated as

$$\varphi_1 \subseteq F_1, \ldots, \varphi_{N_1} \subseteq F_1, \varphi_{N_1+1} \subseteq F_2, \ldots, \varphi_{N_1+N_2} \subseteq F_2, \tag{4-2}$$

where $N_1, N_2 =$ numbers of impulses on the first and the second manoeuvring interval, respectively ($N = N_1 + N_2$).

Find the components $\Delta V_{ri}, \Delta V_{ti}, \Delta V_{zi}, \varphi_i$ ($i = 1, \ldots, N$), which ensure the minimal total manoeuvre delta-v with the constraints 4-1a -4-1f, 4-2:

$$\Delta V = \sum_{i=1}^{N} \Delta V_i = \sum_{i=1}^{N} \sqrt{\Delta V_{ri}^2 + \Delta V_{ti}^2 + \Delta V_{zi}^2}$$

The equations for the primer vector can be presented as

$$\lambda = -\lambda_2 \cos\theta + \lambda_3 \sin\theta + 2\lambda_6, \tag{4-3a}$$

$$\mu = 2\lambda_1 + 2\lambda_2 \sin\theta + 2\lambda_3 \cos\theta - 3\lambda_6\theta, \tag{4-3b}$$

$$\nu = \lambda_4 \sin\theta + \lambda_5 \cos\theta, \tag{4-3c}$$

where $\lambda_1, \lambda_2, \lambda_3, \lambda_4, \lambda_5, \lambda_6$ = arbitrary constants.

Basically, Eq. 4-3 describes a helix. If $\lambda_6 = 0$, the equations will describe an ellipse (a circle) or a line segment (point).

When the primer vector hodograph is the helix ($\lambda_6 \neq 0$), the rendezvous problem total delta-v ΔV_{rdv} exceeds the total delta-v of the transfer problem ΔV_{trf}. Like for the coplanar rendezvous, in this case the impulses of one of the manoeuvring intervals will be braking, while the impulses of the other manoeuvring interval will be boosting.

$\lambda_6 = 0$ ΔV_{rdv} coincides with ΔV_{trf}. The impulses for the transfers between the noncoplanar orbits can be divided into parts and applied on the different manoeuvring intervals. The nature of the solution stays the same, but the time of arrival to the final orbit changes. The rendezvous problem can be solved by the appropriate selection of the velocity impulse division.

The idea of the optimal transfer impulse division for getting the solution of the rendezvous problem is quite natural and was considered in the literature multiple times (Petrov 1985; Jones 1976, 55–90). However, the case when ΔV_{rdv} exceeds ΔV_{trf} (for such solutions the primer vector hodograph is the helix) is not usually considered by the authors or another problem solution is suggested which does not imply the impulse division of the optimal transfer. It is necessary to notice that the traditional method of the transfer problem impulse division has its disadvantages. It cannot be

applied to the problem, in which the different constraints on the impulses of the first and the second manoeuvring intervals must be satisfied; it also cannot be used when the constraints on the drift orbit parameters must be satisfied etc. The methods from the works of Jones (1976, 55–90) and Marec (1968) cannot be applied for the solution to problems with such constraints either.

Remembering the multiple-revolution nature of the considered problem, three calculation algorithms, which ensure that the necessary manoeuvring parameters are obtained, can be suggested. The first algorithm is also based on the solution of the transfer problem, but it appears to be more universal than the algorithms from Petrov (1985) and Jones (1976, 55–90). This will be considered in the second section of this chapter. The second algorithm (where the transfer problem is also solved for each of the manoeuvring intervals) is based on the solution of the minimization problem for the drift orbit elements. The particular case of this algorithm, which is used for the calculation of long-range guidance manoeuvres, is considered in this chapter; the algorithm in general will be considered in Chapter 7. Besides, the optimal nondegenerate solution parameter determination algorithm ($\lambda_6 \neq 0$), which is based on the usage of the necessary optimality conditions, is considered in this chapter.

4.2. Universal Solution Algorithm for the Noncoplanar Rendezvous Problem Based on the Transfer Problem Solution

4.2.1. Manoeuvre Parameter Determination

Due to the multiple-revolution nature of the flyby, the coefficients of the transversal impulse components of the first manoeuvring interval exceed all of the rest coefficients in Eq. 4-1d multiple times, but they only slightly differ from each other. This allows an approximate assessment of the magnitude of the sum of these components (ΔV_{t_1}):

$$\Delta V_{t_1} \approx -\frac{\Delta t}{3\varphi_0}, \tag{4-4}$$

where φ_0 = the angular distance between an arbitrary point of the first manoeuvring interval and the rendezvous point. Then the active spacecraft

orbit semimajor axis magnitude change by the impulses of the first manoeuvring interval can be approximately assessed:

$$\Delta a_I \approx 2\Delta V_{t_I}, \tag{4-5}$$

Also, the active spacecraft orbit semimajor axis magnitude change by the impulses of the second manoeuvring interval can be approximately assessed:

$$\Delta a_{II} \approx \Delta a - 2\Delta V_{t_I}. \tag{4-6}$$

Let Δa^* be $\Delta a^* = |\Delta a_I| + |\Delta a_{II}|$.

The solution of the optimal transfer between the orbits with the orbit element deviations $\Delta e_x, \Delta e_y, \Delta z, \Delta V_z$ and Δa^* (instead of Δa) can be used for the solution of the rendezvous problem. If $\Delta a^* = |\Delta a|$ (this case occurs when Δa_I and Δa_{II} have the same sign), then the obtained in this fashion problem solution will be optimal because its total delta-v coincides with the total delta-v of the transfer problem (corresponds to the case with $\lambda_6 = 0$). If $\Delta a^* > |\Delta a|$, the total delta-v of the found solution is greater than the total delta-v of the optimal solution, to which the primer vector hodograph in the shape of the helix corresponds, but the difference will be small for the multiple-revolution rendezvous.

In order to find the magnitudes of impulses for the rendezvous problem solution, the impulses, which were calculated for the solution of the transfer problem, can be divided as the ratios $\frac{\Delta a_I}{\Delta a^*}$, $\frac{\Delta a_{II}}{\Delta a^*}$ for the first and second manoeuvring intervals, respectively (Baranov 2008, 430–439). For example, the four-impulse solution of the rendezvous problem with the components of the first impulse of the first manoeuvring interval,

$$\Delta V_{t_{I_1}} = \Delta V_{t_1} \frac{\Delta a_I}{\Delta a^*}, \Delta V_{z_{I_1}} = \Delta V_{z_1} \frac{\Delta a_I}{\Delta a^*}, \tag{4-7}$$

and the components of the second impulse of the first manoeuvring interval,

$$\Delta V_{t_{I_2}} = \Delta V_{t_2} \frac{\Delta a_I}{\Delta a^*}, \Delta V_{z_{I_2}} = \Delta V_{z_2} \frac{\Delta a_I}{\Delta a^*}. \tag{4-8}$$

can be obtained from the universal solution (US) to the transfer problem with the components $\Delta V_{t_1}, \Delta V_{z_1}, \Delta V_{t_2}, \Delta V_{z_2}$ (the curved lines *ACK* and *AC*′*K* correspond to it in Fig. 4-1).

Similarly, for the second manoeuvring interval:

$$\Delta V_{t_{II_1}} = \Delta V_{t_1} \frac{\Delta a_{II}}{\Delta a^*}, \Delta V_{z_{II_1}} = \Delta V_{z_1} \frac{\Delta a_{II}}{\Delta a^*}, \tag{4-9}$$

$$\Delta V_{t_{II_2}} = \Delta V_{t_2} \frac{\Delta a_{II}}{\Delta a^*}, \Delta V_{z_{II_2}} = \Delta V_{z_2} \frac{\Delta a_{II}}{\Delta a^*}. \tag{4-10}$$

If the signs of Δa_I and Δa^* coincide on the first manoeuvring interval, then on this interval the angles of the impulse application of the rendezvous problem coincide with the impulse application angles of the transfer problem while, in the contrary case, the angles differ by 180º. Similarly, the equality of signs Δa_{II} and Δa^* on the second manoeuvring interval is checked and the values of the impulse application angles for the rendezvous problem are determined. It is obvious that the revolutions, on which the impulse application angles are situated, should belong to the set manoeuvring intervals.

4.2.2. Solution Existence Domains

The point *D* (Fig. 4-1), which belongs to the line segment *AK* (first the variant of nonintersecting $\Delta a^* > \Delta e$ will be considered), will correspond to the eccentricity vector of the drift orbit of the found solution in the space e_x, e_y.

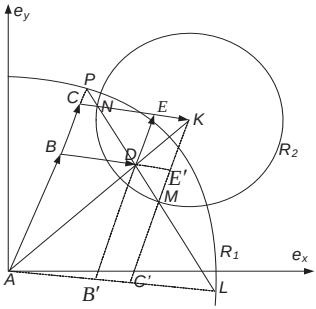

Fig. 4-1. Rendezvous problem solutions obtained from the transfer problem solution

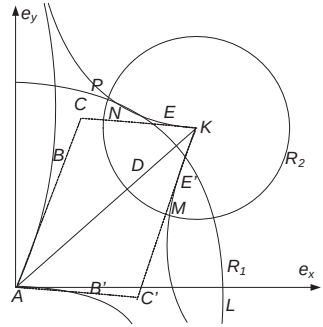

Fig. 4-2. Existence domains for the rendezvous problem solutions

The curved line *ABDEK* corresponds to the transversal impulse components of this solution. If one alters the impulse application order on the first and the second manoeuvring intervals, three more kinds of curved lines – *AB′DE′K*, *ABDE′K*, and *AB′DEK* – can be obtained. These four solutions slightly differ between each other in the conditions of the long-duration rendezvous but, for a small duration, the order of the impulse application matters. The opportunity to use different solutions may be handy from an aspect of keeping the moments of the impulse application in the permitted manoeuvring intervals.

The existence domains of the rendezvous problem solutions, where the total delta-v ΔV_{rdv} of which coincides with the total delta-v of the transfer problem solution ΔV_{trf} ($\Delta a^* = |\Delta a|$), coincide with the existence domains of the CSS and the CAS solutions of the corresponding coplanar rendezvous problem, where the deviations from the plane are not taken into account (depicted in Figs. 3-14a and 3-14b), in the space Δu (the initial phase). In the same way, the existence domains of the solutions, for which the expenditures on ΔV_{rdv} exceed the expenditures on ΔV_{trf} ($\Delta a^* > |\Delta a|$), coincide with the existence domains of the CNS solutions (depicted in Figs. 3-14a and 3-14b) in the space Δu .

The sum of the transversal impulse components of the first manoeuvring interval should be equal to $\Delta a_I / 2$ for the approximated satisfaction of the condition 4-1d:

$$\Delta V_{t_1} + \Delta V_{t_2} = \frac{\Delta a_I}{2}.$$

However, the distribution of the magnitudes of the transversal impulse components within the limits of this sum can be arbitrary and not be limited to the distribution set by eqs. 4-6 and 4-7. Thus, the line segment *MN* (Fig. 4-1) corresponds to the possible values of the drift orbit eccentricity vector. The four-impulse solutions turn to three-impulse solutions at the points *M* and *N*, when only one impulse with the magnitude $\Delta a_{II}/2$ is applied on the second interval. The angle of application of this impulse coincides with the angle of application of the first impulse of the transfer problem universal solution for point *M* or the angle of application of the second impulse for point *N*.

The lateral components should be distributed between the impulses in a fashion when the ratio between the lateral and the transversal components (the same as for the corresponding impulse in the transfer problem) will be preserved for every impulse.

The proportional solution parameters are the easiest to find, even if, for instance, due to the constraints on the drift orbit eccentricity, a solution is needed where the point of the line segment *MN* is different from the point *D* (Fig. 4-1).

The position of the line segment *MN* will be different for the various values of Δu; it will move parallel to itself. For the values $\Delta u \in [\Delta u_{sl}, \Delta u_{sr}]$ (see Section 3.4), the parallelogram *ACKC′* will be the acceptable set for the drift orbit eccentricity vector values in the space e_x, e_y. With $\Delta u = \Delta u_{sl}$, the line segment *MN* degenerates to point *K* and, with $\Delta u = \Delta u_{sr}$ the line segment *MN* degenerates to point *A*.

When Δu becomes greater than Δu_{sr} and keeps on growing, or becomes lesser than Δu_{sl} and keeps on decreasing, Δa^* starts growing (on the interval $[\Delta u_{sl}, \Delta u_{sr}]$, which is constant). At the same time, the radii of both circles R_1 and R_2 start to grow, because Δa_I and Δa_{II}, the signs of which do not coincide (as always, $R_1 = |\Delta a_I|, R_2 = |\Delta a_{II}|$), grow. The line segment continues to correspond to the possible values of the drift orbit eccentricity vector with every concrete value of Δu, but its value will be greater than the value of the line segment, which corresponds to Δu from the interval $[\Delta u_{sl}, \Delta u_{sr}]$ and intersects the same point of line segment *AK*. For the values $\Delta u < \Delta u_{sl}$ and $\Delta u > \Delta u_{sr}$, the acceptable set

for the values of the drift orbit eccentricity vector on the plane e_x, e_y will be the geometric figure (depicted in Fig. 4-2), which holds the parallelogram *ACKC′*.

The universal solution was used during the research on the existence domains as it was the simplest one (see paragraph 2.4), but the analogous picture can be obtained for the existence domains of solutions, as presented in the work of Edelbaum (1967, 66–73).

Let us consider the variant when the orbits intersect and $\Delta a^* = |\Delta a|$. In this case, the circles with the radii R_1 and R_2 on the plane $e_x e_y$ do not intersect (Fig. 4-3). The curved lines *ACK* and *AC′K* correspond to the universal solutions of the transfer problem, and the curved lines *ABDEK*, *AB′DE′K*, *ABDE′K*, and *AB′DEK*, correspond to the proportional solutions of the rendezvous problem. It was mentioned above that the signs of the transversal components of impulses do not coincide for the transfer between the intersecting orbit problem solution. Hence, for example, the solution *AB′DEK* has $R_1 = AB'$-$B'D$ and $R_2 = EK$-DE, and also $MB' = B'D$ and $DE = EN$.

Like in the nonintersecting orbits case, the transversal impulse component magnitude distribution of the first manoeuvring interval within the limits of the sum 4-10 can be arbitrary and not be limited to the distribution set by eqs. 4-6 and 4-7. Thus, the line segment *MN* corresponds to the possible values of the drift orbit eccentricity vector (Fig. 4-3).

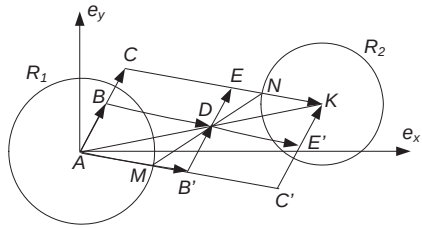

Fig. 4-3. Rendezvous problem solution for nonintersecting orbits.

The four-impulse solution degenerates to the three-impulse solution at the points *M* and *N*. The solution, when only one impulse with the transversal component $\Delta a_I / 2$ and the application angle, which coincides with the application angle of the second impulse of the transfer problem universal solution, is applied on the first interval; this corresponds to point

M. The solution when one impulse with the transversal component $\Delta a_{II}/2$ is applied on the second manoeuvring interval corresponds to point *N*.

Like in the case of a rendezvous on nonintersecting orbits, the position of the line segment *MN* will alter with different values of Δu. The parallelogram *ACKC′* will be the acceptable set for the values of the drift orbit eccentricity vector on the plane e_x, e_y for the values of $\Delta u \in [\Delta u_{sl}, \Delta u_{sr}]$. With $\Delta u = \Delta u_{sl}$, the line segment degenerates to point *K*, and, with $\Delta u = \Delta u_{sr}$, the line segment degenerates to point *A*. When Δu becomes greater than Δu_{sr} and keeps on growing, Δa^* also starts to grow (it was constant on the interval $[\Delta u_{sl}, \Delta u_{sr}]$). At the same time, the radii of both circles R_1 and R_2 start to grow, because Δa_I and Δa_{II}, the signs of which do not coincide, grow. The line segment, which is situated to the left of the point *K*, continues to correspond to the possible values of the drift orbit eccentricity vector with every concrete value of Δu, but its value will be greater than the value of the line segment, which corresponds to Δu from the interval $[\Delta u_{sl}, \Delta u_{sr}]$ and intersects the same point of the line segment *AK*. For the values $\Delta u < \Delta u_{sl}$ and $\Delta u > \Delta u_{sr}$, the acceptable set of the values of the drift orbit eccentricity vector on the plane e_x, e_y will be the unlimited geometric figure, as depicted in Fig. 4-2.

The existence domains of both solutions were investigated with the presumption that Eq. 4-1d was replaced by the approximate Eq. 4-10. It is good enough for understanding the appearance of these areas.

The parameters of any solution from the permitted area can be updated with the help of the iterative procedure, which is analogous to the procedure from Chapter 3 (only value of Δa_I changes). Equation 4-1d should be satisfied with the given accuracy.

It is worth mentioning that the Lambert's problem can be used for the determination of the manoeuvre parameters instead of the aforementioned iterative procedure, since it works effectively enough with the small duration of rendezvous. The magnitudes of the impulse components $\Delta V_{r_i}, \Delta V_{t_i}, \Delta V_{z_i}\ (i = 1,2)$ are determined from the equation system of the six linear equations with the six unknown variables 4-1a - 4.-1f with the fixed moments of the application of two impulses. The optimal solution is found by enumerating possible combinations of φ_1, φ_2. The usage of Lambert's problem on the small manoeuvring intervals is quite reasonable, since it is hard to place more than two manoeuvres on these intervals. Besides, these two manoeuvres are often the part of the estimated earlier

four- or three-impulse manoeuvre. If it is not enough to use two impulses for the optimal solution of the problem and a three- or four-impulse manoeuvring scheme is needed, then the numerical method from the following chapter can be used for manoeuvre parameter determination.

The searching procedure for the optimal multiple-revolution rendezvous problem solution becomes more difficult with the presence of the additional constraints on the angles of application, orientation, and magnitudes of impulses. Such constraints can often be found in practical problems. However, the geometric approach allows finding the optimal analytical solutions in these cases. The algorithm for the solution of this type of problem is described in the Section 4.4.

4.2.3. Example

The four-impulse rendezvous on the noncoplanar orbits is considered. The elements of the initial and target orbits are listed in table 4-1. They are analogous to the orbit elements from example 2.2.8, but the information about the active spacecraft and the target spacecraft latitude argument in the initial moment from example 3.2.3; the numbers of revolutions of both spacecraft on that moment N_{0_i} and N_{0_k}; and the number of revolutions in the rendezvous moment N_{ap_i} and N_{ap_f} are added. The three variants with the different initial locations of the target spacecraft are considered.

Table 4-1

Orbit elements	Initial orbit	Target orbit
$H_{\min}$ km	180	340
$H_{\max}$ km	210	360
u_{prg} deg	20	150
i deg	51.7	51.69
Ω deg	17.49	17.5
u_1 deg	60	5
u_2 deg	60	210
u_3 deg	60	355
N_0 (initial revolution)	1	201
N_{ap} (rendezvous revolution)	17	217

The rendezvous point coincides with the beginning of the 17th revolution.

Let us assume that the manoeuvre sequence is generated on two intervals: the first and the last revolutions of flight. The two impulses, which have the transversal and the lateral components, are applied on each interval.

The alteration of the semimajor axis on the first manoeuvring interval can be determined by the equation

$$\Delta a_I = 2\Delta V_{t_1},$$

where $\Delta V_{t_1} \approx \frac{\Delta t_i}{k_1}$, $k_1 = 4\sin\varphi_1 - 3\varphi_1$. The values of $k_1, \Delta t_i$ were calculated in the example 3.2.3.

The alteration of the semimajor axis on the second manoeuvring interval is $\Delta a_{II} = \Delta a - \Delta a_I$.

For $u_{F_1} = 5^\circ$

$$\Delta a_I = 0.03052705, \Delta a_{II} = -0.007195977, \Delta a_I > 0, \Delta a_{II} < 0.$$

By using the first manoeuvres, the active spacecraft transfers to the orbit with the higher altitude in order to “get caught” by the target spacecraft, and by using manoeuvres of the second interval it lowers to the level of the target spacecraft.

For $u_{F_3} = 210^\circ$, when the phase difference lies in the optimal diapason, the signs of deviations are equal:

$$\Delta a_I = 0.005598495, \Delta a_{II} = 0.01773258, \Delta a_I > 0, \Delta a_{II} > 0.$$

All manoeuvres are accelerating.

For $u_{F_3} = 355^\circ$

$$\Delta a_I = -0.0120339, \Delta a_{II} = 0.03536497, \Delta a_I < 0, \Delta a_{II} > 0.$$

With the use of the first manoeuvres, the spacecraft transfers to the lower orbit in order to catch the target spacecraft.

Let us denote:

$$\Delta a^* = |\Delta a_I| + |\Delta a_{II}|.$$

Let us determine the impulse components $\Delta V_{t_1}, \Delta V_{t_2}, \Delta V_{z_1}, \Delta V_{z_2}$ of the noncoplanar two-impulse transfer. We shall assume that the value Δa^* is the change of the semimajor axis in the calculations of the transfer parameters. The angles of the impulse application can also be taken from the solution of the noncoplanar transfer. The parameters $\Delta V_{t_1}, \Delta V_{t_2}, \Delta V_{z_1}, \Delta V_{z_2}$ in the second case (with the equal signs of Δa_I and Δa_{II}) coincide with the estimated parameters of the noncoplanar transfer problem (example 2.2.8), because $\Delta a^* = \Delta a$.

The distribution of the impulse components $\Delta V_{t_1}, \Delta V_{t_2}, \Delta V_{z_1}, \Delta V_{z_2}$, which were calculated for the noncoplanar two-impulse transfer, is fulfilled in accordance with eqs. 4-7-4-10:

$$\Delta V_{t_{I_1}} = \Delta V_{t_1} \frac{\Delta a_I}{\Delta a^*}, \Delta V_{Z_{I_1}} = \Delta V_{Z_1} \frac{\Delta a_I}{\Delta a^*},$$
$$\Delta V_{t_{I_2}} = \Delta V_{t_2} \frac{\Delta a_I}{\Delta a^*}, \Delta V_{Z_{I_2}} = \Delta V_{Z_2} \frac{\Delta a_I}{\Delta a^*},$$
$$\Delta V_{t_{II_1}} = \Delta V_{t_1} \frac{\Delta a_{II}}{\Delta a^*}, \Delta V_{Z_{II_1}} = \Delta V_{Z_1} \frac{\Delta a_{II}}{\Delta a^*},$$
$$\Delta V_{t_{II_2}} = \Delta V_{t_2} \frac{\Delta a_{II}}{\Delta a^*}, \Delta V_{Z_{II_2}} = \Delta V_{Z_2} \frac{\Delta a_{II}}{\Delta a^*}.$$

1) $u_{F_1} = 5^\circ$

$$\Delta a^* = 0.03772303, T_{F_1} = 87660.38\,\text{s}, \Delta t_1 = 4.458352\,(3823.84\,\text{s})$$
$$\Delta V_{t_{I_1}} = 63.3067\,\text{m/s}, \Delta V_{Z_{I_1}} = -0.7458\,\text{m/s},$$
$$\Delta V_{t_{I_2}} = 54.9230\,\text{m/s}, \Delta V_{Z_{I_2}} = 0.6471\,\text{m/s},$$
$$\Delta V_{t_{II_1}} = -14.9230\,\text{m/s}, \Delta V_{Z_{II_1}} = 0.1758\,\text{m/s},$$
$$\Delta V_{t_{II_2}} = -12.9467\,\text{m/s}, \Delta V_{Z_{II_2}} = -0.1525\,\text{m/s},$$
$$\Delta V_\Sigma = 146.12\,\text{m/s}$$
$$\varphi_1 = 144.9271^\circ, \varphi_2 = 318.3586^\circ,$$
$$\varphi_3 = 144.9271^\circ, \varphi_4 = 318.3586^\circ.$$

In accordance with the aforementioned procedure, the braking impulse application angles are changed by the half a revolution:

$$\varphi_3 = 324.9271^\circ, \varphi_4 = 138.3586^\circ.$$

After the formal application of this procedure, when only the manoeuvre fulfillment necessity on one revolution was taken into account, the application angle of the third impulse becomes greater than the angle of application of the fourth impulse and the impulses must be switched.

$$\varphi_3 = 138.3586^\circ, \varphi_4 = 324.9271^\circ,$$
$$\Delta V_{t_{II_1}} = -12.9467 \text{ m/s}, \Delta V_{Z_{II_1}} = -0.1525 \text{ m/s},$$
$$\Delta V_{t_{II_2}} = -14.9230 \text{ m/s}, \Delta V_{Z_{II_2}} = 0.1758 \text{ m/s}.$$

2) $u_{F_2} = 210^\circ$

$$\Delta a^* = 0.02333108, T_{F_2} = 84537.82 \text{ s}, \Delta t_2 = 0.8176375\,(701.2713 \text{ s})$$
$$\Delta V_{t_{I_1}} = 12.0810 \text{ m/s}, \Delta V_{Z_{I_1}} = -0.2307 \text{ m/s},$$
$$\Delta V_{t_{I_2}} = 9.6017 \text{ m/s}, \Delta V_{Z_{I_2}} = 0.1834 \text{ m/s},$$
$$\Delta V_{t_{II_1}} = 38.2651 \text{ m/s}, \Delta V_{Z_{II_1}} = -0.7309 \text{ m/s},$$
$$\Delta V_{t_{II_2}} = 30.4122 \text{ m/s}, \Delta V_{Z_{II_2}} = 0.5809 \text{ m/s},$$
$$\Delta V_\Sigma = 90.37 \text{ m/s}$$
$$\varphi_1 = 146.6201^\circ, \varphi_2 = 315.9030^\circ,$$
$$\varphi_3 = 146.6201^\circ, \varphi_4 = 315.9030^\circ.$$

3) $u_{F_3} = 355^\circ$

$$\Delta a^* = 0.04739887, T_{F_3} = 82329.17 \text{ s}, \Delta t_3 = -1.757502\,(1507.37 \text{ s})$$
$$\Delta V_{t_{I_1}} = -21.9874 \text{ m/s}, \Delta V_{Z_{I_1}} = -0.2060 \text{ m/s},$$
$$\Delta V_{t_{I_2}} = -24.6193 \text{ m/s}, \Delta V_{Z_{I_2}} = 0.2307 \text{ m/s},$$
$$\Delta V_{t_{II_1}} = 72.3506 \text{ m/s}, \Delta V_{Z_{II_1}} = -0.6780 \text{ m/s},$$
$$\Delta V_{t_{II_2}} = 64.6162 \text{ m/s}, \Delta V_{Z_{II_2}} = 0.6055 \text{ m/s},$$
$$\Delta V_\Sigma = 183.58 \text{ m/s}$$

$$\varphi_1 = 139.1202^\circ, \varphi_2 = 324.3370^\circ,$$
$$\varphi_3 = 144.3370^\circ, \varphi_4 = 319.1202^\circ.$$

Here, the angles' alteration of the braking impulses and the change of the application order of these impulses have already been accounted for.

The solution of the problem for the second variant can be considered as an example of the work of the iterative procedure.

2) $u_{F_2} = 210^\circ$

1st iteration

$\Delta t = 0.8176375\,(701.2713\,\text{s})$ Time used on iteration

$\Delta a_1 = 0.005598495, \Delta a_2 = 0.01773258$

$\Delta a^* = 0.02333108$

1st impulse

$\Delta V_t = 12.08099, \Delta V_z = -0.2307577, \varphi_1 = -97.97196\,(u = 146.6201^\circ)$

2nd impulse

$\Delta V_t = 9.601689, \Delta V_z = 0.1834008, \varphi_2 = -95.01742\,(u = 315.903^\circ)$

3rd impulse

$\Delta V_t = 38.26514, \Delta V_z = -0.730898, \varphi_3 = -3.724182\,(u = 146.6201^\circ)$

4th impulse

$\Delta V_t = 30.41223, \Delta V_z = 0.5809005, \varphi_4 = -0.7696386\,(u = 315.903^\circ)$

$\Delta t_r = 0.8759396\,(751.2758\,\text{s})$ real deviation by time

$\Delta t_n = 0.8176375\,(701.2713\,\text{s})$ nominal deviation by time

$\Delta t_{at} = \Delta t_n - \Delta t_r = -0.05830208\,(-50.00453\,\text{s})$ miss by time on this iteration

$\Delta t = \Delta t + \Delta t_{at} = 0.8176375 - 0.05830208 = 0.7593354$ deviation of time for the next iteration

2nd iteration

$\Delta t = 0.7593354\,(651.2667\,\text{s})$ Time used on iteration

$\Delta a_1 = 0.005128624, \Delta a_2 = 0.01820245$

$\Delta a^* = 0.02333108$

1st impulse

$\Delta V_t = 11.06706, \Delta V_z = -0.2113906, \varphi_1 = -97.97196\,(u = 146.6201^\circ)$

2nd impulse

$\Delta V_t = 8.795837, \Delta V_z = 0.1680083, \varphi_2 = -95.01742\ (u = 315.903^\circ)$

3rd impulse

$\Delta V_t = 39.27907, \Delta V_z = -0.7502651, \varphi_3 = -3.724182\ (u = 146.6201^\circ)$

4th impulse

$\Delta V_t = 31.21808, \Delta V_z = 0.596293, \varphi_4 = -0.7696386\ (u = 315.903^\circ)$

$\Delta t_r = 0.8095131\ (694.3031\,\text{s})$ real deviation by time

$\Delta t_n = 0.8176375\ (701.2713\,\text{s})$ nominal deviation by time

$\Delta t_{at} = \Delta t_n - \Delta t_r = 0.00812438\ (6.968117\,\text{s})$ miss by time on this iteration

$\Delta t = \Delta t + \Delta t_{at} = 0.7593354 + 0.00812438 = 0.7674598$ deviation of time for the next iteration

3rd iteration

$\Delta t = 0.7674598\ (658.2349\,\text{s})$ Time used on iteration

$\Delta a_1 = 0.005183497, \Delta a_2 = 0.01814758$

1st impulse

$\Delta V_t = 11.18547, \Delta V_z = -0.2136523, \varphi_1 = -97.97196\ (u = 146.6201^\circ)$

2nd impulse

$\Delta V_t = 8.889947, \Delta V_z = 0.1698059, \varphi_2 = -95.01742\ (u = 315.903^\circ)$

3rd impulse

$\Delta V_t = 39.16066, \Delta V_z = -0.7480033, \varphi_3 = -3.724182\ (u = 146.6201^\circ)$

4th impulse

$\Delta V_t = 31.12397, \Delta V_z = 0.5944954, \varphi_4 = -0.7696386\ (u = 315.903^\circ)$

$\Delta t_r = 0.8172706\ (700.9566\,\text{s})$ real deviation by time

$\Delta t_n = 0.8176375\ (701.2713\,\text{s})$ nominal deviation by time

$\Delta t_{at} = \Delta t_n - \Delta t_r = 0.0003669154\ (0.314696\,\text{s})$ miss by time on this iteration

$\Delta t = \Delta t + \Delta t_{at} = 0.7674598 + 0.0003669154 = 0.7678267$ deviation of time for the next iteration

4th iteration

$\Delta t = 0.7678267\ (658.5495\,\text{s})$ Time used on iteration

$\Delta a_1 = 0.005185975, \Delta a_2 = 0.0181451$

1st impulse

$\Delta V_t = 11.19082, \Delta V_z = -0.2137545, \varphi_1 = -97.97196\ (u = 146.6201^\circ)$

2nd impulse

$\Delta V_t = 8.894197, \Delta V_z = 0.169887, \varphi_2 = -95.01742\ (u = 315.903^\circ)$

3rd impulse

$\Delta V_t = 39.15532, \Delta V_z = -0.7479012, \varphi_3 = -3.724182\ (u = 146.6201^\circ)$

4th impulse

$\Delta V_t = 31.11972, \Delta V_z = 0.5944142, \varphi_4 = -0.7696386\ (u = 315.903^\circ)$

$\Delta t_r = 0.8176209\ (701.257\ \text{s})$ real deviation by time

$\Delta t_n = 0.8176375\ (701.2713\ \text{s})$ nominal deviation by time

$\Delta t_{at} = \Delta t_n - \Delta t_r = 1.657073e-005\ (0.01421238\ \text{s})$ miss by time on this iteration

$\Delta t = \Delta t + \Delta t_{at} = 0.7678267 + 1.657073e-005 = 0.7678433$ deviation of time for the next iteration

5th iteration

$\Delta t = 0.7678433\ (658.5638\ \text{s})$ Time used on iteration

$\Delta a_1 = 0.005186087, \Delta a_2 = 0.01814499$

1st impulse

$\Delta V_t = 11.19106, \Delta V_z = -0.2137591, \varphi_1 = -97.97196\ (u = 146.6201^\circ)$

2nd impulse

$\Delta V_t = 8.894389, \Delta V_z = 0.1698907, \varphi_2 = -95.01742\ (u = 315.903^\circ)$

3rd impulse

$\Delta V_t = 39.15507, \Delta V_z = -0.7478966, \varphi_3 = -3.724182\ (u = 146.6201^\circ)$

4th impulse

$\Delta V_t = 31.11953, \Delta V_z = 0.5944106, \varphi_4 = -0.7696386\ (u = 315.903^\circ)$

$\Delta t_r = 0.8176368\ (701.2706\ \text{s})$ real deviation by time

$\Delta t_n = 0.8176375\ (701.2713\ \text{s})$ nominal deviation by time

$\Delta t_{at} = \Delta t_n - \Delta t_r = -7.483718e-007\ (-0.0006418635\ \text{s})$ miss by time on this iteration

The initial miss of 701.2713 s becomes 0.00064 s after five iterations, i.e., the error of the arrival in the rendezvous point is less than 3 m.

4.3. Nondegenerate Solution to the Noncoplanar Rendezvous Problem

4.3.1. Numerical Calculation of the Optimal Six-Impulse Solution Parameters

The nondegenerate solution ($\lambda_6 \neq 0$), when the primer vector hodograph is the helix in the space (μ, λ, ν), will now be considered. The six-impulse optimal manoeuvre exists with the particular parameters of this helix. The first impulse is applied in the beginning of the first allowed manoeuvring interval (the helix intersects the sphere in the initial moment of time $\theta = 0$). The second and the third impulses are applied inside the first revolution of the flight in the moment of the osculation of the helix and the sphere. The fourth and the fifth impulses are applied on the last revolution of the flight in the osculating points and the sixth impulse corresponds to the intersection with the sphere in the final moment of time θ_f. As it is shown in the work of Marec (1979), there is no other distribution of the impulses on revolutions. Thus, the first and the last impulses are maximally separated, which allows reducing the total delta-v expenditures on rendezvous, because the spacecraft stays maximally long in the drift orbit.

The osculation of the helix and the sphere in the four inner points is possible if the following helix "symmetry" conditions are satisfied:

$$\mu(0) = -\mu(\theta_f), \lambda(0) = \lambda(\theta_f), \nu(0) = -\nu(\theta_f). \tag{4-11}$$

Such "symmetrical" nature of the helix leads to the impulse application moment symmetry, i.e.,

$$\theta_2 = \theta_f - \theta_5, \theta_3 = \theta_f - \theta_4. \tag{4-12}$$

Thus, it is enough to find the application angles and the impulse orientation of one manoeuvring interval, as similar impulse parameters of the other interval can be found from eqs. 4-11 and 4-12. We have to know the values of the coefficients λ_i ($i = 1....6$), which determine the position of the helix, in order to find these parameters.

Eqs. 4-11 and 1-19 lead to the following equations:

$$
\begin{aligned}
&-\lambda_2 = -\lambda_2 \cos\theta_f + \lambda_3 \sin\theta_f, \\
&-2\lambda_1 - 2\lambda_3 = 2\lambda_1 + 2\lambda_2 \sin\theta_f + 2\lambda_3 \cos\theta_f - 3\lambda_6\theta_f, \quad (4\text{-}13) \\
&\lambda_5 = \lambda_4 \sin\theta_f + \lambda_5 \cos\theta_f,
\end{aligned}
$$

which allow reducing the number of the independent parameters of the helix to three.

Let us remember that, according to Eq. 4-13, it can be concluded that the elements of the pairs λ_2 and λ_3, λ_4 and λ_5, λ_1 and λ_6 should be among these three parameters. Besides, the parameter λ_6 has the biggest influence on the helix behavior, which is why it is reasonable to include it in the list of the independent parameters. The variables $\lambda_3, \lambda_5, \lambda_6$ were chosen as the independent parameters of the helix.

The search for the values $\lambda_3, \lambda_5, \lambda_6$ is fulfilled with the successive use of the two different programs (Baranov and Roldugin 2011). The only entry parameter is the length of the manoeuvring interval θ_f.

The successive usage of two programs allows fully determining the parameters of helix for each θ_f, which osculates the sphere in the four internal points.

Thus, the moments of impulse application and their orientation are determined by the fixed rendezvous duration. The dependencies between the alteration of these manoeuvre parameters and the rendezvous duration, which are rather interesting, can be plotted.

4.3.2. Characteristics of the Optimal Six-Impulse Solution

Fig. 4-4 holds the application moments of the second (lower row) θ_2 and the third (upper row) θ_3 impulses versus the full length of the flyby interval. It is assumed that the first impulse is applied when $\theta_1 = 0$.

It can be seen from the figure that the graphs are practically the same for various θ_f. In order to assess this proximity, it is necessary to draw these dependencies on one figure, by omitting the integer part of the revolutions of the argument θ_f for each of the dependencies before the moments when the six-impulse solution begins to exist.

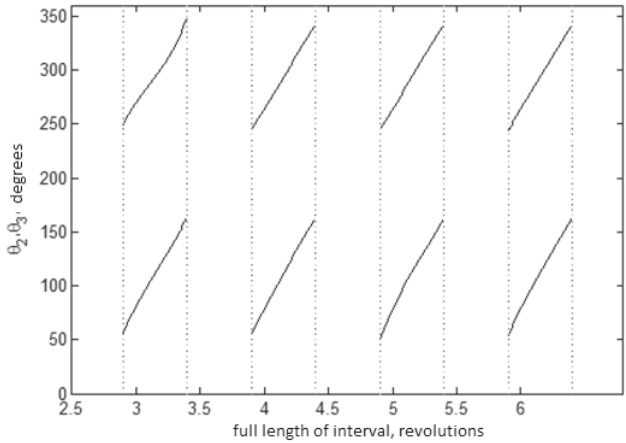

Fig. 4-4. Application moments of the second and the third impulses.

Let us denote the angular part, which will be omitted, as $\bar{\theta}$. For the first dependencies θ_2 and θ_3 $\bar{\theta} = 2$ and for the second ones $\bar{\theta} = 3$, etc. For each of the dependencies the left part of θ_f (let us denote it as θ_f^*), belongs to the interval $\theta_f^* \in [0,2]$. The solutions exist for $\theta_f^* \in [0.9,1.4]$. Let us introduce the variable $\theta^* = 0.5\theta_f^*$ and draw the dependencies between the application moments of the second (θ_2) and the third (θ_3) impulses and θ^*. Figs. 4-5 and 4-6 hold these dependencies, which are obtained by the second piece of software. The legends to each of the figures hold the information about the thrown-away length of the manoeuvring interval $\bar{\theta}$.

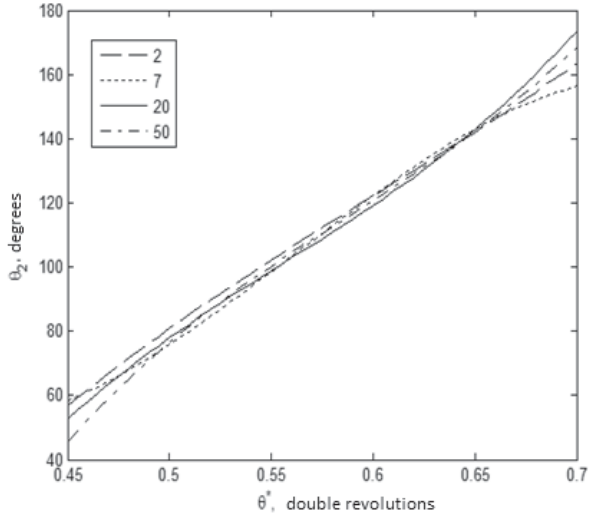

Fig. 4-5. Application moment of the second impulse.

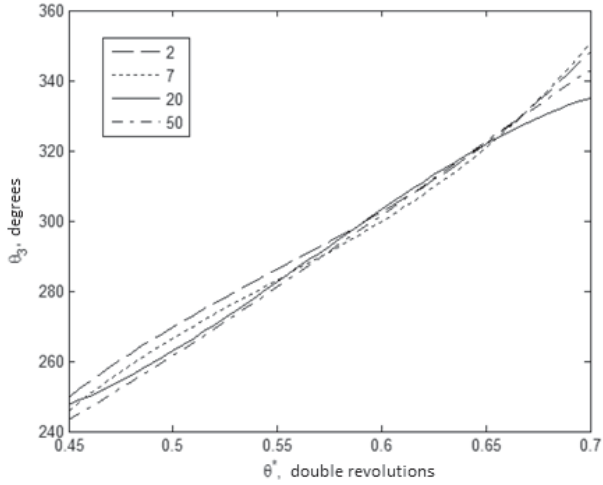

Fig. 4-6. Application moment of the third impulse.

It can be seen from Figs. 4-5 and 4-6 that the dependencies between θ_2, θ_3, and θ^* for the various $\bar{\theta}$ practically coincide. The discrepancies between the curves can be observed when θ^* approaches the end of the nondegenerate six-impulse solution existence interval. It is connected with errors in the determination of the solution parameters, which increase with the degeneration of the helix into the ellipse and with the approach of θ^* to 0.7. The parameter λ_6 becomes zero in this case. The problem with the solution parameter determination for $\theta^* > 0.7$ still exists, but with such a rendezvous duration one can use the results of the previous paragraph, which holds the simple and reliable algorithm of the degenerate solution parameter search for the rendezvous problem, to which the hodograph in the form of ellipse corresponds. As can be seen from the graphs, the difference between the second and the third moments of impulse application is practically half a revolution $\pm 10^\circ$. That is why in the first approximation it can be assumed that the interval between the second and the third (and, hence, between the fourth and fifth) impulses can be half a revolution long.

Figs. 4-7 and 4-8 hold the dependencies between the yaws of the first (β_1) and the second (β_2) impulses and the angles θ^*.

Both graphs demonstrate the same tendency in the alteration of yaws due to $\bar{\theta}$: the slow decrease of their magnitude. The value $\bar{\theta}$, just like in the previous graphs, is depicted in the legend.

The yaws of the second and the third impulses have practically the same magnitudes, but have different signs, due to difference in the impulse application angles (they differ approximately by the half a revolution). The differences of their magnitudes mostly do not exceed 1°.

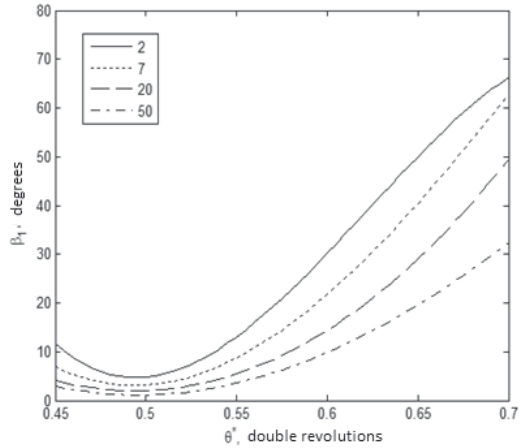

Fig. 4-7. Yaw of the first impulse.

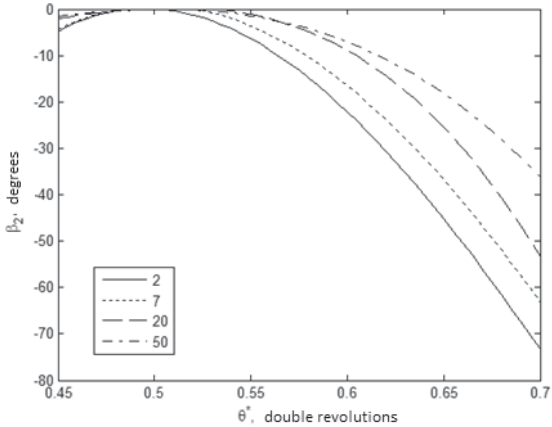

Fig. 4-8. Yaw of the second impulse.

Let us consider the orientation of the impulses in the orbital plane. Fig. 4-9 shows the pitches of the first impulse for the various durations of rendezvous (it is labeled near the type of line).

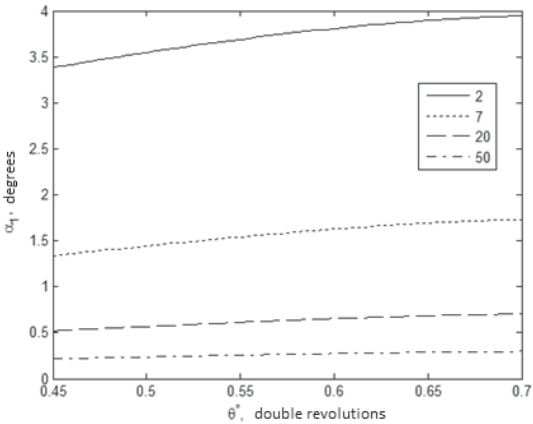

Fig. 4-9. Pitches of the first impulse.

The graph shows that the pitches of impulses are small. For a rendezvous with a duration less or equal to 10 revolutions, the pitch angles do not exceed 1°; a similar result was obtained for rendezvous in coplanar orbits. The same result was obtained for the second and the third impulse pitches. Thus, the impulses in the orbit plane can be assumed to be purely transversal in the first approximation. This supposition is highly accurate (approximately 1°) if the rendezvous duration is longer than 10 revolutions.

4.3.3. Impulse Parameter Approximation with the Help of Analytical Functions

The results obtained in the previous section allow finding the simple analytical equations for the determination of the optimal manoeuvre parameters. It was shown that the impulses within the orbit plane can be considered as purely transversal and the out-of-plane impulse orientation for the second and the third impulses are opposite. Thus, it is necessary to specify only four analytical functions, which approximate the dependencies between the application moments of the second and the third impulses (the problem can be simplified by assuming that they differ by half a revolution as a first guess) and the yaws of the first and the second impulses.

It can be seen from Figs. 4-5 and 4-6, that the application moments of the second (θ_2) and the third (θ_3) impulses do not practically depend on the flyby duration $\overline{\theta}$ (the integer part of the revolutions). Third-degree polynomials are used for the approximation of the dependencies $\theta_2(\theta^*)$ and $\theta_3(\theta^*)$:

$$\begin{aligned}\theta_2(\theta^*) &= 724.8(\theta^*)^3 - 1382.3(\theta^*)^2 \\ &+ 1298.9 \cdot \theta^* - 317.1, \\ \theta_3(\theta^*) &= -35.9(\theta^*)^3 + 180.6(\theta^*)^2 \\ &+ 213.9 \cdot \theta^* + 116.6.\end{aligned} \tag{4-14}$$

Let us remember that θ^* is measured in the fractions of the double revolution, while the moments of impulse application in Eq. 4-14 are measured in the fractions of revolution. In the first approximation, the dependency $\theta_3(\theta^*)$ can be omitted and it can be said that $\theta_3(\theta^*) = \theta_2(\theta^*) + 0.5$.

Basically, the error in approximation does not exceed 3° and, for dependencies with a small number of flyby revolutions, it sometimes gets close to 8° near the boundaries. Such accuracy is enough for the acquisition of an approximate solution. For example, during the use of the numerical methods (Baranov 2008), the step for the impulse application angle enumeration (during the solution of the four-impulse problem) is usually set to 6°.

It can be seen from Figs. 4-7 and 4-8 that the yaws of the first and the second impulses depend on the overall flyby duration. We will use the polynomials of the third order for the approximation of their dependencies on θ^*, but the coefficients will not be constant, as their dependency from $\overline{\theta}$ can also be approximated by third order polynomials:

$$\begin{aligned}\beta_1(\theta^*) &= a_3(\theta^*)^3 + a_2(\theta^*)^2 + a_1\theta^* + a_0, \\ \beta_2(\theta^*) &= b_3(\theta^*)^3 + b_2(\theta^*)^2 + b_1\theta^* + b_0,\end{aligned} \tag{4-15}$$

where

$$a_3 = 0.48 \cdot \overline{\theta}^3 - 44.76 \cdot \overline{\theta}^2 + 1247.41 \cdot \overline{\theta} - 10134.39,$$

$$a_2 = -0.80 \cdot \bar{\theta}^3 + 75.58 \cdot \bar{\theta}^2 - 2127.97 \cdot \bar{\theta} + 18640.44,$$
$$a_1 = 0.44 \cdot \bar{\theta}^3 - 41.96 \cdot \bar{\theta}^2 + 1190.51 \cdot \bar{\theta} - 11002.99,$$
$$a_0 = -0.08 \cdot \bar{\theta}^3 + 7.69 \cdot \bar{\theta}^2 - 219.44 \cdot \bar{\theta} + 2112.89,$$
$$b_3 = -0.23 \cdot \bar{\theta}^3 + 22.91 \cdot \bar{\theta}^2 - 654.31 \cdot \bar{\theta} + 2418.01,$$
$$b_2 = 0.39 \cdot \bar{\theta}^3 - 38.13 \cdot \bar{\theta}^2 + 1116.27 \cdot \bar{\theta} - 5726.06,$$
$$b_1 = -0.21 \cdot \bar{\theta}^3 + 20.71 \cdot \bar{\theta}^2 - 619.14 \cdot \bar{\theta} + 3854.87,$$
$$b_0 = 0.04 \cdot \bar{\theta}^3 - 3.69 \cdot \bar{\theta}^2 + 112.37 \cdot \bar{\theta} - 798.44.$$

The approximation error is less than one degree, which is enough for the acquisition of an acceptable solution.

Thus, with the knowledge of the rendezvous duration (the angular distance between the start of the first manoeuvring interval until the end of the second manoeuvring interval) for the six-impulse manoeuvres, the angles of impulse application and their orientation can be found with the use of the analytical equations obtained on the basis of the necessary optimality conditions. For the first manoeuvring interval, the moment of the application of the first impulse coincides with the beginning of this interval; the application moments of the second and the third impulses relatively to the first impulse are given by Eq. 4-14, the yaws of the first and the second impulses are given by Eq. 4-15, the yaw of the third impulse is opposite to the yaw of the second impulse, and the pitches of all impulses are equal to zero. According to eqs. 4-11 and 4-12, the impulse parameters of the second manoeuvring interval are “symmetrical” to the impulse parameters of the first interval. With the use of this information magnitudes of the impulses are determined from eqs. 4-1a–4-1f.

4.3.4. Comparison of the Six-Impulse Solution with Lambert’s Problem Solution

Let us compare the total delta-v expenditures, obtained with the use of the optimal six-impulse solution and the two-impulse solution.

The two-impulse solution was chosen for the comparison because Lambert’s problem is often used for the rendezvous problem solution. The impulses of the two-impulse solution are situated on the first and last revolutions of the flyby. The possible moments of the impulse application on each of the manoeuvring intervals are enumerated and, for each pair of angles φ_1, φ_2 from eqs. 4-1a–4-1f, the six values $\Delta V_{r_i}, \Delta V_{t_i}, \Delta V_{z_i}$, φ_i (

$i = 1,2$) are determined. By comparing the sums of impulses for various pairs of φ_1, φ_2, the impulse application moments with minimal total delta-v expenditures are found.

The parameters of the six-impulse solutions are determined by eqs. 4-14 and 4-15, and eqs. 4-1a–4-1f. It is assumed that the third impulse is separated from the second one by half a revolution (similarly, the fourth and the fifth impulses are separated from each other by half a revolution), while the first and the sixth impulses are situated on the manoeuvring interval boundaries.

It turned out that the six-impulse solution, which meets the optimality constraints, may not exist, even if the duration of rendezvous belongs to the existence intervals of six-impulse solutions (Fig. 4-4). According to the necessary optimality conditions, the nondegenerate six-impulse solution has the positive transversal impulse components on one manoeuvring intervals and the negative transversal impulse components on the other. However, by using the found moments of application and the orientations of impulses, sometimes one can obtain the solution with the different signs of the transversal impulse components of one manoeuvring interval.

Let us consider an example: when both orbits are circular ($\Delta e_x = \Delta e_y = 0$), the difference between the semimajor axes values is $\Delta a = 0.01$, the deviations between the passive spacecraft orbit plane and the active spacecraft orbit plane are $\Delta z = 0.0001$, $\Delta V_z = 0.0001$, the active satellite is ahead of the passive one ($\Delta u = -50^\circ$ in the rendezvous point), and the total duration of the flyby is $\overline{\theta} = 5$.

By using eqs. 4-14 and 4-15, the six-impulse solution may be found for any flyby duration. The six-impulse solution is more efficient than the two-impulse solution with a duration of up to $\theta^* = 0.33$. Such a duration lies outside of the optimal solution existence diapasons from Fig. 4-4. With $\theta^* = 0.46$, a maximum gain which reaches up to 45% can be obtained. The gain decreases slowly with the decrease of θ^* (with $\theta^* = 0.38$), i.e., on the boundary of optimal solution existence interval (according to the first piece of software) the gain is 41%. On interval $\theta^* \in [0.33, 0.38]$, the necessary conditions are not satisfied (the helix cannot be put inside the sphere), but the signs of the transversal impulse components of one of the manoeuvring intervals coincide, just like it should be in the case of the optimal solution. The advantage of the found six-impulse solution can be confirmed by comparison with the two-impulse solution.

4.3.5. Five-Impulse Manoeuvres

Eqs. 4-14 and 4-15 can be used for the evaluation of five-impulse manoeuvres (Baranov and Roldugin 2012, 441–448). By increasing the duration of the flyby, the zero values of the first or last impulse can be obtained. The interval of the flyby will be greater than the given one but, in fact, due to the manoeuvring start from the second impulse (or end with the fifth impulse); the time of the flyby will meet the problem constraints. In the example considered above, the six-impulse solution with the practically zero first impulse exists when $\theta^* = 0.469$. The second impulse (the first impulse in the five-impulse manoeuvre) is separated from the beginning of the interval with zero impulse of the flyby by 0.2 revolutions. In other words, this manoeuvring scheme corresponds to $\theta^* = 0.369$. This uses either the six-impulse or the five-impulse (derived from the six-impulse solution with $\theta^* = 0.469$) solutions on the interval $\theta^* \in [0.369, 0.469]$. In this case, the helix, which represents the nature of the primer vector hodograph, will start inside the unity sphere, but, nonetheless, it will meet the optimality conditions (4 oscillations and 1 intersection). The length of the interval on which this solution can be used is determined by the distance to the first osculation point.

Fig. 4-10 shows a graph of the total delta-v expenditures (in the dimensionless form) with the use of the six-, five-, and two-impulse manoeuvres.

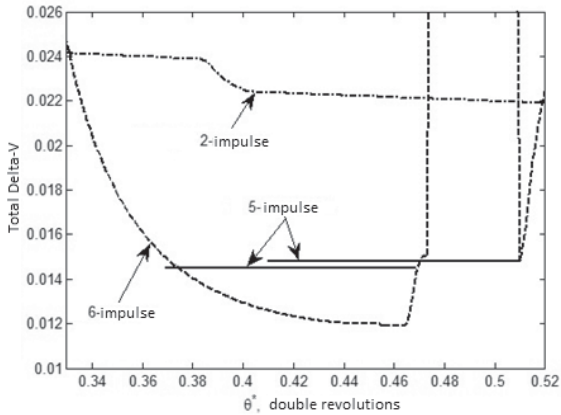

Fig. 4-10. Total delta-v expenditures with the use of six-, five-, and two-impulse manoeuvres.

In Fig. 4-10, the six-impulse solution corresponds to the dashed line, the solution of Lambert's problem corresponds to the dot-and-dash line, and the solid lines correspond to the five-impulse solutions. It can be seen that, with the values of θ^* close to 0.5, the six-impulse solution degenerates, but another five-impulse solution exists with $\theta^* = 0.51$, which allows widening the diapason of θ^*, allowing a gain to be obtained in comparison with the two-impulse solution. With $\theta^* \in [0.51,0.52]$, the six-impulse solution will not be optimal (the first manoeuvring interval contains the accelerating impulse), but it is still more profitable in comparison with the two-impulse solution.

Tables 4-2–4-4 show the parameters of the six- and two-impulse solutions for various values of θ^*.

The tables hold the transversal and the lateral components (ΔV_t and ΔV_z) of the six-impulse solution of the first (*I*) and the second (*II*) manoeuvring intervals; the application moments of the second and the third impulses ($\Delta\varphi_2$ and $\Delta\varphi_3$); the radial, the transversal, and the lateral components of the first and the second impulses of the two-impulse solution (ΔV_{2_I} and $\Delta V_{2_{II}}$); the distance between the application moment of the corresponding impulse and the boundary of the flyby interval ($\Delta\varphi_I$ and $\Delta\varphi_{II}$); and the total delta-v expenditures in both cases (ΔV_6 and ΔV_2).

It can be seen from Table 4-4 that the five-impulse solution does not meet the necessary optimality conditions. Nonetheless, it allows obtaining the considerable gain in the total delta-v expenditures.

Thus, usage of the five-impulse manoeuvres obtained from the six-impulse manoeuvres finds a gain in the total delta-v expenditures and expands the existence domain of the optimal multiple-impulse solutions.

It can be seen that, despite the fact that the optimal multiple-impulse solutions by no means always exist, the six- and five-impulse solutions obtain a considerable gain in the total delta-v expenditures in comparison with the solution to Lambert's problem.

Table 4-2. Impulse parameters with $\theta^* = 0.33$.

ΔV_{t_I}	0	0.0037	0.0049	$\Delta\varphi_2 = 0.0342$
$\Delta V_{t_{II}}$	-0.0003	-0.0033	0	$\Delta\varphi_3 = 0.5719$
ΔV_{z_I}	0.0047	-0.0028	0.0037	$\Delta V_6 = 0.0241$
$\Delta V_{z_{II}}$	-0.0003	0.0025	-0.004	$\Delta V_2 = 0.0241$
ΔV_{2_I}	0.0201	0.0089	-0.001	$\Delta\varphi_I = 0$
$\Delta V_{2_{II}}$	0.0257	-0.0039	0	$\Delta\varphi_{II} = 0.8488$

Table 4-3. Impulse parameters with $\theta^* = 0.38$.

ΔV_{t_I}	0.002	0.0017	0.0049	$\Delta\varphi_2 = 0.0462$
$\Delta V_{t_{II}}$	-0.0005	-0.0014	-0.0018	$\Delta\varphi_3 = 0.6166$
ΔV_{z_I}	0.0019	-0.0006	0.0015	$\Delta V_6 = 0.014$
$\Delta V_{z_{II}}$	-0.0001	0.0004	-0.0016	$\Delta V_2 = 0.0239$
ΔV_{2_I}	0.0072	0.0092	-0.0001	$\Delta\varphi_I = 0$
$\Delta V_{2_{II}}$	0.0178	-0.0042	0.001	$\Delta\varphi_{II} = 0.9443$

Table 4-4. Impulse parameters with $\theta^* = 0.469$.

ΔV_{t_I}	0	0.0029	0.0059	$\Delta\varphi_2 = 0.0342$
$\Delta V_{t_{II}}$	-0.0006	-0.0041	0.009	$\Delta\varphi_3 = 0.5719$
ΔV_{z_I}	0.000001	-0.000018	0.000035	$\Delta V_6 = 0.0145$
$\Delta V_{z_{II}}$	0.000003	0.000026	0.00014	$\Delta V_2 = 0.0221$
ΔV_{2_I}	-0.0227	0.0093	-0.0003	$\Delta\varphi_I = 0$
$\Delta V_{2_{II}}$	0.028	-0.0043	0.003	$\Delta\varphi_{II} = 0.1326$

4.4. Long-Range Guidance Manoeuvre Calculating Algorithm

The long-range guidance manoeuvres have the aim of transferring the spacecraft to the given vicinity of the orbital station, in which the equipment of the autonomous approaching starts to work, which ensures the spacecraft can dock in the station (Petrov 1985). The statement of the long-range guidance manoeuvre evaluation problem differs considerably from the statement of the classic rendezvous problem (another functional, multiple constraints on impulses) but, even for the solution of such unconventional problem, one can use the algorithms from Chapter 3 and from the second paragraph of this chapter.

4.4.1. Problem Statement

To ensure terminal conditions with a high accuracy (necessary during the evaluation of the long-range guidance manoeuvres), the iterative scheme is used from the first chapter. This uses the relatively simple Eq. 4-1 for the determination of the impulse parameters.

During the evaluation of the four-impulse long-range guidance manoeuvres, it is assumed that impulses are applied on the two manoeuvring intervals, where the distance between them is not less than 10 revolutions. The following constraints on the impulse angles on the first manoeuvring interval should be fulfilled:

$$\varphi_1 \subseteq \Phi_1, \varphi_2 \subseteq \Phi_2, \tag{4-16}$$

where Φ_1, Φ_2 = given sets. Usually, they are continuous intervals, starting in the interval of $200^o \div 220^o$ of one revolution and finishing in the interval of $60^o \div 80^o$ of the next revolution. The application angles of the third and the fourth impulses are fixed on the last revolution of flight:

$$\varphi_3 = \varphi_{3_f}, \varphi_4 = \varphi_{4_f} \tag{4-17}$$

As a rule, these impulses are applied one and a half revolution before the rendezvous point.

The orientation of the last two impulses is fixed in order to maintain the satisfaction of condition 4-1d despite the errors in the thrust engines burns:

$$\frac{\Delta V_{r_i}}{\Delta V_{t_i}} = \frac{a_{r_i}}{a_{t_i}}, \Delta V_z = 0 \, (i = 3,4), \tag{4-18}$$

The penalty members are introduced for the first two impulses in the functional of the problem (Petrov 1985):

$$Q_i = k\sqrt{(a_{r_i}\Delta V_{t_i} - a_{t_i}\Delta V_{r_i})^2 + (a_{r_i}^2 + a_{t_i}^2)\Delta V_{z_i}^2},$$

where $a_{r_i} = 2 - 2\cos\varphi_i, a_{t_i} = -3 + 4\sin\varphi_i, k = k^*\delta\psi$, k^* is the set coefficient ($k^* > 0$), and $\delta\psi$ is the given maximum error in the impulse orientation.

The problem can be stated as follows: find the values of $\Delta V_{r_i}, \Delta V_{t_i}, \Delta V_{z_i}, \varphi_i \, (i = 1,..., N)$, which minimize the functional

$$F = \sum_{i=1}^{4}\sqrt{\Delta V_{r_i}^2 + \Delta V_{t_i}^2 + \Delta V_{z_i}^2} + \sum_{i=1}^{2} Q_i$$

with the constraints 4-1a–4-1f and 4-16–4-18.

4.4.2. Solution Algorithm

Let us introduce the additional constraint:

$$\Delta V_{r_1} = \Delta V_{r_2} = 0, \tag{4-19}$$

which simplifies the problem. Let us note that the obtained solution is close to optimal (as was shown in Chapter 3, the optimal multiple-revolution solution, as a rule, has small or zero radial impulse components).

The distance between the rendezvous point and the first manoeuvring interval notably exceeds the magnitudes of the intervals. This is why, as always, one can transit from Eq. 4-1d to the approximate equation, which determines the sum of the transversal impulse components of the first manoeuvring interval:

$$\Delta V_{t_I} = \Delta V_{t_1} + \Delta V_{t_2} \approx -\frac{\Delta t}{3\varphi_0}, \tag{4-20}$$

where φ_0 = some point of the first manoeuvring interval. The sum of the transversal components of the last two impulses can be determined from Eq. 4-1c:

$$\Delta V_{t_{II}} = \Delta V_{t_3} + \Delta V_{t_4} \approx \frac{\Delta a}{2} + \frac{\Delta t}{3\varphi_0}, \tag{4-21}$$

On the plane e_x, e_y, the curved line *ABCDK* (Fig. 4-11), which starts at point *A* and ends at point *K*, corresponds to the four-impulse solution of eqs. 4-1a–4-1c with constraints 4-18 and 4-19.

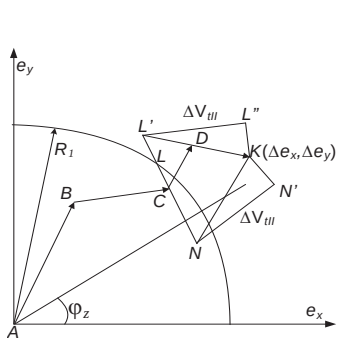

Fig. 4-11. Geometric interpretation of long-range guidance manoeuvres.

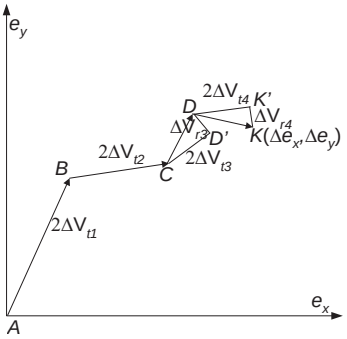

Fig. 4-12. Drift orbit eccentricity vector corresponds to line segment *LN*.

During the mission planning, the initial phase difference Δu between the orbital station and the active spacecraft is chosen in a way that the signs of the transversal components of all the impulses of the optimal solution will coincide (this is possible because the spacecraft deployment orbit always lies inside the station orbit). In this case, it follows from constraint 4-20 that point *C*, which corresponds to the drift orbit eccentricity vector, belongs to the circle of the radius $R_1 = \left|2\Delta V_{t_I}\right|$ with the center in point *A* (Fig. 4-12). According to eqs. 4-17, 4-18, and 4-21, tpoint *C* should also belong to the line segment *L'N* (Fig. 4-12). In this

figure, $L'L''=NN'=\Delta V_{t_{II}}$, $KL''\perp L'L''$, $NN'\perp N'K$, $L''K=\Delta V_{t_{II}}\frac{a_{r_4}}{a_{t_4}}$, $KN'=\Delta V_{t_{II}}\frac{a_{r_3}}{a_{t_3}}$. Thus, point *C* belongs to the line segment *LN*. The positions of *L* and *N* can be made more accurate with the help of the iterative procedure, which differs from the procedures described in Chapter 3, as it is necessary to take into account the radial components of impulses of the second manoeuvring interval. As can be seen from Fig. 4-12, the three-impulse solution with one impulse on the first manoeuvring interval corresponds to point *L*. The unknown magnitudes of the transversal impulse components and the impulse application angle of the first manoeuvring interval can be easily found from eqs. 4-1a–4-1c and 4-20. If Eq. 4-1d cannot be satisfied with a given accuracy using the found manoeuvre parameters, the next iteration is carried out. Eq. 4-1d with the impulse application angle value of the first manoeuvring interval obtained on the previous iteration is used instead of Eq. 4-20 on the second and successive iterations.

The parameters of the manoeuvre, to which point *N* corresponds, are determined in a similar way. It is also a three-impulse manoeuvre, since only the first impulse on the second manoeuvring interval is not equal to zero. There are five unknown variables in the problem: both the impulse application angles of the first interval and the transversal component magnitudes of the three impulses. Hence, the application angle of one of the impulses can be fixed and then the aforementioned iterative procedure can be used.

Let us show that, when the position of the line segment *LN* is known, it is possible to determine the impulse application angles φ_1 and φ_2, where functional *F* is close to its minimal value.

By analyzing the alteration of the sum Q_1+Q_2 (which belongs to functional *F*), it can be shown that its minimum can be obtained if the application angle of at least one of the impulses of the first manoeuvring interval lies in the small vicinity of the node line, $\varphi_i \in G = O_\varepsilon(\varphi_z)$, where $\varphi_z = \operatorname{arctg}\frac{\Delta z}{\Delta V_z} - \pi k$ $(k=1,2,...)$. In this case, the total delta-v expenditures on the orbit plane adjustment are close to the minimum possible values:

$$\Delta i = \Delta V_{z_m} = \sqrt{\Delta z^2 + \Delta V_z^2} \tag{4-22}$$

We will assume that the angles from set *G* belong to one of the intervals Φ_1 or Φ_2. This is acceptable since the length of each of the permitted manoeuvring intervals exceeds half a revolution.

Let us now determine the magnitude of the second impulse application angle of the first manoeuvring interval for the minimal total delta-v $\Delta V_I = \sum_{i=1}^{2} \sqrt{\Delta V_{t_i}^2 + \Delta V_{z_i}^2}$; the application angle of one of the impulses belongs to set *G*. In Fig. 4-13, the *i*-th burn is depicted with the interval with the projections $\left|\Delta V_{t_i}\right|$ and $\left|\Delta V_{z_i}\right|$ on the axes ΔV_t and ΔV_z, respectively. It is obvious that the curved line *APM* corresponds to $\Delta V_I = \sqrt{\Delta V_{t_1}^2 + \Delta_{z_1}^2} + \sqrt{\Delta V_{t_2}^2 + \Delta V_{z_2}^2}$. It follows from eqs. 4-20 and 4-22 that the minimal possible value of ΔV_I is $\Delta V_{Imm} = \sqrt{\Delta V_{t_I}^2 + \Delta V_{z_m}^2}$. It can be obtained if $\frac{\Delta V_{z_1}}{\Delta V_{t_1}} = -\frac{\Delta V_{z_2}}{\Delta V_{t_2}}$ and $\left|\Delta V_{z_1}\right| + \left|\Delta V_{z_2}\right| = \Delta V_{z_m}$ (the line segment *AE* corresponds to such solution in Fig. 4-13). The necessary values of ΔV_{z_1} and ΔV_{z_2} can only be found if the application angles of both impulses of the first manoeuvring interval belong to set *G* (the impulses are applied on the line of the orbit plane's intersection). This is the fourth type of optimal solution from Chapter 2 when the primer vector hodograph degenerates to the line segment. This type of solution exists if the line on plane e_x, e_y with the inclination φ_z to the abscissa axis intersects with the reference frame origin and with the line segment *LN*. If the line does not intersect with the line segment *LN*, then the orbit plane adjustment is fulfilled by the impulse with an application angle that belongs to set *G* (it is applied in the orbit plane intersection line). The magnitude of the lateral component of this impulse is ΔV_{z_m}. For solutions of this type, ΔV_I would be minimal when the transversal impulse component, which alters the orbit plane orientation, is maximum. For example, if the plane is rotated by the second impulse, then *ADE*<*AD'E* with *DM'*>*D'M'* (Fig. 4-13).

It can be easily seen that, in order to have the maximum transversal impulse component, which rotates the orbit plane, it is necessary to have the line segment perpendicular to *LN* in the plane e_x, e_y, which corresponds to the other impulse of the first manoeuvring interval. The

application angle of this impulse should belong to the set

$$\varphi_n = \varphi^* - \frac{\pi}{2} - 2\pi n \,(n = 1,2,...)\,, \qquad \text{where } \varphi^* = \operatorname{arctg} \frac{e_{y_N} - e_{y_L}}{e_{x_N} - e_{x_L}};$$

$e_{x_L}, e_{y_L}, e_{x_N}, e_{y_N}$ = coordinates of the points *L* and *N*, respectively.

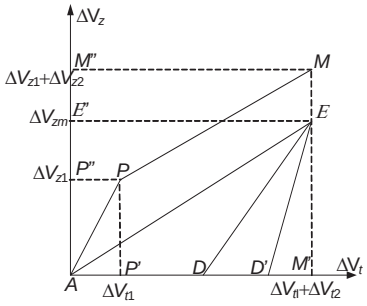

Fig.4-13. Comparison of solutions for the total delta-vs.

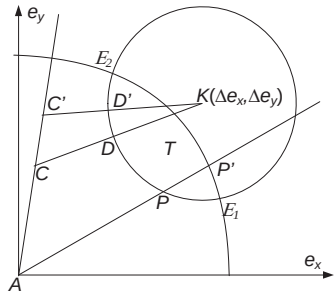

Fig.4-14. Application angles of the third and fourth impulses are not fixed.

If signs of the transversal components do not coincide with each other or the angle φ_n does not belong to the permitted manoeuvring intervals 4-16, then the optimal result will be the solution with the drift orbit, which corresponds with one of the ends of the line segment *LN* c. The boundaries of the line segment *LN* are determined with the condition that the impulse application angles of the first manoeuvring interval belong to the set 4-16.

The total delta-v of the found solution ΔV_Σ was determined with the constraint 4-19 and the condition that the application angle of one of the impulses of the first manoeuvring interval belongs to set *G*, which is why it should be compared with ΔV_m (the minimal possible total delta-v of the transfer to the given rendezvous point). If their difference is lesser than ΔF (the permitted accuracy of determination of the minimum of the functional *F*), the problem is considered to be solved.

In order to find ΔV_m, it is necessary to determine the total delta-v of the manoeuvre (the fixed point of the line segment *LN* corresponds to the drift orbit of this manoeuvre) and then, by varying the position of this point on the line segment *LN*, the value of ΔV_m is determined.

The line, which intersects the points L and N, can be described by the equation $e_y = d + be_x$,

where $d = \left(e_{y_L} - e_{x_L}\right)\dfrac{e_{y_N} - e_{y_L}}{e_{x_N} - e_{x_L}}, b = \dfrac{e_{y_N} - e_{y_L}}{e_{x_N} - e_{x_L}}$.

For this line, the minimal delta-v of the first manoeuvring interval ΔV_{Im} as a function of e_x is given by

$$\Delta V_{Im}(e_x) = \sqrt{\frac{1}{2}}\sqrt{\Delta V_{z_m}^2 + E^2 - \Delta V_{t_I}^2 + \sqrt{\begin{matrix}(\Delta V_{z_m}^2 - E^2 + \Delta V_{t_I}^2)^2 \\ + 4(\Delta V_z(d + be_x) - \Delta z e_x)^2\end{matrix}}},$$

where $E^2 = (d + be_x)^2 + e_x^2$.

The equation for the total delta-v of the transfers without the constraint on the time between the close and almost circular noncoplanar orbits from paragraph 2.2 (the nondegenerate case) was used here.

The total delta-v of the impulses of the second manoeuvring interval ΔV_{II} as a function of e_x is given by

$$\Delta V_{II}(e_x) = \Delta V_{II_L} + \left(\Delta V_{II_N} - \Delta V_{II_L}\right)\frac{e_x - e_{x_L}}{e_{x_N} - e_{x_L}},$$

where $\Delta V_{II_L} = \Delta V_{t_{II}}\left(1 + \left(\dfrac{a_{r_3}}{a_{t_3}}\right)^2\right)^{1/2}, \Delta V_{II_N} = \Delta V_{t_{II}}\left(1 + \left(\dfrac{a_{r_4}}{a_{t_4}}\right)^2\right)^{1/2}$.

By minimizing the total delta-v of the four-impulse manoeuvre $\Delta V = \Delta V_{Im}(e_x) + \Delta V_{II}(e_x)$ on the interval $[e_{x_L}, e_{x_N}]$, one can determine ΔV_m. If $\Delta V_\Sigma - \Delta V_m \le \Delta F$, the solution may be considered to be solved. If this is not the case, the found solution is used as the first guess for the minimization of the functional F with the help of the polytope method from Himmelblau (1975) or with the help of the numerical methods from the next chapter.

The algorithm is also applicable in cases when the impulse magnitudes are limited from below, or when it is needed to have approximately equal impulses of the second manoeuvring interval, etc.

Let us consider, for example, how the algorithm would change if the impulse application angles of the second manoeuvring interval are not fixed. In this case, they can be varied in order to minimize the magnitude of functional *F*. As was shown in Chapter 3, solutions with coinciding signs for the transversal components of all impulses exist, if the circles with the radii R_1 and R_2 intersect (Fig. 4-14). The points, which correspond to the drift orbit parameters of such solutions, should belong to set *T*, which holds the points from the area of the circle intersection. It is necessary to find the point which will ensure the minimal ΔV_I.

If the line with the inclination angle φ_z to the axis e_x intersects the curve E_1E_2 (for example, the line AP' in Fig. 4-14), then, just like in the case for the fixed angles φ_3, φ_4, for any point of the line segment PP', one can obtain the minimal possible $\Delta V_I : \Delta V_{I_{mm}}$ by choosing the variables ratio ΔV_{z_1} and ΔV_{z_2}. The application angle of the third impulse is chosen arbitrarily, and the application angle of the fourth impulse is unambiguously connected with it and can be easily determined.

If the straight line with the inclination angle φ_z does not intersect the curve E_1E_2 (for example, the straight-line AC' in Fig. 4-14), then point *C* needs to be found (*AC* should be maximum with the condition $AC + CD = \Delta V_I$). It can be easily seen that, in order to ensure the maximum value of *AC*, point *D* should belong to the line segment *CK* (Fig. 4-14).

The optimal acceptable transfer *ACDK* has one burn on the second manoeuvring interval. The application angle of this impulse can be evaluated by the following equation:

$$\varphi_3 = 2\operatorname{arctg}\frac{\Delta a\cos\frac{\varphi_z}{2} - \Delta e\cos(\operatorname{arctg}(\frac{\Delta e_y}{\Delta e_x}) - \frac{\varphi_z}{2})}{-\Delta a\sin\frac{\varphi_z}{2} + \Delta e\sin(\operatorname{arctg}(\frac{\Delta e_y}{\Delta e_x}) - \frac{\varphi_z}{2})} - 2\pi n, (n = 1,2,...),$$

where $\Delta e = \sqrt{\Delta e_x^2 + \Delta e_y^2}$.

4.4.3. Examples

Let us consider the solutions to the three problems as examples (Baranov 1990, 61–67). For the solution to problem 1, the velocity impulse application angles of the first manoeuvring interval belong to set *G* and are connected with each other by the equation $\varphi_2 - \varphi_1 = \pi$ (the optimal position of the point *C* on the line segment *LN* is the point of its intersection with the line with the inclination angle φ_z). An additional constraint was introduced for the solution to problem 2: the second manoeuvring interval impulse magnitudes should be approximately equal (point *C* is situated in the middle of the line segment *LN*). The initial conditions of problem 2 practically coincide with the initial conditions of problem 1. For the solution to problem 3, only one of the impulse application angles of the first manoeuvring interval belongs to set *G* (it is necessary to find the optimal point on the line segment *LN*).

The entry data and the solution results for the problems are listed in Tables 4-5–4-9.

Table 4-5

Problem	Δe_y	Δe_x	Δa	Δt	Δz	ΔV_z
1	-23.77	-22.88	108.83	-10,005.87	-12.23	0.36
2	-23.75	-21.56	108.82	-10,003.41	-12.19	0.31
3	-23.96	-22.41	109.06	-10,004.56	-12.05	0.40

Table 4-6

Problem	Φ_1		Φ_2	
	φ_{11} rad	φ_{12} rad	φ_{21} rad	φ_{22} rad
1	-85.217	-79.959	-85.217	-79.959
2	-85.217	-79.959	-85.217	-79.959
3	- 77.79	-73.449	-77.79	-73.449

Table 4-7

Problem	F	ΔV	F_p
1	75.63	57.35	75.68
2	78.24	60.10	75.71
3	74.39	57.72	74.04

Table 4-8

Problem	$-\varphi_1$	ΔV_{r_1}	ΔV_{t_1}	ΔV_{z_1}	$-\varphi_2$	ΔV_{r_2}
1	83.282	0.23	28.36	-8.28	80.140	0.10
2	83.736	0.33	26.38	0	80.136	0.09
3	77.002	0.25	27.80	-12.06	73.449	0.19

Table 4-8 Continued

Problem	ΔV_{t_2}	ΔV_{z_2}	ΔV_{r_3}	ΔV_{t_3}	ΔV_{r_4}	ΔV_{t_4}
1	12.95	3.95	0.0	1.47	5.46	12.87
2	12.06	12.19	0.0	7.75	2.97	7.01
3	15.98	0.0	0.0	2.82	3.37	7.94

Table 4-9

Solution	F	ΔV	$-\varphi_1$	$-\varphi_2$	ΔV_1	ΔV_2	ΔV_3	ΔV_4
1	77.18	59.95	77.774	73.861	31.97	16.27	11.22	0.54
2	76.21	59.64	77.062	73.861	28.62	19.33	0.54	11.16
3	76.20	59.63	77.070	73.861	28.6l	19.33	0.64	11.05
4	74.53	57.86	77.002	73.743	31.00	15.22	0.53	11.11
5	74.39	57.72	77.002	73.449	30.30	15.99	2.82	8.62

Table 4-5 holds the deviations between the initial and the final orbits. The dimensionless deviations were multiplied by $V_0 = 7{,}771\,\text{m/s}$, which corresponds to $r_0 = 6{,}600\,\text{km}$ for descriptive reasons. Table 4-6 shows the manoeuvring intervals, which are allowed for the application of the first two impulses (in radians, starting from the rendezvous point). The application angles of the third and the fourth impulses are fixed: $\varphi_3 = -360^\circ$, $\varphi_4 = -180^\circ$. Table 4-7 shows the values of functional F and

ΔV. The global minimum values of functional F_p, which were obtained with the help of a numerical algorithm, that uses the enumeration of the points from the sets φ_1, φ_2, are listed for the solution accuracy control. This algorithm is presented in Chapter 5.

Table 4-8 shows the solution parameters for each problem. Table 4-9 shows the solution results for all analyzed points of the sets φ_1, φ_2 for problem 3.

Let us consider the solution results for all the problems. In the solution to problem 1, the impulse application angles of the first manoeuvring interval belong to set *G* and the transversal components of all impulses are positive. In this case, the found solution is globally optimal, which can be verified by cross-checking (see the last column of Table 4-7). The small discrepancy in favor of the analytical solution can be explained by the fact that during the numerical solution it is practically impossible to obtain the angles from set *G*.

Sometimes we need to have approximately equal impulse magnitudes of the last manoeuvring interval when we are solving the problem. The suggested algorithm allows finding such solutions: we should use the iterative procedure, which is similar to the procedure from the previous chapter.

During the process of the solution to the second problem, the coefficient $\tilde{k} = \Delta V_{t_4} / (\Delta V_{t_3} - \Delta V_{t_4})$, which determines the position of point *C* on the line segment *LN*, was chosen equal to 0.5. We should take $\tilde{k} = 0.4769$ in order to get equal magnitudes of the third and fourth impulses. During the solution to problem 1, the impulse application angles of the first manoeuvring interval are chosen on the node line and the other one is determined with the help of the iterative procedure. Only one of the angles of set *G* is acceptable: when the orbit plane is changed by the second impulse.

It can be seen from Table 4-8 that the ratio between the lateral component of the second impulse and its magnitude in the solution to problem 2 considerably exceeds the analogous ratios in the solution to problem 1. Thanks to this, the total transfer delta-v increases and, hence, the magnitude of functional *F* for problem 2 also increasesThis conclusion verifies the results listed in Table 4-7.

For solution to problem 3 with the application angles of both impulses of the first manoeuvring interval from set *G*, the signs of the transversal components do not coincide. In accordance with the aforementioned algorithm, it is assumed that only one angle belongs to set *G*, and the

application angle of the other impulse of the first manoeuvring interval should be determined.

Only one point from set G ($\varphi_2 = -73.861$) is suitable for the application of the second impulse of the first manoeuvring interval. With the help of the iterative procedure, one can determine the application angle of the first impulse, with which point N would correspond to the drift orbit parameters. Since the constraint on the minimal possible magnitude of the impulse is used, ΔV_{t_4} is set to its minimal possible value of 0.5 m/s. The solution parameters are given in the first row of Table 4-9. The second row of the table shows the solution parameters; point L corresponds to the drift orbit eccentricity vector. After the determination of the position of the line segment LN, the optimal solution is found (the third row in Table 4-9), which has the line segment on the plane e_x, e_y, which corresponds to the first impulse and is perpendicular to the line segment LN.

Similarly, only one point from set G ($\varphi_1 = -77.002$) is suitable for the application of the first impulse. The solution, which corresponds to point L, exists, and its parameters are presented in the fourth row of Table 4-9. The solution, where the drift orbit eccentricity vector corresponds to point N' ($\Delta V_{t_4} = 0.5$ m/s), and the solution, where the direction of the second impulse on the plane e_x, e_y is perpendicular to the line segment LN', are not acceptable since the angles from set G, which are used in them, do not belong to the permitted manoeuvring interval. The first acceptable angle will be $\varphi_2 = -73.449$. This solution is written in the fifth row of Table 4-9. As was shown, the found solution in this case is optimal among the solutions with the application angle of the first impulse belonging to set G. The comparison between this solution and the third solution from Table 4-9 shows that it is globally optimal, which is why its parameters are listed in Tables 4-7 and 4-8.

The solution time is much smaller in comparison with the numerical algorithms from the works of Petrov (1985), Bazhinov and Yastrebov (1978), and Baranov (1986, 324–327). If the application angles of the third and the fourth impulses are not fixed, then the problem solution time in the presented algorithm does not change, and the numerical algorithms computing the time increase by dozens.

Let us remember that, for illustrative purposes, all the dimensionless values in all of the Tables were multiplied by $V_0 = 7{,}771$ m/s ($r_0 = 6{,}600$ km).

4.5. Comparison of the Solutions Used by NASA, the Russian Mission Control Center, and the Combined Solution

A relatively simple manoeuvring scheme is often offered for the noncoplanar rendezvous solution. The circular orbit is formed by the two impulses of the first manoeuvring interval; the period of which ensures the necessary arrival time to the start of the second interval then, with the help of the impulses from the second interval, the transfer to the rendezvous point on the given orbit is ensured. The lateral impulse, which aligns the orbit planes, is applied on one of these intervals or on the drift revolution on the line of the orbit plane intersection. Such a manoeuvring scheme (we will call it "separate") is attractive due to its simplicity, but it demands excessive total delta-v expenditures. Even manoeuvres in the orbit plane may not be optimal during the implementation of such a scheme. This scheme was used, for example, for the docking of Shuttle[2] with the International Space Station (Fehse 2003, 441–449).

Fig. 4-15 shows an example of when the usage of the circular drift orbit does not increase the total delta-v expenditures. The point with the coordinates (0, 0) should be in set *G* of the intersection of the circles with the radii R_1 and R_2 (let us remember that $R_1 = |\Delta a_I|, R_2 = |\Delta a_{II}|$) for this purpose. The line segments *AB*, *BC*, *CD*, and *DK* correspond to the four impulses by means of which the rendezvous will be performed. However, if the small alteration of the relatively big eccentric vector magnitude (this case is depicted in Fig. 4-16) is needed, the flyby with the circular drift orbit may not be optimal. It can be easily seen that the length of the curved line *ABCDK* (Fig. 4-16), which corresponds to the total delta-v expenditures of the "separate" manoeuvring scheme, will be considerably greater than the sum of the radii R_1 and R_2, which correspond to the total delta-v expenditure of the optimal flyby between the coplanar orbits.

[2] "Shuttle Press Kit: STS-92". Accessed March 25, 2007. http://www.shuttlepresskit.com/STS-92/.

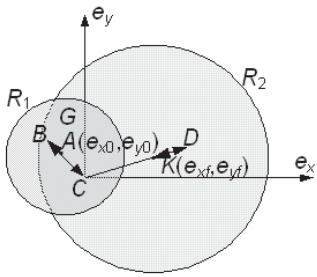

Fig.4-15. Energy is the same for different manoeuvring schemes.

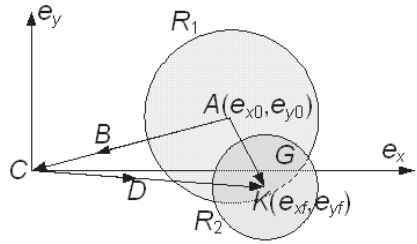

Fig.4-16. Energy differs dramatically from scheme to scheme.

Fig. 4-17 compares the total delta-v expenditures with the accountancy of the expenditures on the orbit plane rotation. Let us suppose that we deal with the case depicted in Fig. 4-15 where the "separate" manoeuvring scheme has the same expenditures on the coplanar rendezvous as the optimal solution. The sum of the impulse transversal components of the first manoeuvring interval is ΔV_{t_I}, and the line segment *AD* corresponds to it (Fig. 4-17). The sum of the transversal impulse components of the second manoeuvring interval is equal to $\Delta V_{t_{II}}$, and the line segment *DN* corresponds to it. The minimal expenditures on the orbit plane rotation are ΔV_{z_m}, and the line segment *AL* corresponds to them. The impulse that changes the orbit plane is situated between the second and the third manoeuvres in the orbit plane. Thus, the curved line *ADPE* corresponds to the "separate" manoeuvring scheme. The curved line *APE* (Fig. 4-17) corresponds to the manoeuvring scheme, which is used for the motion control of the "Soyuz" and the "Progress" spacecrafts, in which the impulses of the first manoeuvring interval have both transversal and lateral components and the impulses of the second interval have only transversal components. If the line with the inclination angle φ_z intersects the line segment *LN* (Fig. 4-12), then the point *P* belongs to the line segment *LE* (Fig. 4-17).

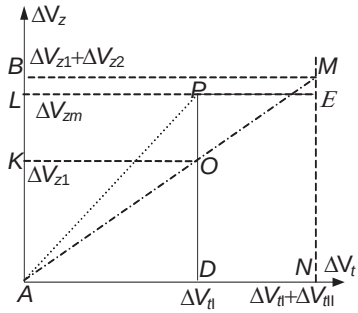

Fig. 4-17. Comparison of solution total delta-vs

The line segment *AM* corresponds to the optimal solution, where the correction of the orbit plane position is fulfilled by all four burns, which have both transversal and lateral components; the line segment *AO* corresponds to the impulses of the first interval, while the line segment *OM* corresponds to the impulses of the second interval.

It is obvious that the length of the curved line *ADPE* is greater than the length of the curved line *APE* and the length of the curved line *APE* is greater than the length of the line segment *AM*. With the decrease in the expenditures on rotation of the orbit plane (with the decrease of the length of the line segment *DP*), the difference in the total delta-v expenditures of all three types of the solution decreases.

Since the time of the launch is usually chosen in a way that the active spacecraft occurs on the target spacecraft orbit plane, the total delta-v expenditures on the orbit plane rotation are considerably less than the expenditures on the alteration of, for example, the orbit semimajor axis. In these cases, all three types of the solution have a close total delta-vs. As it will be shown in Chapter 7, the total delta-v may differ considerably in more complex problems.

4.6. Noncoplanar Rendezvous Achieved by Impulsive Manoeuvring Over a Longer Period of Time

In the aforementioned problems, it was supposed that the manoeuvres were performed on the two separated manoeuvring intervals. There are several, revolutions between these intervals, which are prohibited for the impulse application.

The variants when the thrust engines have a relatively low thrust but when a flyby to the given point is needed to be fulfilled relatively quickly can be often met. In this case, it is necessary to manoeuvre on the big number of the successive revolutions; the number of revolutions that are prohibited for manoeuvring is relatively small and they are needed for the orbit parameter current update. It will be shown in this section that the solution method which applied in the first sections of this chapter is also applicable for this manoeuvring scheme. The magnitudes of all manoeuvres should be approximately the same; this would allow decreasing the total delta-v of the manoeuvres and using the impulsive approximation during the determination of these manoeuvres.

4.6.1. Determining the Length of Subintervals

The whole manoeuvring interval (the number of the revolutions permitted for manoeuvring is N) is divided into two subintervals (N_1 and N_2). Initially, it is assumed that the subintervals have equal lengths ($N_1 = N_2, N_1 + N_2 = N$) with an even N, and differ by one with an uneven N. The interval may be prohibited for the manoeuvring revolutions, which is why the numbers of revolutions on which the manoeuvring is allowed on the subintervals (we will denote them as N_{1_i}, N_{2_j} ($1 \le i \le N_1, 1 \le j \le N_2$), may not be in successive order. During the determination of the genuine values N_1 and N_2, several stages can be distinguished.

Stage 1. The semimajor axis alteration on each of the subintervals is assessed with the help of the equation of time and the general semimajor axis alteration.

Stage 2. The parameters of the two-impulse manoeuvre of the transfer between the orbits are determined (the five equations and the algorithms used can be taken from Chapter 2) with the assumption that the sum alteration of the semimajor axis on both subintervals is corrected; the members of the sum were calculated on the previous stage.

Stage 3. Each of the two estimated manoeuvres are divided between the subintervals, proportionally to the alteration of the semimajor axes on the subintervals.

Stage 4. At this stage, each of two manoeuvres of the subintervals is divided by the number of the revolutions on this subinterval. Thus, the two manoeuvres of the first manoeuvring subinterval are divided by N_1 on equal parts and applied on the different revolutions. Similarly, the

manoeuvres of the second manoeuvring subinterval are divided by N_2 on equal parts ($N_1 + N_2 = N$). The equal duration of the manoeuvres on the revolutions is optimal for the small orbit element alteration.

For example, if the magnitude of the manoeuvres on the revolution of the first subinterval considerably exceeds the magnitude of the manoeuvres on the revolution of the second subinterval, then the number of the manoeuvring revolutions on the first subinterval will be increased by 1, and the number of the manoeuvring revolutions on the second subinterval will be decreased by 1. The transition to the first stage of the calculation is carried out. The procedure ends when the ratio of impulse magnitudes becomes opposite, or when the interval decreases to one revolution. The variant with the lesser magnitude of the manoeuvres on the second interval should be chosen out of the two boundary cases. The results of this procedure are the values of N_1 and N_2.

Each stage is thoroughly considered below.

Stage 1. By using the equations for the time of the arrival to the rendezvous point and for the semimajor axis alteration, the sum magnitudes of the transversal components $\Delta V_{t_1}, \Delta V_{t_2}$ on the first and the second manoeuvring subintervals are assessed:

$$\sum 3\left(2\pi\left(N_{ap} - N_{1_i}\right) - \pi\right)\frac{\Delta V_{t_I}}{N_1} + \sum 3\left(2\pi\left(N_{ap} - N_{2_i}\right) - \pi\right)\frac{\Delta V_{t_{II}}}{N_2} = \Delta t,$$

$$\Delta V_{t_I} + \Delta V_{t_{II}} = \Delta a,$$

where N_{ap} = number of rendezvous revolutions.

Then the magnitude of the spacecraft orbit semimajor axis alteration by the manoeuvres on the first manoeuvring subinterval can be approximately assessed by

$$\Delta a_I \approx 2\Delta V_{t_I},$$

and by the manoeuvres on the second manoeuvring subinterval:

$$\Delta a_{II} \approx \Delta a - 2\Delta V_{t_I}.$$

Stage 2. Similar to the way it was done in the first paragraph of this chapter, a variable $\Delta a^* = \left|\Delta a_I\right| + \left|\Delta a_{II}\right|$ is introduced. The problem

solution to the optimal transfer between the orbits, where the deviations of the elements are the initial deviations $\Delta e_x, \Delta e_y, \Delta z, \Delta V_z$ (Δa^* is taken instead of Δa), is found. Since the correction of the eccentricity vector component deviations $\Delta e_x, \Delta e_y$ and $\Delta z, \Delta V_z$ is fulfilled proportionally to the Δa_I and Δa_{II} correction, such a solution to the transfer problem will be optimal.

The parameters $\Delta V_{t_1}, \Delta V_{z_1}, \varphi_1, \Delta V_{t_2}, \Delta V_{z_2}, \varphi_2$ of this transfer between the noncoplanar orbits can be determined with the help of the algorithm presented in the Section 2.2.7, for example.

Stage 3. In order to find the magnitudes of the impulses which ensure the solution of the rendezvous problem, it is necessary to distribute the impulses, as estimated for the solution of the transfer problem, in the needed proportion. Similar to the way it was done in Section 4.1, the impulses are divided in the proportions $\frac{\Delta a_I}{\Delta a^*}, \frac{\Delta a_{II}}{\Delta a^*}$ for the first and the second subintervals, respectively. The four-impulse solution of the rendezvous problem is obtained after the division of each of the impulses into two parts. The impulse components of the first and the second manoeuvring subintervals can be found by eqs. 4-7-4-10 (Baranov 2008, 430–439).

Stage 4. Each of the manoeuvres of the first manoeuvring subinterval are divided on N_1 equal parts and applied on different revolutions; similarly, the two manoeuvres of the second manoeuvring subinterval are divided on N_2 equal parts.

Then according to the aforementioned algorithm, the magnitudes of impulses on revolutions of the subintervals are compared and the decision about the alteration of the lengths of the subintervals and the return to the first stage is made.

With the optimal initial phase, when $\Delta a_I \approx \Delta a_{II}$, the subinterval lengths are equal. If, for example, due to the big initial phase deviation, the decelerating manoeuvres $\Delta a_I < 0$ and $\Delta a > 0$ on the first subinterval are performed and, hence, $|\Delta a_I| < |\Delta a_{II}|$, then the length of the second subinterval will be considerably greater than the length of the first subinterval. If $\Delta a_{II} < 0$, and $\Delta a > 0$, then the length of the first subinterval will be considerably greater than the length of the second subinterval.

The solution to the rendezvous problem with the impulses applied on the permitted for the manoeuvring revolutions is found after the

implementation of this iterative procedure. The impulse magnitudes, which are applied on one revolution, may differ, but the impulse magnitudes applied on different revolutions on the same latitude argument are approximately the same.

Since the simplified equation system was solved, the necessary accuracy of the arrival time to the given point of the target orbit is provided with the help of the usual iterative procedure.

If the manoeuvre duration of the found solution does not exceed approximately 40º by the latitude argument, the problem is solved; otherwise, the solution should be defined more accurately by switching from the impulsive case to the case with the low thrust during the transfer manoeuvre determination. The manoeuvre parameters can be made more accurate with the help of the iterative procedure from the first chapter.

4.6.2. Example

The multiple-impulse rendezvous on the noncoplanar orbits is solved. The elements of the initial and the target orbits are fully similar to the orbit elements from the example 4.2.3. Just like before, the three variants, which differ from each other by the initial location of the target spacecraft, are considered. It is assumed that the manoeuvring is performed on all revolutions of the flyby except the 8th and the 9th which is why the number of manoeuvres in all variants is 26.

The calculation results:

1) $u_{F_1} = 5^\circ$

The total delta-v of the manoeuvres: 322.930 m/s.

The total delta-v of the coplanar components: 322.91 m/s.

The total delta-v of the lateral components: 6.088 m/s.

The first subinterval holds the revolutions from the 2nd to the 12th; the second subinterval holds the revolutions from the 13th to the 16th. The impulses on the first subinterval are accelerating, while the impulses on the second subinterval are braking (the initial phase is not optimal).

The impulse parameters are listed below: impulse number, revolution, latitude argument of the impulse application, and its radial, transversal, and lateral components.

Impulse	Revolution	u deg	dV_r m/s	dV_t m/s	dV_z m/s
1	2	140.164	0.172	11.990	-0.176
2	2	316.164	-0.161	11.232	-0.053
3	3	140.164	0.173	12.103	-0.178
4	3	316.164	-0.162	11.347	-0.053
5	4	140.164	0.175	12.218	-0.179
6	4	316.164	-0.164	11.464	-0.054
7	5	140.164	0.177	12.337	-0.181
8	5	316.164	-0.166	11.584	-0.054
9	6	140.164	0.178	12.458	-0.183
10	6	316.164	-0.168	11.707	-0.055
11	7	140.164	0.180	12.582	-0.185
12	7	316.164	-0.169	11.832	-0.055
13	10	140.164	0.182	12.709	-0.187
14	10	316.164	-0.171	11.960	-0.056
15	11	140.164	0.184	12.839	-0.188
16	11	316.164	-0.173	12.092	-0.057
17	12	140.164	0.186	12.972	-0.190
18	12	316.164	-0.175	12.227	-0.057
19	13	136.164	0.108	-12.904	-0.096
20	13	320.164	-0.115	-13.785	0.074
21	14	136.164	0.107	-12.773	-0.095
22	14	320.164	-0.114	-13.659	0.073
23	15	136.164	0.106	-12.644	-0.094
24	15	320.164	-0.113	-13.536	0.072
25	16	136.164	0.105	-12.518	-0.093
26	16	320.164	-0.112	-13.417	0.072

2) $u_{F_2} = 210^\circ$

The total delta-v of the manoeuvres: 93.123 m/s.

The total delta-v of the coplanar components: 93.101 m/s.

The total delta-v of the lateral components: 1.778 m/s.

The first subinterval holds the revolutions from the 2nd to the 7th, while the second subinterval holds the revolutions from the 10th to the 16th (the 8th and the 9th revolutions are prohibited for manoeuvring). Both subintervals have accelerating impulses (the initial phase is optimal).

Impulse	Revolution	u deg	dV_r m/s	dV_t m/s	dV_z m/s
1	2	144.046	0.003	0.327	-0.009
2	2	312.046	-0.002	0.259	0.002
3	3	144.046	0.003	0.327	-0.009
4	3	312.046	-0.002	0.259	0.002
5	4	144.046	0.003	0.327	-0.009
6	4	312.046	-0.002	0.259	0.002
7	5	144.046	0.003	0.327	-0.009
8	5	312.046	-0.002	0.259	0.002
9	6	144.046	0.003	0.327	-0.009
10	6	312.046	-0.002	0.259	0.002
11	7	144.046	0.003	0.327	-0.009
12	7	312.046	-0.002	0.259	0.002
13	10	144.046	0.066	7.008	-0.197
14	10	312.046	-0.053	5.589	0.043
15	11	144.046	0.066	7.040	-0.198
16	11	312.046	-0.053	5.622	0.044
17	12	144.046	0.067	7.072	-0.199
18	12	312.046	-0.053	5.656	0.044
19	13	144.046	0.067	7.105	-0.200
20	13	312.046	-0.054	5.691	0.044
21	14	144.046	0.067	7.138	-0.201
22	14	312.046	-0.054	5.725	0.045
23	15	144.046	0.067	7.172	-0.202
24	15	312.046	-0.054	5.761	0.045
25	16	144.046	0.068	7.206	-0.203
26	16	312.046	-0.055	5.796	0.045

3) $u_{F_1} = 355^\circ$

The total delta-v of the manoeuvres: 298.730 m/s.

The total delta-v of the coplanar components: 298.71 m/s.

The total delta-v of the lateral components: 3.199 m/s.

The first subinterval holds the revolutions from the 2nd to the 6th, while the second subinterval holds the revolutions from the 7th to the 16th. The first subinterval has braking impulses, while the second subinterval has accelerating impulses (the initial phase is not optimal).

Impulse	Revolution	u deg	dV_r m/s	dV_t m/s	dV_z m/s
1	2	136.151	0.096	-10.084	0.052
2	2	320.151	-0.103	-10.749	0.171
3	3	136.151	0.096	-10.006	0.051
4	3	320.151	-0.102	-10.674	0.170
5	4	136.151	0.095	-9.931	0.051
6	4	320.151	-0.101	-10.600	0.169
7	5	136.151	0.094	-9.856	0.051
8	5	320.151	-0.101	-10.527	0.168
9	6	136.151	0.093	-9.783	0.050
10	6	320.151	-0.100	-10.456	0.167
11	7	140.151	0.117	12.223	-0.195
12	7	316.151	-0.109	11.426	-0.059
13	10	140.151	0.118	12.338	-0.197
14	10	316.151	-0.110	11.544	-0.059
15	11	140.151	0.119	12.457	-0.198
16	11	316.151	-0.111	11.663	-0.060
17	12	140.151	0.120	12.578	-0.200
18	12	316.151	-0.113	11.786	-0.061
19	13	140.151	0.121	12.702	-0.202
20	13	316.151	-0.114	11.912	-0.061
21	14	140.151	0.123	12.829	-0.204
22	14	316.151	-0.115	12.040	-0.062
23	15	140.151	0.124	12.960	-0.206
24	15	316.151	-0.116	12.172	-0.063
25	16	140.151	0.125	13.093	-0.209
26	16	316.151	-0.118	12.307	-0.063

It can be seen in the case of the optimal initial phase that the total delta-v expenditures are analogous to the expenditures for the case when the impulses are applied on the two separated intervals; however, the optimal phase interval is considerably narrower. With the nonoptimal initial phase (the variants 1 and 3), the total delta-v expenditures are much higher than when the impulses are applied on two separate intervals. For the first variant ($u_{F_1} = 5^\circ$), it is 146.12 m/s and 322.930 m/s, respectively, and, for the third variant ($u_{F_1} = 355^\circ$), it is 183.58 m/s and 298.730 m/s, respectively.

CHAPTER FIVE

NUMERICAL METHODS

The optimal manoeuvre parameter determination problem, which ensures the spacecraft rendezvous on close near-circular orbits with the help of the iterative procedure depicted in the first chapter, can be reduced to a mathematical programming problem.

The analytical methods from the previous chapters and different numerical methods can be used for the solution of this problem. However, due to the considerable number of dimensions and constraints of various kinds, attempts using numerical methods lead to big computing time expenses. That is why it is necessary to bear in mind the peculiarities of the considered problems, which will help to speed up the optimization process.

The numerical method from the works of Baranov (1986, 324–327), Baranov (2008), and Baranov, Gundobin, Ivanov, Kapralov et al. (1992, 26–27), which has been successfully used for many years in the ballistic center of the Keldysh Institute of Applied Mathematics of rhe Russian Academy of Sciences for the manoeuvre determination of the "Soyuz" and "Progress" spacecrafts, as well as the "Kvant", "Priroda" modules and others, is described in this chapter. The method is relatively simple and universal. It has the necessary performance characteristics and ensures the high reliability of the problem solution.

5.1. Problem Statement and General Solution Method

If the influence of the second term of the gravitational field expansion series (c_{20}) is taken into account, Eq. 1-12 will be rewritten as follows (Petrov 1985):

$$\sum_{i=1}^{N} \left\{ \Delta V_{r_i} \sin\left[(1-\gamma)\varphi_i\right] + 2\Delta V_{t_i} \cos\left[(1-\gamma)\varphi_i\right] \right\} = \Delta e_x, \quad \text{(5-1a)}$$

$$\sum_{i=1}^{N}\left\{-\Delta V_{r_i}\cos\left[(1-\gamma)\varphi_i\right]+2\Delta V_{t_i}\sin\left[(1-\gamma)\varphi_i\right]\right\}=\Delta e_y, \quad (5\text{-}1b)$$

$$\sum_{i=1}^{N}2\Delta V_{t_i}=\Delta a, \quad (5\text{-}1c)$$

$$\sum_{i=1}^{N}\left\{\begin{array}{l}2\Delta V_{r_i}\left[1-\cos((1-\gamma)\varphi_i)\right]\\+\Delta V_{t_i}\left[-3(1-\gamma)\varphi_i+4\sin((1-\gamma)\varphi_i)\right]\end{array}\right\}=\Delta t, \quad (5\text{-}1d)$$

$$\sum_{i=1}^{N}(-2\beta\Delta V_{t_i}\varphi_i\cos u_i\sin 2i_0-\Delta V_{z_i}\sin\varphi_i)=\Delta z, \quad (5\text{-}1e)$$

$$\sum_{i=1}^{N}(2\beta\Delta V_{t_i}\varphi_i\sin u_i\sin 2i_0+\Delta V_{z_i}\cos\varphi_i)=\Delta V_z, \quad (5\text{-}1f)$$

where $\beta=-c_{20}\dfrac{3r_e^2}{2r_0^2}$, $\gamma=\dfrac{\beta}{2}(5\cos^2 i_0-1)$, $c_{20}=-1082637\cdot10^{-6}$,

r_e = 6378140 m, i_0, r_0 = inclination and radius of the relative orbit, and u_i = latitude arguments of the impulse application points.

Please note, if the duration of rendezvous is small (less than or equal to several days), a simpler scheme can be used (Eq. 4-1).

The angles of impulse applications should belong to the specified sets

$$\varphi_1\subseteq F_1,\ldots,\varphi_N\subseteq F_N. \quad (5\text{-}2)$$

The sets F_i may be less than the revolution and/or contain the several separate intervals, as it was for the first "Progress" spacecraft. The constraints on the moments of the impulse application are connected with the Earth's visibility zones and the structural aspects of the spacecraft, etc. Sometimes the impulse application angles are fixed. For instance, during the determination of the three- and four-impulse manoeuvres of the "Soyuz" and the "Progress" spacecrafts, it was supposed that the application angles of the third and fourth impulses were fixed on the revolution and half a revolution before the rendezvous point.

The problem of searching for the optimal manoeuvre parameters can be stated as follows: determine $\Delta V_{r_i}, \Delta V_{t_i}, \Delta V_{z_i}, \varphi_i$ ($i=1,\ldots,N$) with the minimal functional

$$W = \sum_{i=1}^{N} \sqrt{\Delta V_{r_i}^2 + \Delta V_{t_i}^2 + \Delta V_{z_i}^2} + \sum_{i=1}^{N} Q_i$$

and the constraints 5-1 and 5-2.

The problem functional can encompass the terms Q_i together with ΔV. The terms Q_i account for the problem peculiarities. It is preferable to have Q_i as the convex functions of impulse components, like ΔV. For example, as was already mentioned in Chapter 4, the functional for the "Soyuz" and the "Progress" spacecrafts will be (Petrov 1985):

$$W = \sum_{i=1}^{N} \sqrt{\Delta V_{r_i}^2 + \Delta V_{t_i}^2 + \Delta V_{z_i}^2} + \sum_{i=1}^{N} k_i \sqrt{(a_{r_i} \Delta V_{t_i} - a_{t_i} \Delta V_{r_i})^2 + (a_{r_i}^2 + a_{t_i}^2) \Delta V_{z_i}^2}.$$

Here, $a_{r_i} = 2 - 2\cos\varphi_i$, $a_{t_i} = -3 + 4\sin\varphi_i$, $k_i = k_i^* \delta\psi$ $(k_i^* > 0)$ are the fixed coefficients, and $\delta\psi$ = the agreed maximum error in the impulse orientation.

Unlike the impulse component space, in the space of the impulse application angle, functional W will have local minimums. Besides, the sets F_i might be rather complex. Consequently, the minimization process is usually fulfilled in two steps (Petrov 1985): firstly, the minimum of the functional is determined for each fixed $\varphi^T = \{\varphi_1, ..., \varphi_N\}$

$$W_m(\varphi) = \min_{\Delta V} W(\varphi, \Delta V) \tag{5-3}$$

over the variables $\Delta V^T = \{\Delta V_{r_1}, \Delta V_{t_1}, \Delta V_{z_1}, ..., \Delta V_{r_N}, \Delta V_{t_N}, \Delta V_{z_N}\}$ and the constraints (Eq. 5-1). On the second step, the global minimum of the functional $W_m(\varphi)$ over the variables $\varphi^T = \{\varphi_1, ..., \varphi_N\}$ is found by enumerating the points out of the acceptable impulse application set $F = F_1 \cdot F_2 \cdot ... \cdot F_N$.

It should be noted that the steps are carried out in turn, and not in a successive manner. A point is taken from set F. By applying the minimization in the space of the impulse components, W_m can be determined and then, after that, another point from set F is taken and the

corresponding W_m can be evaluated, etc. The process continues until the solution is found, which will be optimal in the space of the impulse components and in the space of the impulse application angles.

Each stage of the problem solution will be considered thoroughly in the next two sections.

The found solution is used in the iterative procedure from Chapter 1, which ensures the satisfaction of the terminal conditions with the given accuracy and by taking into account the atmosphere influence, the given number of the harmonics of the gravity field, and the burn duration, etc.

5.2. Minimization with Involved Components of Velocity Impulses

This minimization can be carried out by different methods, but the best option is to avoid it in the first place. For this purpose, the number of the used velocity components should be equal to the number of the system constraints accounted for in 5-1. If there is a need to account for the six equations of the equation system, the six impulse components will be used: four planar and two lateral. All six impulse components are used for the two-impulse problem. It is necessary to omit some of the impulse components for the three- and four impulse problems. As was shown in Chapter 3, it is necessary to omit the radial impulse components for the four-impulse problem. In this case, the values of the transversal impulse components can be determined from Eq. 5-1 unambiguously. In the case of the three-impulse problem, it is necessary to omit the radial impulse components, which are applied on one manoeuvring interval, and then the transversal components and the radial component of the impulse, which is applied on the corresponding manoeuvring interval, can be determined unambiguously from Eq. 5-1 as well. It is necessary to remember that the circle, which corresponds to the transversal components of the two impulses and is performed on a single manoeuvring interval (see 3.3), should not be inside the circle which corresponds to the transversal velocity component of the sole impulse on its interval. It is necessary to change the impulse distribution between the intervals if this situation occurs.

The use of the aforementioned technique of reducing the number of the used components may lead to an increase of ΔV due to the lack of some radial components, but it is compensated by the simplicity and reliability of the obtained solution.

It is a little bit more difficult to deal with the lateral components, as it is not clear which impulses should have these components for the better

result. It is recommended to use the lateral components for the impulses where it was agreed to not use the radial components in the three-impulse problem. For the four-impulse problem, it is necessary to use the lateral components of the impulses of the first manoeuvring interval. Thus, the simpler problem with practically no lateral components will be solved on the second manoeuvring interval (before the docking). If there is a need to decrease the total delta-v, the lateral impulse components should be used on the interval with the greater sum of the transversal components. In the case of a long rendezvous duration and big deviations of RAAN (Ω), the usage of the lateral impulse components of the first manoeuvring interval is almost necessary (see Chapter 7), but it is better to use the lateral impulse components of both manoeuvring intervals. There is another simple option of choosing the optimal lateral impulse components. It will be given later in this text.

If there is a need to find the optimal solution and more than two impulses are used, then minimization in the space of the impulse components is necessary. In order to simplify this, the linear constraints 5-1 are used for the transition to the unconditional minimization in the space of the lesser number of dimensions during the search for $W_m(\varphi)$. In this case, the dimensionality of the minimization space will be reduced by the number of accounted for constraints in the form of equality.

It is important to choose the impulse components as the independent variables. This is obvious for the impulse components, which lie in the orbital plane. The transversal components make a major contribution in the alteration of the orbit elements; their magnitudes alter gradually with the alteration of the impulse application angles, and the radial components are practically always equal to zero. Thus, it is better to use the radial components as independent variables and take their zero values as the starting point of the minimization process. This would allow gradually reducing the number of the minimization steps, which are needed for the minimum determination.

It is harder to deal with the lateral impulse components because it is hard to distinguish a priori the ones that would make the least contribution in the minimization process and, hence, could be used as independent variables. However, if there is an option to alter the purpose of the independent lateral impulse components during the transition from one set of the impulse application angles to another, then there is an option to distinguish the less effective components.

In the case of a long rendezvous duration, the most effective will be the lateral components with the impulse application angles close to equatorial, as the alteration of inclination causes the secular influence on

the alteration of the RAAN. Hence, it is better to use the impulse components with the application angles most distant from the equator as the independent variables.

In the case of a relatively small rendezvous duration (the distance between the manoeuvring intervals does not exceed the several dozens of revolutions), the inclination correction does not noticeably affect the RAAN. In this case, the effectiveness of the lateral component only depends on the proximity of the impulse application angle to the optimal orbit plane correction angle φ_z (the orbit plane intersection line). In Fig. 5-1a, one can find the direction of the optimal orbit plane correction φ_z, the magnitude of the lateral deviation Δi (*AK*), which needs to be corrected ($\Delta i = \sqrt{\Delta z^2 + \Delta V_z^2}$), and the four angles of the impulse application $\varphi_1, \varphi_2, \varphi_3, \varphi_4$. If only the lateral deviation correction is under consideration, the usage of the second and the third lateral components (the curved line *ABK* corresponds to this solution) will be more effective than the usage of the first and the fourth components, because the length of the curved line *ADK* corresponding to this solution is bigger than the length of the curved line *ABK*. Thus, it is optimal to use the lateral impulse components with the application angles mostly close to φ_z and lying on different sides from this direction (Baranov 2008).

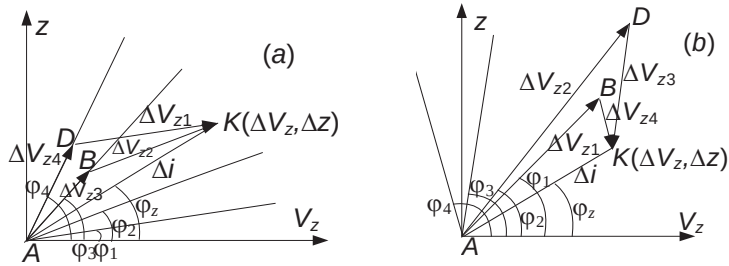

Fig. 5-1. Two-impulse correction of lateral deviation:
(a) impulses are applied on different sides from node line; (b) impulses are applied on one side of node line.

If the impulse application angles lie on one side from the direction φ_z (Fig. 5-1b), then it is necessary to use the closest one and the most distant impulse components instead of the two closest ones. The curved line *ABK* in Fig. 5-1b corresponds to this solution. The curved line *ADK*

corresponds to the solution with the two other components. Its line length is obviously bigger than the length of the curved line *ABK*. Thus, the most effective components are determined. The rest are less effective, and they should be used as the independent variables during the minimization of the functional *W*. Their zero values are taken as the initial point of the minimization process.

Using the same effectiveness assessment of the lateral components, it is possible to avoid the minimization in their space and leave the two most effective ones.

One more conclusion from the above-mentioned examples may be handy. For the correction of the lateral deviations, it is more effective to use the sets of the impulse application angles with the angles that lie on the different sides from the direction φ_z.

During the flight support of a real spacecraft, it is necessary to solve the problems with different numbers of impulses and with different constraints, so the software should be universal enough.

To ensure this utility along the minimization in the space of the impulse components, the following computing scheme is used.

With the help of the matrix *J*, the deviation set is set, which needs to be corrected (from the full deviation vector Δ, which is used in Eq. 5-1, one can turn to the vector with a smaller number of dimensions $\Delta_k = J\Delta$ if needed). The impulse components ΔV_k, which will be used for the problem solution, are set in the corresponding scale with the help of the flags. The influence matrix A_k of these impulse components on the chosen deviations is formed. The constraints 5-1 can be described as

$$A_k \Delta V_k = \Delta_k . \tag{5-4}$$

Another scale holds the impulse components ΔV_i which will be the independent variables in the space of which the optimization will take place. The rest of the components will be the depending variables ΔV_d ($\Delta V_k = \Delta V_i + \Delta V_d$).

The matrix A_k can be divided into the corresponding parts. Constraint 5-4 will be as follows:

$$A_i \Delta V_i + A_d \Delta V_d = \Delta_k . \tag{5-5}$$

From Eq. 5-5, one can find ΔV_d:

$$\Delta V_d = A\Delta V_i + \Delta_k^* \tag{5-6}$$

where $A = -A_d^{-1}A_i$, $\Delta_k^* = A_d^{-1}\Delta_k$.

Thus, the transition to the unconditional minimization W in the space of ΔV_i occurs:

$$W = W(\Delta V_i).$$

The differential derivatives W for the independent variables, which are needed for minimization with the gradient methods, are computed with the use of the analogous scheme and the information from the same scales. Its basis is the derivatives (determined with the analytical equations) of all used impulse components.

If only part of deviations (Δ_k)are zeros, then the rest of the deviations ($\Delta_p = \Delta - \Delta_k$) are added to the minimized functional as penalties

$$W = \sum_{i=1}^{N} \sqrt{\Delta V_{r_i}^2 + \Delta V_{t_i}^2 + \Delta V_{z_i}^2} + \sum_{i=1}^{N} Q_i + \sqrt{\Delta_p^T G \Delta_p},$$

where G = set matrix. For example, an accurate transfer to the vicinity of the orbital station can be demanded, whereas the velocity deviations will not necessarily be zeros. They can be decreased by using the penalties. This situation occurs when the number of the used impulse components is less than the number of terminal constraints.

It is worth mentioning that the conjugate gradient method should be used as the minimization method in the space of impulse components. Its effectiveness for the given class of problems is approximately 10% higher than the effectiveness of the steepest-descent method (Baranov 1982, 172–179).

5.3. Minimization with Involved Angles of Application of Velocity Impulses

The minimization in the space of the impulse application angles (on set F) is more difficult, because the minimization area may contain several separate areas due to the presence of local minimums and due to the fact that the functional value is obtained as a result of the minimization in the

space of the impulse components. This is why it is difficult to use the effective numerical methods. Usually, the simple method of enumeration for the points from the permitted intervals is used, which allows finding the global minimum of the functional W, but it also requires considerable computation time.

The desire to speed up the global minimum search process makes us search for the option to reduce the number of points F, for which the computation of W_m is made. Two methods could be used for this purpose. The first one is geometrical, which uses the results from Chapter 3 and allows us to quickly eliminate nonoptimal points. The second method is based on the determination of magnitude W_m from below.

For the explanation of the first method (Baranov 2008), let us draw, as always, circles with the radii R_1 and R_2 (Fig. 5-2), which correspond to the sum of the transversal impulse components of the first and the second manoeuvring intervals. As was shown in Chapters 3 and 4, for the optimal solution of the multiple-revolution rendezvous problem, the point that corresponds to the eccentricity vector of the drift orbit should belong to area G (the intersection area of the circles, which have the radii R_1 and R_2).

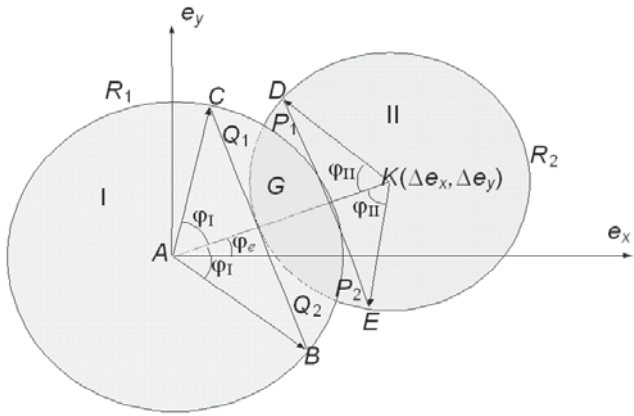

Fig. 5-2. Existence domains of optimal solutions for flybys between nonintersecting orbits.

Thus, it is unnecessary to use the impulse application angles of the first manoeuvring interval, where the point corresponding to the drift orbit eccentricity vector will belong to area I. Similarly, it is unnecessary to use

the impulse application angles of the second manoeuvring interval, where the point corresponding to the drift orbit eccentricity vector will belong to area *II*. Area *I* is a semiplane, which was formed by the line that intersects the points *C* and *B* (*CB* is perpendicular to *AK*) and osculates with the circle in point *K* as its center. Area I does not contain area *G* (Fig. 5-2). Area *II* is a semiplane, which was formed by the line which intersects points *D* and *E* (*DE* is perpendicular to *AK*) and osculates with the circle with the center in point *A*. Area *II* does not contain area *G*.

Thus, the point set from sets *F* is dropped if $\varphi_e + \varphi_I < \varphi_1 < \varphi_e + 2\pi - \varphi_I$ and simultaneously $\varphi_e + \varphi_I < \varphi_2 < \varphi_e + 2\pi - \varphi_I$, or if $0 < \varphi_3 < \varphi_e + \pi - \varphi_{II}$ or $\varphi_e + \pi + \varphi_{II} < \varphi_3 < 2\pi$ and simultaneously $0 < \varphi_4 < \varphi_e + \pi - \varphi_{II}$ or $\varphi_e + \pi + \varphi_{II} < \varphi_4 < 2\pi$, where

$$\varphi_I = \arccos \frac{\Delta e - R_2}{R_1}, \varphi_{II} = \arccos \frac{\Delta e - R_1}{R_2}, \varphi_e = \operatorname{arctg} \frac{\Delta e_y}{\Delta e_x}.$$

One should bear in mind that the angles $\varphi_1, \varphi_2, \varphi_3, \varphi_4$ are negative, which is why these angles should be increased by the value $2\pi k$ in order to make them belong to the interval $[0, 2\pi]$ before the verification of these constraints.

The point set from space *F* is dropped if the impulse application angles of the first interval are situated above line *AK*, and the angles of the impulse application of the second interval lie beneath line *AK* or vice versa. With these transversal impulse application angles, the point which corresponds to the drift orbit eccentricity vector will also not belong to the area *G*.

The solution example, which should be dropped by this criterion (point *C* corresponds to the drift orbit eccentricity vector), can be found in Fig. 5-3. The line segments *AB*, *BC*, *CD*, and *DK* correspond to the impulses of this solution. The impulse application angles of the first interval φ_1, φ_2 lie above line *AK*, and the impulse application angles of the second interval φ_3, φ_4 lie below line *AK*.

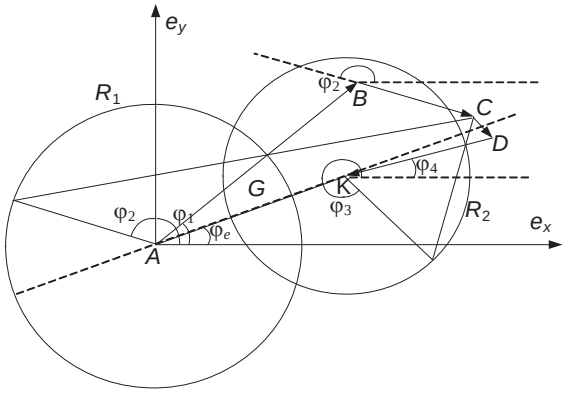

Fig. 5-3. Example of a nonoptimal solution.

Thus, for the existence of the optimal solution, the following conditions are not allowed: the simultaneous satisfaction of $\varphi_e < \varphi_1$, $\varphi_2 < \varphi_e + \pi$,
and $\varphi_e + \pi < \varphi_3$, $\varphi_4 < 2\pi$ or $0 < \varphi_3$, $\varphi_4 < \varphi_e$ or vice versa $\varphi_e < \varphi_3$, $\varphi_4 < \varphi_e + \pi$, and $\varphi_e + \pi < \varphi_1$, $\varphi_2 < 2\pi$ or $0 < \varphi_1$, $\varphi_2 < \varphi_e$.

The other geometrical constructions can be used, which will reduce tset F with the help of the numerical optimization, but one should remember that the algorithm should be simple enough to maintain the advantage in the time over the computation of W_m.

If the circles do not intersect, the point corresponding to the drift orbit eccentricity vector should belong to area D (Fig. 5-4).

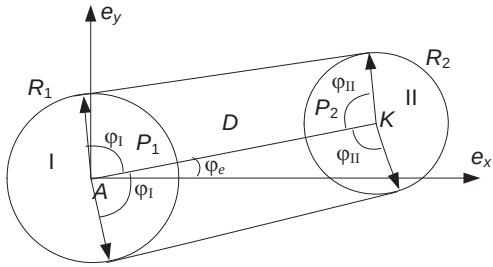

Fig. 5-4. Existence domain of optimal solutions for flybys between intersecting orbits.

By using the algorithm analogous to the aforementioned, the big number of possible points from set F can be dropped during their enumeration for nonintersecting orbits.

The second stage implies dropping the points from areas G or D, for which the solution of the coplanar rendezvous problem is optimal, but the expenditures on the orbital plane altitude correction are substantial. The algorithm from the work of Baranov (1986, 324–327) is used for the drop-off of the points. It uses the assessment from below for the minimized functional W and $L\pi_\tau$ subsequence for the enumeration of the points from set F (Levitan and Sobol 1976). The analytical assessment from below W_n (with a much shorter computation time in comparison with the numerical determination of W_m) gradually reduces the total time for the problem solution. If the value W_n is bigger than the minimum value of the functional W, which was found by this moment, then the numerical search of the minimum in the space of the impulse components (the determination of W_m) for the given set of angles of impulse application may not be fulfilled.

This procedure can be explained with the help of the example from Fig. 5-5. In this figure, the value of the functional W_m is plotted with a solid line, while the value of the assessment from below W_n is plotted with a dashed line. It is necessary to find the minimum of the functional W_m on the interval AF. Let us denote that the enumeration of points from the interval is carried out with a constant step from the point A to the point F. The value W_m will be calculated for all the points before point C. Starting with point C, the value of W_n will be bigger than the value of W_m in point B, and all the points from interval CD will be omitted (the value W_m will not be computed for them).

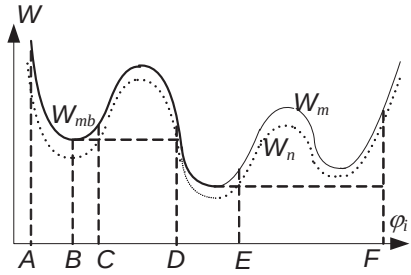

Fig. 5-5. Usage of below assessment of minimized functional.

The further enumeration will cause a drop in the points of the line segment *EF* in a similar fashion.

If $\Delta a^* = |\Delta a|$ (the definition of Δa^* is given in the first paragraph of 4th chapter), then the value

$$W_n = \sqrt{\Delta a^2 + (|\Delta V_{z_i}| + |\Delta V_{z_k}|)^2}, \tag{5-7}$$

can be used for the assessment-from-below for nonintersecting orbits and the value

$$W_n = \sqrt{\Delta e^2 + (|\Delta V_{z_i}| + |\Delta V_{z_k}|)^2}, \tag{5-8}$$

for the intersecting orbits, where Δa = difference between the semimajor axes of the orbits and Δe = module of the difference of the eccentricity vectors, and $\Delta V_{z_i}, \Delta V_{z_k}$ = most effective lateral components of the impulses. The procedure for their determination was presented earlier. Otherwise, the major of values Δa^* or Δe will be used in the equations.

The points of the $L\pi_\tau$ subsequence were chosen for the enumeration of the points from set *F* because they use the capabilities of value W_n in the most efficient fashion. The great thing about the $L\pi_\tau$ subsequence is that every 2^n of its points are evenly spaced in the unit cube of the dimension *N* (Levitan and Sobol 1976). Set *F* can be fitted in the multiple-dimensional rectangle $L = L_1 \cdot L_2 \cdot ... \cdot L_N$, where L_i = line segment of the minimum length, which contains set F_i. If 2^n points of the $L\pi_\tau$ subsequence are taken then, from its characteristics, it follows that, for the *i*-th variable in every $\frac{L_i}{2^n}$ part of line segment L_i, there will be the point of the $L\pi_\tau$ subsequence. Thus, for every *n*, the points of the sequence are equally distributed along t line segment L_i, and, with the increase of *n*, the density of the distribution also increases.

The areas of existence of the local minimums can be easily determined because the consideration of the line segment has smaller and smaller steps each time and not a small constant step starting with its specific part of the line segment. Thus, the current value W_n will be compared with the

value of the functional W close to the global minimum, and the bigger number of points will be omitted.

This option is shown in Fig. 5-6. Let us consider that, after viewing the first four points (they are labeled in the order that corresponds to the order of the $L\pi_\tau$ subsequence), which are evenly distributed on the line segment *AF*, the minimum current value of the functional W_{m_4} will appear to be in the fourth point. For the all subsequent points, the current value of W_n will be compared with W_{m_4} and at least all the points from the line segments *AB*, *CD*, and *EF* will be omitted.

If during the process of the subsequent enumeration one of the points will be in the vicinity of the global minimum (point *M*), this would not allow evaluating W_m for a bigger number of points.

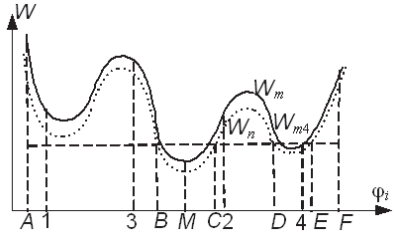

Fig. 5-6. Usage of $L\pi_\tau$ series.

There is one more way to quicken the process of the minimum search in the space of the impulse application angles. Let us consider the problem when the angles of application of the two last impulses are fixed. Then, with the help of the first two impulses, it is necessary to transfer to the line segment *LN* (Fig. 5-7). The *AB* line segment corresponds to the first impulse; *BC* corresponds to the second impulse. By altering the angle of application of the first impulse φ_1 and by determining the corresponding angle of application of the second impulse φ_2, one can obtain φ_2 as a function of φ_1 for the flyby to the point *N*. In Fig. 5-8, this function is plotted with a solid line. Then the analogous function is obtained for the flyby to the point *L*. In Fig. 5-8, this function is plotted with a dotted line. The plotted functions are the boundaries of area *G*.

The optimal angles of the impulse application for the correction of the lateral deviation belong to the set

$$\varphi_z = \varphi_{z_0} - \pi k (k = 1,2,...),$$

($\varphi_{z_0} = \text{arctg}\dfrac{\Delta z}{\Delta V_z}$ = angle between the axis *x* and the line of the orbit plane intersection); the dash-dotted lines in Fig. 5-8 correspond to these angles. If the lines intersect inside area *G* (point *A* and point *B* in Fig. 5-8), then the optimal solution exists with the angles of application for the first and the second impulses belonging to set φ_z. This variant is possible when line *AP* is inclined by angle φ_{z_0} to intersect the line segment *LN* in Fig. 5-7. Thus, it is worth starting to search for the optimal impulse application angles from t angles φ_1 and φ_2, which belong to set φ_z. If such a solution exists, it is optimal. If a solution of this type does not exist, then solutions with only one of the angles φ_2, φ_1, that belong to set φ_z can be considered. After obtaining the close-to optimal solution, we can begin the search for the optimal solution on the whole possible space of the impulse application angles with the help of the aforementioned methods.

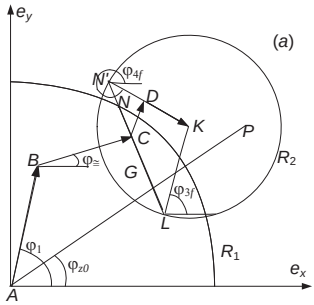

Fig. 5-7. Geometric locus of the eccentricity vector of the transfer orbit.

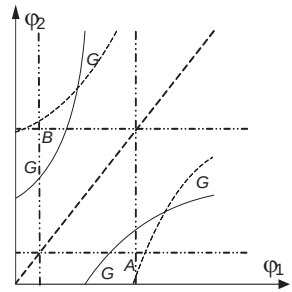

Fig. 5-8. Existence domain of The optimal solutions.

5.4. Graphical Dialog Exploitation

The numerical method is quite universal, and in case the number of used impulse components coincides with the number of terminal constraints, it is also very fast and reliable. The important disadvantage of this method is the lack of explanation as to why this and only this solution

was obtained. Besides, it is impossible to determine the nature of its alteration with, for example, the alteration of the constraints set. It is hard to choose the manoeuvring scheme by only using numerical methods, i.e., it is hard to determine the minimal number of impulses which will be enough for the optimal problem solution, and in which places these impulses should be applied. The numerical methods are more suitable for the determination of the optimal manoeuvre parameters of the given manoeuvring scheme.

The organization of the graphical dialog with the problem helps to eliminate these disadvantages. The first use of the graphical dialog was carried out by A.K. Platonov and P.K. Kazakova (Kazakova and Platonov 1976) during the determination of the manoeuvring parameters for interplanetary transfers. It has proved its effectiveness. During the dialog process, the moments of impulse application were shown on screen for the initial and the target orbits. The manoeuvre parameters were determined by solving Lambert's problem.

The description of the graphical dialog for the interplanetary limited thrust transfer determination is given in the work by Yu.A. Zaharov (Zakharov, 1984). A transition from the impulse solution to the limited thrust problem solution is made with the help of nonlinear programming methods. The use of the graphical dialog was intended for during the spacecraft's flight design stage and during the stage of choosing the spacecraft's characteristics.

The emergency situations which occurred in the orbit during the flight of the "Soyuz" and the "Progress"-type spacecrafts proved the necessity of the development of an effective graphical dialog with the problem, which would enable the ability to quickly choose new manoeuvring schemes that account for the additional constraints caused by emergency situations. Such a dialog was created in the ballistic center of the Institute of Applied Mathematics (Baranov, Gundobin, Ivanov, Kapralov et al. 1992, 26–27).

As was already mentioned in the previous chapters, during the solution of the manoeuvre parameter determination problem for the transfer between close near-circular orbits, it is convenient to demonstrate the impulses on the eccentricity vector component plane. The curved line is plotted on screen. It corresponds to the impulses of the found solution with using the numerical method. Also, two circles are plotted which correspond to sum of the transversal impulse components of each manoeuvring interval. Thus, the illustration on screen is analogous to Figs. 3-3 and 4-12. The relative position of the four-piece curved line and the circles allows us to judge the robustness of the solution against the orbit determination errors and the errors of the impulse performance. This

depends on how deep the point that corresponds to the drift orbit eccentricity vector is situated inside the area of intersection of the circles *G*. How close the impulse angles, which belong to the first manoeuvring interval, to the angles of the optimal correction of the orbit plane (this direction is also shown on the screen), etc., can be estimated. There is an option of setting up the new angles of the impulse application graphically or numerically and returning to the problem for the determination of the new impulse magnitudes. Thus, the additional constraints on the application point and the impulse magnitudes can be accounted for, and the number of used impulses can be reduced, etc.

The realization errors and/or the orientation of the impulses can be accounted for by drawing the corresponding ellipses with the centers at the ends of the vectors, which correspond to the impulses (Fig. 5-9). The errors in the thrust engine burns often lead to emergency situations, which is why they should be accounted for when choosing the manoeuvring scheme in such a situation. The constraint on the transfer orbit altitude can be accounted with the use of a graphical dialog (see Fig. 5-10).

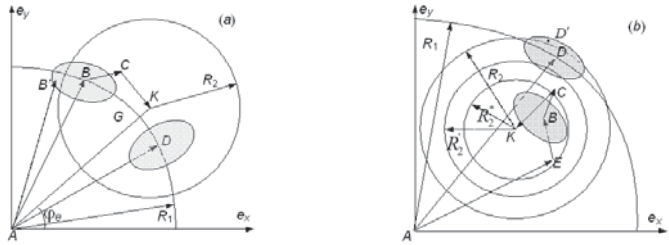

Fig. 5-9. Influence of impulse errors applied on the first manoeuvring interval for the CSS-type solution.

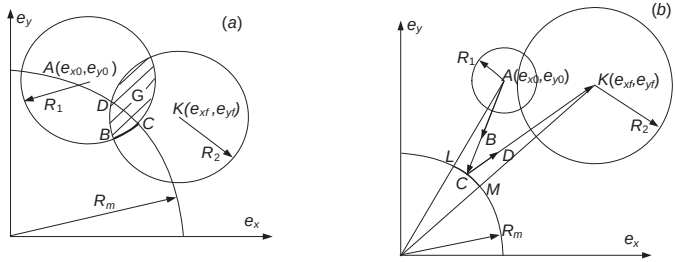

Fig. 5-10. Relative position of circles, which correspond to the sum of the transversal impulse components of the first and the second manoeuvring intervals, and the acceptable values of drift orbit eccentricity vector.

The call of the dialog occurs on the specified iterations. Its usage allows combining the capabilities of the numerical and analytical methods. The dialog is especially effective on the stage of the manoeuvring scheme selection and in case of emergency situations during the flight. If the flight is conducted normally and the predetermined and checked manoeuvring scheme is used, then only the numerical method can be used since only the optimal manoeuvre parameters must be determined.

5.5. Examples

The optimal manoeuvre parameter determination problems, which have been being solved in the ballistic center of the Keldysh Institute of Applied Mathematics of Russian Academy of Sciences during the navigational ballistic support of the flight of the "Soyuz TM-30" spacecraft, are considered in this section (Baranov 2008).

In the moment of deployment of the "Soyuz Tm-30" spacecraft, the difference in the angular position of the spacecraft and the station (the phase difference) was $\Delta u \approx 197^{\circ}$.

The four-impulse problem was solved before the first manoeuvring interval. It was supposed that the fixed impulse with the magnitude 2 m/s was applied on the 17th revolution.

The initial data and the solution results for the four-impulse problem can be found in Example 5-1. The initial conditions of both spacecraft (in the Greenwich rotating reference frame) are listed in the first part of the example. The parameters of the dynamic atmosphere F and a_p and the number of the harmonics for the expansion of series for the Earth's gravity potential, which will be accounted for during the numerical integration of the equations of motion, are set. The target point is set by the revolution number and the latitude argument. Also, the time of its approach to the passive spacecraft is listed. The target vector and the terminal conditions accuracies are specified. The diagonal element nonzero values of the matrices J and J_z indicate the deviations of parameters for the correction.

The second part of the example holds the allowed manoeuvring intervals for the impulse application (they are specified by the revolution number, and the latitude arguments of the left and the right boundaries) and the steps of the point enumeration from these intervals. Please note that the application angles of the third and fourth impulses are fixed one revolution and half a revolution before the rendezvous point. It is specified in the array $V_r V_t V_z$ which impulse components can be used for the

problem solution (the first position corresponds to ΔV_r, the second to ΔV_t, the third to ΔV_z, "1" indicates that the component in the corresponding position should be used, and "0" indicates that is should not be used). The next line indicates which coordinate frame is used for the fixation of the thrust engine orientation during the realization of the corresponding manoeuvre ("0" for the inertial stabilization, "1" for the orbital stabilization). This information is separately listed for every impulse, because sometimes the thrust engine orientation on the different manoeuvring intervals can be fixed in the different coordinate frames. The constraints on the minimum and maximum impulse magnitudes and the minimum angular distance between them are also listed. The last line holds the values of the coefficients k_i for the functional *W*.

The information about the fixed impulses is given in the third part of the example.

The results of the manoeuvre parameter determination, which was obtained on the last iteration (the impulse components and the latitude arguments of its application points), are depicted in the fourth part. The number of the iterations for the problem solution, the values of the functional *W*, the total delta-v expenditures, the sums of the lateral impulse components, the total number of the considered points of the space *F*, and the number of dropped points due to the various criteria are given in the next line.

The information about the manoeuvres obtained after the numerical integration is given in the fifth part. The time of the ignition and the duration of the thrust engine burn, as well as the magnitudes and the orientations of the impulses, are listed. Due to the fact that the orientation of the engine thrusters was fixed in the inertial coordinate frame, the time of the ignition and the orientation of the engine thrusters were chosen in a way that the estimated point of the impulse application was in the middle of the active interval and the thrust engine orientation in this moment was the same as the estimated impulse orientation. The presence of small negative pitches which are proportional to the impulse magnitudes can be explained by this, despite the fact that the radial impulse components were not used. This also explains that the latitude arguments of the moments of the thrust engine ignition (the last column) are slightly smaller than the estimated impulse application moments. Also, the deviations between the spacecraft and the station after the manoeuvre application can be found in this part of the example.

The elements of the orbital station orbit and the elements of active spacecraft orbit in initial moment and after each manoeuvre are given at the end of the example.

Example 5-1

	Orbital station	Spacecraft	Atmosphere parameters Gravity field
Rev.	782	3	F_0 =125.0 a_p = 12.0 *Ngarm* = 8
Date	2000.04.06	2000.04.04	Target point:
Time	85,139.26	104,719.62	rev. latitude arg. deg date Time
X , km	3.159596	5.570846	33. 344.80 2000. 04.06 90048.42
Y , km	-4.262639	-3.503213	Target vector:
Z , km	-4.110163	0.0	R, V_r, V_n, N, Z, V_z (km, m/s)
V_x , km/s	6.286519	2.291193	0.0 0.0 -12.5 0.0 0.0 0.0
V_y , km/s	1.022838	3.694669	accuracies: R, V_r, V_n, N, Z, V_z (km,m/s)
V_z , km/s	3.774388	6.110578	0.100 0.050 0.050 0.500 0.100 0.050
S	0.0390	0.0340	Diagonal matrices J = 1. 1. 1. 1. J_z = 1. 1.

Manoeuvring intervals				
Impulse number N	1	2	3	4
Revolution of interval start	3	3	32	33
Lat. argument of the left boundary, deg.	200.0	200.0	344.8	164.8
Lat. argument of the right boundary, deg.	440.0	440.0	344.8	164.8
Interval enumeration step, deg.	3.0	3.0	0.	0.
Impulse components used ($V_r V_t V_z$)	011	011	010	010
Engine stabilization type (0-inert., 1-orb.)	0	0	0	0
Min. impulse velocity constraint, m/s	0.5	0.5	0.5	0.5
Max. impulse velocity constraint, m/s	60.0	60.0	60.0	60.0
Min. inter-impulse distance constraint, deg.	120.0	120.0	120.0	120.0
Coefficient values k_i	0.007	0.007	0.0	0.0

Fixed impulses:

Impulse number N	Rev	Latitude argument (U)	dV m/s	Yaw	Pitch
3	17	344.8	2.0	0.0	0.0

Approximate solution: impulse components and angles of their application

Impulse number	1	2	3	4
	0.0	0.0	0.0	0.0
$dV_{r_i}\, dV_{t_i}\, dV_{z_i}$	21.25	10.84	6.29	22.38
	-10.95	5.47	0.0	0.0
Revolution, latitude	3.0;	3.0;	32.0;	33.0;
argument	263.0	437.0	344.8	164.8

$N_{it} = 5$ $W = 129.70$ $dV_{sum} = 64.71$ $dV_{zsum} = 16.42$ $N_{all} = 821$

$N_{dV} = 134$

N	date	time	dV	yaw	pitch	T, s	Rev	Lat. argument
1	2000.04.04	115,124.0	23.90	27.26	-1.94	56.6	3	261.06
2	2000.04.04	123,445.1	12.14	333.20	-0.97	28.6	3	436.03
3	2000.04.05	90,615.8	2.00	0.0	0.0	4.7	17	344.80
4	2000.04.06	73,028.1	6.29	0.0	-0.49	14.7	32	344.31
5	2000.04.06	81,501.2	22.38	0.0	-1.74	52.2	33	163.06

Deviations from station: km, m/s

$R = -0.001$ $V_r = 0.008$ $V_n = -12.499$ $N = -0.046$ $Z = 0.0$ $V_z = 0.0$

Rev.	U	$Hmin$	$Umin$	$Hmax$	$Umax$	ω	I	Ω	e
782	344.0	330.0	7.9	341.6	308.7	41.6	51.6687	117.6062	0.00082
3	360.0	192.0	61.2	238.0	264.8	71.5	51.6920	130.1112	0.00369
3	264.0	237.7	261.1	264.3	86.4	258.8	51.6391	129.7626	0.00135
4	78.0	254.6	10.8	274.7	268.8	88.9	51.6315	129.5567	0.00022
17	345.0	253.1	7.9	276.0	256.2	10.5	51.6690	123.9449	0.00152
32	345.0	253.8	5.4	285.5	185.8	357.7	51.6675	117.9373	0.00311
33	166.0	285.1	163.1	337.4	305.7	152.3	51.6688	117.7708	0.00447

Target point

altitude, km	latitude, deg.	longitude, deg.
332.6	-11.9	332.4

After the realization of the first two determined impulses on the third and fourth revolutions and after the orbit determination with the help of the measurements at the 13th–15th revolutions, the three-impulse problem

is solved. Also, the manoeuvre parameters on the 17th revolution and in the last manoeuvring interval are determined. The usage of this initially fixed and then adjustable manoeuvre on the 17th revolution compensates for the errors of the manoeuvre realization of the first manoeuvring interval (primarily their influence on the arrival time to the rendezvous point). It is much harder to compensate for the deviation of this parameter with the manoeuvres on the last manoeuvring interval. The initial data for the solution of the three-impulse problem and the estimated manoeuvre parameters are given in Example 5-2.

Example 5-2

	Orbital station	Spacecraft	Atmosphere parameters		Gravity field	
Rev.	782	15	F_0=125.0	a_p = 12.0	*Ngarm* = 8	
Date	2000.04.06	2000.04.05	Target point:			
Time	85,137.89	44135.78	revolution	latitude arg. deg	date	Time
X , km	3.160009	3.866979	33.0	344.20	2000. 04.06	90037.94
Y , km	-4.262298	5.393846	Target vector:			
Z , km	-4.110167	0.0	R, V_r, V_n, N, Z, V_z (km, m/s)			
V_x, km/s	6.286416	-3.518402	0.0 0.0 -12.5 0.0 0.0 0.0			
V_y, km/s	1.023499	2.514312	accuracies: R, V_r, V_n, N, Z, V_z (km,m/s)			
V_z, km/s	3.774374	6.081848	0.100 0.050 0.050 0.500 0.100 0.050			
S	0.390	0.31559	Diagonal matrices J=1. 1. 1. 1. J_z =1. 1.			

Manoeuvring intervals			
Impulse number N	1	2	3
Revolution of interval start	17	32	33
Lat. argument of the left boundary, deg.	164.0	344.2	164.2
Lat. argument of the right boundary, deg.	410.0	344.2	164.2
Interval enumeration step, deg.	1.0	0.0	0.0
Impulse components used (V_r V_t V_z)	011	010	010
Engine stabilization type (0-inert., 1-orb.)	0	0	0
Min. impulse velocity constraint, m/s	0.5	1.9	1.9
Max. impulse velocity constraint, m/s	60.0	60.0	60.0
Min. inter-impulse distance constraint, deg.	120.0	120.0	120.0
Coefficient values k_i	0.007	0.0	0.0

Approximate solution: impulse components and angles of their application

Impulse number	1	2	3
dV_{r_i}	0.0	0.0	0.0
dV_{t_i}	0.61	7.87	21.47
dV_{z_i}	0.0	0.0	0.0
Revolution, latitude argument (U)	17.0	32.0	33.0
	349.0	344.2	164.2

Nit = 5 *W* = 29.95 *dVsum* = 29.95 *dVzsum* = 0.00 *Nall* = 248

N	Date	Time	*dV*	Yaw	Pitch	*T*, s	Rev.	Latitude argument
1	2000.04.05	90,737.9	0.608	0.0	0.11	1.4	17	348.95
2	2000.04.06	73,014.9	7.868	0.0	-0.62	18.4	32	343.5
3	2000.04.06	81,452.0	21.471	0.0	-1.66	49.9	33	162.54

Deviations from the station: km, m/s

R= 0.0 V_r= 0.0 V_n= -12.500 *N*= 0.0 *Z*= -0.402 V_z=0.052

Rev.	*U*	*Hmin*	*Umin*	*Hmax*	*Umax*	ω	*i*	Ω	*e*
782	344.2	329.6	7.9	341.5	308.7	41.93	51.6685	117.6067	0.00081
15	0.0	257.5	160.9	274.7	271.3	45.32	51.6695	124.9542	0.00120
17	349.0	255.8	13.3	275.4	270.3	29.49	51.6715	123.9506	0.00107
32	344.8	256.9	4.9	285.5	135.3	357.44	51.6686	117.9417	0.00285
33	165.9	285.1	165.9	337.3	305.0	152.20	51.6699	117.7753	0.00446

Target point

Altitude, km	Latitude, deg.	Longitude, deg.
332.7	-12.4	332.1

The two-impulse problem is solved after the application of the manoeuvre on the 17th revolution and the following orbit determination before the last manoeuvring interval on the 31st–32nd revolutions. The initial data for its solution and the determined manoeuvre parameters can be found in Example 5-3.

Example 5-3

	Orbital station	Spacecraft	Atmosphere parameters		Gravity field	
Rev.	782	30	F_0=125.0	a_p= 12.0	*Ngarm*=8	
Date	2000.04.06	2000.04.06	Target point:			
Time	84,937.62	30,537.89	revolution	latitude arg. deg	date	Time
X, km	2.379805	2.004973	33.0	344.20	2000. 04.06	90,037.64
Y, km	-4.351406	6.325135	Target vector:			
Z , km	-4.522517	0.0	R, V_r, V_n, N, Z, V_z (km, m/s)			
V_x , km/s	6.709404	-4.125250	0.0	0.0	-14.54	0.0 0.17 0.0
V_y , km/s	0.459303	1.300320	accuracies: R, V_r, V_n, N, Z, V_z (km, m/s)			
V_z , km/s	3.089667	6.083085	0.100	0.050	0.050	0.500 0.100 0.050
S	0.0390	0.031063	Diagonal matrices J=1. 1. 1. 1. J_z =1. 1.			

Manoeuvring intervals		
Impulse number *N*	1	2
Revolution of interval start	32	33
Latitude argument of the left boundary, deg	284.2	104.2
Latitude argument of the right boundary, deg	404.2	224.2
Interval enumeration step, deg	3.0	3.0
Impulse components used ($V_r V_t V_z$)	111	111
Engine stabilization type (0-inert., 1-orb.)	0	0
Minimum impulse velocity constraint, m/s	0.5	0.5
Maximum impulse velocity constraint, m/s	60.0	60.0
Minimum inter-impulse distance constraint, deg.	120.0	120.0
Coefficient values k_i	0.007	0.007

Approximate solution: impulse components and angles of their application						
Impulse number	1			2		
dV_{ri} dV_{ti} dV_{zi}	-2.15	5.78	-2.19	2.36	21.50	-2.29
Revolution, latitude argument (U)	32	323.2		33	164.2	

N_{it} = 3 W= 29.17 dV_{sum} = 28.30 dV_{zsum} = 4.48 N_{all} = 1410

N	Date	Time	*dV*	Yaw	Pitch	*T*, s	Rev	Latitude Argument
1	2000.04.06	72,513.7	6.545	20.75	-19.15	15.3	32	323.20
2	2000.04.06	81,518.6	21.753	6.09	6.24	50.6	33	164.20

Deviations from the station: km, m/s
R= -0.001 V_r= 0.001 V_n= -14.54 N= 0.002 Z= 0.170 V_z= 0.0

Rev.	*U*	*Hmin*	*Umin*	*Hmax*	*Umax*	ω	*i*	Ω	*e*
782	344.2	330.6	360.0	343.6	300.8	44.95	51.6680	117.6063	0.00078
30	0.0	256.2	10.0	274.6	271.3	42.31	51.6707	118.9471	0.00134
32	324.2	257.5	4.4	279.7	114.9	351.86	51.6715	117.9378	0.00166
33	167.6	277.7	164.2	337.0	306.8	153.62	51.6683	117.7690	0.00506

Target point

altitude, km	latitude, deg.	longitude, deg.
333.0	-12.4	332.12

Let us illustrate the capabilities of the graphical dialog for the analysis and alteration of the obtained solution using the four-impulse problem from Example 5-1.

Figure 5-11 shows the illustration that the operator sees on the monitor after the problem solution at the iteration with the set number (in this case after the fifth iteration).

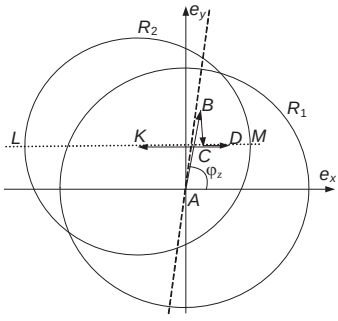

Fig. 5-11. Optimal solution.

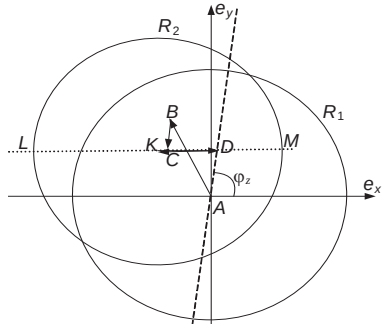

Fig. 5-12. Solution with equalization of the third and the fourth impulses.

Since the application angles of the third and the fourth impulses are fixed on the angles π and 2π before the rendezvous point, the line segment *LM* (from which with the use of the impulses from the second manoeuvring interval the transfer to the final point *K* can be fulfilled) is parallel to the e_x axis and intersects point *K*. The dashed line corresponds to the direction of the orbit plane optimal correction. This line intersects point *A* and is inclined by φ_z to the e_x axis. The curved line *ABCDK* corresponds to the problem solution (the transversal impulse components).

It can be seen that the dashed line intersects the line segment *LM*. As was shown in Section 4.2, the solution with the impulses of the first manoeuvring interval applied in the points of the orbit plane's optimal correction will be optimal (on the line of the orbit plane intersection), and the magnitudes of the lateral components will be proportional to the magnitudes of the transversal impulse components. Indeed, for the solution from Example 5-1, which was obtained with the use of the numerical method, the modules of the ratios of the lateral impulse components to the transversal components for the first and the second impulses are almost equal and the line segments *AB* and *BC*, which correspond to the transversal impulse components, are close to the dashed line. The small deviation from the optimal analytical solution can be explained as follows: the enumeration of impulse application angles was carried out with 3º step, which is why it was impossible to find the exact optimal solution. The line segment C*D* corresponds to the third impulse interval and the line segment *DK* corresponds to the fourth interval. It can be easily seen that the impulses of the second interval (the line segments *CD* and *DK*) of the optimal solution differ from each other by magnitude. It can also be seen from the figure that, in order to obtain the solution with the almost equal impulses of the second manoeuvring interval, it is necessary to reduce the angle of the first impulse application. In this case, the line segment which corresponds to the first impulse will approach point *K*.

There is the option of changing the impulse application angles and using the numerical method for the determination of the impulse magnitudes afterwards in the graphical dialog developed in the ballistic center of the Institute of Applied Mathematics. The angles of application of the first and second impulses, which ensured obtaining the solution with the desired characteristics were chosen using this option (Fig. 5-12). The impulse parameters for this solution and the angles of their application are given in Example 5-4.

Example 5-4

Impulse number	1		2		3		4	
$V_{r_i} V_{t_i} V_{z_i}$:	0.0; 0.45	21.89;	0.0; 16.72	10.09;	0.0; 0.0	14.11;	0.0; 0.0	14.95;
Revolution, latitude argument:	3; 221.0		3; 440.0		32; 344.8		33; 164.8	

$N_{it} = 8$; $W = 70.49$; $dV_{sum} = 70.49$; $dV_{zsum} = 17.16$

For this solution, $CD \approx DK$. The direction of the line segment, which depicts the second impulse, is close to the direction of the dashed line. Hence, this impulse is basically used for the orbit plane correction (this can also be seen by the magnitudes of the lateral impulse components). Since the expenditures on correction of the orbit plane are not distributed proportionally between the first and the second impulses, the total delta-v of the new solution is 5.8 m/s higher in comparison with Example 5-1, but the impulse magnitudes of the last interval are almost the same.

The iterative procedure from Chapter 1 was used for the solution of all the aforementioned problems. The effectiveness of this procedure is clearly seen from the iteration data for the four-impulse problem from Example 5-5. The following information is printed successively: the number of the current iteration (N_{it}); the sum deviation vector (*SVD*), which is used on this iteration in Eq. 5-1 for the manoeuvre parameter determination; the computed components of the impulses (dV_i (V_r, V_n, V_z)) on this iteration; the number of revolutions and the application angles of the impulses (N_i, U_i); and, after the manoeuvre realization, the deviations between the orbit elements of the spacecraft and the orbit elements of the station which were altered by the magnitude of the target vector (*CD*) were obtained. The sum deviation vector (*SVD*) has the dimension of m/s (the coordinate components of the deviation vector are multiplied by the angular velocity along the relative circular orbit). The sum deviation vector which is used on the first iteration coincides with the deviation vector between the uncorrected orbit of the spacecraft and the station orbit, which was depicted at the start of Example 5-5. In order to quicken the converging of the iterative procedure, the angles of the impulse application have been fixed, starting with the third iteration. As can be seen from the solution, the iterative procedure ensures the fulfillment of the terminal constraints rapidly and with a high accuracy (the deviations decrease by an order with each iteration).

Example 5-5

CD initial deviations of spacecraft from station + target vector km, m/s
R = -141.47 V_R = -11.25 V_N = 95.79 N = 17,538.6 Z = 2.635 V_Z = 3.287
N_{it} = 1 *SVD*: 162.504 11.250 -95.792 -20,146.397 3.026 3.287
$V_{r_i} V_{t_i} V_{z_i}$: 0.0 25.45 4.48 0.0 9.68 0.02 0.0 -0.77 0.0
0.0 32.34 0.0
N_i U_i: 3 302.0 3 440.0 32 344.8 33 164.8
CD: R = 15.48 V_R = -25.47 V_N = -11.89 N = -1468.2 Z = -18.07
V_Z = -5.35

N_{it} = 2 *SVD*: 144.713 36.728 -83.893 -18,459.880 -17.729
-2.070
$V_{r_i} V_{t_i} V_{z_i}$: 0.0 25.58 -13.28 0.0 -6.47 4.58 0.0 5.84 0.0
0.0 22.92 0.0
N_i U_i: 3 263.0 3 437.0 32 344.8 33 164.8
CD: R = -1.413 V_R = 17.47 V_N = 1.70 N = 3.443 Z = 1.231
VZ = 0.310

N_{it} = 3 *SVD*: 146.336 19.253 -85.587 -18,463.836 -16.315
-1.760
$V_{r_i} V_{t_i} V_{z_i}$: 0.0 21.12 -10.84 0.0 10.94 5.59 0.0 6.26 0.0
0.0 22.41 0.0
N_i U_i: 3 263.0 3 437.0 32 344.8 33 164.8
CD: R = 0.170 V_R = -0.408 V_N = -0.207 N = 7.379 Z = 0.021
V_Z = -0.007

N_{it} = 4 *SVD*: 146.140 19.661 -85.380 -18,472.312 -16.291
-1.767
$V_{r_i} V_{t_i} V_{z_i}$: 0.0 21.23 -10.91 0.0 10.84 5.48 0.0 6.29 0.0
0.0 22.38 0.0
N_i U_i: 3 263.0 3 437.0 32 344.8 33 164.8
CD: R = 0.002 V_R = -0.044 V_N = 0.001 N = -0.597 Z = -0.010
V_Z = -0.003

N_{it} = 5 *SVD*: 146.138 19.705 -85.382 -18,471.626 -16.302
-1.771

$V_{r_i} V_{t_i} V_{z_i}$: 0.0 21.24 -10.94 0.0 10.83 5.47 0.0 6.29 0.0
0.0 22.38 0.0
N_i U_i: 3 263.0 3 437.0 32 344.8 33 164.8
CD: R = -0.001 V_R = 0.008 V_N = 0.001 N = -0.046 Z = 0.0
V_Z = 0.0

5.6. The Iterative Procedure Taking into Account the Constraints on the Drift Orbit Altitude

The aforementioned procedure can be effectively used for the drift orbit parameter constraint satisfaction and for many other purposes.

Let us consider, for example, its usage for an accurate assessment of the constraint on the drift orbit altitude.

Let us suppose that on the *i*-th iteration the problem has been being solved with the constraint that the altitude of the drift orbit *h* should be higher than the given value h_{m_i}. The solution with the analytically found h_{a_i}, which had met the constraint ($h_{a_i} > h_{m\_i}$), was determined. During the numerical integration of the motion equation system with the accountancy of the estimated impulses, the drift orbit altitude h_i is also estimated, which corresponds to this solution. The deviation between the altitude values determined with the help of the analytical method and the numerical integration $\Delta h = h_{a_i} - h_i$ is determined. On the next $i+1$ iteration, the value $h_{m\_i+1} = h_{\min} + \Delta h$ (where $h_{\min}$ = given minimal drift orbit altitude value) is used as the constraint on altitude.

This technique allows the use of relatively simple equations for the drift orbit altitude determination and the meeting of the constraint for the altitude with the necessary accuracy.

For the determination of the manoeuvre parameters which meet the altitude constraint h_{m_i}, one can use the numerical analytical method from Section 3.6. If the numerical method is used for the problem solution and the number of constraints in the equality form coincides with the number of used impulse components, then the altitude constraint requirement satisfaction is checked for next solution. After the determination of the impulse components for the next point from set *F*, the constraint fulfillment $h_{a_i} > h_{m\_i}$ is checked and, if the constraint is not met, the solution is dropped and, if it is met, the optimality of the found

solution is checked. If the obtained solution is better than the previous ones, it becomes the current optimal solution.

The procedure which is analogous to the procedure of h_{m_i} change is used during the problem solution, when only part of the terminal deviations is needed to make zeros (Δ_k); the other deviations (Δ_p) are added to minimize the functional as penalties.

5.7. The Simplex Method for Manoeuvre Parameter Determination

The simplex method is quite effective for the determination of the optimal manoeuvre parameters on near-circular orbits. The idea of the implementation of the simplex method for the manoeuvre parameter determination was proposed by M.L. Lidov (Lidov 1971, 687–706), and was later developed for manoeuvres with limited thrust in the work of M.L. Lidov and N.M. Teslenko (Lidov and Teslenko 1978, 112–141). The further development of this method in the works of V.P. Gavrilov and E.V. Obuhov (Petrov 1985), Gavrilov and Obukhov (1980, 163-172) allowed solving the problem with the fixed number of impulses. The software by V.P. Gavrilov and E.V. Obuhov has been used for years in the RSC “Energia” for the flight design of the “Soyuz” and the “Progress” spacecrafts. The Mission Control Center (Korolev, Moscow Region) had its own realization of the simplex method. It was realized in 1990 and has been used for many years for the manoeuvre determination of all spacecraft docking in the orbital station. R.R. Nazirov and B.T. Bakshiyan used the simplex method for the manoeuvre parameter determination of interplanetary transfers (Bakshiyan, El'yasberg, and Nazirov 1980; Nazirov and Timokhova 1993, 93–101).

The next step made by A.V. Gavrilov (Gavrilov 1995; Gavrilov 2000) consisted in using the duality theory. This substantially reduced the solution time for the multiple-impulse problem on the stage of the impulse application angle enumeration. A comprehensive description of the simplex method application for the manoeuvring problem solution with the necessary examples was provided by G.A. Kolegov (Kolegov, 2007).

The simplex method has a number of substantial advantages. It solves the problem with the arbitrary number of impulses and the arbitrary set of terminal constraints. It also easily accounts for the constraints on the impulse magnitudes and on the points of their application. The basic advantage of the simplex method is the problem solution speed in comparison with the gradient methods.

The disadvantage of the simplex method (and every numerical method) is the inability of find an explanation for the obtained solution. It is impossible to forecast how the solution will alter with the alteration of the problem conditions. The simplex method is hard to use for the manoeuvre parameter determination on board the spacecraft.

During the multiple calculations for the ATV launch preparation, CNES had some problems with the convergence of the simplex method for the manoeuvre parameter determination. In these cases, the selection of control constants was needed for the complete problem solution. Due to this disadvantage in the simplex method, CNES opted for the simple and reliable method described in this chapter as the basic method for the determination of the ATV manoeuvre parameters (Carbonne, Chemama, Julien, Kudo et al. 2009, 1091–1106). Later, the realization of this method by CNES was used for the manoeuvre parameter determination for the deployment of the satellite formation flying "PRISM". The simplex method with all its numerous advantages is used by CNES for solving research problems (Baranov and Labourdette 2001, 1–20).

The further development of numerical methods for the manoeuvre parameter determination is connected with works by Yu.P. Ulybyshev. By using the inner circle method (Wright, 1997), he was able to spread this approach for the solution to low thrust and combined problems. In these problems, part of the manoeuvre is performed by the main thrusters (these are close to the impulsive manoeuvres), and the rest of the manoeuvres are performed by the docking and the orientation engines. The duration of the latter manoeuvres encompass the substantial part of the revolution. In the works by Yu.P. Ulybyshev, the lengthy active interval is modeled by tens of thousands of pseudo impulses (Ulybyshev 2016, 1-11), (Sokolov and Ulybyshev 1999, 95-100).

There are other effective numerical methods for the optimal manoeuvre parameter determination on near-circular orbits. For example, the method developed by Yu.P. Pavlushevich. A method of the description can be found in the work of Bazhinov and Yastrebov (1978). This method has been used for many years (from 1972 till 1990) in the Mission Control Center for the manoeuvre parameter determination of the spacecraft, which is used to dock in the orbital station.

The effective numerical methods for the rendezvous problem solution can not only be found in mission control centers, but also in universities (Guo-Jin, Hai-Yang, and Ya-Zhong 2007, 185–191). Lambert's problem solution is often the basis for these methods (Chiu and Prussing 1986, 17–22; Guo-Jin, Hai-Yang, Ya-Zhong, and Yong-Jun 2007, 946–952).

CHAPTER SIX

MANOEUVRING WITH LOW-THRUST ENGINES

As described in the previous paragraphs, when determining the manoeuvring parameters, it was supposed that the manoeuvres were being carried out by engines with infinite thrust. This assumption allowed us to model the manoeuvres as impulsive. However, real spacecraft engines always have limited thrust and thus the manoeuvres have restricted duration. If the manoeuvre duration is small in comparison to the period of the orbit, an approximation of the impulse can be treated as being sufficiently accurate. If the manoeuvre duration is several dozens of degrees long according to the latitude argument, and the impulse model is used for the determination of the manoeuvre parameters, one can only rely on the iterative procedure presented in Chapter 1. In some cases this procedure can provide the fulfillment of the terminal conditions even if the duration of the real manoeuvres reaches 45º according to the latitude argument. However, the maximum acceptable manoeuvre duration that ensures the convergence of the iterative procedure depends on the concrete problem and may be far less than 45º. For example, this situation occurs during the solution of the long duration rendezvous problem. In cases where the thrust engines are working during a considerable part of the revolution, the convergence of the iterative procedure breaks and the total delta-v expenditure differs gradually from the impulsive variant. In these cases it is necessary to account for the time of the thrust engine firing during the determination of the manoeuvre parameters.

Sometimes, one may try to detach the impulse solution from the low-thrust solution by orienting it on the engine thrust criterion. This may lead to incorrect conclusions. Engine division by the high and low thrust criteria is rather uncertain, as follows from the text below.

The characteristics of different engines and their classification for high and low thrust have been thoroughly analyzed in the work of Yu. G. Sukhoi (2011):

“In the work of Anonymous (2002) “Recommendation on Cataloging. Cataloging of Production for Federal State Needs. Supplies. List of Confirmed Titles. Russian State Standard” the low-thrust rocket liquid-

fueled engine is designated as an engine with thrust of less than or equal to 1600 N, which is used as the executive element of the control system for flying and descent vehicles. The work of Ivanov (2002) "Encyclopedia Russian Weaponry and Technology. XXI century" describes the applicable scope of a low-thrust rocket liquid-fueled engine for spacecraft. For example, the low-thrust rocket liquid-fueled engine (LTRLFE) 11D428A – 16 (thrust = 130.5 N, thrust specific impulse = 290 s) is used for the transport spacecraft "Soyuz-TM", "Progress-M", and the "Zvezda" service module of the International Space Station. The low-thrust rocket engines (LTRE) 17D51 (thrust = 111 N, thrust specific impulse = 209 s), 11D456 (thrust = 104 N, thrust specific impulse = 252 s), and 11D457 (thrust = 54 N, thrust specific impulse = 254 s) are used on Earth orbit remote sensing satellites. LTRE 11D458 (thrust = 400 N) is used on the upper rocket stage "Briz". LTRE 17D58E has the thrust 13.3 N. There are lots of different types of low-thrust rocket liquid-propellant engines with two-component and single-component fuel. LTRLFE with single-component fuel (hydrogen peroxide and hydrazine) uses a catalyzer for fuel decomposition in addition to the fuel itself. A high-temperature gas, which produces thrust, is the result. The magnitude of the specific impulse is bigger for two-component engines in comparison to single-component ones. The thrust range for low-thrust single-component rocket liquid-fueled engines is vast, ranging from fractions to hundreds of Newtons.

Gas-jet systems (Belik, Belyaev, and Uvarov 1979) have their own range of division on the low-high-thrust scale. Compressed air (air, nitrogen, and argon) in the cylinders is used as the propellant. They are reliable and the simplest of all rocket micro-engines. Their disadvantages include the small specific impulse and decrease in thrust by the moment of fuel depletion. Low-thrust gas-jet systems, as a rule, have thrust of 0.1 to 1 N, and high-thrust systems have thrust of up to 10 N. The ignition duration of a low-thrust gas-jet engine may be in the range of fractions of seconds to several hours. The ignition duration of a high-thrust gas-jet engine is usually limited to minutes.

Electric jet systems are often suitable for geostationary spacecraft, since they allow operation with ultralow thrust for small orbital perturbation compensation. Electric jet engines (EJE) usually differ from the point of view of the generation of accelerated particles: electrostatic, electrothermal, electromagnetic, magnetodynamic, and impulsive (Kvasnikov, Latyshev, Ponomarev-Stepnoy et al., 2001; Gorshkov, 1999, 56-58). Electrostatic engines are divided into ionic and plasmic forms. Impulse engines are based on the use of gas kinetic energy, which appears during solid body vaporization by the electrical charge. Liquids, gases,

and their mixture are used as the propellant in EJE. Recently, considerable results have been achieved in the development of stationary plasmic engines. Various Russian magnetoplasmodynamic engines of the SPD series with different nominal thrust values are known: SPD-35 – 0.01 N, SPD-50 – 0.02 N, SPD-60 – 0.03 N, SPD-70 – 0.04 N, SPD-100 – 0.083 N, SPD-140 – up to 0.3 N, SPD-200 – up to 0.5 N, and SPD-290 – up to 1.5 N. The SPD-35, SPD-50, and SPD-60 engines may be used for small spacecraft of mass 500-1,000 kg; SPD-70 and SPD-100 may be used for medium-sized spacecraft; while SPD-140 may be used for interorbital transportation and heavy geostationary satellite orbit correction.

SPD-200 and SPD-290 engines are suitable for the orbital correction of various satellites, for solution of the deployment and transfer problem, and for use as components of upper stages. The specific impulse of these engines is 1500-2600 s. The summary thrust impulse for SPD-100 engines is approximately 2000 kN·s. SPD-60 engines have been mounted on "Meteor" satellites; SPD-70 has been mounted on "Geizer", "Altair", "Kupon", and "Yamal-100" spacecraft; and SPD-100 has been mounted on "Express-A", "Express-AM", and "Gals" spacecraft (Gorshkov 1999, 56-58). Xenon ionic electric jet engines are widely used abroad including: the "13 sm" (thrust = 0.018 N), the "30 sm" (thrust = 0.092 N), and the "25 sm" (thrust = 0.165 N). The specific impulse of these engines lies in the range of 2565-3800 s. The "13 sm" engines have been mounted on the "Panamsat-5", "Panamsat-6B", "Panamsat-9", "Panamsat-5", and "DirektTV 1R" spacecraft, among others; the "25 sm" engines have been mounted on the "Galaxy 11", "Panamsat-1R", and "Anik F1" spacecraft; the "30 sm" engines on "Deep Space 1" spacecraft. The electrothermal engines DEN-15 with ammonia as the propellant have been mounted on the "Meteor-3", "Meteor-Priroda", "Resurs-O", and "Electro" spacecraft. The power of the ammonia engine is approximately 100-400 W, the nominal thrust = 0.05-0.3 N, the specific impulse = 100-270 s, and the summary thrust impulse reaches up to 500 kN·s. Other models of EJE (D-38, D-55, D-100-1, D-100-2, X-40, T-100, T-160, and KM-45) with thrust of fractions of newtons and a specific impulse of 1300-4200 s are also known (Gorshkov 1999, 56-58; Belikov, Gorshkov, Muravlev, and Shagaida 2007). Electric jet systems allow for ignition durations ranging from several minutes to dozens of hours thanks to their low-thrust capabilities. Thrust can be conveniently divided into low (approximately 0.5-100 N) and ultralow (0.01-0.5 N) from the middle geostationary orbit correction point of view, independently of the engine model used. This criterion is based on the capability/incapability of compensating for middle geostationary satellite weak orbital perturbations during the

maximum perturbations from the Sun and the Moon with a single ignition period".

6.1. Coplanar Low-Thrust Transfers

For real spacecraft, the engine orientation during manoeuvre completion is always practically fixed in the orbital or the inertial coordinate frames. This circumstance leads us to necessarily consider both variants. Furthermore, the algorithm for the determination of the optimal orientation alteration law of the thrust vector in the general case is proposed.

6.1.1. Thrust Vector Constant Orientation in an Orbital Coordinate Frame

Let us consider the variant of fixing the transversal thrust engine orientation in the orbital coordinate frame. The case of primer vector degeneration into the point ($\lambda = 0,\ \lambda_1 = \pm 1,\ \sqrt{\lambda_2^2 + \lambda_3^2} = 0,\ \mu = 1$ or $\mu = -1$, (1-19)) corresponds to this orientation. This means that the transversal thrust vector orbital orientation can be optimal for the long intervals of the thrust engine burns. Just as in the impulsive case, the main result of such a manoeuvre is the alteration of the semimajor axis and, hence, the orientation of the thrust vector is optimal for transfers between nonintersecting orbits.

In order to get closer to the impulsive solution, which is considered foundational, and obtain the optimal solution, the middle of the active interval should coincide with the impulse application point (Braude and Kuzmak 1969, 323-338). This assumption is fair, because the spacecraft mass changes insignificantly during fulfillment of a single manoeuvre and jet acceleration can be considered as the constant. In Fig. 6-1, the orbital arc *AC* ($\Delta\varphi$) corresponds to the active interval and point *B* is the impulse application point, which is situated on the apsidal line of the relative orbit. The impulse size is ΔV_t. Since point *B* is situated in the middle of the arc *AC*, alteration of the eccentricity vector during a long-duration manoeuvre will be in the same direction as in the impulsive case (to point *B*). However, the magnitude of the eccentricity vector alteration caused by the influence of the dimensionless velocity ΔV_t ($\Delta V_t = \Delta V_t^* / V_0$), equally distributed on the interval of the latitude argument $\Delta\varphi$, will be smaller in comparison to its alteration Δe caused by an impulse of the same

magnitude ΔV_t (Fig. 6-1). This is connected to the fact that the more distant from the middle of the active interval part of the arc, on which the impulse δV_t is realized, the more the direction of the performed alteration of the eccentricity vector δe (pointed to the center part of the arc) differs from the necessary direction to point *B* (Fig. 6-1).

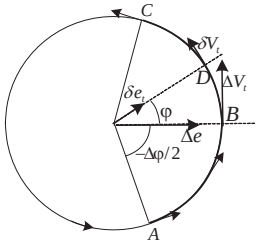

Fig. 6-1. Constant orientation in the orbital coordinate frame

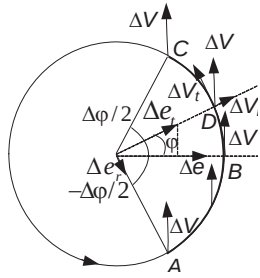

Fig. 6-2. Constant orientation in the inertial coordinate frame

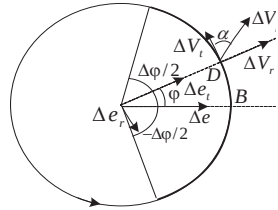

Fig. 6-3. Optimal orientation for eccentricity alteration

Considering that the arc *AC* is symmetrical relative to point *B*, the sum of the eccentricity vector is pointed to point *B*, but its magnitude is smaller in comparison to the impulse case. The alteration to the eccentricity caused by the dimensionless velocity ΔV_t, equally distributed along the latitude argument interval $\Delta\varphi$, can be evaluated as:

$$\Delta e = 2\int_{-\Delta\varphi/2}^{\Delta\varphi/2} \frac{\Delta V_t}{\Delta\varphi}\cos\varphi d\varphi = 4\frac{\sin\frac{\Delta\varphi}{2}}{\Delta\varphi}\Delta V_t, \qquad (6\text{-}1)$$

where φ = the angle between the middle point of the active interval and the current point (Fig. 6-1). It follows from Eq. 6-1 that the increase in duration of the engine firing interval leads to a decrease in eccentricity alteration in comparison to the impulsive case. In table 6-1, one can see the eccentricity alteration decrease (in percent) in comparison to the impulsive case for different values of burn duration (the burn duration is measured, by the latitude argument, in degrees).

Table 6-1

$\Delta\varphi$ deg	20	40	60	80	100	120	140	160	180
Δe %	1.0	2.0	4.5	7.9	12.2	17.3	23.1	29.1	36.3
$\Delta\varphi$ deg	200	220	240	260	280	300	320	340	360
Δe %	43.6	51.0	58.6	66.2	73.7	80.9	87.8	94.1	100

It is assumed that the spacecraft's mass does not practically change during the single manoeuvre and the time Δt that is needed for the alteration of the spacecraft's velocity by the magnitude $V_0\Delta V$ can be evaluated as:

$$\Delta t = \frac{m}{P} V_0 \Delta V, \tag{6-2}$$

where m = spacecraft mass and P = engine thrust.

According to Eq. 6-2, $\Delta\varphi$ is proportional to ΔV :

$$\Delta\varphi = \lambda_0 \Delta t = k\Delta V = \frac{w_c}{w}\Delta V, \tag{6-3}$$

where $\lambda_0 = \frac{V_0}{r_0}$, $k = \frac{mV_0^2}{Pr_0} = \frac{w_c}{w}$, w_c = the centripetal acceleration of the relative circular orbit and ($w_c = \frac{V_0^2}{r_0}$), and w = the acceleration made by the thrust engines ($w = \frac{P}{m}$).

With the help of Eq. 6-3, one can find the orbital eccentricity acceleration caused by the engine firing on the interval $\Delta\varphi$:

$$\Delta e = 4\frac{w}{w_c}\sin\frac{\Delta\varphi}{2}. \tag{6-4}$$

The maximum eccentricity alteration that can be reached after a single firing is:

$$\Delta e^* = 4\frac{w}{w_c}, \tag{6-5}$$

The optimal value is $\Delta\varphi = \pi$. If the thrust orientation has the opposite direction on the other half of the revolution, the sum of the eccentricity alteration will be:

$$\Delta\tilde{e} = 8\frac{w}{w_c}. \tag{6-6}$$

The minimum revolution number n_e, which is needed for the correction of the eccentricity deviation Δe, should meet the constraint:

$$n_e \geq \frac{\Delta e}{\Delta\tilde{e}}. \tag{6-7}$$

Considering that the alteration to the semimajor axis does not depend on the moment of application of the transversal impulse, but rather depends on the magnitude of this impulse $\Delta a = 2\Delta V_t$ (here, Δa is the dimensionless value, as always), the alteration of the dimensionless semimajor axis after the firing of the thrust engine on the interval $\Delta\varphi$ can be found as:

$$\Delta a = \frac{2w}{w_c}\Delta\varphi. \tag{6-8}$$

The maximum semimajor axis alteration on the revolution when the thrust engine works for the whole revolution ($\Delta\varphi = 2\pi$) is:

$$\Delta\tilde{a} = \frac{4\pi w}{w_c}.$$

The minimum number of revolutions n_a, which is necessary for the correction of the deviation of the semimajor axis Δa, should meet the constraint:

$$n_a \geq \frac{\Delta a}{\Delta\tilde{a}}. \tag{6-9}$$

The conditions of transfer to the given orbit can be found from the equation below. Each revolution contains two burns. The centers of the active intervals are situated on the apsidal line of the relative orbit:

$$\begin{aligned} 4\sin\frac{\Delta\varphi_1}{2} - 4\sin\frac{\Delta\varphi_2}{2} &= \frac{w_c\Delta e}{wn}, \\ 2\Delta\varphi_1 + 2\Delta\varphi_2 &= \frac{w_c\Delta a}{wn}, \end{aligned} \tag{6-10}$$

where n = the number of revolutions on which the thrust engines work in the same fashion ($n \geq n_a, n \geq n_e$). The possible magnitudes of alteration of $\Delta a, \Delta e$ are defined more accurately in section 6.1.6.

The values of $\Delta\varphi_1, \Delta\varphi_2$ can be found using Eq. 6-10:

$$\begin{aligned} \Delta\varphi_1 &= \frac{w_c\Delta a}{4wn} + 2\arcsin\frac{w_c\Delta e}{8wn\cos\dfrac{w_c\Delta a}{8wn}}, \\ \Delta\varphi_2 &= \frac{w_c\Delta a}{4wn} - 2\arcsin\frac{w_c\Delta e}{8wn\cos\dfrac{w_c\Delta a}{8wn}}. \end{aligned} \tag{6-11}$$

If $\Delta\varphi_i$ appears to be negative, the orientation of the thrust vector should correspond to the deceleration while performing the manoeuvre.

If the condition for the transfer between the nonintersecting orbits is true:

$$\frac{w_c|\Delta a|}{2wn} > 4\arcsin\frac{w_c\Delta e}{8wn\cos\dfrac{w_c|\Delta a|}{8wn}}, \tag{6-12}$$

then the total delta-v expenditure for transfer with limited thrust is analogous to the expenditure of the impulsive solution and may be estimated as:

$$\Delta V = \frac{|\Delta a|}{2}.$$

The total delta-v expenditure for the transfer with limited thrust exceeds the expenditures of impulsive solutions in the case of transfers between intersecting orbits and transfers between nonintersecting orbits without fulfilling Eq. 6-12. These expenditures can be found by using the equation:

$$\Delta V = \frac{4nw}{w_c} \arcsin \frac{w_c \Delta e}{8wn \cos \dfrac{w_c |\Delta a|}{8wn}}. \tag{6-13}$$

By increasing *n*, we can get closer to the impulse solution for the total delta-v point of view.

6.1.2. Example

It is necessary to determine the parameters for transfer between the orbits with the elements from table 2-1 for low-thrust engines. These initial conditions are analogous to the conditions in Example 2.1.5.

Table 6-2

Orbit elements	Initial orbit	Final orbit
$H_{\min}$ km	180	340
$H_{\max}$ km	210	360
u_{prg} deg	20	150

It is important to know the spacecraft's mass, $m = 300$ kg , and engine thrust, $P = 0.2$ N, in this problem.

The centers of the thrust engine firing intervals $\varphi_{1_c}, \varphi_{2_c}$ are the locations of impulse application during an impulsive transfer (as evaluated in 2.1.5). The assessment of the minimum number of revolutions *n* for manoeuvring can be obtained from the second equation of Eq. 6-10. Only the assessment of the semimajor axis alteration will be used, as this alteration is bigger than the eccentricity alteration.

We use the evident constraint that the angular interval of firing on a single revolution cannot exceed 2π:

$$\varphi_1 + \varphi_2 = \frac{w_c \Delta a}{2wn} < 2\pi \Rightarrow n > \frac{w_c \Delta a}{4w\pi}.$$

Here, $w = \frac{P}{m} = 0.000667 \text{ m/s}^2$ = the acceleration caused by the thrust engines and $w_c = \frac{V_0^2}{r_0} = 9.0 \text{ m/s}^2$ = the centripetal acceleration. We get n = 25. We will add some spare revolutions to the final number of revolutions per manoeuvre in order to account for a possible pause between the manoeuvring revolutions and the inability to get the angles $\Delta\varphi_i$ due to the discrepancy of the arcsine function argument and its range of definition. We thus assume n = 31.

The angular duration of the thrust engine firing intervals can be evaluated by (6-11):

$$\Delta\varphi_1 = \frac{w_c \Delta a}{4wn} + 2\arcsin\frac{w_c \Delta e}{8wn\cos\frac{w_c \Delta a}{8wn}},$$

$$\Delta\varphi_2 = \frac{w_c \Delta a}{4wn} - 2\arcsin\frac{w_c \Delta e}{8wn\cos\frac{w_c \Delta a}{8wn}}.$$

The calculation results are: $\varphi_{1_c} = 180624^\circ$, $\Delta\varphi_1 = 226.012^\circ$, $\Delta V_{t_1} = \frac{w}{w_c}\Delta\varphi = 69.92$ m/s, $\varphi_{2_c} = 360240^\circ$, $\Delta\varphi_2 = 66.069^\circ$, $\Delta V_{t_2} = 20.44$ m/s.

6.1.3. Thrust Vector Constant Orientation in the Inertial Coordinate Frame

Let us consider the variant of the fixed thrust engine orientation in the inertial coordinate frame. In order to get closer to the impulsive solution, which is considered as the basis solution, the middle of the active interval should coincide with the impulse application point (in Fig. 6-2, the orbital arc *AC* also corresponds to the active interval and point *B* is the impulse application point). The thrust vector in the initial moment (point *A*) should be pointed in such a way that at the middle of the active interval (point *B*) it would be directed transversally. With these constraints met, the

alteration of the eccentricity vector will be in the same direction as in the impulsive case, but the magnitude of alteration itself will be smaller. The eccentricity alteration caused by the application of the dimensionless velocity ΔV , which is equally distributed on the interval of the latitude argument $\Delta\varphi$, can be calculated with the help of the equation:

$$\Delta e = \int_{-\Delta\varphi/2}^{\Delta\varphi/2} \frac{\Delta V}{\Delta\varphi}(2\cos\varphi\cos\varphi + \sin\varphi\sin\varphi)d\varphi = \Delta V(\frac{3}{2} + \frac{\sin\Delta\varphi}{2\Delta\varphi}), \quad (6\text{-}14)$$

where $\Delta\varphi$ = the angular magnitude of the active interval. According to Eq. 6-14, the eccentricity alteration is greater in comparison to the fixation of the orientation in the orbital coordinate frame. From table 6-3, one can see the decrease (in percent) of the eccentricity alteration in comparison to the impulsive case for the different values of the thrust engine firing angular duration.

Table 6-3

$\Delta\varphi$ deg	20	40	60	80	100	120	140	160	180
Δe %	0.5	1.99	4.3	7.37	10.9	14.7	18.4	21.9	25.0
$\Delta\varphi$ deg	200	220	240	260	280	300	320	340	360
Δe %	27.4	29.2	30.2	30.4	30.0	29.1	27.9	26.4	25.0

Using Eq. 6-3, one can find the orbital eccentricity alteration for the interval of the thrust engine firing $\Delta\varphi$:

$$\Delta e = \frac{3w}{2w_c}\Delta\varphi + \frac{w}{2w_c}\sin\Delta\varphi. \quad (6\text{-}15)$$

According to Eq. 6-15, the eccentricity vector alteration in the required direction is carried out during the whole revolution ($\Delta\varphi = 2\pi$) with the fixed thrust vector orientation in the inertial coordinate frame.

The maximum eccentricity alteration that can be gained after one revolution is:

$$\Delta\tilde{e} = 3\pi\frac{w}{w_c}, \quad (6\text{-}16)$$

The value will be $\Delta\varphi = 2\pi$.

The minimum number of revolutions n_e, needed for the correction of the eccentricity Δe, should meet the constraint:

$$n_e \geq \frac{\Delta e}{\Delta \tilde{e}}. \tag{6-17}$$

The semimajor axis alteration, caused by application of the relative velocity ΔV, can be evaluated by:

$$\Delta a = 2\int_{-\Delta\varphi/2}^{\Delta\varphi/2} \frac{\Delta V}{\Delta\varphi}\cos\varphi d\varphi = 4\frac{\sin\frac{\Delta\varphi}{2}}{\Delta\varphi}\Delta V. \tag{6-18}$$

This equation is analogous to the eccentricity alteration equation for the fixed thrust engine orientation in the orbital coordinate frame.

Using Eq. 6-3, one can get:

$$\Delta a = \frac{4w}{w_c}\sin\frac{\Delta\varphi}{2}. \tag{6-19}$$

The maximum semimajor axis alteration that can be gained after a single ignition is:

$$\Delta a^* = 4\frac{w}{w_c}, \tag{6-20}$$

The value will be $\Delta\varphi = \pi$. If the thrust vector orientation on the other half of the revolution is opposite, the sum of the semimajor axis alteration will be:

$$\Delta \tilde{a} = 8\frac{w}{w_c}. \tag{6-21}$$

The minimum number of revolutions n_a that are needed for the correction of the semimajor axis deviation Δa should meet the constraint:

$$n_a \geq \frac{\Delta a}{\Delta \tilde{a}}. \tag{6-22}$$

The transfer conditions for the given orbit can be found using the equation below. Each revolution contains two burns. The centers of the active intervals are situated on the apsidal line of the relative orbit and the thrust engine orientation is the opposite:

$$\begin{aligned} &\frac{3}{2}\Delta\varphi_1 + \frac{1}{2}\sin\Delta\varphi_1 - \frac{3}{2}\Delta\varphi_2 - \frac{1}{2}\sin\Delta\varphi_2 = \frac{w_c \Delta e}{wn}, \\ &4\sin\frac{\Delta\varphi_1}{2} + 4\sin\frac{\Delta\varphi_2}{2} = \frac{w_c \Delta a}{wn}, \end{aligned} \tag{6-23}$$

where n = the number of revolutions on which the thrust engine works in the same fashion ($n \geq n_a, n \geq n_e$). The values of $\Delta\varphi_1, \Delta\varphi_2$ can be numerically found from this equation system.

6.1.4. Thrust Vector Optimal Orientation for Eccentricity Vector Alteration

Let us determine the orientation of the thrust vector for the provision of the maximum change in eccentricity. We are only interested in the eccentricity here because we considered the semimajor axis alteration earlier—the thrust vector orientation must be transversal.

The thrust vector orientation at this point of the orbit is determined by the angle α, which counts from the perpendicular to the radius vector (Fig. 6-3). Then, after application of the impulse ΔV_p ($\Delta V_p = \frac{\Delta V_p^*}{V_0}$) at the point φ degrees far from the middle of the active interval (Fig. 6-3), the following alterations of the semimajor axis a and the eccentricity e (in the direction of point B) will occur:

$$\begin{aligned} &\Delta V_t = \Delta V_p \cos\alpha, \Delta V_r = \Delta V_p \sin\alpha, \\ &\Delta e(\varphi) = 2\Delta V_p \cos\alpha \cos\varphi + \Delta V_p \sin\alpha \sin\varphi, \end{aligned} \tag{6-24}$$

$$\Delta\alpha(\varphi) = 2\Delta V_p \cos\alpha. \tag{6-25}$$

According to Eq. 6-24, the maximum eccentricity alteration can be reached if:

$$\operatorname{tg}\alpha = \frac{1}{2}\operatorname{tg}\varphi \tag{6-26}$$

The same result can be obtained if one uses the required optimality conditions. The thrust vector orientation with $\lambda_1 = 0$ (Fig. 6-4), is determined by an equation that is similar to Eq. 6-26:

$$\operatorname{tg}\alpha = \frac{\lambda}{\mu} = \frac{\sqrt{\lambda_2^2 + \lambda_3^2}\sin\varphi}{2\sqrt{\lambda_2^2 + \lambda_3^2}\cos\varphi} = \frac{1}{2}\operatorname{tg}\varphi.$$

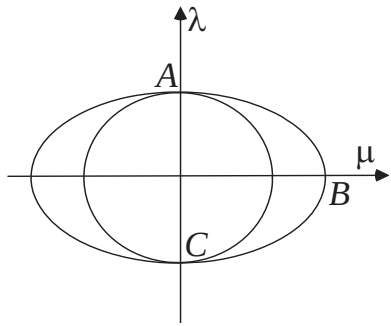

Fig. 6-4. Primer vector hodograph for $k = 1$, $\lambda_1 = 0$

This thrust engine orientation, which corresponds to the primer vector hodograph in the form of an ellipse, meets all the optimality conditions. The ellipse is symmetrical relative to the axis λ. This form ensures maximum eccentricity alteration among all the optimal solutions. Let us remember that for the case of the optimal impulse transfers between the intersecting orbits, when the maximum eccentricity alteration is needed, we use the ellipse (with center in the coordinate frame origin) as the primer vector hodograph. The difference for the case of limited thrust lies in the fact that the primer vector hodograph determines the optimal orientation of the thrust engines not just in the two points where the ellipse and the unit circle osculate, but in all points of the ellipse outside the unit circle (Fig. 6-4).

Hereafter, the thrust engine orientation determined by Eq. 6-26 will be termed “optimal by eccentricity”.

The equation for the eccentricity alteration in this point is given by:

$$\Delta e = \Delta V_p \sqrt{1+3\cos^2\varphi}. \tag{6-27}$$

The alteration of the semimajor axis is calculated by:

$$\Delta a = \frac{4\Delta V_p \cos\varphi}{\sqrt{1+3\cos^2\varphi}}. \tag{6-28}$$

Remembering that $\Delta V_p = \frac{\Delta V}{\Delta\varphi} d\varphi = \frac{w}{w_c} d\varphi,$ the semimajor axis alteration caused by firings on the whole interval will be:

$$\Delta a = \int_{-\Delta\varphi/2}^{\Delta\varphi/2} \frac{4w\cos\varphi d\varphi}{w_c\sqrt{1+3\cos^2\varphi}} = \frac{8w}{\sqrt{3}w_c} \arcsin\left(\frac{\sqrt{3}}{2}\sin\frac{\Delta\varphi}{2}\right). \tag{6-29}$$

The elliptical integral of the second kind is the part of the equation for eccentricity alteration:

$$\Delta e = \int_{-\Delta\varphi/2}^{\Delta\varphi/2} \frac{w}{w_c}\sqrt{1+3\cos^2\varphi} d\varphi = 4\frac{w}{w_c} E\left(\frac{\Delta\varphi}{2}, \frac{\sqrt{3}}{2}\right). \tag{6-30}$$

In tables 6-4 and 6-5, one can see decreases (percent) in the semimajor axis and the corresponding eccentricity alteration (obtained from eqs. 6-29 and 6-30) in comparison to the impulse case for the different values of the angular duration of firing.

Table 6-4

$\Delta\varphi$ deg	20	40	60	80	100	120	140	160	180
Δa %	0	0.5	0.1	2.5	4.0	6.5	10.0	15.5	23.0
$\Delta\varphi$ deg	200	220	240	260	280	300	320	340	360
Δa %	32.5	43.0	53.0	63.0	72.0	80.0	87.5	94.0	100.0

Table 6-5

$\Delta\varphi$ deg	20	40	60	80	100	120	140	160	180
Δe %	0	1.5	3.5	6.0	9.0	12.5	16.0	19.5	23.0
$\Delta\varphi$ deg	200	220	240	260	280	300	320	340	360
Δe %	25.5	27.7	28.2	28.5	28.0	27.0	25.5	24.2	23.0

6.1.5. Comparison of the Effects Caused by Different Thrust Vector Orientations

Figures 6-5 and 6-6 present graphs depicting the semimajor axis and eccentricity alteration plotted against the manoeuvre angular duration for the various types of thrust engine orientation. In the graphs, one can find the dependencies of the orbital orientation (solid line), the inertial orientation (dashed line), and the "optimal for eccentricity" orientation (dotted line). In order to remove the account of engine power and the orbital radius, the variables $\frac{w_c}{w}\Delta a$ and $\frac{w_c}{w}\Delta e$ are used instead of Δa and Δe, which is why the magnitudes of the dimensionless semimajor axis and the eccentricity are greater than 1. In order to get the actual graphs for a specific problem, one should divide the values from these graphs by $\frac{w}{w_c}$.

As can be seen, the curves for the different types of orientation are close to each other for manoeuvre durations of less than or equal to 45°. The semimajor axis and eccentricity alterations are the same as the ones obtained with the equivalent impulse. This explains the effectiveness of the impulse solution for relatively small manoeuvre durations.

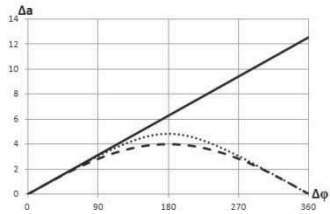

Fig. 6-5. Effectiveness of semimajor axis correction

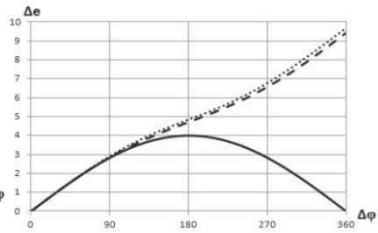

Fig. 6-6. Effectiveness of eccentricity correction

It is important to note that the dependencies for the inertial orientation and "optimal by eccentricity" orientation are close to each other (especially for the eccentricity alteration). It can be seen in Fig. 6-6 that, starting from approximate $\Delta\varphi = 180^\circ$, the graphs of the inertial and the "optimal by the eccentricity" orientations go in parallel with good proximity to each other. This allows the use of the simpler but still effective inertial orientation instead of the challenging "optimal by eccentricity" orientation for cases of large eccentricity deviations. Due to the proximity of the eccentricity alteration for these types of orientation, one can use the approximate Eq. 6-31 (Baranov and Baranov 2010, 115-116), rather than Eq. 6-30 for the "optimal by eccentricity" orientation.

The error will not exceed 0.5 % for these cases:

$$\Delta e = \frac{w}{w_c}\left(\frac{3}{2}\Delta\varphi + \frac{1}{2}\sin\Delta\varphi + 0.04\frac{\Delta\varphi}{\pi}\right), \Delta\varphi \le \pi, \tag{6-31a}$$

$$\Delta e = 1.54\frac{w}{w_c}\Delta\varphi + \frac{w}{2w_c}\sin\Delta\varphi, \Delta\varphi \ge \pi. \tag{6-31b}$$

6.1.6. Geometric Interpretation of Manoeuvres: Domains of Existence of the Observed Solutions

The assessments of the domains of existence of the various solution types, used in the previous paragraphs of this chapter, are rather coarse and do not allow us to get the whole picture. It is preferable to specify the area boundaries in one dimension. Earlier, it was shown to be effective to use the plane e_x, e_y for the geometric interpretation of the manoeuvres. In this chapter, the ratio of the eccentricity alteration to the semimajor axis alteration is significant, not the direction of the eccentricity vector alteration (which is carried out along the apsidal line of the relative orbit). As such, it is necessary to use the coordinate frame, with the semimajor axis alteration marked on the abscissa axis and the eccentricity alteration marked on the ordinate axis.

Let us consider the use of this plane for the impulse solution as an example. The positive transversal impulse ΔV_t (vector *OA* corresponds to it in Fig. 6-7), which is applied at the relative orbit pericenter, causes the equal alteration of the orbital eccentricity and the semimajor axis $2\Delta V_t$. Vector *OD* corresponds to the negative impulse $-\Delta V_t$, which is applied at this point. Vector *OB* corresponds to the positive impulse, the moment of

application of which is half a revolution distant. Vector *OC* corresponds to the negative impulse, which is applied half a revolution later.

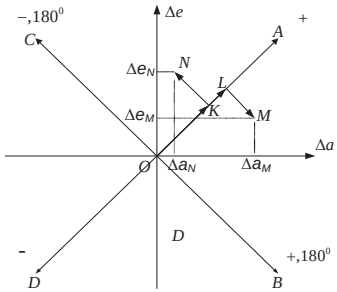

Fig. 6-7. Semimajor axis and eccentricity change by impulses

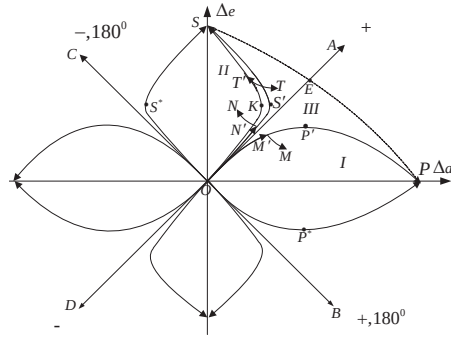

Fig. 6-8. Semimajor axis and eccentricity change by low-thrust engines

Let us consider the transfer to the orbit with deviations between the parameters of the initial and target orbits $\Delta a_M, \Delta e_M$ (point *M* in Fig. 6-7) with the help of two transversal impulses $\Delta V_{t_1}, \Delta V_{t_2}$, which are applied on the apsidal line of the relative orbit (ΔV_{t_2} is applied at the relative orbit's apocenter) and, additionally, $\Delta a_M > \Delta e_M$ (the transfer between the nonintersecting orbits). The impulse magnitudes can be found from the equation system:

$$2\Delta V_{t_1} + 2\Delta V_{t_2} = \Delta a_M,$$
$$2\Delta V_{t_1} - 2\Delta V_{t_2} = \Delta e_M.$$

The curved line *OLM* corresponds to this transfer on plane a, e. Both impulses are positive.

The curved line *OKN* (the second impulse is negative) corresponds to the transfer between the intersecting orbits (for example, to point *N* ($\Delta a_N < \Delta e_N$)).

It is possible to gain the limited eccentricity and semimajor axis alterations on the revolution when using the manoeuvres carried out by engines with limited steady thrust. Line *OP P* (Fig. 6-8) corresponds to the

orbital element alteration with the fixed transversal orientation of the thrust engines in the orbital coordinate frame. Point P' is reached after the thrust engine fires for half a revolution, while point P is reached after the thrust engine fires for a whole revolution. The equation depicting the curve $OP'P$ can be found using eqs. 6-4 and 6-8:

$$\Delta e = 4\frac{w}{w_c}\sin\frac{w_c}{4w}\Delta a.$$

Line OKS corresponds to a constant orientation in the inertial coordinate frame. The equation depicting the curve OKS is derived from eqs. 6-15 and 6-19:

$$\Delta e = \frac{3w}{w_c}\arcsin\frac{w_c\Delta a}{4w} + \frac{w}{2w_c}\sin(2\arcsin\frac{w_c\Delta a}{4w}).$$

Line $OS'S$ corresponds to the close-to-previous orientation, ensuring maximum eccentricity alteration. Points S' and K correspond to the orbital element change for a half-revolution manoeuvre duration. Similarly, the analogous dependencies are presented in the other quadrants (Baranov, Baranov, and Razoumny 2010).

In the second, third, and fourth quadrants one can find the signs "+", "-", and "180º". The plus sign shows the thrust orientation for the acceleration, the minus sign indicates braking, and the "180º" sign indicates that the influence of the manoeuvre, which has a middle 180º distant from the middle of the active interval (the influence of which is depicted in the first quadrant), is shown in the given quadrant.

The orbital orientation of the thrust engines is optimal for reaching the points from the area, restricted with the line $OP'P$ and the abscissa axis (area I). The two manoeuvres should be performed on a single revolution. The middle parts of the manoeuvres are 180º distant from each other and the thrust engine orientation is the same for both manoeuvres. A part of line $OP'P$ corresponds to the first manoeuvre, while a part of line OP^*P corresponds to the second manoeuvre. For example, the transfer to point M is carried out with the use of the trajectory $OM'M$. The values of $\Delta\varphi_1, \Delta\varphi_2$, corresponding to the curves OM' and $M'M$ respectively, can be found using Eq. 6-11.

The orientation of the thrust engines that ensures the maximum eccentricity alteration will be optimal if the transfer to the orbit (to which the point of the area, constrained by the ordinate axis and line $OS'S$ (area

II) corresponds, for example, point *N*) is needed. The constant orientation in the inertial coordinate frame is close to it from the point of view of the effectiveness of eccentricity correction, but it is a little bit less effective for the correction of the semimajor axis. The second fact is less important within the considered area and the "inertial" orientation is more preferable if simplicity of the orientation setting and maintenance is demanded. The trajectory $ON\mathcal{N}$ corresponds to the transfer to point *N* and the transfer is fulfilled with the help of two manoeuvres. A part of line $OS'S$ corresponds to the first manoeuvre, while a part of line OS^*S corresponds to the second manoeuvre. The values $\Delta\varphi_1, \Delta\varphi_2$, which correspond to the curves ON' and $N\mathcal{N}$ respectively, can be found from Eq. 6-23 for the "inertial" orientation, or they can be found by using eqs. 6-29 and 6-31 for the "optimal by eccentricity" orientation.

The orbital transfer, to which the point from area *III* corresponds, constrained by the lines $OS'S$ and $OP'P$ and the line that connects points *S* and *P*, can be carried out with the use of two manoeuvres on a revolution, the centers of which are 180° distant from each other. However, it is better to use the different types of thrust engine orientation for the fulfillment of these manoeuvres. The thrust vector orientation is fixed in the orbital coordinate frame for the application of the first manoeuvre and the thrust orientation is fixed in the inertial coordinate frame for the application of the other manoeuvre. The terms from eqs. 6-10 and 6-23 are included in the equations of the system for the parameter determination of such manoeuvres.

In area *III*, it is possible to transfer to the required point with the use of the single optimal long-duration manoeuvre by changing angle α during the manoeuvre. Manoeuvres of this type are considered in the next paragraph.

6.1.7. Existence Domains of Nondegenerate Solutions in the Case of Optimal Thrust Orientation

Cases in which the primer vector hodograph degenerates to a point and when it is in an ellipse (symmetrical to the λ axis) have been considered. Let us investigate the optimal solutions that correspond to the other ellipse locations. The ellipses, increasing in size, which osculate with the unit circle and are located to its right, are shown in Fig. 6-9.

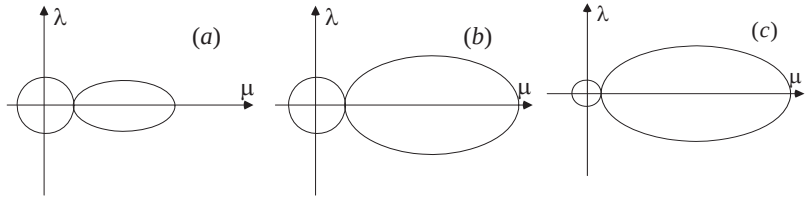

Fig. 6-9. Outer osculation of primer vector hodograph and unit circle

With the increasing size of the ellipse, the ellipse variants (a, b, and c for example) in Fig. 6-9, corresponding to the curves on plane $\Delta a, \Delta e$ (also designated *a*, *b*, *c* in Fig. 6-11), move away bit by bit from the curve $OP\mathcal{P}$ and get closer to the curve $OL\mathcal{L}$, which restrains the area (designated *IV*) of this type of solutions existence.

Similarly, with the increase in the dimensions of the ellipse, which has an inner osculation with the unit circle, variants (d, e, and f in Fig. 6-10, corresponding to the curves designated *d*, *e*, and *f* in Fig. 6-11) move away bit by bit from the curve $OS\mathcal{S}$ and fill the rest of area *III*.

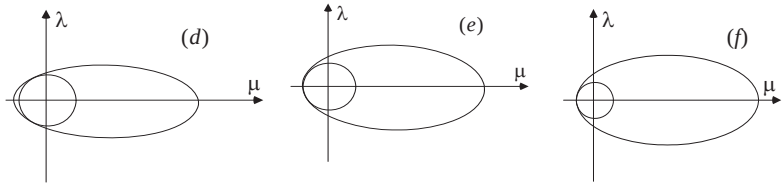

Fig. 6-10. Primer vector hodograph and unit circle inner osculation

The existence domain of this type of solution is designated by the number *V*. The lines, which correspond to ellipses with big dimensions, also move towards the curve $OL\mathcal{L}$, but the upwards curve, connected to the presence of the interval where $\mu<0$, remains. The less that the part of the ellipse, belonging to the left semiplane, the closer the curved line to the curve $OL\mathcal{L}$ and the smaller the upwards curve is.

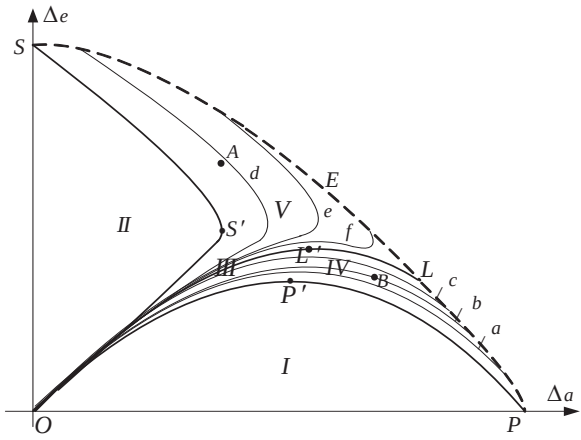

Fig. 6-11. The existence domains of different types of solutions

The curve *OL′L*, which divides the areas *IV* and *V*, can be evaluated approximately using the function (Baranov, Baranov, de Prado and Razumny 2011, 269-279):

$$\Delta e = -0.003\,\Delta a^3 - 0.035\,\Delta a^2 + 1.068\,\Delta a,\ 0 \le \Delta a \le 9.67, \tag{6-32}$$

The *SEP* curve is determined by the equations:

$$\Delta e = 0.001\,\Delta a^3 - 0.081\,\Delta a^2 - 0.593\,\Delta a + 9.69,\quad 0 \le \Delta a < 8.27, \tag{6-33a}$$

$$\Delta e = -0.04\,\Delta a^3 + 1.404\,\Delta a^2 - 14.295\,\Delta a + 55.332,\quad 8.27 \le \Delta a < 12.57, \tag{6-33b}$$

In order to use these results for the specific problem, one should switch from the true dimensionless deviations $\Delta a^*, \Delta e^*$ to the variables $\Delta a, \Delta e$, which are used in these equations:

$$\Delta a = \frac{w_c}{w}\Delta a^*,\ \Delta e = \frac{w_c}{w}\Delta e^*.$$

The information concerning the boundary *SEP* is very important, as it allows the rather accurate assessment of the possibility of transferring between orbits with the use of a single manoeuvre per revolution (or whatever number of revolutions *n* will be necessary for the manoeuvring) without the direct calculation of the manoeuvre parameters.

Corresponding to the arbitrary values k, λ_1, the curves on plane a, e stay within the boundary limits of area *III*. This reminds us of the fact that with the use of the optimal thrust vector orientation, the points of areas *I* and *II* can be reached with only two burns.

6.1.8. Parameter Determination of the Optimal Nondegenerate Solution

Let us consider the manoeuvre parameters (duration and law of change for angle α) that ensure the given alterations of the orbital elements Δa_0 and Δe_0.

It follows from the necessary optimality conditions that

$$tg\,\alpha = \frac{\lambda}{\mu} = \frac{k \sin\varphi}{2(\lambda_1 + k\cos\varphi)}, \tag{6-34}$$

The cosine and the sine of angle α can be found by:

$$\begin{aligned} \cos\alpha &= \frac{2(\lambda_1 + k\cos\varphi)}{\sqrt{4\lambda_1^2 + 8\lambda_1 k\cos\varphi + 3k^2\cos^2\varphi + k^2}} \\ \sin\alpha &= \frac{k\sin\varphi}{\sqrt{4\lambda_1^2 + 8\lambda_1 k\cos\varphi + 3k^2\cos^2\varphi + k^2}} \end{aligned} \tag{6-35}$$

Using eqs. 6-35, 6-24, and 6-25 we obtain the following equations for the alterations of the semimajor axis and eccentricity:

$$\Delta a = \int_{-\Delta\varphi/2}^{\Delta\varphi/2} \frac{4(\lambda_1 + k\cos\varphi)}{\sqrt{4\lambda_1^2 + 8\lambda_1 k\cos\varphi + 3k^2\cos^2\varphi + k^2}}\, d\varphi, \tag{6-36}$$

$$\Delta e = \int_{-\Delta\varphi/2}^{\Delta\varphi/2} (2\frac{2(\lambda_1 + k\cos\varphi)\cos\varphi}{\sqrt{4\lambda_1^2 + 8\lambda_1 k\cos\varphi + 3k^2\cos^2\varphi + k^2}} + \\ + \frac{k\sin^2\varphi}{\sqrt{4\lambda_1^2 + 8\lambda_1 k\cos\varphi + 3k^2\cos^2\varphi + k^2}})d\varphi. \quad (6\text{-}37)$$

The following algorithm for the determination of k, λ_1 and $\Delta\varphi$ is proposed (Baranov, Baranov, de Prado and Razumny 2011, 269-279). It is determined to which area the point $(\Delta a_0, \Delta e_0)$ belongs. If it is area *I*, then $\Delta\varphi_1, \Delta\varphi_2$ can be found from Eq. 6-11. If it is area *II*, then $\Delta\varphi_1, \Delta\varphi_2$ can be found from Eq. 6-23, which is used in the case of the fixed thrust vector orientation in the inertial coordinate frame, or from eqs. 6-29 and 6-31 in the case of the optimal by eccentricity orientation. We are interested in the case when the point $(\Delta a_0, \Delta e_0)$ belongs to the areas *IV* or *V*.

The search for a solution consists of the successive repetition of the three stages. In the first stage, a point from the dimension k, λ_1 is taken, which sets the location of the ellipse and the law of change for angle α. This point can be rather accurately specified, as areas *IV* and *V* are preliminarily divided into known subareas. In the next stage, $\Delta\varphi$ is determined, which corresponds to the part of the ellipse outside the unit circle (Fig. 6-12). The ellipse now intersects the circle because the transfer to the inner point of areas *IV* and *V* is considered and, hence, the manoeuvring is fulfilled for the part of the revolution that corresponds to the part of the ellipse outside the circle.

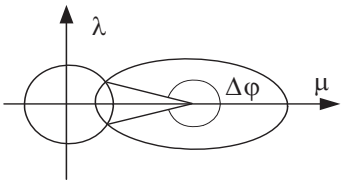

Fig. 6-12. Primer vector hodograph for points of area *III*

The value found for $\Delta\varphi$ determines the limits of integration. At the third stage, the integrals 6-36 and 6-37 are calculated. The problem is solved if the determined values of $\Delta a_c, \Delta e_c$ coincide with $\Delta a_0, \Delta e_0$ with the desired accuracy. Otherwise, we return to the first stage, i.e. to a new

point from area k, λ_1 is taken. In the vicinity of the optimal solution, the steps of enumeration in area k, λ_1 and the integration step are decreased in order to provide the necessary accuracy for the problem's solution.

The problem of the deviations from area *III* can be solved with the use of two manoeuvres and the alteration of the thrust vector orientation, but the benefit of decreasing the number of manoeuvres will disappear and it is also a lot easier to realize the fixed orientation of the thrust engines (the alternative solution).

The algorithm used to determine the parameters of the manoeuvre with the alteration to the thrust vector orientation described in this paragraph can also be used on the active interval of the upper stage for the determination of its thrust vector.

6.1.9. Number of Revolutions with Activated Propulsion

The minimum number of revolutions $n_{\min}$ needed for the flyby to a given orbit, can be found with the help of Eq. 6-33, to determine the outer boundary of area *III*. The deviations $\Delta a_0 / n_{\min}$ and $\Delta e_0 / n_{\min}$ (point *E* corresponds to them in Fig. 6-13) should belong to area *III*. By increasing the number of revolutions *n* on which the manoeuvring is fulfilled and, hence, by shifting point *E* deeper into area *OSP*, the fuel expenditures for the flyby can be reduced.

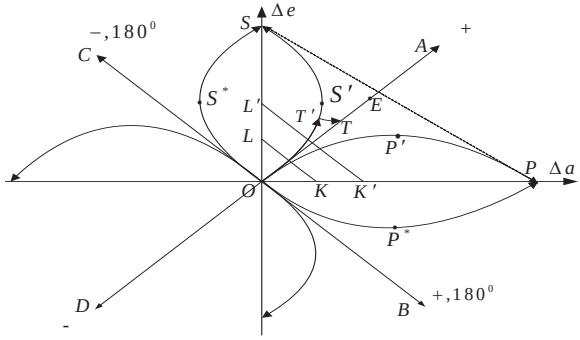

Fig. 6-13. Semimajor axis and eccentricity alteration by different types of thrust engine orientation

As can be seen in Fig. 6-13, with a manoeuvre duration of less than or approximately equal to 45º by the latitude argument, the lines, which correspond to all three considered thrust engine orientations, practically

coincide, and the total delta-v expenditure coincides with the expenditures in the impulsive case. This is one of the explanations for the good convergence of the iterative procedure with the impulse manoeuvre parameter determination in the impulsive statement and the manoeuvre duration that does not exceed 45º during manoeuvre modeling.

In Fig. 6-13, area *OKL* correspond to the orbital elements that can be obtained with the help of these manoeuvres. Thus, it is not necessary to increase the number of flyby revolutions and decrease the manoeuvre duration to less than one-eighth of a revolution. The discrepancy in the impulsive solution for eccentricity alteration will be less than 10 % for all considered thrust engine orientations for a manoeuvre duration of less than or equal to 90º. The discrepancy in the semimajor axis alteration from the impulsive case with the "optimal by eccentricity" orientation will be less than 5 %, or less than 10 % for the inertial orientation. Thus, manoeuvres of durations ranging from 45º to 90º are effective enough. In Fig. 6-13, area *KLL′K′* corresponds to the orbital elements, which can be obtained with the help of these manoeuvres. If the duration of the manoeuvre is half of a revolution, the discrepancy from the impulsive case for the eccentricity and the semimajor axis alteration (except for the orbital orientation) will be greater than 20 %. It is necessary to increase the number of manoeuvring intervals in order to transfer the goal-point from area *K′L′SP* to area *OK′L′*. In the general case, the choice of the number of revolutions *n* on which the spacecraft manoeuvres should allow us to find a compromise between the desire to reduce the time of the transfer to the given orbit (the decrease in *n*) and the desire to decrease the total delta-v expenditure (the increase in *n*).

6.1.10. Distribution of Orbit Element Correction within Active Revolutions

As discussed in the previous sections, equal alterations of the semimajor axis and the eccentricity should be performed on each *n* revolutions at which the thrust engines operate. The results in tables 6-1 to 6-4 show that manoeuvre effectiveness decreases with an increase in their angular duration in a nonlinear fashion. This means that we can suppose that the angular manoeuvre duration on each revolution should be equal. Thus, the right terms in eqs. 6-10 and 6-23 for different manoeuvre revolutions should be equal to each other.

Let us suppose that the number of revolutions *n* on which firing should occur is determined. Then, the average semimajor axis and eccentricity

alterations should be $\Delta a_n = \frac{\Delta a}{n}, \Delta e_n = \frac{\Delta e}{n}$. Remembering that the angular duration of the manoeuvres on each revolution should be equal and using Eq. 6-6 one can obtain the alteration of the semimajor axis Δa_f for the last manoeuvring revolution:

$$\frac{w_{c_m} \Delta a_n}{w} = \frac{w_{c_f} \Delta a_f}{w}, \tag{6-38}$$

where w_{c_m}, w_{c_f} = the centripetal accelerations for the middle and final manoeuvring revolutions, respectively. Let $\Delta r = r_f - r_0$ be the difference between the average radii of the set and the initial orbits (the average radius is the radius of the circular orbit with the same period as the considered orbit).

Then

$$\frac{\Delta a_n}{r_m^2} = \frac{\Delta a_f}{(r_m + \frac{\Delta r}{2})^2},$$

where $r_m = \frac{1}{2}(r_0 + r_f)$. Neglecting the values of the second order of smallness, one obtains:

$$\Delta a_f = \Delta a_n (1 + \frac{\Delta r}{r_m}).$$

The necessary semimajor axis alteration on the manoeuvring revolution with the number *i* can be determined by:

$$\Delta a_i = \Delta a_n (1 + \frac{\Delta r}{r_m} (\frac{2i}{n} - 1)).$$

The analogous equation can be obtained for the eccentricity alteration.

The supposition about the equal angular duration of the manoeuvres is simple enough and, at the same time, more accurate than the supposition about the equal alteration of the orbital elements on each manoeuvring revolution.

Egorov, Grigoriev, and Ryzhov (2005) determined, with the use of the numerical method, the linear dependency of the duration (by the angular duration) of the active intervals during the flybys between the distantly located circular orbits.

6.2. Coplanar Low-Thrust Rendezvous

6.2.1. Rendezvous in Coplanar Nonintersecting Orbits

The apsidal solutions from the previous paragraph can be used for the solution of the rendezvous problem on coplanar orbits. It is supposed that the thrust engines allow the performance of all necessary manoeuvring on two intervals, the magnitudes of which gradually become smaller than the distances between them. Initially, it is supposed that the two manoeuvres are performed on each manoeuvring interval.

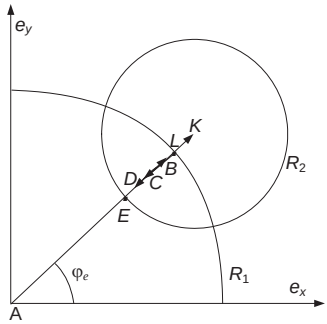

Fig. 6-14. Rendezvous on coplanar nonintersecting orbits

Line segments *AB*, *BC*, *CD*, and *DK* (Fig. 6-14) contingently correspond to the four manoeuvres (it is not correct to say that line segment $2\Delta V_t$ corresponds exactly to the manoeuvre). Point *C* corresponds to the drift orbit eccentricity vector.

Each manoeuvre of the first manoeuvring interval can be divided into m_1 equal parts, applied on different revolutions. Similarly, the manoeuvres of the second manoeuvring interval can be divided into m_2 equal parts.

In the impulsive case, if all solutions (for these solutions, the points of line segment *EL* (Fig. 6-14) correspond to the drift orbital eccentricity vectors) have equal total delta-v expenditures; then, for the case of the

limited thrust solution, the total delta-v may depend on the location of point *C* on line segment *EL*. Let *x* be the distance from point *A* to point *C* (*AC* = *x*), then $CK = \Delta e - x$. The solution of the rendezvous problem (for this solution, point *C* corresponds to the drift orbit eccentricity vector) may be represented as the solution and involves the combination of the two transfer problems on each of the manoeuvring intervals with the alteration of the orbital elements $\Delta a_1 = 2\Delta V_{t_I}$, $\Delta e_1 = x$ and $\Delta a_2 = 2\Delta V_{t_{II}}$, $\Delta e_2 = \Delta e - x$, respectively, where ΔV_{t_I} and $\Delta V_{t_{II}}$, which can be found by the equations:

$$\Delta V_{t_I} \approx -\frac{\Delta t}{3\varphi_{10}}, \tag{6-39}$$

$$\Delta V_{t_{II}} \approx \frac{\Delta a}{2} + \frac{\Delta t}{3\varphi_{10}}, \tag{6-40}$$

and φ_{10} = is the first permitted arbitrary point for the manoeuvring interval (the radii of the circles are $R_1 = 2\left|\Delta V_{t_I}\right|$ and $R_2 = 2\left|\Delta V_{t_{II}}\right|$).

Since $|\Delta a| > \Delta e$ for the nonintersecting orbits, then it is necessary to choose the transversal thrust engine orientation in the orbital coordinate frame for the fulfillment of the manoeuvre. The maximum alteration of the orbital semimajor axis occurs in this case.

Using Eq. 6-10, we can write:

$$\begin{aligned}
&\frac{4w}{w_c}\sin\frac{w_c\Delta V_{t_{I_1}}}{2w} - \frac{4w}{w_c}\sin\frac{w_c\Delta V_{t_{I_2}}}{2w} = \frac{x}{m_1},\\
&\Delta V_{t_{I_1}} + \Delta V_{t_{I_2}} = \frac{\Delta V_{t_I}}{m_1},\\
&\frac{4w}{w_c}\sin\frac{w_c\Delta V_{t_{II_1}}}{2w} - \frac{4w}{w_c}\sin\frac{w_c\Delta V_{t_{II_2}}}{2w} = \frac{\Delta e - x}{m_2},\\
&\Delta V_{t_{II_1}} + \Delta V_{t_{II_2}} = \frac{\Delta V_{t_{II}}}{m_2},
\end{aligned} \tag{6-41}$$

where m_1 and m_2 = the numbers of parts for the division of the transversal manoeuvring components of the first $\Delta V_{t_{I_1}}, \Delta V_{t_{I_2}}$ and the second $\Delta V_{t_{II_1}}, \Delta V_{t_{II_2}}$ manoeuvring intervals.

With the help of Eq. 6-11, the magnitudes of the manoeuvres $\Delta V_{t_{I_1}}, \Delta V_{t_{I_2}}$, $\Delta V_{t_{II_1}}, \Delta V_{t_{II_2}}$ can be found from the following equation system:

$$\begin{aligned}
\Delta V_{t_{I_1}} &= \frac{\Delta V_{t_I}}{2m_1} + \frac{2w}{w_c}\arcsin\frac{w_c x}{8wm_1\cos\dfrac{w_c\Delta V_{t_I}}{4wm_1}},\\
\Delta V_{t_{I_2}} &= \frac{\Delta V_{t_I}}{2m_1} - \frac{2w}{w_c}\arcsin\frac{w_c x}{8wm_1\cos\dfrac{w_c\Delta V_{t_I}}{4wm_1}},\\
\Delta V_{t_{II_1}} &= \frac{\Delta V_{t_{II}}}{2m_2} + \frac{2w}{w_c}\arcsin\frac{w_c(\Delta e - x)}{8wm_2\cos\dfrac{w_c\Delta V_{t_{II}}}{4wm_2}},\\
\Delta V_{t_{II_2}} &= \frac{\Delta V_{t_{II}}}{2m_2} - \frac{2w}{w_c}\arcsin\frac{w_c(\Delta e - x)}{8wm_2\cos\dfrac{w_c\Delta V_{t_{II}}}{4wm_2}},
\end{aligned} \tag{6-42}$$

If $|\Delta a|$ gradually exceeds Δe, and the signs of Δa_1 and Δa_2 coincide (in the impulse case, the AS solution type is optimal), then the total delta-v of the manoeuvres ΔV can be found by:

$$\Delta V = m_1\left(\left|\Delta V_{t_{I_1}}\right| + \left|\Delta V_{t_{I_2}}\right|\right) + m_2\left(\left|\Delta V_{t_{II_1}}\right| + \left|\Delta V_{t_{II_2}}\right|\right) = \frac{|\Delta a|}{2}. \tag{6-43}$$

If the signs of Δa_1 and Δa_2 do not coincide (in the impulse case the CNS solution type is optimal) and $|\Delta a_1| + |\Delta a_2|$ gradually exceeds Δe, then the manoeuvres ΔV can be found by:

$$\Delta V = m_1\left(\left|\Delta V_{t_{I_1}}\right| + \left|\Delta V_{t_{I_2}}\right|\right) + m_2\left(\left|\Delta V_{t_{II_1}}\right| + \left|\Delta V_{t_{II_2}}\right|\right) = \frac{|\Delta a_1|}{2} + \frac{|\Delta a_2|}{2}. \quad (6\text{-}44)$$

The same solution can be used for intersecting orbits when the CNS type solution will be optimal in the impulsive case.

Equations 6-43 and 6-44 can be used when the point corresponds to the drift orbit eccentricity vector. This point is close to the middle of line segment *EL*. In those cases, when $|\Delta a|$ is bigger than Δe, but their values are close, and for the points that are close to the boundaries of line segment *EL*, the total delta-v of the manoeuvres will be higher due to the bigger expenditures on the alteration of eccentricity.

6.2.2. Rendezvous in Coplanar Intersecting Orbits

The variant when the CNS type solution is optimal in the impulsive case (the circles, which have the radii R_1 and R_2, intersect) was considered earlier. Let us consider the variant when the CAS type solution will be optimal in the impulse case (the circles, which have the radii R_1 and R_2, do not intersect).

In the impulse case, all solutions of the rendezvous problems on the coplanar intersecting orbits (for these solutions the points of line segment *EL* correspond to the drift orbit eccentricity vector in Fig. 6-15), have equal total delta-v expenditures. In the case of limited thrust, the total delta-v of the solution depends on the location of point *C* on line segment *EL*. As for the rendezvous problem on nonintersecting orbits, we denote *x* as the distance from point *A* to point *C* (*AC* = *x*), such that $CK = \Delta e - x$.

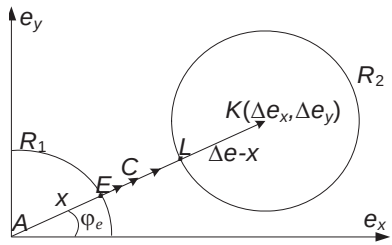

Fig. 6-15. Rendezvous on coplanar intersecting orbits

The rendezvous problem solution (in this solution, point *C* corresponds to the drift orbit eccentricity vector) presented here also involves the

combination of the two solutions of the transfer problems with the alteration of the orbital elements $\Delta a_1 = 2\Delta V_{t_I}$, $\Delta e_1 = x$ and $\Delta a_2 = 2\Delta V_{t_{II}}$, $\Delta e_2 = \Delta e - x$, respectively, where ΔV_{t_I} and $\Delta V_{t_{II}}$ can be evaluated by eqs. 6-39 and 6-40. Let us suppose that the fixed transversal orientation of the thrust engines in the orbital coordinate frame is used. Since the eccentricity correction is crucial for the intersecting orbits, by using Eq. 6-13, one can obtain the total delta-v value of the apsidal solution of the rendezvous problem:

$$\Delta V = \Delta V_1 + \Delta V_2 = \frac{4w}{w_c}\arcsin k_1 x + \frac{4w}{w_c}\arcsin(k_2\Delta e - k_2 x), \quad (6\text{-}45)$$

where ΔV_1 and ΔV_2 = the total delta-v expenditures of the transfer problem solution on the first and second manoeuvring intervals, respectively:

$$k_1 = \frac{w_c}{8w\cos\dfrac{w_c|\Delta a_1|}{8w}}, \quad (6\text{-}46)$$

$$k_2 = \frac{w_c}{8w\cos\dfrac{w_c|\Delta a_2|}{8w}}, \quad (6\text{-}47)$$

w_c = the centripetal acceleration of the support circular orbit and w is the acceleration caused by the thrust engine.

The minimum ΔV is obtained for the value:

$$x = \Delta e_1 = \frac{\Delta e}{2} + \frac{k_2^2 - k_1^2}{2k_1^2 k_2^2 \Delta e}. \quad (6\text{-}48)$$

With the knowledge of Δe_1 and Δe_2, and the help of Eq. 6-11, one can obtain the impulse magnitudes on the first and second manoeuvring intervals.

Similarly, the solution can be obtained for the problem when different thrust engines are used on the first and second manoeuvring intervals or different sets of identical thrust engines are used. In this case, there will be different values of w for the first and second manoeuvring intervals, and

the optimal value of x will be determined from the solution of the second-degree equation.

After the solution of a relatively simple problem with the use of the fixed orientation in the orbital coordinate frame, one can assess the characteristics of the solution and, if considerable eccentricity alteration is needed and the duration of the manoeuvres exceeds 100º, a turn to the "optimal" orientation. In this case there will be a single dimension minimization by x, and for every fixed x the two equation sets (similar to Eq. 6-38) will be solved numerically.

6.2.3. Rendezvous Achieved by Manoeuvring During Each Revolution

In some cases, several dozens or even hundreds of revolutions are needed for a flyby to the vicinity of the target spacecraft and the manoeuvring scheme is not specified. The problem consists of the provision of a rendezvous with the spacecraft and the demand for reducing the rendezvous time without a considerable increase in fuel expenditure becomes important. In order to meet these constraints, the spacecraft should manoeuvre in a practically uniform fashion during the greater part of the transfer revolutions and, hence, there are not two apparent manoeuvring intervals, unlike the abovementioned cases. The following relatively simple and reliable algorithm for the solution of this problem can be proposed.

The solution process starts with the determination of the minimum number of revolutions needed for the flyby to reach the target orbit. For this purpose, the transfer problem is solved with the help of one of the methods from section 6.1. The minimum number of revolutions n necessary for the optimal transfer to the target orbit is obtained as a result.

After modeling the flyby with $2n$ calculated manoeuvres, one can discover that the spacecraft will be in the target orbit by the end of the flyby, but with an angular deviation along the orbit Δu_f because the rendezvous condition has not yet been used. Let us suppose that, in the initial moment of time, the active spacecraft is situated on a lower orbit in comparison to the target spacecraft orbit ($a_f > a_0$, where a_f, a_0 = the semimajor axes of the target spacecraft and the active spacecraft orbits, respectively). This is the most typical case, but if the opposite variant occurs ($a_f < a_0$), it is considered in a similar way. If $a_f > a_0$, then it is supposed that $\Delta u_f > 0$ is always the case (the target is located ahead of the active spacecraft). For example, if the latitude argument of the target

spacecraft is $u = 210^\circ$, and the latitude argument of the active spacecraft is $u = 215^\circ$, then, in the estimated moment of the rendezvous, $\Delta u_f = 355^\circ$; and vice versa, if $a_f < a_0$, then it is the case that $\Delta u_f < 0$ (the target spacecraft is behind the active spacecraft). Let us designate the phase deviation of the two spacecraft in the initial moment of time as Δu_0 and designate the phase deviation after the transfer manoeuvres on the last revolution of the flight as Δu_f. If the phase deviation in the initial moment of time was $\Delta u_{opt} = \Delta u_0 - \Delta u_f$ instead of Δu_0, then it would have been optimal; the initial phase deviation and the solution of transfer problem would have also been the solution of the rendezvous problem. Since Δu_0 differs from Δu_{opt}, it is necessary to add *m* revolutions to the number of total revolutions for the flyby in order to solve the rendezvous problem. These revolutions are situated at the beginning of the flyby, with no manoeuvring performed on them. Due to the presence of the difference in the periods $\Delta P = P_f - P_0$ (here P_f = the target orbit period and P_0 = the initial orbit period), the active spacecraft will decrease the desynchronization of the angular locations along the orbit per one passive revolution by the magnitude Δu_1:

$$\Delta u_1 = 2\pi \frac{\Delta P}{P_0}. \tag{6-49}$$

The magnitude *m* should be greater than the integer part of the ratio Δu_f to Δu_1 by one:

$$m = \text{int}\left(\frac{\Delta u_f}{\Delta u_1}\right) + 1.$$

As such, due to the flight on the first passive revolutions, the active spacecraft will be a little ahead of the target spacecraft.

In Fig. 6-16, point *K* corresponds to the location of the active spacecraft after the fulfillment of the transfer manoeuvres; point *L* corresponds to the location of the target spacecraft in this moment; the phase desynchronization is Δu_f; the alteration of the phase distance per passive revolution is Δu_1; point *K'* corresponds to the location of the

active spacecraft after the addition of *m* passive revolutions; and the new phase desynchronization after the addition of the passive revolutions is Δu_{f_n}.

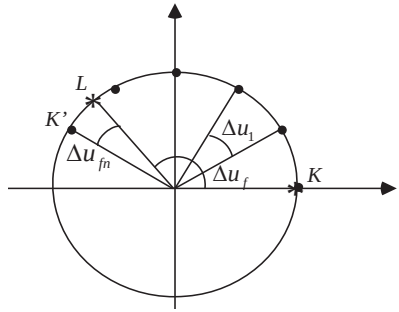

Fig. 6-16. Relative position of spacecraft in orbit

In fact, the addition of the initial passive revolutions allows us to start the manoeuvres at the moment of approximately optimal phase desynchronization. However, since *m* is an integer, not all the desynchronization Δu_f can be eliminated solely by choosing this number. The value *m* is chosen from among the neighbouring values. The chosen value must ensure the transfer of the active spacecraft ahead of the target spacecraft. For the situation depicted in Fig. 6-16, *m* = 5.

In order to eliminate Δu_{f_n} (the rest of the angular desynchronization), one should move the part of the manoeuvre ΔV_{t_1} from the last revolution to the last of the first *m* revolutions, and decrease the performance of the previous manoeuvre of magnitude ΔV_{t_L} by the magnitude ΔV_{t_1} on the last revolution. All in all, the alteration to the orbital element will remain practically the same, but the angular position will change at the end of the flight duration due to the fact that the active spacecraft would fly *n* revolutions on a higher orbit.

The necessary value of ΔV_{t_1} can be found by the equation:

$$6\pi(n+1)\Delta V_{t_1} = \Delta u_{f_n}. \tag{6-50}$$

The error that occurs during the use of this simplified scheme of determination can be eliminated with the help of the iterative procedure.

On the next iteration, the additional substitution of the value ΔV_{t_1} by value ΔV_{t_2}, which allows us to eliminate the new phase deviation $\Delta u_{f_{m_2}}$, can be evaluated by using the analogous equation:

$$\Delta V_{t_2} = \Delta u_{f_{m_2}} / 6\pi(n+1). \tag{6-51}$$

After elimination of the phase deviation, the found solution is made more accurate with the help of the iterative procedure from Chapter 1 in order to fulfill the terminal conditions with the given tolerance. Each iteration of this outer iterative procedure contains the inner iterative procedure, ensuring the fulfillment of the phase condition with the given accuracy.

6.2.4. Example

Table 6-6 presents the initial conditions for the active spacecraft and the target spacecraft, located on a higher orbit. The mass of the active spacecraft is 300 kg and the thrust is 0.1 N.

Table 6-6

Orbital elements	Initial orbit	Target orbit
a km	6,566	6,721
E	0.0022845	0.00248787
ω deg	20.0	30.0
u deg	60.0	5.0
N rev	1	1
Date	2014.06.25	2014.06.25
Time	43,120.065	43,120.065

For the solution of the transfer problem, the active spacecraft requires 52 revolutions while the target spacecraft makes 50 revolutions in the same time. The two manoeuvres are performed on each of the 52 revolutions. The thrust engine orientation is fixed by the transversal component in the orbital coordinate frame. The latitude argument of the middle of the first manoeuvre is 89.03º and the latitude argument of the middle of the second manoeuvre is 269.03º. The angular duration of the first manoeuvre is 246.14º, while the second manoeuvre has the duration of 102.11º. The transversal component of the first manoeuvre on the

revolution is 1.23 m/s, the transversal component of the second manoeuvre on the revolution is 0.51 m/s, and the total delta-v of all the manoeuvres is 90.35 m/s. The phase miss with these manoeuvring parameters is $\Delta u_f = 334133^\circ$. In order to eliminate this miss, 27 passive revolutions are added at the start of the flyby. After this, the phase miss becomes $u_{f_n} = -0.166^\circ$. In order to eliminate the remaining miss, the magnitude of the first manoeuvre on the last revolution of the flight is reduced by 0.016 m/s, while the magnitude of the second manoeuvre on the last revolution is reduced by 0.0066 m/s. These parts of the manoeuvres are added on the 28th revolution (the first manoeuvring revolution). After these adjustments, the phase miss practically becomes zero $\Delta u_{f_n} = -8.28 \cdot 10^{-13}$ degrees.

6.3. Noncoplanar Low-Thrust Transfer

Two options are usually used for the change of the orbital plane orientation. The scheme with a spacecraft having two sets of engines (one set of engines is responsible for manoeuvres in the orbital plane; the other set of engines is responsible for the alteration of the orbital plane orientation) is widely used. The manoeuvres in the orbital plane and the orbital plane rotating manoeuvres are performed separately. This variant, which provides simple and reliable although not optimal control, is widely used in the control of geostationary spacecraft and satellite constellations etc.

Optimal control can be realized for the spacecraft with the ability to set the orientation of the thrust vector in the required direction and changing the orientation according to the manoeuvre realization program. A rather sophisticated system for motion control around the center of mass is needed for this. However, one can use the close-to-optimal and easy-realizable control process as depicted in the second part of this paragraph.

6.3.1. Plane Orientation Alteration Manoeuvre

Firstly, let us consider the first, simpler manoeuvring scheme. Since the in-plane manoeuvres and the orbital plane rotating manoeuvres are not connected to each other, they can be considered separately.

The change in the orbital plane orientation, caused by the lateral velocity ΔV_z, can be evaluated by the equation:

$$\Delta i = \int_{-\Delta\varphi/2}^{\Delta\varphi/2} \frac{\Delta V_z}{\Delta\varphi}\cos\varphi d\varphi = 2\frac{\sin\frac{\Delta\varphi}{2}}{\Delta\varphi}\Delta V_z, \qquad (6\text{-}52)$$

where $\Delta\varphi$ = the angular duration of the active interval and φ = the angle between the middle of the active interval and the current point. The middle of the active interval is situated on the line of the orbital plane intersection (Fig. 6-17).

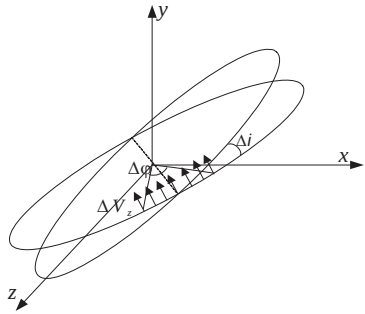

Fig. 6-17. Alteration of the orbital plane orientation

Using the equation $\Delta\varphi = \frac{w_c}{w}\Delta V$, we obtain:

$$\Delta i = 2\frac{w}{w_c}\sin(\frac{\Delta\varphi}{2}). \qquad (6\text{-}53)$$

This equation differs from eqs. 6-4 and 6-19 by the multiplier (2 instead of 4, since the influence of the lateral component is 2 times less than the transversal one). Equation 6-4 depicts the alteration of eccentricity in the conditions of the orbital orientation of the thrust engines. Equation 6-19 depicts the alteration of the semimajor axis in the conditions of the inertial orientation of the thrust engines. This fact is very important and will be used multiple times. For example, one can determine the decrease (in percent) of the alteration of the angle between the orbits in comparison to the impulse case depending on the duration of the thrust engine firing interval in table 6-1.

It is easy to realize the presented manoeuvre because it is enough to maintain the orbital or its inertial orientation. The engine's axis is directed along an axis that is perpendicular to the orbital plane and the middle of the thrust engine firing interval coincides with the point of the optimal impulse correction of the lateral deviation (which can be evaluated by Eq. 1-14b).

6.3.2. Simultaneous Changing of All Orbit Elements

In order to obtain an optimal transfer between the noncoplanar orbits, it is necessary to combine the orbital plane orientation alteration with the corrections for the eccentricity vector and the semimajor axis. In the general case, the primer vector hodograph, which determines the optimal orientation of the thrust engines, will be an ellipse with the dimensions λ, μ, ν. It is difficult to discover and realize the optimal solution and we need to enable the rather complicated alteration of the thrust engine orientation during manoeuvre fulfillment. The control in the conditions of the fixed orientation in the orbital and/or the inertial coordinate frame is easy enough to realize. The problem solution will be searched for with this additional constraint.

The impulse solution is taken as the basis (denoted as the basic solution), just as in the case of transfers between coplanar orbits. The solution with only transversal and lateral impulse components is chosen from the domain of two-impulse solutions for the problem of optimal transfer between near-circular noncoplanar orbits in Chapter 2. The angle of application of one of the impulses is enumerated in the given interval. The enumeration of the angle is carried out extremely thoroughly in the vicinity of the optimal impulse solution. Once the angle is fixed, the other manoeuvre parameters are determined unambiguously using eqs. 2-2a to 2-2c, 2-14a, and 2-14b. This solution can be used for the arbitrary deviations of the orbital elements of the initial and given orbits. The rest of the solutions from Chapter 2 exist for their respective areas.

Let us suppose that the basic solution consists of two impulses with the magnitudes $\Delta V_1, \Delta V_2$; the two angles of the impulse application φ_1 and φ_2; and the components $\Delta V_{t_1}, \Delta V_{z_1}$ and $\Delta V_{t_2}, \Delta V_{z_2}$. The thrust engine orientation is adjusted by the angles β_i:

$$\operatorname{tg}\beta_1 = \frac{\Delta V_{z_1}}{\Delta V_{t_1}}, \operatorname{tg}\beta_2 = -\frac{\Delta V_{z_2}}{\Delta V_{t_2}}. \tag{6-54}$$

The lateral component of the first impulse will alter the orbital plane orientation by $\Delta i_1 = \Delta V_{z_1} = \Delta V_1 \sin \beta_1$, and the transversal component will alter the eccentricity by $\Delta e_1 = 2\Delta V_{t_1} = 2\Delta V_1 \cos \beta_1$ and the semimajor axis by $\Delta a_1 = 2\Delta V_{t_1} = 2\Delta V_1 \cos \beta_1$.

Let us consider the variant when the thrust engine maintains a constant orientation in the orbital coordinate frame during manoeuvre fulfillment. We suppose (as always) that the moment of the middle passage of the manoeuvre coincides with the moment of impulse application. The acceleration made by the thrust engines in the transversal direction is $w_t = w \cos \beta$, while the acceleration in the lateral direction is $w_l = w \sin \beta$.

From the equation:

$$\Delta i_1 = \Delta V_{z_1} = \Delta V_1 \sin \beta_1 = 2 \frac{w \sin \beta_1}{w_c} \sin(\frac{\Delta \varphi_1}{2}) \quad (6\text{-}55)$$

we can find the duration of the first manoeuvre $\Delta \varphi_1$:

$$\Delta \varphi_1 = 2 \arcsin \frac{w_c \Delta V_1}{2w}. \quad (6\text{-}56)$$

The same value $\Delta \varphi_1$ can be obtained using the equation for eccentricity:

$$\Delta e_1 = 2\Delta V_{t_1} = 2\Delta V_1 \cos \beta_1 = 4 \frac{w \cos \beta_1}{w_c} \sin(\frac{\Delta \varphi_1}{2}),$$

$$\Delta \varphi_1 = 2 \arcsin \frac{w_c \Delta V_1}{2w}.$$

Similarly, the duration of the second manoeuvre $\Delta \varphi_2$ can be found:

$$\Delta \varphi_2 = 2 \arcsin \frac{w_c \Delta V_2}{2w}.$$

Since each manoeuvre provides the required alteration of the orbital elements $\Delta e_1, \Delta i_1$ and $\Delta e_2, \Delta i_2$, the corresponding elements of the given orbit will be identical to the elements in the impulse case. Complexity arises due to the fact that the alteration of the semimajor axis will be

greater than necessary because the orbital orientation is more effectively altered than the eccentricity.

Thus, after manoeuvre fulfillment, the deviations in the eccentricity vector and the planar orientation for the initial and given orbits will be eliminated, but the error in the adjustment of the required semimajor axis will remain. This error can be eliminated with the help of the iterative procedure presented in Baranov and Karatunov (2016, 284-295).

Let us suppose that the initial deviation of the semimajor axis was $\Delta a_0 = a_f - a_0$ (for example, $\Delta a_0 > 0$). This deviation Δa_0 and the deviations $\Delta e_{x_0}, \Delta e_{y_0}, \Delta i_0, \Delta \psi_0$ have already been used for the determination of the manoeuvring parameters. The angle $\Delta \psi_0$ between the line of the orbital plane intersection and the apsidal line of the relative orbit can be obtained using Eq. 1-14c.

The new semimajor axis a_1 ($a_1 > a_f$) is formed after the realization of the estimated manoeuvres. On the next iteration, the deviations $\Delta a_1 = \Delta a_0 + a_f - a_1, \quad \Delta e_{x_0}, \Delta e_{y_0}, \Delta i_0, \Delta \psi_0$ will be used for the determination of the manoeuvring parameters; on the next, the following will be used $\Delta a_2 = \Delta a_1 + a_f - a_2,$ etc. The process continues until the semimajor axis is formulated with the required accuracy.

If, for example, the transfer between the nonintersecting orbits ($\Delta a > \Delta e$) is considered, then such an iterative procedure will lead to a successive decrease in the semimajor axis of the ellipse in Fig. 2-2. Thus, the impulse magnitudes, which stand as a base for the solution with constant limited thrust, will decrease while the angle between them will increase.

We will suppose now that the thrust maintains a constant orientation in the inertial coordinate frame during manoeuvre realization.

Using Eq. 6-56, one can determine the manoeuvre duration, which will ensure the same orbital plane rotation as the basic impulse. Since the alteration of the semimajor axis in the inertial coordinate frame orientation is presented by the same equation as the eccentricity alteration in the orbital orientation, the found manoeuvre duration will ensure the necessary alteration of the semimajor axis. However, the eccentricity alteration will differ from the desired one. Since the basic impulses are not situated on the apsidal line of the relative orbit, the error will occur both in the magnitude and the orientation of the eccentricity vector.

In order to form the given orbit, one would need to apply the iterative procedure, during which the projections of the eccentricity vector will

alter. The process of their alteration is analogous to the process of the semimajor alteration described earlier.

As shown in the first paragraph of this chapter, sometimes, in order to obtain a close-to-optimal solution, it is necessary to use the fixed thrust engine orientation in the orbital coordinate frame for the first manoeuvre and the inertial coordinate frame for the second manoeuvre. In this case, for a manoeuvre performed in the orbital coordinate frame we will add the error in forming of the set semimajor axis, while for a manoeuvre performed in the inertial coordinate frame, we will add the error in forming the given eccentricity vector. Thus, in order to obtain the exact solution, it is necessary to use the iterative procedure, including both the eccentricity vector projections and the semimajor axis alterations.

The solutions from this paragraph ensure we get the size and orientation of the desired orbit with the necessary accuracy. These results are close enough to the optimal solution, since the rotation of the initial orbital plane is combined with the alterations to its eccentricity vector and semimajor axis. In order to get the solution based on the exact equations of motion with the accountancy of the influence of the noncentral gravitational field and the atmosphere etc., it is necessary to use the iterative procedure from Chapter 1. Each iteration of the outer iterative procedure uses the inner iterative procedure from this paragraph, which allows us to find the approximate solution with the necessary accuracy.

6.3.3. Example

We determine the transfer parameters with the use of the low-thrust engine. Table 6-7 presents the parameters of the initial and target orbits. These parameters are identical to the parameters from Example 2.2.8. The mass of the spacecraft $m = 300$ kg and the engine thrust $P = 0.2$ N.

Table 6-7

Orbital elements	Initial orbit	Target orbit
$H_{\min}$ km	180	340
$H_{\max}$ km	210	360
u_{prg} deg	20	150
i deg	51.7	51.69
Ω deg	17.49	17.5

After assessing the required number of manoeuvring revolutions, 56 revolutions was decided on.

Due to the fact that the initial parameters for this example and Example 2.2.8 coincide, one can use the calculation results:

$$\Delta a = 0.02333\ ,\Delta e_x = -0.00344\ ,\Delta e_y = -0.00004\ ,\Delta e = 0.00345\ ,$$
$$\Delta\Omega = 0.01^\circ, \Delta i = -0.01^\circ, \Delta\gamma = -0.0127^\circ, u_z = -38.1240^\circ,$$
$$\varphi_z = 180^\circ + u_z = 141.8760^\circ.$$

In determining the manoeuvre parameters, the calculated orbital element deviations are divided by the number of manoeuvring revolutions.

The solution procedure consists of the enumeration of the first impulse application angles; the determination of the rest impulse solution parameters for each angle (the second angle and the impulse components); and the parameter determination of all long-duration manoeuvres with the help of the iterative procedure. A comparison of the solutions with the different values of the first angles can help to find the optimal solution. Such a solution was found for the angle $\varphi_1 = -206.3^\circ$. Table 6-8 presents the alterations of the solution parameters per iteration, which correspond to this angle. The second column presents the values of the second angles of the impulse solution (the middle part of the long-duration manoeuvre). The third and fourth columns present the angular durations of the manoeuvres (in degrees). The fifth column presents the values of the semimajor axes (in km), which are used in the calculations. The sixth column presents the error in the semimajor axis correction. The seventh, eighth, ninth, and tenth columns present the impulse components. The columns between the fifth to the tenth columns present the summed values for all the manoeuvring revolutions. This allows us, for example, to control the total miss in forming the semimajor axis. It can be seen that the required value of the semimajor axis is formed with an acceptably high level of accuracy.

Table 6-8

	$-\varphi_2$	$\Delta\varphi_1$	$\Delta\varphi_2$	Δa	δa	ΔV_{t_1}	ΔV_{t_2}	ΔV_{z_1}	ΔV_{z_2}
1	35.1	105.2	76.26	155.00	-18.86	50.88	39.47	0.59	2.30
2	36.5	90.16	64.28	136.13	7.04	45.35	34.01	0.27	1.98
3	35.9	95.53	68.65	143.17	-2.28	47.41	36.05	0.39	2.10
4	36.1	93.76	67.22	140.89	0.78	46.74	35.39	0.35	2.06
5	36.1	94.36	67.71	141.67	-0.26	46.97	35.61	0.36	2.07
6	36.1	94.16	67.54	141.41	0.09	46.90	35.54	0.36	2.07

6.3.4. Microsatellite Transfer to the Final Sun-Synchronous Orbit

The microsatellite transfer problem is considered here as an example. The spacecraft is transferred from the deployment orbit to the operational sun-synchronous orbit with an altitude of 491 km. Due to the fulfillment of different technological operations, it is possible to carry out the manoeuvres from the 50th revolution onwards only. In order to reduce the influence of error in the orbital determination, which was carried before the start of manoeuvres, and the influence of the error connected to the realization of the estimated manoeuvres, the required alteration of the orbital elements was divided according to the proportions 0.8:0.2 between the first and second manoeuvring intervals. The first interval starts on the 50th revolution and the second manoeuvring interval starts on the 85th revolution. The shaped orbit was controlled in the ascending node for the 93 revolutions. Updating the orbit after the fulfillment of the first interval manoeuvre and subsequent recalculation of the second interval manoeuvring parameters help to gradually increase the accuracy of shaping the given orbit.

The relatively small flight duration (43 revolutions) between the start of the first manoeuvring interval and the checkpoint, with sufficiently high altitudes of the initial and target orbits, allow us to use the iterative procedure for the problem solution from Chapter 1. The manoeuvring parameters were determined with the help of the simplest motion model (the central gravitational field and the linearized motion equations) using the algorithm from 6.3.2. The orientation of the thrust engine was fixed in the orbital coordinate frame. The influence of the gravity field 8*8 and the atmosphere dynamic model were used during the prognosis.

Tables presenting the initial data and the determination results can be found below.

Table 6-9

Orbital elements	Initial orbit	Target orbit
$H_{\min}$ km	418.330	511.000
$H_{\max}$ km	420.355	511.100
u_{prg} deg	218.918	0.134000
i deg	97.5940	97.5440
Ω deg	11.1200	17.1900
N_{rev}	1.00000	1.00000
u_{lat} deg	93.7500	0.100000
S	0.783330E-02	0.671130E-02
T s	448.28006	966.07807
Data	2012.04.25	2012.05.01
Time	43,120.065	42,118.065

Table 6-9 presents the elements of the initial and target orbits, including: the minimum and maximum orbital altitudes; the pericenter argument; the inclination and RAAN; the revolution number; the latitude argument; the ballistic coefficient; and the date and time of the initial conditions.

Table 6-10 presents the characteristics of a small spacecraft and its thrust engine, including: thrust N; the specific impulse; the small spacecraft's mass in kg; the minimum time between manoeuvres s; and the minimum and maximum manoeuvre durations s.

Table 6-10

Thrust	Specific impulse	Weight	ΔT	$T_{\min}$	$T_{\max}$
0.20	2,060.0	300.0	600.0	0.25	3,600.0

The first number in table 6-11 is the number of revolutions reached by which the given orbit must be shaped. The next two numbers are the revolution numbers, which determine the start of the first and second manoeuvring intervals. The fourth numbers shows the quantity of revolutions prohibited for the manoeuvring, the next two numbers are the numbers of these revolutions. The orbital parameters and the magnitudes of the remaining manoeuvres can be recalculated on these prohibited revolutions.

Table 6-11

N_f	N_1	N_2	N	N_{11}	N_{21}
93.0	50.0	85.0	2.0	55.0	91.0

Table 6-12 presents the accuracies of the target orbital element, adjusting: the eccentricity vector projections; the semimajor axis in km; the time in seconds; the inclination in degrees; and the RAAN in degrees. If the corresponding number equals 0, this element is not corrected. The second line of the table presents the deviations between the final and the given target orbit.

Table 6-12

e_x	e_y	a	T	i	Ω
0.000250	0.000250	0.010000	0.000000	0.000500	0.000000
-0.000002	0.000000	-0.004580	10.825450	0.000000	-0.068249

Table 6-13 presents the impulse solution parameters, which are used for the quality assessment of the obtained solution with low thrust. The total delta-v impulse, the sums of the transversal components, and the lateral components and angles, which determine the moments of the optimal eccentricity vector correction and alteration of the orbital plane orientation, are shown. These five parameters help to understand the problem physics.

Table 6-13

dVimp	*dVinpln*	*dVoutpl*	*UEopt*	*UZopt*
41.53	41.02	6.51	263.2	0.0

For the sake of comparison, table 6-14 gives the total delta-v impulse and the summed manoeuvring impulse for the “separate” correction scheme. In this scheme, the manoeuvres for the alteration of the orbital elements in the plane and manoeuvres for the orbital plane rotation are performed separately. The sum impulses for these manoeuvres can be found in the second and third columns of the table, respectively. The total number of manoeuvres required and the number of revolutions on which they are performed are listed further. The separate manoeuvring scheme is widely used today for the manoeuvring of small spacecraft with low thrust.

Table 6-14

dVsp	*dVinpln*	*dVoutpl*	*Nman*	*Nrev*
47.56	41.02	6.55	42	14

Table 6-15 presents the parameters of the basic solution, including: the total delta-v impulse; the sums of the transversal and lateral components; the total number of manoeuvres; and the number of iterations needed for shaping the given orbit with the required accuracy.

Table 6-15

dV	*dVinpln*	*dVoutpl*	*Nman*	*Niter*
42.30	41.02	7.71	38	6

Table 6-16 presents analogous data about manoeuvres on the first and second manoeuvring intervals.

Table 6-16

dV	*dVinpln*	*dVout*	*Nman*	*Rt*
33.60	33.03	6.18	30	0.8
8.70	8.57	1.53	8	0.2

Table 6-17 presents the number of each manoeuvre; the number of revolutions; and the latitude arguments of the start and end of the current manoeuvre, as well as the yaw and pitch, setting the orientation of the thrust vector and the magnitude of the equivalent impulse.

Table 6-17

Nman	*REV_bg*	*U_bg*	*REV_fn*	*U_fn*	*Yaw*	*Pitch*	*dVi*
1	50	138.55	50	248.05	10.50	0.00	1.162
2	50	295.45	51	36.99	-10.69	0.00	1.078
…	…	…	…	…	…	…	…
29	65	138.55	65	248.05	10.50	0.00	1.162
30	65	295.45	66	36.99	-10.69	0.00	1.078
31	85	139.24	85	245.61	10.21	0.00	1.128
32	85	297.16	86	36.13	-10.02	0.00	1.048
…	…	…	…	…	…	…	…
37	88	139.24	88	245.61	10.21	0.00	1.128
38	88	297.16	89	36.13	-10.02	0.00	1.048

Table 6-18 presents information for each manoeuvre, including: the date and time of the start and end; the manoeuvre duration in minutes; and the small spacecraft's mass after the manoeuvre.

It can be noted that the total delta-v expenditures for the impulse and low-thrust solutions are practically identical, indicating the high quality of the solution accounting for the thrust engine firing duration. The total delta-v is considerably higher for the traditional "separate" solution.

Table 6-18

Manoeuvre	Date_bg	Time_bg	Date_fn	Time_fn	dT	Mass
1	2012.04.28	85,324.5	2012.04.28	92,147.2	28.38	299.83
2	2012.04.28	93,407.0	2012.04.28	100,028.3	26.35	299.68
…	…	…	…	…	…	…
29	2012.04.29	82,041.1	2012.04.29	84,922.5	28.69	295.35
30	2012.04.29	90,149.1	2012.04.29	92,828.6	26.66	295.19
31	2012.04.30	154,954.8	2012.04.30	161,748.2	27.89	295.03
32	2012.04.30	163,120.9	2012.04.30	165,721.3	26.01	294.88
…	…	…	…	…	…	…
37	2012.04.30	203,340.2	2012.04.30	210,137.6	27.96	294.09
38	2012.04.30	211,511.8	2012.04.30	214,116.1	26.07	293.93

CHAPTER SEVEN

SATELLITE CONSTELLATION AND FORMATION FLYING DEPLOYMENT

The algorithms presented in the previous chapters can be used for the determination of satellite manoeuvring parameters for satellites in constellations. However, the manoeuvres of such satellites, in certain cases, have peculiarities that need to be accounted for.

Despite the variety of satellite constellations, two types of problems for optimal manoeuvring need to be solved. These are: how to deploy the satellite constellation with the desired configuration; and how to maintain this configuration.

The satellite constellation configuration maintenance problem will be considered in the next chapter. The problem of satellite constellation initialization, which is similar to the classical rendezvous problem, is considered in this chapter. Each satellite is considered separately in terms of how it needs to move to a set position in the target orbit for a fixed time duration. Unlike the classical rendezvous problem, the satellite's transfer time to a fixed orbital point is not strictly limited and can be chosen from across a considerably wide range. The problem becomes more complicated if the satellite is required to be transferred to an orbit with a RAAN (right ascension of ascending node) that differs by several or even dozens of degrees from the initial orbital RAAN.

7.1. Changing a Spacecraft's Position in a Constellation Operating in Circular Orbits

Here, a satellite constellation is considered with the satellites situated on several circular orbits that have equal radii and inclinations, but differ in terms of their RAANs. The major part of real functioning satellite constellations belong to this type, including the "Global Navigation Satellite System (GLONASS)", "Global Positioning System (GPS)", and "Iridium". The conclusions about the optimal satellite transfer strategy from one system position to another, which will be examined further, are

general in form and may be implemented in every satellite constellation of this type.

Let us suppose that there is a spare satellite in one of the planes. This satellite should be placed in a vacant position in its orbit, in an orbit that has a different RAAN, or designated as the service satellite situated in this position. Let us consider the different variants of transferring a satellite to a new position in order to select the optimal manoeuvring scheme with simultaneous fulfillment of the following contradictory criteria: the flyby time to a new position, which needs to be reduced, and the minimization of ΔV expenditure, which increases with a decrease in flyby time.

7.1.1. Positional Change in Orbit

First, let us consider the transfer of a satellite to another location in the same orbit, but Δu degrees distant from the initial one ($|\Delta u| \le 180^0$, $\Delta u > 0$, if the new location is situated ahead of the initial one). Hereafter, the angle Δu will be measured in fractions of a revolution; its maximum value cannot exceed 0.5.

It is supposed that the transfer is fulfilled at N revolutions of the target point flight. The number of flyby revolutions is chosen so that the satellite would not move much away from the initial orbit. The variant of a sizeable shift from the initial orbit and the rapid return to it is considered in the work of G. G. Raykunov (Raykunov, 2002).

Using Eq. 3-1d, one can obtain the transversal impulse component ΔV_t, which is necessary for the required change in the orbital period:

$$\Delta V_t \approx -\frac{\Delta u}{3N} V_0, \tag{7-1}$$

where $V_0 = \sqrt{\frac{\mu}{a}}$ = the satellite's velocity of motion along a circular orbit of radius a. The moment of impulse application is arbitrary.

An impulse of the same magnitude and opposite direction is applied on the final revolution at the apocenter (if $\Delta u > 0$) or at the pericenter (in the opposite case) in order to return to the circular orbit. Thus, the total delta-v expenditure ΔV will be:

$$\Delta V \approx \frac{2|\Delta u|}{3N} V_0. \tag{7-2}$$

The total delta-v expenditure is considerable for the small duration of the satellite's transfer to the desired point and the number of flyby revolutions N will increase with its decrease. It would appear that zero expenditure could be obtained with a further increase of N, but this is not the case. The orbital semimajor axis is changed by the transfer to a new position and, thus, a deviation between the RAANs $\Delta\Omega$ occurs thanks to different orbital evolutions under the influence of a noncentral gravitational field. The known equation for the alteration of the RAAN per revolution $\delta\Omega$ due to the influence of the second member of the expansion of the gravitational field potential in series by the spherical functions of the geocentric latitude is used for the calculation of this deviation:

$$\delta\Omega = -\frac{2\pi\varepsilon}{\mu p^2}\cos i, \tag{7-3}$$

where i = the orbital inclination, p = the focal parameter ($p = a$ for circular orbits), $\varepsilon = 2.634\cdot 10^{10}\ \text{km}^5/\text{s}^2$, and $\mu = \gamma M = 3.986028\cdot 10^5\ \text{km}^3/\text{s}^2$ (M = the mass of the planet and γ = the gravitational constant). In order to assess $\delta\Omega$, we will name its values for the several groups of circular orbits with different altitudes above the Earth's surface: h = 330 km: $\delta\Omega = 0.521\cos i$ deg; h = 1,400 km: $\delta\Omega = 0.394\cos i$ deg; and h = 20,000 km: $\delta\Omega = 0.034\cos i$ deg.

The semimajor axis and eccentricity will be altered by Δa and Δe, respectively, due to the application of impulse ΔV_t. By neglecting the magnitude $\Delta a\Delta e$ (it will be further shown that it is necessary to have a circular drift orbit, i.e. $\Delta e = 0$), we can write that $p = a + \Delta a$. By expanding the equation for $\delta\Omega$ by Δa in series and taking the member of the first order of smallness, one can obtain the equation for the alteration $\delta\Omega$ due to the alteration of a by Δa:

$$\delta\Omega^* = -\frac{2\pi\varepsilon}{\mu p^2}\cos i\left(-\frac{2\Delta a}{a}\right) = -2\delta\Omega\frac{\Delta a}{a}.$$

Since $\Delta a = 2a\dfrac{\Delta V_t}{V_0}$ (Eq. 3-1c), the equation for alteration $\delta\Omega$ due to the application of ΔV_t is given by:

$$\delta\Omega^* = -4\delta\Omega\frac{\Delta V_t}{V_0}. \tag{7-4}$$

The difference between the target orbit RAAN and the drift orbit RAAN increases by $\delta\Omega^*$ every revolution. Thus, the deviation after N revolutions can be determined by the equation:

$$\Delta\Omega = -4\delta\Omega N\frac{\Delta V_t}{V_0}. \tag{7-5}$$

By expressing ΔV_t in terms of Δu from Eq. 7-1, one can obtain the final equation for the deviation between RAANs:

$$\Delta\Omega = \frac{4}{3}\delta\Omega\Delta u. \tag{7-6}$$

For example, the orbital plane rotation can reach up to $\Delta\Omega = 0.262\cos i$ deg for an orbit of altitude h = 1,400 km and $\Delta\Omega = 0.022\cos i$ deg for an orbit of altitude h = 20,000 km for the alteration of the satellite's position by half a revolution.

In order to assess the impulse required to compensate for the deviation between the RAANs, we find the deviations of Δi and $\Delta\Omega$, which are the given by the application of the binormal impulse ΔV_z (at the point of the orbit with the latitude argument u) (Fig. 7-1).

The binormal impulse causes an orbital plane rotation by the angle:

$$\Delta\gamma = \frac{\Delta V_z}{V_0}. \tag{7-7}$$

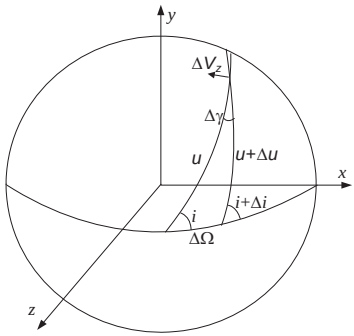

Fig. 7-1. Orbital plane orientation correction

The following equation can be written with the help of the sine theorem for the spherical triangle:

$$\frac{\sin\Delta\gamma}{\sin\Delta\Omega}=\frac{\sin(180^\circ-(i+\Delta i))}{\sin u}. \tag{7-8}$$

By taking into account the smallness of $\Delta\gamma$, Δi, and $\Delta\Omega$, we can obtain the final equation for the change in RAAN (Nazarenko and Skrebushevsky 1981):

$$\Delta\Omega=\frac{\sin u}{\sin i}\Delta\gamma=\frac{\sin u}{\sin i}\frac{\Delta V_z}{V_0}. \tag{7-9}$$

The following equation can be written with the help of the cosine theorem for the spherical triangle:

$$\cos(180^\circ-(i+\Delta i))=-\cos\Delta\gamma\cos i+\sin\Delta\gamma\sin i\cos u. \tag{7-10}$$

The equation for the change in orbital inclination can be obtained from Eq. 7-10:

$$\Delta i=\cos u\Delta\gamma=\cos u\frac{\Delta V_z}{V_0}. \tag{7-11}$$

The velocity impulse should be applied at the maximum distance from the equatorial points ($u = 90^\circ$ or $u = 270^\circ$, the orbital apex or vertex) in order to effectively compensate for the deviation of Ω in the problem without causing deviation by *i*. The magnitude of the impulse lateral component ΔV_{z_Ω} is determined by the equation:

$$\Delta V_{z_\Omega} \approx \frac{\sin i}{\sin u}\Delta\Omega V_0 = \frac{4}{3}\frac{\sin i}{\sin u}\delta\Omega\Delta u V_0. \qquad (7\text{-}12)$$

Let us suppose that the flyby to the given position starts at the orbital apex and ends *N* revolutions afterwards, also at the apex, i.e. a two-impulse flyby is used. Let us divide the found lateral component into two equal parts between these impulses; then, the equation for the total delta-v of all the manoeuvres will be given by (Baranov and Terekhova 1993):

$$\Delta V = 2\sqrt{\Delta V_t^2 + (\frac{1}{2}\Delta V_{z_\Omega})^2} = \frac{2}{3}|\Delta u|V_0\sqrt{\frac{1}{N^2} + 4\delta\Omega^2\sin^2 i}. \qquad (7\text{-}13)$$

The expenditure on correcting the angle between the orbital planes exceeds the expenditure for the correction of the along-the-orbit position, which results in this angle with big numbers of *N* if the value $1/N$ is less than $2\delta\Omega\sin i$.

A two-impulse scheme, similar to the scheme in the work of Pollard (2000, 1-39), has been considered, but has not been sufficiently investigated to give an optimal solution. The evolution of the pericenter position, as well as the evolution of the RAAN, should be taken into account. The pericenter will not be at the apex on the final revolution, since it changes its position on each revolution by the following magnitude:

$$\delta\omega = \frac{\pi\varepsilon}{\mu p^2}(5\cos^2 i - 1). \qquad (7\text{-}14)$$

Due to this shift in the pericenter position, one impulse, applied at the apex of the last manoeuvring interval, will not be enough to shape the circular orbit. It is necessary to change the location of the impulse to the apsidal point; however, this change will lead to an increase in expenditure on RAAN correction. In reality, this change is small and commensurable with the change in RAAN.

The use of the four-impulse system, where every impulse is divided into two equal parts, helps to preserve minimal total delta-v, which can be determined using Eq. 7-13. The impulses in the four-impulse scheme are applied at the apex and the vertex of the first and last revolutions. The component sums of these impulses for each of the intervals are equal in magnitude to the corresponding impulse components of the two-impulse scheme; however, the lateral components have equal signs.

With such a manoeuvring scheme, the drift orbit will have zero eccentricity, and the points, at the maximum distance from the equator, can be used again at the end of the flyby for the impulse application.

The orbit T_1, which is the drift orbit for the two-impulse transfer to a new operational position (the single-impulse transfer from the operational orbit T_0 to drift orbit T_1), is depicted in Fig. 7-2 by the dashed line. The two-impulse transfer from the operational circular orbit T_0 to the drift orbit T_f is depicted by the dotted line. The interim orbit is T_2. A return to the operational orbit is fulfilled with the help of the transfer T_3, depicted by the dash-dot line.

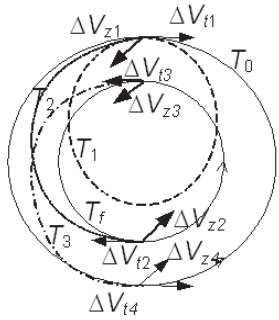

Fig. 7-2. Four-impulse flyby to the drift orbit

There is another opportunity to eliminate the deviation occurring between the RAANs. This involves the use of deviations in the evolution of orbits with different inclinations. If the drift orbit has a different inclination, then its influence on the RAAN may be compensated for by the influence of the semimajor axis alteration.

For the alteration of the inclination, optimally we apply the impulse on the equator at the ascending or descending nodes. If the impulse is applied at the ascending orbital node, then the magnitude of its lateral component

ΔV_{z_i}, necessary for the required change in inclination, can be found from the equation:

$$Nk\frac{\Delta V_{z_i}}{V_0} \approx \Delta\Omega, \tag{7-15}$$

where $k = \frac{2\pi\varepsilon}{\mu p^2}\sin i = \Omega$ per change in revolution caused by alteration of the inclination by the magnitude $\Delta i = \frac{\Delta V_{z_i}}{V_0}$. The equation for k was obtained by differencing of the equation for $\delta\Omega$ by i. Thus, the equation for ΔV_{z_i} can be written as:

$$\Delta V_{z_i} = \frac{4\delta\Omega\Delta u}{3Nk}V_0. \tag{7-16}$$

Taking into account the relationship between k and $\delta\Omega$, which can be stated $k = -\delta\Omega \mathrm{tg} i$, one can get the final equation for ΔV_{z_i}:

$$\Delta V_{z_i} = -\frac{4\Delta u}{3N\mathrm{tg}i}V_0. \tag{7-17}$$

This equation is true for the ascending node and the sign of ΔV_{z_i} will be opposite for the descending node.

The high level of effectiveness of this method with i close to 90º (in this case $\Delta V_{z_i} \approx 0$) can be explained by the fact that the magnitude of $\Delta\Omega$ will be small and the alteration of the RAAN evolution together with the alteration to the inclination is considerable.

Taking into account that it is necessary to obtain the initial inclination at the end of the flyby, the equation for the total delta-v expenditure is given by (Baranov 2008, 215-218):

$$\Delta V = 2\sqrt{\Delta V_t^2 + \Delta V_{z_i}^2} = \frac{2|\Delta u|}{3N}V_0\sqrt{1+\frac{16}{\mathrm{tg}^2 i}}. \tag{7-18}$$

Equations 7-1 and 7-17 allow us to compare ΔV_t and ΔV_{z_i}. If the orbital inclination satisfies the condition $\mathrm{tg}i < 4$, then the expenditure on the correction of the orbital plane positional deviation that occurs will be greater than the expenditure on the position of the satellite's along-the-orbit correction, which caused it, with any magnitude of *N*.

The aforementioned methods are interesting because the impulses are applied in known locations (at the equator or the orbital points most distant from the equator). However, the combination of both methods is optimal when the impulses are applied at some interim point of the revolution u_0. Let us determine the magnitude u_0 for a set number of flyby revolutions *N*. The magnitude of the impulse lateral component ΔV_z, applied with the latitude argument *u*, which is used for the compensation of the deviation between RAANs $\Delta\Omega$, can be determined by the equation:

$$(Nk\cos u + 2\frac{\sin u}{\sin i})\frac{\Delta V_z}{V_0} = \frac{4}{3}\delta\Omega\Delta u. \qquad (7\text{-}19)$$

On the second manoeuvring interval, the impulses are applied at the symmetrical points relative to the apex in relation to the impulse application points of the first manoeuvring interval ($u_{0_{II}} = \pi - u_{0_I}$). This is connected to the necessity of changing the orbital inclination to its initial value by the impulses of the second manoeuvring interval. In the meantime, the same Ω change, which was fulfilled by the impulses of the first manoeuvring interval, should be fulfilled by those of the second manoeuvring interval; this explains the coefficient 2 in the second addend.

The magnitude of ΔV_z is minimal if the value in the brackets is at its maximum and *u* must be equal to u_0, so that:

$$u_0 = \mathrm{arctg}\frac{2}{Nk\sin i}. \qquad (7\text{-}20)$$

One can obtain the equation for the optimal value ΔV_z:

$$\Delta V_z = \frac{4\delta\Omega\Delta u}{3\sqrt{N^2(\delta\Omega\mathrm{tg}i)^2 + \frac{4}{\sin^2 i}}}V_0. \qquad (7\text{-}21)$$

Taking into account that the lateral components of the same magnitude are applied at the end of the flyby, the equation for total delta-v will be given by the equation (Baranov and Terekhova 1993):

$$\Delta V = 2\sqrt{\Delta V_t^2 + \Delta V_z^2} = \frac{2}{3}\left|\Delta u\right| V_0 \sqrt{\frac{1}{N^2} + \frac{4\delta\Omega^2 \sin^2 2i}{N^2 \delta\Omega^2 \sin^4 i + 4\cos^2 i}}. \quad (7\text{-}22)$$

7.1.2. Examples

Figure 7-3 presents the dependencies between total delta-v, which is needed for the satellite's change in position by 180º along the orbit and the number of revolutions N. The upper three lines are plotted for the Globalstar satellite constellation ($h \approx$ 1,430 km, $i \approx 52^\circ$) and the lower line is plotted for the GLONASS system ($h \approx$ 19,500 km, $i \approx 64.2^\circ$). The distribution of ΔV as a function of N in the case of along-the-orbit deviation correction with $\Delta u = 180^\circ$ (Eq. 7-2) is plotted with dots. The distribution of ΔV versus N in the case of simultaneous correction of Δu and $\Delta\Omega$ ($\Delta\Omega \approx 0.16^\circ$) with the impulse application at the points of the orbit most distant from the equator (Eq. 7-13) is plotted with the dashed line. The distribution of $\Delta V(N)$ in the case of the simultaneous optimal correction of Δu and $\Delta\Omega$ (Eq. 7-22) is plotted with the solid line.

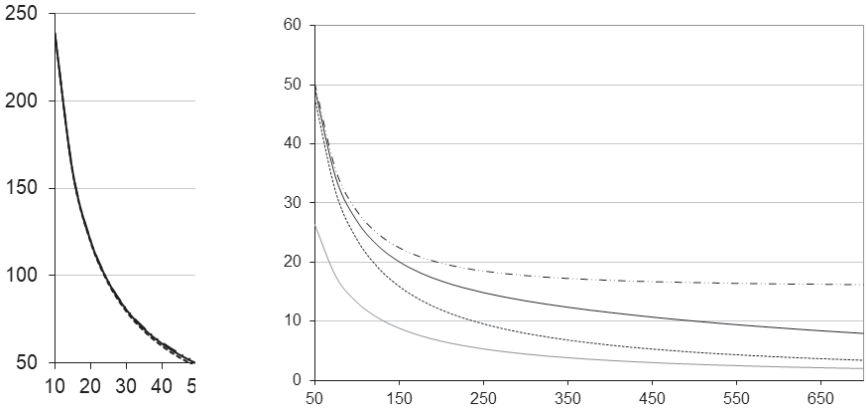

Fig. 7-3. Total delta-v expenditure necessary for satellite transfer by 180º along the orbit as a function of the number of flight revolutions

It can be seen that, in the case of the Globalstar satellite constellation, a rapid decrease in ΔV, up to approximately the 200th revolution, with an increase in N occurs. The further increase in N leads to an insignificant gradual decrease of ΔV marked by the solid and the dotted lines and, in the case where the impulses are applied at those points of the orbit most distant from the equator (the dashed line), the expenditure of ΔV does not practically decrease.

The three analogous dependencies practically merge into one for GLONASS, as depicted by the dash-dot line 4. This is connected to the smallness of $\delta\Omega$ for such high orbits and hence the small magnitude of the deviation of $\Delta\Omega$ that occurs ($\Delta\Omega \approx 0.01^{\circ}$), which can remain uncorrected, or, if necessary, be corrected at the orbital points most distant from the equator.

Thus, for the satellite constellations in low Earth orbits (LEO), different manoeuvring strategies can be used depending on the flyby duration. With a flyby duration of less than or equal to 100 revolutions, the velocity impulses can be applied at the apex or vertex of the orbit and the total delta-v expenditure will not exceed 25 m/s for the satellite transfer along the orbit by 180º. With a duration of more than 1,000 revolutions, the impulses can be applied on the equator and the expenditure will be less than 5 m/s. The combined strategy is optimal for medium durations. This conclusion is true for the following satellite constellations: Iridium ($h \approx$ 780 km); Orbcomm ($h \approx$ 800 km); and Globalstar ($h \approx$ 1,430 km).

The optimal approach sees the application of impulses at the apex or vertex of the orbit for satellite constellations in medium orbits: GPS ($h \approx$ 20,100 km) and GLONASS ($h \approx$ 19,500 km).

7.1.3. Compromise Flight Duration

According to the graphs in Fig. 7-3, a rapid decrease in ΔV occurs with an increase in N; however, a further increase in N leads to an insignificant gradual decrease in ΔV. The moment of the descent rate of change of ΔV may be considered as a compromise number of the revolutions of the standby between the flyby time and the expenditure of ΔV in its fulfillment.

Figure 7-4 presents the isochronal dependency of ΔV versus N for the altitudes 700 km and 2,500 km. It can be seen that the point of intersection of the two lines lies in the area of the interest.

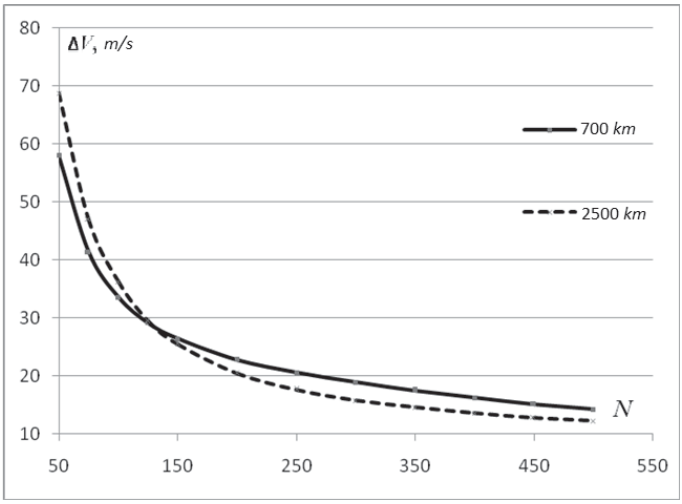

Fig. 7-4. Velocity expenditure as a function of isochronal *N* for various heights

This point can be calculated analytically (Baranov and Grishko 2013, 289-312):

$$N = \sqrt{\frac{-\xi \pm \sqrt{\xi^2 - 4\gamma\alpha}}{2\gamma}}, \tag{7-23}$$

where: $\gamma = A \cdot K + C \cdot K - A \cdot P \cdot D - A \cdot P \cdot F$

$\xi = A \cdot M + B \cdot K + C \cdot M - B \cdot P \cdot D - B \cdot P \cdot F - A \cdot P \cdot E$

$\alpha = B \cdot M - B \cdot P \cdot E$

$\beta = -2\pi\varepsilon / \mu, A = \beta^2 \sin^4 i, B = 4p_1^4, C = 4\beta^2 \sin^2 2i,$

$D = T_1^2 T_2^2 \beta^2 \sin^4 i, E = 4T_2^4 p_2^4, F = 4T_1^2 T_2^2 \beta^2 \sin^2 2i,$

$K = T_1^4 \beta^2 \sin^4 i, M = 4T_2^2 T_1^2 p_2^4, P = p_1 / p_2,$

T_1 and T_2 = the periods of the two compared orbits and p_1 and p_2 = their focal parameters. After the application of Eq. 7-23, we find that the curves intersect twice in the general case. For example, Eq. 7-23 gives the values $N_1 = 81$ and $N_2 = 554$ revolutions for the altitudes 300 and 700 km, respectively. The principal change in the descent dynamics of the function $\Delta V(N)$ occurs at point N_1, which can be considered the point of flyby

duration compromise. During the investigation of the applicability of Eq. 7-23, it was found that for all orbits the curves in Fig. 7-4 intersect only when the inclination of the initial orbit is less than 70º. This can be explained by the fact that with inclinations close to 90º, the multiplier cos*i* from the equation for the RAAN precession rate turns out to be close to zero and hence the influence of the altered semimajor axis on the secular drift of the RAAN is decreased. As such, with inclinations exceeding 70º, the choice of the standby compromise number of revolutions in the interim orbit is necessary to fulfill (by orienting on the graph) the dependency between the total delta-v expenditure and the number of flyby revolutions.

This analytical search for a compromise between total delta-v expenditure on the flyby and its duration may be useful in designing complex multiple-tiered satellite constellations and satellite servicing constellations, etc.

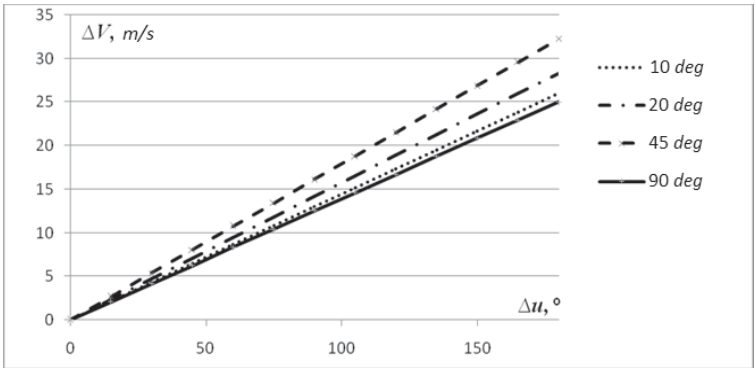

Fig. 7-5. Total delta-v expenditure as a function of Δ*u* for various inclinations

Figure 7-5 presents the total delta-v expenditure necessary for the elimination of phase desynchronization for satellite constellations at altitudes of 700 km, for different inclinations and with a flyby duration of 100 revolutions (the optimal manoeuvring scheme is used in which Δ*V* is calculated with the help of Eq. 7-22). It can be seen that the maximum total delta-v expenditure is reached with inclinations close to 45º and the minimum is reached on either the polar or equatorial orbits.

7.1.4. Satellite Transfer to Another Operational Plane

The variant is possible when it is necessary to transfer a satellite to a location with a different latitude argument and in a different operational plane. This means that it is necessary to correct both deviations by the latitude Δu and the deviation between RAANs $\Delta\Omega$, which can reach up to several dozens of degrees, just like Δu.

The direct correction of the considerable deviation between the RAANs demands considerable total delta-v expenditure. The influence of the gravitational field's noncentrality can be used for its decrease. The deviation between the RAANs, which occurs during movement along orbits with different semimajor axes, may be compensated for, to a great extent, by the initial deviation between the RAANs, leading to a considerable decrease in the total delta-v of the manoeuvres. For a considerable decrease in total delta-v, it is necessary to have the difference of several revolutions between the number of the flight revolutions of the satellite and the target point (we will denote this difference n).

Let us suppose that the orbit to which we wish to transfer the satellite has a smaller RAAN value than the orbit on which the satellite is initially situated ($\Delta\Omega < 0$). By engaging a transversal retrofire at the beginning of the flyby, one can achieve a double effect. Firstly, due to the decrease in the focal parameter p, the $|\delta\Omega|$ of the drift orbit increases, and thus the difference between the RAANs will decrease with each new revolution of the flight. Secondly, with a relatively long flyby duration, the satellite will fly n revolutions more than the target point (due to the smaller period of the obtained orbit), which will additionally help to considerably decrease the deviation between the RAANs thanks to the rotation of the orbit on the additional revolutions of the flight. In this example, it is necessary to consider Δu as the positive value, which changes in the range [0,1], not in the range [-0.5,0.5] unlike the first part of this paragraph.

The equality condition of the time spent on different numbers of revolutions of the satellite's flight and the target point can be written as follows:

$$(P - \Delta P)(N + n) = P(N - \Delta u), \tag{7-24}$$

where P = the circular orbit period and ΔP = the period alteration due to the transversal component impulses of the first manoeuvring interval. By substituting the expression for the period $P = \frac{2\pi a}{V_0}$ and the period change

$\Delta P = \frac{\Delta u a}{V_0} = -3\frac{2\pi\Delta V_t}{V_0}\frac{a}{V_0}$ in Eq. 7-24, one can find the sum of the transversal impulse component of the first manoeuvring interval ΔV_{t_1} :

$$\Delta V_{t_1} = -\frac{\Delta u + n}{3(N+n)}V_0.$$

This expression can be obtained from Eq. 3-1d.

Let us consider the combined strategy for the correction of the deviation between the RAANs, with which the impulses are applied in some optimal locations: the first with latitude u and the second in a location half a revolution distant from the first one. Taking into account eqs. 7-5 and 7-19, the equation, which depicts the change in Ω, can be written:

$$\begin{aligned} &-4(N+n)\delta\Omega\frac{\Delta V_{t_1}}{V_0} - ((N+n)\delta\Omega \mathrm{tg} i\cos u \\ &-2\frac{\sin u}{\sin i})\frac{\Delta V_z}{V_0} = \Delta\Omega - \delta\Omega n. \end{aligned} \tag{7-25}$$

The change in Ω due to the different numbers of flight revolutions n has been accounted for in the right part of the equation; the member, which accounts for the difference in the evolution of Ω due to the motion of orbits with different values for the semimajor axes, has been added to the left part of the equation.

Just as before, it is supposed that two impulses are applied at the beginning of the flyby (the first manoeuvring interval) and two impulses are applied at the end of the flyby (the second manoeuvring interval).

For the optimal value of the impulse lateral component application angle, one gets the expression:

$$u_0 = \mathrm{arctg}\frac{2}{(N+n)\delta\Omega \mathrm{tg} i\sin i}, \tag{7-26}$$

which practically coincides with the analogous equation for u_0 for the case of a satellite's transfer to a new location in the same orbit. This leads us to the statement that the conclusions about the optimal manoeuvring

strategies, made for the first problem, are true for the problem of satellite transfer to another working plane as well.

By substituting the expression for ΔV_{t_1} in Eq. 7-25, and assuming that the impulse velocity is applied at the optimal point u_0, one can obtain the equation for ΔV_z:

$$\sqrt{(N+n)^2 \delta\Omega^2 \mathrm{tg}^2 i - \frac{4}{\sin^2 i}} \frac{\Delta V_z}{V_0} = -\Delta\Omega + \delta\Omega n + \frac{4}{3}\delta\Omega(\Delta u + n),$$

from which the summed magnitude of the lateral impulse components of the first manoeuvring interval can be obtained:

$$\frac{\Delta V_z}{V_0} = \frac{3\Delta\Omega - (4\Delta u + 7n)\delta\Omega}{3\sqrt{(N+n)^2 \delta\Omega^2 \mathrm{tg}^2 i + \frac{4}{\sin^2 i}}}. \qquad (7\text{-}27)$$

Thus, the equation for the sum of expenditure is given by (Baranov 2008, 215-218):

$$\Delta V = \frac{2}{3} V_0 \sqrt{\frac{(\Delta u + n)^2}{(N+n)^2} + \frac{(3\Delta\Omega - (4\Delta u + 7n)\delta\Omega)^2}{(N+n)^2 \delta\Omega^2 \mathrm{tg}^2 i + \frac{4}{\sin^2 i}}}. \qquad (7\text{-}28)$$

It can clearly be seen that ΔV has approximately the same dependency on *N*, just as in the case of the first problem.

The function of *n* has a more complex nature, but the search for an optimal value n_{opt} is relatively simple because it is close to the value:

$$n^*_{opt} = \frac{3\Delta\Omega - 4\Delta u \delta\Omega}{7\delta\Omega}, \qquad (7\text{-}29)$$

which minimizes the second addend in Eq. 7-28.

Sometimes the variable $\Delta\Omega / \delta\Omega$ is used for the assessment of n_{opt}, as it is widely thought that the major part of the deviation Ω should be compensated due to the different numbers of flight revolutions. The real n_{opt} is more than two times smaller than $\Delta\Omega / \delta\Omega$, which is connected to

the considerable decrease in the deviation between the RAANs on the coincident number of flight revolutions due to the difference *p*. It is worth remembering that *n* is an integer, hence, the deviation between the RAANs cannot be eliminated solely by choosing the proper value of *n*, but the remaining part of the deviation will not exceed $0.5\delta\Omega$ and can be easily eliminated with the help of ΔV_z.

7.1.5. Examples

We can consider a satellite's transfer to the neighboring plane for the Globalstar satellite constellation as an example of the usage of Eq. 7-28. The difference between the RAAN values of the neighboring planes of this constellation is 45º and the optimal *n* for the satellite transfer to the neighboring plane is $n_{opt} \approx 70$ revolutions. The dependency between ΔV and the number of revolutions of flight *N* is depicted in Fig. 7-6.

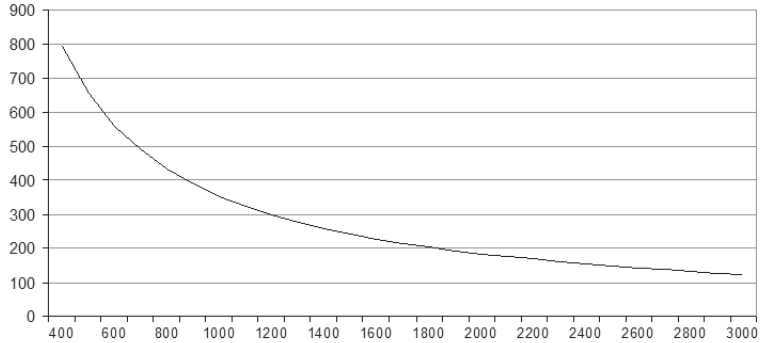

Fig.7-6. Total delta-v expenditure needed for the alteration of the RAAN by 45° as a function of the number of flight revolutions (the orbital altitude is 1,400 km)

For GLONASS $n_{opt} \approx 3{,}000$ revolutions; thus, the optimal flyby will take many thousands of revolutions, which speaks to the ineffectiveness of using such a scheme to change the RAAN for satellite constellations in high orbits. It is necessary to launch the satellite to the desired plane.

7.1.6. Total Delta-V as a Function of the Difference in the RAAN

Total delta-v expenditure as a function of the desynchronization of the RAANs has a close-to-linear nature, but strongly depends on the orbital inclination; the expenditure rate of increase rapidly rises for the range of the values $i \in [60^{\circ};90^{\circ}]$ (Fig. 7-7).

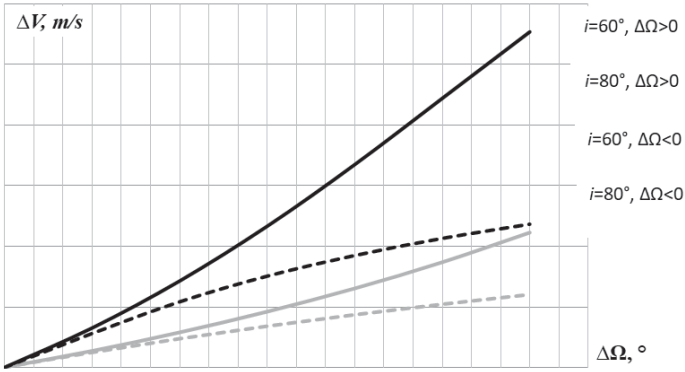

Fig. 7-7. Total delta-v expenditure as a function of RAAN desynchronization with various inclinations, an altitude of 700 km, and N = 1,000 including planar rotation in the direction of natural precession ($\Delta\Omega<0$) or opposite direction ($\Delta\Omega>0$)

Figure 7-8 gives the results of calculating the various inclinations in the small range of angles $\Delta\Omega$. The function of total delta-v expenditure in this case is represented by a curve with decreasing oscillations; moreover, the intensity of these oscillations depends on both the inclination and the magnitude of the semimajor axis (the nature of the function is similar). It can be seen in Fig. 7-8 that the oscillations are stronger for the inclinations 20-40º. Based on Fig. 7-8, the following important conclusion can be made with the fixed inclination and the altitude of the initial orbit it is possible to transfer the spacecraft in the plane, with a big value in the RAAN deviation, but with a smaller total delta-v expenditure on the transfer; moreover, the difference for the medium inclinations can reach up to 20 m/s (up to 86 %). This is explained by the fact that parameter n is an integer in its distribution, which eliminates the possibility of accurately compensating the deviation between the RAANs by one phasing operation

in the orbital plane and the correction of the leftside deviation between the RAANs is needed.

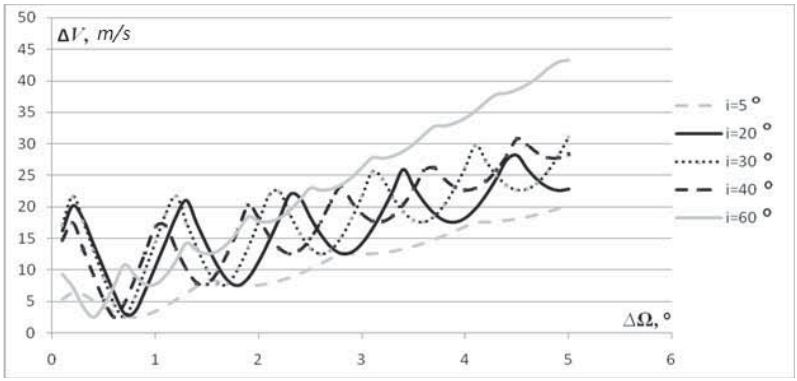

Fig. 7-8. Velocity expenditures as a function of the desynchronization between the RAANs for various inclinations (altitude 700 km and N = 1,000 revolutions)

The fractional part of n as a function of the angle between the planes for the altitude 700 km is depicted below. The graph in Fig. 7-9 unambiguously connects the fractional part of n with the oscillation amplitudes of the flyby delta-v expenditures (Fig. 7-8): in cases where the difference in the number of revolutions of the flight n is close to the integer value and the planes can be almost aligned by phasing, the function $\Delta V(\Delta\Omega)$ receives its minimums.

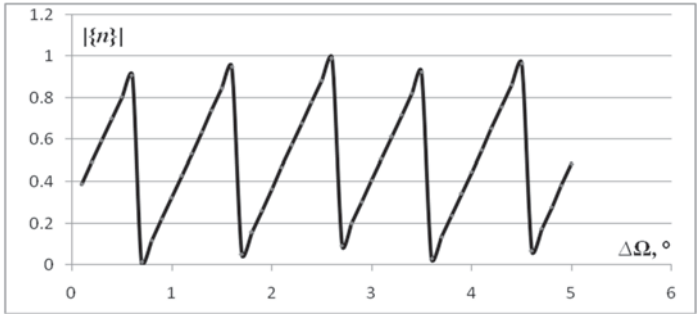

Fig. 7-9. The fractional part of the absolute value of n as a function of the angle between planes for altitude 700 km and N = 1,000 revolutions

Let us note the following circumstance: the sign of $\Delta\Omega$ needs to be accounted for during the assessment of flyby total delta-v expenditure (in Fig. 7-8, $\Delta\Omega > 0$). Figure 7-10 presents the curves for the total delta-v expenditure for two inclinations (30º and 60º) for the case of planar rotation by the angle 0.1-5º in the direction of the RAAN precession and the opposite direction, for the altitude 700 km.

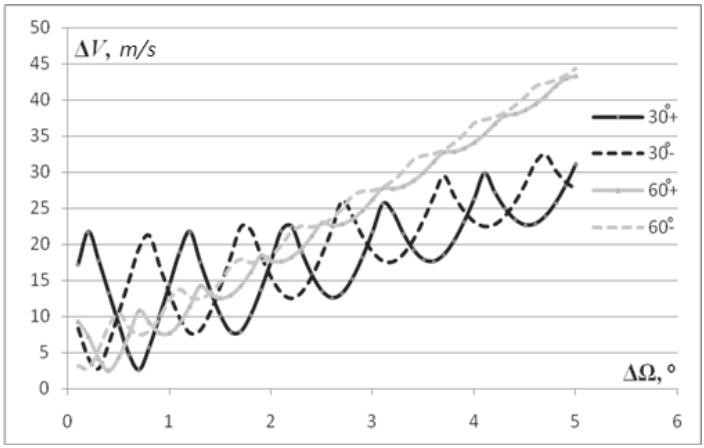

Fig. 7-10. Velocity expenditures needed for planar rotation for inclinations 30º and 60º in the direction of precession (-) and in the opposite direction (+)

It can be seen from the graph in Fig. 7-10 that, in the case of planar rotation against the direction of precession, the curve of total delta-v expenditure will be in the counter phase with curve oscillations, obtained for the concurrent rotation (a very important regular pattern), but a small shift takes place due to the negative influence of the RAAN evolution.

The influence of the direction of the planar rotation is also noticeable in the dependency between total delta-v and the number of flyby revolutions for different values of the orbital desynchronization angle by the RAAN (Fig. 7-11). With an increase in the value of the required angle of planar rotation, this influence becomes more noticeable in the area of relatively small *N*. The planar rotation in the node line's natural direction of precession allows, for example, obtaining a gain of 100 m/s in the case of 450 standby revolutions (≈ 31 days) with the required planar rotation angle of 30º.

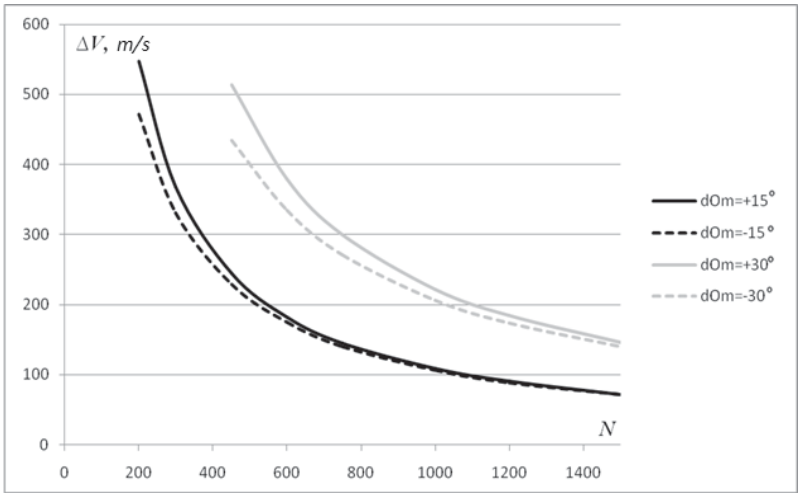

Fig. 7-11. Delta-v expenditure as a function of the number of revolutions for various directions and alteration to the RAAN magnitudes for an altitude of 700 km

The conducted analysis of the satellite's orbital transfer, which has a substantial deviation between the RAANs, allows us to choose the optimal strategy of such a transfer. The investigated dependency between the total delta-v of the flyby and the deviation between the RAANs may be used in choosing the optimal space debris removal strategy.

7.2. Universal Algorithm for Manoeuvring Parameter Determination during Satellite Constellation Deployment

The problem of satellite transfer to a desired point in the target orbit (the target point) is considered primarily in its general statement, with the initial and target orbits having close, but different values for the semimajor axes, eccentricities ($e < 0.05$), and inclinations. The deviation between the RAANs may be arbitrary by magnitude. Problems of this type occur during the initialization of a satellite constellation and its maintenance; the de-orbiting of several satellites by one spacecraft; and soil delivery from other planets and their satellites, etc.

The complexity of this problem consists not only of the difficulty in determining the manoeuvring parameters (such as the solution of the usual rendezvous problem of fixed duration, considered in chapters 3 and 4), but

also in finding the optimal number of revolutions *N* of the target point flight and the difference in the numbers of revolutions of the flight for the active spacecraft and the target point *n*. The optimal choice of these variable values and the drift orbit parameters allows us to practically eliminate the whole magnitude of the initial desynchronization of the RAANs due to the influence of the noncentrality of the gravitational field. This gradually reduces the total delta-v expenditure necessary for the transfer of a satellite to a given point.

Due to the long rendezvous duration, it is necessary to eliminate the considerable deviations in the RAAN and the problems of convergence that appear during the use of the iterative procedure, ensuring the fulfillment of the terminal conditions with the desired accuracy. This iterative procedure is presented in Chapter 1. In addition, the orbit's eccentricity is not only directly changed by the impulses of the first manoeuvring interval (like in rendezvous of small and medium durations), but also through the alteration of the orbital evolution due to the transversal and lateral components of the impulses, complicating the problem significantly.

7.2.1. Difference in the Number of Revolutions: Active and Passive Spacecraft

During the problem solution, we will assume that the duration of the rendezvous is fixed (the target point flight revolution number *N* is fixed). The problem in this statement is in itself both interesting and important and if we had a quick enough solution, we could enumerate the values of *N* with the set step in the range of interest and solve the problem for every *N*. This allows us to choose *N*, providing the necessary compromise in reducing both the rendezvous duration and the total delta-v expenditure, which, as a rule, increases with the decrease in rendezvous duration. The decision about the optimal solution *N* is made by the operator, who seeks to solve the problem through the analysis of the total delta-v expenditure versus the flyby duration.

With the fixed value of *N*, the problem solution starts with a determination of the difference in the active spacecraft and target point *n* numbers of revolutions of the flight. Once this difference is defined, the analog of the conventional rendezvous problem is obtained, during the solution of which it is still necessary to take into account the influence of the gravitational field's noncentrality.

The determination of optimal *n* is also carried out with the help of the iterative procedure described as "outer". The iterative procedure from

Chapter 1, which is used for the fulfillment of the terminal conditions with the given accuracy, is described as “inner”.

The approximate value of *n* is determined at the first stage with the condition that only some of the orbital elements are corrected. Let us denote the difference between the semimajor axes, the latitude arguments, the inclinations, and the RAANs of the target and active spacecraft orbits in the initial moment of time as $\Delta a_0, \Delta u_0, \Delta i_0, \Delta\Omega_0$, respectively. We denote the sum of the transversal components of the impulse on the first and second manoeuvring intervals as ΔV_{t_I} and $\Delta V_{t_{II}}$, respectively. It is suggested that the first manoeuvring interval is the first revolution and second manoeuvring interval is the last revolution of active spacecraft flight.

Let us start with the case when Δi_0 is small enough and the change in inclination does not take part in the change of Ω. It is suggested that only the impulse transversal components are used for the solution at this stage.

Taking into account Eq. 7-5, the conditions for compensating the deviations $\Delta a_0, \Delta u_0, \Delta\Omega_0$ in 7-24 have been approximately given (Baranov 2001, 113; Baranov and Labourdette 2003, 130-142):

$$2\frac{\Delta V_{t_I} + \Delta V_{t_{II}}}{V_0} = \frac{\Delta a_0}{a_0}, \tag{7-30a}$$

$$-3(N+n)\frac{\Delta V_{t_I}}{V_0} = -3N\frac{\Delta V_{t_I} + \Delta V_{t_{II}}}{V_0} + \Delta u_0^* + n, \tag{7-30b}$$

$$-4(N+n)\delta\Omega\frac{\Delta V_{t_I}}{V_0} = -4N\delta\Omega\frac{\Delta V_{t_I} + \Delta V_{t_{II}}}{V_0} + \Delta\Omega - \delta\Omega n, \tag{7-30c}$$

here, $\Delta u_0^* = \frac{\Delta u_0}{2\pi}$. It is also suggested that $\Delta\Omega = \Delta\Omega_0$ in the beginning and $\Delta\Omega = \Delta\Omega_0 + \Delta\Omega_1$ (where $\Delta\Omega_1$ = deviation of RAANs after the first iteration) after the first iteration of the outer iterative procedure etc.

The expression for *n*, which does not depend on the magnitudes of the impulses, can be found from the second and third equations:

$$n = \frac{3\Delta\Omega}{7\delta\Omega} - \frac{4}{7}\Delta u_0^*. \tag{7-31}$$

This relatively simple expression for *n* allows us to make several important conclusions. Firstly, *n* does not depend on the rendezvous

duration *N*. As we will further see, it is not exactly true for accurate solutions, but the dependency is indeed weak. Secondly, as previously noted, the found value for *n* is two times smaller than the simplest assessment of $\Delta\Omega / \delta\Omega$. The initial phase desynchronization Δu_0 adds the addend, which does not exceed half a revolution, but, during calculation, *n* is rounded up and the deviation Δu_0 may change *n* by unit.

The sum of the impulse transversal components of the first manoeuvring interval depends on the rendezvous duration and can be found from eqs. 7-30a and 7-30b:

$$\frac{\Delta V_{t_I}}{V_0} = \frac{N\Delta a_0}{2(N+n)a_0} - \frac{\Delta u_0^* + n}{3(N+n)}, \tag{7-32a}$$

$$\frac{\Delta V_{t_{II}}}{V_0} = \frac{\Delta a_0}{2a_0} - \frac{\Delta V_{t_I}}{V_0}. \tag{7-32b}$$

A more accurate value of *n* can be obtained if the change in inclination is accounted for. Let us denote the sum of the impulse lateral components of the first and second manoeuvring intervals ΔV_{z_I} and $\Delta V_{z_{II}}$, respectively. By supposing that the impulses are applied at the equator and taking into account Eq. 7-15, the following equation system is obtained (Baranov and Baranov 2008):

$$2\frac{\Delta V_{t_I} + \Delta V_{t_{II}}}{V_0} = \frac{\Delta a_0}{a_0}, \tag{7-33a}$$

$$-3(N+n)\frac{\Delta V_{t_I}}{V_0} = -3N\frac{\Delta V_{t_I} + \Delta V_{t_{II}}}{V_0} + \Delta u_0^* + n, \tag{7-33b}$$

$$\frac{\Delta V_{z_I} + \Delta V_{z_{II}}}{V_0} = \Delta i_0, \tag{7-33c}$$

$$\begin{aligned} &-4(N+n)\delta\Omega\frac{\Delta V_{t_I}}{V_0} - (N+n)\delta\Omega\,\mathrm{tg}i\frac{\Delta V_{z_I}}{V_0} = \\ &-4N\delta\Omega\frac{\Delta V_{t_I} + \Delta V_{t_{II}}}{V_0} - N\delta\Omega\,\mathrm{tg}i\frac{\Delta V_{z_I} + \Delta V_{z_{II}}}{V_0} + \Delta\Omega - \delta\Omega n \end{aligned} \tag{7-33d}$$

The number of variables is greater than the number of equations in Eq. 7-33. Selecting n as an independent variable, one can obtain the expressions for the impulse components:

$$\Delta V_{t_I} = V_0 \left[\frac{N\Delta a_0}{2(N+n)a_0} - \frac{\Delta u_0^* + n}{3(N+n)} \right], \tag{7-34a}$$

$$\Delta V_{t_{II}} = V_0 \frac{\Delta a_0}{2a_0} - \Delta V_{t_I}, \tag{7-34b}$$

$$\Delta V_{z_I} = \frac{V_0}{N+n} \left[N\Delta i_0 - \frac{4(\Delta u_0^* + n)\delta\Omega + 3(\delta\Omega n - \Delta\Omega)}{3\delta\Omega \mathrm{tg} i} \right], \tag{7-34c}$$

$$\Delta V_{z_{II}} = V_0 \Delta i - \Delta V_{z_I}. \tag{7-34d}$$

The value n will be optimal with the minimal function:

$$\Delta V = \sqrt{\Delta V_{t_I}^2 + \Delta V_{z_I}^2} + \sqrt{\Delta V_{t_{II}}^2 + \Delta V_{z_{II}}^2}.$$

It is not difficult to conduct single-dimensional optimization; moreover, a good initial value for n can be determined with the help of Eq. 7-31.

The numerical and numerically analytical (which is more preferable thanks to the long rendezvous duration) integration of the equations of motion for the target point and the active spacecraft's transfer to the target point is fulfilled after the determination of n. The target point is given by the number of revolutions and the latitude argument. The deviations of the orbital elements are calculated and the manoeuvring parameters, ensuring the adjustment of all the elements of the target orbit except for the RAAN, are determined.

During the determination of the manoeuvring parameters, it is supposed that the inclination correction distribution between the manoeuvring intervals (the inclination of the drift orbit, calculated during the determination of optimal n) is preserved. The multiple iterations of the inner iterative procedure are fulfilled in order to make the deviations of the corrected elements small enough. After that the magnitude of the left deviation between the RAANs $\Delta\Omega_1$ is analyzed. If $|\Delta\Omega_1| > |\delta\Omega^*|$, where $\delta\Omega^* = \Delta\Omega_0 / n$, such that the accuracy of the model used for the

determination of n is not enough, $\Delta\Omega_0$ should be substituted with $\Delta\Omega_1$ and the next iteration of the outer iterative procedure should be conducted (with updated n). The flowchart of the n determination algorithm is given below.

Evaluation of the difference in the number of revolutions of flight n

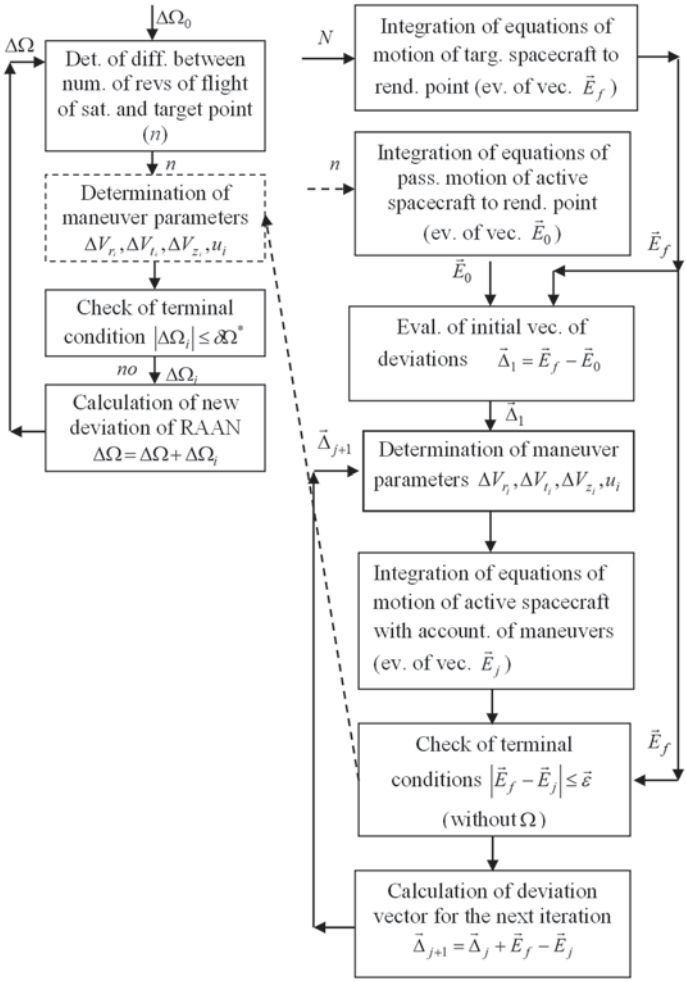

7.2.2. Change of Semimajor Axis and Eccentricity Vector

When the final value for n is found, we can switch to determining the manoeuvring parameters, which ensure the adjustment of all elements of the target orbit. As with a medium duration rendezvous, the solution will be searched for in the form of a solution that combines the two transfer problems; however, the peculiarities, connected to the noncentrality of the gravitational field, must be taken into account.

Figure 7-12 gives the target point orbital eccentricity vector in the rendezvous moment—vector *OK*; the active spacecraft orbital eccentricity vector in the initial moment of rendezvous—vector *OA'*; and the rendezvous final moment—vector *OA*. The optimal direction of eccentricity correction is set by vector *AK*.

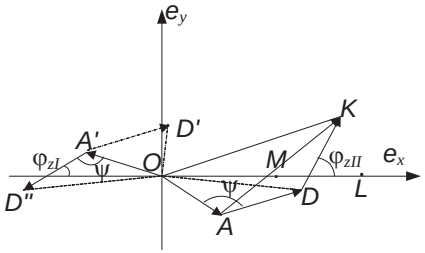

Fig. 7-12. Eccentricity vector correction

Let us suppose that the target point is set on the equator with inclination i corrected and Ω uncorrected; such a variant is used, for example, for the first iterations of the outer iterative procedure. In this case, the optimal direction of the orbital plane correction coincides with the direction of axis e_x. Let us suppose that vector *OL* corresponds to the magnitude of the required inclination change.

With the help of eqs. 7-32a and 7-32b, the change in distribution of the semimajor axes $\Delta a_I, \Delta a_{II}$ by the impulse transversal components of the first and second manoeuvring intervals is assessed. This assessment is rather accurate thanks to the long duration of the rendezvous.

By setting the positions of point *M* on line segment *OL* and point *D* on plane e_x, e_y, i.e. by distributing the inclination and eccentricity vector correction between the manoeuvring intervals, the two transfer problems are obtained. Solving these problems, the optimal values of the total delta-

v of each of the transfers (ΔV_{trf_I} and $\Delta V_{trf_{II}}$) can be found and, hence, the rendezvous total delta-v $\Delta V = \Delta V_{trf_I} + \Delta V_{trf_{II}}$ can be found too. The optimal solution of the rendezvous problem can be obtained by varying the positions of points *M* and *D* (Baranov and Baranov 2009, 256-262).

There is no need to account for the influence of the noncentrality of the gravitational field during the determination of $\Delta V_{trf_{II}}$ for the second manoeuvring interval. The alteration of the semimajor axis is determined by Eq. 7-32b. The alteration of the eccentricity vector is set by vector *DK* and the alteration of the orbital plane is set by vector *ML*. The angle between these vectors $\varphi_{z_{II}}$ is known (Fig. 7-12). The transfer problem (searching for $\Delta V_{trf_{II}}$) is determined and one of the methods from the 2nd paragraph of the Chapter 2 can be used for its solution.

Accounting for the influence of the noncentrality of the gravitational field is necessary for the determination of ΔV_{trf_I} for the first manoeuvring interval. We get vector *OD′*, which, as can easily be seen, differs in magnitude from the desired vector *OD*, if we change the active spacecraft orbital eccentricity vector, which it had at the initial moment in time (vector *OA′*), by the seemingly required vector *AD*. In order to find the vector that needs to be corrected, one should draw line segment *AD* from *OA′* with the same angle ψ between vector *AD* and vector *OA*. Then, we will get the desired vector *OD″*, which will take the place of vector *OD* after evolution. The drift orbit, shaped by the impulses of the first manoeuvring interval, should have the eccentricity vector *OD* right before the second manoeuvring interval. As we can see, the magnitude of the eccentricity alteration is equal to the magnitude of vector *OD* at the moment of performance of the first interval manoeuvre, but the direction gradually changes. The angle between the eccentricity vector's optimal direction of correction and the optimal direction of the orbital plane correction changes too. The angle φ_{z_I} differs from angle $\varphi_{z_{II}}$ (Fig. 7-12). The difference between angles φ_{z_I} and $\varphi_{z_{II}}$ explains the necessity of searching for the optimal position of point *D* in the vicinity of line segment *AK*, not on line segment *AK* itself. Let us remember that, in the medium duration rendezvous problem, the optimal position of point *D* can easily be determined: for example, it divides line segment *AK* proportionally to ΔV_{t_I} and $\Delta V_{t_{II}}$. After determination of the position of point *D″*, the transfer problem for the first manoeuvring interval is

determined: it is necessary to transfer from point A' to point D'' with angle φ_{z_1} between the optimal orbital plane change in direction and the required alteration to the eccentricity vector. One of the methods from the second paragraph of Chapter 2 can also be used for its solution.

7.2.3. Orbital Plane Rotation

During the simultaneous correction of the inclination and the RAAN optimal direction of the orbital plane correction can be different for different intervals too.

In Fig. 7-13a, the difference between the orbital inclinations Δi_0, which needs to be corrected, has been put on the abscissa axis. The deviation between the RAANs, which remains after the correction of the eccentricity vector, the semimajor axis, and the position along the orbit (let us denote it as $\Delta\Omega_r$) has been placed on the ordinate axis.

There are two ways of performing deviation correction between the RAANs $\Delta\Omega_r$.

Let us assume that, during the determination of optimal *n*, it was found that the magnitude of the inclination change by the impulses of the first manoeuvring interval should be equal to Δi_n; and by the impulses of the second manoeuvring interval: $\Delta i_0 - \Delta i_n$. Such a distribution of inclination correction should lead (due to orbital evolution) to the alteration of the RAAN at the rendezvous point by the magnitude $\Delta\Omega_n$.

In Fig. 7-13a, the influence of the alteration of the inclination Δi_n on the alteration of the RAAN is plotted by line segment *LM*. The angle between line segment *LM* and the abscissa axis depends on $N+n$ and on $\delta\Omega \mathrm{tg} i$ (it depends on the flight duration and the rate of orbital evolution).

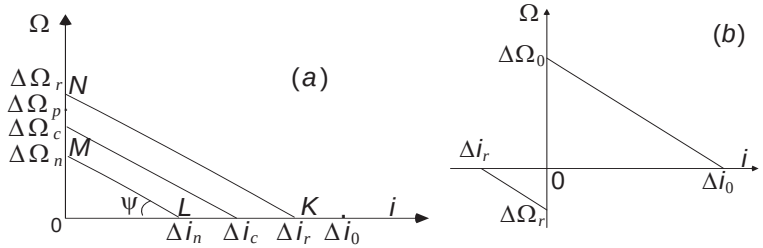

Fig. 7-13. Orbital plane orientation correction

Thus, the deviation between the RAANs $\Delta\Omega_r - \Delta\Omega_n$ remains after the correction of the planar orbital elements and the inclination.

In order to completely eliminate the deviations between the RAANs, the lateral components of the impulses of the first manoeuvring interval should alter the inclination by Δi_r, not Δi_n. In order to find Δi_r, line segment *NK*, which is parallel to line segment *ML*, should be plotted from point $N\ (0, \Delta\Omega_r)$. This is a method of RAAN correction with the help of the inclination. The deviation between the RAANs can be eliminated completely through the lucky choice of the inclination of the drift orbit (Δi_r) without correcting the deviation between the RAANs. This is a simple and reliable method, but it may be nonoptimal from the total delta-v expenditure point of view.

The combined method appears to be more universal and optimal (Baranov and Baranov 2009, 256-262). Let us assume that the impulses of the first manoeuvring interval alter the inclination by Δi_c and the impulses of the second manoeuvring interval alter the inclination by $\Delta i_0 - \Delta i_c$. The alteration of the inclination by Δi_c will lead to the alteration of the RAAN by $\Delta\Omega_c$. The deviation $\Delta\Omega_r - \Delta\Omega_c$ remains, as Δi_c does not coincide with Δi_r. The correction of the deviation $\Delta\Omega_r - \Delta\Omega_c$ is conducted in the usual way and it is optimal to distribute it between the manoeuvring intervals. For example, on the first manoeuvring interval $\Delta\Omega_p - \Delta\Omega_c$ may be corrected simultaneously with the correction of Δi_c (Fig. 7-13a) and on the second manoeuvring interval $\Delta\Omega_r - \Delta\Omega_p$ may be corrected simultaneously with the correction of $\Delta i_0 - \Delta i_c$. It is obvious that, in this case, the optimal points for the orbital plane rotation will shift from the equator and will be different for the first and second manoeuvring intervals. By altering Δi_c, and by altering $\Delta\Omega_p$ for each Δi_c, different variants of alteration of the orbital plane on the first and second manoeuvring intervals are obtained. Since the optimal directions of eccentricity vector correction are also different on the first and second manoeuvring intervals, the opportunity to bring the near optimal directions of the corrections of the eccentricity vector and the orientation of the orbital plane on each of the intervals, hence, the decrease of the total delta-v of the transfers ΔV_{trf_I} and $\Delta V_{trf_{II}}$ arises.

It is worth mentioning that, sometimes, the deviation of *i* needs to be increased for the sake of a decrease in the deviation between the RAANs

(Fig. 7-13b). This happens when $\Delta\Omega_r$ and $\Delta\Omega_0$ have different signs, where $\Delta\Omega_0$ corresponds to the alteration of the RAAN due to the change in inclination by the impulses of the first manoeuvring interval by the magnitude Δi_0. In this case, it is necessary to enumerate the points from interval $[\Delta i_r, \Delta i_0]$, not from interval $[0, \Delta i_0]$, for obtaining the optimal value of Δi_c (Fig. 7-13b).

7.2.4. General Algorithm for Getting the Precise Solution to the Problem

The flowchart of the problem solution algorithm is given below.

The solution consists of three embedded iterative procedures. The outer procedure is used for the determination of the optimal difference in the number of revolutions of flight *n*. The inner procedure is used for the fulfillment of the terminal conditions with the desired accuracy (for each of the fixed values of *n*). The third procedure ensures the transfer to the desired orbit for a fixed time with the required accuracy and the approximate determination of the manoeuvring parameters.

The manoeuvring parameters, which ensure the adjustment of all orbital elements except the RAAN, are calculated during updating of the value *n*. Once the optimal value of *n* is found, all orbital elements including the RAAN are corrected in the inner and the third procedures. This solution is the final problem solution.

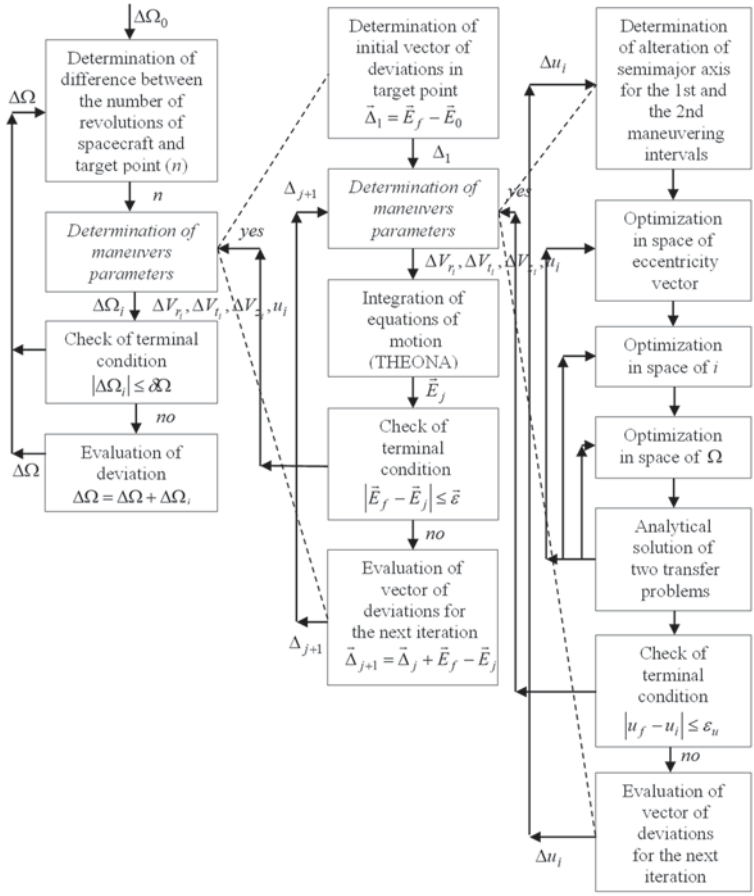

7.2.5. Examples of Algorithm Application in the Mars Sample Return Mission Project

The method for calculating the manoeuvring parameters for a long duration rendezvous, described in this paragraph, was realized in the form of a piece of software entitled “GAMA”. The numerical analytical integration of high accuracy of the equations of motion “THEONA” was used for the propagation of the motion of the spacecraft in the software (Golikov 1990; Golikov 2008). A detailed description of the numerical analytical prognosis procedure “THEONA” can be found in the first paragraph of Chapter 10. The combination of the two numerical analytical

methods in one program allows us to obtain the solution of the most complex problems in some dozens of seconds, including the analysis of the dependency between the total delta-v expenditure of the manoeuvres and the rendezvous duration. During the development of the "GAMA" software, considerable difficulties had to be overcome, connected, first of all, with the poor convergence of the inner iterative procedure with the long duration of the rendezvous (several months). To demonstrate the capabilities of the "GAMA" software and the aforementioned method, the two rendezvous problems on the orbit of Mars and the two problems of the satellite transfer to the required positions in the satellite constellations in Earth orbit will be considered.

In the project "Mars sample return mission" (Bollman, D'Amario, Lee, and Roncoli et al. 1999), the return vehicle would have to successively "grab" two capsules with soil in Mars orbit. It was assumed that the first capsule, delivered by a previous spacecraft, would be deployed in Mars orbit two years before the arrival of the return vehicle. This is why there is the possibility of considerable desynchronization of the RAANs of the return vehicle and the capsule orbits. The deviation $\Delta\Omega = 182^{\circ}$ was considered in problem 1. The second capsule would be delivered by the spacecraft itself, but, due to its long stay on the surface of Mars and due to the fact that the return vehicle was grabbing the first capsule at that time, a considerable deviation between the RAANs would also occur ($\Delta\Omega = 80^{\circ}$). The project was not realized, but the problems remain interesting due to their complexity. The statements and solution results are presented in the work of Bollman, D'Amario, Lee, and Roncoli et al. (1999). This allows us to compare the results obtained with the help of different methods. This possibility was already used in the work of Breeden, Guinn, and Ocampo (2001, 1-20), in which the solution of one of the problems considered in the work of Bollman, D'Amario, Lee, and Roncoli et al. (1999) is depicted. The results, obtained in Bollman, D'Amario, Lee, and Roncoli et al. (1999), Breeden, Guinn, and Ocampo, (2001, 1-20), and the results, obtained with the help of the "GAMA" software (Baranov and Labourdette 2003, 130-142; Baranov and Baranov 2009, 256-262) are listed in table 7-1.

In the work of Bollman, D'Amario, Lee, and Roncoli et al. (1999), the solution for both problems was searched for with the help of the traditional method for NASA[3] (Fehse 2003, 441-449), with individual correction of the orbital plane orientation and other elements. Solutions of this type we

[3] "Shuttle Press Kit: STS-92". Accessed March 25, 2007. http://www.shuttlepresskit.com/STS-92/.

will term “separate”. NASA used 10 impulses and 320.8 m/s of total delta-v with a rendezvous duration of 123.9 days for the solution of problem 1 (the 3rd row in table 3-1). The “GAMA” software used 6 impulses and 233.7 m/s of total delta-v with a rendezvous duration of 123.1 days for the “separate” solution. The information about the solution is listed in the second row of table 3-1 and the solution parameters are presented in Example 1-1.

At the beginning of Example 1-1, the orbital elements of the active and target spacecraft are presented, including: the minimal and maximum altitudes above the surface of Mars, *Hmin* and *Hmax*; the pericenter argument ω; the inclination *i* and the RAAN; and the number of revolutions and the latitude argument *Nrev* and *Ulat*, respectively. The total delta-v of the manoeuvres and, separately, the total delta-v expenditure on manoeuvring in the orbital plane and the orbital plane rotation, the number of iterations of the inner iterative procedure, needed for the solution of the whole problem (with updated *n*) and the solution of the problem with a fixed value of *n*, are further listed. The parameters of each of the manoeuvres are also listed in the rows, including: the number of revolutions and the latitude argument of the impulse application moment and its components. Then, the duration of the rendezvous (in days), the value of *n*, and, separately, the active and target spacecraft number of flight revolutions, are listed. The next row gives the distribution between the manoeuvring intervals of the total delta-v expenditure on altering the eccentricity vector and the rotation of the orbital plane. At the end of the example case, the given accuracies of fulfilling the terminal conditions and the deviations in the rendezvous point between the orbits, shaped with the manoeuvres, and the given target orbit are presented.

The apsidal four-impulse solution was used, which is why the four inner impulses are purely transversal. The application angles of one manoeuvring interval differ by 180º; however, as has already been shown, the directions of optimal eccentricity correction are different for the first and second manoeuvring intervals. The two impulses, listed in the last column, are used for the alteration of the orbital plane. They correct only the inclination (both applied on the equator), but, through the correct choice of their magnitude deviation between the RAANs, they can be fully eliminated. The four transversal impulses can solve the coplanar rendezvous problem. As shown in Chapter 3, we can use three impulses, but the four-impulse apsidal solution is more universal as there is no need to analyze on which of the intervals the two impulses should be applied. Furthermore, by using four impulses, one can obtain a solution that is less

sensitive to the errors of impulse realization and the knowledge of the orbital parameters (see paragraph 3.9).

In the solution given by Bollman, D'Amario, Lee, and Roncoli et al. (1999), the five transversal impulses ensure the required evolution of the orbital plane for the elimination of the main difference between the RAANs, but do not solve the rendezvous problem completely—they only ensure the transfer to an orbit 0.5 km lower than the given orbit. At this moment, a difference in position along the orbit may be half a revolution long. As such, the necessary standby on this close orbit is fulfilled in order to let the active spacecraft catch up with the target spacecraft (the standby can take up to two weeks), after this a transfer to the desired orbit in the limited vicinity of the target spacecraft is made with help of two additional impulses. During this final phasing a deviation between the RAANs occurs; the special impulse, applied at the orbit apex is used for its correction. These additional impulses explain the big difference in the number of impulses used, presented in the two compared solutions. The general discrepancy in the total delta-v expenditures is connected to the different eccentricity vector deviation correction schemes (see paragraph 4.5).

The optimal total delta-v expenditure solution can be obtained, if the use of all components of every impulse is permitted (a "combined" solution). Such a solution, obtained with the help of the "GAMA" software is listed in Example 1-2. Four impulses are needed for the problem solution (the magnitude of the second impulse is only 0.54 m/s), ΔV = 202.4 m/s. The information about this solution is listed in the first row of table 3-1.

A close solution, in term of the attributes (the fourth row in table 3-1; 3 impulses; ΔV = 199.52 m/s; and a rendezvous duration of 133.04 days), was obtained in the work of Breeden, Guinn, and Ocampo (2001, 1-20) using the numerical method. The expenditures are slightly smaller, but the rendezvous duration is longer. The total delta-v expenditure can be decreased by increasing the rendezvous duration. Such a combined solution, obtained with the help of the "GAMA" software is listed in Example 1-3. Four impulses are used in this solution: ΔV = 194.6 m/s; the duration of the flyby is 144.7 days; and the parameters of the solution are listed in the fifth row of table 3-1.

The universal method (the impulses do not have radial components), leading to practically the same (the second decimal place of percent greater) total delta-v expenditures as the optimal Edelbaum solution (Edelbaum 1967, 66-73), but ensuring a more rapid convergence of the iterative procedures, was used during the search for the combined

solutions on each of the manoeuvring intervals for the determination of the optimal transfer manoeuvring parameters.

The total delta-v expenditure decreases as the rendezvous duration increases. The high performance of the "GAMA" software allows us to find compromise values for these parameters. There is an option to enumerate the target spacecraft flight revolution number (N_f) during calculation. For every N_f, the problem is solved and the values of total delta-v and other manoeuvring parameters are found (Example 1-4) (Baranov and Baranov 2009, 256-262). The total solution time will be considerably smaller in comparison to the solution of the succession of problems with fixed N_f. Analysis of the calculation results from Example 1-4 shows that a truly close-to-optimal rendezvous duration was chosen in the work of Bollman, D'Amario, Lee, and Roncoli et al. (1999). Specifically, on the interval from 1,350 to 1,400 revolutions of the target spacecraft's flight, the dependency between total delta-v and rendezvous duration decreases considerably. It is not particularly effective to increase the rendezvous duration further.

For the second rendezvous problem in Mars orbit, the optimal combined solution (Example 2-1), the separate solution (Example 2-2), and the solution with the enumeration of the number of target spacecraft flight revolutions (Example 2-3, 800 to 1,800 revolutions with a step of 200) are presented. The obtained results can be compared to the results given by Bollman, D'Amario, Lee, and Roncoli et al. (1999) with the help of table 7-2.

The calculation results, listed in Example 2-3, show that, for the second problem in the work of Bollman, D'Amario, Lee, and Roncoli et al. (1999), the optimal rendezvous duration was chosen as well, since, specifically on a target spacecraft flight interval of 1,200 to 1,400 revolutions, the dependency between total delta-v and rendezvous duration decreases considerably.

The impulse manoeuvres were supposed to have been used in all the aforementioned examples, as there was no information given about the types of engines used.

PROBLEM 1

Example 1-1

	initial orbit	target orbit
Hmin km	250.0	500.0
Hmax km	1,400.0	700.0
ω deg	4.0	184.0
i deg	45.0	46.0
Ω deg	2.0	184.0
Nrev	1	1
Ulat deg	184.0	184.0

dV = 233.68 m/s *dVinpln* = 184.68 m/s *dVoutpl* = 49.00 m/s
Niter = 95 16

Nimp	*Nrev*	*Ulat*	*dVrd*	*dVtr*	*dVlt*
1	1	180.00	0.0	0.0	-47.09
2	2	185.22	0.0	54.93	0.0
3	3	5.22	0.0	0.15	0.0
4	1,221	36.48	0.0	-0.67	0.0
5	1,222	216.48	0.0	-128.92	0.0
6	1,222	0.00	0.0	0.0	1.91

N_days: 123.1 *n* = -169.0 *REVfnlTG* = 1392 *REVfnlCH* = 1223
*U*1*opt* = 185.2 *E*1*opt* = 109.57 *E*2*opt* = 256.5 *Z*1*opt* = 47.09
*Z*2*opt* = 1.91

Given tolerances of terminal condition fulfillment

e_x	e_y	*a*	*t*	*i* deg	Ω deg
0.0001	0.0001	0.01	0.1	0.0005	0.0005

Deviations in the rendezvous point after manoeuvre fulfillment

Δe_x	Δe_y	Δa	Δt	Δi deg	$\Delta\Omega$ deg
0.0000199	0.0000008	0.0011981	-0.0932687	0.0000011	0.0000036

Example 1-2

dV = 202.39 m/s *dVinpln* = 184.22 m/s *dVoutpl* = 56.66 m/s
Niter = 93 15

Nimp	*Nrev*	*Ulat*	*dVrd*	*dVtr*	*dVlt*
1	2	186.10	0.0	54.09	-47.41
2	3	306.19	0.0	0.54	0.09
3	1,221	210.05	0.0	-78.71	-5.47
4	1,222	224.74	0.0	-50.86	3.66

N_days: 123.1 *n* = -169.0 *REVfnlTG* = 1,392 *REVfnlCH* = 1,223
*U*1*opt* = 183.6 *E*1*opt* = 107.66 *E*2*opt* = 257.14 *Z*1*opt* = 47.5
*Z*2*opt* = 2.1

Δe_x	Δe_y	Δa	Δt	Δi	$\Delta\Omega$
0.0000002	-0.0000002	-0.0000124	-0.0400580	-0.0000013	-0.0000171

Example 1-3

dV = 194.59 m/s *dVinpln* = 186.35 m/s *dVoutpl* = 53.82 m/s
Niter = 79 14

Nimp	*Nrev*	*Ulat*	*dVrd*	*dVtr*	*dVlt*
1	2	188.50	0.0	50.13	-21.05
2	3	11.30	0.0	-12.81	4.56
3	1,461	195.93	0.0	5.72	-0.71
4	1,462	5.09	0.0	-117.67	27.48

N_days: 144.7 *n* = -173.0 *REVfnlTG* = 1,636 *REVfnlCH* = 1,463
*U*1*opt* = 184.6 *E*1*opt* = 125.88 *E*2*opt* = 246.60 *Z*1*opt* = 25.6
*Z*2*opt* = 28.1

Δe_x	Δe_y	Δa	Δt	Δi	$\Delta\Omega$
-0.0000001	0.0000004	-0.00024	-0.0424021	0.0000052	-0.0000115

Example 1-4

dV = 205.66 m/s *dVinpln* = 183.11 m/s *dVoutpl* = 60.77 m/s
Niter = 73 14

Nimp	*Nrev*	*Ulat*	*dVrd*	*dVtr*	*dVlt*
1	2	189.67	0.0	50.87	-47.84
2	3	34.56	0.0	-2.08	0.67
3	1,279	244.60	0.0	-126.83	-6.51
4	1,280	84.65	0.0	3.30	-5.73

N_days: 128.2 *n* = -169.0 *REVfnlTG* = 1,450 *REVfnlCH* = 1,281
*U*1*opt* = 185.6 *E*1*opt* = 105.56 *E*2*opt* = 259.90 *Z*1*opt* = 48.5
*Z*2*opt* = 2.2

Δe_x	Δe_y	Δa	Δt	Δi	$\Delta\Omega$
-0.0000008	0.0000003	0.0000469	0.0951869	0.0000012	0.0000456

Nrevtg	*dV*	*dVinpln*	*dVoutpl*	*n*
1,050	293.40	284.35	51.11	-168.0
1,100	275.40	266.82	51.52	-168.0
1,150	259.69	251.39	54.81	-169.0
1,200	245.23	235.24	55.75	-169.0
1,250	231.92	221.97	56.34	-170.0
1,300	219.46	210.91	53.97	-172.0
1,350	208.59	196.96	55.30	-171.0
1,400	206.87	187.01	51.38	-169.0
1,450	205.66	183.11	60.76	-169.0

Table 7-1

	PROBLEM 1			
	Number of manoeuvres	ΔV m/s	%	Time days
GAMA (comb.)	4	202.39	100	123.1
GAMA (sep.)	6	233.68	115.5	123.1
NASA (sep.)	10	320.8	158.5 (137.3)	123.9
UT&JetPL (comb.)	3	199.52	98.6	133.04
GAMA (comb.)	4	194.6	96.1	144.7

PROBLEM 2

Example 2-1

	initial orbit	target orbit
Hmin km	475.6	446.8
Hmax km	724.4	553.2
ω deg	279.3	238.4
i deg	46.0	45.0
Ω deg	80.2	1.2
Nrev	1	1
Ulat deg	356.5	105.8

dV = 145.36 m/s *dVinpln* = 130.35 m/s *dVoutpl* = 56.14 m/s
Niter = 73 11

Nimp	*Nrev*	*Ulat*	*dVrd*	*dVtr*	*Vlt*
1	2	190.96	0.00	-42.60	6.48
2	3	348.66	0.00	-41.48	-25.61
3	1,430	322.68	0.00	28.90	-2.50
4	1,431	260.91	0.00	17.35	1.53

N_days: 116.9 *n* = 59.0 *REVfnlTG* = 1,374 *REVfnlCH* = 1,433
U1opt = 86.0 *E1opt* = 16.30 *E2opt* = 40.14 *Z1opt* = -51.1 *Z2opt* = -2.2

Given tolerances of terminal condition fulfillment

Δe_x	Δe_y	Δa	Δt	Δi	$\Delta\Omega$
0.0001	0.0001	0.01	0.1	0.0005	0.0005

Deviations in the rendezvous point after manoeuvre fulfillment

Δe_x	Δe_y	Δa	Δt	Δi	$\Delta\Omega$
0.0000002	0.0000001	0.000023	-0.0148	-0.0000002	-0.000001

Example 2-2

dV = 181.74 *dVinpln* = 130.84 *dVoutpln* = 50.91 *Niter* = 86 16

Nimp	*Nrev*	*Ulat*	*dVrd*	*dVtr*	*Vlt*
1	1	180.00	0.0	0.0	46.34
2	2	265.26	0.0	-83.76	0.0
3	3	85.26	0.0	-0.11	0.0

4	1,430	48.07	0.0	44.10	0.0
5	1,431	228.07	0.0	2.86	0.0
6	1,432	0.00	0.0	0.0	-4.55

N_days: 116.9 *n* = 59.0 *REVfnlTG* = 1,374 *REVfnlCH* = 1,433
*U*1*opt* = 85.3 *E*1*opt* = 167.31 *E*2*opt* = 82.47 *Z*1*opt* = 46.3 *Z*2*opt* = -4.5

Δe_x	Δe_y	Δa	Δt	Δi	$\Delta\Omega$
-0.0000005	0.0000086	0.0004194	-0.0837062	0.0000011	0.000012

Example 2-3

dV = 125.47 *dVinpln* = 112.10 *dVoutpl* = 55.34 *Niter* = 30 10

Nimp	*Nrev*	*Ulat*	*dVrd*	*dVtr*	*dVlt*
1	2	347.32	0.0	-43.37	-24.18
2	3	196.98	0.0	-31.32	18.18
3	1,859	174.50	0.0	33.43	11.68
4	1,860	60.77	0.0	3.96	-1.28

N_days: 153.2 *n* = 62.0 *REVfnlTG* = 1,800 *REVfnlCH* = 1,862
*E*1*opt* = 22.39 *E*2*opt* = 32.04 *Z*1*opt* = -41.0 *Z*2*opt* = -12.2

Nrevtg	*dV*	*dVinpln*	*dVoutpl*	*n*
800	203.00	193.26	55.37	58.0
1,000	176.27	166.28	56.06	60.0
1,200	156.45	145.34	54.29	60.0
1,400	145.78	130.06	62.01	60.0
1,600	134.80	119.72	59.00	61.0
1,800	125.46	112.10	55.34	62.0

Table 7-2

	PROBLEM 2			
	Number of manoeuvres	ΔV m/s	%	Time days
GAMA (comb.)	4	145.36	100	116.9
GAMA (sep.)	6	181.74	125	116.9
NASA (separate)	10	219.6	151 (120.8)	116.9

7.2.6. Example of Algorithm Application in the Globalstar Deployment Problem

The "GAMA" software is especially effective for manoeuvring parameter determination during the deployment and station-keeping of satellite constellations. Table 7-3 presents the dependency between total delta-v, required for the satellite transfer to the neighboring operational plan and the number of target point revolutions of the flight for the "Globalstar" satellite constellation, and, separately, the total delta-v expenditure on manoeuvring in the orbital plane and the orbital plane rotation.

Table 7-3

N	T *days*	ΔV m/s	ΔV_{inpln}	ΔV_{outpln}
800	63.2	534.06	517.97	114.12
1,000	79	425.86	395.79	147.78
1,200	94.8	342.34	337.59	56.68
1,400	110.6	290.17	285.17	53.41
1,600	126.4	252.63	249.33	40.61
1,800	142.2	223.76	218.81	46.42
2,000	158	201.21	199.46	25.78
2,200	173.8	182.32	179.21	33.06
2,400	189.6	166.99	164.41	28.64
2,600	205.4	154.13	151.93	25.41
2,800	231.2	143.93	143.03	15.67

The altitude of the initial and target orbits is 1,414 km; the inclination is $i = 52^\circ$; and the angle between the orbital planes is $\Delta\Omega = 45^\circ$.

The solution, corresponding to a flyby duration of 2,400 revolutions, is listed in Example 3-1.

Example 3-1

	initial orbit	target orbit
*H*min km	1,410.0	1,412.0
*H*max km	1,418.0	1,416.0
*U*prg deg	10.0	90.0
i deg	52.000	52.001
gOMG deg	45.0	90.0
Nrev	1.0	1.0
Ulat deg	15.50	105.80

dV = 166.99 *dVinpln* = 164.42 *dVoutpl* = 28.65 *Niter* = 86 8

Nimp	*Nrev*	*Ulat*	*dVrd*	*dVtr*	*dVlt*
1	2	191.66	0.0	42.3301	-6.2140
2	3	15.24	0.0	41.8784	9.7993
3	2,317	162.37	0.0	-40.1753	6.0814
4	2,318	342.36	0.0	-40.0335	-6.5529

7.3. Manoeuvre Parameters for Multiple-Tiered Constellation Deployment

7.3.1. Multiple-Tiered Satellite Constellation Characteristics

In recent times, much attention has been paid to multiple-tiered satellite constellations (Kozlov, Razoumny, and Razoumny 2015, 200-204; Kozlov, Razoumny, and Razoumny 2015, 196-199; Ulybyshev 2015, 311-322; Ulybyshev 2016, 1-11), in which satellites are located in circular orbits of different radii. The satellites are divided into several groups, each of which is a conventional single-tiered satellite constellation; their combination gives a constellation with novel attributes. The difference in the precession rates of their orbital planes occurs with considerably different values of the semimajor axes of differently tiered orbits. As a result, different secular drifts of the RAANs occur, leading to a continuous increase in the difference between the orbital plane angles. These orbits of different tiers must have different inclinations in order to have equal secular RAAN drifts. The semimajor axes $a_{\max}$ and the inclinations $i_{\max}$ of the orbits of one tier can be connected to the semimajor axes a_m and inclinations i_m of another tier by following the approximate equation:

$$\frac{\cos i_{\max}}{a_{\max}^{7/2}} = \frac{\cos i_m}{a_m^{7/2}}. \tag{7-35}$$

Hereafter, we will term these orbits with different semimajor axes, but the same evolution of RAANs as “synchronized”.

Equation 7-35 is true for an arbitrary value of the initial deviation of the RAANs, which is why the satellite orbits on different tiers maintain an equalized relative spatial configuration.

Figure 7-14 gives graphs of the dependencies between the inclination deviations Δi and the altitude differences Δh for the orbits, which have different inclinations. The altitude of all orbits is h = 600 km. Similar graphs for orbits at an altitude of h = 1,100 km are depicted in Fig. 7-15. It is assumed that the altitude of the differently tiered orbits will be greater by Δh and hence the deviations of inclinations Δi should be negative. Similar graphs can be found in Kozlov, Razoumny, and Razoumny (2015, 200-204).

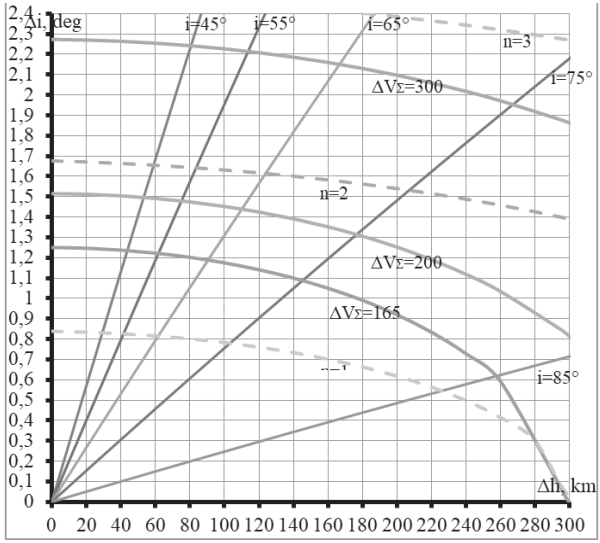

Fig. 7-14. Inclination as a function of altitude for lower tier orbits with altitude h = 600 km

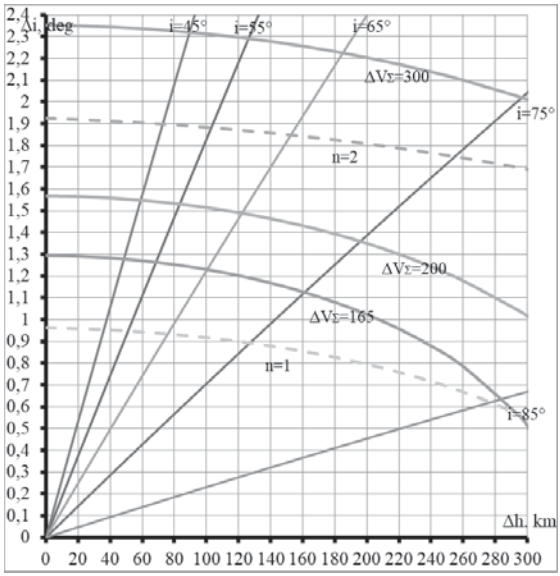

Fig. 7-15. Inclination as a function of altitude for lower tier orbits with altitude h = 1,100 km

7.3.2. Estimation of the Delta-V Required for Changing an Altitude Shell

For a flyby from the synchronized orbit to an orbit of another tier (such a problem occurs during satellite constellation initializations), it is necessary to correct for differences in altitude and inclination. The total delta-v expenditure for such an impulse transfer ΔV_Σ is lower than the assessments of total delta-v expenditure for the solution of the real flyby problem, in which the phase correction and manoeuvre realization with the help of the low-thrust engines are taken into account. The total delta-v expenditure on the impulse transfer can be found using the equations:

$$\Delta V_t = \frac{V_0}{2r_0}\Delta a,$$

$$\Delta V_z = V_0 \Delta i,$$

$$\Delta V_\Sigma = \sqrt{\Delta V_t^2 + \Delta V_z^2}.$$

Using the expression for ΔV_Σ, one can find the dependency between Δi and Δh for the fixed expenditures of ΔV_Σ:

$$\Delta i = \sqrt{\frac{\Delta V_\Sigma^2}{V_0^2} - \frac{\Delta h^2}{4r_0^2}}. \tag{7-36}$$

Such lines for $\Delta V_\Sigma = 165\,\text{m/s}$, $\Delta V_\Sigma = 200\,\text{m/s}$, and $\Delta V_\Sigma = 300\,\text{m/s}$ are depicted in figs. 7-14 and 7-15.

A more accurate assessment of the necessary ΔV_Σ expenditure can be obtained if the real manoeuvre duration (when the manoeuvres are fulfilled with the help of low thrust engines) is taken into account. Since the correction of the deviation between the semimajor axis Δa and the inclination Δi is fulfilled, optimally we perform the two equal manoeuvres on the revolution, the middle of which is located on the node line.

The angular duration of the manoeuvre $\Delta\varphi$ and the angle β, which sets the orientation of the thrust engines in the orbital coordinate frame, can be found from the equation system:

$$\frac{\Delta a}{2n} = \frac{2w\cos\beta}{w_c}\Delta\varphi, \tag{7-37}$$

$$\frac{\Delta i}{2n} = 2\frac{w\sin\beta}{w_c}\sin(\frac{\Delta\varphi}{2}), \tag{7-38}$$

here, n = the number of revolutions on which equal manoeuvres are performed.

Recalculating $\Delta\varphi$ of one of the manoeuvres into ΔV of all the manoeuvres with the help of equation:

$$\Delta V = 2n\frac{w}{w_c}\Delta\varphi, \tag{7-39}$$

one can find the real total delta-v expenditure needed for the transfer to the synchronized orbit.

Using the equation:

$$\left(\frac{\Delta a w_c}{4nw\Delta\varphi}\right)^2 + \left(\frac{\Delta i w_c}{4nw\sin(\frac{\Delta\varphi}{2})}\right)^2 = 1, \qquad (7\text{-}40)$$

we can find the dependency between Δi and Δh for a firing duration of one revolution (n = 1), two revolutions (n = 2), and three revolutions (n = 3). These dependencies are plotted with dashed lines in figs. 7-14 and 7-15. Thus, the areas, which can be reached by continuous manoeuvring during one or two revolutions, can be determined.

7.3.3. Optimal Initial Phase Range

The alteration of ΔV during the transition from the impulsive model to the real engine thrust model has been determined. The correction of the difference between the phases $\Delta\psi$ should be accounted for in the next stage (during satellite constellation deployment). The rate of the maximum approach along the orbit, when the difference between the phases is equal to zero (during maintenance) or to the set value (during deployment), is of special interest. Figure 7-16 shows the dependency between the rendezvous number for a one-year time interval and the deviation by altitude.

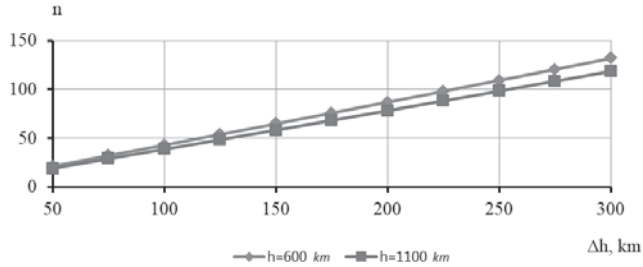

Fig. 7-16. Number of rendezvous as a function of altitude

Figure 7-17 gives the time between the two neighboring rendezvous as a function of deviation by altitude. It can be seen that the time between the rendezvous is small with a big difference between the altitudes and for which the total delta-v expenditure is considerable. The medium heights are a compromise with both the total delta-v expenditures being relatively small and the possibility of the rendezvous arising sufficiently often.

In the initial moment of flyby, if $\Delta\psi \approx 0$, then it is necessary to transfer to the target orbit immediately (for impulsive manoeuvres). In the initial moment of the flyby, if $\Delta\psi > 0$ and the phase difference does not exceed the magnitude, which can be eliminated due to passive flight on the revolutions left before the moment of rendezvous, then the expenditures on the rendezvous do not exceed the expenditures on the transfer between orbits. The range of the optimal phases for the impulse transfers, which depends on the difference between the orbital semimajor axes and the flyby duration, is determined in this fashion. With a considerable or small initial phase difference, expenditure on the rendezvous will be greater than expenditure on transfer (see sections 1.5.2 and 3.5).

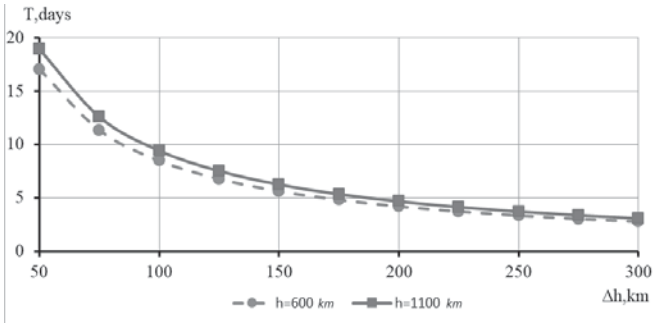

Fig. 7-17. Time between rendezvous as a function of the difference in altitudes

The assessment of the angular difference between the two spacecraft is used in many problems. For example, it is used in the problem of dangerous approach hazard assessment (Baranov and Karatunov 2012; Baranov and Karatunov 2016). For the controlled time interval, if the assessed distance along the orbit exceeds the permitted one, then a collision with this object is impossible. The distance along the orbit exceeds the permitted one if it is greater within the boundaries of the interval and the point of the zero angular distance is outside the interval.

7.3.4. Manoeuvring Calculations in the Problem of Multiple-Tiered Constellation Deployment

The peculiarities of flyby between synchronized orbits involve the presence of a small deviation between their eccentricities Δe, as each one is small by itself, there are considerable deviations between the semimajor axes Δa and, especially, the deviations between Δi. The manoeuvres under consideration are rendezvous manoeuvres of medium duration (since there is no significant deviation between the RAANs, there is no need to consider the long rendezvous duration). If the manoeuvre duration is relatively small, then the algorithms from chapters 4 or 5 can be used for their parameter determination.

7.4. Manoeuvring Parameters in Satellite Formation Flying

The methods from the first and second sections of this chapter may be used successfully in the determination of the manoeuvring parameters during the initialization of satellite groups (satellite formation flyings). The two problems of satellite formation flying initialization are considered in this section. With the help of the equations, developed in the first section, the initialization problem for the atmospheric tomography cluster has been solved; with the help of the "GAMA" software, the "Aqua Train" problem of satellite formation flying initialization has been solved as well.

7.4.1. Deployment of the Cluster for Atmospheric Tomography

The problem of initializing the cluster, which consists of four microsatellites (the weight of each one does not exceed 30 kg) is considered. The cluster is designed for atmospheric tomography.

The satellites of the cluster should be placed in an orbit with an inclination $i = 56^\circ$; an altitude $h = 550$ km; and with the satellite positions: $u_1 = 0^\circ, u_2 = 5^\circ$, $u_3 = 24.75^\circ$, and $u_4 = 34.75^\circ$. The positions of the satellites are shown in Fig. 7-18 by asterisks.

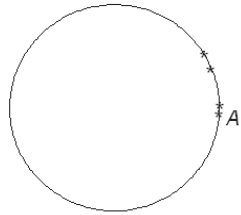

Fig.7-18. Atmospheric tomography satellite formation flying

It is assumed that, in the initial moment, the launch vehicle delivers all the satellites to a single point in the given orbit and it is necessary to deploy the satellites to their operational positions.

The total delta-v expenditure (ΔV) necessary for the change in the microsatellite positions at half the maximum distance between them by the latitude argument in this cluster, depending on the number of the revolutions of the flyby, were calculated.

Table 7-3

Nrev	**days**	ΔV_t	ΔV_{omg}	ΔV_i	ΔV_{iomg}	ΔV_z	U_{opt}
20	1.326	12.210	12.366	35.132	12.249	0.980	6.591
30	1.990	8.140	8.373	23.421	8.198	0.977	84.893
40	2.653	6.105	6.412	17.566	6.182	0.974	83.205
50	3.316	4.884	5.263	14.053	4.979	0.971	81.529
60	3.979	4.070	4.518	11.711	4.183	0.966	79.867
70	4.642	3.488	4.003	10.038	3.618	0.961	78.222
80	5.306	3.052	3.629	8.783	3.198	0.955	76.596
90	5.969	2.713	3.349	7.807	2.874	0.948	74.993
100	6.632	2.442	3.133	7.026	2.617	0.940	73.412
110	7.295	2.220	2.963	6.388	2.408	0.932	71.858
120	7.958	2.035	2.827	5.855	2.235	0.924	70.330
130	8.622	1.878	2.717	5.405	2.089	0.915	68.832
140	9.285	1.744	2.626	5.019	1.965	0.906	67.363
150	9.948	1.628	2.550	4.684	1.858	0.896	65.924
160	10.611	1.526	2.486	4.391	1.765	0.886	64.517
170	11.275	1.436	2.432	4.133	1.682	0.875	63.143
180	11.938	1.357	2.386	3.904	1.609	0.865	61.801
190	12.601	1.285	2.346	3.698	1.543	0.854	60.492
200	13.264	1.221	2.311	3.513	1.484	0.843	59.216

210	13.927	1.163	2.281	3.346	1.430	0.832	57.972
220	14.591	1.110	2.255	3.194	1.380	0.821	56.762
230	15.254	1.062	2.231	3.055	1.335	0.809	55.584
240	15.917	1.017	2.211	2.928	1.293	0.798	54.439
250	16.580	0.977	2.192	2.811	1.254	0.787	53.325
260	17.243	0.939	2.176	2.702	1.218	0.776	52.243
270	17.907	0.904	2.161	2.602	1.184	0.765	51.191
280	18.570	0.872	2.148	2.509	1.153	0.754	50.170

With this approach, ΔV expenditures for the other microsatellites of the cluster will be slightly smaller or equal (for one microsatellite) to the calculated ΔV expenditures. All the spacecraft will have to manoeuvre, but, firstly, this will provide for a steady fuel expenditure and, secondly, the deployment errors can be eliminated.

The first column of table 7-3 shows the number of revolutions between the first and last manoeuvres (N_{rev}); the second column gives the microsatellite transfer durations to the desired positions in days (days); the third column presents the sum of the impulse transversal components, needed for the required change in satellite position (ΔV_t); the fourth column shows the sum of the impulse lateral components, performed at the apex or vertex of the orbit, needed for direct correction of the deviation occurring between the RAANs (ΔV_{omg}); the fifth column gives ΔV for similar manoeuvres on the equator (ΔV_i); the sixth column presents ΔV for the manoeuvres fulfilled at the optimal locations for the orbital plane rotation (ΔV_{iomg}); the seventh column presents the sum of the lateral components of the manoeuvres from the previous column (ΔV_z); and the eighth column gives the optimal angle for the orbital plane rotation (u_{opt}).

The graphs in figs. 7-19 and 7-20 show the variable changes from the table in the dependency of the number of revolutions of the flyby.

It follows from the above that the compromise duration of the initialization of the cluster lies in the range of 100 to 200 revolutions and the total delta-v expenditures decrease from $\Delta V = 2.62\,\text{m/s}$ to $\Delta V = 1.48\,\text{m/s}$. The expenditures of ΔV start to increase rapidly with shorter durations and the additional increase in duration does not lead to a significant decrease in ΔV.

Research into the problem has shown that, for low-thrust engines, the preferable manoeuvre duration does not exceed one eighth of a revolution. If the manoeuvre duration exceeds this magnitude with the chosen thrust

engines, it is recommended that it be divide it into two parts, which will be performed on different revolutions. With the large number of revolutions, needed for optimal cluster initialization, such a division is always possible and does not significantly influence the results of the calculation.

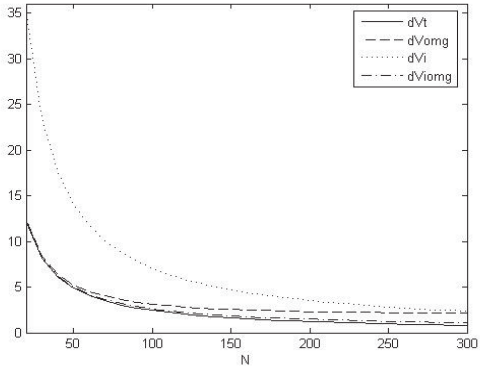

Fig.7-19. Total delta-v expenditures with different schemes of cluster initialization (i = 56°, h = 550 km, and satellite location change relative to the cluster's center Δu = 17.375°)

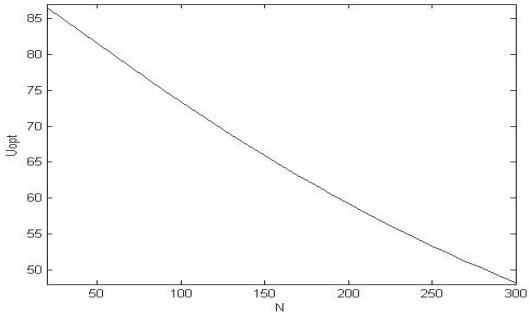

Fig.7-20. Latitude argument alteration for optimal correction impulse application points

7.4.2. Manoeuvres for "Aqua Train" Formation Flying

With the help of the "GAMA" software, one of the problems of satellite transfer in formation flying "Aqua Train" was considered. This satellite group consists of six satellites located on identical orbits, but with shifts in the RAANs and the latitude arguments. The approximate location of the satellites is shown in Fig. 7-21 by asterisks.

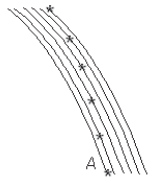

Fig.7-21. Satellite location in the formation flying "Aqua Train"

Table 7-4 gives the ΔV expenditures for satellite transfer from one operational position in the group to another as a function of transfer duration. The solution, which corresponds to a flyby duration of 1,540 revolutions, is depicted in example 3-1.

Table 7-4 (Aqua Train)

N	T days	ΔV m/s	ΔV_{inpln} m/s	ΔV_{outpln} m/s
340	23.3	180.58	138.61	112.07
490	33.6	124.15	88.49	81.71
640	43.9	93.61	69.68	55.27
790	54.15	78.77	58.05	44.94
940	64.4	66.67	50.11	34.07
1,090	74.7	57.85	39.78	30.84
1,240	85.02	52.58	35.99	26.08
1,390	95.3	47.78	29.43	24.22
1,540	105.6	44.69	24.82	23.45

Example case 3-1 (Aqua Train)

	initial orbit	target orbit
Hmin km	663.0	705.0
Hmax km	663.1	705.1
ω_{prg} deg	53.968	77.149
i deg	98.0800	98.2055
Ω deg	263.28	266.04
Ulat deg	0.0	30.0

dV = 44.69 m/s *dVinpln* = 24.82 m/s *dVoutpl* = 23.46 m/s
Niter = 30 11

Nimp	*Nrev*	*Ulat*	*dVrd*	*dVtr*	*dVlt*
1	2	184.95	0.0	0.024	-3.52
2	3	11.08	0.0	0.316	16.43
3	1,552	179.71	0.0	10.703	1.37
4	1,553	1.70	0.0	13.779	-2.14

N_days: 105.6 *n* = 15.0 *REVfnlTG* = 1,540 *REVfnlCH* = 1,555

In the aforementioned examples, it was necessary to place the satellites at considerably large distances from each other. In this case, when the satellites should be located at small distances from each other, the manoeuvring strategy during satellite formation flying initialization differs slightly. The assessment of satellite collision hazards during their transfer to the desired positions in the group becomes of great significance. The use of a target vector may help to reduce this hazard, ensuring the safe direction of the flight to the satellite formation flying procedure. The use of the final target vector will allow the occupation of the desired position in the satellite formation flying procedure. The emphasis should also be on compensating manoeuvre fulfillment errors. One of the algorithms for the determination of manoeuvre initialization in closely located satellite formation flying procuress was described in the work of Baranov, Boutonnet, Escudier, and Martinot (2005, 913-920).

As a rule, the satellites make the desired formation flying manoeuvres with the help of low-thrust engines. The method determining such manoeuvres is presented in Chapter 6. This method is simple and reliable enough to be used during the design of onboard algorithms for the determination of the manoeuvring parameters for in the initialization of satellite formation flying.

CHAPTER EIGHT

STATION-KEEPING OPTIMIZATION FOR A SATELLITE CONSTELLATION

The two main keeping strategies for the given configuration of a satellite constellation can be distinguished as absolute and relative. With absolute station-keeping, the motion of each satellite complies with some programmed motion, which allows an assessment of the manoeuvre parameters of each satellite to be performed independently from the locations of the other satellites in the constellation. Coordinated movements for all satellites from the constellation are ensured with relative station-keeping. It is considerably more economical than the absolute one, as there is no need for constant element correction in orbit, as they change in practically the same fashion for all satellites. For example, the semimajor axes of all orbits may decrease under the atmosphere influence practically in the same fashion, but the relative satellite angular distances, which determine the constellation configuration, will be almost constant. The considerable alterations of the semimajor axes do not have to be corrected, and only maintaining the slowly changing angular configuration of the constellation is required. Relative station-keeping is a more complex problem as it is necessary to take the positions of all other elements of the constellation into account during one of the satellite manoeuvre parameter calculations.

8.1. Relative Station-Keeping for a Satellite Constellation

8.1.1. Maintenance Problem Statement

This chapter considers the manoeuvre parameter determination problem, in which the keeping of the given satellite constellation configuration is ensured. The satellites are situated on several circular orbits, which have the same radii and inclinations, but different values of RAANs. The relative deviations between the satellites and their nominal values by the latitude argument u, the RAAN Ω, and the inclination i are

required to be smaller than the given values of δu, $\delta\Omega$, and δi on the fixed time interval (the station-keeping interval). The constraints of the minimum and maximum magnitudes of the manoeuvres, as well as the number performed within the fixed time interval, should be taken into account; the constant expenditure of fuel by the satellites from the satellite constellation should also be considered.

The satellite orbit elements are not fixed, and only their relative angular distances, which determine the constellation configuration, are important. Thus, relative constellation configuration keeping is considered.

8.1.2. Calculation for the Basic Orbit Elements

We will denote the base orbits as orbits, where the differences in their values for controlled parameters comply with the nominal values. If elements (u, Ω, i) for one of the base orbits are known, then the elements for all other base orbits are determined unambiguously from the nominal satellite location conditions.

For example, let us consider the 6-satellite constellation (STARSYS). The initial conditions are listed in Table 8-1 (Bernussou, Brousse, Dufour, Foliard et al. 1997). The nominal latitude angular distances between the satellites in one plane are $u_d = 180^\circ$, and the locations of the satellites in the different planes differ by $u_m = 120^\circ$.

Table 8-1

Satellite	*a* km	*i* deg	Ω deg	*u* deg
11	7,377.178	52.9992	0.057	10.043
12	7,377.004	52.9994	0.134	189.913
21	7,378.914	52.9995	120.025	130.085
22	7,379.607	53.0010	119.945	310.057
31	7,378.106	52.9998	240.011	250.120
32	7,378.647	52.9989	239.925	69.847

Let us put all the satellites at one point, which, for example, corresponds to the position of satellite 11. For this purpose, we will subtract the nominal angular distances u_d and/or u_m from the latitude arguments of the other satellites: $u_{11_p} = u_{11} = 10.043^\circ$, $u_{12_p} = u_{12} - u_d = 9.913^\circ$, $u_{21_p} = u_{21} - u_m = 10.085^\circ$, $u_{22_p} = u_{22} - u_d - u_m = 10.057^\circ$

, $u_{31_p} = u_{31} - 2u_m = 10.120^\circ$, and $u_{32_p} = u_{32} - u_d - 2u_m + 360^\circ = 9.847^\circ$. Let us find the value of the normalized base latitude argument u_{bp} with equal by magnitude maximum deviations from it. It can be easily seen that u_{bp} is equal to the arithmetic mean of the minimum and maximum values of u_p. In this case, the maximum value is u_{31_p}, and the minimum value is u_{32_p}; hence, $u_{bp} = 9.9835^\circ$. The maximum deviations are $\Delta u_{\max_0} = \pm 0.1365^\circ$. By knowing u_{bp} from the normalized base orbit, the latitude arguments of the base orbits of all satellites can be easily calculated. The nominal angular distances u_d and/or u_m should be added for this purpose: $u_{11_b} = u_{bp} = 9.9835^\circ$, $u_{12_b} = u_{bp} + u_d = 189.9835^\circ$, $u_{21_b} = u_{bp} + u_m = 129.9835^\circ$, $u_{22_b} = 309.9835^\circ$, $u_{31_b} = 249.9835^\circ$, and $u_{32_b} = 69.9835^\circ$. A similar procedure is also applied for the determination of the base values of the RAANs. By substituting $\Omega_d = 0$ and $\Omega_m = 120^\circ$, we get $\Omega_{11_b} = 0.0295^\circ$, $\Omega_{12_b} = 0.0295^\circ$, $\Omega_{21_b} = 120.0295^\circ$, $\Omega_{22_b} = 120.0295^\circ$, $\Omega_{31_b} = 240.0295^\circ$, and $\Omega_{32_b} = 240.0295^\circ$. The base value of the inclination is easier to find; it is the same for all satellites in the constellation and is $i_b = 52.99995^\circ$. Thus, the elements of all base orbits in the initial moment of time are found.

A similar algorithm is applied if the satellite planes are distributed on nonequal but known nominal angular distances from each other. The transition to the elements of the normalized base orbit is convenient because we can only deal with one value of each kind of element despite the number of satellites in the constellation. These parameters determine the positions of all base orbits.

8.1.3. The General Algorithm for the Maintenance Problem Solution

It can easily be seen that if the maximum deviations between the controlled elements of the orbits and the calculated values of the corresponding elements of the base orbits are less than half of the keeping accuracy of the constellation configuration, then the relative deviations of the controlled elements of an arbitrary pair of satellites will be less than the

given values of $\delta u, \delta\Omega, \delta i$, which is necessary according to the problem conditions. It is suggested that at the beginning of the station-keeping interval the constellation configuration meets the given constraints. The goal of the fulfillment of the manoeuvre is to ensure that these constraints will be met at the whole station-keeping interval.

Since the dependencies between the Ω, u and time are close to the linear nature for the near-circular orbits, then the dependency between the mutual deviations of these elements and time is also close to the linear nature. This suggests that, if at the beginning and at the end of the station-keeping interval the satellite-controlled parameters deviate from the corresponding parameters of their own base orbits by a value lower than the half of the necessary constellation station-keeping accuracy then this constraint is also fulfilled inside the station-keeping interval. If this constraint is fulfilled for all orbit elements of each satellite from the constellation then the mutual deviations by each of the controlled parameters of the orbits between two arbitrary satellites will not exceed the permitted values ($\delta u, \delta\Omega, \delta i$). For brevity, the vicinities of the base orbit elements $\left[-\frac{\delta u}{2}, \frac{\delta u}{2}\right]$, $\left[-\frac{\delta\Omega}{2}, \frac{\delta\Omega}{2}\right]$, and $\left[-\frac{\delta i}{2}, \frac{\delta i}{2}\right]$ we will denote as $\left[-\frac{\delta}{2}, \frac{\delta}{2}\right]$.

Thus, the control problem for the mutual deviations on all station-keeping intervals is equivalent to the simpler problem of the transfer of each satellite to the vicinity $\left[-\frac{\delta}{2}, \frac{\delta}{2}\right]$ of their base orbit at the end of the station-keeping interval.

This suggests using the following algorithm for the problem solution (Baranov and Baranov 2009, 48–54). A point in the space of elements of the normalized base orbit in the end of the station-keeping interval is chosen. The elements of the base orbits for each satellite in this moment are determined. The impulse parameters, which ensure the optimal (by the total delta-v expenditures) transfer to the vicinity $\left[-\frac{\delta}{2}, \frac{\delta}{2}\right]$ of the base orbit, are calculated for each satellite. The value of the problem functional, which corresponds to the given point of the space of elements of the normalized base orbit, is determined. The functional alteration in comparison with its value in the previous point is analyzed and the transfer

to the next point in the space of elements of the normalized base orbit is fulfilled.

The parameter searching process for the optimal base orbit at the end of the station-keeping interval (the transfer to the next point) can be fulfilled with, for example, the help of the numerical method and the polytope method (Himmelblau, 1975), or by a simple enumeration with a constant step, since the search area is relatively limited.

The procedure ends when the optimal position of the normalized base orbit is found at the end of the station-keeping interval. The manoeuvre calendar, which ensures satellite transfers to the vicinity of the base orbits that correspond to this point, will be the problem solution.

The supposition about the control sufficiency of the constellation status at the beginning and the end of station-keeping interval means that only the information about its orbit and elements of the base orbits during the initial manoeuvre parameter determination of each satellite are used and that it does not take the other satellite motion into account, which simplifies the problem considerably. The information about the motions within the constellation is used for the manoeuvre calendar update, if some of the constraints are not met, such as when the number of satellites performing the manoeuvres on one revolution exceeds the permitted one.

In order to find the initial point for the minimization process, the initial conditions of all satellites are adjusted at the end of the station-keeping interval and the values of the controlled parameters u, Ω, i are determined. By subtracting the nominal difference between the RAAN and latitude arguments, the parameters are adjusted to the vicinity of the corresponding values of one of the satellites (a similar procedure to find these values was described above). Then the mean arithmetical inclination values, the normalized latitude arguments, and the RAANs, which are used as the initial point for the minimization of the parameters of the normalized base orbit in space, are calculated.

The parameters of the normalized base orbit are optimal if the functional is minimal (Baranov and Golikov 1999, 482–485):

$$F = \sum_{j=1}^{n} \frac{\Delta V_j}{\Delta V_j^*} \tag{8-1}$$

where n = number of satellites, ΔV_j^* = impulse for j-th satellite, and ΔV_j = sum impulse, which is necessary for the transfer of this satellite to the vicinity of its base orbit. The minimization of such a functional equally

distributes fuel expenditures between the satellites. The functional minimization suggested by G.V. Mozhaev also ensures the uniform distribution of expenditures:

$$F = \sum_{j=1}^{n} \frac{1}{\Delta V_j^* - \Delta V_j}. \tag{8-2}$$

The application of this functional is especially effective when the satellites are low on fuel. Naturally, solutions with $\Delta V_j^* - \Delta V_j < 0$ are not considered. Other functionals can be used in which ΔV_j^* and ΔV_j are present, or the functional of the conventional type $F = \sum \Delta V_j$ can be minimized.

8.1.4. Manoeuvre Parameter Determination

During the manoeuvre parameter determination, it is supposed that just the transversal and the lateral components of impulses are used, as it is enough to only have these two variables in combination with the optimal angle of the impulse application to ensure the satellite transfer to the required point in space u, Ω, i with the help of a single manoeuvre.

Taking eqs. 1–12.d, 7-11, and 7-25 into account, the equation system for the determination of the impulse application point latitude argument u_j and its transversal and lateral components ΔV_{t_j} and ΔV_{z_j} will be as follows:

$$(-3U_j + 4\sin U_j)\frac{\Delta V_{t_j}}{V_0} = \Delta u_j, \tag{8-3a}$$

$$\cos u_j \frac{\Delta V_{z_j}}{V_0} = \Delta i_j, \tag{8-3b}$$

$$-4U_j \delta\Omega \frac{\Delta V_{t_j}}{V_0} - (U_j \delta\Omega \mathrm{tg} i \cos u_j - \frac{\sin u_j}{\sin i})\frac{\Delta V_{z_j}}{V_0} = \Delta\Omega_j, \tag{8-3c}$$

where $\Delta u_j, \Delta\Omega_j, \Delta i_j$ = deviations between the controlled parameters of *j-th* satellite, calculated at the end of the station-keeping interval and the

parameters of the base orbit in this point; u_j = impulse application point latitude argument; and U_j = angle between this point and the point at which the deviations are calculated.

The single-impulse scheme will be considered, since the decrease of the used impulse number is also important for the station-keeping process, as well as the problem functional minimization, and the corrected deviations and the impulses are usually small. However, if the keeping of the initial deviation by *i*, or even its increase, allows decreasing the deviation by Ω, and hence ΔV_j, then it will be optimal to use the two-impulse scheme for the transfer from the first paragraph of Chapter 7.

If the impulse magnitude is greater than the permitted one, then it is divided into several impulses applied on the different revolutions. If the impulse magnitude is less than the permitted one, then the impulse application point can be shifted to the revolution with the greater number; this will lead to a transversal component increase. If the constraint violation of one of the parameters happens before the minimum impulse application moment, then it is applied before the constraint violation and then the sliding mode may occur.

If only the inclination is corrected, the impulse is applied on the equator, but if only the RAAN is corrected and the satellite constellation is located on the considerable distance from the Earth (see the first paragraph of Chapter 7), then the impulse is applied in the orbit apex or vertex. These are the optimal points for the correction of the corresponding parameters. The number of the revolution, on which the impulse is applied, does not matter. If only the position along the orbit is corrected, then the impulse is applied at the apsidal point, which provides the maximum orbit eccentricity decrease. Herein the impulse is applied on the revolution, which is the nearest to beginning of the constellation configuration keeping interval.

If both deviations by the latitude argument and by the RAAN or the deviation by the inclination are corrected, then the impulse is applied in the orbit apex or vertex or on the equator of the closest to the beginning of station-keeping interval revolution. The point is chosen according to the capability of the orbit eccentricity decreasing in this particular case.

If during the constellation configuration keeping process or during its initialization the orbit of one of the satellites obtains a considerably high eccentricity value, it may need to be corrected. In this case, the two impulses should be used in order to optimally correct all orbit elements. Firstly, the impulse components and the optimal angle of the orbit plane rotation are found from Eq. 8-3, and then the parameters of the two impulses are determined with the help of the equations for the optimal

transfer between the close near-circular orbits. The deviation of the semimajor axes Δa used in these equations can be evaluated as follows:

$$\Delta a = 2a\frac{\Delta V_{t_j}}{V_0}, \tag{8-4}$$

and the angle of the needed orbit rotation can be determined by

$$\Delta\gamma = \frac{\Delta V_{z_j}}{V_0}, \tag{8-5}$$

where $\Delta V_{t_j}, \Delta V_{z_j}$ = impulse components, which was determined using Eq. 8-3.

8.1.5. Iterative Procedure Application

With the help of iterative procedure (which is similar to the procedure from the first chapter), the impulse parameter update is fulfilled in order to adjust the base orbit parameters with the necessary accuracy. Each satellite is considered separately at this stage.

The target orbit used in the iterative procedure coincides with the base orbit on the first iteration. After the determination (in the linear notation) of the parameters of the impulses, which shape the target orbit, the numerical (L'vov and Stepanyantz 2000, 9–14) or analytical numerical (Golikov 1990; 2008) propagation of the satellite motion for the accurate determination of the parameters of almost any shaped orbit at the end of the station-keeping interval is fulfilled. (Due to the large number of the satellites which can be in the constellation, the long station-keeping intervals, and the multiple prognosis application, the use of the numerical analytical prognosis is, undoubtedly, preferable for this problem). The deviations between these parameters and those of the base orbit are determined; if these deviations are greater than the acceptable ones, then the target orbit parameters are altered by the magnitudes of the calculated deviations. Then the impulse parameters, which should shape the new target orbit, are calculated, and then the deviations between the shaped orbit and the base orbit are calculated, etc. The process continues until the deviations will not be lower by K times the needed accuracy of the constellation configuration keeping (usually K = 10). This procedure, which allows eliminating the inaccuracies of the linear approach during the impulse determination, is repeated for every satellite from the constellation.

Despite the small impulse magnitude, the use of iterative procedures is necessary, since station-keeping intervals may be very long, and small errors in the impulse magnitude may lead to considerable deviations in the destination point.

8.1.6. Target Point Selection

The choice of the base orbit as the target point is the simplest one and ensures fulfillment of the terminal condition. However, it is often preferable to use the closest boundary to the permitted diapason as the target point, and not its middle part (Baranov and Baranov 2009, 48–54). This decreases the ΔV expenditures and increases the corrected orbit element in the permitted diapason duration stay, because this element can change from one boundary to another through the whole permitted diapason, but not half of it.

For example, let us consider the latitude argument alteration for the 4-satellite constellation. Figure 8-1 shows the normalized latitude arguments in the initial station-keeping moment $u_{1_p}, u_{2_p}, u_{3_p}, u_{4_p}$ and in the final moment $u_{1_{pf}}, u_{2_{pf}}, u_{3_{pf}}, u_{4_{pf}}$ (if the correction was not fulfilled). The point u_{bp} corresponds to the latitude argument of the normalized base orbit in the initial moment, and the point u_{bp_f} corresponds to the selected value of the base orbit latitude argument in the final moment of time. The permitted swath (the permitted diapason) is restricted by dashed-and-dotted lines, which intersect the points d_0 and d_f, as well as b_0 and b_f ($d_0 - u_{bp} = u_{bp} - b_0 = d_f - u_{bp_f} = u_{bp_f} - b_f = 0.5\delta u$).

The satellite latitude argument alteration by time and without their motion correction is shown with dashed lines. The latitude argument alteration after the manoeuvre fulfillment is shown with solid lines. As can be seen, the closest boundary of the permitted diapason was chosen as the target point, and not the base orbit latitude argument u_{bp_f}.

According to Eq. 8-3a, the expenditures on the correction of the deviation by the latitude argument *u* are proportional to the magnitude of this deviation. Hence, the expenditures needed for the correction of all deviations by *u* are proportional to the sum of the distances from the points $u_{1_{pf}}, u_{2_{pf}}, u_{3_{pf}}, u_{4_{pf}}$ to the target points.

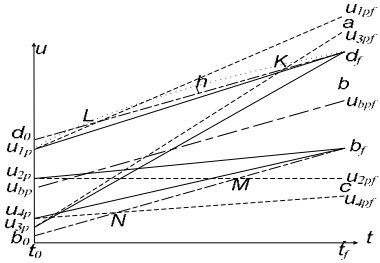

Figure 8-1. Satellite latitude argument alteration on the station-keeping interval. The alteration of latitude arguments before manoeuvre fulfillment are depicted by dashed lines, and the alteration of latitude arguments after manoeuvre fulfillment are depicted by solid lines.

We will denote that $u_{1_{pf}} - u_{3_{pf}} = a, u_{3_{pf}} - u_{2_{pf}} = b, u_{2_{pf}} - u_{4_{pf}} = c$. If the latitude argument of the normalized base orbit $u_{bp_f} \in [u_{3_{pf}}, u_{2_{pf}}]$ is the target point for all the satellites, then the sum of the distances to this point $\sum \left| u_{ip_f} - u_{bp_f} \right|$ is equal to $a + 2b + c$ and does not depend on the location of the point u_{bp_f} on the interval $(u_{3_{pf}}, u_{2_{pf}})$. This is a very important peculiarity, which can be used effectively. For example, if one of the boundary points, $u_{3_{pf}}$ or $u_{2_{pf}}$, is taken as u_{bp_f}, then the corresponding satellite will not have to manoeuvre; hence, the total number of used impulses decreases without the alteration of the manoeuvre total delta-v. The interval for the search for the optimal value of u_{bp_f}, which is necessary to search for in the diapason $[u_{3_{pf}}, u_{2_{pf}}]$, also considerably decreases.

If the point u_{bp_f} is shifted by *x* from the interval $(u_{3_{pf}}, u_{2_{pf}})$, but still belongs to the interval $(u_{4_{pf}}, u_{1_{pf}})$, then the sum will be $a + 2b + c + 2x$. If the point u_{bp_f} is chosen in a way that neither point $u_{3_{pf}}$ nor point $u_{2_{pf}}$ belong to the interval (d_f, b_f), and the target points are the nearest to the boundaries d_f and b_f (like in Fig. 8-1), then the sum will be $a + 2b + c - 2\delta u$, and it still does not depend on the concrete location of

point u_{bp_f}. Thus, the usage of the boundaries d_f and b_f as target points helps to decrease the ΔV by a magnitude of $\frac{2\delta u}{3U}V_0$. The duration of the stay in the permitted diapason after the station-keeping interval (since drift will occur in the direction set by the correction, i.e., from the closest boundary to the permitted diapason to the furthest) also increase. The disadvantage of the boundary usage as the target point is the increase in the probability of crossing the limits of the permitted diapason inside the station-keeping interval. This is mostly probable, when the solid line is close to the dashed-and-dotted line, i.e., when the initial and the final points lie on one side from the line $u_{bp}u_{bp_f}$. These are the lines $u_{1_p}d_f$ and $u_{4_p}b_f$ in Figure 8-1. Let us draw the real alteration of the latitude argument of the first satellite with a dotted line. As can be seen, inside the station-keeping interval the satellite gets out of the permitted diapason by the maximum value *h*. In order to eliminate this violation, the target point can be moved by the corresponding value inside the permitted diapason. The determination of the boundary violation of the permitted diapason and the shift of the target point are carried out during the process of the iterative fulfillment of the terminal conditions. It is worth mentioning, that, by benefiting from the number of impulses (when one of the satellites does not manoeuvre), we lose the duration of the station-keeping because the satellite will be outside of the given diapason after the end of the station-keeping interval. But, if the satellite is low on fuel and it is undesirable to manoeuvre, then the manoeuvre-avoiding option becomes the key.

It can also be shown that, if the manoeuvre number is uneven, then it is optimal to bring the latitude arguments of all satellites to the vicinity of the latitude argument of the "inner" satellite (the big and small values of the latitude arguments have an equal number of satellites). If we drop the fourth satellite in Figure 8-1 (we leave three satellites in the constellation), then the latitude arguments of the first and the second satellites should be brought to the vicinity of point $u_{3_{pf}}$.

Sometimes it is suggested to choose one of the satellites and synchronize the motion of the other satellites in the constellation to it (to choose "the leader"). In this case, all maintained parameters of the other satellite orbits accord with the leader-satellite orbit parameters. But, as the aforementioned example shows, it is optimal to bring each orbit parameter of the satellites to the "inner" value of this parameter. The "inner" values

of the different parameters may belong to various satellites. Thus, it is optimal to choose the fictive satellite as the leader with the maintained orbit parameters as the "inner" parameters relating to various satellites de facto. This is a simplified approach, but it shows the possible nonoptimality of the concrete satellite choice as the leader-satellite. The parameters of such a fictive satellite may be used as the initial guess for the numerical search of the optimal values, to which it is necessary to bring all the satellite parameters. It is worth remembering that the values of all parameters are calculated at the end of the station-keeping interval, and not at its beginning. And that this is the moment when the parameters of the fictive satellite are determined.

8.1.7. Manoeuvring Interval Determination

Figure 8-1 reveals the speed of the deviation correction using the latitude argument for the chosen position of the normalized base orbit at the end of the station-keeping interval u_{bp_f}. The extreme points of the manoeuvre are the intersection points of the dashed and dash-and-dot lines (point *L*, point *K*, point *M*, and point *N*). The closest boundary of the permitted diapason cannot be used as the target point during the manoeuvre at these moments of time, because the solid line will coincide with the boundary dash-and-dot line, and the probability of leaving the permitted diapason will be high.

The orbit inclinations *i* practically do not alter on the whole station-keeping interval. It is necessary to quickly bring it to some average value (which will also decrease the absolute values of the deviations by *i*) in order to prevent the secular drifts by Ω. For some satellites, it is worth refraining from correcting the inclination, if the keeping of the initial deviation by *i* will decrease the initial deviation by Ω.

Figure 8-2 shows the possible alteration of Ω for each of four considered earlier satellites. The alteration of Ω after the latitude argument and inclination corrections is plotted with dashed lines. It is obvious that, for the third and the fourth satellites with the chosen value of Ω_{bp_f}, the correction Ω may not be conducted, since the values of $\Omega_{3_{pf}}$ and $\Omega_{4_{pf}}$ occur in the permitted diapason (d_f, b_f).

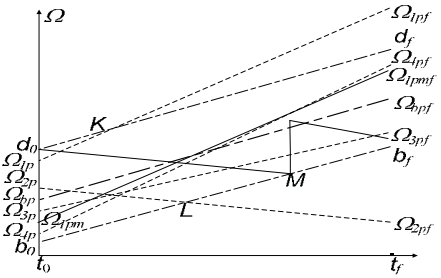

Figure 8-2. Alteration of satellite RAANs on the station-keeping interval. The alteration of RAANs is shown as a dashed line (before manoeuvres) and a solid line (after manoeuvres).

For the first satellite, the dashed line $\Omega_{1_p}\Omega_{1_{pf}}$ intersects the boundary of the permitted diapason (the dash-and-dot line $d_0 d_f$); therefore, it is necessary to alter Ω before the critical point *K*. It is necessary to do this in the initial moment by combining the corrections of the other deviations, which lead to the decrease of the impulse number, and manoeuvre ΔV. The change of Ω has a "leaping nature", and the new value after the impulse will be $\Omega_{1_{pm}}$, and the line $\Omega_{1_{pm}}\Omega_{1_{pmf}}$, which belongs to the permitted area, corresponds to the later alteration. The point inside the permitted diapason (d_f, b_f) was chosen as the target in order to prevent the constraint violation immediately after the station-keeping interval ends.

The situation stays the same for the second satellite, but the alteration of Ω in the initial moment is limited by the value $d_0 - \Omega_{2_p}$, which is why it is necessary to conduct the new correction of Ω in the point *M*.

The impulse parameter search procedure is repeated for every satellite, until all satellites from the constellation will not be able to have their parameters brought to their base orbits.

The near-optimal solution can be obtained with the help of numerical methods. However, it is practically impossible to account for the aforementioned physically understandable options for the ΔV decrease and the number of impulses while using numerical methods (as a rule, the simplex method should be used [Bernussou, Brousse, Dufour, Foliard et al. 1997; Bernussou, Dufour, and Lasserre 1996, 169–174; Fedorov, Malyshev 2001, 45–46), since the deviations are checked at equally distant

moments of time and not in moments when the actual station-keeping constraint violations occur.

After determining the full manoeuvre calendar, the constraint fulfillment is checked for all the satellites from the constellation inside the station-keeping interval. The first priority is to control the constraint fulfillment for the total number of manoeuvres during the given manoeuvring interval. If the manoeuvre number exceeds the given value, the exceeding part is transferred to a later time. The first priority is to perform the manoeuvres without the transversal impulse component (because they can be conducted on any revolution), while the second priority is performing satellite manoeuvres with considerable fuel consumption and impulses close to the minimum possible magnitudes. When the manoeuvre calendar is formed, the combined integration of the equations of motion for all the satellites is conducted taking the calculated impulses into account. The maximum deviations of the controlled parameters inside the station-keeping interval are estimated. If the assumption about the linear dependency of the deviations is not accurate enough, and the corrected orbit elements exceed the permitted ones for some satellite deviations, then the target points for these elements are shifted or additional impulses, which decrease these deviations, are calculated.

The value of the functional F is determined for the fully prepared manoeuvre calendar and the decision about stopping the problem solution is made, or the new values of the normalized base orbit elements are adjusted, and then the manoeuvre calendar determination procedure, which would correspond to this orbit, is repeated.

8.1.8. Examples

Table 8-2 shows the results of the manoeuvre calendar determination (Baranov and Baranov 2009, 48–54) for the satellite constellation; the initial conditions of which can be found in Table 8-1.

The configuration of the constellation was maintained for an interval of six months; the deviations of the controlled parameters should not exceed 0.1°. The sum keeping expenditures are $\Delta V = 2.485$ m/s.

As can be seen from the table, the only deviation is corrected by the latitude argument; the deviations of i and Ω stay in the permitted diapason even without the corrected impulse application. The position of the base orbit at the end of the keeping interval was chosen so that satellite 31 was not manoeuvring at all.

Table 8-2

Satellite	Rev	u_i deg	ΔV_t m/s	ΔV_z m/s
11	3	330.4	0.476	0.0
12	2	150.5	0.528	0.0
21	4	151.7	-0.418	0.0
22	1	331.2	-0.801	0.0
31	6	35.7	0.0	0.0
32	5	330.5	-0.261	0.0

The manoeuvre calendar determination method considered in this paragraph ensures the satellite station-keeping for the time interval from several days to twenty-four months. The problem peculiarities are taken into account during the calculation, which allows using the minimal manoeuvre number and performing them during optimal moments of time. The method is primarily suitable for the calculation of the satellite constellation station-keeping manoeuvres at altitudes of 800 to 1,500 km, but the deviation by the latitude argument correction strategy is also applicable for satellite constellations at altitudes of approximately 20,000 km, since it has a universal nature.

The algorithm presented by Y.P. Ulybyshev can be used for the manoeuvre parameter determination of the satellite constellation configuration relative station-keeping at high altitudes, when, for example, the solar and lunar attractions are considerable (Ulybyshev 1998, 109–115). In the works by G.V. Mozhaev (Mozhaev 2001, 634–647) and R.F. Murtasin (Murtazin 1998, 173–182), problems similar to the one investigated in this paragraph are considered. It was supposed in these works that the manoeuvres are performed in the initial (Mozhaev 2001, 634–647) or the initial and final moments of time (Murtazin 1998, 173–182). The constellation status was not controlled in the interim moments. A comparison between the relative and the absolute station-keeping strategies was conducted using concrete satellite constellations as examples. It was shown that the relative station-keeping needs fewer manoeuvres and less total delta-v expenditures.

8.2. Absolute Station-Keeping for a Satellite Constellation

8.2.1. General Solution Scheme

Despite the costs of absolute station-keeping, it is used far more often in real satellite constellations, where the station-keeping motion of each

satellite is accorded with some programmed motion. This allows the manoeuvres of each satellite to be estimated independently from the other satellite motion in the constellation. During the station-keeping, the satellite parameters must belong to the given diapason via each of the controlled orbit elements (which must be within the given dimensions). When the satellite reaches one of the boundaries of the box during the process of its evolution, it is transferred to the opposite boundary by the manoeuvres. The periodicities of the transfer by various elements may significantly differ. For example, in low earth orbits we have to increase the altitude far more often than correct the other elements. When we correct an orbit element which has reached its limit, this does not mean we do not have to correct the other maintained orbit elements. It is optimal that, in this moment, the other orbit elements are corrected proportionally to their sum alterations on the whole station-keeping interval. The algorithms described in the previous chapters may be used for the manoeuvre determination close to both the impulse and long-duration manoeuvres. As a rule, they are the transfer manoeuvres described in Chapters 2 and 6.

8.2.2. Maintenance of the Semimajor Axis and Inclination

Let us consider the problem of the spacecraft orbit semimajor axis and inclination keeping (Baranov and Wang 2015, 68-83) in a two given vicinities—$[-\delta a, \delta a]$, $[-\delta i, \delta i]$—with their nominal values (a_0, i_0) at the given time interval T_k (e.g. one year).

Three stages can be distinguished within the solution to spacecraft operational orbit station-keeping problem: the parameter selection of the "rational" orbit on which the spacecraft will start functioning; the determination of the moment of exceeding the constraints by the operational orbit parameters; and the parameter determination of the manoeuvres that transfer the spacecraft to "rational" orbit.

We will call this a "rational" orbit, which stays for the longest time within the permitted vicinity of the nominal orbit during the evolution process. In order to determine the parameters of the rational orbit, it is necessary to investigate the evolution of the maintained orbit. The figures in section 8.2.3 show the dependencies between the alterations of the maintained elements and eccentricity, as well as the time required for various orbits. All orbit elements suffer from short period alterations, and the eccentricity and the inclination also periodically alter within sufficiently greater magnitudes. These are several times smaller than the station-keeping interval. The monotonous decrease of the semimajor axis

takes place for orbits sensitive to atmospheric drag; a continuous decrease of the inclination takes place for sun-synchronous orbits.

If there are no strict demands for the accuracy of the given orbit keeping, there is no need "to fight" with the short-period perturbations. If there are no severe constraints on the given orbit station-keeping accuracy, then there is no sense in reacting to the short period perturbations. However, they need to be accounted for when choosing the "rational" orbit in order to not cross the upper boundary of the permitted diapason in the short time interval. For example, it is desirable to put the "rational" orbit semimajor axis $a_{rational}$ as the maximum value of the maintained orbit semimajor axis minus the value of the doubled magnitude of the short-period alteration of the semimajor axis Δa_{k_p} (the shift) plus several per cent from this value, and minus Δa_m = the methodical accuracy of the orbit elevation problem solution.

$$a_{rational} = a_0 + \delta a - 2(1 + 0.05)\Delta a_{k_p} - \Delta a_m. \tag{8-6}$$

Thus, in the initial moment the "rational" orbit semimajor axis is close to the upper permitted boundary, but this is slightly lower for the prevention of the constraint on the maximum value violation of the operational orbit semimajor axis due to the short-period perturbations. The shift is approximately 250 m for the orbits with the altitudes from 270 to 1,100 km. The similar shift values are 0.001° for the inclination and 0.0005 for the eccentricity. Subsequently, the orbit semimajor axis will reach its lower boundary by decreasing under the atmospheric drag influence.

In the program which determines the station-keeping manoeuvre parameters, the numerical integration of the spacecraft equations of motion is fulfilled on the first stage with the use of the exit function, which controls the constraint on the semimajor axis magnitude in the ascending node of the orbit; the inclination value is also controlled and the short-period oscillations of both element magnitudes are determined. It is preferable to have the orbit parameters close to the "rational" orbit parameters in the initial moment of time. For example, when the constraint on the semimajor axis lower value is reached, the exit out of the integration occurs. The parameters of the manoeuvres, which alter the semimajor axis, are evaluated in order to return its value to that of the "rational" orbit semimajor axis. It is optimal to correct the inclination in

this moment proportionally to its sum alteration on the whole station-keeping interval.

Let us assume that after the time ΔT from the beginning of the station-keeping (or from the previous elevation) the orbit elevation necessity occurred again. The inclination is changed by the angle Δi for the time ΔT. The time T remains before the end of the station-keeping interval. It can be assumed that the inclination will be more altered by the angle $\Delta i^* = \Delta i \cdot T / \Delta T$ for the time left. The total inclination alteration will be $\Delta i^* + \Delta i$ by the end of the station-keeping interval. Let us put Δi_m as the maximum permitted inclination alteration on the station-keeping interval $T + \Delta T$ ($\Delta i_m = i_0 \pm \delta i - i_n$, i_n = inclination in the beginning of the interval ΔT; the sign of δi is chosen so that the signs of Δi and Δi_m will coincide). Thus, the exceedance, which is necessary to correct the interval $T + \Delta T$, is $\Delta i_k = \Delta i^* + \Delta i - \Delta i_m$. The exceedance part, which needs to be combined with the altitude elevation, is $\Delta i_k \cdot \Delta T / (T + \Delta T)$. Thus, in this moment, it is essential to correct the deviation of $\Delta i_{\Delta T}$ (not Δi) along with the altitude increase:

$$\Delta i_{\Delta T} = \Delta i - \Delta i_m \frac{\Delta T}{T + \Delta T}. \tag{8-7}$$

If

$$\left|\Delta i\right| < \left|\Delta i_m\right| \frac{\Delta T}{T + \Delta T}, \tag{8-8}$$

then the inclination may not be corrected. When condition 8-8 is not fulfilled and the semimajor axis correction needs to be combined with the inclination correction, it is essential to perform the manoeuvres in the vicinity of the equator.

When the inclination is not corrected and only the semimajor axis increase needs to be fulfilled (which may be corrected at any point of orbit), its eccentricity may be decreased by placing the altitude increase manoeuvre in the orbit apocenter.

The manoeuvring always starts on the revolution before the one where one of the parameters goes out of the boundaries of the permitted diapason.

After the manoeuvre calculation and modeling, the numerical analytical prognosis for the newly formed orbit will be fulfilled again and the next moment of the operational orbit parameter boundary violation will then be found. The process ends when the given time of the station-keeping interval ending is reached.

One variant of orbit absolute keeping with the help of low-thrust engines will be considered in paragraph 8.2.5.

8.2.3. Orbit Evolution Features

The real orbit element alteration needs to be found in order to select the correct station-keeping strategy. With the help of the numerical analytical integration of the equations of motion and "THEONA" (Golikov 1990; Golikov 2008), the dependencies of the element alteration of the various orbits were obtained. Figures 8-3–8-11 show graphs of the obtained semimajor axes alterations, as well as the eccentricity and the inclination for orbits with an initial altitude of 700 km, which have the initial inclinations 51.6°, 63.8°, and 98° for the following time intervals: 3 revolutions, one week, and one year.

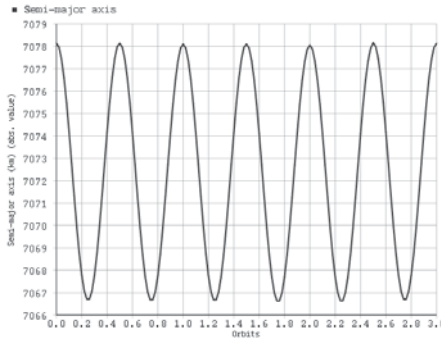

Short-period inequalities for 3 revolutions

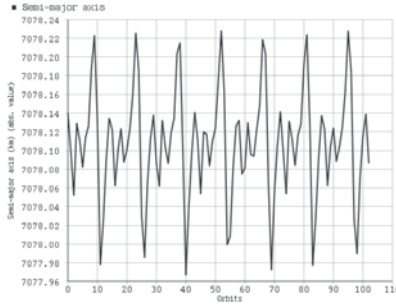

Short-period inequalities for 1 week

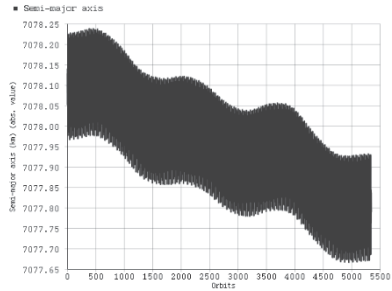

Short-period inequalities for 1 year

Figure 8-3. Orbit semimajor axis evolution (Inclination 51.6°)

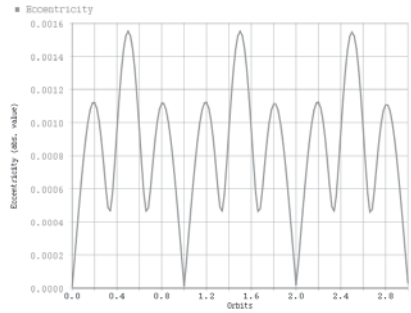

Short-period inequalities for 3 revolutions

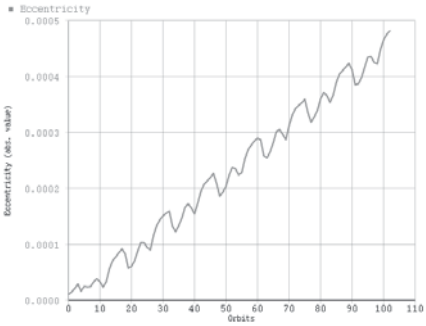

Short-period inequalities for 1 week

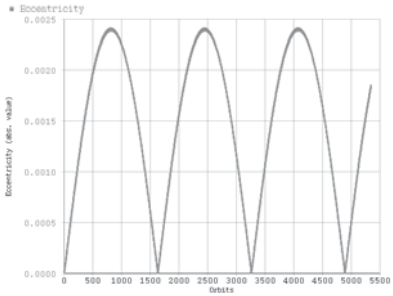

Short-period inequalities for 1 year

Figure 8-4. Orbit eccentricity evolution (Inclination 51.6°)

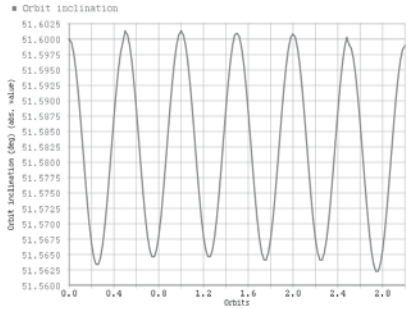

Short-period inequalities for 3 revolutions

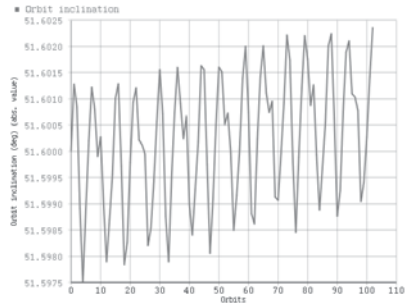

Short-period inequalities for 1 week

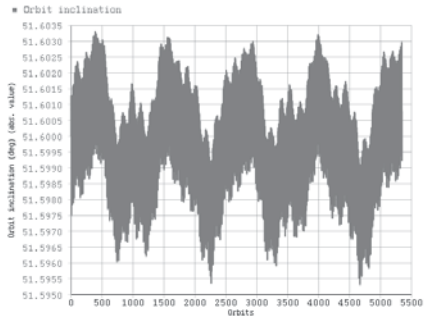

Short-period inequalities for 1 year

Figure 8-5. Orbit inclination evolution (Inclination 51.6°)

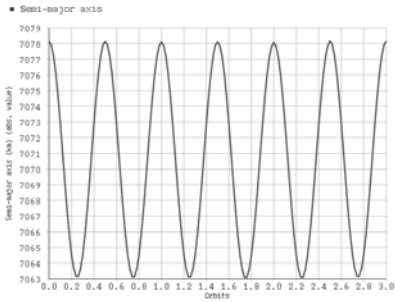

Short-period inequalities for 3 revolutions

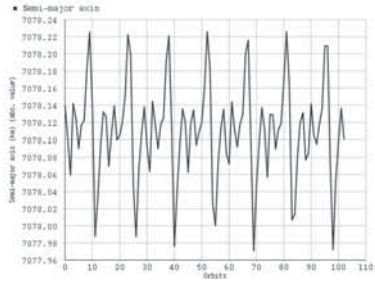

Short-period inequalities for 1 week

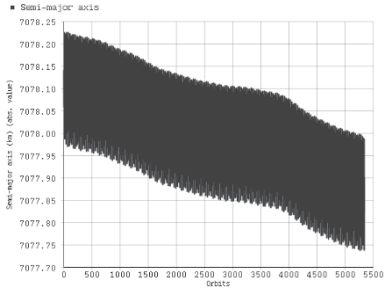

Short-period inequalities for 1 year

Figure 8-6. Orbit semimajor axis evolution (Inclination 63.8°)

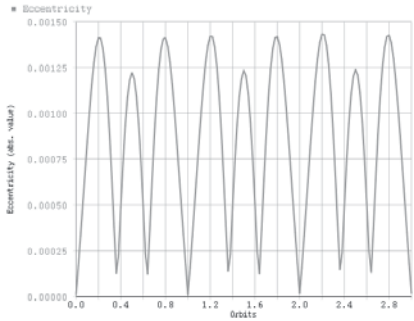

Short-period inequalities for 3 revolutions

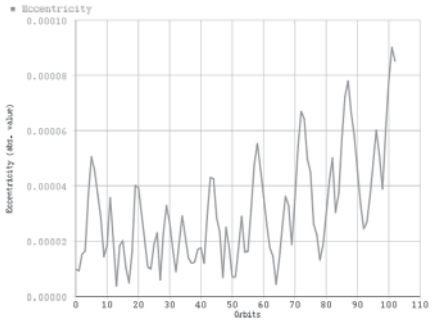

Short-period inequalities for 1 week

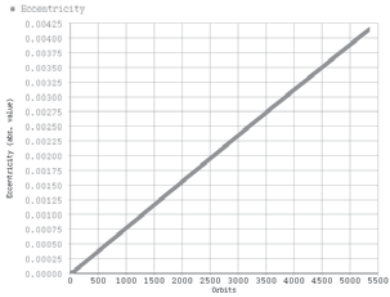

Short-period inequalities for 1 year

Figure 8-7. Orbit eccentricity evolution (Inclination 63.8°)

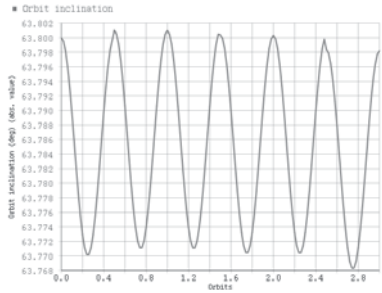

Short-period inequalities for 3 revolutions

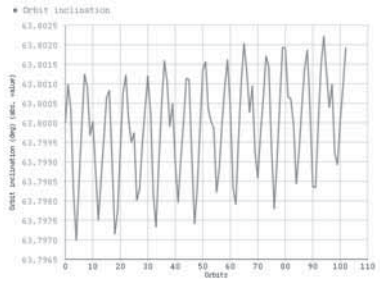

Short-period inequalities for 1 week

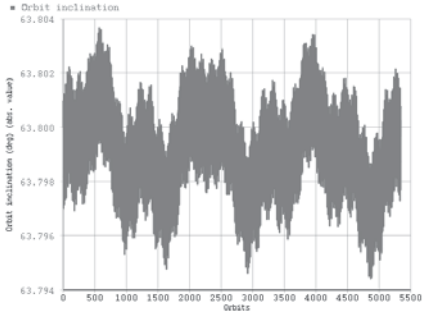

Short-period inequalities for 1 year

Figure 8-8. Orbit inclination evolution (Inclination 63.8°)

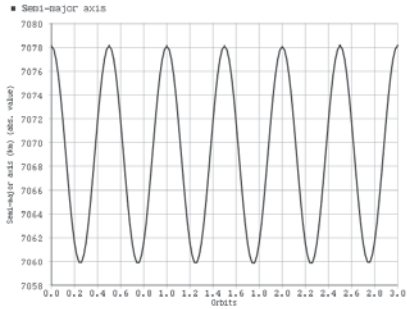

Short-period inequalities for 3 revolutions

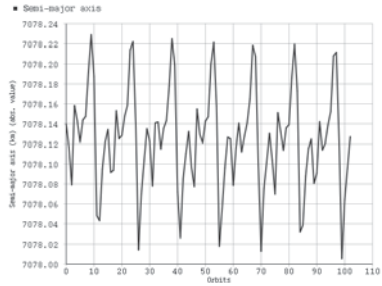

Short-period inequalities for 1 week

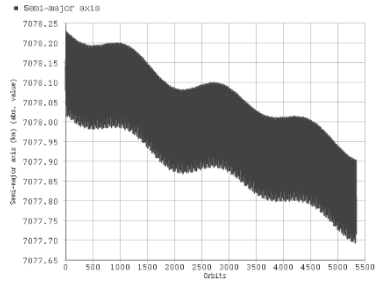

Short-period inequalities for 1 year

Figure 8-9. Orbit semimajor axis evolution (Inclination 98°)

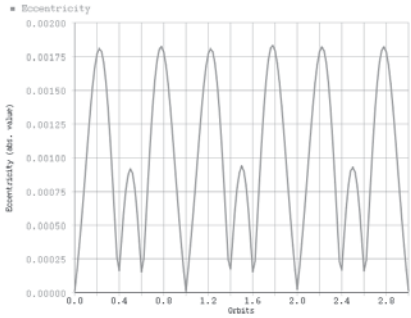

Short-period inequalities for 3 revolutions

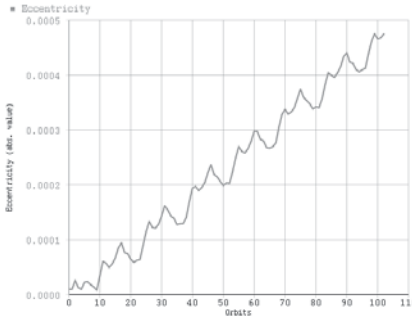

Short-period inequalities for 1 week

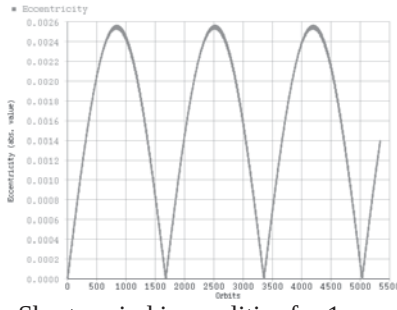

Short-period inequalities for 1 year

Figure 8-10. Orbit eccentricity evolution (Inclination 98°)

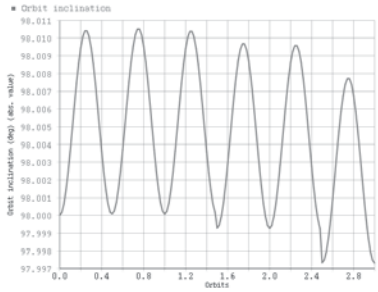

Short-period inequalities for 3 revolutions

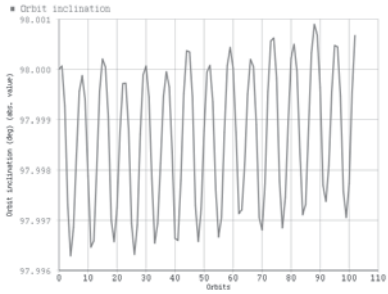

Short-period inequalities for 1 week

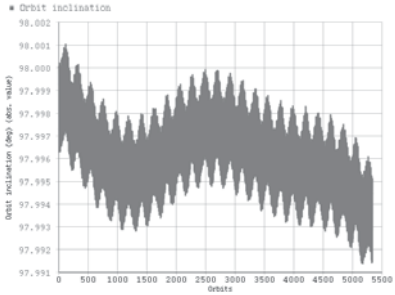

Short-period inequalities for 1 year

Figure 8-11. Orbit inclination evolution (Inclination 98°)

The spacecraft orbit elements change under the influence of the gravity field, the Earth's atmospheric drag, and the Sun and Moon's gravity fields.

8.2.4. Analytical Orbit Propagation

In a number of cases, there is a necessity for the simplest analytical assessment of the orbit element alteration. These questions were sufficiently investigated in works by various authors.

The spacecraft orbit altitude constantly decreases due to the atmospheric drag. The altitude alteration *h* can be estimated with the help of the approximate equation for the small eccentricity value orbits (Vallado, 2007):

$$\dot{h} = -C_x S \rho \sqrt{\mu a} / m_{sc}, \tag{8-7}$$

where C_x = drag coefficient; S = spacecraft cross-section, m^2; m_{sc} = spacecraft mass, kg; ρ = atmospheric density on spacecraft flight altitude, $\mathrm{kg/m}^3$; a = orbit semimajor axis, km; μ = 398,603; and the Earth's gravitation constant, $\mathrm{km}^3/\mathrm{s}^2$. Let us consider the calculation example of *h* with the help of the aforementioned equation with the use of the atmospheric density model NRLMSISE-00 for the following inputs: S = 2.5 m^2, a = 6,890.396 km. The current value of the solar activity index $F_{10,7}$ coincides with the average value and is equal to 125 units; the average value of the geomagnetic index is a_p = 12.0. By neglecting the dependency between the atmospheric density and the time and latitude, one can calculate the atmospheric density (Baranov and Wang 2015, 68–83) on the altitude h = 512,396 km, which turns out to be equal to $\rho = 2.18 \cdot 10^{-13}$ $\mathrm{kg/m}^3$, and $\dot{h} = -1.53 \cdot 10^{-4}$ m/s = –13.2 m/day.

The Sun always stays on one side of the sun-synchronous orbit and its attraction leads to the orbital plane position alteration, i.e., it changes the orbit inclination. In case of sun-synchronous orbits. the expression for the secular perturbations of the inclination *i* can be found by (Cour-Palais and Kessler 1978, 2637–2646):

$$\frac{di}{dt} = \frac{3n_s^2}{16n} \sin i (1 + \cos i_s)^2 \sin(2u_s - 2\Omega) \tag{8-8}$$

where, i_s = solar declination; u_s = solar right ascension; n_s = solar mean angular velocity; Ω = RAAN; and n = spacecraft mean motion. If the solar local time is 21:00, then $2u_s - 2\Omega = 90^\circ$ and, for a sun-synchronous

orbit with latitude $h = 512.396$ km, $di/dt = -0.04^\circ$/year. The orbit inclination decreases due to the gravitational attraction of the Sun, which leads to the RAAN precession rate alteration:

$$\frac{d\Omega}{dt} = -\frac{3}{2} J_2 n \left(\frac{R_e}{a} \right)^2 \cos i, \tag{8-9}$$

where J_2 = the coefficient for the second zonal harmonic in the geopotential expansion and R_e = the Earth's equatorial radius. In combination with the initial errors, this leads to a considerable deviation between the solar local time of the ascending node passage and the estimated active spacecraft lifetime.

8.2.5. Sun-Synchronous Orbit Maintenance for a Microsatellite

In this sun-synchronous orbit station-keeping problem, the microsatellite needs to be in the diapason with altitudes of 510–512] km. The solar local time (SLT) on the latitude 40° must be within the range of 10 or 11 hours. The station-keeping is fulfilled with a seven year long interval. The manoeuvres are fulfilled with the fixed orientation of the thrust engines in the orbital coordinate frame.

During the manoeuvre calculations, it is assumed that the orbit plane is not changed by the manoeuvres and the microsatellite in a relatively large diapason for SLT is ensured by the choice of an optimal initial inclination orbit.

The problem solution process consists of the successive repetition of two stages.

The numerical analytical propagation for the satellite motion was fulfilled in the first stage. The influence of the gravity field 8*8 and the dynamic atmospheric model were taken into account. During the prognosis process, the orbit altitude and the SLT were controlled. At the moment when the lower boundary reaches the permitted diapason in the ascending node by its altitude, the manoeuvre determination problem was used to determine the manoeuvre parameters, which transfer the satellite to the "rational" orbit. The iterative procedure from Chapter 1 was used for the calculations since a small orbit altitude alteration is needed, which can be achieved by using the manoeuvres in one revolution.

The calculation results for the orbit station-keeping manoeuvres are listed below (see Tables 8-3–8-9).

Table 8-3 shows the initial orbit elements, the minimum and the maximum orbit altitudes, the pericenter argument, the inclination and the RAAN of the orbit, the revolution number, the latitude argument, the ballistic coefficient, and the initial condition's date and time.

Table 8-4 shows the characteristics of the microsatellite and its engines: thrust N, specific impulse, microsatellite mass kg, minimal time between the ending of one manoeuvre and beginning of another s, and minimal and maximum manoeuvre durations s.

Table 8-3

Orbital elements	Initial orbit
Hmin km	511.80
Hmax km	511.83
Uprg deg	0.1340
i deg	97.5473
gOMG deg	17.1900
Nrev	1
Ulat deg	0.1000
S_{ball}	0.78330000E-02
Date	2012.05.01
Time	42,118.065

Table 8-4

Thrust	Specific Impulse	Weight	ΔT	Tmin	Tmax
0.20	2,060.0	300.0	600.0	0.25	3,600.0

Table 8-5 shows the solution parameters: the sum impulse including all manoeuvres, the total number of the orbit elevations, and the total number of performed manoeuvres.

Table 8-6 shows the number for each manoeuvre; the revolution; and the latitude arguments of its beginning and ending; the yaw and the pitch, which form the thrust vector orientation; and the equivalent impulse magnitude.

Table 8-5

d*V*	Nlift	Nman
36.60	38.0	76.0

Table 8-6

Nman	REVbg	U_bg	REVfn	U_fn	Yaw	dVi
1	1,082	9.28	1,082	55.27	0.00 0.00	0.485
2	1,082	189.28	1,082	235.27	0.00 0.00	0.485
3	2,223	58.74	2,223	103.37	0.00 0.00	0.470
4	2,223	238.74	2,223	283.37	0.00 0.00	0.470
5	2,861	162.50	2,861	213.34	0.00 0.00	0.536
6	2,861	342.50	2,862	33.34	0.00 0.00	0.536
…	…	…	…	…	…	…
71	32,809	27.04	32,809	72.23	0.00 0.00	0.476
72	32,809	207.04	32,809	252.23	0.00 0.00	0.476
73	35,454	23.57	35,454	68.55	0.00 0.00	0.474
74	35,454	203.57	35,454	248.55	0.00 0.00	0.474
75	37,717	76.85	37,717	121.71	0.00 0.00	0.473
76	37,717	256.85	37,717	301.71	0.00 0.00	0.473

Table 8-7 shows the dates and times of the start and end of each manoeuvre, the duration in minutes, and the values of the microsatellite mass after the manoeuvres.

Table 8-7

Nman	DATE_bg	TIME_bg	DATE_fn	TIME_fn	dT	Mass
1	2012.07.11	74,827.5	2012.07.11	80,031.6	12.07	299.93
2	2012.07.11	83,547.6	2012.07.11	84,756.3	12.15	299.86
3	2012.09.24	101,629.0	2012.09.24	102,810.0	11.70	299.79
4	2012.09.24	110,347.0	2012.09.24	111,535.0	11.80	299.72
5	2012.11.05	102,743.0	2012.11.05	104,107.0	13.40	299.64
6	2012.11.05	111,508.0	2012.11.05	112,830.0	13.36	299.57
…	…	…	…	…	…	…
71	2018.03.30	90,113.4	2018.03.30	91,306.9	11.89	295.02
72	2018.03.30	94,835.0	2018.03.30	100,029.4	11.91	294.95
73	2018.09.20	104,313.0	2018.09.20	105,501.0	11.81	294.88
74	2018.09.20	113,033.0	2018.09.20	114,225.0	11.87	294.81
75	2019.02.16	92,030.4	2019.02.16	93,217.8	11.79	294.74
76	2019.02.16	100,750.0	2019.02.16	101,940.0	11.83	294.67

Table 8-8 shows the distribution of the total delta-v expenditures versus years. Their inequality is connected with different solar activity levels.

Table 8-9 provides information about the SLT for the beginning and ending station-keeping, as well as the orbit elevations

Table 8-8

Year	1	2	3	4	5	6	7
$dV_{\Sigma i}$	6.77	8.80	7.68	5.73	2.84	2.85	1.89

Table 8-9

Nrev	DATE	SLT	Nrev	DATE	SLT	Nrev	DATE	SLT
1	2012.05.01	10.20	1,081	2012.07.11	10.26	2,222	2012.09.24	10.32
2,860	2012.11.05	10.35	3,468	2012.12.15	10.38	4,272	2013.02.06	10.41
4,896	2013.03.19	10.44	5,443	2013.04.24	10.46	6,035	2013.06.02	10.48
6,857	2013.07.26	10.51	7,692	2013.09.19	10.54	8,209	2013.10.23	10.56
8,680	2013.11.23	10.57	9,288	2014.01.02	10.59	9,970	2014.02.16	10.60
10,548	2014.03.26	10.62	11,064	2014.04.29	10.63	11,688	2014.06.09	10.64
12,539	2014.08.04	10.65	13,330	2014.09.25	10.67	13,846	2014.10.29	10.67
14,332	2014.11.30	10.68	15,000	2015.01.13	10.69	15,760	2015.03.04	10.69
16,383	2015.04.14	10.70	17,067	2015.05.29	10.70	18,192	2015.08.11	10.70
19,134	2015.10.12	10.70	19,863	2015.11.29	10.70	20,926	2016.02.07	10.70
22,005	2016.04.18	10.69	23,480	2016.07.24	10.67	25,090	2016.11.07	10.65
26,852	2017.03.03	10.62	28,721	2017.07.04	10.58	30,743	2017.11.14	10.52
32,808	2018.03.30	10.46	35,453	2018.09.20	10.35	37,716	2019.02.16	10.25
38,838	2019.05.01	10.19	-	-	-	-	-	-

As can be seen, 36.6 m/s will be needed for the seven-year orbit altitude keeping, and the SLT changes in the diapason from 10.2 to 10.7 hours.

If necessary, the dispersion of the SLT during the microsatellite functioning process can be reduced due to the inclination correction.

8.3. Station-Keeping for the Satellite Formation Flying TerraSAR-X–TanDEM-X

The satellite formation flying (FF) “TerraSAR-X–TanDEM-X” can serve as an example of successful initialization and station-keeping with a high accuracy in the given satellite formation flying configuration. The Satellite “TerraSAR-X” (TSX) was launched on June 15, 2007, and the satellite “TanDEM-X” (TDX) was launched on June 21, 2010. The satellites were manufactured by the Astrium GmbH corporation. The project was initially financed by the German Federal Ministry of Economics and Technology, and the German Space Agency (DLR) was the satellite owner and operator.

The satellite formation flying mission required the development of a high-accurate global digital model of altitudes, which is now used in scientific research and for commercial ventures.

8.3.1. Deployment of Formation Flying

After the deployment, the TDX was 16,000 km away from the TSX along the orbit. The TDX transfer to the TSX vicinity was fulfilled from June 22 till July 19. It took 23 manoeuvres with total delta-v 6.5 m/s. The fuel economy was achieved thanks to the RAAN deviation correction with the help of the inclination alteration. This was presented in the previous chapter. The special space debris collision avoidance manoeuvres were fulfilled during the flight process (these are described in the following chapter). Due to the phasing manoeuvres, the TDX turned out to be 20 km distant along the orbit from the TSX.

8.3.2. Safe Configuration for Formation Flying

Even a relatively small deviation between the satellite orbit semimajor axes gradually leads to the considerable alteration of their relative positions along the orbit, and, hence, to the constellation collapse. In this case, the use of the different values of the inclinations or the semimajor axes also leads to the constellation configuration collapse due to the increase of deviation by RAANs. It is possible to ensure the safe and long-lasting functioning of the closely positioned satellites in formation flying due to the dispersal of orbit tracks in the plane perpendicular to the velocity vector and/or their shift along the motion trajectory. For example, for the initialization of the steady satellite formation flying, one can use the RAAN difference and the eccentricity vector difference. The RAAN difference will lead to the safety shift in the lateral direction in the vicinity of the equator; however, this shift will be eliminated in the orbit apex and vertex. This situation can be fixed with the help of the difference in the eccentricity vector directed to the orbit apex or vertex. Then there will be a maximum relative shift in the radial direction at the points most distant from the equator. By choosing the proper values of these two deviations, it can be demonstrated that the guided satellite (the TDX in our case) would have an almost circular trajectory in the plane perpendicular to the guiding satellite velocity vector relative to the guiding (TSX) satellite.

After the fulfillment of the initialization manoeuvres, the TDX satellite appeared 20 km distant along the orbit from the TSX, 300 m vertically distant (in the orbit apex), and 1,305 m horizontally distant (on the equator) (i.e., the monostatic formation). The trajectory, which uses the guided satellite in this configuration in the plane perpendicular to the velocity vector of the guiding satellite, is depicted in Figure 8-14 with dashed lines. The horizontal shift of 1.3 km on the equator intersection

was chosen for the prevention of the track shift, which is caused by the 2.6 s desynchronization in time taken to reach the equator. This is caused by the 20 km desynchronization along the orbit. This configuration was used from July 22 to October 10.

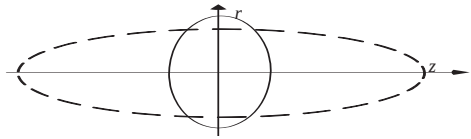

Figure 8-12. Deviation between the guided and guiding satellites in the plane perpendicular to the velocity vector.

Later it was changed to a configuration where the deviation in the horizontal direction was decreased to 362 m and in the vertical direction was increased to 400 m (the bistatic formation). The trajectory, which corresponds to this configuration, is depicted in Figure 8-12 with a solid line. Since the deviation along the equator was decreased to 362 m, the track shift prevention deviation along the orbit must be decreased to 5.5 km, which corresponds to the difference in time when reaching the equator (0.72 s).

According to the equations from section 1.4.1, in order to get a radial shift of 400 m in the apex, the radial impulse directed upwards should be applied on the equator:

$$\Delta V_r = \frac{\Delta r}{r_0} V_0 = \frac{0.4}{6886} 7609.2 \approx 0.5 \text{ m/s}.$$

This impulse will cause the eccentricity change:

$$\Delta e = \frac{\Delta V_r}{V_0} = \frac{0.5}{7609.2} = 0.000066.$$

Due to the influence of this impulse, a shift in the satellite along the orbit in the descending node will occur (it will be behind the guiding satellite). This will happen because the guided satellite flies on a higher orbit from the ascending to the descending node

$$\Delta n = \Delta u r_0 = -4\frac{\Delta V_r}{V_0} r_0 \approx 1600 \text{ m}.$$

The distance between the satellites along the orbit increases in the descending node up to 7.1 km.

The guided satellite will fly closer to the Earth on a trajectory arc lower than the plane of the equator, and the lag of 1600 m will be compensated.

The necessary shift by the RAAN will be ($\Delta\Omega$)

$$\Delta\Omega = \frac{\Delta r}{r_0} = \frac{0.4}{6886} = 0.000053.$$

Hence, $\Delta\Omega \approx 0.003\text{deg}$.

Due to the influence of these deviations, the satellite relative trajectory lies on the surface of the cylinder with a radius of 400 m and a length of 1600 m.

Table 8-10 shows the orbit parameters of the guiding (object 1) and the guided (object 2) satellites, the deviations of the eccentricity vectors, and the RAANs which correspond to the calculated deviations.

The projections of the trajectory on the plane perpendicular to the guiding satellite velocity vector, on the plane of its orbit, and on the plane perpendicular to its radius-vector (which uses a guided satellite for the given initial conditions) are depicted in Figures 8-13–8-15. Figure 8-16 shows the inclination changes for the time in the orbital coordinate frame.

Table 8-10

	Object 1	Object 2
a	6,892.93	6,892.93
e_x	0.000468	0.000468
e_y	0.001238	0.001171
i	97.44	97.44
Omg	66.733	66.736
U	360.0	359.95
Date	2005.01.07 20:31:56.14	2005.01.07 20:31:56.14
Ball.coef.	0.01	0.01

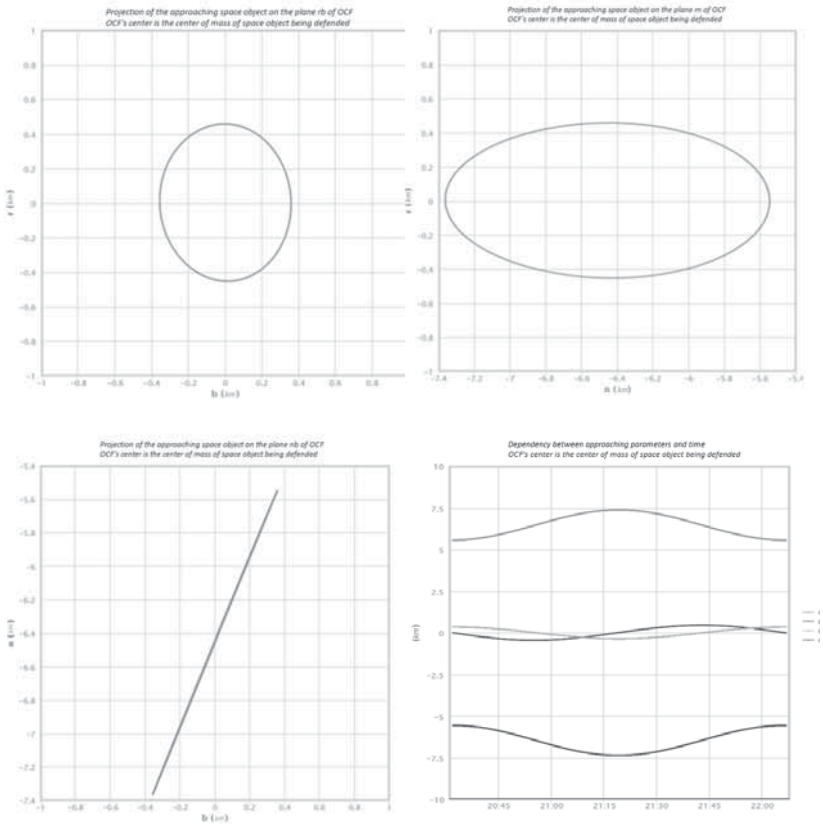

Figures 8-13–8-16. Deviation between the guided and the guiding satellite in the orbital coordinate frame: in plane r,b; in plane r,n; and in plane n,b. Deviations in the orbital coordinate frame by time (dR), by radius (dr), in a lateral direction (db), and along the orbit (dn).

The relative trajectory of motion for the guided satellite along the surface of the cylinder is depicted in Figure 8-17 with a thick solid line; the trajectory of motion of the guiding satellite is depicted with a thick dashed line. The position of the guiding satellite is marked with an asterisk (point *B*).

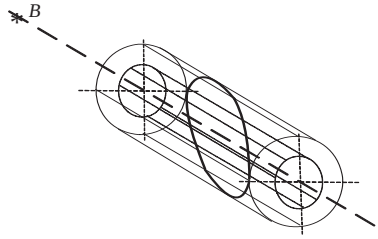

Figure 8-17. Guided satellite trajectory relative to the guiding satellite trajectory

8.3.3. Maintenance of Formation Flying with a Given Configuration

The satellite formation flying operational configuration station-keeping problem is divided into two sub-problems. In the first sub-problem, it is necessary to provide the synchronized station-keeping of the operational orbit for each satellite from the formation flying. In the second sub-problem, it is necessary to provide the configuration of the satellite position inside the formation flying.

The TSX nominal orbit was chosen to be eleven days. The current orbit should lie within the tube of the radius 250 m around the nominal orbit (in Figure 8-17 the tube base and its generatrixes are plotted with dotted lines). It is very important that the manoeuvres performed by the guiding satellite must not drag it out from a circle with a radius of 250 m in the plane perpendicular to the velocity vector. Thus, not less than 150 m remains between the TSX and the TDX in the plane perpendicular to the satellite motion direction, which ensures safe satellite motion. In order to meet the constraint of 250 m in the plane perpendicular to the satellite motion direction, the semimajor axis alteration must not exceed 250 m ($\Delta V_t < 0.16\,\text{m/s}$), the inclination alteration $\Delta i < 0.002^\circ (\Delta V_z < 0.27\,\text{m/s})$, the eccentricity alteration $\Delta e < 0.00004$ ($\Delta V_r < 0.31\,\text{m/s}$, $\Delta V_t < 0.16\,\text{m/s}$), and the RAAN alteration $\Delta\Omega < 0.002^\circ$ ($\Delta V_z < 0.27\,\text{m/s}$).

Depending on the solar activity the manoeuvres of the current trajectory keeping in the given vicinity of the nominal orbit had to be performed within periods from 2 days to 2 weeks. In order to maintain the given satellite formation flying configuration, it is necessary to simultaneously perform identical manoeuvres for the orbit keeping of both guiding and guided satellites. If the semimajor axis and/or the inclination

are corrected for orbit keeping, then the single impulse applied in the vicinity of the equator will be enough. These two or three impulses have to be used when correcting the previous parameters with the simultaneous correction. Hence, simultaneous successions have to be performed.

The detailed description of this project is given in multiple articles. The numerical two satellite flight modeling with an analysis of the manoeuvre application periodicity depending on the maintenance accuracy of the operational orbit and the given configuration was conducted in (Baranov and Chernov 2019, 220–228).

CHAPTER NINE

MANOEUVRING ISSUES IN THE SPACE DEBRIS PROBLEM

Manoeuvring issues play an important role in the space debris problem. Most of the enormous volume of work connected to space object cataloguing is needed for predicting spacecraft collisions with space objects and the further calculation and application of collision avoidance manoeuvres. Collisions with moving space objects are especially dangerous due to the lack of information about their future movements. In this case, it is necessary to have a technique for estimating the already applied active spacecraft manoeuvres and how to predict future manoeuvres.

9.1. Collision Avoidance Manoeuvres

An orbit shaped by the target manoeuvres should not only be suitable for the tasks assigned to the spacecraft, but also to keep it safe from collisions with space debris and active space objects. The danger of collision can be eliminated using special collision avoidance manoeuvres or by modifying the target manoeuvres themselves.

While calculating which approaches are dangerous, we have to look at the problem from two sides. On the one hand, we should not fail to account for a dangerous approach and, on the other, we should not exaggerate the danger approach criterion otherwise there will be too many false alarms. Reacting to these false alarms will lead to the excessive expenditure of the spacecraft's resources.

9.1.1. Dimensions of the Satellite Safety Zone

Spacecraft orbits are determined and predicted using a space tracking system that looks 72 hours ahead so as to determine possible approaches. The collision probability p_c is calculated according to this interval. If the

collision probability $p_c > 0.0001$, then a collision avoidance manoeuvre needs to be applied. Such avoidance measures should push the spacecraft out of the danger zone. In this problem, we let the dimensions of the danger zone be $r_{\min}$ by the radius, $n_{\min}$ along the orbit, and $b_{\min}$ in the lateral direction.

Space objects moving towards the spacecraft are the most dangerous, as the relative velocity in low Earth orbits can be as high as 15.5 km/s. The components of relative velocity that have the biggest magnitude are the transversal and lateral ones. The radius vector component does not exceed 1 km/s, even for highly eccentric orbits.

The space object's velocity relative to the spacecraft's velocity can be evaluated by:

$$\vec{V}_{rel} = \vec{V}_{SO} - \vec{V}_{SC}.$$

Its projections along the axes of the orbital coordinate frame, connected to the spacecraft and fixed at the moment of supposed collision, are denoted V_{rel_r}, V_{rel_n}, and V_{rel_b}. The safe zone dimensions, $r_{\min}$, $n_{\min}$, and $b_{\min}$, are determined, first of all, by the error calculation of the dangerous approach time Δt (Melnikov 2009). This error occurs because of an inaccuracy in determining the orbits of the spacecraft and the space object. It is hard to predict the motion of a space object because its mass-inertial characteristics and shape are unknown. Errors also arise from inaccuracies in determining the atmospheric influence etc.

The transversal deviation caused by the error Δt can be found as the multiplication of Δt and V_{rel_n}:

$$n_{\min} = \Delta t V_{rel_n}.$$

The maximum deviation for Δt = 1 s is approximately $n_{\min} = 15.5\,\text{km}$.

For the lateral deviation, we get:

$$b_{\min} = \Delta t V_{rel_b}.$$

The maximum relative speed in this direction is 8 km/s; hence, the maximum lateral deviation for Δt = 1 s is approximately $b_{\min} = 8\,\text{km}$.

Similarly, for the radial direction:

$$r_{\min} = \Delta t V_{rel_r},$$

and the maximum deviation in this direction for Δt = 1 s is approximately $r_{\min} = 1\,\text{km}$.

Narrowing the safe zone is possible only by decreasing Δt. This can be achieved by decreasing the error in orbital determination and increasing the frequency of searching and identifying dangerous approaches; the prediction errors decrease as the motion prediction interval narrows.

There are many algorithms that can help discover the dimensions of the prohibited area more accurately. For example, this problem has been investigated in Estes and Foster (1992), Patera and Peterson (2003, 233-237), Foster and Stansbery (2003), Kelly and Picciotto (2005), Byram, Slater, and Williams (2006, 1140-1146), and Klinkrad (2007, 955-962).

9.1.2. Single-Impulse Avoidance Manoeuvres

Usually, collision avoidance (in relation to a space object) is performed using a special collision avoidance manoeuvre. The manoeuvre parameter calculation method in this case is already well known (Melnikov, 2009).

Different manoeuvring schemes can be applied. Along-the-orbit avoidance is most frequently used so long as there is the opportunity to apply the manoeuvre several revolutions before an expected collision. This avoidance procedure is fulfilled by a transversal manoeuvre. A similar manoeuvre applied half or one and a half revolutions before collision results in avoidance by altitude. Avoidance by altitude can also be fulfilled using a radial manoeuvre. This is less effective, but leaves the orbital period unchanged.

Let us suppose that the transversal impulse ΔV_t is applied $\Delta\varphi_1$ degrees before the expected location of collision. The minimum magnitude of the impulse $\Delta V_{t_{\min_n}}$, which can push the spacecraft along the orbit and out of danger $n_{\min}$, can be calculated as:

$$\begin{aligned} (3\Delta\varphi_1 - 4\sin\Delta\varphi_1)\Delta V_{t_{\min_n}} &= \lambda n_{\min}, \\ \Delta V_{t_{\min_n}} &= \frac{\lambda n_{\min}}{3\Delta\varphi_1 - 4\sin\Delta\varphi_1}, \end{aligned} \tag{9-1}$$

where λ = the angular velocity of the motion along the circular drift orbit and $\Delta\varphi_1$ = the angle between the moment of impulse application and the possible moment of collision ($\Delta\varphi_1 > 0$).

In the case of forward firing, the spacecraft will reach the collision point after the space object ($n > 0$); if retrofiring is used, the spacecraft will reach the collision point earlier ($n < 0$). In both cases, safe spacecraft motion is ensured.

If a collision avoidance manoeuvre is urgently needed, it is effective to apply it half or one and a half revolutions before the point of the estimated collision, dragging the spacecraft out of the danger zone by altitude. We can estimate the magnitude of the manoeuvre $\Delta V_{t_{\min_r}}$, which is to be applied $\Delta\varphi_2$ degrees before the point of the estimated collision by the equations:

$$\begin{aligned} 2(1-\cos\Delta\varphi_2)\Delta V_{t_{\min_r}} &= -\lambda r_{\min}, \\ \Delta V_{t_{\min_r}} &= -\frac{\lambda r_{\min}}{2(1-\cos\Delta\varphi_2)}. \end{aligned} \tag{9-2}$$

By substituting $\Delta\varphi_2 = \pi$, we can get the minimum manoeuvring magnitude:

$$\Delta V_{t_{r_{\min}}} = -\frac{1}{4}\lambda r_{\min}. \tag{9-3}$$

With the use of an accelerating impulse, the spacecraft will go up above the space object, while the use of the braking impulse will force the spacecraft to go below the space object. Let us remember that $r_{\min}$ can be evaluated as follows: $r_{\min} = r_{SO} - r_{SC}$.

The angular distance $\Delta\varphi_1$ between the impulse application point and the estimated collision point, ensuring the equal effectiveness of both strategies, can be found by:

$$\frac{\lambda|n_{\min}|}{|3\Delta\varphi_1 - 4\sin\Delta\varphi_1|} = \frac{1}{4}\lambda|r_{\min}|. \tag{9-4}$$

Assuming that $\Delta\varphi_1$ contains the integer revolution number *N*, we get:

$$N = \frac{4|n_{\min}|}{6\pi|r_{\min}|}. \tag{9-5}$$

Using this equation, one can determine that, for the aforementioned values $n_{\min}$ and $r_{\min}$, and $\Delta\varphi_1$ greater than three revolutions, the strategy utilizing along-the-orbit drag becomes more valuable.

Transversal impulses are used in the compared strategies. This allows us to combine collision avoidance manoeuvres with orbital elevation manoeuvres, which occasionally need to be fulfilled for Earth remote sensing spacecraft, the International Space Station (ISS), and other spacecraft.

However, there are a number of cases for which changing the orbital period is prohibited; for example, if the spacecraft is in the phasing orbit and the approach is in process, specifically, when the ISS is maintaining the necessary initial phase for the docking spacecraft. In these cases, transversal impulses cannot be applied. Instead, radial impulses, which keep the orbital period unchanged, must be used.

The influence of the radial impulse component on orbital altitude at the estimated moment of collision can be described as:

$$-\lambda\Delta r = \sin\varphi\Delta V_r.$$

As such, in order to drag the spacecraft out of the danger zone by changing its altitude, one should apply an impulse with magnitude:

$$\Delta V_{r_{\min}} = \frac{-\lambda r_{\min}}{\sin\varphi}. \tag{9-6}$$

The magnitude of the impulse will be minimal with $\varphi = \pm\frac{\pi}{2}N, N \in Z$:

$$\Delta V_{r_{\min}} = \lambda r_{\min} \tag{9-7}$$

if it is applied one quarter of a revolution earlier $(\Delta V_r > 0)$ or three quarters of a revolution after $(\Delta V_r < 0)$ the approach point. For safety's sake, it is necessary to reschedule this impulse to the previous revolution.

It can be seen that the use of transversal impulses is four times more effective than the use of radial impulses in dragging a spacecraft out of the danger zone by changing its altitude. Hence, where there are no other constraints, the use of transversal impulses for collision avoidance manoeuvres is more preferable.

At the moment of minimum distance, there are deviations in the positions between the spacecraft and the space object, which we will denote $\Delta r, \Delta n, \Delta b$. If the collision avoidance manoeuvre drags the spacecraft towards the space object, for example, if the manoeuvre increases the spacecraft's altitude and the space object was initially higher than the spacecraft, then it is necessary to increase the orbital altitude by Δr. In this case, if the manoeuvre leads to a decrease in the spacecraft's orbital altitude, the magnitude of altitude alteration can be decreased by Δr.

9.1.3. Geometric Interpretation of the Satellite Safety Zone

In the previous section, we examined the case where the avoidance of a collision with a space object was fulfilled through the use of an additional special manoeuvre. However, it is not always possible to do this. This technique is mainly used when spacecraft perform rendezvous manoeuvres. For instance, the "Soyuz" and "Progress" spacecraft will have communication-free revolutions after fulfilling the first two (performed on the 2nd or 3rd revolution) of a series of four connected rendezvous manoeuvres (see section 5.3). The communication-free revolutions cannot be used for the manoeuvres. If the phased orbit shaped by the first two manoeuvres is dangerous because of possible collisions, there will be no possibility of changing it. The only way to resolve this is to recalculate the rendezvous problem solution with the use of the additional constraint so that the spacecraft will not go through the danger area after the application of the first two impulses.

A safe orbit can be obtained by changing the orbital phase eccentricity due to the fact that the magnitude of the semimajor axis after the application of the first interval impulses is determined by the problem conditions (the initial phase difference Δu). The aforementioned special radial impulse also solves the problem by changing the orbital eccentricity. The radial impulse does not change the semimajor axis.

Let us determine the boundaries of the area on the plane e_x, e_y from which the orbital phasing eccentricity vector should be moved in order to avoid a collision with the space object. We assume that the phasing orbit

has eccentricity e_0, the pericenter argument ω_0, and the semimajor axis a_0. A collision with the space object occurs when the latitude argument reaches u_0. The orbital radius at this point can be evaluated as follows:

$$r_0 = \frac{a_0(1-e_0^2)}{1+e_0\cos(u_0-\omega_0)}.$$

In order to avoid a collision with the space object at the point with the latitude argument u_0, the orbital radius should be increased to $r_0+\Delta r_{\min}$ at the possible collision point (upwards drag) or decreased to $r_0-\Delta r_{\min}$ (downwards drag), where $\Delta r_{\min}$ = the distance of safe drag. By evaluating the value *e* for the different values of ω using the equation:

$$r_0+\Delta r_{\min} = \frac{a_0(1-e^2)}{1+e\cos(u_0-\omega)}, \tag{9-8}$$

one can calculate the outer boundary of the prohibited area. Using the equation:

$$r_0-\Delta r_{\min} = \frac{a_0(1-e^2)}{1+e\cos(u_0-\omega)}, \tag{9-9}$$

one can calculate its inner boundary. Thus a collision can be avoided by dragging the eccentricity vector of the phasing orbit shaped by the first interval manoeuvres out of the prohibited area.

Figure 9-1 presents the example of the prohibited area of the phasing orbit with the semimajor axis $a_0 = 10{,}000\,\text{km}$, eccentricity $e_0 = 0.3$, and the pericenter argument $\omega_0 = 0^\circ$. The collision occurs at the latitude argument $u_0 = 30^\circ$. It is supposed that the spacecraft's altitude at the collision point should be changed by $\Delta r_{\min} = 600\,\text{km}$ (higher or lower). This distance gradually exceeds the usual one used for collision avoidance, but helps to describe the prohibited area.

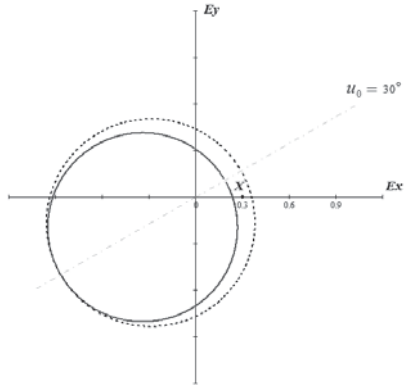

Fig. 9-1. Prohibited area overview

The dashed line designates the prohibited area's line of symmetry. The angle between this line and the e_x axis equals u_0. The inner boundary of the prohibited area is represented by the solid line and the outer boundary is represented by the dotted line. Point *X* is related to the phasing orbit (e_0, ω_0). It can be seen that the boundaries of the prohibited area have a common point (Fig. 9-1) that corresponds to the turning of the elliptical orbit into a parabola ($e = 1$). The dimensions of the prohibited area are proportional to $\Delta r_{\min}$. The dependency between *e* and ω is depicted in Fig. 9-2.

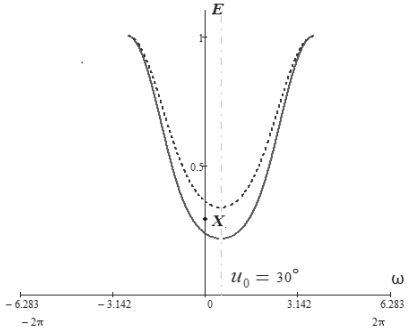

Fig. 9-2. Gaps of boundaries of the prohibited area on plane ω, *e*

In Fig. 9-3, one can see the prohibited areas for the angles $u_0 = 100^\circ$ and $u_0 = 210^\circ$.

It can be seen that the axis of symmetry of the prohibited area rotates around the datum point of the coordinate frame. The dimensions and the position of the prohibited area also change.

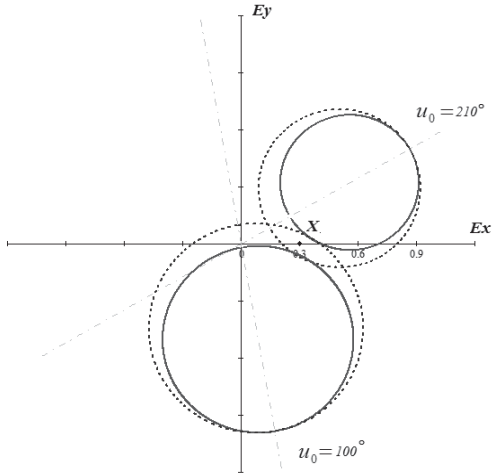

Fig. 9-3. Location of the prohibited area for the angles $u_0 = 100°$ and $u_0 = 210°$

As previously noted, the real magnitude of the value $\Delta r_{\min}$ is far smaller than the one used here in the examples. In Fig. 9-4, one can see the prohibited area for the phasing orbit of the "Soyuz" spacecraft with the semimajor axis $a_0 = 6{,}660\,\text{km}$, the eccentricity $e_0 = 0.005$, and the pericenter argument $\omega_0 = 135^\circ$. The orbital station rendezvous point is $u_0 = 358^\circ$ and a collision occurs when $u_0 = 135^\circ$. The necessary condition is $\Delta r_{\min} = 3\,\text{km}$. As we can see, for the appropriate range of eccentricity alteration (in the vicinity of point $X(e_{x_0}, e_{y_0})$), the prohibited area is restricted by almost straight lines. The width of the prohibited area is $2\Delta e$, where Δe can be evaluated as:

$$\Delta e = \Delta r_{\min} / r_0. \tag{9-10}$$

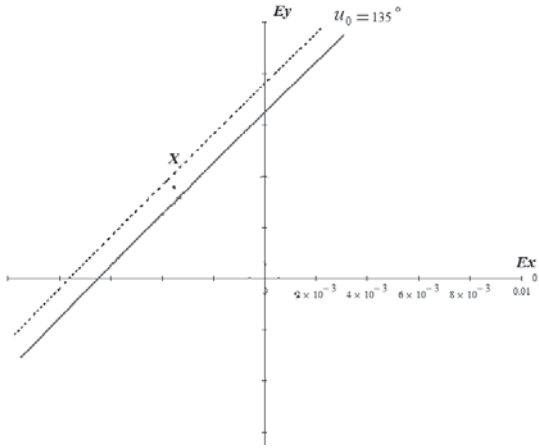

Fig. 9-4. Location of prohibited area in real conditions for angle $u_0 = 135°$

Let us determine the position of the prohibited area in accordance with the latitude argument of the collision. For this purpose, let us draw the several prohibited areas with $u_0 = 0^\circ, 45^\circ, 90^\circ, 135^\circ$ on the single coordinate plane. In Fig. 9-5, one can see that altering angle u_0 leads to the rotation of the prohibited area around point $X(e_{x_0}, e_{y_0})$. The composition of several areas determines the area in which multiple spacecraft collisions are possible.

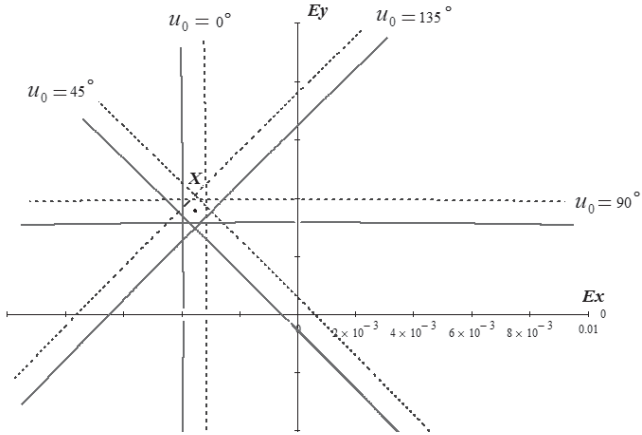

Fig. 9-5. Orientation of the prohibited area for different u_0

The use of the prohibited areas obtained allows us to find the rendezvous problem's solution with the help of algorithms from chapters 3, 4, and 5. This solution helps to avoid collisions in the phasing orbit. It is especially effective to use the graphical dialog for the manoeuvre parameter determination problem from Chapter 5 for these purposes. The example of the use of these areas for the "Soyuz" spacecraft manoeuvre parameter recalculation is presented in an article by the author.

9.2. Assessment of Manoeuvres Performed by an Active Space Object

The problem of propagating the motion of the manoeuvring spacecraft appears while keeping the space object catalogue. To solve this problem, one should know how to estimate the realized manoeuvres using the orbits obtained on the basis of trajectory measurements. The assessment of the performed manoeuvres together with further motion propagation of the active space object and accounting for future analogous manoeuvres allows us to gradually increase the accuracy of calculating dangerous approaches with this object. Manoeuvre assessment is also necessary for a proximity assessment of the protected spacecraft and the manoeuvring space object on the manoeuvring interval. This manoeuvre assessment allows the development of more precise orbital parameters in the case of determining the terminal orbit with considerable errors. In addition, the information obtained during the space object manoeuvre assessment

(information about acceleration during the manoeuvre), together with the information gathered during its passive motion, allows us to discover some of the manoeuvring space object's characteristics, such as its mass or engine thrust.

The existing methods of assessment of the performed manoeuvres (Alfriend, Kamensky, Stepanyants, and Tuchin 2009, 3-22; Borovin, Stepanyantz, Tuchin, and Tuchin et al. 2012) require a lot of processing time to obtain results. They are suitable for arbitrary orbits and due to the problem's complexity are based on the simple enumeration of the definable parameters. Space object manoeuvres in near-circular orbits are described in this book. This simplifies the problem and allows us to use analytical and numerical analytical methods for its solution. In addition, the scope of application is insignificantly narrowed as most real manoeuvring space objects are situated in near-circular orbits. The time for solving the problem decreases by several orders, speeding up the updating of the manoeuvring space objects catalogue. The high response speed is important because the regular manoeuvre assessment has to be performed for a large number of real manoeuvring space objects.

9.2.1. Manoeuvre Parameter Reconstruction: General Solution Method

The two state vectors of manoeuvring space objects for the two moments of time are already known. The magnitude and orientation of the impulses that have changed orbit and the times of thruster firing need to be assessed. If the moments of time are not distant to each other, then it is fair to assume that one or two manoeuvres were performed during that interval. For longer time intervals with several possible manoeuvres, it is almost impossible to restore the magnitudes and moments of manoeuvre application. Only minimal total delta-v expenditures can be assessed with the help of the algorithms from chapters 2, 3, 4, and 6.

It is supposed that only single and double-impulse manoeuvres will be assessed further. The assessment algorithms for close to impulsive manoeuvres and manoeuvres performed by low-thrust engines differ gradually from each other and need to be considered individually. The final determination of the manoeuvre parameters is made by the iteration procedure described in Chapter 1.

The assessment methods for close-to-impulsive manoeuvres are mostly well-developed.

The problem of assessing the single-impulse manoeuvring parameters with good accuracy for the initial and target orbits is the simplest one. If

the accuracy of determining the orbits is poor, an uncertainty occurs in the assessed impulse parameter selection. Lambert's problem is usually used for the assessment of the two-impulse manoeuvring parameters (Alfriend, Kamensky, Stepanyants, and Tuchin 2009, 3-22). The use of the numerical analytical methods from the previous chapters allows us to gradually speed up the process of two-impulse velocity parameter determination. The two sub-problems can be distinguished for the two-impulse manoeuvre problem:

1) Parameter determination of the two connected impulse coplanar manoeuvres;

2) Parameter determination for the two connected impulse manoeuvres that caused the alteration of all orbital elements.

Nowadays, mostly numerical methods with simple enumeration of the definable parameters with a constant step are used for the assessment of manoeuvres performed by low-thrust engines (Alfriend, Kamensky, Stepanyants, and Tuchin 2009, 3-22; Borovin, Stepanyantz, Tuchin, and Tuchin et al. 2012). The use of the analytical and numerical analytical methods from Chapter 6 for long-duration manoeuvre assessment also helps to gradually speed up the solution of the problem, thus making it possible to use this method in the technological cycle of calculating and keeping the catalogue of near-Earth space objects. In the case of a manoeuvre performed by low-thrust engines, the proposed method helps not only to determine the manoeuvre parameters, but also to determine the magnitude of acceleration made by the thruster engine.

For *long-duration* manoeuvres, the problem stated in the general case can be divided into several simple sub-problems:

1) Determine the parameters of the manoeuvre that results in the alteration of the semimajor axis and/or eccentricity vector;

2) Determine the parameters of the manoeuvre that causes the orbital plane rotation;

3) Determine the parameters of the combined manoeuvre that alters all orbital elements;

4) Determine the parameters of the two connected long duration coplanar manoeuvres;

5) Determine the parameters of the two independent long duration coplanar manoeuvres;

6) Determine the parameters of the two long duration independent manoeuvres that alter all orbital elements.

Determination of Orbital Parameter Alteration: Accounting for the Influence of the Impulse

The first step of the solution is the calculation of the orbital parameter deviation vector Δ caused by the working of the thrust engines.

In order to determine the deviation vector Δ, it is necessary to undertake a prognosis of the initial state vector up to the moment t_2. The prognosis is performed with all perturbations except engine thruster firing. Then the difference between the elements of the terminal orbit and the orbit obtained after the calculation of the prognosis. The components of the deviation vector $\Delta = (\Delta a, \Delta e_x, \Delta e_y, \Delta t, \Delta z, \Delta V_z^*)^T$ were determined in section 1.1.2.

In the case where the thrust engine firing interval is small in comparison to the space object orbital period, the following assumption can be made: the orbital parameter change was instantaneous. This assumption allows us to write out the conditions for reaching the desired point of the terminal orbit in the form of eqs. 1-12a to 1-12f for manoeuvres in the vicinity of the circular orbit.

In the case of a single-impulse manoeuvre, the definable variables are $\Delta V_{r_1}, \Delta V_{t_1}, \Delta V_{z_1}, \varphi_1$ as the components of the first impulse and the angle of its application. For the two-impulse case, the unknown variables are $\Delta V_{r_1}, \Delta V_{t_1}, \Delta V_{z_1}, \varphi_1, \Delta V_{r_2}, \Delta V_{t_2}, \Delta V_{z_2}, \varphi_2$ as the parameters of the first and second impulses.

9.2.2. Single-Impulse Manoeuvre Assessment in the Case of Accurate Orbital Determination

The simplest method is the variant of the close-to-impulse manoeuvre, performed in a single ignition with both orbits having been determined with acceptable accuracy. The solution includes the search for the minimum distance between the object positions in the initial and target orbits with further evaluation of the difference between the velocity vectors at this moment.

9.2.3. Single-Impulse Manoeuvre Assessment with Inaccuracies in Orbital Determination

In practice, one has to deal with the initial data errors while determining the realized manoeuvres. These inaccuracies are connected to

errors in determining the initial and terminal orbits (especially concerning the terminal orbit, which has, by default, fewer measurements). Accounting for the stochastic nature of the trajectory information makes the problem more complex, but helps us get to a more trustworthy solution. The coplanar and noncoplanar cases are described further.

Impulsive Coplanar Manoeuvre

Let us state that the realized impulse does not have radial components. According to eqs. 1-12a to 1-12c, the radial impulse components do not take part in changing the semimajor axis and are twice as inefficient in altering the eccentricity vector as the transversal ones. This is why this component is barely used in manoeuvres for orbital maintenance. Thus, the assumption that the determined manoeuvre has zero radial components (i.e. $\Delta V_r = 0$) is acceptable.

In Fig. 9-10, point *K* with coordinates $\Delta e_x, \Delta e_y$ corresponds to the end of the eccentricity vector difference between the initial and target orbit eccentricity vectors $\Delta\bar{e} = \bar{e}_f - \bar{e}_0$. The angle of transversal impulse application, which allows us to correct the deviation of the eccentricity vector, is designated φ_e. Following on from eqs. 1-12a and 1-12b, and the magnitude of the impulse, which produces the necessary eccentricity alteration:

$$\Delta V_t = V_0 \frac{\left|\Delta\bar{e}\right|}{2} = V_0 \frac{\Delta e}{2}.$$

Let us draw a circle with radius *R* ($R = \frac{\Delta a}{r_0} = \frac{a_f - a_0}{r_0}$), which is the dimensionless difference between the semimajor axes of the initial and terminal orbits. The circle's center is situated at the center of the coordinate frame. If there are no orbital definition errors, point *K* would have belonged to the circle because $\frac{\Delta a}{r_0} = \frac{2V_t}{V_0} = \Delta e$.

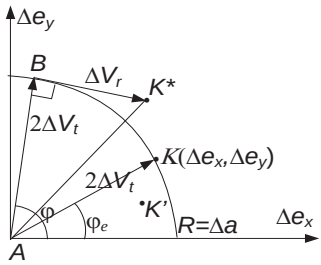

Fig. 9-10. Single-impulse coplanar transfer

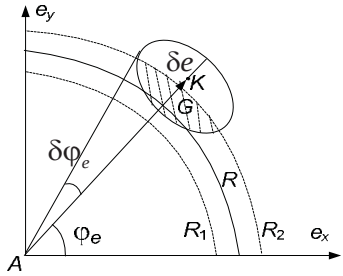

Fig. 9-11. Influence of the error on the determination of the difference between the semimajor axes and the difference between the eccentricity vectors

Due to errors in determining the semimajor axis and eccentricity vector of each orbit, point *K* may not belong to the circle. If the point is inside the circle (point *K'* in Fig. 9-10), then the orbits do not intersect ($|\Delta a| > \Delta e$) and the single-impulse solution does not exist. If point *K* is outside the circle (point K^* in Fig. 9-10), then the initial and terminal orbits intersect ($\Delta e > |\Delta a|$) and the single-impulse solution exists and the impulse has a radial component (BK^* in Fig. 9-10). In order to obtain a trustworthy transversal solution, one has to account for errors in determining the semimajor axis and eccentricity vector.

Let us designate δa as the maximum error in the determination of the dimensionless difference of the semimajor axes. We will draw two concentric circles with radii $R_1 = R - \delta a$ and $R_2 = R + \delta a$. In Fig. 9-11, these circles are drawn with dashed lines. The area between the dashed circles corresponds to the acceptable values of the dimensionless difference between the semimajor axes. Let us draw an ellipse, which will constrain the area, corresponding to the acceptable values of the difference between the eccentricity vectors. One of the semi axes of this ellipse is determined by the maximum error in the absolute value of the eccentricity vector difference δe, while the other one is determined by the maximum error in the angular position of the eccentricity vector difference $\delta\varphi_e$. The intersection of the area constrained by the ellipse and the area between the dashed circles is the shaded area *G*, the points of which correspond to possible single-impulse transversal solutions for acceptable eccentricity

alteration (Baranov, Karatunov, Razoumny, and Vikhrachev 2017, 141-149). If the areas do not intersect, the single-impulse solution is not possible and two-impulse solutions should be considered.

In order to assess the parameters of the determined impulse, one should also take into account the error in the determination of the manoeuvre application time. The angle φ_t corresponds to the moment of time when the spacecraft will be on the same revolution and the same latitude argument, as if it moved forward along the initial orbit and backwards along the target orbit. The maximum error in determining this angle is $\delta\varphi_t$. The intersection of the sector $[\varphi_t - \delta\varphi_t, \varphi_t + \delta\varphi_t]$ with area *G* will give us the shaded area *P* (Fig. 9-12) with acceptable single-impulse transversal solutions. The smaller the error in the orbital determination, the closer the angles φ_t and φ_e will be.

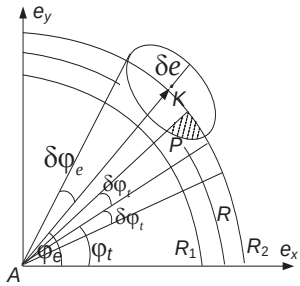

Fig. 9-12. The influence of the error in determining the difference between the semimajor axes, errors in determining the eccentricity vectors, and errors in determining the impulse application time

There will be one point from area *P* that will determine the problem solution. The problem solution can be the point that is determined rapidly and ensures a minimal difference in the probability of adjusting each orbital element.

For example, the impulse application angle φ_{imp} can be found from the equation:

$$\frac{\delta\varphi_e}{\varphi_e - \varphi_{imp}} = \frac{\delta\varphi_t}{\varphi_{imp} - \varphi_t}.$$

Thus, φ_{imp} will be:

$$\varphi_{imp} = \frac{\delta\varphi_t\varphi_e + \delta\varphi_e\varphi_t}{\delta\varphi_e + \delta\varphi_t}.$$

For the determination of point *K* with this angle, we can use the equation:

$$\frac{\delta e_{imp}^2}{\delta e^2} + \frac{(\varphi_e - \varphi_{imp})^2}{\delta\varphi_e^2} = 1$$

One should find the maximum error δe_{imp} in terms of the difference between the absolute magnitude of the eccentricity vector during impulse application with the angle φ_{imp}:

$$\delta e_{imp} = \frac{\delta e}{\delta\varphi_e}\sqrt{\delta\varphi_e^2 - (\varphi_e - \varphi_{imp})^2}$$

Then, from the equation:

$$\frac{x}{\delta a} = \frac{CD - x}{\delta e_{imp}},$$

one can determine *x*:

$$x = \frac{CD\delta a}{\delta e_{imp} + \delta a},$$

where *CD* = the distance between a circle of radius *R* and an ellipse with axis *x* starting from this circle and determining the position of point *K*.

Impulse Noncoplanar Manoeuvre

Let us suppose that the assessed impulse has both transversal and lateral components. The angle φ_z, which determines the position of the orbital plane line of intersection, is the application angle of the impulse lateral component. If the orbits have been determined without errors, then the application angles of the transversal and lateral components coincide

with each other and $\varphi_e = \varphi_z$. If there were errors in the orbital determination, the angle of optimal eccentricity correction φ_e and the angle of orbital plane rotation φ_z do not coincide, although in the real impulse case they should.

Let us call $\delta\varphi_z$ the maximum determination error of the angle on which the orbital plane rotation was performed. The lines between the angles $\varphi_z - \delta\varphi_z$ and $\varphi_z + \delta\varphi_z$ determine the acceptable area for the impulse application angle of the orbital plane rotation. If this area has common points with area *P* (we will designate the intersection area for these two areas *L*; in Fig. 9-13, this is depicted as the hatched section), then the single-impulse solution exists. If not, one should move to the determination of two-impulse solution parameters.

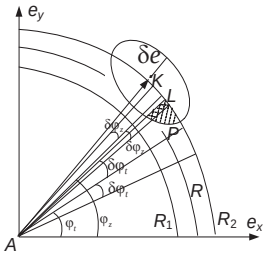

Fig. 9-13. The influence of the error in determining the difference between the semimajor axes, the eccentricity vectors, and the moment of the impulse lateral component application

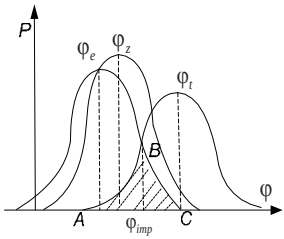

Fig. 9-14. Probability distributions of the impulse application angle for the correction of the eccentricity vector φ_e, the angle of the impulse application moment φ_t, and the angle of the orbital plane rotation start φ_z

Figure 9-14 gives the probability distributions for the impulse application angles for the correction of the eccentricity vector φ_e, the angle of the orbital plane rotation start φ_z, and the angle of the impulse application moment φ_t. It can be easily seen that the acceptable angles for the application should belong to line segment *AC*. The angle φ_{imp} is chosen in accordance with point B (here, the probability density for both angles is equal). Then, δe_{imp} is determined for the found angle etc.

The magnitude of the dimensionless lateral impulse component can be found as:

$$\Delta V_z = \Delta\gamma,$$

where γ = the angle between the nominal orbital planes.

9.2.4. Assessment of Two Finite-Burn Manoeuvres

In cases where the single-impulse solution does not exist, one should consider determination of the two-impulse solution parameters. By altering the angles φ_1 and φ_2 in the range corresponding to the time interval between the epochs of the initial and target orbits, and solving Eq. 1-12 for each pair of angles (in order to find the impulse components), lots of solutions with different values of total delta-v ensuring the flyby from the initial to the target orbit can be obtained. The final result is the solution with the lowest energy cost. We call this approach the full enumeration method. This is the traditional approach for solving the two-impulse manoeuvre assessment problem (Alfriend, Kamensky, Stepanyants, and Tuchin 2009, 3-22; Borovin, Stepanyantz, Tuchin, and Tuchin et al. 2012).

Usually the solution of Lambert's problem is used, but, as will be shown later, the solution can be obtained more easily by using Eq. 1-12. The number of the enumeration variants gradually grows with the increase in the time interval between the epochs of the initial and target orbits. Even if the simple Eq. 1-12 is used instead of calculating Lambert's problem, the calculation time gradually increases. This makes it difficult to use the traditional approach in the technological cycle of keeping the space object catalogue.

The assumption about impulse orientation can also help reduce the computation time. As a rule, the assessed manoeuvres are not rendezvous manoeuvres, but are variations of simple transfer manoeuvres. The semimajor axis change and/or the eccentricity vector change are the goal of using such manoeuvres while manoeuvring in the orbital plane. As already mentioned, the radial components are hardly used in orbital maintenance manoeuvres. Thus, it can be assumed that the estimated manoeuvres do not have radial impulse components, i.e. $\Delta V_{r_1} = 0$, $\Delta V_{r_2} = 0$. The radial components, which may occur as result of errors in setting up the required orientation of the thrust engines, usually do not exceed 2 % of the impulse magnitudes. These components do not alter the semimajor axis and practically do not influence the time of the flyby up to its end point. They can also be omitted during the manoeuvre assessment,

as will be shown in one of the examples in section 9.2.9. As such, the solution of the two-impulse problem is feasible in searching for the class of manoeuvres that only have transversal and lateral components. The search algorithm for this solution can be stated as follows (Baranov and Karatunov 2016, 284-295). The different application angles of the first impulse are selected on a single revolution interval. The angle φ_{1_f} is the current value of φ_1. Then, with the help of eqs. 2-2a to 2-2c, the magnitudes of the transversal components $\Delta V_{t_1}, \Delta V_{t_2}$ and the second impulse application angle φ_{2_f} are found. The lateral components $\Delta V_{z_1}, \Delta V_{z_2}$ can be found using eqs. 2-14a and 2-14b. The obtained solution will be acceptable for all combinations of the angles $\varphi_{1_n} = \varphi_{1_f} + 2\pi n$, $\varphi_{2_n} = \varphi_{2_f} + 2\pi n$, and $n \in N$ on the interval of the revolutions between t_1 and t_2. Only pairs of angles that ensure the solution of Eq. 1-12d with the given tolerance Δt_f are considered. Thus, we obtain not only a solution with the minimal total delta-v (the traditional criterion), but also the solution, which fulfils the demand that the flyby will miss the target orbit at a value not greater than the given value Δt_f. The solution, which ensures a practically zero time miss, exists because the real orbital change was caused by impulses with zero radial components. The solution time with this approach is much smaller than the solution time with the method of full enumeration, as the basic enumeration of angle φ_1 is made only on one revolution and angle φ_2 can be found using Eq. 2-2c. There is no need to use enumeration to find φ_2. Further consideration of the different combinations of angles $\varphi_{1_n}, \varphi_{2_n}$ for different revolutions requires only the computation of the left part of Eq. 1-12d for each pair.

This method gradually exceeds the method of direct enumeration. It is much faster and has the same or even better accuracy. A comparison of the accuracy and performance of these two methods can be found in section 9.2.8.

If the orbits are determined with considerable errors, no special solution is proposed, as the suggested two-impulse solution allows us to solve the problem.

9.2.5. Manoeuvres Performed by Low-Thrust Engines in the Case of Accurate Orbital Determination

As was mentioned in Chapter 6, the real spacecraft thrust engine orientation is fixed in the orbital or inertial coordinate frame during manoeuvring. For a spacecraft with low-thrust engines, the manoeuvres are usually applied with fixed orientation of the thrust engines in the orbital coordinate frame. It is supposed further that this orientation of the thrust engines is used for the manoeuvre parameter assessment problem solution.

The alteration of the eccentricity and the dimensionless semimajor axis caused by the firing of the thrust engines on the angular interval $\Delta\varphi$ can be found using eqs. 6-4 and 6-8:

$$4\sin\frac{\Delta\varphi}{2} = \frac{w_c}{w}\Delta e, \tag{9-11}$$

$$2\Delta\varphi = \frac{w_c}{w}\Delta a. \tag{9-12}$$

After the division of Eq. 9-11 by 9-12, we get the equation for the determination of $\Delta\varphi$:

$$\frac{\Delta e}{\Delta a} = \frac{2\cdot\sin(\frac{\Delta\varphi}{2})}{\Delta\varphi}. \tag{9-13}$$

By solving the transcendental Eq. 9-13, one can find the duration of the thrust engine firing $\Delta\varphi$. Then, with the use of eqs. 9-11 or 9-12, the acceleration of the spacecraft caused by the thrust engine firing can be found ($w = \frac{P}{m}$):

$$w = \frac{w_c}{2\Delta\varphi}\Delta a.$$

The manoeuvre delta-v ΔV_t can be found as follows:

$$\Delta V_t = \frac{w}{w_c} V_0 \Delta\varphi. \tag{9-14}$$

The position of the active interval φ_e, which coincides with the impulse application moment in the optimal impulse solution (Braude and Kuzmak 1969, 323-338) is determined by:

$$\varphi_e = \operatorname{arctg}\left(\frac{\Delta e_y}{\Delta e_x}\right). \tag{9-15}$$

Lateral Manoeuvre Assessment

The middle part of the active interval of such a manoeuvre should be on the line of intersection of the initial and target orbits. The angle φ_z, which determines the position of the orbital intersection line, can be found using the equation:

$$\operatorname{tg}\varphi_z = -\frac{\Delta z}{\Delta V_z^*}.$$

If the orbital plane rotation is set by the deviations $\Delta\Omega, \Delta i$, then φ_z can be found as:

$$\operatorname{tg}\varphi_z = \sin i \frac{\Delta\Omega}{\Delta i}$$

The active interval angular duration can be determined with the use of Eq. 6-53:

$$\Delta\varphi_z = 2\arcsin\left(\frac{w_c \Delta\gamma}{2w}\right). \tag{9-16}$$

where $\Delta\gamma$ = the angle between the orbital planes, which is calculated by Eq. 1-14d:

$$\Delta\gamma = \sqrt{\Delta z^2 + \Delta V_z^{*2}}.$$

The lateral impulse magnitude is determined by:

$$\Delta V_z = \frac{w}{w_c} V_0 \Delta\varphi_z .$$

Assessment of Long-Duration Manoeuvres Altering All Orbital Elements

Let us look at the case when the correction of the orbital coplanar and noncoplanar elements occurs simultaneously. To perform this manoeuvre, the thrust vector is rotated by the angle β out of the orbital plane. We have the following components of the thrust vector:

$P_t = P\cos\beta$ (thrust vector transversal component);
$P_z = P\sin\beta$ (thrust vector binormal component).

The ratio of the thrust vector to mass (w) will also have two components:

$$w_t = \frac{P_t}{m}; w_z = \frac{P_z}{m}. \tag{9-17}$$

The full acceleration magnitude is:

$$w = \sqrt{w_t^2 + w_z^2} .$$

It is supposed that during the manoeuvre, the orientation of the thrust vector in respect of the orbital coordinate frame cannot change.

The duration of the active interval $\Delta\varphi$ can be found from Eq. 9-13, and then w_t can be found using Eq. 9-12:

$$w_t = \frac{\Delta a}{2\Delta\varphi} w_c . \tag{9-18}$$

w_z can be found with the knowledge of $\Delta\varphi$ from Eq. 9-16:

$$w_z = \frac{\Delta\gamma}{2\sin\left(\frac{\Delta\varphi}{2}\right)} w_c. \tag{9-19}$$

The next step is to find the thrust vector orientation:

$$\beta = \operatorname{arctg}\left(\frac{w_z}{w_t}\right). \tag{9-20}$$

The components of delta-v can be determined with the use of eqs. 9-21 and 9-22:

$$\Delta V_t = \frac{w_t}{w_c} V_0 \Delta\varphi, \tag{9-21}$$

$$\Delta V_z = \frac{w_z}{w_c} V_0 \Delta\varphi. \tag{9-22}$$

The manoeuvre's magnitude ΔV can be calculated with the equation:

$$\Delta V = \sqrt{\Delta V_t^2 + \Delta V_z^2}.$$

The middle parts of the active intervals for eccentricity alteration and the orbital plane rotation should coincide if these alterations were caused by a single manoeuvre. However, due to the errors in orbital determination, these moments may slightly fail to coincide. In this case, the results obtained for the determination of the moment of impulse application with the errors in the orbital determination can be used for the determination of the active interval center (see section 9.2.3).

Another approach for the assessment of long-duration manoeuvres is the full enumeration of parameters such as the start and end times of thrust engine firing, the thrust vector orientation, and the magnitude of acceleration made by the thrust engines, with further selection of the solution, which will ensure the necessary alteration of the orbital elements (Alfriend, Kamensky, Stepanyants, and Tuchin 2009, 3-22; Borovin, Stepanyantz, Tuchin, and Tuchin et al. 2012). Meanwhile, the number of steps, with which the calculation of the orbital element changes are

performed, is equal to $\frac{n_{\varphi}^2 n_{\beta} n_w}{2}$, where n_{φ} = the number of the steps of enumeration for the time of the thrust engine firing start and end; n_{β} = the number of enumeration steps for the thrust vector orientation; and n_w = the number of enumeration steps for acceleration. Thus, it can be stated that the method proposed in this section demands reduced calculation time in comparison to the method presented in Alfriend, Kamensky, Stepanyants, and Tuchin (2009, 3-22) and Borovin, Stepanyantz, Tuchin, and Tuchin et al. (2012).

9.2.6. Manoeuvres Performed by Low-Thrust Engines with Inaccuracies in Orbital Determination

Coplanar Manoeuvres

If there are errors in the determination of the initial and target orbits (especially errors in the determination of the target orbit), the procedure for determining the single long-duration manoeuvre parameter problem solution gradually changes.

It is supposed that the acceleration caused by the active space object thrust engine firing *w* was calculated before, as a result of the assessment of the single long-duration manoeuvre parameters with the use of the algorithm depicted in section 9.2.5 with the initial and target orbits determined with high precision.

In Fig. 9-15, one can find the area between the dashed circles that corresponds to the acceptable values of the dimensionless difference between the semimajor axes. Also, the ellipse that constraints the area, corresponding to the acceptable values of the eccentricity vector difference, is shown in the figure. Unlike the case which was considered in section 9.2.3, the area constrained with dashed circles and the area constrained with the ellipse may not intersect, and the ellipse will be inside the smaller circle. According to eqs. 9-11 and 9-12, this is connected to less effective eccentricity correction for long-duration manoeuvre conditions. However, the solution with a single ignition can take place in this case as well.

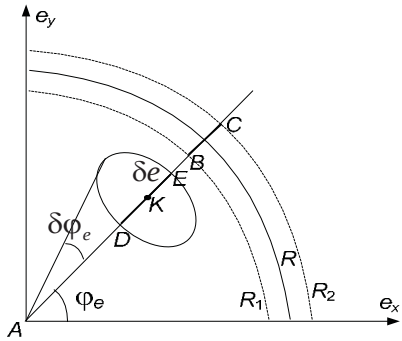

Fig. 9-15. Determination of the influence of the semimajor axis difference error and eccentricity vector differences

Unlike the impulsive case, it is hard to determine the time of the manoeuvre's middle. This is why angle φ_t is not used. If a manoeuvre that does not change the orbital plane is considered, then angle φ_e is agreed as the middle of the angular interval of the thrust engine firing. This is because the middle of the long-duration manoeuvre should coincide with the optimal impulse manoeuvre application angle (Braude and Kuzmak 1969, 323-338).

The algorithm of the manoeuvre parameter assessment consists of the enumeration of the points of line segment *BC* (Fig. 9-15) with some steps. The angular duration of manoeuvre $\Delta\varphi_i$, which ensures the corresponding alteration of the semimajor axis, is estimated for every value Δa_i from line segment *BC* with the use of Eq. 9-12. Then, with the help of Eq. 9-11, the eccentricity alteration caused by this manoeuvre is found. If the found value of the eccentricity Δe_i belongs to line segment *DE*, then the found solution is acceptable. The goal is to find the solution that has the maximum close propagation distributions $p_{\Delta a}(\Delta a_i)$ and $p_{\Delta e}(\Delta e_i)$. The angular duration of the manoeuvre $\Delta\varphi_i$, which corresponds to Δa_i, is the problem solution. The middle of the active interval is determined by the angle $\varphi_{imp} = \varphi_e$.

Noncoplanar Manoeuvres

Let us suppose that the assessed parameter has both transversal and lateral components. In this case, the middle part of the orbital plane rotating optimal manoeuvre should coincide with angle φ_z, which determines the position of the initial and target orbital plane intersection line. If there are errors in orbital determination, then the angle of the optimal eccentricity correction φ_e and the angle of optimal orbital plane rotation φ_z do not coincide. The angular difference $\delta\varphi_z$ is the maximum error in the determination of angle φ_z. The lines with the inclines $\varphi_z - \delta\varphi_z$ and $\varphi_z + \delta\varphi_z$ determine the area that is acceptable for the middle of the manoeuvre, which rotates the orbital plane. If this area has common points with the area constrained by the ellipse (we will designate it the area of intersection of the two areas *P*, shaded in Fig. 9-16), then the solution with one long-duration manoeuvre can exist; otherwise we have to consider the two manoeuvre parameter determination.

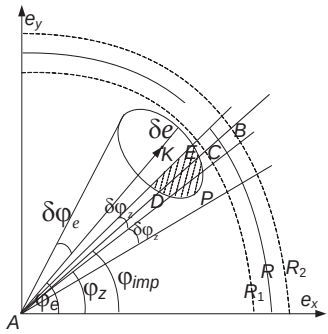

Fig. 9-16. The influence of the error in determining the difference between the semimajor axes, the difference between the eccentricity vector, and the errors in angle φ_z, which determine the orbital plane rotation

Angle φ_{imp} can be taken as the middle of the angular manoeuvring interval and can be found by:

$$\frac{\delta\varphi_e}{\varphi_e - \varphi_{imp}} = \frac{\delta\varphi_z}{\varphi_{imp} - \varphi_z}.$$

We get:

$$\varphi_{imp} = \frac{\delta\varphi_z\varphi_e + \delta\varphi_e\varphi_z}{\delta\varphi_e + \delta\varphi_z}.$$

The later angular duration of the manoeuvre, which ensures the corresponding alteration of the semimajor axis $\Delta\varphi_i$, is calculated for each value Δa_i (from line segment *BC*, see Fig. 9-16). The equation system 9-23 to 9-25 should be solved and the values $\Delta\varphi_i, w_t, w_z$ can be found:

$$w_t = \frac{\Delta a_i}{2\Delta\varphi_i} w_c. \tag{9-23}$$

$$w_z = \frac{\Delta\gamma}{2\sin\left(\frac{\Delta\varphi_i}{2}\right)} w_c, \tag{9-24}$$

$$w = \sqrt{w_t^2 + w_z^2}, \tag{9-25}$$

where $\Delta\gamma$ = the nominal angle between the orbital planes. Then, by using Eq. 9-26:

$$\Delta e_i = 4\frac{w_t}{w_c}\sin\frac{\Delta\varphi_i}{2}, \tag{9-26}$$

one can find the eccentricity alteration caused by this manoeuvre. If the found eccentricity value Δe_i belongs to line segment *DE* (Fig. 9-15), the solution is acceptable. The goal is to find an acceptable solution with maximum close probability densities $p_{\Delta a}(\Delta a_i)$ and $p_{\Delta e}(\Delta e_i)$. The angular manoeuvre duration $\Delta\varphi_i$, which corresponds to a value such as Δa_i, is the problem solution. The middle part of the active phase is determined by the angle φ_{imp}. The thrust vector orientation can be found using Eq. 9-20.

If the engine thrust is unknown, the problem should be solved the same way as in the case of precise orbital determination.

9.2.7. Two-Impulse Coplanar Manoeuvres Over a Longer Period of Time

As in the previous section, it is assumed that the thrust engines maintain a constant transversal orientation in the orbital coordinate frame (as the most effective one) during the manoeuvres. The proposed solution method allows us to account for the orientation in the inertial coordinate frame as well, but the orbital orientation is considered because it is met more frequently in practical contexts.

There are two approaches for the application of the two long-duration manoeuvres: the realization of the connected manoeuvre with the purpose of the semimajor axis and eccentricity vector alteration; and the realization of the two independent manoeuvres (each of the manoeuvres causes the alteration of one orbital parameter).

If two optimal connected manoeuvres ate performed, the center of the angular interval $\Delta\varphi_1$, on which the first manoeuvre is performed, should be situated on angle φ_e, which is optimal for the application of the first impulse in the impulse solution:

$$\mathrm{tg}\varphi_e = \frac{\Delta e_y}{\Delta e_x},$$

The center of the angular interval of the second manoeuvre should be half a revolution further on.

In accordance with eqs. 9-11 and 9-12, the transfer conditions on the given orbit can be described as:

$$\begin{cases} 4\sin\dfrac{\Delta\varphi_1}{2} - 4\sin\dfrac{\Delta\varphi_2}{2} = \dfrac{w_c\Delta e}{w} \\ 2\Delta\varphi_1 + 2\Delta\varphi_2 = \dfrac{w_c\Delta a}{w} \end{cases} \tag{9-27}$$

It is supposed that the acceleration $w = P/m$, produced by the thrust engines, was determined earlier when the assessment of the single manoeuvre was fulfilled.

Using Eq. 9-27, one can find the manoeuvre angular durations $\Delta\varphi_1$ and $\Delta\varphi_2$:

$$\Delta\varphi_1 = \frac{w_c \Delta a}{4w} + 2\arcsin\frac{w_c \Delta e}{8w\cos\dfrac{w_c \Delta a}{8w}},$$

$$\Delta\varphi_2 = \frac{w_c \Delta a}{4w} - 2\arcsin\frac{w_c \Delta e}{8w\cos\dfrac{w_c \Delta a}{8w}}.$$

Negative $\Delta\varphi$ means that the thrust vector should be transversal and directed towards the space object's motion during manoeuvring (i.e. braking occurs).

Thus, the transfer problem solution has been obtained, but, in fact, the rendezvous problem should be solved. In order to solve the rendezvous problem, we select the impulse application order and the manoeuvring revolutions using enumeration, and compare the time deviations.

If the manoeuvres are performed individually, it is more complicated. It is not necessary for the middle parts of the manoeuvres to be divided by half a revolution. The first part of the assessment algorithm of such manoeuvres is analogous to the assessment algorithm of the two small duration manoeuvres. The application angle of the first impulse $\varphi_1 = \varphi_{1_f}$ is fixed on one of the revolutions of the allowed interval between the moments of the initial condition fixation. Then, the transversal components and the application angle of the second impulse φ_{2_f} are determined using eqs. 2-2a to 2-2c.

As with the previous case, it is supposed that the middle points of the angular intervals with long-duration manoeuvres coincide with the optimal solution impulse application angles.

$\Delta\varphi_1$ can be found from the equation:

$$\Delta e_1 = 4\frac{w}{w_c}\sin\frac{\Delta\varphi_1}{2},$$

where Δe_1 = the eccentricity alteration made by the first manoeuvre of the impulse solution. $\Delta\varphi_1$ is the necessary angular duration of the first manoeuvre that leads to eccentricity alteration made by the first impulse. Similarly, the angular duration of the second manoeuvre $\Delta\varphi_2$ is:

$$\Delta\varphi_2 = 2\arcsin\frac{w_c\Delta e_2}{4w}.$$

Each manoeuvre causes a necessary change in eccentricity in the required direction. Thus, the desired eccentricity vector will be formed after the manoeuvres.

The problem remains that the semimajor axis alteration will be greater than needed. According to eqs. 9-11 and 9-12, it changes more efficiently than the eccentricity in conditions of long duration and the fixed orientation of the thrust engines.

This difference can be eliminated with the help of the following iteration procedure. Let us suppose that the initial semimajor axis deviation was $\Delta a_0 = a_f - a_0$ (for example, $\Delta a_0 > 0$). This deviation Δa_0 and deviations $\Delta e_{x_0}, \Delta e_{y_0}$ are used in determining the manoeuvre parameters.

After the realization of the estimated manoeuvres, the new semimajor axis a_1 will be obtained. Its value exceeds the required one. On the next iteration, the deviations $\Delta a_1 = \Delta a_0 + a_f - a_1$, $\Delta e_{x_0}, \Delta e_{y_0}$ (the semimajor axis deviation will be smaller than the original one) will be used; on the next iteration $\Delta a_2 = \Delta a_1 + a_f - a_2$, the values will be used etc. The process continues until the semimajor axis is obtained with the desired accuracy.

Thus, for the fixed angle φ_{1_f}, the target orbit transfer problem is solved with the use of two long-duration manoeuvres.

The enumeration continues with the angles φ_{1_f}, ensuring the solution of Eq. 1-12d with the desired accuracy Δt_f. This allows us to find the solution with the minimum total delta-v and the target orbit transfer time miss does not exceed the given Δt_f. Thus, the transfer problem solution and even the rendezvous problem solution will be obtained.

As we can see, the enumeration of angle φ_{1_f}, just as in the impulsive case, is made by one unknown variable and only on one revolution.

9.2.8. Two-Impulse Noncoplanar Manoeuvres Over a Longer Period of Time

The solution results from the previous simpler impulsive problem are used, just as with the transition from the coplanar two-impulse solution to the solution with long intervals of thrust engine firing.

Similarly, φ_{1_f} is enumerated (the first impulse application angle) and the impulsive solution is searched for each value of the angle φ_{1_f} with the algorithm from section 9.2.4. Let us suppose that the impulsive solution consists of two impulses with magnitudes $\Delta V_1, \Delta V_2$, the impulse application angles φ_{1_f} and φ_2, and the components $\Delta V_{t_1}, \Delta V_{z_1}, \Delta V_{t_2}, \Delta V_{z_2}$. The orientation of the thrust engines is adjusted by the angles β_i:

$$\mathrm{tg}\beta_1 = \frac{\Delta V_{z_1}}{\Delta V_{t_1}}, \mathrm{tg}\beta_2 = \frac{\Delta V_{z_2}}{\Delta V_{t_2}}.$$

The lateral component of the first impulse will change the orbital plane orientation $\Delta\gamma_1 = \Delta V_{z_1} = \Delta V_1 \sin\beta_1$, while the transversal component will lead to the alteration of the eccentricity $\Delta e_1 = 2\Delta V_{t_1} = 2\Delta V_1 \cos\beta_1$ and the semimajor axis $\Delta a_1 = 2\Delta V_{t_1} = 2\Delta V_1 \cos\beta_1$.

The acceleration made by the thrust engines in the transversal direction is $w_t = w\cos\beta$, while in the lateral direction it is $w_z = w\sin\beta$.

As in the previous section, we find the angular duration of the manoeuvre, which will alter the eccentricity by means of the first manoeuvre, corresponding to the alteration caused by the first impulse:

$$\Delta e_1 = 2\Delta V_{t_1} = 4\frac{w_t}{w_c}\sin\frac{\Delta\varphi_1}{2},$$

$$\Delta e_1 = 2\Delta V_1 \cos\beta_1 = 4\frac{w\cos\beta_1}{w_c}\sin\frac{\Delta\varphi_1}{2},$$

$$\Delta V_1 = 2\frac{w}{w_c}\sin\frac{\Delta\varphi_1}{2},$$

$$\Delta\varphi_1 = 2\arcsin\frac{w_c\Delta V_1}{2w}.$$

The calculated long-duration manoeuvre will rotate the orbital plane by angle $\Delta\gamma$, which can be found using the equation:

$$\Delta\gamma = 2\frac{w}{w_c}\sin(\frac{\Delta\varphi}{2}).$$

The angular duration of the manoeuvre leading to the required orbital plane rotation can be evaluated independently:

$$\Delta\gamma_1 = \Delta V_{z_1} = \Delta V_1 \sin\beta_1 = 2\frac{w\sin\beta_1}{w_c}\sin(\frac{\Delta\varphi_1}{2}),$$

$$\Delta\varphi_1 = 2\arcsin\frac{w_c\Delta V_1}{2w}.$$

The same value $\Delta\varphi_1$ was evaluated after using the eccentricity equation. Thus, the required alteration to the eccentricity and the orbital plane rotation with the given manoeuvre duration can be obtained.

Similarly, the duration of the second manoeuvre $\Delta\varphi_2$ can be found. The required eccentricity vector will be formed and the orbital plane rotation will be done with the known manoeuvre durations. The error arising in the adjustment of the semimajor axis can be eliminated by the iteration procedure, which is analogous to the procedure from the previous section.

9.2.9. Examples

A program for the numerical integration of the spacecraft equations of motion accounting for the firing of the thrusters was used to formulate the initial conditions and can be used for the quality assessment of the aforementioned algorithms. The initial spacecraft state vector and the manoeuvre parameters provided the initial conditions for this program. The spacecraft terminal state vector after all manoeuvres was obtained. Then, the initial and the final state vectors were used in the program, which uses the aforementioned algorithms and gives assessed values for the manoeuvring parameters. These assessed values were compared to the

desired ones, which were used in the motion prognosis program. Based on this comparison, a conclusion about the magnitude of the error in the assessment of the manoeuvre parameters was made.

Two initial orbits were considered. Orbit 1 is a low Earth orbit, while orbit 2 is a geostationary orbit. The orbital elements are described in table 9-1.

The calculation results can be found in tables 9-2 to 9-9 (Baranov and Karatunov 2016, 284-295; Baranov, Karatunov, Razoumny, and Vikhrachev 2017, 141-149). In the tables, ΔV = the manoeuvre delta-v; β = yaw; θ = pitch; $\Delta\varphi$ = manoeuvre angular duration; and w = spacecraft acceleration made by the thrusters (indexes 1 and 2 near the parameters denote the number of manoeuvres to which they belong).

The initial orbital parameters for both variants can be found in table 9-1.

Table 9-1. Test orbit initial parameters

Orbital elements	Orbit 1	Orbit 2
a km	6,662.813	42,168.262
e_x	0.003335	-0.000021
e_y	0.000524	0.000134
i deg	51.72082	0.15140
Ω deg	97.72594	84.06768
*U*deg	0.014097	151.36502
Date	2012.09.20	2014.04.14
Time	02:04:13.683	21:07:26.540

Table 9-2 presents the results of the two assessments of single noncoplanar small-duration manoeuvres. This assumption can be explained by the ratio of the spacecraft thrust and mass (P = 2,940; N (300 kg(f)); m = 7,127 kg) and the impulse magnitude (ΔV < 26 m/s). The manoeuvres were applied in orbit 1.

As is clear, the parameters of such manoeuvres can be estimated with high accuracy. This is the case not only for the magnitude and the orientation of the impulse, but also for the moment of impulse application.

Table 9-2. Assessment of single-impulse noncoplanar short manoeuvres for orbit 1

Manoeuvre parameters	Given values	Assessment result	Errors
Test 1			
ΔV m/s	25	24.99	0.04%
φ deg	0	0.03	-
β deg	330	329.94	0.02%
Time	2:49:31.8	2:49:32.1	0.3 sec
Test 2			
ΔV m/s	12.5	12.49	0.08%
φ deg	0	0.04	-
β deg	45	45.04	0.09%
Time	2:49:16.7	2:49:17.3	0.6 sec

The results of the assessments of the single coplanar and noncoplanar long-duration manoeuvres can be found in tables 9-3 and 9-4 (Baranov and Karatunov 2016, 284-295). The spacecraft mass = 7,127 kg; the engine thrust in case of the coplanar manoeuvres = 132.3 N (13.5 kg(f)); and the engine thrust in the case of noncoplanar manoeuvres = 122.5 N (12.5 kg(f)). It can easily be seen that the parameters of such manoeuvres have been assessed with a high level of accuracy.

The assessment results for the two dynamic operations are described in table 9-5 for low orbit 1. Each operation consisted of the two small-duration manoeuvres. This assumption can be explained by the ratio of the spacecraft's thrust and mass (P = 2,940; N (300 kg(f)); m = 7,127 kg) and the magnitude of the impulse (ΔV < 26 m/s). For the sake of comparison, the assessment was made using the traditional method of full enumeration and the quick method proposed in this work.

The search interval for the impulse application moments for test 7 was approximately 3 hours in length: 2012.09.20 6:04:13.6835 – 2012.09.20 9:14:00.0000.

The search interval for test 8 was much longer (approximately 15 hours): 2012.09.20 06:04:13.6835 – 2012.09.20 21:14:00.0000.

The angle selection step for tests 7 and 8 was 1º and the maximum phase error for the quick method was 1 second.

As can be seen, the use of the quick method for orbit 1 allowed us to reduce the time of computation by several orders and increase the accuracy of the manoeuvre assessment.

Table 9-6 presents two examples, which have reference solutions with the small pitches of the impulses. The pitch was 1º in test 3 and 2º in test

4. These examples imitate the impulses, performed with respective errors in the thruster orientation. As a result, the error in the determination of each impulse does not exceed 8 % for the quick method and can reach up to 27 % for the traditional method. The total delta-v can be estimated to an even higher level. The quick method gives a value of approximately 2.5 % for the determination error, while the value for the traditional method is 6.5%. The time of the impulse application can also be estimated more accurately using the quick method.

Table 9-7 gives the results of manoeuvre assessment for the geostationary orbit (orbit 2).

The search interval for tests 11 and 12 was: 2014.04.14 21:07:26.5421 – 2014.04.15 21:00:00.0000.

The angle selection step was 0.1º and the maximum phase error was 20 s.

The manoeuvre parameters can be assessed more accurately for orbit 2. This can be explained by the difference in the orbital periods.

There are practically no errors in the impulse assessment for the geostationary orbit. The impulses have radial components.

Tables 9-8 and 9-9 show the results of the two-impulse long-duration manoeuvre assessment.

The spacecraft mass = 7,127 kg and the engine thrust in tests 13 and 14 = 98 N (10 kg(f)). The engine thrust in tests 15 and 16 = 5.9 N (0.6 kg(f)).

The search interval for tests 13 and 14 was: 2012.09.20 06:04:13.6835 – 2012.09.20 09:14:00.000.

The search interval for tests 15 and 16 was: 2014.04.14 21:07:26.5421 – 2014.04.15 21:00:00.000.

The angle selection step for tests 13 and 14 = 1°.

The angle selection step for tests 15 and 16 = 0.1°.

The maximum phase error in tests 13 and 14 was 1 s.

The maximum phase error in tests 15 and 16 was 20 s.

We can also note that the manoeuvre parameters have been assessed with high accuracy and a very short time period.

There is no comparison with the solutions of other types as only single long-duration manoeuvres were assessed in the works of Alfriend, Kamensky, Stepanyants, and Tuchin (2009, 3-22) and Borovin, Stepanyantz, Tuchin, and Tuchin et al. (2012).

Table 9-3. Assessment of single-impulse coplanar long-duration manoeuvres for orbit 1

Manoeuvre parameters	Given values	Assessment result	Errors
Test 3			
ΔV m/s	25	24.94	0.2%
$\Delta\varphi$ deg	89.13	86.12	3.4%
$W\ 10^{-2}$ m/s^2	1.858	1.917	3.1%
Time of manoeuvre start	2:51:00.0	2:51:47.0	47 sec
Time of manoeuvre end	3:13:33.2	3:13:28.0	5.2 sec
Test 4			
ΔV m/s	12.5	12.49	0.1%
$\Delta\varphi$ deg	44.66	43.65	2.2%
$W\ 10^{-2}$ m/s^2	1.858	1.903	2.4%
Time of manoeuvre start	2:51:00.0	2:51:15.5	15.5 sec
Time of manoeuvre end	3:02:13.2	3:02:11.9	1.3 sec

Table 9-4. Assessment of single-impulse noncoplanar long-duration manoeuvres for orbit 1

Manoeuvre parameters	Given values	Assessment result	Errors
Test 5			
ΔV m/s	25	24.65	1.4 %
β deg	45	44.29	1.6 %
$\Delta\varphi$ deg	96.47	94.66	1.9 %
$W\ 10^{-2}$ m/s^2	1.720	1.726	0.4 %
Time of manoeuvre start	2:49:01.6	2:45:46.7	3:14.9
Time of manoeuvre end	3:13:12.2	3:09:29.6	3:42.6

Table 9-4 continued

Manoeuvre parameters	Given values	Assessment result	Errors
Test 6			
ΔV m/s	12.5	12.35	1.2 %
β deg	45	44.44	1.5 %
$\Delta\varphi$ deg	48.24	46.96	2.7 %
$W\ 10^{-2}$ m/s^2	1.720	1.747	1.6 %
Time of manoeuvre start	2:49:01.6	2:45:41.6	3:20.0
Time of manoeuvre end	3:01:06.3	2:57:21.4	3:44.9

Table 9-5. Assessment of two-impulse short manoeuvres for orbit 1

Impulse parameters	Reference	Traditional method	Errors	Quick method	Errors
Test 7					
Time of 1st impulse	2012.09.20 6:14:00.00	2012.09.20 06:12:31.06	01:28.94	2012.09.20 06:14:08.52	00:08.52
ΔV_1 m/s	10.5	12.07	15.0%	11.25	7.1%
β_1 deg	45	47.60	5.8%	46.10	2.4%
θ_1 deg	0	-14.38	-	0	-
Time of 2nd impulse	2012.09.20 8:22:30.00	2012.09.20 08:23:53.66	01:23.66	2012.09.20 08:22:55.65	00:25.65
ΔV_2 m/s	15.0	14.26	4.9%	14.91	0.6%
β_2 deg	315	317.41		315.24	0.1%
θ_2 deg	0	0.63	-	0	-
$\sum\Delta V$ m/s	25.5	26.33	3.2%	26.15	2.5%
Comp. time	-	2.521 s	-	0.003 s	-

Table 9-5 continued

Impulse parameters	Reference	Traditional method	Errors	Quick method	Errors
Test 8					
Time of 1st impulse	2012.09.20 18:14:00.00	2012.09.20 18:12:27.39	01:22.61	2012.09.20 18:14:08.45	00:08.45
ΔV_1 m/s	10.5	11.90	12.3%	11.25	7.4%
β_1 deg	45	46.04	2.3%	46.11	2.5%
θ_1 deg	0	-15.95	-	0	-
Time of 2nd impulse	2012.09.20 20:22:30.00	2012.09.20 20:24:05.12	01:35.12	2012.09.20 20:22:55.48	00:25.48
ΔV_2 m/s	15.0	14.49	10.2%	14.91	0.6%
β_2 deg	315	316.43	0.5%	315.24	0.1%
θ_2 deg	0	0.92	-	0	-
$\sum\Delta V$ m/s	25.5	26.39	3.5%	26.16	2.6%
Comp. time	-	57.839 s	-	0.005 s	-

Table 9-6. Assessment of two-impulse short manoeuvres with radial impulse components for orbit 1

Impulse parameters	Reference	Traditional method	Errors	Quick method	Errors
Test 9					
Time of 1st impulse	2012.09.20 6:14:00.00	2012.09.20 06:11:27.75	02:32.25	2012.09.20 06:14:08.53	00:08.53
ΔV_1 m/s	10.5	13.35	2.85 (27.1%)	11.33	0.83(7.9%)
β_1 deg	45	49.04	4.04(9.0%)	46.33	1.33(3.0%)
θ_1 deg	1	-25.19	26.19	0	1
Time of 2nd impulse	2012.09.20 8:22:30.00	2012.09.20 08:24:38.87	02:08.87	2012.09.20 08:22:52.47	00:22.47
ΔV_2 m/s	15.0	13.82	1.18(7.9%)	14.83	0.17(1.1%)
β_2 deg	315	319.21	4.21(1.3%)	315.39	0.39(0.1%)
θ_2 deg	1	-1.17	2.17	0	1
$\sum\Delta V$ m/s	25.5	27.17	1.67(6.6%)	26.16	0.66(2.5%)
Comp. time	-	2.521 s	-	0.003 s	-

Table 9-6 continued

Impulse parameters	Reference	Traditional method	Errors	Quick method	Errors
Test 10					
Time of 1st impulse	2012.09.20 6:14:00.00	2012.09.20 06:11:30.77	02:29.23	2012.09.20 06:14:23.62	00:23.62
ΔV_1 m/s	10.5	13.37	2.87(27.3%)	11.02	0.52(6.0%)
β_1 deg	45	48.99	3.99(8.7%)	44.41	0.59(1.3%)
θ_1 deg	2	-25.12	27.12	0	2
Time of 2nd impulse	2012.09.20 8:22:30.00	2012.09.20 08:24:38.86	02:08.86	2012.09.20 08:23:00.54	00:30.54
ΔV_2 m/s	15.0	13.78	1.22(8.1%)	15.13	0.13(0.7%)
β_2 deg	315	319.18		313.93	1.07(0.3%)
θ_2 deg	2	-0.82	2.82	0	2
$\sum\Delta V$ m/s	25.5	27.15	1.65(6.5%)	26.16	.66(2.5%)
Computation time	-	2.521 s	-	0.003 s	-

Table 9-7. Assessment of two-impulse short manoeuvres for orbit 2

Impulse parameters	Reference	Traditional method	Errors	Quick method	Errors
Test 11 (coplanar manoeuvre)					
Time of 1st impulse	2014.04.15 08:00:00.00	2014.04.15 08:04:21.91	4:21.91	2014.04.15 08:00:40.66	0:40.66
ΔV_1 m/s	10.5	10.52	0.02 (0.2%)	10.52	0.02 (0.2%)
β_1 deg	180	179.95	0.05 (0.0%)	179.95	0.05 (0.0%)
θ_1 deg	0	0.10	0.10	0	0
Time of 2nd impulse	2014.04.15 20:00:00.00	2014.04.15 20:01:58.52	1:58.52	2014.04.15 19:59:21.25	0:38.75
ΔV_2 m/s	15.0	14.97	0.03 (0.0%)	14.97	0.03 (0.0%)
β_2 deg	180	179.96	0.04 (0.0%)	179.97	0.03 (0.0%)
θ_2 deg	0	0.05	0.05	0	0
$\sum\Delta V$ m/s	25.5	25.49	0.01 (0.0%)	25.49	0.01 (0.0%)
Computation time	-	57.163 s		0.146 s	
Test 12					
Time of 1st impulse	2014.04.15 08:00:00.00	2014.04.15 07:56:17.92	3:42.18	2014.04.15 07:58:09.13	1:50.87
ΔV_1 m/s	10.5	10.40	0.10 (1%)	10.32	0.18 (1.7%)
β_1 deg	45	44.88	0.22 (0.5%)	44.44	0.56 (1.2%)
θ_1 deg	0	0.49	0.49	0	0
Time of 2nd impulse	2014.04.15 20:00:00.00	2014.04.15 20:02:26.30	2:26.30	2014.04.15 20:01:10.69	1:10.69
ΔV_2 m/s	15.0	15.10	0.10 (0.7%)	15.17	0.17 (1.1%)
β_2 deg	315	315.06	0.06 (0.0%)	314.76	0.24 (0.0%)
θ_2 deg	0	1.23	1.23	0	0
$\sum\Delta V$ m/s	25.5	25.50	0	25.49	0.01
Computation time	-	54.556 s		0.145 s	

Table 9-8. Assessment of two-impulse long-duration manoeuvres for orbit 1

Impulse parameters	Reference	Solution	Error
Test 13			
Time of 1st manoeuvre start	2012.09.20 06:14:00.00	2012.09.20 06:12:47.88	1:12.12
Time of 1st manoeuvre end	2012.09.20 06:26:41.74	2012.09.20 06:25:59.37	0:42.37
$\Delta\varphi_1$ deg	50.6	52.5	1.9 (3.8%)
ΔV_1 m/s	10.50	10.51	0.01 (0.0%)
β_1 deg	45	43.77	1.23 (2.7%)
Time of 2nd manoeuvre start	2012.09.20 8:45:00.00	2012.09.20 08:44:18.95	0:41.05
Time of 2nd manoeuvre end	2012.09.20 9:03:03.52	2012.09.20 09:02:46.80	0:16.72
$\Delta\varphi_2$ deg	72.23	73.50	1.27 (1.8%)
ΔV_2 m/s	15	14.22	0.78 (5.2%)
β_2 deg	315	313.42	1.58 (0.5%)
Computation time		0.13 s	
$\sum\Delta V$ m/s	25.5	24.73	0.77 (3.0%)
Test 14 (coplanar manoeuvre)			
Time of 1st manoeuvre start	2012.09.20 06:14:00.00	2012.09.20 06:13:12.63	0:47.37
Time of 1st manoeuvre end	2012.09.20 06:26:41.74	2012.09.20 06:26:36.71	0:05.03
$\Delta\varphi_1$ deg	50.6	53.8	3.2 (6.3%)
ΔV_1 m/s	10.50	10.66	0.16 (1.5%)
β_1 deg	180	183.73	3.73 (2.1%)

Time of 2nd manoeuvre start	2012.09.20 8:45:00.00	2012.09.20 08:44:46.56	0:13.44
Time of 2nd manoeuvre end	2012.09.20 9:03:03.52	2012.09.20 09:02:47.24	0:16.28
$\Delta\varphi_2$ deg	72.23	72.32	0.09 (0.0%)
ΔV_2 m/s	15	13.9	1.1 (7.3%)
β_2 deg	180	179.77	0.33 (0.0%)
Computation time		0.14 s	
$\sum \Delta V$ m/s	25.5	24.56	0.94 (3.7%)

Table 9-9. Assessment of two-impulse long-duration manoeuvres for orbit 2

Impulse parameters	Reference	Solution	Error
Test 15			
Time of 1st manoeuvre start	2014.09.15 06:30:00.00	2014.09.15 06:33:27.26	3:27.26
Time of 1st manoeuvre end	2014.09.15 10:01:35.64	2014.09.15 09:55:39.01	5:56.63
$\Delta\varphi_1$ deg	52.37	50.23	2.14 (4.1%)
ΔV_1 m/s	10.50	9.70	0.80 (7.6%)
β_1 deg	45.00	43.05	1.95 (4.3%)
Time of 2nd manoeuvre start	2014.09.15 17:30:00.00	2014.09.15 17:25:06.17	4:53.83
Time of 2nd manoeuvre end	2014.09.15 22:30:58.72	2014.09.15 22:39:26.57	8:27.65
$\Delta\varphi_2$ deg	74.50	78.09	3.59 (4.8%)
ΔV_2 m/s	15	14.39	0.61 (4.1%)
β_2 deg	315	313.45	1.55 (0.5%)

Computation time		0.64 s	
$\sum \Delta V$ m/s	25.5	24.09	1.41 (5.5%)
Test16 (coplanar manoeuvre)			
Time of 1st manoeuvre start	2014.09.15 06:30:00.00	2014.09.15 06:25:54.38	4:04.62
Time of 1st manoeuvre end	2014.09.15 10:01:35.64	2014.09.15 09:58:23.64	3:12.00
$\Delta\varphi_1$ deg	52.37	53.92	1.55 (3.0%)
ΔV_1 m/s	10.50	10.14	0.36 (3.4%)
β_1 deg	180.00	179.49	0.51 (0.3%)
Time of 2nd manoeuvre start	2014.09.15 17:30:00.00	2014.09.15 17:25:23.41	4:36.59
Time of 2nd manoeuvre end	2014.09.15 22:30:58.72	2014.09.15 22:27:16.84	3:41.88
$\Delta\varphi_2$ deg	74.50	76.61	2.11 (2.8%)
ΔV_2 m/s	15	13.87	1.13 (7.5%)
β_2 deg	180	179.64	0.36 (0.0%)
Computation time		0.63 s	
$\sum \Delta V$ m/s	25.5	24.00	1.5 (5.9%)

Table 9-10 presents the results of the assessment of two single-impulse coplanar manoeuvres with errors in orbital determination (Baranov, Karatunov, Razoumny, and Vikhrachev 2017, 141-149). The second column gives the assessment results obtained without accounting for errors in orbital determination. The third one shows the assessment results obtained while accounting for errors in the initial and target orbital determination. Finally, the fourth one gives the magnitudes of the impulses planned for application. As we can see, the proposed method allows us to gradually increase the accuracy of the manoeuvre parameter assessment. Furthermore, if the calculated impulse is applied for the initial orbit, one can obtain the target orbit, which will be far closer to the real orbit than the one that was obtained using the measurements.

Table 9-10. Assessment of two single-impulse coplanar manoeuvres with the presence of the errors in orbital determination

Manoeuvre parameters	Without accounting for uncertainty	Accounting for uncertainty	Reference
Test 1 (Electro-L2)			
ΔV m/s	0.410	0.419	0.419
ΔV_t m/s	-0.392	0.419	0.419
ΔV_r m/s	-0.118	0	-
ΔV_z m/s	-0.016	0	-
Manoeuvre duration	18:07:33	18:08:17	18:09:54
Test 2 (Luch-5V)			
ΔV m/s	0.155	0.107	0.105
ΔV_t m/s	-0.134	-0.107	-0.105
ΔV_r m/s	0.002	0	-
ΔV_z m/s	-0.061	0	-
Manoeuvre duration	07:49:47	06:01:51	06:18:25

This algorithm can be used for the assessment of the impulses required for a given spacecraft orientation. It is impossible to sequence the thrusters that rotate the spacecraft perfectly. An impulse that affects the motion of the spacecraft's center of mass occurs and the assessment and the further accounting for these impulses will help increase the accuracy of motion prognosis for these spacecraft.

CHAPTER TEN

LARGE SPACE DEBRIS POPULATION DECREASE

There are two ways of mitigating overcrowding in the near space region. The first way focuses on preventing an increase in the number of space objects. For this purpose, it is necessary to transfer decommissioned spacecraft to appropriate disposal orbits (DOs). The second way is to clear space objects, especially large ones, from populated orbits. These two problems are considered in this chapter.

10.1. Manoeuvres Forming an Orbit with Fixed Time of Ballistic Existence

In solving the disposal problem, it is necessary to transfer various passive objects to a disposal orbit (DO) where they will no longer be a danger for active space objects. For the geosynchronous (GEO) region, such "graveyard" orbits are located above the geostationary orbits (250-350 km). In the case of the low Earth orbit (LEO) region, the parameters of the DO should ensure that the passive object orbital lifetime is less than or equal to the given value T_{exist}. According to "GOST (State All-union Standard) of Russia 52925-2008: Items of Space System Engineering: Basic Demands of Spacecraft for the Restriction of Technogenic Pollution of Near-earth Space" (anonymous 2008), T_{exist} is recommended as being no more than 25 years for all spacecraft at altitudes of less than 2,000 km after the active phase of the flight has been completed.

The spacecraft transfer to the low Earth DO manoeuvre parameter determination problem can be divided into two sub-problems. In the first problem, it is necessary to determine an orbit with reduced ballistic existence; in the second, it is necessary to determine the spacecraft transfer manoeuvre parameters for this DO. Two main types of DO can be distinguished. In the first case, an elliptical orbit is shaped with the use of a single braking impulse applied at the apocenter. Its pericenter is located

in the upper layers of the atmosphere. In the second case, a circular orbit is shaped by two braking impulses applied at the orbital apocenter and pericenter. The orbit is situated in the upper layers of Earth's atmosphere. The first case has lower fuel costs; however, the DO's apogee stays in the operational altitudes of active space objects. Hence, a spacecraft transferred to an elliptical DO will be dangerous for active space objects with orbits that are lower than the apocenter of the DO. As such, one of the problems considered involves the assessment of how quickly the elliptical DO's apogee will leave the active space object operational area. The transfer to a circular orbit immediately drags the spacecraft out of the active space object operational orbit area and the altitude of this orbit is higher than the altitude of the elliptical DO pericenter.

Due to the fact that the magnitudes of the impulses used to adjust the DO are quite large, and their precision falls at the end of the spacecraft existence period, it is necessary to divide these impulses into individual parts and apply them on different revolutions but with the same latitude arguments. This improves the accuracy of orbital determination after application of the velocity impulse and helps us better calculate the probability of a possible collision with space debris during orbital shaping. If there is a danger of collision, manoeuvres lowering the orbit can be rescheduled to future revolutions or performed earlier. Due to the considerable magnitudes of the manoeuvres, any changes to the times of manoeuvre execution will be made significantly more efficient in terms of collision avoidance.

10.1.1. Spacecraft Motion Simulation over a Long Time Interval

It is necessary to predict the motion of a spacecraft for a period of 25 years when selecting its DO. This results in considerable restrictions on the method of propagation. On the one hand, it is necessary to ensure a high level of prognostic accuracy; on the other hand, it needs to be quick enough to reduce the total computing time of the problem solution.

Modelling the spacecraft motion can be done very effectively using the TRACE software. This software is based on the numerical analytical THEONA spacecraft motion theory developed at the Keldysh Institute of Applied Mathematics of the Russian Academy of Sciences (Golikov 1990; Golikov 2008). The software realization has high accuracy and is 100-300 times faster than usual the method of numerical integration. The error is several centimeters per revolution along the orbit and less than a

millimeter in the lateral direction in comparison to the method of numerical integration.

The basic principles of THEONA numerical analytical theory can be briefly described as follows. As a drift orbit, we take the accurate solution of the generalized problem of two fixed centers—Euler's orbit. This type of solution takes into account the most significant effects of the gravitational field, determined by the second, third, and, partially, the fourth zonal harmonics of the gravitational potential. Therefore, Euler's orbital elements are used in differential equations of motion. The element selection in THEONA allows avoidance of the singularities typical for near-circular orbits: the satellite orbit latitude argument is selected as an independent variable. The satellite trajectory is divided into revolutions. Each revolution begins at one ascending node and ends at the next ascending node. For near-equatorial orbits, another variant of the "revolution" and nonsingular orbital elements are provided. Here, the integration variable is also angular, but it represents the sum of the latitude argument and the RAAN.

The choice of Euler's orbit as the drift orbit allows us to include the most significant disturbing factors in the interim motion of the satellite. The other dynamic effects are taken into consideration using the numerical analytical integration of differential equations for Euler's orbital elements.

The force model used for the calculation and propagation of spacecraft motion using the THEONA numerical analytical methods considers the most modern Russian standards:

- The Earth's gravitational field model PZ-90. The maximum degree and order of the model are defined by default at the point of software initialization, but they can also be changed by the operator. It is also possible to use the EGM2008 model from the IERS Conventions 2010 (ed. IAU 2009), adopted as an international standard.
- The dynamic model of Earth's atmosphere density GOST R 25645.166-2004.
- Solar and lunar gravitational influence.
- Solar radiation pressure taking the Earth's cylindrical shadow into account.
- Tidal forces, caused by changes to the Earth's surface.

The THEONA force model is practically the same as force models that are used in the numerical integration of the exact equations of orbital motion.

The fundamental astronomical and geodetic constants from the IERS Conventions 2010 (ed. IAU 2009 XXVI GA) are used as built-in

parameters. The Russian standards for corresponding constants (PZ-90.02) are also used.

The table of the exact ephemeris of the Sun and the Moon in the coordinate frame J2000 corresponds to the model DE405 created by JPL (Jet Propulsion Laboratory). The calculation of the position of the Sun and the Moon (to account for the gravitational influence of the external stellar bodies and the solar radiation pressure) can be carried out using this table or the approximate analytical equations depending on the TRACE software user selection. This selection is fixed at the point of initialization of the software for the calculation and prediction of the spacecraft's orbital parameters.

THEONA uses the cylindrical shadow model from the celestial body that has the orbiting satellite while considering the light pressure (from direct solar radiation). The light pressure force affecting the satellite is proportional to the light pressure coefficient. This coefficient depends on the satellite surface reflection coefficient and its figure.

Consideration of the tidal forces is limited (Love's model) with the tidal potential of "elastic" Earth, accounting for solar and lunar motion.

Also, the motion of the active spacecraft as it executes manoeuvres (impulsive and low-thrust) is provided in the THEONA numerical analytical prediction method.

Numerical analytical integration is carried out by the method of "step by step/revolution by revolution" summation of the orbital element perturbations calculated analytically within the revolution. Thus, this calculation scheme allows the tracking of changes to the orbital elements (long-period and secular) without the difficulties that arise in the classic methods of the general perturbation theory. The method of summing "revolution-by-revolution" makes it possible to take into consideration changes in physical parameters: the solar activity indices and the geomagnetic disturbance and minor motion (the pole, precession, and motion of nutation) of the Earth etc. Moreover, the spacecraft's orbit may significantly change (the manoeuvres, collisions, changes in spacecraft orientation and, hence, in the force model, etc.) during its mission. The new trajectory parameters require recalculation of the orbit and, hence, the orbital elements need to be updated. THEONA has no difficulty in dealing with these cases in contrast to analytical theories.

The short-period perturbations at the required time (or angular variable value) are calculated to make a prediction within the current revolution. The calculation of all (secular, long-period, and short-period) perturbations is carried out separately for each perturbing factor by the analytical integration of the perturbed motion of Lagrange-type or Newton-type

equations. At the same time, the special function recurrent relations of the THEONA numerical analytical theory that it uses allow us to realize rapid calculation. They are designed for the effective functioning of the whole THEONA extrapolator circuit accounting for all the features of the revolution per revolution summation of the analytic integrals.

In addition to the functions known from celestial mechanics, new special functions have been proposed:

- The orbit inclination functions are used for calculating the gravitational perturbations from the central (main) celestial body, external celestial bodies, and solar radiation pressure. They are directly expressed in terms of Jacobi's polynomial functions $P_{mk}^{n}(\cos i)$ from group representation theory. The basic inclination functions $Q_{mk}^{n}(\cos i)$ differ from the well-known Kaula's inclindation functions only by the normalization that optimizes the recurrence relations. The new additional inclination functions $\overline{Q}_{mk}^{n}(\cos i)$ were created to take into account the members of the third order of minority (approximately 10^{-9} for Earth's gravitational potential) in the inequalities caused by the noncentrality of Earth's gravitational field.
- The functions of two arguments $G_m^n(\alpha, e)$, their connection with Jacobi's functions $P_{mk}^{n}\left(\frac{1}{\sqrt{1-e^2}}\right)$ (from group representation theory), and cylindrical Bessel functions of the first kind $J_k(\alpha e)$ can be expressed as an infinite scalar product with index *k*:

$$G_m^n(\alpha, e) = \sum_{k=-\infty}^{\infty} J_k(\alpha e) \cdot P_{m-\alpha,k-\alpha}^{n}\left(\frac{1}{\sqrt{1-e^2}}\right).$$

The second argument of these functions is the orbital eccentricity *e*. The first argument, in accounting for the perturbations from the main celestial body's gravitational field, is a multiple of the ratio of the main celestial body's rotational angular velocity to the satellite's mean motion. When taking into account the influence of the gravitational forces from external celestial bodies, as well as the solar radiation pressure, the first argument of the function $G_m^n(\alpha, e)$ is a multiple of the ratio of the satellite's mean motion to the angular velocity of the external celestial body around the central one.

In the THEONA numerical analytical theory, the proposed functions $G_m^n(\alpha, e)$ are used when taking into account the gravitational perturbations, the solar radiation pressure, and the tidal forces. These functions are efficient in terms of integrals with respect to the latitude argument, true anomalies, or true longitudes.

Hansen's coefficients $X_{n,m}^{(k)}$ are a particular case with the first integer argument:

$$X_{n,m}^{(k)} = \left(1 - e^2\right)^{\frac{n+1}{2}} \cdot G_{k-m}^{-(n+2)}(k, e).$$

- The attached Legendre functions with noninteger superscripts $P_n^{\lambda}(x)$ can be used to take into account atmospheric braking more effectively than the associated Legendre functions with the integer indices since they do not require the additional approximation of the Earth's atmospheric density model. At the same time, they work both for understanding the distribution of the density over the height and to take into account the midday effect—the angle between the direction to the satellite and the "afternoon hump" in the planet's atmosphere.

  For all special functions used in THEONA, a scheme for their recurrent calculation has been developed. It allows us to implement fast calculations without using large conserved data arrays. This is especially effective for use in manoeuvring problems (TRACE software implementation).

  The TRACE software created using the THEONA propagator returns results in Cartesian coordinates in the Greenwich coordinate frame, fixed at a given time and in the osculating orbital Keplerian elements. Moreover, the accuracy of the obtained spacecraft state vector (the position and velocity) allows, if necessary, for us to proceed to numerical integration and back. This can be used in the calculation of manoeuvring tasks for short time intervals $t \in [t_{start}; t_{end}]$ (accurate short propagation).

10.1.2. Orbital Evolution with Fixed Time of Ballistic Existence

The results presented below were obtained using the numerical analytical method for propagation, which allows us to evaluate the dependencies between the various parameters ensuring the lowering of an

orbit when selecting its DO (Baranov, Budyansky, Chernov, and Golikov 2015, 4-19).

First of all, it is necessary to estimate when the spacecraft should be inserted into the selected DO. The nature of orbital lowering depends on the distribution of the atmospheric density at the current moment in time. This may be due to a seasonal effect (i.e. when the Sun is above or below the ecliptic), changes in solar activity, and geomagnetic disturbances. As a rule, these factors are taken into account in dynamic Earth atmospheric models by Russian and foreign scientists. Since the geomagnetic disturbance index cannot be predicted for more than a few days, its changes should not be used for long-term orbital motion propagation. At the same time, the solar activity indices for several years ahead are provided by various physics research centers around the world. The American center NOAA provides prognostic data of the current solar cycle of solar activity on a daily basis and also assesses the parameters for the next 11-year cycle. The spacecraft's orbital lowering rate also varies at different seasons.

Table 10-1 gives the dependency of the circular orbital altitude (the second option selecting the operational orbit) versus the time of its initialization (spacecraft deployment).

Here, we present the results of analysis of shaping a circular spacecraft orbit for two types of orbits with the different inclinations: 98º and 51.6º. If the initialization time is "delayed", the required altitude of the initial orbit decreases (see lines 1-7 and 8-14). This is explained by the fact that, in 2013-2015, the average index of solar activity increased (in the first half of the 11-year solar cycle) and an "early" spacecraft would pass through the thicker atmosphere over a longer time interval. At the same time, a seasonal effect can also be observed: the change rate in the autumn/spring period is slowing (see lines 2-3 and 4-5).

Table 10-1

№	Inclination deg	S (bal)	Year	Season	Date	Altitude km
1	98	0.03	2013	summer	2013.06.22	687.029
2				autumn	2013.09.22	685.351
3				winter	2013.12.21	685.512
4			2014	spring	2014.03.21	683.213
5				summer	2014.06.22	683.164
6				winter	2014.12.21	680.951
7			2015	summer	2015.06.22	679.167
8	51.6	0.03	2013	summer	2013.06.22	671.341
9				autumn	2013.09.22	670.871
10				winter	2013.12.21	669.772
11			2014	spring	2014.03.21	668.803
12				summer	2014.06.22	667.963
13				winter	2014.12.21	666.175
14			2015	summer	2015.06.22	664.737

Figure 10-1 displays a graph showing the described dependency of the spacecraft operational orbital altitude with different inclinations versus deployment date. The altitude implies a 25 year lifetime. The spacecraft ballistic coefficient is 0.03.

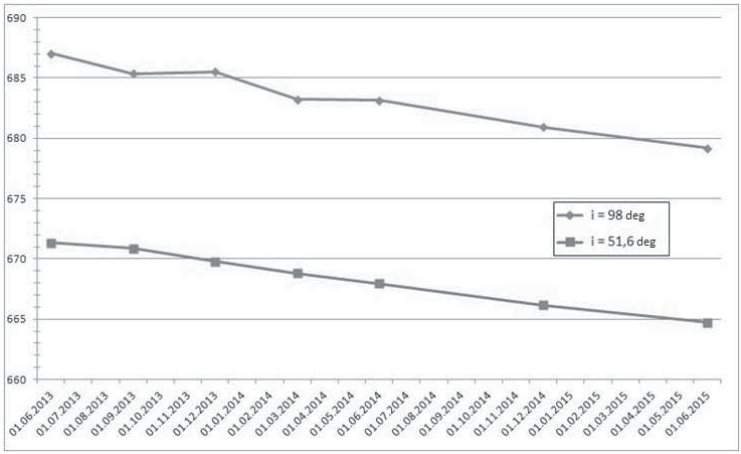

Fig. 10-1. Operational orbital altitude as a function of the deployment date

Table 10-2 shows the calculation results for the circular DO altitude (the second option in initial orbit selection) with the different ballistic coefficients: S (bal) = 0.18; 0.03; 0.005.

Table 10-2

#	Inclination deg	S (bal)	Year	Season	Date	Altitude km
1	98	0.18	2013	summer	2013.06.22	816.886
2	98	0.03	2013	summer	2013.06.22	687.029
3	98	0.005	2013	summer	2013.06.22	541.172
4	51.6	0.18	2013	summer	2013.06.22	802.061
5	51.6	0.03	2013	summer	2013.06.22	671.341
6	51.6	0.005	2013	summer	2013.06.22	540.094

The difference in altitude of the required orbits is significant: 162-175 km between the spacecraft with the biggest and the smallest ballistic coefficients. It is no coincidence that such values for the ballistic coefficients are chosen in the proposed test as they reflect the range for almost all the spacecraft used.

In addition to the circular orbit, another orbit can also be chosen as the spacecraft DO—an elliptical, eccentric orbit with a given altitude of apogee. In order to get the parameters of such an orbit, it is necessary to find the perigee altitude of a DO ensuring a fixed degradation time. In the case of an elliptical DO, the perigee altitude should be lower than in the first variant with a circular DO. This perigee altitude decreases with the augmentation of the given apogee altitude.

Table 10-3 shows the calculated results of the altitude required for a 25 year satellite lifetime with different ballistic coefficients and different specified orbital apogee altitudes. The spacecraft deployment starting date was June 22, 2013.

The lowering of the DO initial minimum altitude allows us to quickly lower the altitude of the orbital apogee into the thick layers of atmosphere. Thus, the DO leaves the area of operational orbits of active space objects sooner, reducing hazards to the active space objects with orbits lower than the DO apocenter. Further orbital lowering is similar to the variants with lower initial values of the given apogee altitude.

Table 10-3

Initial orbit	Initial inclination deg	Perigee altitude km		
		Ballistic coefficient S (bal) = 0.03	Ballistic coefficient S (bal) = 0.18	Ballistic coefficient S(bal) = 0.005
Near-Circular	98	687.031	816.886	541.172
	51.6	671.341	802.061	540.094
Apogee altitude 800 km	98	658.728	-	537.531
	51.6	625.571	-	532.219
Apogee altitude 1,100 km	98	616.639	774.837	519.231
	51.6	614.228	769.414	517.300
Apogee altitude 1,500 km	98	580.110		504.115
	51.6	579.868	743.301	503.301

The graph below presents a comparison of similar orbits with degradation for the initial circular orbit variant, as well as elliptical orbits with given apogee altitudes of 800 km and 1,000 km. The evolution of the maximum altitudes of the considered orbits is shown.

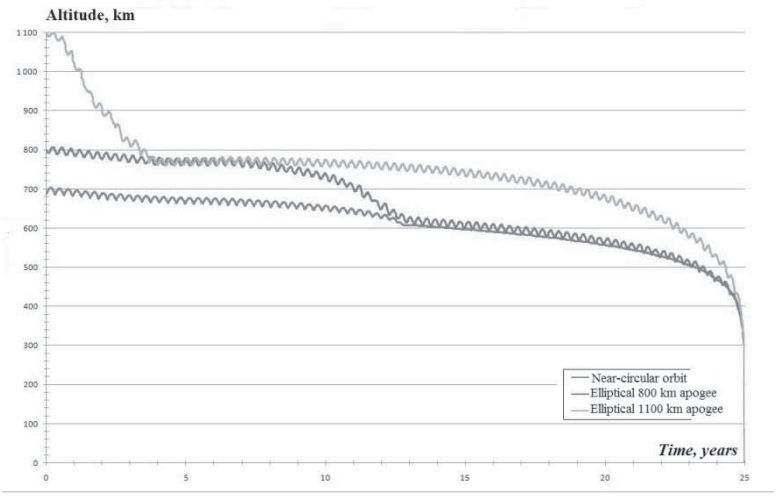

Fig. 10-2. Comparison of orbital altitude evolution versus time for circular and elliptical DOs (apogee altitude)

The rapid lowering of the "high" orbit with an initial apogee altitude of 1,100 km in the first 4 years makes it possible to argue that the variant of the high elliptic DOs may be interesting in terms of saving fuel (the fuel cost reduction on the manoeuvring for spacecraft deployment to the required orbit).

It is necessary to perform the calculations using the high-performance software for the DO selection scheme and the deployment of the spacecraft to this orbit. It is also required for the determination of the orbital degradation time and the moment of time of leaving the spacecraft's maximum orbital altitude from the spacecraft operational orbit area in the real project.

The following two graphs demonstrate the nature of spacecraft orbital degradation during 25 years for both the considered variants of the initial DO: the circular and the elliptical. In the pictures, besides the average altitude, the maximum and minimum spacecraft orbital altitudes are shown.

The eccentricity decreases with time for the elliptical orbit and altitude lowering into the thicker layers of the atmosphere tends to be the same as for the circular orbital evolution.

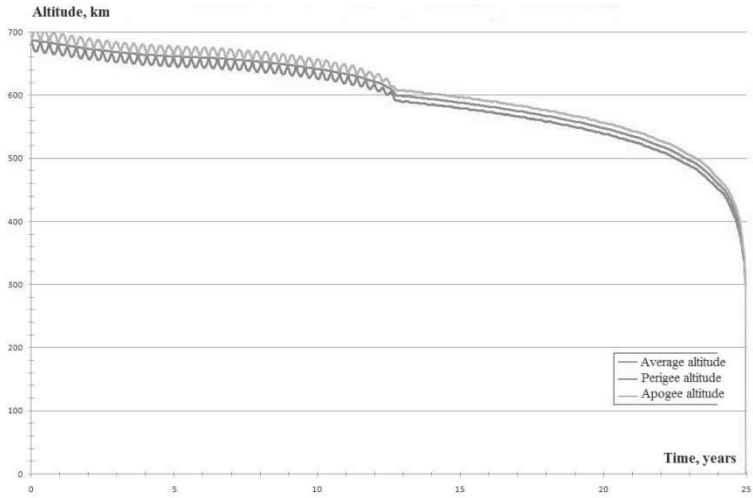

Fig. 10-3. Near-circular orbital degradation versus time (inclination 98°)

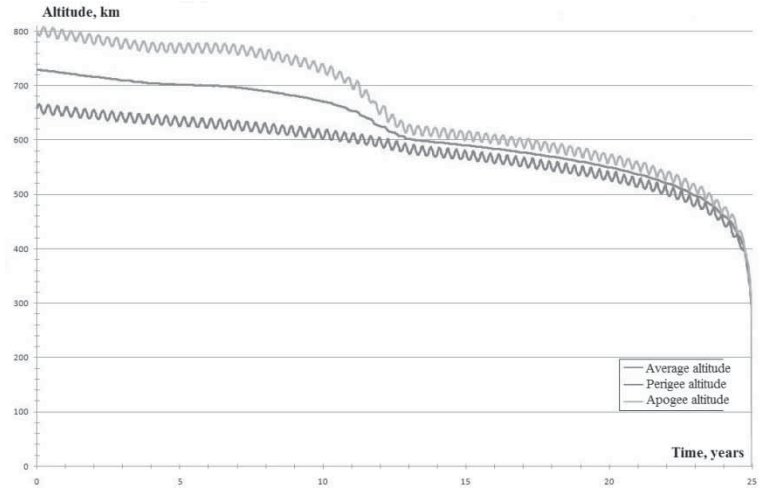

Fig. 10-4. Elliptical orbital degradation versus time (inclination 98º)

10.1.3. Parameter Determination Algorithm for an Orbit with Fixed Time of Ballistic Existence

An iterative procedure for the determination of the spacecraft's orbit with the exact (less than 1 hour) specified interval of existence time, uses the effective TRACE extrapolator based on the THEONA numerical analytical theory. Its high performance and accuracy make it possible to form a multiple-iteration process without facing the difficulties in predicting spacecraft motion over long time intervals.

The input data for the iterative procedure are:

- The spacecraft's initial orbital parameters (the semimajor axis a, the eccentricity e, the inclination i, the perigee argument ω, the RAAN Ω, the initial moment of time t_0, and the latitude argument u_0) and the spacecraft's characteristics (mass, ballistic coefficient, and coefficient of solar radiation pressure).
- The duration of the disposal time interval T_L. The spacecraft enters the thicker layers of the atmosphere (with the following descent) at the fixed moment in time with acceptable accuracy.
- The DO selection mode (the circular or elliptical orbit with a fixed apogee). In both variants, the orbital plane remains unchanged (the inclination and the RAAN) at the initial moment in time. For the

elliptical DO, the apogee point and the altitude (the geocentric distance) of the apogee are also fixed. The initial moment of time is preserved.

Thus, the boundary equation is solved $Ah_0 = h_{\min}$, where $h_{\min}$ = the altitude of the spacecraft's entry into the denser layers of the Earth's atmosphere and A = the operator, which depends on the time of the spacecraft's existence T_L in the orbit and the fixed parameters Q of the desired DO.

While searching for the circular DO, the fixed orbit parameters are:

$Q = \{i_0, \Omega_0\}$ at the initial moment of time t_0, while searching for the elliptical DO.

$Q = \{h_\alpha, \omega_0, i_0, \Omega_0\}$ at the initial moment of time t_0, where h_α = the orbital apogee altitude.

In both cases, it is convenient to use $a_0 = a(t_0)$ instead of $h_0 = h(t_0)$.

Taking into account the close to exponential dependence between the atmospheric density $\rho(h) = \exp\left(-\frac{h-h_0}{H}\right) \cdot \rho(h_0)$ and the altitude h above the Earth's surface, it is more effective to consider the equation with another operator and a logarithmic variable $\ln(h_0 - h_H)$ or $\ln(a_0 - a_H)$.

At each iteration, the satellite's motion is propagated until it enters the denser layers of the lower atmosphere and falls down towards Earth's surface (Event 1), or until the specified time interval passes (Event 2). If these two events coincide (with permissible tolerance), it is supposed that the iteration procedure is complete and the desired initial parameters of the spacecraft DO have been found.

The algorithm and methods of the iterative procedure for searching for the DO can be described as follows:

1. Cross-checking of the event iterative procedure variants available for the initial spacecraft.
2. A decrease (or increase, depending on the previous event) of the spacecraft orbit's initial semimajor axis $a_0 = a(t_0)$ with a big step until the change of the event variant occurs.
3. In the case of a big interval between the values of the previous $a_0^{(n-1)}$ and the current step $a_0^{(n)}$, the golden section method is realized (dichotomy method optimization) for the acquisition of the new $a_0^{(n+1)}$.

4. In the case of the small interval between $a_0^{(n-1)}$ and $a_0^{(n)}$, the secant method or chord method is used depending on the specific characteristics of the algorithm. If Event 1 occurs on the current step, the calculation of the direction of the secant while accounting for perturbations in the semimajor axis due to atmospheric deceleration calculated for the prognosis of the initial revolutions is realized. This quickens the convergence of the iterative process.
5. The iterations are repeated until full convergence is achieved, i.e. until both events occur with acceptable accuracy. The convergence of the iterative process is monitored with the possibility of changing its methods, which were described above.

As an explanation, the boundary equation with operator A can be represented as a function for Event 1: $t(Q, h_{\min}, h_0) = T_L$; or for Event 2 as: $h(Q, T_L, h_0) = h_{\min}$.

The results (the output data) of the iterative procedure algorithm:

- The altitude $h_0 = h_\pi(t_0)$ of the DO perigee at the initial moment of time t_0. The perigee altitude coincides with the constant orbital altitude $h_0 = h(t_0)$ for the circular orbit.
- The number of revolutions carried out in the DO until the critical altitude ("the fall"). This data can be used in reports and results analysis (in particular, in graphs or tables).

10.1.4. Manoeuvre Parameter Determination Algorithm for Transfer to an Orbit with Fixed Time of Ballistic Existence

Using the magnitude of the circular DO radius r_f and the pericenter radius of the elliptical DO $r_{\pi f}$ from the previous section, it is possible to calculate the total delta-v expenditure needed for the adjustment of the corresponding DO.

The elliptical orbital semimajor axis alteration can be found using the equation

$$\Delta a = \frac{2a^2 V}{\mu} \Delta V_T, \tag{10-1}$$

where ΔV_T = the impulse tangential component and V = the velocity at the location of impulse application. According to the equation, it is

necessary to orient the impulse tangentially to the orbit for optimal alteration of the semimajor axis. The maximum alteration can be gained by application of the impulse at the orbital pericenter where the spacecraft velocity has its maximum value.

Before the start of the main calculation, the velocity at the initial orbital apogee is calculated, along with the apogee and perigee radii:

$$V_\alpha = \sqrt{\frac{\mu}{p}}(1-e),$$
$$r_\alpha = a(1+e),$$
$$r_\pi = a(1-e).$$

One braking impulse applied in the initial orbital apogee is used for the shaping of the elliptical DO. The magnitude of the impulse can be found by:

$$\Delta V_t = \frac{(r_{\pi f} - r_\pi)\mu}{4a^2 V_\alpha}. \tag{10-2}$$

Two braking impulses are used for the second type solution in forming the circular DO. The first of the impulses is applied at the initial orbital apogee and the second one is applied at the orbital perigee, obtained after the application of the first impulse. The magnitude of the first impulse applied at the apogee can be found by:

$$\Delta V_{t_1} = \frac{(r_f - r_\pi)\mu}{4a^2 V_\alpha}. \tag{10-3}$$

Then the semimajor axis a_n, the focal parameter p_n, the eccentricity e_n of the orbit shaped by the first impulse, and the velocity at the perigee $V_{\pi n}$ are found:

$$a_n = \frac{1}{2}(r_\alpha + r_f),$$

$$e_n = \frac{r_\alpha - r_f}{r_\alpha + r_f},$$

$$p_n = a_n(1-e_n^2),$$

$$V_{\pi n} = \sqrt{\frac{\mu}{p_n}}(1+e_n).$$

The magnitude of the second impulse, applied at the orbital perigee obtained after the application of the first impulse, can be found as follows:

$$\Delta V_{t_2} = \frac{(r_f - r_\alpha)\mu}{4a_n^2 V_{\pi n}}. \tag{10-4}$$

If the initial orbit is circular, then additional constraints should be taken into account while choosing the moment of transfer from the orbit. For example, one should choose an orbit which generally avoids collisions with space debris.

10.1.5. Example

The problem of manoeuvre parameter determination for a spacecraft's transfer to a DO can be solved in two steps. The first step involves the determination of an orbit with a reduced time of ballistic existence. The second step involes the determination of the actual manoeuvre parameters to transfer the spacecraft to this orbit. The two options for shaping the orbit with the reduced time of ballistic existence have been realized. In the first case, the elliptical orbit is adjusted by the application of a single braking impulse at the apocenter. Its pericenter is situated in the denser layers of the atmosphere. In the second case, the circular orbit is shaped by the application of two braking impulses—at the apocenter and the pericenter. It is situated in the even thicker layers of the atmosphere.

The algorithms for the determination of the DO parameters and the manoeuvre parameters that shape the DO were described earlier.

Table 10-4 presents the elements of the initial spacecraft orbit. Table 10-5 gives the spacecraft parameters of: engine thrust (*P*); spacecraft mass (*kg*); specific impulse (*I*); existence time of the DO (*dT*); the orbital elements printing step (*dN*); the accuracy of the DO adjustment (*epsR*); and the accuracy of the DO existence time (*epsT*).

Table 10-4

H_{min} km	H_{max} km	ω deg	u deg	i deg	Ω deg	N	Date	Time	S (bal)
707.7	750.3	0	72	98	50	1	2013.01.01	043000.15	0.0045

Table 10-5

P N	m kg	I s	dT days	dN	mode	epsR km	epsT days
3,000	7,000	0.023	9,131	3,000	2	0.001	1

Information about the transversal braking manoeuvre (Baranov, Budyansky, Chernov, and Golikov 2015, 4-19), which transfers the spacecraft to the elliptical orbit, can be found in table 10-6, including: the date and time of the start of manoeuvring; its magnitude; the number of revolutions for the manoeuvre application; and the latitude arguments of its beginning and end.

Table 10-6

Date	Time	dVm/s	Revolution	U_in	U_ta
2013.01.01	45822.8	71.55	2	174.95	185.05

Table 10-7 gives information about the two transversal braking manoeuvres, which transfer the spacecraft to a circular orbit.

Table 10-7

Manoeuvre	Date	Time	dV m/s	Revolution	U_in	U_ta
1	2013.01.01	45,850.4	47.90	2	176.62	183.38
2	2013.01.01	54,643.3	59.19	2	355.74	364.26

Below, we find the information about the evolution of the circular and elliptical orbital elements with a 12,000 revolution step (Baranov, Budyansky, Chernov, and Golikov 2015, 4-19).

The ballistic coefficient: 0.4500000000000D-02.

The solar radiation coefficient: 0.3500000000000D-09.

The evolution of the formed circular DO

Revolution Semimajor axis Eccentricity Argument of perigee Inclination RAAN Argument of latitude Time Flight duration Altitude of perigee

0 0.691518526288D+01 0.188963633604D-02 0.534077652727929D+02 0.9798980982053D+02 0.4998835802642D+02 0.2079163930186D+00 0.3869483449816D+00 0.6737776267169D+00 0.5191467727679D+00

12,000 0.6910050637D+01 0.99626895852D-03 0.97675731382D+02 0.9798681758181D+02 0.161677850795D+03 0.1200020791639D+05 0.6902365575951D+00 0.794476952433D+03 0.5174040573780D+00

24,000 0.69045256152D+01 0.17642920474D-02 0.5264659611D+02 0.97988180283D+02 -0.8543534012577D+02 0.2400020791639D+05 0.1272884399222D+00 0.15873735431D+04 0.5093786551627D+00

36,000 0.68984083484D+01 0.12147105789D-02 0.9581586601D+02 0.97984775341D+02 0.28772504210D+02 0.3600020791639D+05 0.75160647230D+00 0.23792727749D+04 0.5044609776106D+00

48,000 0.68915398165D+01 0.1513560635D-02 0.4693031706D+02 0.9798319080282D+02 0.14448699096D+03 0.4800020791639D+05 0.4569529980653D-01 0.317003765099D+04 0.4983694254986D+00

60,000 0.68837999432D+01 0.15692059216D-02 0.8693337542D+02 0.97984573775D+02 -0.9810855747773D+02 0.6000020791639D+05 0.600908254738D+00 0.395952909260D+04 0.4880257878580D+00

72,000 0.68746542153D+01 0.10688947970D-02 0.4866613792D+02 0.97984268041D+02 0.2121055056212D+02 0.7200020791639D+05 0.97688345646D+00 0.4747587858528D+04 0.4842600476981D+00

84,000 0.6864018972D+01 0.1747816097D-02 0.70246607D+02 0.9797954810D+02 0.1427778386D+03 0.8400020791639D+05 0.3987172583D+00 0.55339666134D+04 0.468034014978D+00

96,000 0.6850988423D+01 0.1088092563D-02 0.8351860256D+02 0.97978995099D+02 -0.92957745893D+02 0.9600020791639D+05 0.65934499690D+00 0.631834067892D+04 0.45849168772D+00

108,000 0.6833781483D+01 0.1348714535D-02 0.5312903244D+02 0.9797836567636D+02 0.347462338653D+02 0.108000207916D+06 0.699654008843D+00 0.7100175424764D+04 0.441384506914D+00

120,000 0.6809484442D+01 0.1610268829D-02 0.6796995206D+02 0.97974781525D+02 0.16725486801D+03 0.12000020791D+06 0.27286508923D+00 0.78784892161D+04 0.41456741851D+00

132,000 0.6763956514D+01 0.1473728186D-02 0.7866936324D+02
0.979682073356D+02 -0.524058950951D+02 0.132000207916D+06
0.550028992118D+00 0.865114296932D+04 0.369315631040D+00
139,573 0.6518598360D+01 0.6637589020D-03 0.2019154822D+02
0.97930094998D+02 0.140965354553D+03 0.141000207916D+06
0.81188654224D+00 0.913143598161D+04 0.131977512142D+00

The evolution of the elliptical orbit

0 0.698300893939907D+01 0.23641198941D-01
0.377324001414D+01 0.9798970932014D+02 0.4998792065997D+02
0.2118375662256D+00 0.3329191174416D+00
0.6737770013786D+00 0.4365476667912D+00
12,000 0.697130821036D+01 0.206665984686D-01 -
0.136684079987D+03 0.9798653713232D+02 0.1471525460116D+03
0.1200021183756D+05 0.6336642014066D+00
0.8056102272414D+03 0.4407849960690D+00
24,000 0.696004050022D+01 0.219267241667D-01
0.794645134932D+02 0.97983352282208D+02 -
0.11327332902293D+03 0.24000211837566D+05
0.45671568048419D+00 0.16085835701008D+04
0.42353845961942D+00
36,000 0.694824990590D+01 0.183332692905D-01 -
0.707421722178D+02 0.97983265094289D+02 -
0.11211388146403D+02 0.36000211837566D+05
0.94559381308499D+00 0.24095504739073D+04
0.43738256021135D+00
48,000 0.693543479024D+01 0.188557098128D-01
0.120943138911D+03 0.97983072289462D+02
0.93474685414810D+02 0.48000211837566D+05
0.13310166721930D+00 0.32084243765405D+04
0.41871106677928D+00
60,000 0.692212780045D+01 0.161662067919D-01 -
0.440936036024D+02 0.97980213151987D+02 -
0.15898563073397D+03 0.60000211837566D+05
0.25084808515384D+00 0.4005036380218D+04
0.42793255247802D+00
72,000 0.690705780952D+01 0.159891438168D-01
0.123727903817D+03 0.97978789158900D+02 -
0.48300702027612D+02 0.72000211837566D+05

0.88504246552474D+00 0.4799181491725D+04
0.41045768514320D+00
84,000 0.689049144014D+01 0.127885229966D-01 -
0.640357956355D+02 0.97972912852217D+02
0.65859025846478D+02 0.84000211837566D+05
0.64955866942182D+00 0.55906238269624D+04
0.41915043568269D+00
96,000 0.687147050470D+01 0.133690209724D-01
0.809328236263D+02 0.97974377385835D+02 -
0.17604559527898D+03 0.96000211837566D+05
0.25392688997089D+00 0.6379047711272D+04
0.39548862687624D+00
108,000 0.684889647758D+01 0.916118511227D-02 -
0.14887412646D+03 0.97969547364881D+02 -
0.53228668831080D+02 0.10800021183756D+06
0.68754771491512D+00 0.7163888028791D+04
0.39886179535013D+00
120,000 0.681821152587D+01 0.791173060441D-02 -
0.22530022704D+02 0.97963043269527D+02
0.75679477060619D+02 0.12000021183756D+06
0.83711257798131D+00 0.79441739332999D+04
0.38260601229904D+00
132,000 0.676011617528D+01 0.610290374228D-02
0.51041811480D+02 0.97954666432225D+02 -
0.14580580772984D+03 0.13200021183756D+06
0.23680918919853D+00 0.8717434169407D+04
0.33612002482384D+00
135,000 0.672780453941D+01 0.482607282465D-02
0.59407342434D+02 0.97952018476325D+02
0.71634231611012D+02 0.13500021183756D+06
0.79273351724259D+00 0.89087388864899D+04
0.31212370854329D+00
138,531 0.651134593280D+01 0.508719801598D-03
0.260863630465D+02 0.97918439161084D+02 -
0.28915308313555D+02 0.14100021183756D+06
0.57465186133049D+00 0.9131503988132D+04
0.12475769843603D+00

This information allows us to present the dependencies between the orbital elements and the time or number of revolutions of the spacecraft flight. The graphs of the alteration of the perigee altitude (Fig. 10-5), the

semimajor axis (Fig. 10-6), and the apogee (Fig. 10-7) of the two estimated DOs can be found below.

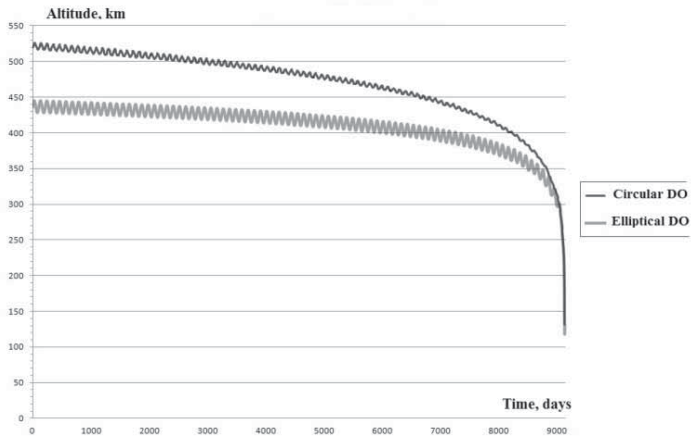

Fig. 10-5. Evolution of DO perigee altitude versus time

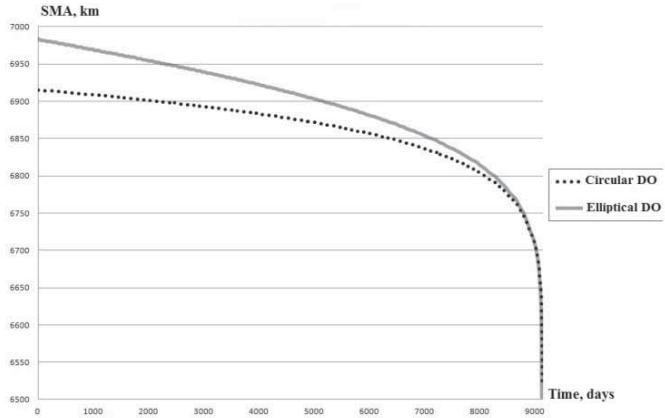

Fig. 10-6. Evolution of the DO semi-major axis versus time

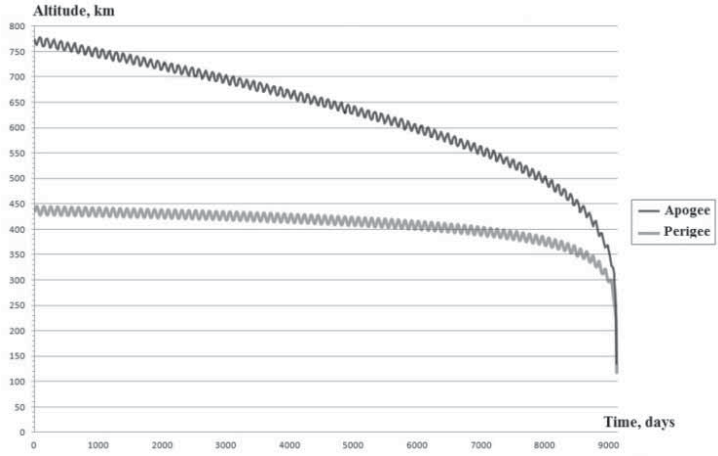

Fig. 10-7. Evolution of DO apogee and perigee altitude versus time

10.2. Active Debris Removal Problem

In order to stop overcrowding in the near space environment, decommissioned spacecraft and large-size space debris (LSSD) should be transferred to appropriate DOs. Above all, the final stages of launch vehicles (LV), upper stages, and large spacecraft should all be transferred to DOs. Collisions of LSOs with other space objects are accompanied by the generation of considerable quantities of debris with high kinetic energy (Johnson and Liou 2009, 1407-1415). This can lead to snowballing growth in dangerous space objects. This effect is known as the Kessler syndrome (Cour-Palais and Kessler 1978, 2637-2646; Johnson and Liou 2009, 1407-1415).

According to the results of research (Lewis and White 2014, 1195-1206; Johnson and Liou 2009, 1407-1415), the removal of 3-5 LSOs a year from the near-Earth orbit environment in combination with the fulfillment of Inter-Agency Space Debris Coordination Committee requirements (Crowther, Lewis, Stokes, and White 2012, 62-68) is the only way to stop snowballing growth in space debris. It is worth mentioning that the accuracy of these recommendations should be treated with caution due to the complexity of spacecraft motion propagation over long time periods. This is primarily connected to errors in solar activity forecasting.

There are lots of current projects for returning LSOs. Schemes in which a service spacecraft or a space vehicle collector (SV-collector) remove several LSOs at one go are the most effective.

The first scheme implies the successive flyby of some objects and their collection, or the autonomous control of small spacecraft and fuel supplies in the exhaust sections of LSOs (thrust de-orbit kits (TDKs)) that can provide sufficient deceleration for the transfer of an LSO to an orbit with reduced time of ballistic existence.

The second scheme implies the use of one SV-collector, which manoeuvres between objects and drags them to the DO with the help of its engines. It is less effective, but allows for a faster transfer on to the next object. In this section, both schemes are considered and a comparison is made.

10.2.1. Geometry of Large Space Debris Objects

Table 10-8 presents the geometrical characteristics of some objects of the aforementioned type. Based on the analysis in this table, the conclusion can be made that a minimal cross-section exceeds 5 m^2 (Baranov and Grishko 2014, 39-48).

Table 10-8

Object Type	Diam.	Len.	Min. cross-section	Max. cross-section
	m		m^2	
“Proton” launch vehicle 3rd stage	4.098	4.11	13.19	16.84
“Soyuz” launch vehicle 3rd stage	2.66	6.745	5.56	17.94
“Zenit” launch vehicle 2nd stage	3.9	10.4	11.95	40.56
“Ariane 5” launch vehicle 2nd stage	3.96	3.356	12.32	13.29
“Agena-A” 2nd stage	1.52	4.73	1.81	7.19
“Briz” upper stage	2.49	2.654	4.87	6.61
“Fregat” upper stage	3.35	1.5	8.81	5.025
“Centavr” upper stage	3.05	12.68	7.31	38.67

10.2.2. Compact Groups of Large Space Debris Objects in the LEO Region

Several compact groups of LSOs in the LEO region can be distinguished due to the target attributes of spacecraft launches. Looking through the NORAD catalogue[4], one can distinguish five groups of objects with sectional areas of more than 5 m^2 in LEO (Baranov and Grishko 2014, 39-48) (table 10-9).

The semimajor axis value interval does not exceed 50 km for orbits of the second, third, and fourth groups. This value is less than 90 km for the first group.

The last group has appeared due to spacecraft being launched into sun-synchronous orbits. Hence, the inclination of the spacecraft in this group is a function of altitude. The altitude alters in the range of 527 km.

Approximately 50 m/s is needed for a 100 km alteration of orbital altitude by spacecraft in the specified groups. However, approximately 130 m/s is needed for an orbital plane rotation of 1º. As such, the most crucial aspect is the difference in inclination, which was used to distinguish these five groups. Besides the inclination, one can find the number of LSOs in the group and the range of the change in their semimajor axis values.

Table 10-9

Group	Group elements Inclination deg	Semimajor axis diapason km	Number of LSOs in a group
1	71	7,193-7,281	23
2	74	7,122-7,152	11
3	81	7,211-7,262	28
4	83	7,318-7,358	52
5	97-100	6,973-7,500	46

The groups were determined using the space object catalogue for November 21st, 2013. All the estimates of these objects are attribute-based and these attributes are used for the determination of the capability and effectiveness of different schemes for large space debris recovery.

[4] "NORAD Satellite Catalog". Accessed November 21, 2013. http://www.celestrak.com/satcat/search.asp

10.2.3. A Portrait of RAAN Deviation Evolution

The current mutual orientation of orbital planes must be known in order to design appropriate flyby schemes for the objects of the specified LSO groups. Direct consideration of the dynamic pattern of RAAN alteration leads to complications in the analysis of the flyby scheme problem because the orbital planes rotate at close rates. A parameter that is more static and that characterizes the orbital plane position should be chosen. This parameter should be connected to the corrected deviations. The RAAN deviation for all objects (indexes *i*) from the RAAN of the specially chosen object with the fixed number $k \in 1; m$ (m = number of objects in the group) $\Delta\Omega_{i_k} \in [-\pi, +\pi]$ can be chosen. With this approach, the dependencies $\Delta\Omega_{i_k}(t)$ for orbits with close parameters (mostly in groups 1-4) will be lines with small inclination angles, and the relative angular distance $\Delta\Omega_{i_k}(t)$ will alter slowly over time. It is better to choose an object with number *k*, which is the reference for relative angular distance determination, so that the majority of the lines $\Delta\Omega_{i_k}(t)$ will have an angular coefficient with one sign.

The graphs of RAAN evolution for the specified groups can be found in figs. 10-8 to 10-12 (for a time span of 10 years). These deviations need to be corrected during successive flybys from one LSO to another. Analysis of these deviations allows us to choose an optimal flyby scheme for the LSO.

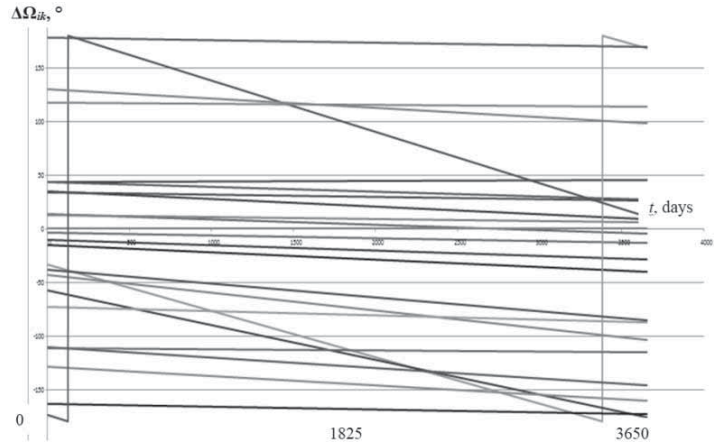

Fig. 10-8. RAAN deviation evolution for elements of group 1

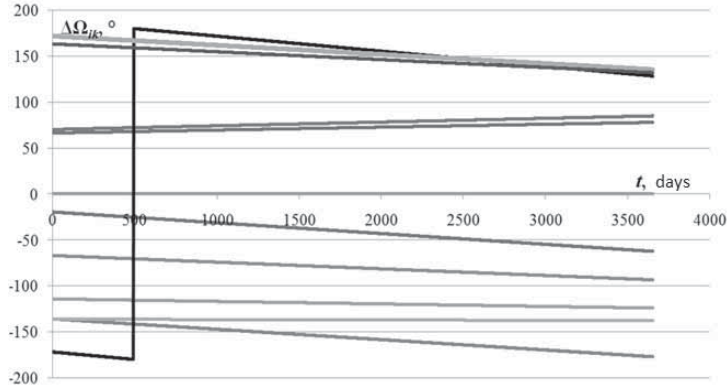

Fig. 10-9. RAAN deviation evolution for elements of group 2

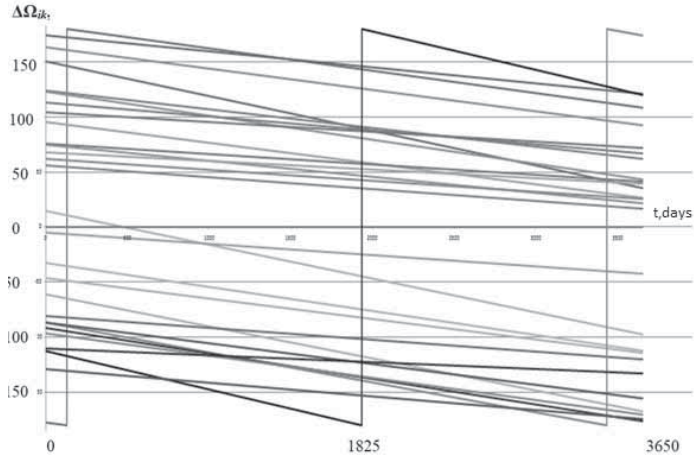

Fig. 10-10. RAAN deviation evolution for elements of group 3

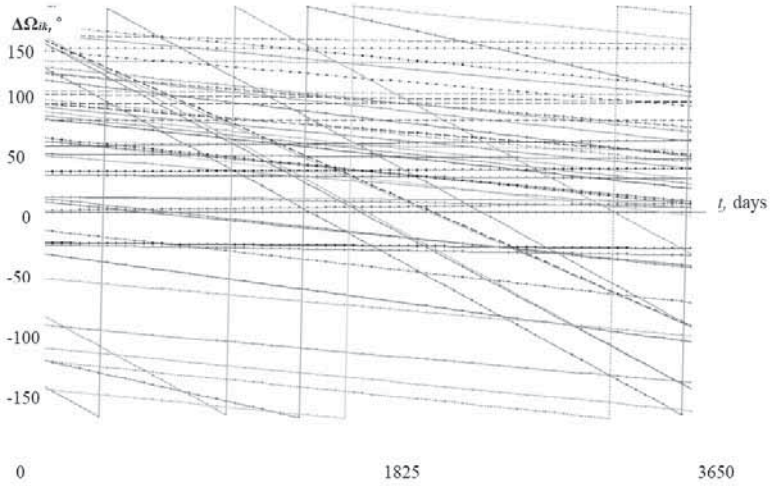

Fig. 10-11. RAAN deviation evolution for elements of group 4

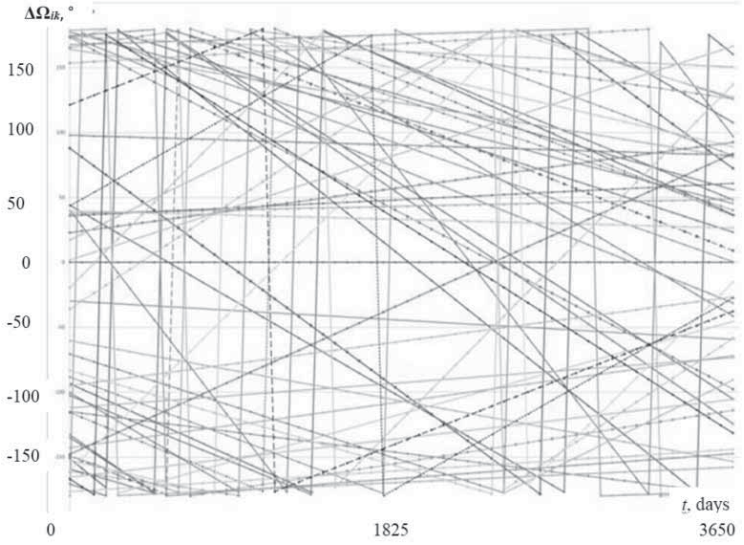

Fig. 10-12. RAAN deviation evolution for elements of group 5

10.2.4. First De-Orbiting Variant: Estimation of Delta-V Budget Required for Flights between Objects

If the evolution of the RAAN deviations primarily described quasi-parallel lines (figs. 10-8 to 10-10), the flyby between the three LSOs would demand the following action sequence. After the flyby of the SV-collector to the vicinity of object 1 for the injection of the TDKs into the exhaust section, the manoeuvring SV-collector fulfills the flyby to object 2 (Fig. 10-13). For this purpose the transfer of the SV-collector from the orbit of object 1 to a drift orbit using the impulse ΔV_1 is fulfilled. The impulse here denotes, as a rule, two ignitions on one revolution. After reaching the desired drift orbital plane orientation and the required phase difference, the SV-collector is transferred to the vicinity of object 2 with the help of impulse ΔV_2 in order to inject the TDKs into the exhaust section of this object. The aforementioned actions are repeated with the help of impulses ΔV_3 and ΔV_4 to reach object 3, etc.

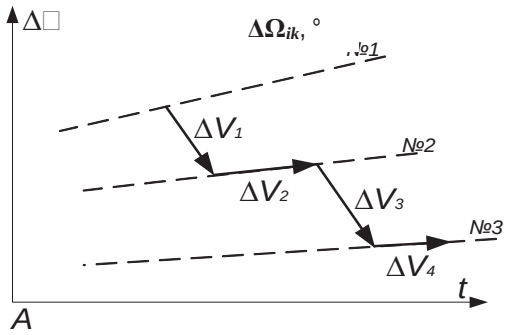

Fig. 10-13. Flyby between orbits on RAAN deviation evolution for the case when the LSO orbits for a group have small mutual deviations Δa and Δi

During the determination of ΔV_1 and ΔV_2, it is supposed that the initial and target orbits have close but different values for the semimajor axes (the difference Δa_0); that small inclination deviations are possible (Δi_0); and that the deviation of the RAANs $\Delta\Omega_0$ may be arbitrary. The difference in eccentricity is small and does not effect the solution type; it can be neglected while assessing the total delta-v of the manoeuvres. It is supposed that impulses with transversal and binormal components are applied at the equator on two manoeuvring intervals, which are situated on the first and last flyby revolutions. It is also supposed that the flyby is fulfilled using N revolutions of the LSO flight. Due to the transversal components of the two impulses of the first manoeuvring interval, the semimajor axis alters in order to compensate for the initial moment deviation of the latitude argument Δu_0^* and the necessary difference in the number of revolutions of the flyby n while moving on the new (phasing) orbit. Also, due to the task-orientated alteration of the orbital precession rate, a substantial part of the RAAN angular difference $\Delta\Omega_0$ is eliminated. The binormal components of impulses, which are needed for the compensation of the inclination difference Δi_0, are also distributed between the manoeuvring intervals so that they can affect the precession rate of the phasing orbit.

The required values for the sum of the transversal and lateral impulse components of the first $\Delta V_{t_I} = \Delta V_{t_{I_1}} + \Delta V_{t_{I_2}}$, $\Delta V_{z_I} = \Delta V_{z_{I_1}} + \Delta V_{z_{I_2}}$ and the

second $\Delta V_{t_{II}} = \Delta V_{t_{II_1}} + \Delta V_{t_{II_2}}$, $\Delta V_{z_{II}} = \Delta V_{z_{II_1}} + \Delta V_{z_{II_2}}$ manoeuvring intervals can be found using eqs. 7-34a- to 7-34c:

$$\Delta V_{t_I} = V_0 \left[\frac{N\Delta a_0}{2(N+n)a_0} - \frac{\Delta u_0^* + n}{3(N+n)} \right],$$

$$\Delta V_{t_{II}} = V_0 \frac{\Delta a_0}{2a_0} - \Delta V_{t_I},$$

$$\Delta V_{z_I} = \frac{V_0}{N+n} \left[N\Delta i_0 - \frac{4(\Delta u_0^* + n)\delta\Omega + 3(\delta\Omega n - \Delta\Omega_0)}{3\delta\Omega \mathrm{tg} i} \right],$$

$$\Delta V_{z_{II}} = V_0 \Delta i_0 - \Delta V_{z_I},$$

where $\delta\Omega$ = the RAAN alteration of the LSO orbit per single revolution.

The functional minimum should be found while transferring from the current position to the next LSO:

$$\Delta V = \sqrt{\Delta V_{t_I}^2 + \Delta V_{z_I}^2} + \sqrt{\Delta V_{t_{II}}^2 + \Delta V_{z_{II}}^2}.$$

The difference between the number of flight revolutions of the active spacecraft and the target revolutions n in the first approximation can be found as follows:

$$n = \frac{3\Delta\Omega}{7\delta\Omega} - \frac{4}{7}\Delta u_0^*. \tag{10-5}$$

Single-dimension optimization for n can be fulfilled numerically and Eq. 10-5 gives a good initial guess for this parameter. It is worth remembering that n is an integer value, thus, by choosing n, we cannot eliminate the whole RAAN deviation, but the remaining part does not exceed $1/2\delta\Omega$.

10.2.5. Duration of Flight to the Next Object in Line

The number of flyby revolutions between the two objects N can either be fixed or it can be chosen by knowing the magnitude of the difference in the RAANs, which is more preferable because the real spatial distribution of the LSOs is taken into account. The total delta-v expenditure decreases

with an increase in flyby duration. However, some temporal constraints occur during the process of choosing the flyby scheme. This can be the result of technical issues as well as an unwillingness to wait too long. Thus, the compromise value for the flyby duration should be seached for in the area where ΔV expenditures start to reduce rapidly with an increase in N.

The dependency between N and $\Delta\Omega_{i_k}$, which helps find the compromise value of N, can be obtained for each LSO group based on a visual analysis of the graphs $\Delta V(N)$ (Fig. 10-14) for various values of $\Delta\Omega_{i_k}$.

It is necessary to draw a slowly ascending convex curve on the coordinate plane ΔV, N, which would intersect the graphs $\Delta V(N)$, plotted for the different $\Delta\Omega_{i_k}$ in the compromise area. Using the intersection points, one can get the dependency $N(\Delta\Omega_{i_k})$, which can be approximated with fairly good accuracy (for LSO group 4) using the linear function (Baranov and Grishko 2015, 639-650):

$$N(\Delta\Omega_{i_k}) = 69.32\left|\Delta\Omega_{i_k}^{\circ}\right| + 250.6 \qquad (10\text{-}6)$$

It is obvious that the described approach for searching for the flyby revolution compromise number is not very convenient. On the other hand, the analytical dependency for the revolution compromise number search cannot be obtained for this problem, unlike with the case of a flyby in the orbital plane described in Chapter 7.

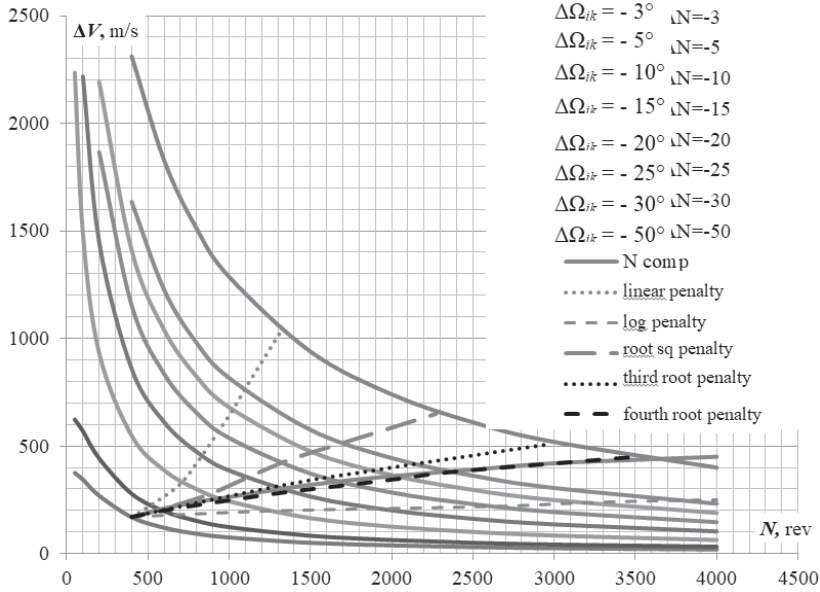

Fig. 10-14. Total delta-v expenditure as a function of the number of flyby revolutions from various $\Delta\Omega_{ik}$ for LSO group 4

The following approach can be suggested as an alternative. The total delta-v expenditure in the considered problem is mostly formed by the magnitude of the RAAN deviation. This magnitude can be evaluated using Eq. 7-28:

$$\Delta V = \frac{2}{3} V_0 \sqrt{\frac{(\Delta u_0^* + n)^2}{(N+n)^2} + \frac{(3\Delta\Omega_0 - (4\Delta u_0^* + 7n)\delta\Omega)^2}{(N+n)^2 \delta\Omega^2 \mathrm{tg}^2 i + \dfrac{4}{\sin^2 i}}}.$$

The first guess for n can be found by:

$$n_{opt} = \frac{3\Delta\Omega_0 - 4\Delta u_0^* \delta\Omega}{7\delta\Omega},$$

Equation 7-28 can be transformed to:

$$\Delta V = \frac{2}{3} V_0 \frac{\Delta\Omega_0}{7\delta\Omega N + 3\Delta\Omega_0} \tag{10-7}$$

One possibility for obtaining an analytical solution for N is the use of the functional:

$$F = \Delta V(N,...) + f(N) \tag{10-8}$$

In Eq. 10-8, the second term is the penalty function, which increases with the argument increase, unlike the case of the first term. The analysis of different variants (linear, logarithmic, and power penalty functions, Fig. 10-14) shows that the best variants for the LSO group 4 appear when this function has the following form (Baranov, Grishko, Lapshin, and Medvedevskikh 2016, 229-236):

$$f(N) = k\sqrt[4]{N} \tag{10-9}$$

where $k \approx 0.233917$.

The compromise value N can be obtained from the equation:

$$-56V_0\delta\Omega\Delta\Omega_0\sqrt[4]{N^3} + k(7\delta\Omega N + 3\Delta\Omega_0)^2 = 0 \tag{10-10}$$

10.2.6. Successive Transfer Scheme for a Group of Orbits with Close Semimajor Axes and Inclinations

In the next stage, it is necessary to determine the order of flyby elements for each group. The configuration of the first three groups, the orbital elements of which are close due to the values of the semimajor axes and inclinations, hardly changes over time for the evolution of the RAAN deviations. This allows us to use the successive flybys of these objects in the direction of a natural RAAN precession (Baranov, Grishko, and Mayorova 2015, 307-317). Before each new flyby, a search for an object with the least total delta-v expenditure for the flyby with a given number of revolutions N from the current position is carried out. The total delta-v expenditures are basically determined by the angular difference $\Delta\Omega_{i_k}$. The start of the flyby (the first object) is chosen so as to exclude the flyby between the two neighboring objects that are most distant in terms of the orbital RAAN. As the flyby of the whole group will take a

considerable time to complete, the relative angular positions of the orbits of the final objects may change after the flyby time passes. This should be taken into account and the RAAN values of the final objects should be recalculated after every flyby.

10.2.7. Examples of Calculations for Groups 1, 2, and 3

Let us consider the active spacecraft manoeuvre total delta-v determination for the flyby for LSO group 3 (Baranov and Grishko 2015, 639-650) as an example.

The objects in this group have orbits with inclinations of approximately 81º. The identification numbers of the elements of group 3 in the NORAD catalogue[5] and some fixed orbital elements as of November, 2013 can be found in table 10-10.

[5] "NORAD Satellite Catalog". Accessed November 21, 2013. http://www.celestrak.com/satcat/search.asp

Table 10-10

NORAD ID	*a* km	Ω	*i*
		deg	
13771	7,242	35.277	81.2
7493	7,231	26.186	81.3
5732	7,244	15.762	81.2
5918	7,218.5	2.758	81.2
7275	7,225.5	336.582	81.3
7210	7,239	334.788	81.2
8846	7,235	325.465	81.3
6393	7,243	316.731	81.3
9904	7,245	308.01	81.2
5118	7,242	288.046	81.3
11963	7,232	287.289	81.3
12457	7,245	280.591	81.3
13403	7,240.5	274.718	81.3
11166	7,239	268.278	81.3
7364	7,220.5	226.695	81.2
8800	7,262	212.623	81.3
8027	7,240	207.415	81.3
13719	7,215.5	180.447	81.3
9482	7,245.5	166.249	81.2
11608	7,224	151.181	81.2
8520	7,262	132.137	81.2
7715	7,227.5	126	81.2
6257	7,245	125.895	81.2
4420	7,236	121.222	81.2
9662	7,242.5	116.194	81.2
10515	7,248.5	102.624	81.3
12646	7,211.5	100.14	81.2
7575	7,235.5	83.823	81.3

The difference in RAANs between the orbits of the last (7575) and the first (13771) objects at the moment the flyby starts is 48.5º (maximum). In table 10-10, the LSOs of this group are given in descending order by RAAN so as to exclude the most expensive flyby.

Table 10-11

Flyby order with fixed number of revolutions $N = 1{,}000$	ΔV m/s	Flyby order with flexible number of revolutions	Flexible number of revolutions $N(\Delta\Omega_{ik})$	Duration days	ΔV m/s
1	*2*	*3*	*4*	*5*	*6*
1-2	211	1-2	1,293	91.6	167
2-3	222	2-3	1,483	105.1	149
3-4	325	3-4	1,968	139.5	182
4-5	499	4-5	2,601	184.3	189
5-6	57	5-6	770	54.6	108
6-7	144	6-7	752	53.3	129
7-8	155	7-8	1,005	71.2	139
8-9	289	8-9	2,007	142.2	167
9-10	320	9-10	1,591	112.7	174
10-11	89	10-11	885	62.7	137
11-12	48	11-12	367	26	26
12-13	168	12-13	1,185	84	153
13-14	156	13-14	1,093	77.5	147
14-16	985	14-16	4,896	346.9	213
16-17	340	16-17	2,576	182.5	199
17-15	56	17-15	2,044	144.8	177
15-18	791	15-18	3,499	247.9	209
18-19	207	18-19	1,117	79.2	128
19-21	521	19-21	2,141	151.7	169
21-20	132	21-26	2,306	163.4	193
20-23	231	26-23	1,243	88.1	147
23-26	107	23-20	422	29.9	61
26-24	168	20-25	1,555	110.2	156
24-25	3	25-24	679	48.1	113
25-22	58	24-22	1,026	72.7	145
22-28	341	22-27	5,456	386.6	232
28-27	564	27-28	6,457	457.6	204
ΔV_Σ m/s	**7,187**				**4,213**
Total duration	**27,000 revs 1,913.3 days**		**52,417 revs**	**3,714.3 days**	

Calculation of the total delta-v expenditure for flyby manoeuvres with a fixed number of revolutions N = 1,000 (columns 1 and 2), and the

expenditures for the flybys with the use of the "compromise" number of revolutions *N* depending on the RAAN difference (columns 3-6), can be found in table 10-11.

The aforementioned method was also implemented for the calculation of the total delta-v expenditure for the flyby manoeuvres of LSO groups 1 and 2 (Baranov and Grishko 2015, 639-650). The results of these calculations can be found in tables 10-12 and 10-13, respectively.

Table 10-12

Flyby order with fixed number of revolutions *N = 1,000*	ΔV m/s	Flyby order with flexible number of revolutions	Flexible number of revolutions $N(\Delta\Omega_{ik})$	Duration days	ΔV m/s
1	*2*	*3*	*4*	*5*	*6*
1-2	14	1-2	504	35.7	16
2-3	123	2-3	1,349	95.6	94
3-4	11	3-4	598	42.4	21
4-5	257	4-5	2,520	178.5	105
5-7	158	5-7	1,709	121	90
7-8	65	7-8	1,009	71.5	68
8-9	100	8-9	1,285	91	81
9-10	77	9-10	1,100	77.9	73
10-12	338	10-12	3,225	228.5	122
12-13	92	12-13	1,369	97	76
13-11	135	13-15	2,134	151.2	94
11-15	211	15-11	1,263	89.5	134
15-14	121	11-14	1,501	106.3	90
14-17	378	14-17	1,528	108.3	183
17-16	105	17-16	1,710	121.2	96
16-18	213	16-18	2,122	150.3	99
18-19	343	18-19	2,905	205.8	104
19-21	230	19-21	2,313	163.9	102
21-20	540	21-23	6,303	446.6	118
20-22	176	23-22	1,241	87.9	82
22-23	18	22-20	5,346	378.8	162
23-6	1,104	20-6	3,805	269.6	223
ΔV_Σ m/s	**4,809**				**2,233**
Total duration	**22,000 revs 1,558.7 days**		**46,839 revs**	**3,318.5 days**	

Columns 1 and 3 show the LSO pairs for the flyby. Columns 2 and 6 present the total delta-v expenditures needed for the fulfillment of this flyby with a fixed number of revolutions *N* and "compromise" *N*, respectively. Columns 4 and 5 give the values of the best "compromise" flyby duration—the number of revolutions *N* and the flyby duration in days, respectively. According to table 10-11, the use of the "compromise" number of revolutions allows a decrease in the total delta-v expenditures approximately by half, but even in this case the total delta-v expenditures exceed 4 km/s, which is too high for modern spacecraft.

Table 10-13

Flyby order with fixed number of revolutions *N = 1,000*	ΔV m/s	Flyby order with flexible number of revolutions	Flexible number of revolutions $N(\Delta\Omega_{ik})$	Duration days	ΔV m/s
1	*2*	*3*	*4*	*5*	*6*
1-2	57	1-2	633	43.9	89
2-3	836	2-3	5,026	348.8	183
3-4	306	3-4	2,066	143.4	176
4-5	612	4-5	3,517	244	182
5-6	616	5-6	3,429	237.9	192
6-8	290	6-8	1,749	121.4	152
8-7	69	8-7	1,216	84.4	150
7-9	530	7-9	3,324	230.7	196
9-10	180	9-10	855	59.3	116
10-11	101	10-11	819	56.8	104
ΔV_Σ m/s	**3,597**				**1 ,540**
Total duration	**10,000 revs 693.9 days**		**22,634 revs**	**1,570.6 days**	

The work of Castronuovo (2011, 848-859) is very interesting because it offers a comprehensive review of all questions connected to LSO return. This work suggests the use not only of an SV-collector with two manipulators and TDKs onboard, but also spacecraft-refuelers. The spacecraft-refueler will be injected into the orbit of the basic SV-collector when the latter runs out of fuel and TDK supplies. The SV-collector docks with the spacecraft-refueler, refuels its tanks, gets more TDKs, and continues its flyby for the remaining LSOs. According to the results from Castronuovo (2011, 848-859), the mass of the SV-collector in this model

would be approximately 600 kg. The fuel supplies for each spacecraft would allow the expenditure of up to 2,500 m/s total delta-v and the number of TDKs on each spacecraft-refueler could be up to 6 or 7.

If the potential of total delta-v supplies is under consideration, then one SV-collector and one spacecraft-refueler would be enough to engage in a flyby with all the objects of group 3. However, the number of TDKs needed exceeds the real number twice as much for one spacecraft-refueler, which is why two more spacecraft-refuelers would be needed. As such, a part of the fuel supplies on these spacecraft-refuelers would need to be replaced with more TDKs.

A delta-v budget of 2,233 m/s is needed for a flyby of the 23 LSOs of group 1. These total delta-v expenditures would be acceptable for the SV-collector described in Castronuovo (2011, 848-859), but the number of TDKs needed is too big, hence, two more spacecraft-refuelers would be required. Part of the fuel supplies would have to be replaced with TDKs on the SV-collector and the spacecraft-refuelers.

A delta-v budget of 1,540 m/s would be needed for a flyby of the 11 LSOs of group 2. The total delta-v expenditure of the SV-collector would be higher than needed, but the number of TDKs would be insufficent for a flyby of all objects of the group. Hence, one more spacecraft-refueler would be needed.

10.2.8. Diagonal Transfer Scheme for a Group of Orbits with different Semimajor Axes and Inclinations

Groups 4 and 5 have a considerable number of objects with orbital differences in terms of semimajor axis and inclination. These are enough to result in the presence of intersections between the lines of relative difference in the RAANs (figs. 10-11 and 10-12). In Fig. 10-15, one can find the lines, corresponding to objects with the hypothetical numbers 1, 2, and 3.

After approaching object 1, being in its orbit, it is enough to apply only one impulse ΔV_1 to approach object 2 in the moment of orbital plane RAAN coincidence; furthermore, a single impulse ΔV_2 should be applied for the subsequent approach to object 3. Hence, the number of ignitions in the interval of the flyby from object 1 to object 3 may be reduced by 2. The total delta-v expenditure also decreases because there is no need to correct the RAAN deviations.

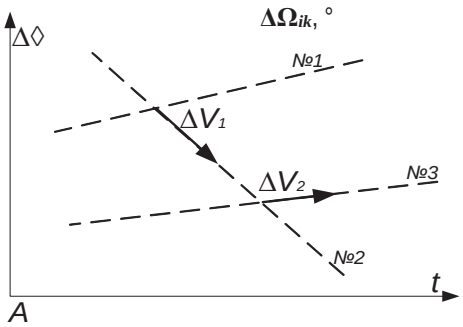

Fig. 10-15. Flyby variants in the evolution of RAAN deviations for the case when the LSO orbital parameters in the groups have substantial mutual deviations of Δa and Δi

Let line $\Delta\Omega_{i_k}(t)$, which corresponds to one of the orbits and intersecting the two lines and thus to the different orbits, be "diagonal". We have the opportunity to find several branches that contain a number of successions of the diagonals, allowing the completion of a flyby to the greatest number of LSOs in the group. The suggested solution will be termed the "diagonal" from hereon.

The moment where the lines intersect $\Delta\Omega_{i_k}(t)$ in the evolution of the RAAN deviations means that the orbits of corresponding LSOs have equal RAAN values. As such, the orbits of these objects may vary only in terms of their semimajor axes, eccentricity vectors, inclinations, and latitude arguments. The numerical and numerical-analytical algorithms for the solution of the small and medium duration rendezvous problem, which can be used for the determination of the approach manoeuvres with new objects, can be found in chapters 4, 5, and 6.

10.2.9. Search of Diagonal Solutions

As can easily be seen, the direct deviations of RAANs $\Delta\Omega_{i_k}(t)$ in Fig. 10-12 chaotically intersect multiple times. As such, a successive flyby of the objects of group 5 becomes ineffective. In order to address the branches-solutions of the search problem, under the condition of a large number of lines and mutual intersections, it is good to use some graph theory elements.

In order to find the diagonal solution of the flyby problem to an LSO inside the group, it is necessary to get the T_{ij} = matrix of line intersection $\Delta\Omega_{i_k}(t)$, analogous to the classical connectivity matrix (Zarubin and Krischenko, 2004):

$$T = \begin{bmatrix} \infty & t_{1,2} & - & \dots & t_{1,46} \\ t_{2,1} & \infty & \dots & \dots & \dots \\ - & \dots & \infty & \dots & \dots \\ \dots & \dots & \dots & \dots & \dots \\ t_{46,1} & \dots & \dots & \dots & \infty \end{bmatrix}$$

The matrix T is symmetrical and its diagonal has the symbol "∞", representing the coincidence of the lines $\Delta\Omega_{i_k}(t)$. If the intersection point of the lines $\Delta\Omega_{i_k}(t)$ and $\Delta\Omega_{j_k}(t)$ exists, then the coordinate t is shown as the element t_{ij}; if there are no intersection points or the intersection occurs when $t \to \infty$, then the dash is set as the matrix element. The search for a diagonal solution is fulfilled with the help of the iterative algorithm of the graph node run. The solution should meet the following criteria:

- The graph nodes should be in the range $\Delta\Omega_{i_k} \in [-\pi, +\pi]$.
- The direction of the increase in branch length should coincide with the increase in *t*.
- Each intersection point (graph node) contains two entries and two exits, and it is unlikely that three or more lines $\Delta\Omega_{i_k}(t)$ will intersect in one node.
- Each line $\Delta\Omega_{i_k}(t)$ may be used only once.
- The longer branch has priority;
- If the branches have equal lengths, priority will be assigned to the branch with the lesser angular coefficient module sum of the lines used $\Delta\Omega_{i_k}(t)$.

Using the diagonal solution, the flyby duration to the next LSO is entirely determined by the mutual remoteness of the intersection points of the lines $\Delta\Omega_{i_k}(t)$ for the evolution of the RAAN deviations.

Three cycles are used in searching for a solution with diagonal transfers.

The inner cycle. Let us designate the point at which the motion from the object starts as 1. In the first line of matrix *T*, it is necessary to find the first element $t_{1,l} \neq "\infty"$ and $t_{1,l} \neq "-"$. Let us call this element $t_{1,2}$. Impulse ΔV_1, which is needed for the flyby to a new orbit should be found. After acquiring ΔV_1, we should designate $t_{1,l} = t_{m,1} = "-"$ and $m, l = 1,...,n$, in order to exclude further usage of the 1st branch, and also assign the value "–" to all $t_{m,l}$, being $t_{m,l} < t_{1,2}$. After the transition to line 2, it is necessary to find the first element $t_{2,1} \neq "\infty"$ and $t_{2,1} \neq "-"$. The process continues until there is no further option to find the element $t_{m+1,l}$ from the node $t_{m,l}$ with the necessary constraints, or *l* reaches 46 (the number of LSOs in group 5), i.e. where the end of the branch with maximum length is found. If there is no option to proceed further, it is necessary to write the numbers of objects of the branch, the total delta-v expenditures, and the last pair $t_{m,l}$ from matrix *T*, assign it the value "–" and continue searching the branches until the algorithm leads to the elements with the coordinates [1;1]. The aim of the inner cycle is to determine the branch of maximum length with the start of the flyby from the first object.

The middle cycle. After fixing the longest branch with the start in the first object and the total delta-v expenditure, it is necessary to call the inner cycle for line 2 starting at object 2. This is repeated *n* times. The longest branch for the first SV-collector, which works with the use of the "diagonal" scheme, can be chosen from *n* interim variants. The goal of the middle cycle is to determine the priority starting point and the priority branch originating from this point, determining the first problem solution.

After the work of the middle cycle and sorting of the found branches according to length, the situation may occur when several obtained solutions have maximum length for the current configuration of matrix *T*. In this case, it is necessary to compare the energy expenditures of the flybys of these branches indirectly. In the evolution of RAAN deviations, the angle between the lines $\Delta\Omega_{i_k}(t)$ is determined by the difference in their angular coefficients, which depend on the magnitudes of the focal parameter and inclination. Hence, the bigger the differences in Δp and Δi of two object orbits, the bigger angle will shape the corresponding lines $\Delta\Omega_{i_k}(t)$. This is why it is necessary to estimate the sum of the alteration of the angular coefficients in the transfer from one object to another for every branch found as an indirect energy assessment.

Thus, at the end of the middle cycle, the branch with maximum length and the least sum of alteration of the angular coefficients is chosen. The LSOs that form the example case are "dragged out" from the initial matrix T_0 and the search for the branch of maximum length among the remaining objects within the outer cycle is carried out.

The outer cycle. It is necessary to "drag out" all the elements from the initial matrix T_0, which were used in the first solution found, and repeat the inner and middle cycles. The goal of the outer cycle is to get the set of all possible "diagonal" branches, which will then be arranged in descending order by length, encompassing the maximum number of objects.

After the fulfillment of three cycles, a part of the objects is encompassed by the "diagonal" transfers and the flyby of the rest of the LSOs can be estimated with the help of the aforementioned successive scheme, as used in determining the flyby for the first three groups of LSOs.

10.2.10. Example Calculations for Group 5

The LSO orbits of group 5 have inclinations in the range of 97.1-100.4º. Apart from the region of near-Earth space with a high probability of collisions, the area of sun-synchronous orbits needs special attention (Castronuovo 2011, 848-859). The information about the LSOs of group 5 for November, 2013 is listed in table 10-14; the objects are in descending order by RAAN. As a result of the aforementioned algorithm, the implementations of the two diagonal solutions were found, encompassing 30 (18 and 12) LSOs out of 46 (Baranov, Grishko, Lapshin, and Medvedevskikh 2016, 242-250).

Table 10-14

	NORAD ID	*a* km	Ω	*i*
			deg	
1	27940	7,052	170.1286	97.8
2	7946	7,430.5	169.7677	100.1
3	20323	7,105	166.1984	97.1
4	27006	7,367.5	165.7893	99.2
5	28932	6,979.5	163.8276	98.3
6	28059	7,090.5	149.0105	98.7
7	11081	7,315.5	143.212	99.7

8	32959	7,125.5	127.9842	99
9	33500	6,989	126.2109	98.3
10	13778	7,235	106.7009	100.1
11	25979	6,973.5	96.3879	98.2
12	2174	7,495.5	90.2609	100.4
13	27601	7,159	65.798	98.5
14	32063	7,098.5	55.4669	98.2
15	26387	7,042	42.8234	98.1
16	27422	7,166.5	37.8068	98.3
17	20791	7,291	31.147	99.2
18	36089	7,100	23.6017	98.1
19	16615	7,159	14.203	98.8
20	28499	7,005.5	11.2445	98.2
21	29713	6,995	351.2681	97.6
22	21610	7,129.5	343.3011	98.8
23	21689	7,259	338.5724	99.5
24	37932	7,191	336.9718	98.4
25	25400	7,178.5	336.8603	98.3
26	10704	7,308	333.6947	98.8
27	28050	7,208.5	327.0023	98.5
28	815	7,173	325.7258	99.9
29	23343	7,013.5	325.2177	98.2
30	20443	7,139.5	320.7193	98.8
31	27387	7,144	315.5157	98.3
32	25732	7,205	309.6141	98.9
33	31114	7,200	306.3191	98.4
34	19468	7,253.5	304.8742	99
35	25261	7,153.5	303.4229	98.4
36	22830	7,159.5	300.7151	98.8
37	25861	7,008.5	300.5517	97.9
38	27432	7,217	300.2821	98.8
39	28651	7,027.5	299.5225	97.8
40	18961	7,262	298.1063	99.3
41	23561	7,139.5	293.7485	98.7
42	38341	6,999.5	291.5595	98.5
43	23828	7,191	290.3812	98.6
44	23324	7,207.5	279.5703	98.9

Columns 1 and 4 of table 10-15 give the obtained branches (the object numbers corresponding to the flyby order); columns 2 and 5 give the total

delta-v expenditures of the flyby to the respective object; and columns 3 and 6 give the flyby time in days. It is supposed that a separate active spacecraft was used for each branch.

Table 10-15

First Solution	ΔV m/s	Duration days	*Second Solution*	ΔV m/s	Duration days
1	2	3	4	5	6
37-38	161	60	30-26	87	161
38-40	77	5	26-32	54	244
40-33	127	52	32-25	83	88
33-35	24	16	25-36	67	52
35-41	41	100	36-10	174	1,270
41-24	48	497	10-13	221	448
24-34	94	130	13-15	81	122
34-21	228	303	15-17	193	78
21-3	89	429	17-1	221	554
3-5	177	171	1-29	57	1
5-27	124	51	29-4	225	458
27-8	83	213	-	-	-
8-28	127	52	-	-	-
28-16	209	331	-	-	-
16-44	90	30	-	-	-
44-18	123	146	-	-	-
18-46	69	356	-	-	-
$\Delta\mathbf{V}_\Sigma$, m/s per branch	**1,891**			**767**	
Duration per branch days		**2,942**			**3,476**
$\Delta\mathbf{V}_\Sigma$ m/s	**2,658**				

According to table 10-15, the total delta-v expenditure obtained for the first branch is 1,891 m/s and 767 m/s for the second. One SV-collector and two spacecraft-refuelers would be needed for the flyby of the first branch. The total delta-v budget is enough for a flyby of the whole branch, but the tanks of deployable modules would need to be refueled. One SV-collector and one spacecraft-refueler would have to be used for the flyby of the second branch.

For a 30 object flyby, a delta-v budget of 2,658 m/s is sufficient. Thus, the presence of the diagonal intersections of RAAN deviation evolution

allows a decreasing number of manoeuvres to be performed and total delta-v expenditure in the flyby of objects of the group in comparison to the successive flyby used for groups 1-3.

The results of determining the successive flyby of the LSOs, which were not encompassed by the diagonal solution, are listed in table 10-16.

Table 10-16

Flyby order	Number of Revolutions $N(\Delta\Omega_{i_k})$	Duration days	ΔV m/s	Flyby duration on one full fuel tank	ΔV m/s on one fuel tank
1	*2*	*3*	*4*	*5*	*6*
2-6	1,669	118.2	248	11,439 revolutions 810.1 days	2,190
6-7	660	46.7	387		
7-9	1,350	95.6	247		
9-11	2,368	167.7	282		
11-12	1,185	83.9	681		
12-14	4,207	298	345		
14-20	706	50	187	12,893 revolutions 913.1 days	2,260
20-19	406	28.8	242		
19-23	970	68.7	356		
23-22	804	56.9	113		
22-42	1,599	113.3	200		
42-31	6,068	429.8	361		
31-43	693	49	265		
43-39	1,373	97.2	137		
39-45	274	19.4	399		
ΔV_{Σ} m/s			**4,450**		
Duration	**24,332 revolutions**	**1,723.2 days**			

The data in the first column shows the LSO pair for the flyby. The second column gives the values for the compromise flyby duration N calculated by Eq. 10-10. The third column shows the duration of the corresponding flyby in days. The fourth column gives the total delta-v expenditures for the fulfillment of these flybys.

A velocity expenditure of 4,450 m/s is needed for a flyby of 16 objects. Pushing (de-orbiting or DO transfer) of these objects can be fulfilled with the use of one active spacecraft and one spacecraft-refueler. The

distribution results of the LSOs and the spacecraft are listed in the 5th and 6th columns.

10.2.11. Example Calculations for Group 4

The LSO identification numbers for group 4 in the NORAD catalogue[6] and some elements of their orbits for November, 2013 are depicted in table 10-17. The orbits of the objects of this group have an inclination of approximately 83º, the semimajor axis has the range of 7,318-7,358 km.

Table 10-17

	NORAD ID	*a* km	Ω	*i*
			deg	
1	11289	7,329.5	73.6622	82.9
2	21131	7,334.5	340.672	82.8
3	24678	7,340.5	172.2879	82.9
4	22208	7,342.5	94.1841	82.9
5	26819	7,343.5	263.8941	83
6	21876	7,346	83.1548	83
7	18710	7,348	142.5439	83
8	22007	7,349	241.8947	83
9	12682	7,349.5	118.766	82.9
10	24955	7,350.5	252.8786	83
11	25569	7,351	265.5485	82.9
12	27819	7,351	109.5972	83
13	20509	7,351.5	272.864	82.9
14	21231	7,352.5	171.8711	82.9
15	32053	7,356	167.4046	83
16	23774	7,356.5	111.474	83
17	11327	7,358	230.8018	82.9
18	15100	7,319.5	19.4841	82.5
19	15517	7,318	318.0135	82.5
20	16409	7,318	236.493	82.5
21	16736	7,318	263.3544	82.5
22	17242	7,323	257.8371	82.5
23	18313	7,320.5	260.4844	82.6

[6] "NORAD Satellite Catalog". Accessed November 21, 2013. http://www.celestrak.com/satcat/search.asp

24	22784	7,323	257.1819	82.6
25	6829	7,345.5	194.4667	82.9
26	10918	7,345	121.9273	82.9
27	11586	7,339	225.249	82.9
28	11681	7,351.5	201.9585	82.9
29	14085	7,348.5	236.6751	82.9
30	15360	7,347	197.7759	82.9
31	16799	7,345	232.311	82.9
32	18130	7,348	340.261	82.9
33	20528	7,360.5	204.5554	82.9
34	20805	7,350.5	208.2701	82.9
35	21153	7,350.5	351.6455	82.9
36	22308	7,350.5	315.5031	82.9
37	22591	7,344.5	191.6403	82.9
38	23466	7,355	52.1648	82.9
39	24773	7,358.5	159.5764	82.9
40	25592	7,356.5	250.7425	82.9
41	25893	7,347.5	174.8071	82.9
42	27535	7,355	11.261	82.9
43	8597	7,352.5	204.1671	83
44	8874	7,353.5	145.1377	83
45	10461	7,347	160.6361	83
46	11668	7,351	190.146	83
47	16728	7,347	123.5242	83
48	19325	7,344	171.2448	83
49	19922	7,345	212.7931	83
50	23180	7,342.5	81.2198	83
51	27437	7,347.5	215.7	83
52	28381	7,342	123.4479	83

The evolution of RAAN deviations for LSO group 4 (fig. 10-11) is a combination of quasi-parallel and inclined lines $\Delta\Omega_{i_k}(t)$. Hence, the most effective combination would involve the diagonal solution with the successive flyby. First of all, diagonal solutions (the branches reaching as many LSOs as possible) are considered, because their realization needs far smaller total delta-v expenditures. There are two such solutions in the given example (Baranov and Grishko 2015, 5450-5462), the flyby order and the required total delta-v expenditures are shown in table 10-18.

The first and fourth columns present the numbers of overflown objects between which the flyby is performed. The third and sixth columns give

the total delta-v expenditures necessary for the flyby. The flyby duration between two objects within every branch is given in the second and fifth columns.

The duration of each branch coincides with the range for the RAAN deviation evolution: 3,148 and 3,522 days, respectively. The total delta-v expenditures are 540 and 358 m/s, respectively. In the first branch, 12 spacecraft are flown by and in the second branch 10 objects are flown by. One SV-collector and one spacecraft-refueler are enough for the flyby of one branch. One SV-collector is enough for the second branch.

Table 10-18

First Solution	Duration, days	ΔV, m/s	*Second Solution*	Duration, days	ΔV, m/s
1	*2*	*3*	*4*	*5*	*6*
48-3	88	19	29-22	409	54
3-14	9	15	22-17	81	55
14-15	290	19	17-24	102	43
15-20	653	67	24-27	254	41
20-39	309	56	27-43	528	19
39-21	469	56	43-31	752	19
21-7	75	66	31-18	714	54
7-23	363	54	18-30	617	54
23-16	439	55	30-45	65	19
16-19	392	67	-	-	-
19-52	61	66	-	-	-
Duration, days using branch 1	**3,148**		Duration, days using branch 2	**3,522**	
$\Delta\mathbf{V}_{\Sigma}$, m/s using branch 1	**540**		$\Delta\mathbf{V}_{\Sigma}$, m/s using branch 2	**358**	
$\Delta\mathbf{V}_{\Sigma}$, m/*s* of diagonal solution	**898**				

Once the parameters of the two diagonal solutions are determined, the encompassed LSOs are no longer considered. The evolution of the RAAN deviations for the last 30 objects presents the same basic appearance as LSO groups 1-3.

The results of calculating the successive LSO flyby, not encompassed by the diagonal solutions, are listed in table10-19. The data from the first column show the LSO pairs between which the flyby is performed. The

second column gives the flyby compromise duration values calculated using Eq. 10-10. The third column presents the duration of the corresponding flyby in days. The fourth column shows the total delta-v expenditures needed for the fulfillment of this flyby.

From table 10-19, it follows that the total delta-v expenditure exceeds 7 km/s even in the case of the "compromise" choice of the flyby revolution number. The "drag" (de-orbiting or DO transfer) of these objects could be fulfilled using one active spacecraft and three SV-collectors. The distribution results for the LSOs and the spacecraft can be seen in the 5th and 6th columns.

Table 10-19

Flyby order	Number of Revolutions $N(\Delta\Omega_{ik})$	Duration, days	ΔV, m/s	Flyby duration on one full fuel tank	ΔV, m/s on one fuel tank
1	*2*	*3*	*4*	*5*	*6*
1-11	750	54.3	241	6,640 revolutions 480.7 days	1,836
11-5	334	24.2	106		
5-10	990	71.7	272		
10-40	482	34.9	166		
40-8	756	54.7	253		
8-51	2,049	148.3	385		
51-49	472	34.2	174		
49-34	807	58.4	239		
34-33	387	28	128	7,358 revolutions 532.6 days	1,936
33-28	540	39.1	199		
28-46	671	48.6	236		
46-25	464	33.6	163		
25-37	459	33.2	167		
37-41	1,352	97.9	318		
41-44	1,620	117.2	348		
44-47	1,865	135	377		
47-12	1,105	80	291	7,436 revolutions 538.1 days	1,745
12-26	353	25.5	102		
26-9	343	24.8	100		
9-6	1,958	141.7	378		
6-50	492	35.6	181		
50-4	317	22.9	72		

4-13	2,083	150.8	385		
13-38	785	56.8	236		
38-42	3,046	220.5	420	8,695 revolutions 629.3 days	1,701
42-35	1,784	129.1	364		
35-32	1,144	82.8	295		
32-36	1,821	131.8	364		
36-2	900	65.1	258		
ΔV_{Σ}, m/s			**7,218**		
Duration	**30,129 revs**	**2,180.7 days**			

10.2.12. Second De-Orbiting Variant: Parameters of Disposal Orbits

The second scheme of LSO removal implies the use of a spacecraft manoeuvring between the objects and transferring them successively to DOs with the help of its thrust engines. The capture of an LSO is fulfilled with a specially developed unit (Iutkin and Trushliakov 2013, 56-61; Emanuelli, Ronse, Tintori, and Trushlyakov 2012, 185-218).

Determination of the disposal orbit. It has been agreed internationally that LEO spacecraft should remain in a DO for no longer than 25 years. Two types of DOs can be distinguished for the considered LSO groups: an elliptical orbit with its pericenter in the upper layers of the atmosphere and a circular orbit that is entirely situated in the upper layers of the atmosphere. The transfer to the circular orbit "pushes" the spacecraft out of the operational area of the active spacecraft. The altitude of this orbit is higher than the altitude of the elliptical DO.

Table 10-20 gives the elements of the circular and elliptical DOs, calculated for LSOs with an average ballistic coefficient value of 0.045. The algorithm described in the first paragraph of this chapter was used. The perigee argument was 45º for the elliptical orbits and the initial date for propagation was December 1st, 2013. The third column presents the radii of the circular DOs. The fourth column gives the semimajor axes, while the fifth gives the eccentricities of the elliptical DOs, corresponding to the lower (Min) boundary of the orbital semimajor axes values for orbits of each group. The sixth column presents the semimajor axes and the seventh gives the eccentricities of the elliptical DOs, corresponding to the upper (Max) boundary of the orbital semimajor axes values for the orbits of each group.

Table 10-20

Inclination deg	a_{min} - a_{max} km	R km	Min a km	min e	max a km	max e
71	7,193-7,281	6,912.7	7,000.3	0.0275	7,040.2	0.0341
74	7,122-7,152	6,912.7	6,969.6	0.0219	6,981.9	0.0243
81.3	7,211-7,262	6,913.1	7,007.5	0.0291	7,030.5	0.0329

According to table 10-20, the semimajor axis of the circular DO for all LSOs from the first three groups is practically the same: 6,912.7 km. If the value of the semimajor axis of the LSO lies inside the boundaries of the respective range (column 2), the orbital element linear interpolation from columns 4-7 should be implemented for the correct determination of the elliptical DO elements.

In Fig. 10-16, the relative evolution of the circular DO plane for one of objects of group 2 is shown by the dashed line.

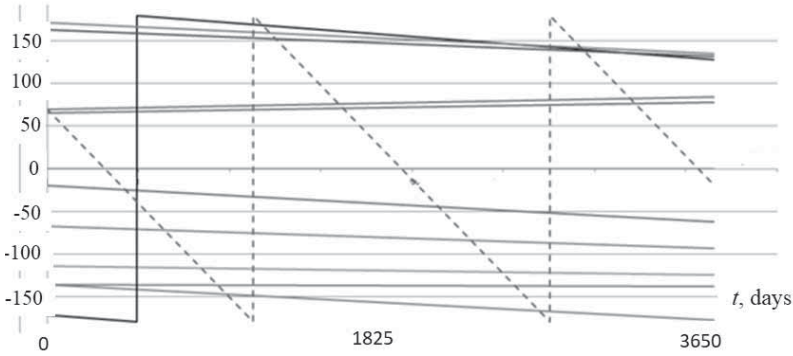

Fig. 10-16. RAAN deviation evolution of elements of group 2

Manoeuvring strategy. If the RAAN deviation evolution describes mainly quasi-parallel lines (Fig. 10-16), the following sequence of actions should be done in order to fulfill the flyby between two LSOs using the second scheme. After the deployment of the active spacecraft in the vicinity of object 1, the approach to and then capture of this object occurs. Then, with the help of impulse ΔV_1, the compound unit "active spacecraft

+ LSO" is pushed from the orbit of object 1 to the DO of object 1. For the circular DO, unlike the elliptical one, the impulse will be denoted as two ignitions localized on one revolution. The manoeuvre determination algorithm, which drags the LSO to the DO, is described in the first paragraph of this chapter. After shaping the DO, object 1 separates from the active spacecraft, which temporarily stays on this orbit until the planes of the DO and the orbit of the next LSO coincide in terms of their RAANs. Once the RAANs coincide, the transfer of the active spacecraft in the vicinity of object 2 is fulfilled with the help of impulse ΔV_2 (the determination algorithm for these manoeuvres is described in chapters 4, 5, and 6). Then, the described actions should be repeated. The points of line intersection in the RAAN deviation evolution correspond to the coincidence of the orbital planes by RAANs. In this case, the line corresponding to the next object and the dashed line intersect.

10.2.13. Example Calculations for Groups 1, 2, and 3

The results of the flyby manoeuvre determination for groups 1-3 are described in tables 10-21 to 10-23 (Baranov, Chernov, and Grishko 2016, 48-64). Each table consists of two parts, which differ from each other by the type of DO to which the LSO will be transferred. All objects within one group have been sorted in descending order by initial RAAN values and enumerated in order for the flybys for the first scheme.

The delivery of the first active spacecraft to the first object is fulfilled using a launch vehicle. The succession of further flybys in the case of a circular DO is shown in the first column. As the configuration of orbital planes on the RAAN deviation evolution in the case of the first three groups does not change with time, the initial orbital RAAN order of the objects, in general, corresponds to the succession of flybys, though with some exceptions. The second column gives the duration of the active spacecraft in the previous object's DO before continuing the flyby to the current object. The third column shows the total delta-v expenditures necessary for the flyby from the previous object DO to the current object. The fourth column presents the total delta-v expenditures needed for the transfer of the current object to its DO. The fifth column gives the summed-up total delta-v needed for the flyby to the current object and its transfer to the DO. Similar data can be found in columns 6-10 for the elliptical DO.

Table 10-21

Circular DO					Elliptical DO				
Flyby order	Duration at DO, days	Transfer from DO to object	Transfer to DO	∑Δ*V*, m/s	Flyby order	Duration at DO, days	Transfer from DO to object	Transfer to DO	∑Δ*V*, m/s
1	***2***	***3***	***4***	***5***	***6***	***7***	***8***	***9***	***10***
1	0	0	162	162	1	0	0	108	108
2	0.1	165	165	330	2	0.2	112	110	222
3	24.1	159	158	317	3	36.6	109	106	215
4	4.5	161	161	322	4	6.4	109	107	216
5	58.5	159	159	318	5	88.4	106	107	213
6	1.8	161	161	322	6	2.1	108	107	215
7	37.5	162	162	324	7	55.7	108	108	216
8	12.3	160	160	320	8	19.3	107	107	214
9	20.1	159	159	318	9	31.1	106	107	213
10	15.6	158	158	316	10	24.1	106	106	212
12	72.3	150	150	300	12	111.7	99	102	201
11	10.5	240	192	432	13	31.6	106	104	210
13	6.6	202	153	355	11	5.5	193	124	317
14	58.7	226	193	419	14	68.8	125	124	249
15	13.4	198	160	358	15	5.1	169	107	276
17	110.2	161	161	322	17	162.4	108	108	216
16	8.8	157	157	314	16	21.5	103	105	208
18	52.1	157	157	314	18	76.6	106	106	212
19	93.4	160	160	320	19	131.9	109	107	216
21	53.2	160	160	320	21	79.9	107	107	214
20	75.4	242	195	437	20	198.9	202	126	328
22	58.8	213	157	370	22	34.5	192	106	298
23	18.7	161	161	322	23	14.1	110	108	218
Total ΔV, m/s		3,871	3,761	**7,632**	Total ΔV, m/s		2,700	2,507	**5,207**
Total duration, days	**806.6**				Total duration, days	**1,206.4**			

Table 10-22

Circular DO					Elliptical DO				
Flyby order	Duration at DO, days	Transfer from DO to object	Transfer to DO	$\sum\Delta V$, *m/s*	Flyby order	Duration at DO, days	Transfer from DO to object	Transfer to DO	$\sum\Delta V$, *m/s*
1	***2***	***3***	***4***	***5***	***6***	***7***	***8***	***9***	***10***
1	0	0	125	125	1	0	0	88	88
2	16.7	124	124	248	2	23.7	88	88	176
3	299.7	129	129	258	3	426.4	93	91	184
4	104.8	122	122	244	4	163	84	87	171
5	200.3	125	125	250	5	274.7	89	88	177
6	191.8	121	121	242	6	261.9	85	86	171
8	91.2	129	128	257	8	122.8	95	90	185
7	42.8	122	122	244	7	88.2	84	87	171
9	187.2	114	113	227	9	280.1	82	81	163
10	42.4	116	116	232	10	37.2	85	83	168
11	32.3	124	124	248	11	40.4	92	88	180
Total ΔV, m/s		1,226	1,349	**2,575**	Total ΔV, m/s		877	957	**1,834**
Total duration, days	**1,209.2**				Total duration, days	**1,718.4**			

As can be seen in tables 10-21 to 10-23, the duration of the group flyby with the use of the elliptical DO is on average 1.5 times longer in comparison to the use of the circular DO. However, in this case the total delta-v expenditure is 1.5 times less. The group flyby durations with object transfers to the elliptical DOs will be 3.3, 4.7, and 8.7 years, which is acceptable for modern space systems.

The flyby characteristics depend on the initial object for the flyby in the case of the 4th and 5th groups. Successive analysis of the variants allows us to choose the optimal initial object. The results of the optimal flyby manoeuvre determination for groups 4 and 5 are shown in tables 10-24 and 10-25.

Table 10-23

Circular DO					Elliptical DO				
Flyby order	Duration at DO, days	Transfer from DO to object	Transfer to DO	∑Δ*V*, m/s	Flyby order	Duration at DO, days	Transfer from DO to object	Transfer to DO	∑Δ*V*, m/s
1	***2***	***3***	***4***	***5***	***6***	***7***	***8***	***9***	***10***
1	0	0	175	175	1	0	0	116	116
2	50.7	170	169	339	2	75.9	111	113	224
3	66.1	177	176	353	3	102.7	120	116	236
4	88.9	163	163	326	4	148.5	103	109	212
5	131.3	167	167	334	5	174.8	114	111	225
6	21.1	174	173	347	6	39.6	119	115	234
7	33.3	172	171	343	7	35.5	114	114	228
8	42.3	175	175	350	8	57.5	118	116	234
9	80.8	177	177	354	9	146.9	118	116	234
10	81.4	175	175	350	10	100.3	116	116	232
11	21.5	170	170	340	11	45.8	110	113	223
12	16.8	177	177	354	12	8.5	120	116	236
13	42.2	174	174	348	13	70.6	114	115	229
14	40.6	173	173	346	14	63.9	114	115	229
16	265.3	185	185	370	16	360.4	127	121	248
17	89.5	174	174	348	17	185.4	110	115	225
15	17.3	164	164	328	15	149.4	106	110	216
18	213.2	162	161	323	18	261.3	108	108	216
19	62.1	177	177	354	19	70.9	125	117	242
21	128.7	185	185	370	21	145.8	125	121	246
20	48.1	166	166	332	26	154.9	115	117	232
23	55.9	177	177	354	20	64.7	106	111	217
26	16.3	179	178	357	23	4.3	121	116	237
25	54.3	175	175	350	25	111.1	115	116	231
24	0.3	172	172	344	24	25.6	112	114	226
22	12.1	168	168	336	22	53.6	110	112	222
28	94.4	172	172	344	28	20.4	117	114	231
27	163.3	160	159	319	27	500.2	103	107	210
Total ΔV, m/s		4,661	4,828	**9,489**	Total ΔV, m/s		3,091	3,200	**6,291**
Tot.dur., days	**1,937.8**				Tot.dur., days	**3,178.5**			

Table 10-24

Circular DO					Elliptical DO				
Flyby order	Dur. at DO, days	Total ΔV, m/s			Flyby order	Dur. at DO, days	Total ΔV, m/s		
		Transf. from DO to object	Transf. to DO	∑Δ*V*, *m/s*			Transf. from DO to object	Transf. to DO	∑Δ*V*, *m/s*
1	2	3	4	5	6	7	8	9	10
18	0	0	214	214	18	0	0	136	136
42	35.1	238	232	470	42	49.1	162	145	307
35	109.1	230	230	460	35	178.4	142	144	286
32	64.1	229	229	458	32	105.0	142	143	285
2	17.2	222	222	444	2	49.8	137	140	277
36	111.1	230	230	460	36	149.5	148	144	292
19	125.6	220	214	434	1	380.4	144	144	288
1	85.2	236	230	466	5	16.4	144	142	286
5	25.3	227	226	453	11	56.3	146	144	290
11	17.1	230	230	460	10	20.4	144	144	288
10	34.4	230	230	460	19	3.1	157	135	292
40	43.4	233	233	466	40	60.8	163	145	308
8	18.9	229	229	458	8	3.8	142	143	285
29	75.5	229	229	458	29	169.3	144	143	287
17	17.9	234	234	468	17	14.5	148	145	293
31	12.1	227	227	454	31	40.7	139	142	281
23	30.1	218	215	433	51	14.4	144	143	287
51	8.0	234	228	462	49	37.4	142	142	284
24	8.8	222	216	438	43	45.3	146	144	290
27	1.3	228	224	452	27	3.4	139	141	280
49	9.5	227	227	454	33	85.1	151	146	297
21	26.3	223	214	437	34	14.3	141	144	285
43	6.9	240	231	471	46	17.3	144	144	288
22	22.6	226	216	442	28	38.8	145	144	289
34	8.7	236	230	466	30	60.9	142	143	285
33	2.5	235	235	470	25	37.6	142	142	284
28	30.7	230	230	460	23	25.0	148	136	284
46	10.5	230	230	460	15	2.8	162	145	307
30	23.1	228	228	456	37	2.6	140	142	282
25	21.4	227	227	454	241	17.9	143	137	280
37	17.9	227	227	454	48	4.9	156	142	298
15	48.6	233	233	466	45	80.3	143	143	286
48	3.8	227	227	454	14	40.4	146	144	290
20	17.2	223	214	437	41	2.9	142	143	285
41	15.3	234	228	462	44	53.0	146	144	290

14	5.3	231	231	462	3	14.6	138	141	279
45	9.1	228	228	456	39	4.2	150	146	296
3	16.8	225	225	450	7	35.0	141	143	284
39	29.4	234	234	468	21	69.5	156	135	291
44	22.3	232	231	463	22	14.7	138	137	275
7	27.8	229	229	458	47	54.7	162	143	305
47	110.1	228	228	456	52	34.9	140	141	281
52	13.9	226	226	452	16	10.3	149	145	294
16	28.4	233	233	466	12	55.3	142	144	286
12	25.6	230	230	460	9	150.2	144	143	287
26	32.1	227	227	454	26	5.5	141	142	283
9	4.8	229	229	458	6	110.3	143	142	285
6	118.0	228	228	456	20	28.4	155	135	290
50	22.0	226	226	452	50	10.9	161	142	303
4	22.0	226	226	452	4	135.2	142	142	284
13	162.0	219	219	438	38	265.2	148	147	295
38	29.9	232	232	464	13	47.4	132	138	270
Total ΔV, m/s		11,675	11,801	**23,476**	Total ΔV, m/s		7,446	7,394	**14,840**
Tot.dur., days	**1,784**				Tot.dur., days	**2,928**			

Table 10-25

Circular DO					Elliptical DO				
Flyby order	Dur. at DO, days	Total ΔV, m/s			Flyby order	Dur. at DO, days	Total ΔV, m/s		
		Transf. from DO to object	Transf. to DO	∑Δ*V* m/s			Transf. from DO to object	Transf. to DO	∑Δ*V* m/s
1	2	3	4	5	6	7	8	9	10
10	0	0	171	171	10	0	0	116	116
9	71	247	42	289	9	92.4	253	25	278
8	97.3	147	115	262	3	94.8	180	69	249
3	6.7	272	104	376	11	238.8	176	19	195
11	321.5	149	34	183	1	331.6	102	49	151
1	245.4	92	76	168	4	94.9	279	163	442
4	54.6	300	238	538	7	514.7	151	145	296
7	238.3	222	213	435	2	35.5	208	184	392
6	32.8	163	96	259	6	14.3	210	64	274
2	26.3	325	270	595	8	72.2	91	76	167
5	82.2	257	41	298	33	114.9	139	104	243
45	192.3	365	291	656	39	121.1	111	40	151

33	6.9	260	153	413	45	41.9	392	199	591
39	60.0	103	63	166	26	13.6	195	142	337
26	142.0	246	209	455	25	80.3	127	96	223
46	32.9	102	94	196	27	76.9	114	107	221
43	16.2	149	149	298	43	14.0	99	100	199
25	3.6	148	142	290	31	16.0	102	83	185
27	34.2	160	158	318	24	5.4	109	100	209
35	4.5	130	129	259	35	16.9	81	87	168
31	2.9	125	124	249	21	72.6	141	28	169
24	28.2	149	149	298	28	65.8	325	94	419
21	68.5	115	45	160	46	42.9	209	62	271
37	372.2	66	52	118	37	21.3	123	33	156
28	110.4	297	139	436	38	351.8	185	110	295
38	14.5	217	162	379	16	102.1	122	92	214
34	96.3	183	181	364	18	95.8	78	67	145
44	6.1	158	157	315	34	29.6	188	123	311
16	16.9	157	136	293	44	50.3	100	106	206
18	44.6	105	101	206	5	163.5	106	22	128
32	497.3	188	156	344	32	244.7	161	105	266
41	80.9	125	122	247	14	91.7	126	67	193
14	37.9	120	100	220	41	236.3	118	82	200
36	128.5	154	132	286	13	141.5	95	89	184
13	100.1	138	132	270	36	22.6	107	89	196
40	11.7	213	185	398	15	95.7	132	45	177
15	32.2	173	70	243	17	163.1	226	136	362
17	65.1	246	200	446	40	55.5	122	126	248
29	43.0	143	55	198	29	108.9	181	35	216
30	500.1	146	122	268	30	1,067.0	128	82	210
19	113.4	132	132	264	19	27.3	92	89	181
20	170.1	102	51	153	20	346.3	105	32	137
22	219.5	141	117	258	22	915.7	125	78	203
12	488.7	366	301	667	12	469.8	334	206	540
23	10.6	218	184	402	23	256.9	164	125	289
42	238.9	144	48	192	42	740.9	158	29	187
Total ΔV, m/s		8,158	6,141	**14,299**	Total ΔV, m/s		7,070	4,120	**11,190**
Tot.dur., days	**5,167**				Tot.dur., days	**7,970**			

10.2.14. Comparison of the Flyby Results Obtained by the Other Authors Using the Second Scheme

The LSO flyby using the second scheme is examined to the fullest extent possible in the work of Braun, Flegel, Gelhaus, and Kebschull et al. (2013, 1638-1648) for active spacecraft types with chemical or electro-rocket engines. Despite the use of different approaches for the propagation of orbital motion in the work of Baranov, Budyansky, Chernov, and Golikov (2015, 4-19) and Braun, Flegel, Gelhaus, and Kebschull et al. (2013, 1638-1648), similar results were obtained. These results are connected to the determination of the duration for which the DO apogee is in the operational zone of the spacecraft orbits: the DO apogee for the considered LSO groups descends to an altitude less than 700 km in approximately 10 years time. Meanwhile, the risk of collision of an object transferred to the elliptical DO with other objects during this time is 50 % less in comparison to the initial value calculated for the initial LSO orbit (Braun, Flegel, Gelhaus, and Kebschull et al. 2013, 1638-1648). The statement about the excessively long duration of the passive standby of the active spacecraft in the DO is not exactly correct (Braun, Flegel, Gelhaus, and Kebschull et al. 2013, 1638-1648). As can be seen in tables 10-21 to 10-23, this has been fully determined by the current configuration of the group object orbital planes and may vary from several hours to several months. The required total delta-v expenditure for the transfer of 5 objects with similar orbits is 200-300 m/s less in comparison (Braun, Flegel, Gelhaus, and Kebschull et al. 2013, 1638-1648). This can be explained by the choice of an optimal manoeuvring scheme. The elliptical DOs have similar parameters in both cases.

10.2.15. Comparison with Results of Flyby Manoeuvre Determination for Groups 1-5 Using the First Variant

The results of the flyby for the first three groups using the two schemes and the results of the flyby for the last two groups using the first scheme (with the branch subdivision) are listed in table 10-26. In the third and fourth columns, the first value is for the flyby using the first scheme and the second value is for the flyby using the second scheme. Total delta-v expenditures for the LSO flyby in the case of the first and third groups with the use of the second scheme exceed total delta-v expenditures with the use of the first flyby scheme by 2.4 and 1.5 times, respectively. The total delta-v expenditures in the case of the second group are slightly higher too. The first group flyby time with the use of the second scheme is

2.8 times smaller than the flyby time with the first scheme. The flyby durations in the case of the second and third groups with the use of both schemes are practically the same. It is not entirely valid to compare the flybys of the fourth and fifth groups: with the use of the first scheme the flyby is carried out simultaneously by the three spacecraft. The second scheme flyby suggests that the active spacecraft will perform the de-orbiting manoeuvre while being attached to a captured object with a mass of up to 1 ton. Hence, even if the required total delta-v is the same for both schemes, the realization of the second scheme will demand a bigger fuel budget and, thus, a greater number of spacecraft-refuelers in comparison to the first scheme.

Table 10-26

Group	Object number	Total ΔV m/s	Flyby duration days	Number of spacecraft for the first scheme
1	23	2,233/5,207	3,318/1,206	1 SC+2 (1) Spare
2	11	1,540/1,834	1,570/1,718	1 SC+1 (0)
3	28	4,213/6,291	3,744/3,179	1 SC+3 (1) Spare

Table 10-26 continued

Group	Object number	Total ΔV m/s	Flyby duration days	Number of spacecraft for the first scheme
4	12	540	3,148	1 SC+1 (0) Spare
	10	358	3,522	1 SC
	30	7,218	2,180	1 SC+3 (2) Spare
5	18	1,891	2,942	1 SC+2 (1) Spare
	12	767	3,476	1 SC+1 (0) Spare
	16	4,450	1,723	1 SC+1 (0) Spare
Column Total	160			9 SC+14 (5) Spare

It is only possible to approximately determine the required number of refuelers for the second scheme at the stage of preliminary analysis; however, it is clear that it will be at least 10. Thus, the advantage of the second scheme is the reduced duration of object flyby in the case of the first three LSO groups. At the same time, the first scheme is poorer in the aspects of energy costs and the number of additional refuels.

10.2.16. Conclusions on Flyby Strategy for All Five Groups Using 2 De-Orbiting Variants

The following conclusions can be made.

Using the NORAD catalogue of space objects, five compact groups of LSOs can be distinguished. The elements of the groups have orbits with close inclinations.

The RAAN deviation evolution, plotted for the specific LSO group, allows us to choose an adequate strategy for the flyby of objects of this group: the strategy of consequent flybys (groups 1-3) or the strategy of a combination of diagonal and consequent flybys (groups 5 and 4).

The use of optimal manoeuvring schemes (from the chapter 7) and the compromise flyby duration (the algorithm is described in this paragraph) allow us to gradually reduce the total delta-v expenditures in the case of the consequent flyby.

The use of the diagonal flyby scheme allows us to reduce the number of performed manoeuvres and the total delta-v expenditures for the flyby to the objects of the group in comparison to the consequent flyby.

The advantage of the second scheme is the reduced duration of the object flyby. At the same time, it is poorer in terms of energy costs and the number of additional refuels required.

Nine SV-collectors and 14 spacecraft-refuelers are needed for the removal of approximately 160 objects of the five considered groups using the first scheme (Castronuovo 2011, 848-859).

At present, some works[7] imply the use of up to 25 TDKs on one SV-collector, which is clearly redundant for the removal of LSOs from their orbits (Lewis and White 2014, 1195-1206). However, the number of TDKs (6-7 units) on one SV-collector is clearly not enough (Castronuovo 2011, 848-859). If the number of TDKs is increased up to 11-12 units, the number of spacecraft-refuelers necessary for LSO flybys for all groups can be decreased from 14 to 5.

The necessary total delta-v budget for one spacecraft (2,300 m/s) was determined with high accuracy in Castronuovo (2011, 848-859).

To maintain the pace of annual LSO removal (4-5 objects), having at least two functioning SV-collectors is recommended.

It is better to solve the problem of LEO decontamination in an integrated fashion by removing several compact groups of LSOs

[7] "Rocket Space Company Ad AstraTM, Low Earth Orbit Large Debris Removal Using VASIMR®".
http://www.adastrarocket.com/aarc/SpaceCleaner

simultaneously. Thus, the spacecraft used for cleaning LEOs should have total delta-v of 2,300 m/s and 12 TDKs on board.

10.2.17. Optimal Schemes for Flybys between Space Debris Objects in Geostationary Orbits

The problem of re-orbiting space debris objects (SDO) from the vicinity of the GEO region is also extremely important. The problem of determining the transfer schemes between space debris objects in the vicinity of the GEO region with the goal of their transfer to disposal orbits (DO) has been considered. It was supposed that an active spacecraft-collector (SV-collector) performs flybys between target objects (87 upper stages). Two re-orbiting variants were considered. For the first re-orbiting variant, each target object is re-orbited into a DO with special detachable modules—TDKs mounted on the SV-collector. For the second variant, the object is pushed to a DO by the collector itself, which then moves to a new space debris object from the previous object's DO.

The geometrical peculiarities of relative orbit positioning in the near-equatorial region and two transfer schemes between space objects were considered. For the first scheme, a transfer is executed when the orbits have the same inclination near the equator and for the second scheme when the orbit of the next object has the smallest inclination.

The calculations show that both schemes are practically equivalent in terms of both average ΔV for a transfer and flyby duration; however, not all objects under consideration can be covered during the transfer in the moment of coincidence of inclination.

Distinct from low orbits (in which it is preferable to use TDKs), it is more beneficial to follow the second variant for re-orbiting SDOs from the GEO region (i.e. using the SV-collector itself without TDKs). This problem has been thoroughly considered in Baranov and Chernov (2019, 220-228) and Estes and Foster (1992).

BIBLIOGRAPHY

1. Agapov, V., Baranov, A., Stepanyantz, V., Tuchin, A. 2010. “Identification of Manoeuvres Executed by Low-Thrust Engines”. *8th US/Russian Space Surveillance Workshop Space Surveillance Detecting and Tracking Innovation Maui Hawaii*.
2. Akhmetshin, R., Efimov, G., Egorov, V., Eneev, T. et al. 1997. “Trajectory-Ballistic Analysis of Flights of Spacecraft with Low-Thrust Engines to Asteroids and Comets”. In *Intellectual Systems of Autonomous Craft for Space and Ocean*, edited by D. Goldin. Moscow: Institute of Control Sciences of Russian Academy of Sciences.
3. Akhmetshin, R., Efimov, G., Eneev, T., Yegorov, V. 2000. “Asteroid and Comet Rendezvous Missions Using Low-Thrust Nuclear Propulsion”. *International Journal of Space Politic, Science and Technology*, No. 5: 279-305.
4. Akhmetshin, R., Beloglazov, S., Belousova, N., Efimov, G., Egorov, V., Glazkov A., and Guschin V.1985."Optimization of Spacecraft With Low- and High-Thrust Propulsion Systems Transfers to Asteroids and Comets". *Preprint M.V. Keldysh Institute of Applied Mathematics of SU Academy of Sciences*, No. 144.
5. Akim, E., Golikov, A. 1994. “NA-Theory: The Precise Method for Prediction of the Satellite Motion in the Earth’s Atmosphere”. *9th International Symposium on Space Dynamics*.
6. Akim, E., Golikov, A. 1993. “Numeric-Analytical Satellite Theory”. *8th International Symposium on Space Flight Dynamics.*
7. Alexeev, K., Bebenin, G., and Yaroshevsky, V.1970. *Spacecraft Manoeuvring*. Moscow: Mashinostroenie.
8. Alfriend, K., Kamensky, S., Stepanyants, V., Tuchin, A. 2009. “Algorithm of Automatic Detection and Analysis of Nonevolutionary Changes in Orbital Motion of Geocentric Objects”. *AAS/AIAA Astrodynamics Specialist Conference*: 3–22.
9. Alvarez, S., Carter, T. 2000. “Quadratic-Based Computation of Four-Impulse Optimal Rendezvous near Circular Orbit”. *Journal of Guidance, Control and Dynamics*, No. 1: 109–117. https://doi.org/10.2514/2.4493

10. Anonymous. 2002. *Recommendation on Cataloging. Cataloging of Production for Federal State Needs. Supplies. List of Confirmed Titles. Russian State Standard*. Moscow.
11. Anonymous. 2008. *GOST (State All-union Standard) of Russia 52925-2008: Items of Space System Engineering: Basic Demands to Spacecraft for Restriction of Technogenic Pollution of Near-earth Space*. Moscow.
12. Appazov, R. and Ogarkov, V.1976."Research of Optimal Multiple-Impulse Transfers with Fixed Time between Close Near-Circular Orbits". *Cosmic Research*, No. 2.
13. Bakshiyan, B., El'yasberg P., Nazirov, R. 1980. *Motion Determination and Correction*. Moscow: Science.
14. Baranov A., Labourdette P. 2001. "Strategies for On-Orbit Rendezvous Circling Mars". *AAS/AIAA Astrodynamics Specialist Conference*: 1–20.
15. Baranov A., Labourdette P. 2003. "A Software for Rendezvous between Near-Circular Orbits with Large Initial Ascending Node Difference". *Proceedings of the 17th International Symposium on Space Flight Dynamics*: 130–142.
16. Baranov, A. Jr, Baranov A. 2008. "Satellite Constellation Deployment Manoeuvres". *Proceedings of the 5th International Workshop on Constellations and Formation Flying*.
17. Baranov, A. Jr., Baranov, A., de Prado, A., Razumny, V. 2011. "Optimal Low-thrust Transfers Between Close Near-Circular Coplanar Orbits". *Cosmic Research*, No. 3: 269–279. https://doi.org/10.1134/S0010952511030014.
18. Baranov, A. Jr., Baranov, A., Razoumny, V. 2010. "Formation and Maintenance of the Orbit with Small Spacecraft Thrusters". *Preprint M.V. Keldysh Institute of Applied Mathematics of Russian Academy of Sciences*, No. 52.
19. Baranov, A. Jr., Baranov, A. 2009. "Maintenance of Given Configuration of Satellite Constellation". *Cosmic Research*, No. 1: 48–54
20. Baranov, A. Jr., Baranov, A. 2009. "The Algorithm for Calculating the Parameters of Manoeuvres of Formation of Satellite Systems". *Cosmic Research*, No. 3: 256–262.
21. Baranov, A. Jr., Baranov, A. 2010. "Manoeuvring With Steady Low-Thrust". *Actual Problems of Russian Cosmonautics, Proceedings of XXXIV Academic Readings on Cosmonautics*: 115-116.

22. Baranov, A. Jr. 2008. “Change of Spacecraft Position in a Satellite System”. *Cosmic Research*, No. 3: 215–218. https://doi.org/10.1134/S0010952508030040
23. Baranov, A., Wang, L. 2015. “Optimal Maintenance of Spacecraft with Low-Thrust Engines on Sun-Synchronous Orbit”. *Bauman Moscow State Technical University Bulletin. Mashinostroenie Series*, No. 2: 68–83.
24. Baranov, A., Boutonnet, A., Escudier, B., Martinot, V. 2005. “Optimal Invariant Spacecraft Formation Deployment with Collision Risk Management”. *Journal of Spacecraft and Rockets*, No. 5: 913-920. https://doi.org/10.2514/1.6236
25. Baranov, A., Boutonnet, A., Escudier, B., Martinot, V., Noailles, J. 2003. “Optimal Analytical Solution for Invariant Spacecraft Formation Initialization”. *Proceedings of the Third International Workshop on Satellite Constellations and Formation Flying*.
26. Baranov, A., Boutonnet, A., Escudier, B., Martinot, V., Noailles, J. 2003. “Optimal Small Formation Flying Initialization in Circular Orbit”. *Proceedings of the 17th International Symposium on Space Flight Dynamics*: 83–96.
27. Baranov, A., Budyansky, A., Chernov, N., Golikov, A. 2015. “Choice of the Low-altitude Disposal Orbits and Transfer of Obsolete Spacecraft to Them”. *Bauman Moscow State Technical University Bulletin. Mashinostroenie Series*, No. 4: 4-19. https://doi.org/10.18698/0236-3941-2015-4-4-19.
28. Baranov, A., Chen, D., Grishko, D., Khurkina O. 2020. “Optimal transfer schemes between space debris objects in geostationary orbit”. *Acta Astronautica*, V. 169: 23–31. https://doi.org/10.1016/j.actaastro.2020.01.001
29. Baranov, A., Chernov, N., Grishko, D. 2016. “Flyby of Large-Size Space Debris Objects Situated at LEO With Their Successive De-Orbiting”. *Science and Education. Bauman Moscow State Technical University. Electronic journal*, No. 4: 48-64. https://doi.org/10.7463/0416.0838417.
30. Baranov, A., Chernov, N. 2019. “Energy Cost Analysis to Station Keeping for Satellite Formation Type ‘TerraSAR-X–TanDEM-X’”. *RUDN Journal of Engineering Researches*, No. 3: 220-228. https://doi.org/10.22363/2312-8143-2019-20-3-220-228
31. Baranov, A., Garanin O., Grishko, D., Ryltsova E. et al. 2018. “Flights between space debris objects in the vicinity of the geostationary orbit”. *KIAM Preprint #190*: 1–27. https://doi.org/10.20948/prepr-2018-190

32. Baranov, A., Golikov, A. 1999. “Optimal Manoeuvres for Station Keeping for a Given Configuration of the Satellite Constellation”. *Proceedings of the 14th International Symposium on Space Flight Dynamics*: 482–485.
33. Baranov, A., Grishko, D. 2015. “Ballistic Scheme Selection for Manoeuvring Inside a Constellation with Continuously Changing Configuration”. *Proceedings of the 66th International Astronautical Congress, IAC 2015*, V. 7: 5450–5462.
34. Baranov, A., Grishko, D., Lapshin V., Medvedevskikh, V. 2016. "Solution of the flyby problem for large space debris at sun-synchronous orbits". *Cosmic Research*, No. 3: 229–236. https://doi.org/10.1134/S0010952516030011.
35. Baranov, A., Grishko, D., Mayorova, V. 2013. “Estimation of Delta-V Expenses, Necessary for Maintenance and Replenishment of Satellite Constellations on Circular Orbits”. *Engineering journal: Science and Innovations*, No. 3.
36. Baranov, A., Grishko, D., Mayorova, V. 2015. “The Features of Constellations Formation and Replenishment at Near-Circular Orbits in Noncentral Gravity Fields”. *Acta Astronautica*, V. 116: 307–317. https://doi.org/10.1016/j.actaastro.2015.06.025.
37. Baranov, A., Grishko, D. 2013. “Problems of minimizing summary characteristic velocity required for maintenance and replenishment of satellite systems at non-coplanar circular orbits”. *Science and Education. Bauman Moscow State Technical University. Electronic journal*, No. 9: 289–312.
38. Baranov, A., Grishko, D. 2014. “Ways of Energetic Expenses Decreasing for Flybys Between Satellite Constellation Elements”. *Polet*, No. 8: 39–48.
39. Baranov, A., Grishko, D. 2015. “Ballistic Aspects of Large-Size Space Debris Flyby at Low-earth Near-Circular Orbits”. *Journal of Computer and Systems Sciences International*, No. 4: 639–650. https://doi.org/10.1134/S106423071504005X
40. Baranov, A., Gundobin, I., Ivanov D., Kapralov M., Terehova E. 1992. “Spacecraft Orbital Motion Control in the Program of Manned Flights”. *Proceedings of XVI Scientific Readings on Cosmonautics, section Applied Celestial Mechanics and Motion Control*: 26–27.
41. Baranov, A., Karatunov, M., Razoumny, Y., Vikhrachev, V. 2017. “A Geometric Method of Near-Circular Orbit Determination after Single Correction”. *Journal of Computer and System Sciences International*, No. 1: 141–149.

42. Baranov, A., Karatunov, M. 2012. “Optimization Method of Searching for Dangerous Approaches on Near-Earth Orbits”. *Molodezhny nauchno-technichesky vestnik*, No. 5.
43. Baranov, A., Karatunov. 2016. “Techniques of Identification and Evaluation of Spacecraft Approaches to Space Debris”. *Engineering Journal: Science and Innovation*, No. 4.
44. Baranov, A., Karatunov, M. 2016. “Estimation of Parameters of Two Coupled Manoeuvres Performed by an Active Space Object”. *Journal of Computer and System Sciences International*, No. 2: 284–295. https://doi.org/10.1134/S1064230716010068.
45. Baranov, A., Labourdette P. 2002. “Strategies for On-Orbit Rendezvous Circling Mars”. *Advances in the Astronautical Sciences*, V. 109.
46. Baranov, A., Roldugin, D. 2011. “Optimal six- and five-impulses rendezvous on near-circular noncoplanar orbits”. *Preprint M.V. Keldysh Institute of Applied Mathematics of Russian Academy of Sciences*, No. 57.
47. Baranov, A., Roldugin, D. 2012. “Six-Impulse Manoeuvres for Rendezvous of Spacecraft in Near-Circular Noncoplanar Orbits”. *Cosmic Research*, No. 6: 441–448. https://doi.org/10.1134/S0010952512050012.
48. Baranov, A., Terekhova E. 1993. “Optimal in Terms of Primer Vector Four-Impulse Rendezvous in the Vicinity of Circular Orbit”. *Preprint M.V. Keldysh Institute of Applied Mathematics of Russian Academy of Sciences*, No. 7.
49. Baranov, A., Terekhova E. 1995. “ Optimal Four-Impulse Rendezvous in Coplanar Near-Circular Orbits”. *Cosmic Research*, No. 4: 382-387.
50. Baranov, A. 1986. “Algorithm for Calculating of Parameters of Four-Impulse Transitions Between Close Almost-Circular Orbits”. *Cosmic Research*, No. 3: 324–327.
51. Baranov, A. 1989. “Geometric Solution of the Problem of a Rendezvous on Close Nearly Circular Coplanar Orbits”. *Cosmic Research*, No. 6: 689–697.
52. Baranov, A. 1990. “An Algorithm for Calculating Parameters of Multiple-orbit Manoeuvres in Remote Guidance”. *Cosmic Research*, No. 1: 61–67.
53. Baranov, A. 2001. “Optimal Transitions Between the Orbits That Have Significant Deviations of Longitude of the Ascending Node”. *Proceedings of the 25 Scientific Readings on Cosmonautics.*
54. Baranov, A. 2008. “Methods of Calculating Manoeuvre Parameters for Rendezvous with Orbital Station”. *Preprint M.V.*

Keldysh Institute of Applied Mathematics of Russian Academy of Sciences, No. 6: 32.

55. Baranov, A. 2008. “Numerical Analytical Determination of Parameters of Manoeuvres of Multiple-Revolution Spacecraft Rendezvous on Close Near-Circular Noncoplanar Orbits”. *Cosmic Research*, No. 5: 430–439.
56. Baranov, A. 2012. “Near-Circular-to-Near-Circular Flybys”. In *Encyclopedia Mashinostroenie, Vol. IV-22, Rocket and Space Engineering. Book 1*, edited by Legostaev, Victor, 141–151. Moscow: Mashinostoenie.
57. Baranov, A.1982."Optimal Rendezvous on Close Quasi-Circular Noncoplanar Orbits". *Proceedings of VI Scientific Readings on Cosmonautics, Institute for the History of Science and Technology of SU Academy of Sciences*:172–179.
58. Baranov, A.1985."A Geometric Solution of Impulsive Multiple-Revolution, Between Close Near-Circular Coplanar Orbits Transfer Problem".*Preprint M.V. Keldysh Institute of Applied Mathematics of SU Academy of Sciences*, No. 64.
59. Bartenev, V., Krasilshikov, M., Lebedev, A., Malyshev, V., Malyshev, V., Reshetnev, M. 1988. *Control and Navigation of Artificial Earth Satellites on Near-Circular Orbits*. Moscow.
60. Battin, R. 1966. *Astronautical Guidance*. New York: McGraw Hill Book Company.
61. Battin, R. 1977. “Lambert’s Problem Revisited”. *AIAA Journal*, V. 15: 707-713. https://doi.org/10.2514/3.60680
62. Bazhinov, I., and Yastrebov, V. 1978. *Navigation During the Joint Soyuz and Apollo Spacecraft Flight*. Moscow: Science.
63. Beletsky, V., Egorov, V. 1964. “Interplanetary Transfers with Steady Thrust”. *Cosmic Research*, No. 3: 360–391.
64. Belik, N., Belyaev, N., Uvarov, E. 1979. *Spacecraft Jet Propulsion Control Systems*. Moscow: Mashinostroenie.
65. Belikov, M., Gorshkov, O., Muravlev, V., Shagaida, A. 2007. “Electric Propulsion System on Base of Hall’s Engine KM-45 for GSAT-4 Spacecraft”. *IAC 2007 (58 International Astronautical Congress)*.
66. Bernussou, J., Brousse, P., Dufour, F., Foliard, J., Lamy, A., Lasserre, E., Lefebre, L., Vincent, M. 1997. “Relative Station Keeping Optimization for Starsys Constellation”. *Proceedings of the XII International Symposium on Space Flight Dynamics.*
67. Bernussou, J., Dufour, F., Lasserre, E. 1996. “Optimization and Simulation of the Station Keeping of an Homogeneous Satellite

Constellation". *2nd World Automation Congress (WAC'96)*: 169–174.
68. Bobronnikov, V., Fedorov, A., Krasilshikov, M., Malyshev, V., Nesterenko, O. 2001. "A Program Complex for Analysis, Synthesis and Control of Space Systems". *International Conference on Space–2001 Space without Weapons–Arena of Peaceful Cooperation in the XXI Century*: 43–45.
69. Bollman, W., D'Amario, L., Lee, W., Roncoli, R., Smith, J. 1999. "Mars Orbit Rendezvous Strategy for the Mars 2003/2005 Sample Return Mission". *AAS/AIAA Astrodynamics Specialist Conference*: 1–19.
70. Boltyansky, V., Gamkrelidze, R., Mishenko, E., Pontryagin, L. 1983. *Mathematical Theory of Optimal Processes: 4th edition*. Moscow: Nauka.
71. Borovin, G., Stepanyantz, V., Tuchin, A., Tuchin, D., Zakhvatkin, M. 2012. "Identification of Manoeuvres Performed With Low-Thrust". *Engineering journal: Science and Innovations*, No. 2.
72. Braude, A., Kuzmak, G. 1969. "An Approximate Determination of Optimal Flybys in Small Vicinity of Circular Orbit". *Cosmic Research*, No. 3: 323–338.
73. Braun, V., Flegel, S., Gelhaus, J., Kebschull, C. et all. 2013. "Active Debris Removal of Multiple Priority Targets". *Advances in Space Research*, No. 9:1638-1648. https://doi.org/10.1016/j.asr.2012.12.003.
74. Breeden, J., Guinn, Joe, Ocampo, Cesar. 2001. "Rendezvous Options and Dynamics for the Mars Sample Return Mission". *AAS/AIAA Astrodynamics Specialist Conference*: 1–20.
75. Bulynin, Y. 2008. "Ballistic Support of Orbital Motion Control of Geostationary Spacecraft on Different Operational Stages". *13 International Scientific Conference: System Analysis, Control and Navigation*: 73–74.
76. Bushuev, E., Krasovski, A. 1969. "A Geometric Solution of Impulsive, Between Close Near-Circular Orbits Transfer Problem". *Cosmic Research*, No. 4: 485–489.
77. Byram S., Slater G., Williams T. 2006. "Collision Avoidance for Satellites in Formation Flight". *Journal of Guidance, Control, and Dynamics*, No. 5: 1140–1146. https://doi.org/10.2514/1.16812.
78. Byrkov, B., Razoumny, Y. 1992. "A Solution of Solid Multiple Earth Coverage Problem with the Use of Artificial Earth Satellite Swath". *Issledovanie Zemli iz kosmosa*, No. 1: 62–68.

79. Carbonne, D., Chemama, F., Julien, E., Kudo, G., Labourdette, P., Laurent, S. 2009. “Manoeuvre Plans for the First ATV Mission”. *AAS/AIAA Astrodynamics Specialist Conference*: 1091–1106.
80. Carbonne, D., Goester, J., Labourdette, P. 2007. “ATV Phasing and Post-Escape”. *European workshop on space mission analysis, ESOC*.
81. Castronuovo, M. 2011. “Active space debris removal—A preliminary mission analysis and design”. *Acta Astronautica*, No. 9-10: 848-859. https://doi.org/10.1016/j.actaastro.2011.04.017.
82. Chao, C., Schmitt, D. 1991. “Eliminating GPS Stationkeeping Manoeuvres by Changing the Orbital Altitude”. *Journal of the Astronautical Sciences*, No. 2.
83. Chernov, A., Chernyavsky, G. 2004. *Earth Remote Sensing Orbits: Lections and Exercises*. Moscow: Radio and Communication.
84. Chiu, J., Prussing J. 1986. “Optimal Multiple-Impulse Fixed-Time Rendezvous Between Circular Orbits”. *Journal of Guidance, Control and Dynamics*, No. 1: 17–22. https://doi.org/10.2514/3.20060
85. Cour-Palais, B., Kessler, D. 1978. “Collision Frequency of Artificial Satellites: The Creation of a Debris Belt”. *Journal of Geophysical Research*, V. 83: 2637–2646. https://doi.org/10.1029/JA083iA06p02637
86. Crowther, R., Lewis, H., Stokes, H., White, A. 2012. “Synergy of Debris Mitigation and Removal”. *Acta Astronautica*, No. 1: 62–68. https://doi.org/10.1016/j.actaastro.2012.06.012
87. Dashkov, A., Kubasov, V. 1979. *Interplanetary Transfers*. Moscow: Mashinostroenie.
88. Doll, J., Gobetz, F., 1969. “A Survey of Impulsive Trajectories”. *AIAA Journal*, No. 5: 801-834. https://doi.org/10.2514/3.5231
89. Dubrovski, Y., Shershneva, N., Zhuravlev, K. 2005. “Ballistic Modeling and Perspective Hydrometeorological Spacecraft Operational Orbits Determination”. *Electromechanics Issues*, V. 102: 220–234.
90. Edelbaum, T. 1967. “Minimum Impulse Transfer in the Vicinity of a Circular Orbit”. *Journal of the Astronautical Sciences*, No. 2: 66–73.
91. Egorov, V. 1965. *Spatial Problem of Reaching the Moon*. Moscow: Nauka.
92. Egorov, V., Grigoriev, I., Ryzhov, S. 2005. “Optimization of Multiple-Revolution Interorbital Spacecraft Transfers”. *Preprint*

M.V. Keldysh Institute of Applied Mathematics of Russian Academy of Sciences, No. 63.
93. El'yasberg, P.1965. *Introduction to the Theory of Flight of Artificial Earth Satellites*. Moscow: Nauka.
94. Emanuelli, M., Ronse, A., Tintori, C., Trushlyakov, V. 2012. "A Space Debris Removal Mission Using the Orbital Stage of Launchers". *Dynamics of Systems, Mechanisms and Machines*, No. 2: 185–218.
95. Ermilov, Y., Ivanova, E., Panushin, S. 1977. *Control of Spacecraft Approaching*. Moscow: Nauka.
96. Escobal, P. 1970. *Methods of Orbit Determination*. Moscow: Mir.
97. Estes, H, Foster J. 1992. "A Parametric Analysis of Orbital Debris Collision Probability and Manoeuvre Rate for Space Vehicles". *NASA/JSC-25898*: 1–17.
98. Fedorov, A., Malyshev V. 2001. "A Program Complex for Spacecraft Manoeuvres Determination". *International Conference on Space–2001 Space without Weapons–Arena of Peaceful Cooperation in the XXI Century*: 45–46.
99. Fehse, W. 2003. *Automated Rendezvous and Docking of Spacecraft*. London: Cambridge University Press.
100. Foster, J., Stansbery, E. 2003. "Fundamentals of Debris Collision Avoidance". *54th International Astronautical Congress of the International Astronautical Federation, the International Academy of Astronautics, and the International Institute of Space Law*. https://doi.org/10.2514/6.IAC-03-IAA.5.3.03
101. Frayssinhes, E., Lansard, E., Palmade, J-L. 1998. "Global Design of Satellite Constellations: A Multiple-Criteria Performance Comparison of Classical Walker Pattern and New Design Patterns". *Acta Astronautica*, No. 9: 555–564. https://doi.org/10.1016/S0094-5765(98)00043-5
102. Gavrilov, A. 1995. "Search of Functional Global Minimum for Solution of Spacecraft Linear Manoeuvre Problem". *Rocket-Space Technics, Research and Technology Bulletin*, No. 1.
103. Gavrilov, A. 2000. "Using Branch-and-Bound Method for Rendezvous Problem Solution". *Proceedings of the XV International Symposium on Space Flight Dynamics.*
104. Gavrilov, V., Obukhov, E. 1980. "Correction Problem with Fixed Number of Impulses". *Cosmic Research*, No. 2: 163–172.
105. Gavrilov, V., Obukhov, E., Skoptsov, A., Zaslavsky, G. 1975. "An Algorithm of Solution of Some Two-Impulse Correction

Problems". *Preprint M.V. Keldysh Institute of Applied Mathematics of SU Academy of Sciences*, No. 125.

106. Golikov, A. 1990. "Numerical-Analytical Theory of Motion of Artificial Satellites of Celestial Bodies". *Preprint M.V. Keldysh Institute of Applied Mathematics of SU Academy of Sciences*, No. 70.
107. Golikov, A. 2008. "Semi-analytical Theory THEONA & Constellation Motion Analysis". *5 International Workshop on Constellations and Formation Flying, MAI Proceedings*.
108. Golubev, Y. 2010. "Brachistichrone with Friction". *Journal of Computer and Systems Sciences International*, No. 5: 41–52.
109. Gorshkov, O. 1999. "Native Electric Jet Engines Today". *News of Cosmonautics*, No. 7: 56–58.
110. Grigoriev, I., Zapletin, M. 2009. "Constructing Pontryagin Extremals for Optimal Control Problem of Asteroid Flyby". *Automation and Remote Control*, No. 9: 1499-1513. https://doi.org/10.1134/S0005117909090045.
111. Grigoriev, I., Zapletina, E., Zapletin, M. 2007. "First ACT Global Trajectory Optimization Competition: Results Found at Moscow State University". *Acta Astronautica*, No. 9: 758–762. https://doi.org/10.1016/j.actaastro.2007.03.002
112. Grodzovski, G., Ivanov, Y., Tokarev, V. 1966. *Space Flight Mechanics with Low-Thrust*. Moscow: Nauka.
113. Gross, L., Prussing, J. 1974. "Optimal Multiple-Impulse Direct Ascent Fixed-Time Rendezvous". *AIAA Journal*, No. 7: 885-889. https://doi.org/10.2514/3.49376
114. Guojin, T., Jin, Z., Yazhong, L. 2013. "Survey of Orbital Dynamics and Control of Space Rendezvous". *Chinese Journal of Aeronautics*, No. 1: 1–11. https://doi.org/10.1016/j.cja.2013.07.042.
115. Guo-Jin, T., Hai-Yang, L., Ya-Zhong, L., Yong-Jun, L. 2007. "Optimization of Multiple-Impulse, Multiple-Revolution, Rendezvous-Phasing Manoeuvres". *Journal of Guidance, Control and Dynamics*, No. 4: 946-952. https://doi.org/10.2514/1.25620.
116. Guo-Jin, T., Hai-Yang, L., Ya-Zhong, L. 2007. "Hybrid Approach to Optimize a Rendezvous-Phasing Strategy". *Journal of Guidance, Control and Dynamics*, No. 1: 185–191. https://doi.org/10.2514/1.20232.
117. Guzman, J., Hughes, S., Mailhe, L. 2003. "A Comparison of Trajectory Optimization Methods for the Impulsive Minimum

Fuel Rendezvous Problem". *Advances in the Astronautical Sciences*, V. 113: 85–104.
118. Han, C., Xie, H. 2004. "Study on Multi-Revolution Lambert Transfer Algorithm for Rendezvous". *Chinese Space Science and Technology*, No. 5: 9–13.
119. Handelsman, M., Lion, P. 1968. "Primer vector on fixed-time impulsive trajectories". *AIAA Journal*, No. 1: 127–132. https://doi.org/10.2514/3.4452.
120. Herrick, S. 1978. *Astrodynamics*. Moscow: Radio and Communication.
121. Himmelblau. 1975. *Applied Nonlinear Programming*. Moscow: Mir.
122. Hironori, S. 2014. "Evaluation of a Satellite Constellation for Active Debris Removal". *Acta Astronautica*, No. 1: 136–144. https://doi.org/10.1016/j.actaastro.2014.08.026.
123. Il'in, V., Kuzmak, G. 1976. *Optimal Flight of Spacecraft*. Moscow: Nauka.
124. Iutkin, E., Trushliakov, V. 2013. "Overview of Means for Docking and Capture of Large-scale Space Debris Objects". *Omsk Scientific Bulletin*, No. 2: 56–61.
125. Ivanov, S, ed. 2002. *Encyclopedia Russian Weaponry and Technology. XXI century. Vol. 5 Space-Borne Spacecraft-Carried Weapons*. Moscow: Weaponry and Technology Publishing.
126. Ivashkin, V., Raykunov, G. 1991. "Optimization of the two-impulse rendezvous manoeuvre of two spacecraft in circular orbit under constraints". *Cosmic Research*, No. 3: 352–374.
127. Ivashkin, V., Raykunov, G. 1994. "Multiple-Impulse Two Spacecraft Rendezvous Trajectories in Circular Orbits". *Cosmic Research*, No. 3: 33–46.
128. Ivashkin, V. 1975. *Optimization of Space Manoeuvres With Constraints on Distances to Planets*. Moscow: Nauka.
129. Ivashkin, V. 2012. "Some Impulsive Transfers". In *Encyclopedia Mashinostroenie, Vol. IV-22, Rocket and Space Engineering. Book 1*, edited by Legostaev, V. Moscow: Mashinostroenie.
130. Jezewski, D., Rozendaal, H. 1968. "An Efficient Method for Calculating Optimal Free-Space N-Impulse Trajectories". *AIAA Journal*, No. 11: 2160–2165.
131. Johnson N., Liou J. 2009. "Characterization of the cataloged Fengyun-1C fragments and their long-term effect on the LEO environment". *Advances in Space Research*, V. 43: 1407–1415. https://doi.org/10.1016/j.asr.2009.01.011.

132. Jones, J. 1976. “Optimal Rendezvous in Neighborhood of a Circular Orbit”. *Journal of the Astronautical Sciences*, No. 1: 55–90.
133. Kazakova, R., Platonov, A. 1976. “Orbit Design System in Applied Problems of Celestial Mechanics”. *Preprint M.V. Keldysh Institute of Applied Mathematics of SU Academy of Sciences*, No. 106.
134. Kelly B., Picciotto S. 2005. “Probability Based Optimal Collision Avoidance Manoeuvres”. *AIAA 2005-6775, Space 2005 forum*. https://doi.org/10.2514/6.2005-6775
135. Klinkrad, H. 2007. “On-orbit risk reduction-collision avoidance”. *Journal of Aerospace Engineering*, No. 6: 955-962. https://doi.org/10.1243/09544100JAERO171
136. Kolegov, G. 2007. *Selected Sections of Artificial Earth Satellite Space Ballistics*. Korolev: Tsniimash.
137. Kolegov, G., Melnikov, E. 1990. “Long-Term Manoeuvre Planning for Space Complex Operational Orbit Adjustment”. *Bulletin of SU Academy of Sciences, Series Cybernetics*, No. 3: 158–165.
138. Konstantinov, M. 1997. “Optimization of Low-Thrust Transfer between Noncoplanar Elliptic Orbits”. *Paper IAF-97-A.6.06*.
139. Kozai, Y. 1959. “The Motion of a Close Earth Satellite”. *Astronomical Journal*, V. 64: 367–377.
140. Kozlov, P., Razoumny, V., Razoumny, Y. 2015. “A Method for Calculating Parameters of Compound Satellite Constellations on Circular and Elliptic Nodally Synchronized Orbits”. *Scientific and Technical Volga Region Bulletin*, No. 3: 196-199.
141. Kozlov, P., Razoumny, V., Razoumny, Y. 2015. “Analyzing Parametric Relations for Circular and Elliptic Nodally Synchronized Orbits”. *Scientific and Technical Volga Region Bulletin*, No. 3: 200–204.
142. Kriz, J. 1976. “A Uniform Solution of the Lambert Problem”. *Celestial Mechanics*, V. 14: 509–513. https://doi.org/10.1007/BF01229061
143. Kvasnikov, L., Latyshev, L., Ponomarev-Stepnoy, N. et al. 2001. *Aircraft Engines*. Moscow: MAI.
144. L’vov, D., Stepanyantz, V. 2000. “An Effective Algorithm for Solution of Differential Equations of Motion System”. *Mathematical Modeling*, No. 6: 9–14.
145. Lawden, D. 1966. *Optimal Trajectories for Space Navigation*. Moscow: Mir.

146. Lebedev, V. 1968. *Motion Determination of Spacecraft with Low-Thrust*. Moscow: VTs of SU Academy of Sciences.
147. Levitan, Y., Sobol, I. 1976. “Acquisition of Points Equally Distributed in Multiple-Dimensional Cube”. *Preprint M.V. Keldysh Institute of Applied Mathematics of SU Academy of Sciences*, No. 40.
148. Lewis, H., White, A. 2014. “An Adaptive Strategy for Active Debris Removal”. *Advances in Space Research*, No. 8: 1195–1206. https://doi.org/10.1016/j.asr.2014.01.021
149. Lidov, M. 1971. “Mathematical Analogy between Some Optimal Problems of Trajectory Corrections and Selection of Measurements and Algorithms of Their Solution”. *Cosmic Research*, No. 5: 687–706.
150. Lidov, M., Teslenko, N. 1978. “Optimization of Some Problems Solution of Spacecraft Flight Control Using Method of Descent by Parameter”. In *Mathematical Support of Space Experiments*, edited by P. El'yasberg, 112–141. Moscow: Nauka.
151. Marec, J-P. 1968. “Contribution a L’Etude des Rendezvous Multi-Impulsionnels, Optimaux, -de Dureee Moyenne, Entre Orbits Quasi-Curculaires, Proches, non Coplanaires”. *2nd International Colloquin on Methods of Oprimization*.
152. Marec, J-P. 1979. *Optimal Space Trajectories*. Amsterdam-Oxford-New York: Studies in Astronautics; V.1. Elsevier Sci. Pub. Co.
153. Melnikov, E. 2004. “Manoeuvring Strategy for Manned International Space Station”. *Cosmonautics and Rocketry*, No. 37: 176–186.
154. Melnikov, E. 2009. *Construction of International Space Station: Planning and Actual Status*. Korolev: Tsniimash.
155. Mozhaev, G. 1968. "Continuous Earth Surface Coverage Satellite Constellation Obit Optimization Problem". *Third All-Union Meeting on Theoretical and Applied Mechanics. Annotation of Papers*.
156. Mozhaev, G. 1972,1973. “Earth Continuous Coverage Problem and Kinematically Right Satellite Constellations I, II”. *Cosmic Research*, No. 6: 833-843, No. 1:59–68.
157. Mozhaev, G. 2001. “Solution of Some Problems of Optimization of Processes of Flexible Motion Correction of Satellite Constellations I, II”. *Cosmic Research*, No. 5: 518-530, No. 6:634–647.

158. Murtazin, R. 1998. “Algorithm of Spacecraft Motion Control for Low Earth Satellite Communication Constellations”. *Journal of Computer and Systems Sciences International*, No. 2: 173–182.
159. Murtazin, R. 2012. “Ballistic Support of Rapid Spacecraft-Orbital Station Approaching Schemes”. *Cosmic Research*, No. 4: 142–149.
160. Murtazin, R. 2013. “Spacecraft Launched From Earth with Lunar Orbital Station Rendezvous Scheme”. *Proceedings of XXXVIII Academic Scientific Readings on Cosmonautics*.
161. Murtazin, R. 2014. “Fast Orbital Station Access to Orbital Station for Modern Spacecraft Scheme”. *Cosmic Research*, No. 2: 162–175.
162. Nazarenko, A., Skrebushevsky, B. 1981. *Satellite Constellation Evolution and Stability*. Moscow: Mashinostroenie.
163. Naziriov, R., Timokhova, T. 1993. “Elliptic Orbits Optimal Linear Correction”. *Automatics and Telemechanics*, No. 3: 93–101.
164. Ohotsimsky, D., Sikharulidze, Yu. 1990. *Fundamentals of Space Flight Mechanics*. Moscow: Nauka.
165. Patera, R., Peterson, G. 2003. “Space Vehicle Manoeuvre Method to Lower Collision Risk to an Acceptable Level”. *Journal of Guidance, Control, and Dynamics*, No. 2: 233–237. https://doi.org/10.2514/2.5063
166. Petrov, B., ed. 1985. *Flight Navigation Support for Salut-6 – Soyuz – Progress Orbital Complex*. Moscow: Nauka.
167. Petukhov, V. 2004. “Optimization of Multi-Orbit Transfers between Noncoplanar Elliptic Orbits”. *Cosmic Research*, No. 42: 250-268. https://doi.org/10.1023/B:COSM.0000033300.18460.a4.
168. Petukhov, V. 2008. “Optimization of Spacecraft Interplanetary Trajectories with Perfectly Regulated Engine by Method of Continuation”. *Cosmic Research*, No. 46: 219-232. https://doi.org/10.1134/S0010952508030052.
169. Petukhov, V. 2012. “Method of continuation for optimization of interplanetary low-thrust trajectories”. *Cosmic Research*, No. 50: 249-261. https://doi.org/10.1134/S0010952512030069
170. Pitkin, E. 1968. “A General Solution of Lambert Problem”. *Journal of the Astronautical Sciences*, No. 5: 270–271.
171. Pollard, J. 2000. “Simplified Analysis of Low-Thrust Orbital Manoeuvres”. *Aerospace report, no. TR-2000(8566)-10, SM-TR-0031*: 1–39.

172. Prussing, J. 1969. “Optimal four-impulse fixed-time rendezvous in the vicinity of a circular orbit”. *AIAA Journal*, No. 5: 928-935. https://doi.org/10.2514/3.5246.
173. Prussing, J. 1970. “Optimal Two- and Three-Impulse Fixed-Time Rendezvous in the Vicinity of a Circular Orbit”. *AIAA Journal*, No. 7: 1221-1228. https://doi.org/10.2514/2.7041.
174. Prussing, J. 2000. “A Class of Optimal Two-Impulse Rendezvous Using Multiple-Revolution Lambert Solutions”. *Journal of the Astronautical Sciences*, No. 2: 31–148.
175. Raykunov, G. 2002. *Ballistic Support of Servicing of Aircraft Constellations on Circular Orbits*. Moscow: PJSC “Institut podgotovki kadrov mashinostroeniya i priborostroeniya”.
176. Razoumny, Y. 1993. “On Optimization of Design and Ballistic Parameters of Constellations for Periodic Coverage”. *Issledovanie Zemli iz kosmosa*, No. 1.
177. Rylov, Y. 1985. “Control of Spacecraft from the Satellite Constellation with the Help of Electric Jet Engines”. *Cosmic Research*, No. 5: 691–714.
178. Saulsky, V. 2005. “Multisatellite systems with linear structure and their application for continuous coverage of the earth”. *Cosmic Research*, No. 43: 34–51. https://doi.org/10.1007/s10604-005-0017-5.
179. Shen, H., Tsiotras P. 2003. “Optimal Two-Impulse Rendezvous Using Multiple-Revolution Lambert Solutions”. *Journal of Guidance, Control and Dynamics*, No. 1: 50-61. https://doi.org/10.2514/2.501
180. Sikharulidze, Y. 1982. *Aircraft Ballistics*. Moscow: Nauka.
181. Sokolov, A., Ulybyshev, Y. 1999. “Many-revolution, low-thrust manoeuvres in vicinity of geostationary orbit”. *Journal of Computer and Systems Sciences International*, No. 2: 95–100.
182. Soloviev, Ts., Tarasov, E. 1973. *Interplanetary Flight Forecasting*. Moscow: Mashinostroenie.
183. Sukhanov, A. 1988. “A Universal Solution of Lambert’s Problem”. *Cosmic Research*, No. 4: 483–491.
184. Sukhoi, Y. 2011. *Geostationary Satellite Orbit Correction*. Moscow: Sputnik+.
185. Suslov, G. 1946. *Theoretical Mechanics*. Moscow: Gostechizdat.
186. Trofimov, Y. 2014. “Optimal Multiple-Impulse Solution of Problem of Circular Orbit Phasing”. *Actual Problems of Russian Cosmonautics, Proceedings of XXXVIII Academic Readings on Cosmonautics*: 140–141.

187. Tuchin, A. 2004. “Parameter Determination of the Spacecraft Motion by Results of Measurements Provided a Noise is in Dynamic System”. *Preprint M.V. Keldysh Institute of Applied Mathematics of Russian Academy of Sciences*, No. 2.
188. Ulybyshev, S. 2015. “Combined satellite systems for continuous global coverage in equatorial and polar circular orbits”. *Cosmic Research*, No. 53: 311–322. https://doi.org/10.1134/S0010952515040085.
189. Ulybyshev, S. 2016. “Design of Unhomogeneous Satellite Constellations for Continuous Global Coverage on Equatorial and Near-Polar Circular Orbits”. *Cosmic Research*, No. 4: 1–11.
190. Ulybyshev, Y. 1998. “Long-Term Formation Keeping of Satellite Constellation Using Linear-Quadratic Controller”. *Journal of Guidance, Control and Dynamics*, No. 1: 109–115. https://doi.org/10.2514/2.4204.
191. Ulybyshev, Y. 1999. “Near-Polar Satellite Constellations for Continuous Global Coverage”. *Journal of Spacecraft and Rockets*, No. 1: 92-99. https://doi.org/10.2514/2.3419.
192. Ulybyshev, Y. 2008. “Optimization of Multiple-Regime Approaching Trajectories with Constraints”. *Cosmic Research*, No. 2: 135–147.
193. Ulybyshev, Y. 2012. “Optimization of Interorbital Low-Thrust Transfers with Constraints”. *Cosmic Research*, No. 5: 403–418.
194. Vallado, D. 2007. *Fundamentals of Astrodynamics and Applications*. New York: Microcosm Press Hawthorne and Springer.
195. Walker, J. 1971. “Some Circular Orbit Patterns Providing Continuous Whole Earth Coverage”. *Journal of British Interplanetary Society*, No. 11: 369–384.
196. Wright, S. 1997. *Primal-Dual Interior-Point Methods*. Philadelphia: Society for Industrial and Applied Mathematics. https://doi.org/10.1137/1.9781611971453.
197. Zakharov, Y. 1984. *Interorbital Spacecraft Design*. Moscow: Mashinostroenie.
198. Zarubin, V., Krischenko, A., ed. 2004. *Discrete Mathematics. Mathematics in Technical University*. Moscow: Bauman Moscow State Technical University Publishing.